DOCTORAL THESIS

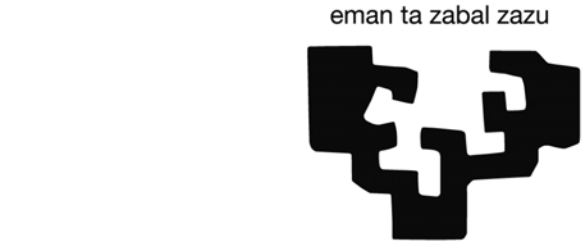

Universidad del País Vasco

Euskal Herriko Unibertsitatea

Algorithms for colour image processing based on neurological models

Submitted by:

Mrs. Estibaliz Garrote Contreras

In fulfilment of the degree of Doctor granted by the University of the Basque Country, European Doctorate.

Directed by

Dr. Pedro Mª Iriondo Bengoa.

Bilbao, January 2011

ISBN: 978-84-694-5841-9

DOCTORAL THESIS

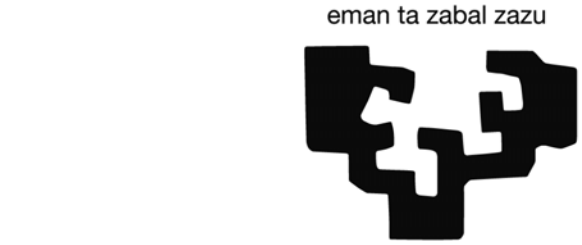

Universidad del País Vasco

Euskal Herriko Unibertsitatea

Algorithms for colour image processing based on neurological models

Submitted by:

Mrs. Estibaliz Garrote Contreras

In fulfilment of the degree of Doctor granted by the University of the Basque Country, European Doctorate

Directed by

Dr. Pedro Mª Iriondo Bengoa.

Bilbao, January 2011

To Borja who crossed an ocean for me

Acknowledgments:

First, I would like to gratefully acknowledge my thesis director, Dr. Pedro Mº Iriondo, whose invaluable help has made this thesis possible. Thank you for all the times you helped me straighten diffuse thoughts and to put me back on the right track, for your critical thinking and for sharing with me the need to establish clear goals in research.

Second, I would like to thank the research team at CBCL at MIT that is directed by Professor Tomaso Poggio, who provided me with first hand access to some of the best visual models that are being developed at this time. Especially, to Dr. Thomas Serre, who invited me to his new lab at Brown University and Dr. Gadi Geiger, for their enthusiasm and dedication. To professor John Mollon at the Vision Lab at Cambridge University who set me in colour theory and mostly for being a laudable example as a researcher, for his dedication to science, his attention to detail and his zeal. To Professor Anya Hurlbert at the Institute of Neuroscience at Newcastle University for granting me the opportunity to learn new fields within colour perception theory.

I would like to thank the support provided by TECNALIA RESEARCH & INNOVATION, and especially to INFOTECH´s unit director, Mrs. Ana Ayerbe, for her support towards research and for her vision to broaden and expand to new international horizons in order to grow as a technology centre.

I would also like to thank the Basque Government who has provided financial support through the ETORTEK programme for my research stays in the Massachusetts Technical Institute (MIT) and Cambridge University. Thank you for the commitment to provide researchers with the opportunity to make a research stay in renowned international groups.

I would also like to thank the support provided by my workmates at INFOTECH, thanks for your patience throughout this time.

Finally, I would like to thank the support provided by my parents, for teaching me to be inquisitive and to not settle with what is already known. To my siblings for their support and patience, especially to Raquel, who came to visit me in Boston and Cambridge when I needed it most. To all my friends who I have been unable to see in these last months of the thesis, thank you for not forgetting me. And last, to Borja, who has suffered most with this thesis. Thank you for providing me with support in those days when the system didn't seem to function, for encouraging me to continue and for reminding me the usefulness of research for society.

Abstract—.

Colour image processing is nowadays mostly achieved through the extrapolation of algorithms developed for images in grey levels into three colour planes, either RGB or some transformed planes, such as HSI, CIELAB... These techniques provide reliable solutions only in simple situations. As colour is a perception and not a characteristic inherent to objects, this thesis has developed new bioinspired algorithms for colour image processing.

The work of this thesis has joined elements in colour theory and processing undertaken in the human visual system. A new functional model of the retina has been developed where each cell type has been characterised according to its connections, distribution and size. A retina architecture has been created which provides detailed information about its cell elements and organisation. This has allowed the creation of a retina model that generates a set of parallel output channels as happens in the human retina. The level of detail provided in the model has allowed the characterisation of each of the pathways with a precision that is not present in existing models described in scientific publications.

The development of a colour processing model requires the combination of a functional retina model with colour appearance models. This union has achieved a new algorithm for colour image processing that provides colour attributes, such as: hue, lightness, brightness, saturation, chroma, colourfulness as well as edge detection components both in chromatic as well as achromatic components. The results provided by this model have been compared with CIECAM02 model's ones and have obtained noticeably better results in the "*ab*" plane and in the attributes calculated on Munsell colour samples. The colour processing model is backed by its results and has allowed identifying output channels of the retina that make up the usual "a", "b" and "A" channels in colour appearance models.

This model entails a step forward on colour processing techniques that shall be of great use for image segmentation, characterisation and object identification.

Key Words — Colour image processing, neuroinspired models, computational modelling, colour appearance models.

Abstract—

Colour image processing is nowadays mostly achieved through the extrapolation of algorithms developed for images in grey levels into three colour planes, either RGB or some transformed planes, such as HSI, CIELAB... These techniques provide reliable solutions only in simple situations. As colour is a perception and not a characteristic inherent to objects, this thesis has developed new bioinspired algorithms for colour image processing.

The work of this thesis has joined elements in colour theory and processing undertaken in the human visual system. A new functional model of the retina has been developed where each cell type has been characterised according to its connections, distribution and size. A retina architecture has been created which provides detailed information about its cell elements and organisation. This has allowed the creation of a retina model that generates a set of parallel output channels as happens in the human retina. The level of detail provided in the model has allowed the characterisation of each of the pathways with a precision that is not present in existing models described in scientific publications.

The development of a colour processing model requires the combination of a functional retina model with colour appearance models. This union has achieved a new algorithm for colour image processing that provides colour attributes, such as: hue, lightness, brightness, saturation, chroma, colourfulness as well as edge detection components both in chromatic as well as achromatic components. The results provided by this model have been compared with CIECAM02 model's ones and have obtained noticeably better results in the "*ab*" plane and in the attributes calculated on Munsell colour samples. The colour processing model is backed by its results and has allowed identifying output channels of the retina that make up the usual "a", "b" and "A" channels in colour appearance models.

This model entails a step forward on colour processing techniques that shall be of great use for image segmentation, characterisation and object identification.

Key Words - Colour image processing, neuroinspired models, computational modelling, colour appearance models.

Index

Chapter I

Introduction

Throughout the History of Humankind great effort has been placed towards the research and development of intelligent systems. Although the beginnings were set early in Antiquity, the development and proliferation of electronic computational systems have paved the way towards the development and application of artificial intelligence [RICH_94].

On the other hand and more common place every time, natural models are analysed in search of new solutions and strategies. This set of activities can be encompassed within the convergence of biology, computational and cognitive systems. The works being undertaken in this convergence can be grouped, as the EC notes, in four great areas [EC_07]:

- New computational paradigms derived from models of the representation of knowledge and of the processing capacity of biological systems or of biological processes.
- Biomimetic artifacts that allow developing high-performance bioinspired devices.
- Two-directional interfaces between electronic or electromechanical devices and living organisms.
- Bio-hybrid systems that integrate biological components with artificial components.

This thesis focuses its research within the first area of work, new computational paradigms, more specifically, those applicable to the field of machine vision.

Sight is one of the senses, if not the sense, that provides most information to human beings. Machine vision arose as the field of knowledge that aims to automate image processing and its identification. Bio-computational works that are currently being carried out in this field are focusing on the analysis of hierarchical sequence of the processes that living beings use. The first element of this sequence is the retina, which is organised in a series of stratified layers. The light signals reach the first layer that is composed of photoreceptors, which in the case of a human being are over 105 million photoreceptors. The output signals of the retina are transmitted through the optic nerve which is made up of axons belonging to 1 million ganglion cells. These signals are transmitted to different areas of the central visual system: LGN, V1, V2…. where they combine different features of the captured image in the retina, to finally generate the visual perception [BEAR_06]. In order to carry out this analysis, within the computational approach, work is being carried out in the following lines:

- Measurement and study of the visual signal: modulation, intensity and activation times [MART_06, BI_98, BOOT_98, KREI_06].
- Analysis of the models and activation areas when presented different controlled stimuli [DOWN_01, HIRS_06, BOOT_98].

- Modelling of the processing pathways: movement detection, location of objects in a scene, object recognition, colour evaluation, etc. [SERR_07a, SERR_07b, SERR_06, BURK_86].

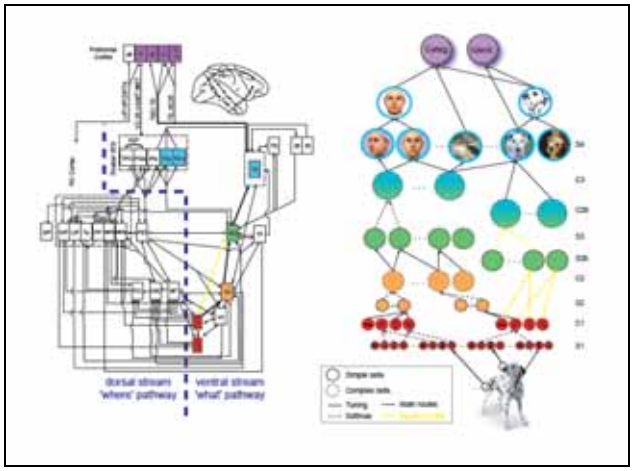

Figure 1.1. Visual processing model example. Source: [SERR_06]

Studies dealing with colour processing and analysis can be set within the information pathways modelling [BURK_06, HUNG_05].

Most research done in the field of machine vision works with images in gray levels. At first, this was due to the difficulty in obtaining colour images as well as the computation cost involved in increasing the number of input data. However, when the capacity to capture colour images improved and the computational capacity underwent a spectacular improvement, the main problem appeared: how to represent and/or measure a colour in order to make absolute and/or relative evaluations about it? For example, how to establish whether a colour is darker or lighter than another?

As J.C. Maxwell demonstrated, a single colour can be represented by three values. The most common is the use of red, green and blue hues (RGB: red, green, blue). The difficulty lies in transforming these three hues into colour attributes. Throughout time, multiple and varied proposals to measure and represent colour have been set forth (see [KUEH_03] for a compilation). These works have helped to increased our knowledge while at the same time have confirmed the existing lack of knowledge about colour, its behaviour and the way living beings perceive it. However, it is important to highlight that at this moment, one of the main points of agreement on colour is the fact that it is a perception rather than a physical characteristic of elements.

1. Motivation and Trajectory

For several years, I have been working in the field of Machine Vision. My first project was related to the identification of metals based on their colour. This was my first experience in colour and thus with the difference between the colours we perceive and the R, G and B values that are provided by a colour camera. I learnt the importance of taking into account the influence of lighting and the different spaces for colour modelling. Since then, I have worked with transformation to other colour spaces and with automated learning systems capable of adapting to the variations caused in real environments. I reached a point where I realised that most colour evaluations are based on what people perceive: the printing technician, the marketing personnel, the quality control manager... Therefore, I realised that in order to tackle colour applications of greater complexity I needed to have a more in-depth knowledge of the way in which human beings see and hence, perceive colour. This was the idea with which I began my doctorate research. As this is clearly a cross-disciplinary issue (involving biology, anatomy, information science, optics....), the collaboration with other research groups was necessary. I made a world-wide analysis of the different groups researching in this field. This analysis leads me to undertake different research stays. The first took place in 2008 at the research group at MIT: Center for Biological & Computational Learning (CBCL) directed by Dr. Tomaso Poggio, where a model of the human visual system is being developed. After a year-long stay in Boston, I began to complement those areas which I wanted to include within the model in this thesis. In order to achieve this, during 2009-2010, I made research stays at the University of Cambridge in the Vision Lab directed by Dr. John Mollon, expert in colour theory. Afterwards, I went to the Institute of Neuroscience at Newcastle University codirected by Dr. Anya Hurlbert, expert in colour constancy and psychophysicist. My last stay was at Brown University in the Serre Lab with Dr. Thomas Serre, who has developed a computational model for object recognition based on the visual system.

This thesis compiles both the work undertaken in these last years as well as the collaborations with the aforementioned research groups. Given the breadth of the field and the limitations placed on existing knowledge, the section on future works sets out shall be the ongoing journey of research that began with that first project on metals.

2. Aim of the Thesis

The aim of this thesis is to develop bioinspired algorithms for the processing of colour images. As colour is a perception, **the aim of this thesis is to analyse the way in which the human visual system process colour information and to define algorithms that make use of this analysis**. In turn, this objective can be divided into two areas:

- The hierarchical and sequential analysis of visual information processing modes as pertains to colour, performed by the human retina in order to build a **functional model of the retina**.
- The definition of a **colour processing model** to work with real images based on the retina model.

At this time, most capture and visualisation digital systems work with red (R), green (G) and blue (B) colour components. However, human beings analyse colours mainly through their hue (H), saturation (S) and intensity (I), as for example dark orange. There are multiple transformations between both spaces of representation, which, as a general rule, have been developed for the comparison or measurement of one or two colours in highly controlled environments. Bioinspired algorithms provide a new possibility for the processing of colour information which shall be especially useful for making comparisons between colours, which is to be able to measure the similarity of two colours not based on its RGB numerical difference but rather on measure that are closer to those used by human perception.

On the one hand, not being able to compare two colours reliably means not having stability in the segmentation of objects due to colour, while on the other hand, means having great difficulty when linking elements in image or video sequences.

Therefore, in order to fulfil the aims of this thesis, the following elements must be looked at:

- Study of colour: colour perception is a complex element which is associated with elements associated with both the observer as well as the environmental conditions. Therefore the following elements must be analysed: influence of the illumination and the influence of surrounding stimuli.
- Study of the physiological component involved in the process of perception and processing of colour, specifically, the sequence of processing related to the retina as the first element of the visual system.

- Modelling of the processing chain in the retina based on the neurons that make up the retina, its connections and chromatic and spatial characteristics.
- Development of a colour processing model with a nucleus that is bioinspired in the developed retina model and based on the theory of colour appearance models.
- Experimentation and testing of the results obtained by the models. The retina model shall be compared with biological measurements and the colour processing model with other existing colour perception models.

3. Content of the Thesis

This thesis is divided into 8 chapters that provide a detailed description of the different areas included in this work.

Chapter I is dedicated to the introduction of the thesis and its objectives. Chapter II provides a general framework of the knowledge in which to develop this research. General information on colour, its representation and measurement are presented; as well as the structure of the visual system from the retina to the different visual areas of the cortex related with colour information.

Chapter III shows the different colour models, the way to tackle the representation of colour based on physical measurements and its relation with the way of perceiving colour by human beings as well as the different factors that influence colour perception: lighting, background colour, intensity of the scene...

Chapter IV looks at the study of different types of elements present in the chain that originates in the retina and which reaches the first areas of the cortex. This Chapter deals with the study of the different types of neurons present in the retina and the different information channels generated in it.

Chapter V briefly looks at the post-retina stages in the visual system: the lateral geniculate nucleus and the cortex. There will be a discussion on the different existing areas and the general connections. The aim is to be able to place the retina model, object of this thesis, within a global context of visual processing as well as to lay the groundwork for future works.

Chapter VI present the functional model of the retina based on the research undertaken in the previous chapter. The different cell layers in the model, its structure, connections as well as the hypothesis and simplifications employed in its development, are shown. Once the model has been

established, a set of test stimuli are defined and the signals generated by each cell type when presented these stimuli are analysed against real measurements on retinas. Finally, the images generated in each cell type when presented several example stimuli are shown.

Chapter VII looks at the colour processing model based on the functional retina model of the previous chapter and on colour appearance models analysed in chapter III. A colour data base and a reference model are selected in order to analyse the results obtained after the application of the colour processing model. A final section is included which shows the results of the application of the colour processing model to real images.

Finally, Chapter VIII sets out the final conclusions and main contributions of this thesis as well as future works.

Chapter II

General knowledge and basic facts

This chapter sets forth general knowledge and data that will act as the basis for the following chapters.

First, some general knowledge on the measurement and description of colour will be presented. A brief description of the elements which are part of colour perception, scale types and the ways to measure colour differences shall be presented. These set the groundwork for Chapter III that will show the most relevant models in the colour representation including its characteristics and evolution.

Second, some basic concepts are laid out on the nervous system, such as its components, structure, signal transmission means and functional areas. These are the general ideas that are the basis of the works that shall be set forth in Chapters IV through VI.

1. Introduction to colour

What is colour and how should it be defined? As it is an everyday element in our daily life, its description should be simple. However, at times one can find curious situations, for example, when two people describe the colour of an object, one identifying it as greenish blue while the other describing it as bluish green. Who is right? Aren't they seeing the object in the same manner? Or is it simply a language problem?

Colour models were developed in order to resolve this and other questions. At the beginning of the 17th century, Aquilonius set out the first model which represented different colours in a continuous manner, ranging from white to black. New models were developed in later research carried out by I. Newton (1660) and J.W. Goethe (1810) among others. In the 19th century, J.C. Maxwell (1872) identified red, green and blue colours as primary colours. In the 20th century, A. H. Munsell (1915) proposed the first three-dimensional model which recognised hue, luminance and saturation.

In 1931, with several possible models available, the Comission Internationale de l'Eclairage - International Commission on Illumination (CIE) established a world wide colour standard, based on the reference established by the Maxwell model (see figure 2.4 chromaticity diagram).

The studies on colour have continued searching for a description that solves the problem of the computation of colour and provides a physiological interpretation thus answering new queries that arise with the advances both in technology as well as in those fields which use colour.

1.1 Perception and representation of colour

"A colour space belongs in the domain of psychology. The description of stimuli that under standard conditions result in perception of colours in that space is an aspect of physics."

R.G Kuehni 2003

Colour is a perception that is generated through physical stimuli. Hereunder are the elements and processes that influence this perception.

The human visual system builds images of the surrounding environment through the light that reaches the retina. Radiation is a form of energy. The part which is commonly associated with the word light corresponds to the visible spectrum, which ranges from 400nm to 760 nm.

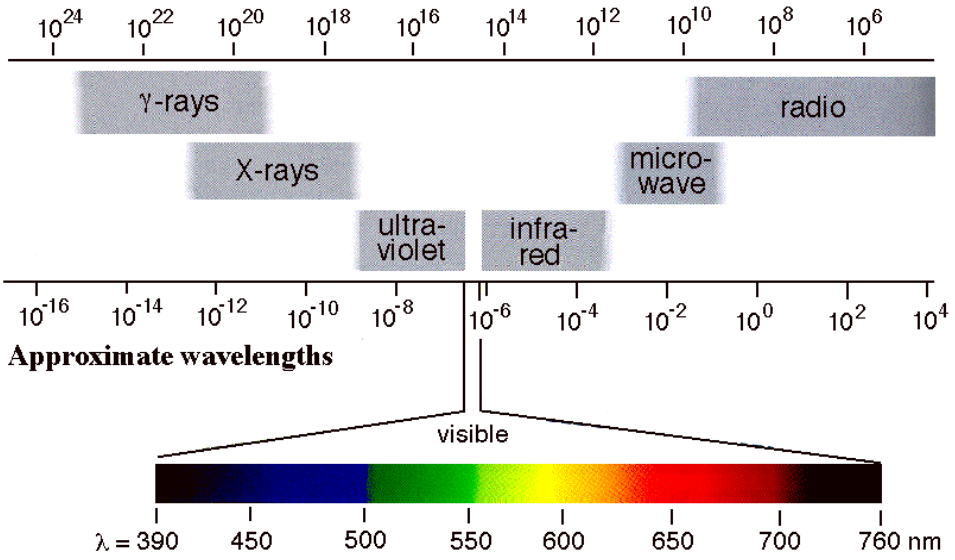

Figure 2.1. Electromagnetic radiation spectrum. Source: [BUDZ_02]

Light reaches objects and these transmit, reflect, absorb and/or modify it. The equation which sets out radiation is written as:

$$\text{Emitted Radiation}_{object}(\ ) = \text{Received}(\lambda) * C_{object}(\lambda) + \text{Emitted}_{object}(\lambda); \qquad \text{Eq. 2.1}$$

Where $C_{object}(\lambda)$ represents the behaviour of the object (reflection, refraction…).

As one can observe, this equation is specific for each wavelength. The eyes of living beings do not have the capacity to individually capture each wavelength. They are made up of

photoreceptors sensitive to specific bands of the spectrum. The human eye has 2 types of photoreceptors: rods and cones. Rods work in low light conditions while cones work in bright light conditions. There is only one type of rod and three types of cones that respond to the three different bands of light.

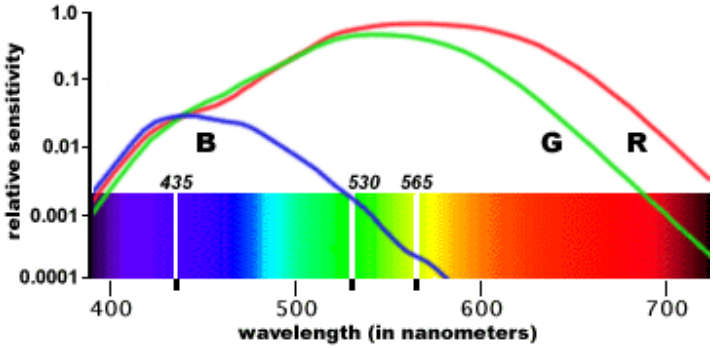

Figure. 2.2. Spectral sensitivity of the cones in the human eye. Source: [VOS_91]

Colour perception is deemed to be caused by cones as more than one type of absorption band is needed.

Figure 2.2 shows how the human eye has greater sensitivity to green, which is in the centre of the visible spectrum, than to red or blue. Experiments show that human beings are capable of distinguishing more levels of green than of blue or red.

If one takes into account that the human eye is capable of distinguishing up to 10 million colours and that colour is a psychological sensation, then it is clear that colour is going to be difficult to define. For this, different scales and associated systems can be used. As a general rule, the simplest scales are the nominal scale that assign a name to each element (for example, red, and green, blue...) and the ordinal scales that specifies the order of the elements that make up the scale (for example the tristimulus system CIE XYZ). Other types are the interval scales that define the size of the interval of each magnitude in every point of the scale (for example, Munsell's colour system).Ratio and absolute scales are more elaborate scales. In the first case, both the ratio as well as the interval are directly linked to colour attributes (for example, the length in metres). In the second case, all its elements reflect colour attributes. The applicability of these types of scales to colour is a matter which raises controversy [KUEH_03, WYSZ_00].

On the other hand, from the perspective of colour perception, a series of attributes have been defined. Those most widely used are:

- Lightness or luminance, that is, the amount of light. One can verify that the colour of an object is not the same when in shade or in sunlight.
- Hue: defines a colour such as red, green, blue, yellow...
- Saturation, which is the level of white in colour, for example, rose colour would have low saturation while red would have high saturation.

Hue and saturation are know as chromaticity features. The following figure is an example of the representation of these attributes.

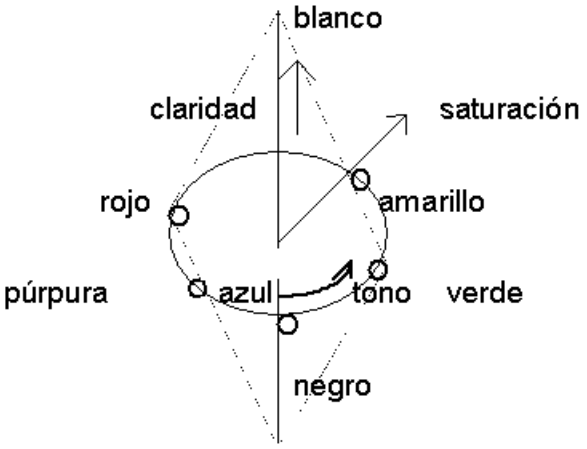

Figure 2.3. Colour representation model.

When lightness, the quantity of light, is increased, all hues tend to be seen as white. Likewise, if light is decreased, then they will tend to be seen as black. Figure 2.2 show the different hues going around the circumference, showing greater saturation as they gain distance from the centre of the circle. Based on this scheme, a widely used representation model, known as HSI, can be obtained which defines hue, saturation and intensity.

An important issue is the measurement of the difference between two colours. Metrics are defined in order to compare colours and measure their differences in a mathematical manner, which can be accomplished through more or less complex expressions based on the representation space. For example, in the RGB and HSI space, this can be done in a simple manner, as follows:

$$\Delta S_1 = \{(\Delta R)^2 + (\Delta G)^2 + (\Delta B)^2\}^{1/2} \quad \text{(Eq. 2.2)}$$

$$\Delta S_2 = \{(\Delta H)^2 + (\Delta S)^2 + (\Delta I)^2\}^{1/2} \quad \text{(Eq. 2.3)}$$

There is a threshold in colour differentiation, which is, given a specific colour, how much must this colour change in order to be perceived as a different colour by a standard observer? McAdam established these limits in an experimental manner (see Figure 2.4). These can be represented as those areas where:

$$\Delta S < \Delta S_0 \text{ (threshold of differentiation)} \qquad \text{(Eq. 2.4)}$$

The problem arises when evaluating these regions. If a system would be uniform, then the areas of uniform colour would be circumferences. However, in the spaces currently in use, they do not adjust to that geometry. It is because of this that new transformations are being sought which will really generate a uniform space.

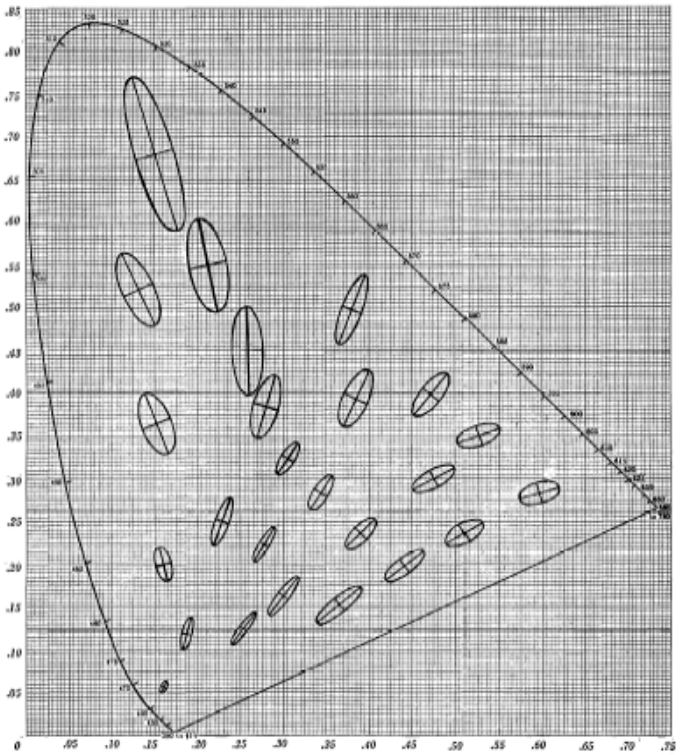

Figure 2.4. MacAdam Ellipses. Representation of experimental data on threshold differentiation obtained when evaluating colours and their variations by an average observer in the CIE 1931XY colour space. Source: [MACA_42]

2. Neuroscience

Neuroscience aims to study the nervous system in order to know and understand human behaviour, ranging from intelligence to emotions. Neuroscience encompasses diverse fields that study the nervous system: biology, medicine, psychology, chemistry, physics, computer science....

2.1 Structure and components of the nervous system

This section shows the structure and main components of the human nervous system.

2.1.1. Cells

The main types of cells that make up the nervous system are neurons and glial cells.

Neurons

Neurons are the basic functional units of the nervous system which respond to stimuli and transmit and process information. A neuron is made of [YOUNG_97]:

- A body known as soma or perikaryon: which is the metabolic centre of the cell.
- A set of extensions:
  - The axon: is responsible of transmitting signals to other neurons (excitatory or inhibitory), muscle cells or glandular cells. They can be covered by a myelin sheath that is periodically punctuated by the nodes of Ranvier. This sheath increases the transmission speed. Its size can range from microns up to one metre.
  - Dendrites: are responsible for receiving signals and transmitting them to the body of the neuron. Its size can range from microns up to 1 mm.

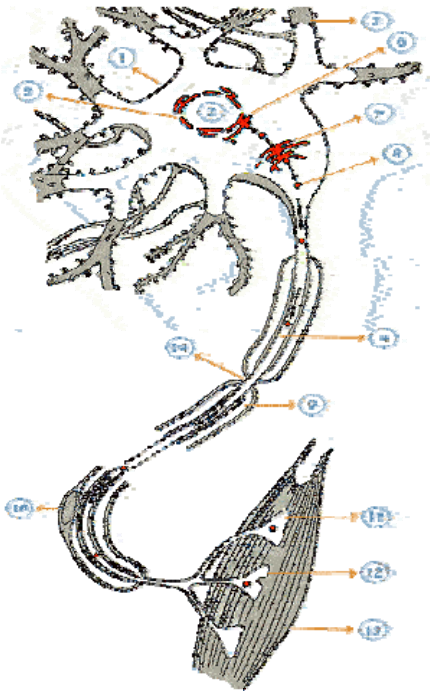

1. Cell body
2. Nucleus
3. Dendrite
4. Myelin axon
5. Nuclear sheath
6. Endoplasmic reticulum
7. Golgi apparatus
8. Synaptic vesicle
9. Myelin sheath
10. Schwann cell
11. Nervous endings
12. Neuro-muscular synapse
13. Skeletal muscle
14. Node of Ranvier

Figure 2.5. Diagram of a neuron. Source: [PUC]

Based on the configuration of the neurites, neurons can be classified according to the following types [BEAR_06]:

- Unipolar: with only one axon which divides itself, they are found in some ganglia.
- Bipolar: made up of a dendrite and an axon. Are found in visual, auditory and vestibular pathways.
- Multipolar: with one axon and between 2 and 12 dendrites.

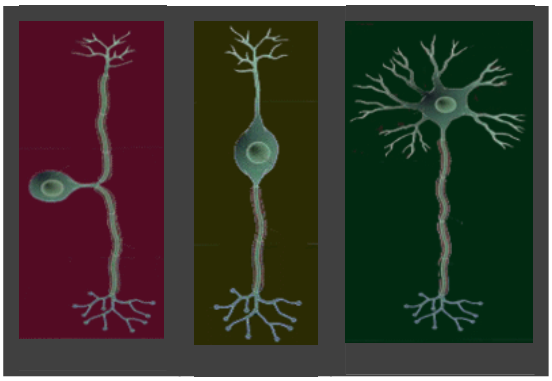

Figure 2.6. Examples of a) unipolar neuron, b) bipolar neuron, c) multipolar neuron: Source: [IIBC_99]

They can also be classified according to the function they perform [BEAR_06]:

- Sensory or afferent neurons: responsible for transmitting input signals from the receptors.
- Association neurons or interneurons: responsible for connecting neurons.
- Motor or effector neurons: responsible for transmitting output signals to the organs.

Neurons communicate through synapses. There are two types of synapses: electrical and chemical, the latter being most common in the nervous system. An electrical synapse is generated by the direct transmission of ions in the gap junctions, thus producing an electrical connection. A chemical synapse is caused through a chain of processes modulated by differences in voltage and chemical components.

Neural signal transmission is accomplished either through the exchange of sodium and potassium ions or through neurotransmitters.

Neurotransmitters are substances that are released in the nervous endings and activate a physiological reaction of a second neuron, when they reach, in a sufficient number, the receptors of that neuron. There are different types of neurotransmitters which have their associated receptors.

Amino acid	Amines	Peptides
Gamma-aminobutyric acid	Acetylcholine	Cholecystokinin
Glutamate	Dopamine	Dynorphy
Glycine	Epinephrine	Enkephalis (Enk)
	Histamine	N-acetylaspartylglutamate (NAAG)
	Norepinephrine	Neuropetide Y
	Serotonin	Somatostatin
		Substance P
		Thyrotropin –releasing hormone
		Vasoactive intestinal peptide

Table 2.1. Neurotransmitter classification: Source: [BEAR_06]

The main transmission mechanism consists in the generation of differences of potential. When the action potential is surpassed, the transmission process is triggered. The following figure shows the resting potential, the action potential and the refractory period that follows activation.

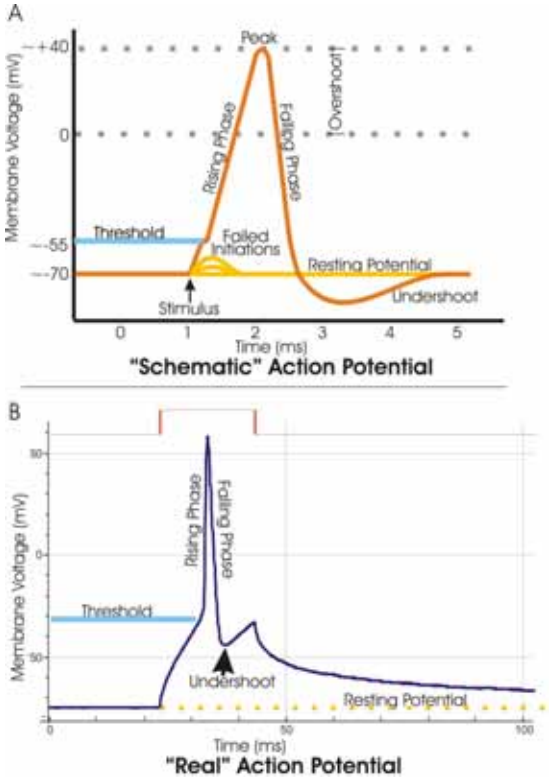

Figure 2.7. Action potential. Source: [WIKI]

Besides neurotransmitters, neuropeptides are another type of substance which ease or hinder the release of neurotransmitters.

Glial cells

The nervous system, besides being made up of neurons, is also made up of glial cells. They are responsible for providing physical and nutritional support to the neurons as well as acting as their protection. There are different types of glial cells: astrocytes, oligodendroglial and Schwann cells. The quantity of glial cells is between 10 and 50 times greater than that of neurons.

Neuron groupings

Anatomists have given different names to the neuron and axon groupings. The following provides the most common terms [BEAR_06]:

- Neuron groups:
  - Grey matter: generic name for neuron collections within the central nervous system.
  - Cortex: set of neurons that group into a thin sheet, generally used for brain groupings.

- Nucleus: grouping of neurons that are clearly distinguishable, usually in the internal areas of the brain.
- Substantia: group of neurons in the internal areas of the brain whose borders are less demarcated than in the case of the nucleus
- Locus: a well-defined small set of neurons.
- Ganglion: grouping of neurons in the peripheral nervous system.

■ Axon groups:

- Nerve: set of axons in the peripheral nervous system or the optic nerve inside the central nervous system.
- White matter: set of axons in the central nervous system.
- Tract: set of axons in the central nervous system that share origin and destination.
- Bundle: axons that share the route but not necessarily the origin and destination.
- Capsule: axons that connect the cerebrum with the brain stem.
- Commissure fibres: any set of axons that connect both sides of the brain.
- Lemniscus: tract that runs along the telencephalon.

In order to provide a better global view of the nervous system from a computational standpoint, it is noteworthy to provide a classification of nerves in accordance with the transmission speed, as this establishes the importance of the times of each signal.

Nerve type		Function	Transmission Speed (m/s)	Diameter (microns)
A	Alpha	Transmission of orders to the muscles	60 -120	12 -20
	Beta	Tactition and pressure	30 -70	6-12
	Gamma	Muscular situation	15 - 30	2 – 8
	Delta	Pain, coldness and tactition	12 - 30	2 - 6
B		Preganglionic autonomous connection	3 -15	1- 3
C		Pain, temperature, mechanoreceptors and reflex arcs	0.5 - 1	0.5 – 2

Table 2.2. Nerve types according to their transmission speed. Source: [GOWI_00]

2.1.2. Structure of the nervous system

The nervous system was developed in response to the need for movement. It is made up of the following [SCHÜ_07, BEAR_06]:

- The central nervous system.
- The peripheral nervous system.

The following provides a description of each of these parts, especially the central nervous system which is responsible for the most important control tasks.

Central nervous system

The central nervous system (CNS) is responsible for managing the voluntary actions of an individual. Two types of matter can be differentiated: gray and white. The first consists of the nucleus of neurons while the latter consists of nervous fibers. It is composed of the brain and the spinal cord. In turn, the brain is divided into the following regions [NATI_08, SFN, IQB_02, BEAR_06, DOWS_07]:✱:

- Prosencephalon, which is made up of:
  - Telencephalon: the brain is its main part. The cerebral cortex or cortex is the most relevant part. It is characterized by its gyri and sulci. The human brain has a great number of these, which attests to its level of development.

  - Diencephalon which is composed of:
    - Thalamus: responsible for temporarily storing sensory data that will later be sent to the brain. It is believed that it also performs processing and synthesis of data tasks.

    - Hypothalamus: regulates the body temperature, thirst, hunger, fear, aggression, dreams and emotional expression mechanisms.

    - Pituitary gland: responsible for generating and releasing hormones that regulate the metabolism.

✱ Image source: [DOWS_07]

- Mesencephalon: responsible for connecting and communicating parts of the brain with the spinal cord, including optic and olfactory nerves.
- Rhombencephalon is subdivided into:
  - Cerebelum: responsible for keeping the balance and coordinating body movements.

  - Medulla oblongata: is an extension of the spinal cord.

  - Protuberance or Pons Varolii: is a transmission and communication system.

Some of these elements are also grouped forming specific groupings such as:

- Brain stem: composed by the mesencephalon, the Pons Varolii and the medulla oblongata. It connects the superior area of the CNS to the spinal cord. It is responsible for vital functions such as breathing, digestion and blood circulation through the control of involuntary muscles.

- Limbic system: composed of parts of the thalamus, hypothalamus and mesencephalon among others. It is responsible for functions such as memory, attention and learning.

  Due to its function, the hippocampus must be mentioned as it plays an important role in memory, including the transfer between short and long term memory.

Last, the spinal cord is made up of a central conduct and the nervous tissue which encloses it. Its main task is the transmission of nervous stimuli although it also processes signals, as happens with reflexive acts.

Peripheral nervous system

The peripheral nervous system (PNS) is responsible for connecting the CNS with the body organs. The PNS is subdivided into two parts:

- The somatic peripheral nervous system, which mainly deals with voluntary control of movements and tactition. It is made up of twelve pair of cranial nerves and two pair of spinal nerves.

  Spinal nerves are made up of 31 pair of nerves: 8 cervical, 12 thoracic or dorsal, 5 lumbar, 5 sacral and 1 coccygeal pair; which when emerge from the medulla are joined in what is known as spinal nerve plexus: cervical plexus, brachial plexus, intercostals or thoracic nerves, lumbar plexus and sacral plexus.

  The cranial nerves emerge from the base of the brain. In general, cranial pairs have a mixed nature: sensory and motor. The first two belong to the CNS while the others belong to the PNS. The following are these pairs [RAMO_08, BEAR_07]:

  - Olfactory: sense of smell.
  - Optic: sense of sight.
  - Oculomotor: movement of the eyes and eyelids and constriction of the pupil.
  - Trochlear: acts on the eye muscles.
  - Trigeminal: transmits facial information and controls chewing muscles.
  - Abducens: acts on the eye muscles.
  - Facial: conveys taste sensations of part of the tongue and controls the facial expression muscles.
  - Vestibulocochlear: sense of hearing and balance.
  - Glossopharyngeal: controls the movement of throat muscles, salivary glands, sense of taste on the tongue and pressure changes in the aorta.
  - Vagus: provides the parasympathetic control of the heart, lungs and abdominal organs, pain sensation in the viscera and the muscular control of the throat.
  - Spinal accessory: controls the movements of the throat muscles and the neck.
  - Hypoglossal: controls the tongue movement.

- The vegetative or autonomic peripheral nervous system: responsible for controlling autonomic or involuntary actions. In turn, it is subdivided into two systems:

  - The sympathetic nervous system: responsible for activating the system when facing dangerous elements.

– The parasympathetic nervous system: responsible, among other tasks, of regulating calm and promoting digestion.

Organ	Sympathetic	Parasympathetic
Eyes	Pupil dilation	Pupil constriction
Salivary glands	Decrease in salivary secretion	Increase in salivary secretion
Heart	Increase in heart beat	Decrease in heart beat
Lungs	Decrease in bronchial secretion and dilation of the bronchioles	Increase in bronchial secretion and constriction of the bronchioles
Gastrointestinal tract	Decrease in secretion and mobility	Increase in secretion and mobility
Pancreas	Decrease in exocrine secretion	Increase in exocrine secretion
Skin	Vasoconstriction, sweat secretion, hair erection	Has no effect

Table 2.3. Listing of different actions that the sympathetic and parasympathetic systems have on organs. [GUYT_06]

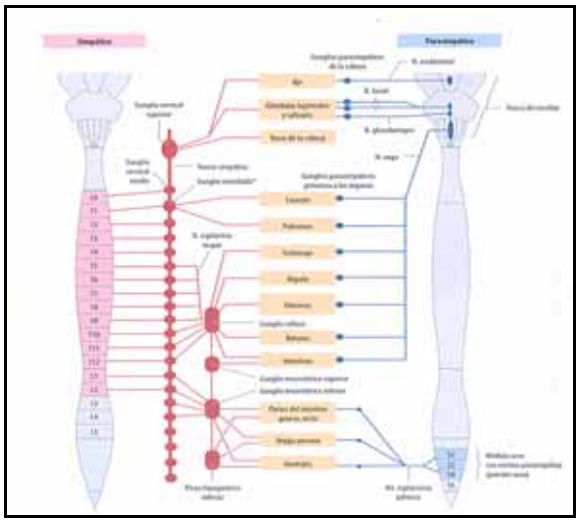

Figure 2.8. Organisation of the sympathetic and parasympathetic nervous systems. Source: [HERR]

2.2 Functional processes and areas

The different parts of the nervous system group themselves to undertake processes. The following are some of the most relevant functions performed by the nervous system [MIT_02]:

- Stimuli capture:
  - Sensory.
  - Transmission.
- Processing:
  - Perception and recognition.
  - Memory and learning.
  - Thought and awareness.
  - Motor control.
  - Language.

The following expounds these areas.

2.2.1 Stimuli capture

The stimuli receptors are a key part of the nervous system. The signals perceived by the sensors are characterised by the following elements:

- The intensity is modulated through the signal frequency and by the number of activated receptors.
- Duration, which creates decrease of sensibility to stimuli which are constant during a certain period of time.
- Location, the signal of the adjacent receptors maintains the proximity when reaching the brain, except in the gustatory and olfactory receptors. In order to more clearly define the location of the stimuli, lateral inhibition processes are activated. In the case of the visual system, the receptive field for each neuron is established. This is the visual space area that directly influences that neuron.

- Sensor type. The following table show receptor types and their features:

Type	Stimuli	Receptor type	Specific receptor
Vision	Light	Photoreceptor	Cones, rods
Hearing	Pressure waves through air	Mechanoreceptor	Cochlea cells
Balance (Equilibrium)	Head movement	Mechanoreceptor	Semicircular canal cells
Tactition	Mechanical, thermal, chemical	Mechanoreceptor, thermoreceptor, chemical receptors	Dorsal root cells
Taste	Chemicals	Chemical receptors	Gustative papillae
Olfaction	Chemicals	Chemical receptors	Olfactory neurons

Table 2.4. Receptor types. Source: [KAND_95]

2.2.2 Processing

Towards the end of the 18th century, the first studies were carried out on the specialisation of the different areas of the nervous system. Since then, numerous discoveries and research have followed. It was established that there are different ways of transmission for sensory signals and for the motor activation, as well as different channels and transmission speeds adapted to the needs of each task. In a parallel manner, the different regions of the brain have been identified and classified with techniques which range from the study of patients with neurological injuries, psychoneurological experiments, animal testing and more recently, the use of new techniques of monitoring neuronal activity (computed tomography, magnetic resonance imaging (MRI), positron emission tomography (PET) and functional magnetic resonance imaging (fMRI).✱✱

An example of brain's areas classification is that proposed by Brodmann based on cellular and organisational differences.

✱✱ As a historical note,the acceptance of the neuron as the functional unit of the brain was achieved through the experiments of Santiago Ramón y Cajal and Camillo Golgi's stain method.

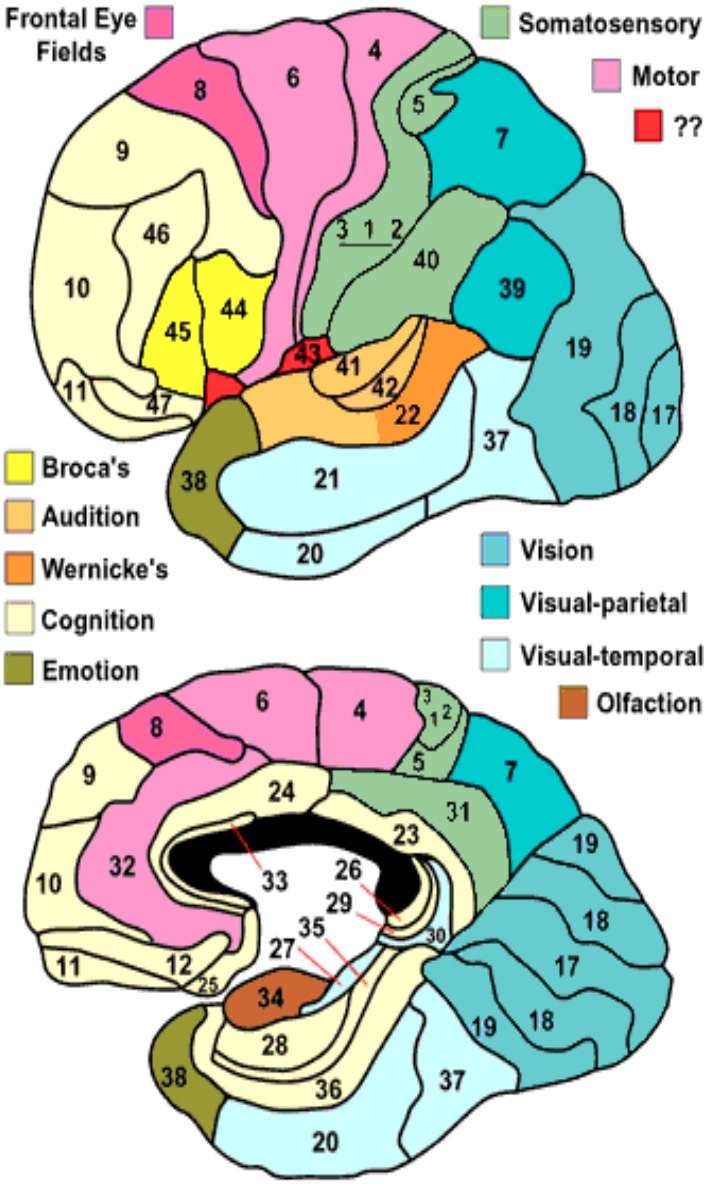

Figure 2.9. Areas of the brain. Source: [DUBI]

Work is also being carried out on the identification of the functions performed in each area. Areas have been related to specific tasks, such as those linked to vision or movement control, and grouped in different units [BEAR_06].

Type	Cortex	Areas
Motor	Primary motor	4
	Premotor and supplementary areas	6
Sensory	Somatosensory	1,2,3
	Visual	17, 18, 19
	Taste	43
	Auditory	41, 42
Associative	Posterior parietal	5, 7
	Inferotemporal	20,21,37
	Prefrontal	9, 10, 46

Table 2.5 Example of areas and associated functions.

Data processing has a structure organised both in series as well as in parallel. This means that signals are transmitted in series from the sensory cells until higher order neurons and that are processed in parallel, for example: in the case of visual information, colour, shape and movement are processed in parallel. The following are the elements of the visual system.

2.2.2.1 Visual Processing

In the visual system, the processing stream begins in the retina, where there is an enormous variety of cells (ranging from 50 to 100according to[WASS_04] or over 55 (mammals) according to [MASL_01]). One can identify, within this great variety, two types of structures based on the direction of the signal transmission: vertical and lateral, as well as 5 main types of neurons organised in layers [NASS_09]:

- Photoreceptors: light sensitive cells. There are two types: cones and rods.
- Horizontal cells: establish lateral connections.
- Bipolar cells: there are 10 different types.
- Amacrine cells: establish lateral connections.
- Ganglion cells: their axons join to form the optic nerve.

One of the most relevant characteristics of the retina is that it is the beginning of parallel information processing, that is, through the optic nerve there is a transmission of "image planes" that represent shapes, movement, colour... which are present in the reality that we perceive.

Estimates show that there are over 20 circuits in the human retina which give rise up to 13 different pathways [NASS_09].

Signals from each eye are transmitted through the optic nerve, are combined in the optic chiasm and continue through the optic track. The following figure shows this structure.

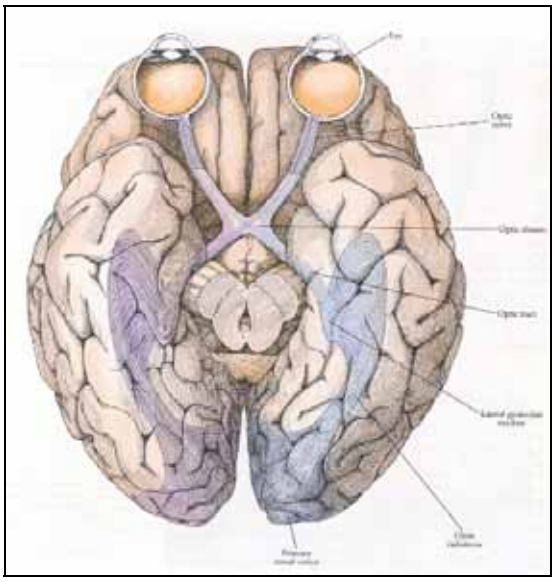

Figure 2.10. Visual system. Source: [Hoge_01]

Most ganglions' axons reach the lateral geniculate nucleus (LGN) in the dorsal thalamus. (Other destinations are the hypothalamus, the pretectum in the mesencephalon and the superior colliculus in the tectum). The se are projected from here towards the visual cortex. The first element is the primary visual area or V1. Although the functions performed in this area are not totally established, it is believed that two processing streams begin from this area (once again there is parallel processing) [MISH_83, DEYOE_88]:

- The dorsal stream is associated with movement and action recognition. From V1 is projected towards V2, V3 and MT. [ALBR_84, GIES_03, MAUN_83, MISH_83]
- The ventral stream is associated with object recognition. From V1 is projected towards V2 and V4 [UNGE_94, TANA_96, LOGO_96]. The processing of colour is deemed to follow this same path. At times it is specifically known as colour stream [CONW_05, LENN_88].

The following illustration shows a possible diagram of parallel visual processing.

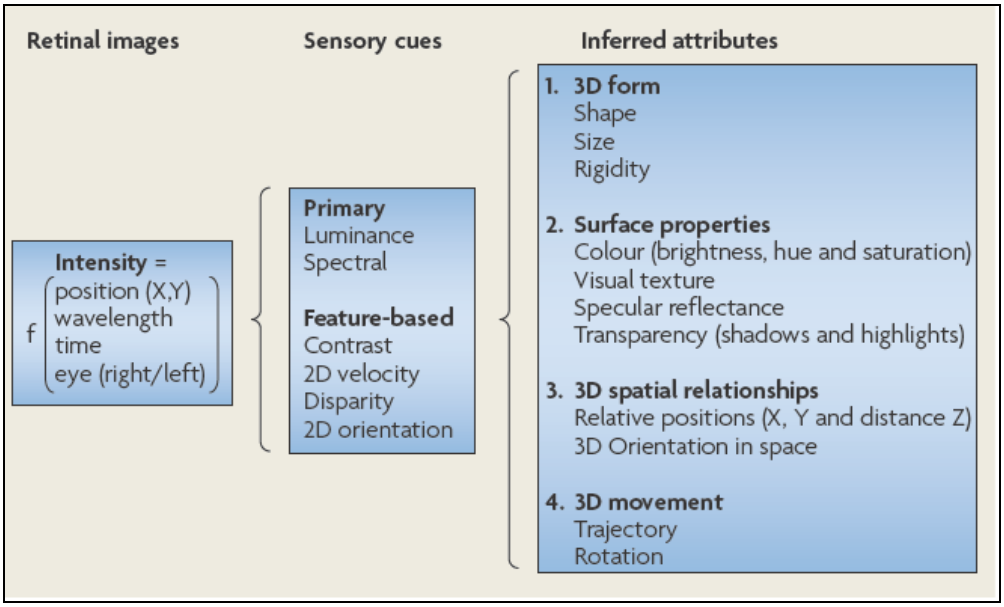

Figure 2.11. Conceptual summary of the visual pathways. Source: [NASS_09] modified from the original [DEYO_88].

3. Conclusions

This chapter has set forth general knowledge on the fields of colour description and measurement and neuroscience that will act as a basis and reference for upcoming chapters.

The section dealing with colour has set out elements that are part of colour perception, such as light, objects and the visual system. From the colour modelling perspective, there has been a brief description of the different types of scales and basic data related with the quantification of the difference between two colours and its associated problem. Emphasis has been placed on the fact that colour is a type of perception.

The nervous system, which is the core of neuroscience as a multidisciplinary discipline, involves chemical, physical, biological, medical and computational elements. It has been presented above. A description has been provided of the cells that compose it, its grouping and communication systems as well as the high level structures. Finally, we have described the main primary components of the visual system.

Chapter III

Colour models

"For the rays (of light) to speak properly are not coloured. In them there is nothing else than a certain power and disposition to stir up a sensation of this or that colour." Isaac Newton 1730

The search for ways to define and characterise colour has been a commonplace concern throughout the history of humankind. This chapter looks at different colour and distance measurement models that have been proposed throughout time. This review is very important when trying to establish the structure of the colour model that is the aim of this thesis. This analysis shall permit to identify some of the factors that influence colour perception in a specific area, the ways to establish the characteristics of the experiments as well as to study different proposals to measure colour distance.

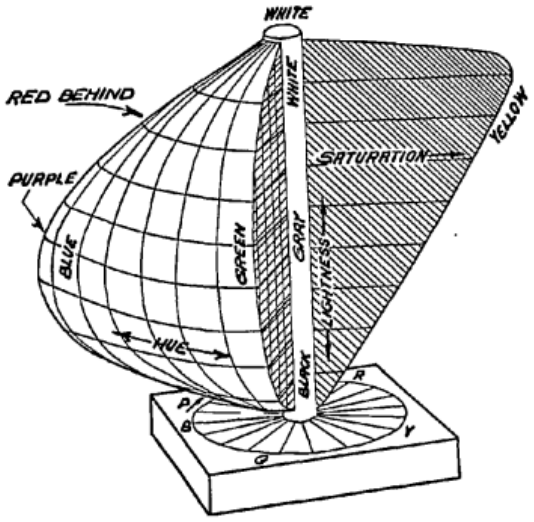

Figure 3.1. Example of colour space. Source: [HUNT_58]

Additionally, there are different singularities detected in colour behaviour. These types of effects have been the object of many studies and at times have been used to check the goodness of fit of colour models. Therefore, on the one hand, they provide the possibility to identify factors that influence the different parameters that characterise colour, while on the other, provide a means of evaluation.

1. Introduction

The study of colour and its evaluation have been approached in different ways based on the specific needs that had to be answered:

- Art: the study of harmony between colours, the capacity to reproduce them and combine pigments, the control of light and shadows…
- Science: study of the relationship between the light stimulus and the perception of colour, analysis of neurological elements and processes involved in perception, description of the main components of the spectrum for colour perception, the influence of different types of surfaces, orientation and texture...
- Manufacturing processes: production control (capacity to produce elements in accordance with a colour standard), capacity to transfer design colours to the final product (depending on the material, pigments produce different colour perceptions), standard measurements (capacity to compare different manufacturers)...

These studies have given rise to three different approaches when describing the colour space:

- The physical representation of colours, that is, through samples of each colour, such as Munsell's Atlas of the Natural Colour System (NCS).

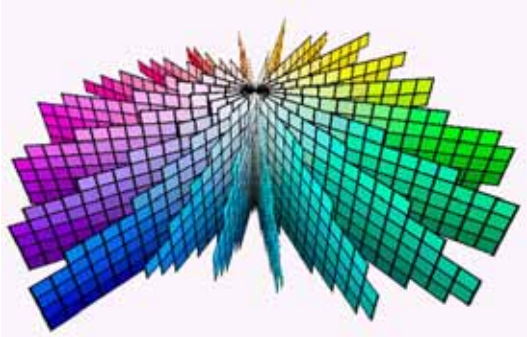

Figure 3.2. Munsell's Atlas. Source:
[http://www.codeproject.com/KB/directx/d3dmunsell/Munsell3D.gif]

- Evaluation of physical magnitudes regarding luminous stimuli, such as CIE XYZ or the photoreceptor space: lms.

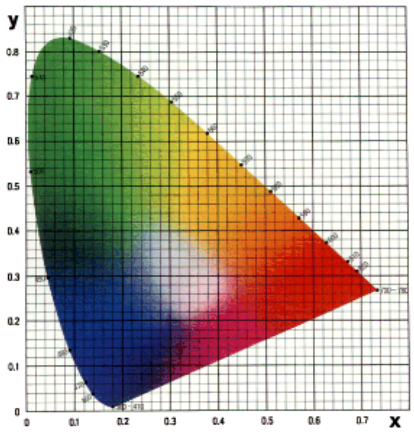

Figure 3.3. Chromaticity diagram. Source:

[http://escience.anu.edu.au/lecture/cg/Color/CIEChromaticityDiagram.en.html]

- Description of the geometry of colour space and its attributes based on physical measurements. Such as CIELAB or HUNT94.

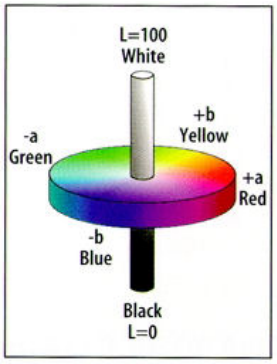

Figure 3.4. CIELAB space. Source:

[http://www.cs.sfu.ca/CC/365/mark/material/notes/Chap3/Chap3.3/Chap3.3.html]

2 History

The following is a chronological presentation of the events and discoveries that have set milestones in the evolution of colour knowledge and its attributes.

The beginning

There are texts with over 2,600 years with references to colour characterisation (Jenofanes, Plato, Aristotle...) that describe what they deemed as fundamental colours and their sources. As early as

the Middle Ages, the first attempts to define scales appeared, such as Avicenna's sequences or Theophilus' book entitled *De diversias atribus* that described colour techniques. In the 17th century, Forsius presented a colour description through the use of what is considered to be the first colour circle.

The scientific approach

> *"I have put down many things simply to indicate the way of thinking about colors that belongs to this theory of triple sensation. We are indebted to Newton for the original design, to Young for the suggestion of a means of working it out, to Helmholtz for a rigorous examination of the facts on which it rests, and to Professor Grassmann for an admirable theoretical exposition of the subject."*
>
> James Clerk Maxwell 1856

I. Newton discovered that when natural light entered a prism, it splits into a range of colours. He also provided the description of the concept of saturation and colour tone by means of a circle. At the end of the 17th century, the fact that three colours can create the rest (technique that began to be used in book printing) was established. It should be noted that, at first, this was thought to be an inherent feature of light.

In the 18th century, J.H. Lambert published his book *Potometri.* G. Palmer postulated the existence of three different types of light and three particles associated to these types in the retina and J. Elliot set forth the existence of elements that are tuned to specific stimuli. This century saw the confirmation of the existence of people with deficiencies in colour perception [KUEH_03]. Three-dimensional colour models began to appear in this time (for example, the double tetrahedron of T. Mayer that was built on the basis of three primary colours).

Early in the 19th century, based on existing principles, T. Young proposed the primary colour theory in which light is a wave and continuous in nature. He also established the existence of three types of sensors in the retina where each is activated by a "pure" colour: red, green and violet.

New colour models were set forth in this period. P. O. Runge introduced the extension of a colour model to two cones which had a colour circle as a common basis, similar to the model proposed by J. W. Goethe. M. Klotz formulated the possibility of the use of a cylindrical model while M. Chevreul proposed the use of a hemisphere whose base was divided into 72 colour hues, with a white centre and a black dome.

Other scientists, such as J.F. Herbart and P. Bouguer began to study the intensity of light and the capacity of perceiving differences. G. T. Fechner introduced the term psychophysics and postulated that sensations can not be measured only the stimuli or the differences in perception when presented different stimuli. Aware of the studies of E. H. Weber on the perception of differences between stimuli, in his book *Elemente der Psychopysik*, he established the relation ship between perception and stimulus in what is today known as the Weber-Fechner law [UÑA_04]:

$$d\gamma = Kd\beta / \beta \qquad \text{(eq. 3.1)}$$

Where γ represents perception and β the stimulus.

C. Doppler placed the three primary colours (yellow, blue and red) in three orthogonal axis, where the combination space was 1/8 of the sphere.

In the middle of the 19th century, H. L. F. Von Helmholtz established the difference between mixes of additive and subtractive colours. Furthermore, he was one of the precursors of trichromatic colour vision set out by T. Young.

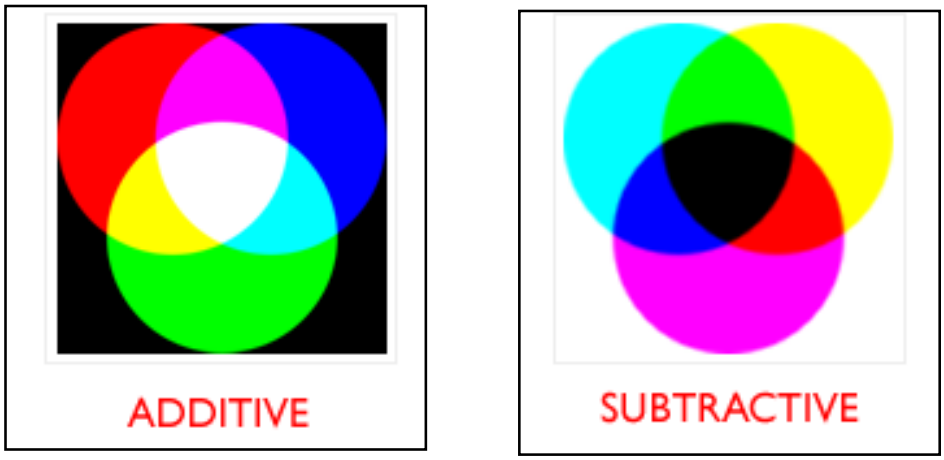

Figure 3.5. Sample of additive and subtractive colour mix. Source:
[http://www.searchfreefonts.com/articles/the-anatomy-of-web-fonts.htm]

H. Grassman proposed that visual perception could be defined by three attributes: hue, brightness and saturation and set out what is known today as the Grassmann's laws on additive, scalar and associative properties of metamers [SHEV_03].

J. C. Maxwell measured the proportions of each primary colour that is generated by the visible spectrum, a precursor of current colorimetric functions. He set out the non-existence of a light

that exclusively activates one of the types of sensors and set forth the use of colour blind observers in order to determine the characteristics of each sensor.

M. J. S. Schultze postulated the theory in which cones are responsible for day vision and rods for night vision. A. König and C. Dieterici obtained perception curves for pronatopes and deuteranopes.

Towards the latter part of the 19th century, K. E. K. Hering proposed the existence of four primary colours: yellow, blue, red and green. Each of these was placed in a semi-axis, grouped in opposing colours: yellow v. blue and red v. green.

At this time, with the existence of two types of theories (3 or 4 primary colours), new proposals were made that looked at the complementariness of both through their sequential application: zone theory (J. Kries, F. Donders).

The 20th century to the present day

In the early 20th century, A. H. Munsell created an ordered colour atlas, organised by hue, lightness and a new concept known as chroma (which indicates the amount of colour presence), creating a three-dimensional figure (see Figure 3.2).

In 1923, E. Q. Adams propounded the existence of two types of sensory processes: activation and inhibition.

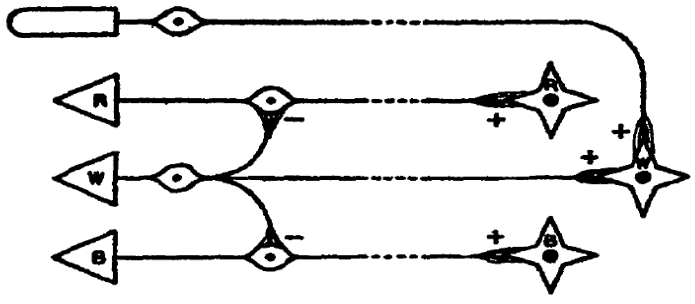

Figure 3.6. Diagram of the nervous connections of a normal observer propounded by Adams.
Source: [ADAM_23]

W. Ostwald proposed a base with three basic colours: yellow, blue and red. He applied Hering's colour equation: colour + white + black =1 and scaled the colours in accordance with the Weber-Fechner law. Some time later, R. Luther and N. D. Nyberg propounded a colour solid that included concepts of colour opponency [KUEH_03].

In 1924, the Commission Internationale de l'Eclairage (CIE) propounded the photopic luminous efficiency function V(λ) for the standard observer.

In 1931, the CIE defined the tristimulus values {X, Y, Z} for a standard observer and a 2º field of view as well as some standard illumination sources. This standard has allowed the characterisation of the stimulus based on their XYZ values and their use is widely accepted. In 1964, it established the standard observer CIE 1964 10º.

Until the mid 20th century, the theory of the existence of three primary colours was predominant. The beginning of measurements of neurons in the visual system led to the verification of the existence of activation and inhibition processes which in turn established the complexity of the human colour processing. The four colour theory was backed by the results obtained in retina cell measurements of several animals that showed processes with colour opponency (R. Granit, G. Svaetichin). These results gave a boost to the development of zone theories.

Later, the study and measurement of the sensitivity curves of the three types of retina cones was begun. Nowadays are known as L, M and S (originally R, G and B).

The following years saw the undertaking of multiple experiments in the retina (1981 Zremer and Gouras showed the existence of simple opponent ganglion cells), in the lateral geniculate nucleus (LGN) (1986 Wiesel, Hubel, DeValois et al. identified different cell types) and in the cortex (1982Hubel and Livingstone detected the presence of colour related blobs). These and many other experiments have contributed towards the increased knowledge on colour perception in the visual system and shall be seen in greater detail in chapters IV and V).

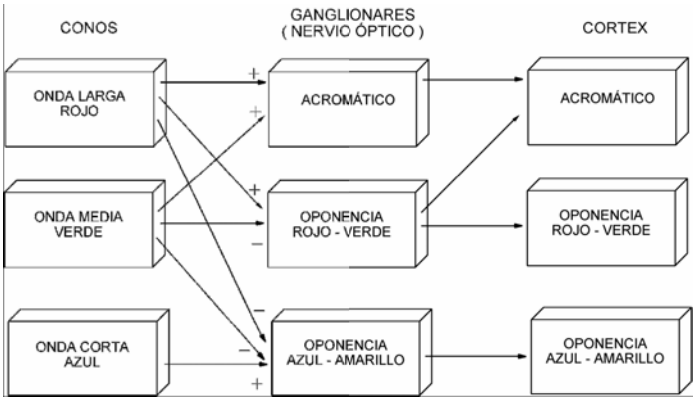

Figure 3.7. Schematic drawing that shows possible interactions between cones towards ganglions and cortex. Source: [URTU_06] original de [ZREN_81].

In 1976, the CIELAB and CIELUV standards were published in order to ease colour difference measurement.

In 1988 T. Indow showed, through a multidimensional study, that in simplified viewing conditions, hue, lightness and chroma are the only necessary attributes to represent a colour [KUEH_03].

In 1997, CIE proposed a new model, CIECAM97, in order to encompass the most relevant existing models. Later, in 2002, CIE presented the CIECAM02 model as an update of CIECAM97.

3 Basic concepts

Before describing colour models, some basic terminology related with colour perception, input data to the models and some singularities that happen in colour perception must be provided.

3.1 Colour terminology

The following is a set of terms and concepts that are necessary in order to work in the field of colour perception [WYSZ_00, LENN_88]:

- Related colour: colour perceived as belonging to an area in relation with other colours.
- Independent colour: colour perceived in a isolated area.
- Hue: colour attribute denoted by the following terms: red, yellow...
- Unique hues are those hues that can only be described by a specific term, such as red versus orange that can be described as yellowish red.
- Brightness: colour attribute by which a colour can appear more or less intense or than can seem to emit more or less light.
- Lightness: colour attribute by which a colour seems to emit more or less light in comparison with a white colour stimulus.
- Chromaticness: colour attribute by which it can seem more or less colourful. The term colourfulness is also used.

- Chroma: colour attribute that reflects the difference with an achromatic stimulus of the same luminosity.
- Saturation: colour attribute that establishes the difference with an achromatic stimulus without taking into account its brightness.
- Luminance: is defined as the luminous intensity per unit of surface in a given direction.
- Aperture colour: colour shown in solitary.
- Surface colour: colour belonging to an object.

3.2 Description of the input values to the models

Most colour space proposals since 1931 work with the CIE {X,Y,Z} tristimulus values. Therefore, it is essential to set forth the characteristics of these.

It is important to define the matching concept between stimuli. It is the state in which these stimuli produce the same neural state. This can be expressed in the following manner: two mixtures are said to seem alike when given three primaries{ P_1, P_2, P_3} and a test light S and its radiant energies P_S, $P_{S,1}$, $P_{S,2}$, $P_{S,3}$, the following is met [SHEV_03]:

$$P_S S \oplus P_{S,3} P_3 \equiv P_{S,1} P_1 \oplus P_{S,2} P_2 \qquad \text{(eq. 3.2)}$$

Where ≡means visually identical and ⊕ the physical mixture of the components.

In order to characterise a colour, its coordinates in a three-dimensional space are defined by three colour sources known as the primary colours. These coordinates are measured comparing the two parts in which a circle is divided and which have two colour combinations projected in them: the stimulus to be measured (colour to be measured) and the weighted combination of three colour sources, known as primary colours. The quantity of each source that equals the perception of both parts of the circle are the colour coordinates of that colour for that set of primaries. In order to perform the tests, the sources must be independent and spectral or near spectral in order to produce the greatest colour gamut.

One of the properties of this three dimensional space is that it can define another set of primaries and calculate the transformation of a Q set to another P:

$$P = A * Q \qquad \text{(eq. 3.3)}$$

A being the representation vectors of set P in the space defined by set Q.

These tristimulus are lineal transformations of the space generated by the three primary illumination sources used in the experiments.

In 1931, CIE proposed a transformation known as XYZ tristimulus that complies with the following requirements:

a) $X(\lambda)Y(\lambda)\,Z(\lambda) \geq 0 \;\forall\; \lambda$ (eq. 3.4)

b) $Y(\lambda) = V(\lambda)^1 \;\forall\; \lambda$ (eq. 3.5)

The proposed transformation generates a set of primaries that are not physically feasible.

The XYZ values can be projected in a two dimensional space known as the chromaticity diagram (see figure 3.3):

$$x = \frac{X}{X+Y+Z}$$
$$y = \frac{Y}{X+Y+Z} \qquad \text{(eq. 3.6)}$$
$$z = 1-x-y$$

If the set of wavelengths of the visible spectrum are represented in this diagram, one can obtain the loci spectrum that can be seen below:

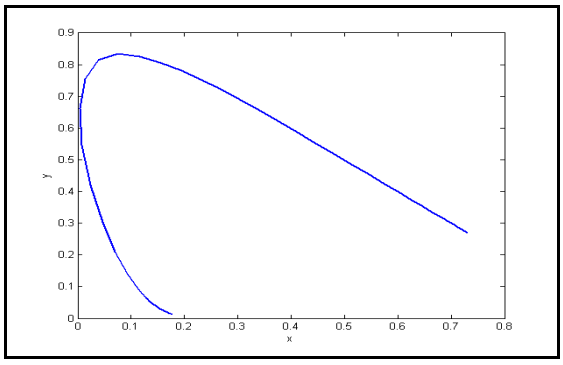

Figure 3.8. Representation of the loci spectrum in the chromatic diagram.

In 1964, the standard observer was proposed for a 10º field of view. This was based on the measurements of Stiles & Burch (1959) and Speranskaya (1959, 1961) and is known as $\{X_{10}\ Y_{10}\ Z_{10}\}$.

On the other hand, from a biological perspective, one can calculate the perception curves of the cones known as cone fundamentals using the assumption established by König where people with

[1] Photopic luminous efficiency

colour detection defects have a reduced version of average vision. Several tabulations of these values known as {M(λ), L(λ), S(λ)} have been set forth. Their names are due to the relation between the photoreceptors and the range of wavelengths of its main wave: long, medium and short.

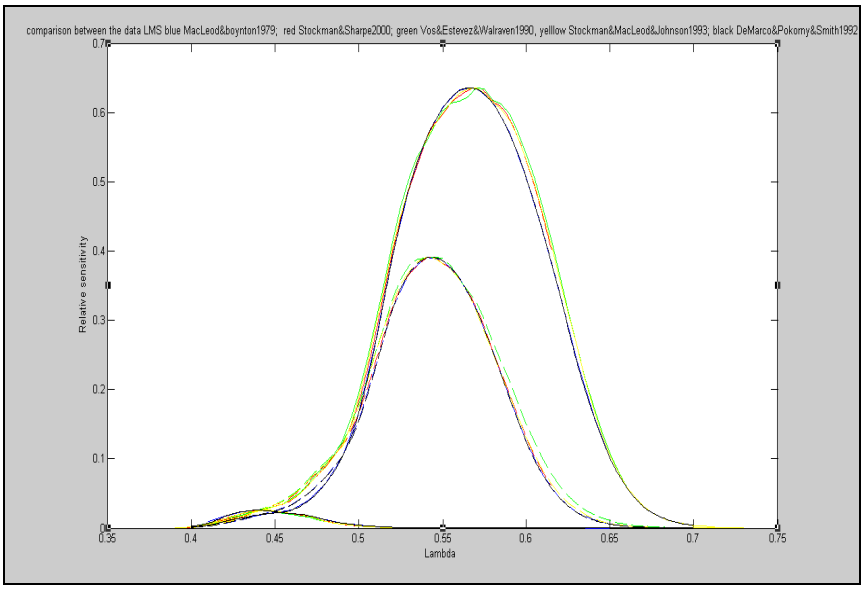

Figure 3.9. Different cone fundamentals: blue) MacLeod & Boynton 1979; red) Stockman & Sharpe 2000; green) Vos & Estevez & Walraven 1990; yellow) Stockman & MacLeod & Johnson 1993; black) DeMarco & Pokorny & Smith 1992. All normalised to the maximum values of Smith & Pokorny (1975).

Similar to the xy chromaticity diagram, one can select a plane within the LMS space. Given the characteristics of these measurements, MacLeod and Boynton (1979) proposed a plane that is directly related with visual perception. They assume that S does not contribute to the brightness that they express as Y= L+M and this way choose a plane of equal luminance (l, s) where:

$$l = L/(L+M) \qquad \text{(eq. 3.7)}$$

$$s = S/(L+M) \qquad \text{(eq. 3.8)}$$

In a similar manner as happens with the chromaticity diagram, the set of wavelengths of the visible spectrum can be represented as follows.

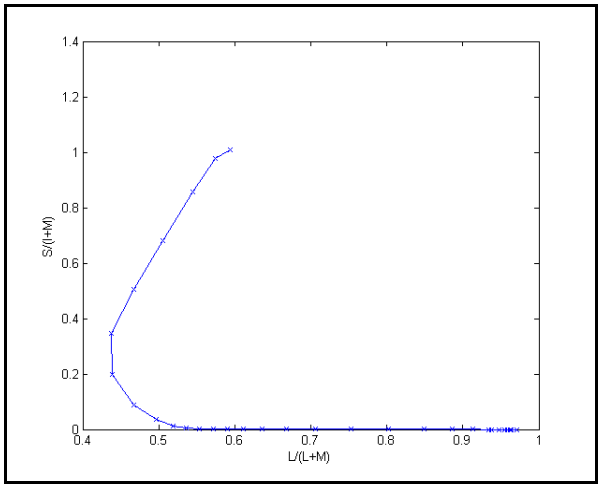

Figure 3.10. Representation of the loci spectrum in the MacLeod-Boynton diagram. Data obtained from [MACL_79].

Although the values in figure 3.9 seem similar when represented in the MacLeod-Boynton space, one can notice its differences.

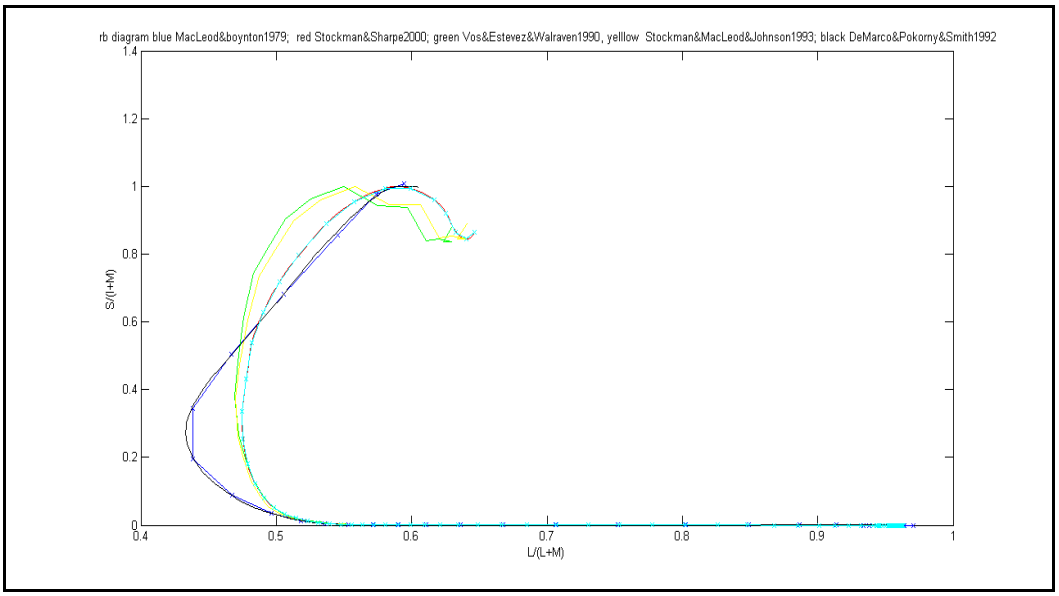

Figure 3.11. Representation of the loci spectrum in the MacLeod & Boynton space: blue) MacLeod & Boynton (1979; red) Stockman & Sharpe 2000; green) Vos & Estevez & Walraven 1990; yellow) Stockman & MacLeod & Johnson (1993; black) DeMarco & Pokorny & Smith (1992). All normalised to the maximum values of Smith & Pokorny (1975).

Finally, a measurement element that is also used is the photopic luminous efficiency V(λ) which can be measured: by comparing the brightness matching of the two halves of a circle that contains a white sample and a stimulus to be evaluated until it matches the brightness perception or by the

flicker method, where the white sample and the stimulus to be evaluated are alternatively shown in time until no oscillation is observed [BOYN_96]. In 1924, CIE proposed a standard for this measurement. Later, the values were updated as they considered that this standard had errors in short wavelengths. CIE proposed a new standard based on the both the corrections made by Judd in 1951 as well as the later corrections made by Vos in 1978.

Both in the XYZ as well as the V case, the calculated values are averages between different observer groups. In any case, one must emphasize that each observer would have different values, this being the main sources of variation among observers [STOC_03]:

- Variations in photopigments: mainly in L and M.
- Differences in photopigment density.
- Differences in filters: lens and the pigment of the macula.

3.3 Colour effects

This section presents the elements that influence the final colour perceived by an observer as well as some of the non-linear behaviours in the colour perception process. Several factors influence this process that can be either sensory or cognitive in nature (related with the observer's previous knowledge) [FAIR_04]:

- Consumption and regeneration of photopigments when presented a high intensity stimulus.
- Transition from cones to rods when presented different intensity levels.
- Control of the gain factor in photoreceptors, independently in each type of photoreceptor and in other cells in the retina.
- Changes in the influence areas of each photoreceptor: the set of surrounding photoreceptors that influence each photoreceptor varies according to the general conditions of the system.
- Spatial and temporal opponency: influence of adjacent stimuli both in time as well as in space

- Control of gain factors in high level mechanisms.
- Signal feedback processes.
- Signal compression.
- Cognitive interpretation of what is perceived, for example the colour memory of an object whereby a colour tends to be associated to that object (eg. such as a banana and yellow).
- Colour constancy: process by which colours are perceived as constant when facing changes.
- Capacity to separate the effect of the illumination: the process by which an observer has previous knowledge on what he sees and is capable of eliminating the illumination colour.

The following are the most influential effects in the final perception of a colour [FAIR_04]:

- Simultaneous contrast, by which a colour depends on its surrounding area.

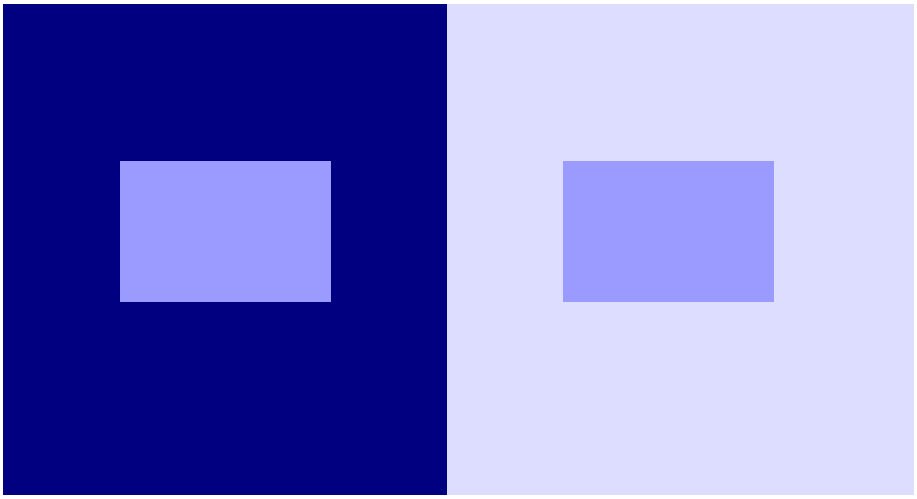

Figure 3.12. Example of simultaneous contrast. The two interior squares are exactly the same colour.

- Crispening: the effect that is produced when two samples are compared against a background that has a colour similar to the object.

Figure 3.13. Example of crispening. The central area shows a greater difference between the two interior squares although the same pairs of squares are present in all three scenarios.

- Spreading: an object apparently blends with the background when decreasing its size or increasing its spatial frequency.

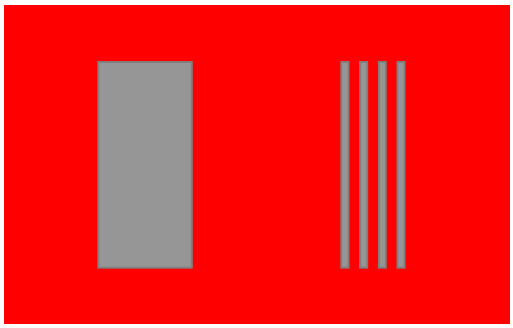

Figure3.14. Example of spreading. If observed at a distance, the bars merge with the background creating another colour.

- The Abney effect: the change in the perceived hue when white light is added to a monochromatic colour source.

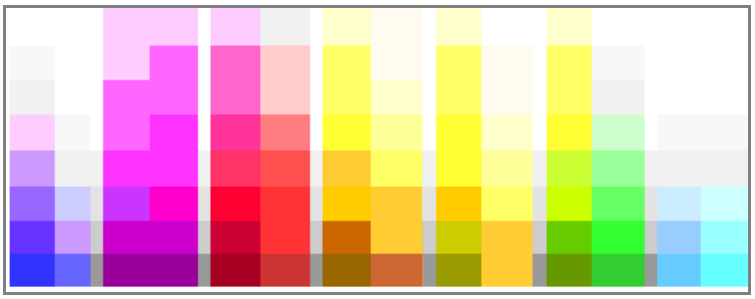

Figure 3.15. Example of the Abney effect. One can notice how colour varies in some columns as the white mixture is increased. Source: [WIKI_10]

- Bezold-Brücke shift: the perceived hue depends on the brightness. Contrary to what might be thought, one can't know the exact hue of a given wavelength.

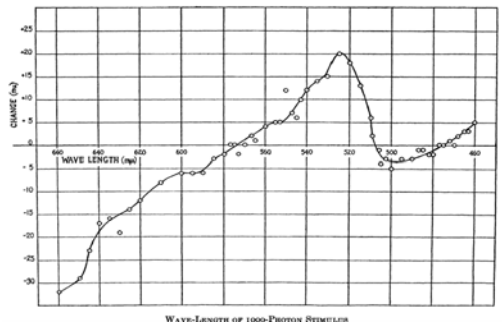

Figure 3.16. Bezold-Brücke shift that shows the change in wavelength necessary to create the same hue when increasing the brightness. Source: [PURD_31]

- Helmholtz-Kohlrausch effect: this effect shows that luminance is not the same thing as brightness. The following graph shows constant brightness curves and their dependence on hue and saturation within a constant luminance level

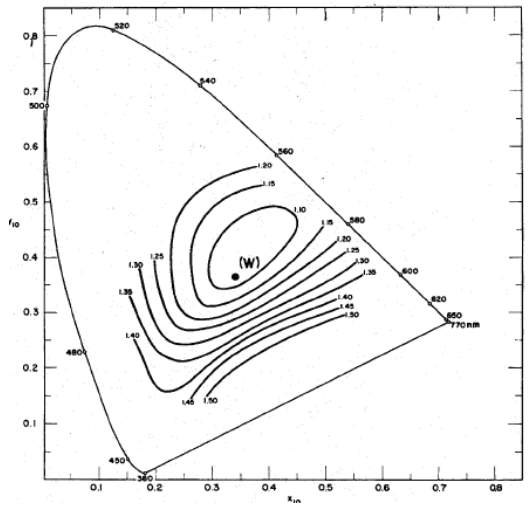

Figure 3.17. Helmholtz-Kohlrausch effect. A representation of the constant brightness curves with constant luminance level Source: [KUEH_03]

- Hunt effect: the chromaticity contrast increases with the level of luminance.
- Stevens effect: the brightness contrast increases with an increase in luminance. As luminance increases, darker colours seem darker and lighter colours seem lighter.

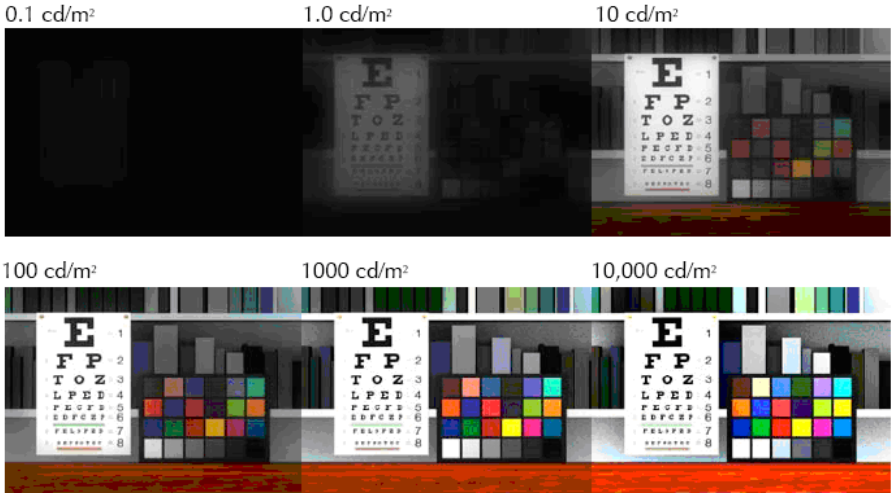

Figure 3.18. Examples of Hunt and Stevens effects. Source: [FAIR_04a]

- The Helson-Judd effect is an effect that rarely happens in daily situations. When an element is lit with monochromatic light, lighter objects than the background have the hue of the source light while darker objects have the complementary hue of the illumination source.
- Surround effect: contrast increases when the luminance of the surrounding increases. At the same time a decrease in surrounding luminance increases the colour brightness. In 1967, Bartleson and Breneman proposed a series of equations that model this effect.

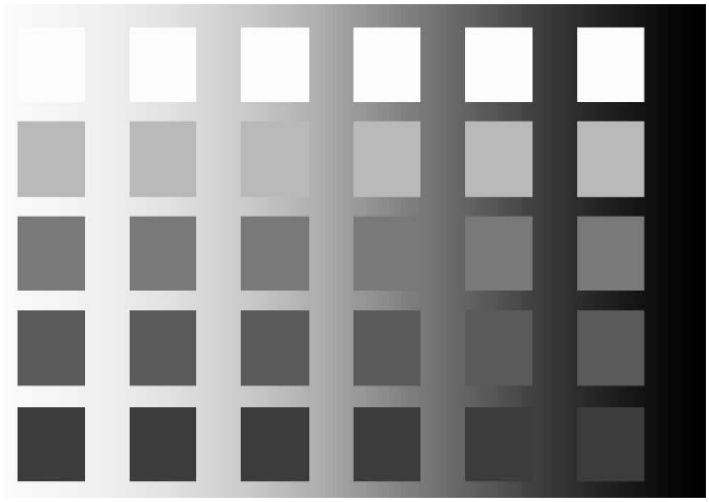

Figure 3.19. Example of the surround effect. Source: [FAIR_04a]

4 Main colour models

The following shows the main proposals to specify colour appearance:

- Direct evaluation systems or models: only take into account the measurements taken on the element to be evaluated.
- Joint evaluation models: include context information.

4.1 Direct evaluation systems or models

Colour spaces: define a set of physical measurements of the element to be measured. Within this type of system one can find examples such as the aforementioned CIE XYZ, or spaces related with artificial systems such as RGB, CMY, HSV...

Ordered colour systems: specify the colour appearance for a set of colours [KUEH_03]:

- Munsell colour system: composed of a set of colour chips ordered according to three attributes: value, chroma (Munsell's) and hue (Munsell's). The hue is a circular system with 10 main hues that in turn are subdivided into 10 sub-areas. Chroma measures the purity of colour, The value 0 belongs to the greys. The 'value' is the lightness attribute and ranges from 0 (black) to 10 (white). The scales of all attributes have been defined in order to represent homogeneous perceptual differences and can be organised within a cylindrical three-dimensional space. New versions have been published since the 1907 original, as for example in 1915 (atlas), in 1929 (book of color), in 1943 (renotations) and in 1967 (re-renotations) in order to improve the perceptual homogeneity. It is designed to be seen with CIE C illuminant (type of illuminant established by CIE) and by the 2º standard observer. The tristimulus from Munsell samples have been measured (in controlled lighting and background conditions). One must mention that despite having a structure based in homogeneous differences, it can not truly measure colours that either vary more than one attribute or have very small variations.

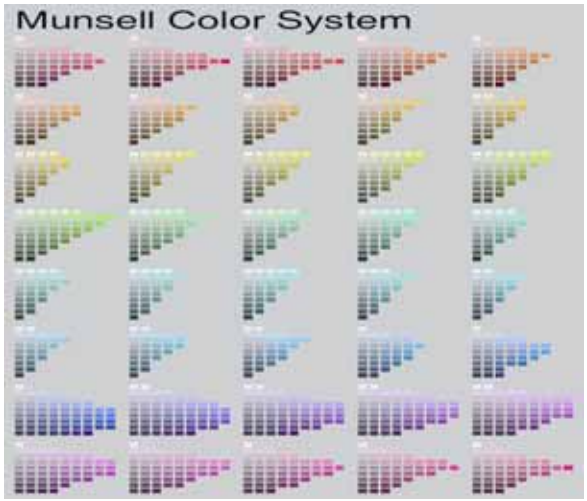

Figure 3.20. Munsell's Colour Chart. Source: [www.jaimetreadwell.com]

- Swedish natural colour system (NCS): is based on the fact that a human being is capable of defining the content of one or two fundamental colours (red, green, blue and yellow) and the quantity of white and black that are present in the samples to be evaluated. Its basis is the opponency pathways of the human visual system. In order to evaluate a colour, certain restrictions are applied: a colour can not be red and green or blue and yellow at the same time and the relation with white and black must add up to 100. Therefore, a colour is defined by 3 values: relation with black, chromaticness and hue. This system is designed for a D65 illumination (illuminant type established by CIE) and a 10º standard observer.

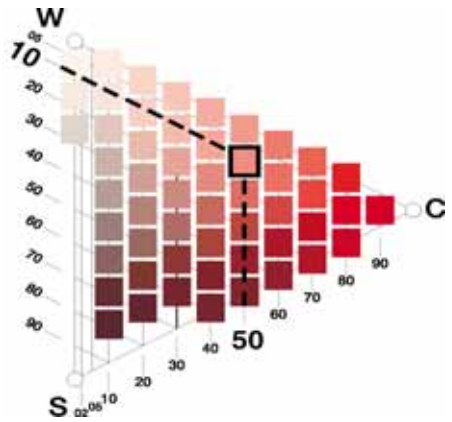

Figure 3.21. Colour sample in the Swedish natural colour system. The marked colour is S 10 (black level) 50 (chromaticness) Y90R (hue).

Source:[www.colourworkshop.co.za/images/NCS_image005.jpg]

- OSA uniform colour scale (OSA-UCS): the purpose of this scale is to obtain a system where the perception differences between adjacent elements are equal irrespective of the variation of one or several of its attributes (Δs= Δcolour). It has a regular- rhombohedral structure with three variables: L, j and g. The positive values in the j axis represent yellow hues while the negative values represent blue hues and the positive values in the g axis represent green hues while the negative values represent magenta. J and g are non-linear combinations (cube roots) based on XYZ CIE 10º tristimulus. The complete equations can be found in [MACA_74]. It is designed to be seen with CIE C illuminant and by the 2º standard observer.

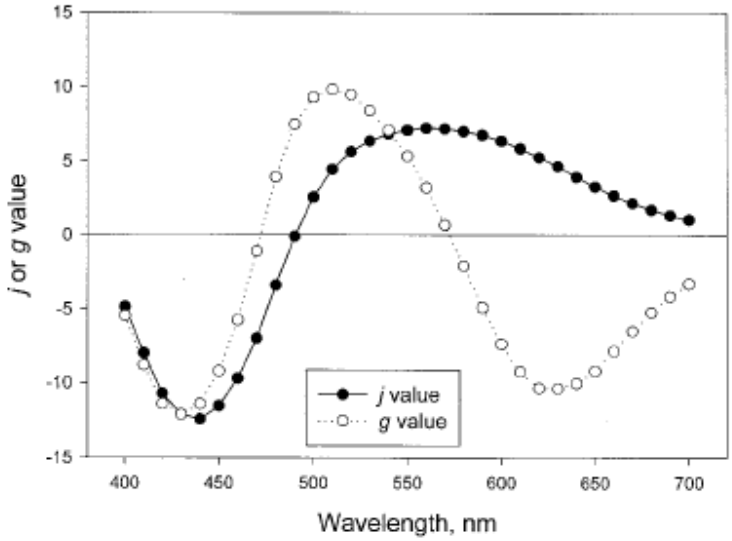

Figure 3.22. Representation of the j and g values of the OSA-UCS for visible spectrum wavelengths. Source: [KUEH_03]

- MÜLLER-JUDD: Müller (1930) proposed the stages theory and Judd (1949, 1951b) developed it. They defined three main stages [KUEH_03]:

    1. Initial photoreceptor stage: there are three types of absorption spectra that can be expressed as linear combinations of the CIE 1931 standard observer:

    $$f_1 = 3.1956\ X + 2.4478\ Y - 0.6434\ Z$$

    $$f_2 = -2.5455\ X + 7.0492\ Y + 0.4963\ Z \qquad \text{(eq. 3.9)}$$

    $$f_3 = 5.000\ Z$$

    2. Intermediate chemical stage: generates the chromatic opponent signals.

$\alpha_1(\lambda) = f_1 - f_1$ {yellowish red – bluish green} (eq. 3.10)

$\alpha_2(\lambda) = 0.0151 f_1 + 0.3849 f_2 - 0.4000 f_3$ {greenish yellow- reddish blue}

3. Final stage towards the optic nerve:

$\beta_1 = \alpha_1 - 0{,}6265\ \alpha_2$ {red – green}

$\beta_2 = \alpha_2 - 0.1622\ \alpha_1$ {yellow – blue} (eq. 3.11)

$\beta_3 = 0.0075 f_1 + 0.1912 f_2 + 0.0013 f_3 + 0.0810 \alpha_1 + 0.0024 \alpha_2$ {white –black}

The following diagram shows the different phases of this model.

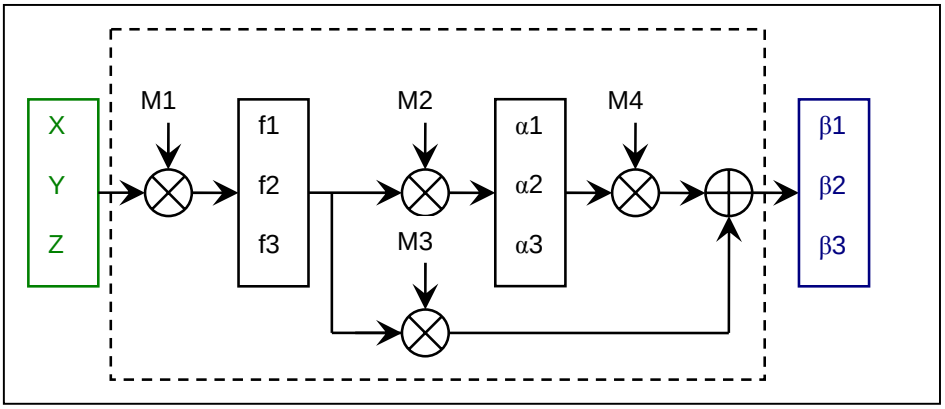

Figure 3.23. Müller-Judd model diagram. Where M1-M4 are the matrices that represent the linear transformations (green inputs, blue outputs).

4.2 Joint evaluation models

Colour perception depends on multiple other factors besides the XYZ or LMS values of the point to be measured, such as, the state of adaptation of the observer, the spatial and temporal structure of the stimulus, the task that is being performed by the observer... [SHEV_03]

The joint evaluation systems that try to characterise the final colour appearance are known as colour appearance models. Most of them follow these steps:

- Use of a sample's XYZ values in order to calculate the chromatic adaptation transform that models the adaptation to the environment (background, luminance,...).

- Define a dynamic response function: where the linear signal is adapted to its compressed form of non-linear nature.
- Combine the signals in an achromatic pathway and several chromatic pathways.
- These input signals are used to calculate the output values: hue, lightness, brightness, chroma, saturation and colourfulness.[2]

The following figure shows a diagram of these phases.

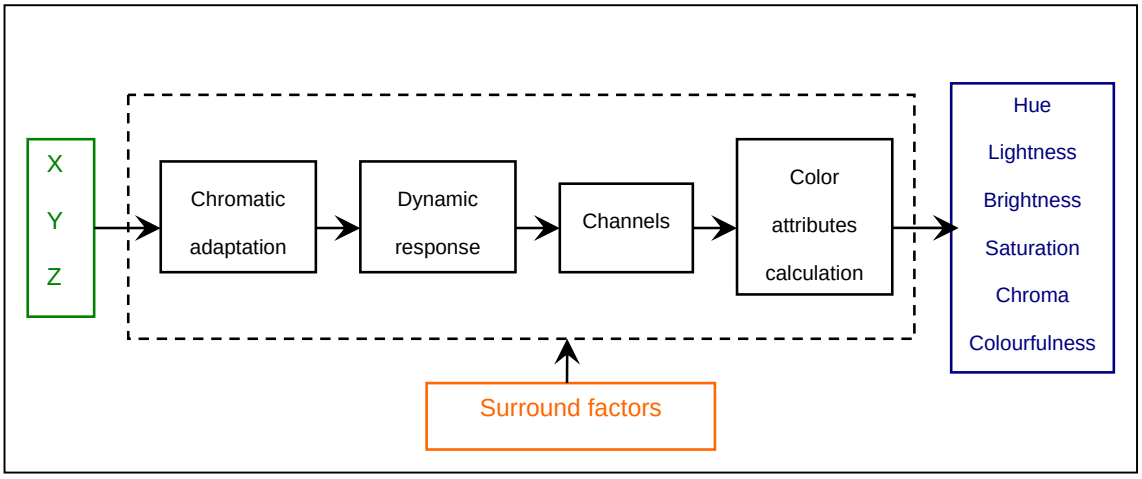

Figure 3.24. Generic diagram of the colour appearance model.

The following shows chronologically the most relevant models both due to its performance as well as by the links established with neurological data.

HURVICH-JAMESON

Hurvich and Jameson (1955-1956) established a psychological specification colour system. This model is based on Hering's colour opponency theory and on the evaluation of the colour levels that annul the perception of a complementary colour. Monochromatic lights of unique colour wavelengths were used for the calculations: blue, green and yellow plus an arbitrary source of red. The study was made with several trichromats and dichromats with different levels of illumination and chromatic adaptation. This model is significant because it took into account two

[2] Not all spaces include all these elements

factors: possible luminance changes and chromatic adaptation. The model defines colour attributes of hue, saturation and brightness. [HURV_55, JAME_55, HURV_56, JAME_56]

They began by calculating the values of four basic pathways: blue, green, yellow and red based on XYZ values.

$$\begin{aligned} B &= 13.0682Y + 0.2672Z \\ G &= -0.6736X + 14.0018Y + 0.004Z \\ Y &= -0.0039X + 13.4680Y - 0.1327Z \\ R &= 0.3329X + 13.0012Y - 0.0011Z \end{aligned} \qquad \text{(eq. 3.12)}$$

The next step is to calculate opponency values: yellow v. blue, red v. green and white v. black (the last one proportional to the perceived brightness).

$$\begin{aligned} y - b &= k_1(nY - lB) \\ r - g &= k_2(pR - mG) \\ w - bk &= k_3(0.5lB + 0.5mG + nY + pR) - k_4\left(\frac{0.5}{l}B + \frac{0.5}{m}G + \frac{1}{n}Y + \frac{1}{p}R\right) \end{aligned} \qquad \text{(eq. 3.13)}$$

With l= Bo/Ba; m=Go/Ga; n=Yo/Ya; p=Ro/Ra. With {Bo, Go, Yo, Ro} being the values of equal energy stimulus and {Ba, Ga, Ya, Ra} the values of the stimulus that the system is adapting to.

Last, hue and saturation are established by:

$$H = \frac{|y-b|}{|y-b|+|r-g|} \quad \text{o} \quad H = \frac{|r-g|}{|y-b|+|r-g|} \qquad \text{(eq. 3.14)}$$

$$S = \frac{|y-b|+|r-g|}{|y-b|+|r-g|+|w-bk|}$$

The space of representation has the following shape:

Figure 3.25. Representation of the Hurvich and Jameson space. Source: [HURV_56]

The model diagram is shown below:

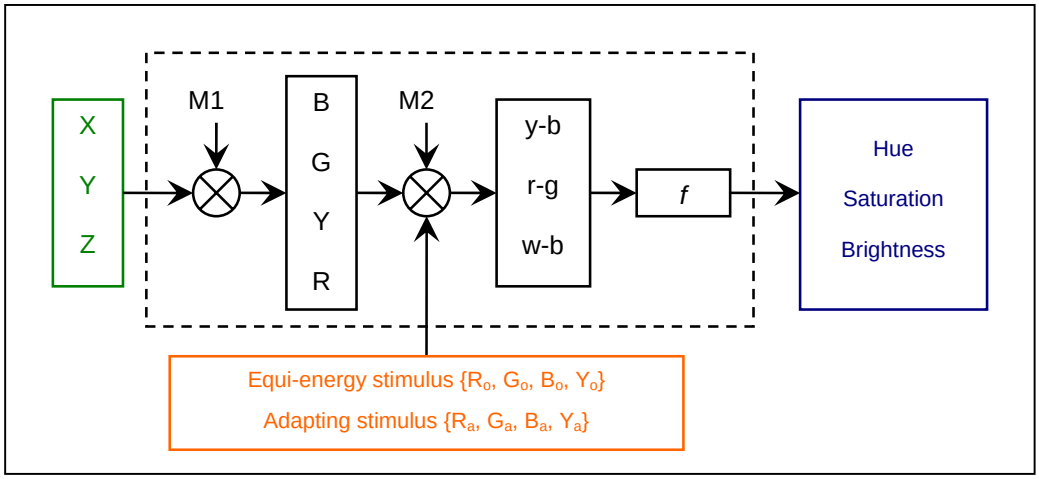

Figure 3.26. Jameson and Hurvich model diagram. Where M1 and M2 are the matrices that represent the linear transforms and *f* the non-linear transform (green inputs, blue outputs, orange system parameters).

One of the main contributions of Jameson and Hurvich was the influence of the adaptation processes.

GUTH

In 1972, Guth proposed the first version of his colour evaluation model. Throughout the years improvements on this first model have been set forth. The following is the 1991 version, known as model CA90, as it includes the main elements of the model and provides a overall vision.

- It begins with the values of the three types of cones calculated by Smith and Pokorny. It normalises the values L:M:S with the ratios 0.55:1:0.66 (values that are not related to the distribution of different types of photoreceptors). Lastly, adds a noise component to the signal and applies a gain factor control:

$$I' = I\left[1 - 0.99\frac{I}{\sigma + I}\right] \qquad \forall \quad I \in \{L, M, S\} \qquad \text{(eq. 3.15)}$$

  Where I represents the stimulus values and σ is a gain factor control.

  Where the stimulus has a background, then:

$$I' = I\left[1 - 0.99\frac{I^*_{p1\bullet estímulo+p2\bullet fondo}}{\sigma + I^*_{p1\bullet estímulo+p2\bullet fondo}}\right] \quad \forall \ \ I \in \{L, M, S\} \qquad \text{(eq. 3.16)}$$

Where $I^*_{p1\bullet estímulo+p2\bullet fondo}$ represent the effect of the weighted combination $\{p_1, p_2\}$ of the stimulus and the background.

- The signals are combined in a second stage according to the following:

$$D_1 = -0.077L' + 0.013M' + 0.091S'$$
$$T_1 = 0.8845L' - 0.7258M' \qquad \text{(eq. 3.17)}$$
$$A_1 = 0.42L' + 0.3108M'$$

- Then, a compression is applied:

$$J' = J/(0.008+J) \quad \forall \ \ J \in \{A_1, T_1, D_1\} \qquad \text{(eq. 3.18)}$$

- A calculation is made of the brightness and the differences between two points can be measured in the following manner:

$$Brightness = \sqrt{A'^2_1 + T'^2_1 + D'^2_1}$$
$$\Delta E = \sqrt{\Delta A'^2_1 + \Delta T'^2_1 + \Delta D'^2_1} \qquad \text{(eq. 3.19)}$$

- Then, hue and saturation are calculated:

$$D_2 = D_1$$
$$T_2 = 0.388\ T_1 + D_1 \qquad \text{(eq. 3.20)}$$
$$A_2 = 0.1\ A_1$$

Aplying, the compression (equation 3.18), results the following:

$$Saturation = \frac{\sqrt{T'^2_2 + D'^2_2}}{A'_2}$$
$$Hue = \frac{T'_2}{D'_2} \qquad \text{(eq. 3.21)}$$

The following figure shows the proposed model.

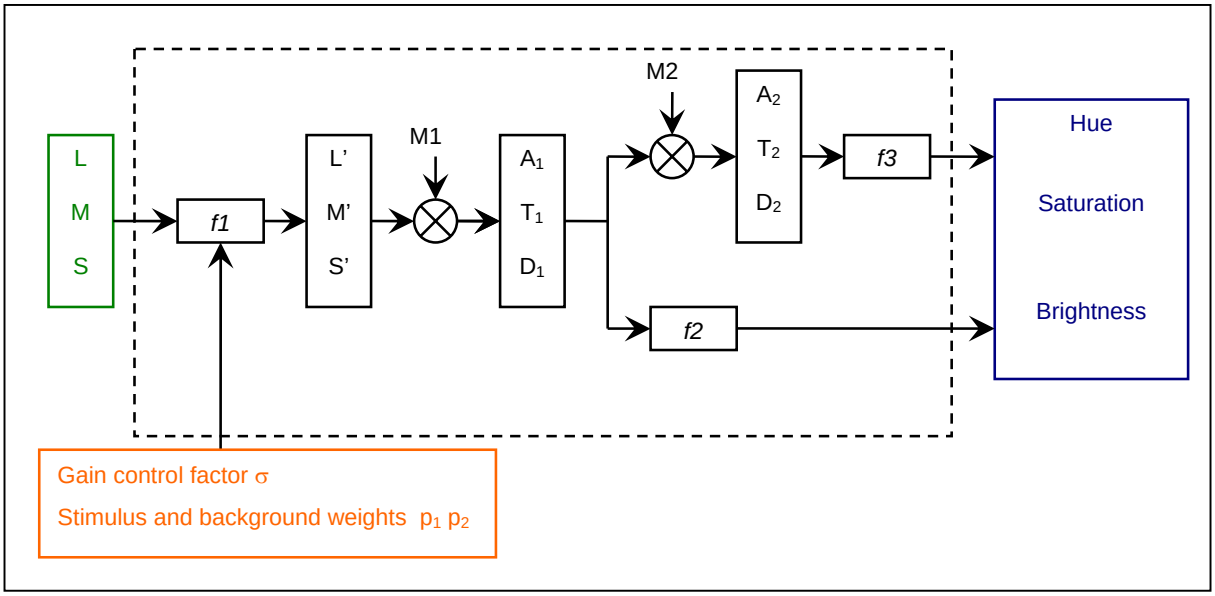

Figure 3.27. Guth model diagram. Where M1 and M2 are the matrices that represent the linear transforms and *f1*, *f2* y *f3* are non-linear transforms (green inputs, blue outputs, orange system parameters).

This model predicts the Bezold-Brücke shift, the Abney effect and the Helmholtz-Kohlrausch effect.

It is noteworthy to point out that this system can model a large number of effects, which in his own words *"…model does make a large number of excellent predictions, its most important contribution may be its suggestion that many perplexing results are straightforward consequences of nonlinear gain controls operating at the receptor level…"* [GUTH_91]

CIELAB

CIELAB or CIE 1976 L*a*b*. In 1976 CIE proposed the CIELAB colour space in order to meet the need to control the quality in manufacturing processes. Based on the CIE 1931 XYZ, it defines three colour attributes L*, a* and b* in order to measure slight colour variations.

- L* represents lightness.

$$L^* = 116\, f\left(\frac{Y}{Y_n}\right) - 16 \qquad \text{(eq. 3.22)}$$

- a* is the measurement of the colour position between red and green.

$$a^* = 500\left[f\left(\frac{X}{X_n}\right) - f\left(\frac{Y}{Y_n}\right)\right] \quad \text{(eq. 3.23)}$$

- b* is the measurement of the colour position between yellow and blue

$$b^* = 200\left[f\left(\frac{Y}{Y_n}\right) - f\left(\frac{Z}{Z_n}\right)\right] \quad \text{(eq. 3.24)}$$

With $\{X_n\ Y_n\ Z_n\}$ are the coordinates of the reference white and

$$f(s) = \begin{cases} 7.787(s) + \dfrac{16}{116}, & s \le 0.008856 \\ s^{1/3}, & s > 0.008856 \end{cases} \quad \text{(eq. 3.25)}$$

The distance between two points is defined as:

$$\Delta E^*_{ab} = \{(\Delta L^*)^2 + (\Delta a^*)^2 + (\Delta b^*)^2\}^{1/2} \quad \text{(eq. 3.26)}$$

Afterwards, new distance measurements have been proposed such as ΔE^*_{94}:

$$\Delta E^*_{94} = \{(\Delta L^*/k_L\ S_L)^2 + (\Delta C^*_{ab}/k_C S_C)^2 + (\Delta H^*_{ab}/k_H\ S_H)^2\}^{1/2} \quad \text{(eq. 3.27)}$$

Where:

$$C^*_{ab} = \sqrt{a^{*2} + b^{*2}}$$

$$H^*_{ab} = \arctan\left(\frac{b^*}{a^*}\right)$$

$S_L = 1$;

$S_C = 1 + 0.045C^*_{ab}$

$S_H = 1 + 0.015C^*_{ab}$

The following requirements must be met in order to use this measurement: use of a D65 illuminant, 1000lux illumination and an achromatic background with L*=50.

Munsell's samples are habitually used as an example of homogeneous colour distribution. The following figure shows the a* and b* values for sets of constant chroma or hue with a value=5.

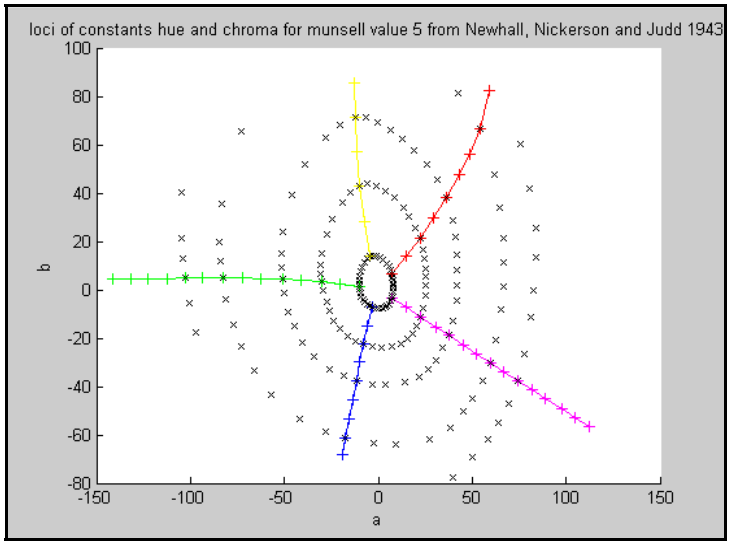

Figure 3.28. Munsell samples with constant chroma (each point of the ovals in black) and constant hue (each point set of the same colour), for a value=5 in CIELAB space.

The following diagram shows the different phases of this model.

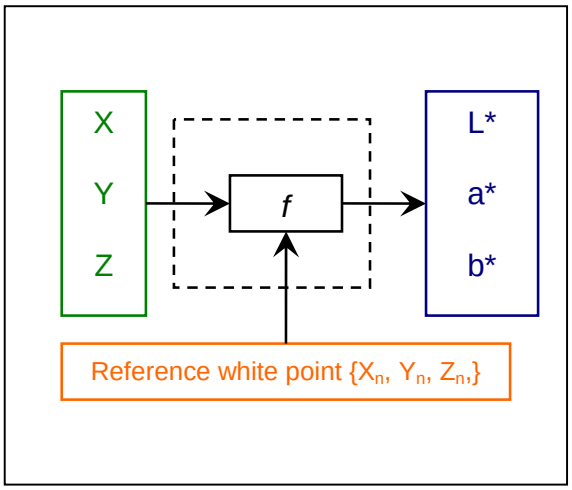

Figure 3.29. CIELAB model diagram. Where *f* represents non-linear transforms (green inputs, blue outputs, orange system parameters).

As can be seen in figure 3.28, the CIELAB model improves the homogeneity in colour distribution although it doesn't achieve a perfect space. The biggest advantage of this model lies in its simplicity and its parameters. Because of this, it is one of the most widely used models nowadays.

CIELUV

CIELUV was created for the same purpose as CIELAB. The colour attributes are defined according to the following:

- L* represents the lightness:

$$L^* = 116\, f\left(\frac{Y}{Y_n}\right) - 16 \qquad \text{(eq. 3.28)}$$

  Where F is described in equation 3.25.

- The chromaticity parameters are:

$$u^* = 13L^*(u' - u_n') \qquad \text{(eq. 3.29)}$$

$$v^* = 13L^*(v' - v_n') \qquad \text{(eq. 3.30)}$$

Where $u' = \frac{4X}{X + 15Y + 3Z}$; $v' = \frac{9Y}{X + 15Y + 3Z}$ and $\{Y_n\ u_n'\ v_n'\}$ are the reference white values.

The distance is defined as:

$$\Delta E^*_{uv} = \{(\Delta L^*)^2 + (\Delta u^*)^2 + (\Delta v^*)^2\}^{1/2} \qquad \text{(eq. 3.31)}$$

The following shows a representation of Munsell samples with constant hue or chroma and a value=5 in the CIELUV space.

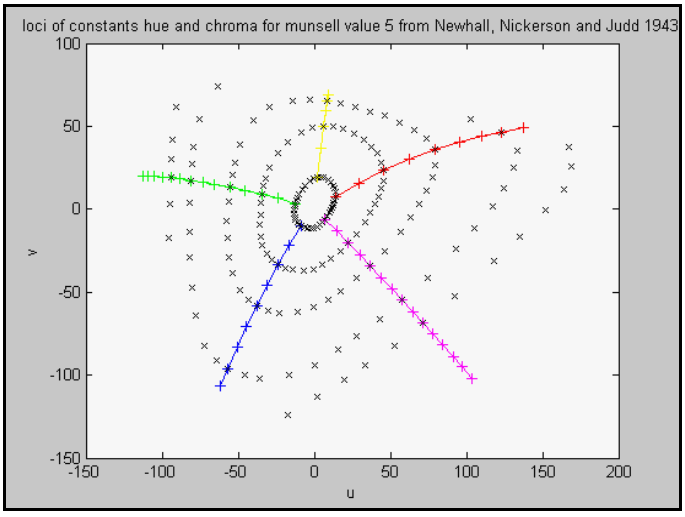

Figure 3.30. Munsell samples with constant chroma (each point of the ovals in black) and constant hue (each point set of the same colour), for a value=5 in CIELUV space.

The following figure shows a diagram with the different phases of this model.

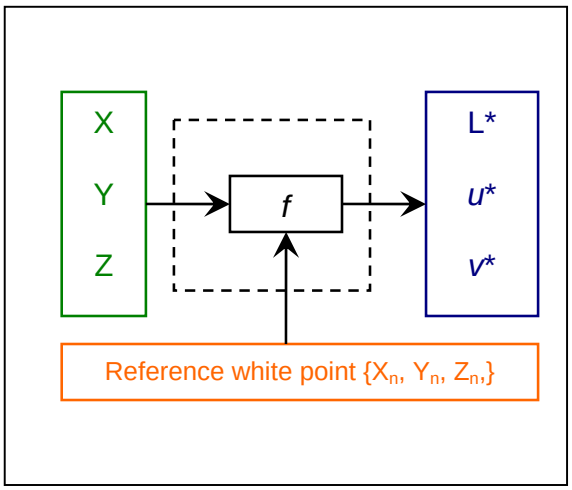

Figure 3.31. CIELUV model diagram, where *f* represents non-linear transforms (green inputs, blue outputs, orange system parameters).

Figure 3.30 shows that, as happens with the CIELAB model case, the CIELUV model improves the homogeneity of the colour space but does not achieve the desired structure. Due to its simplicity, it is nowadays a widely used model. It was proposed, along with CIELAB, neither is clearly better overall and each has specific areas of application where its use is better suited.

NAYATANI

Nayatani et al. proposed in 1981 a colour appearance model to be used in the design and evaluation of lighting systems. Multiple modifications have been set forth on the first version. The system set forth in [NAYA_86] is presented as the aim of this description is to analyse the proposed structure and its main steps. The following is a diagram of the proposed model.

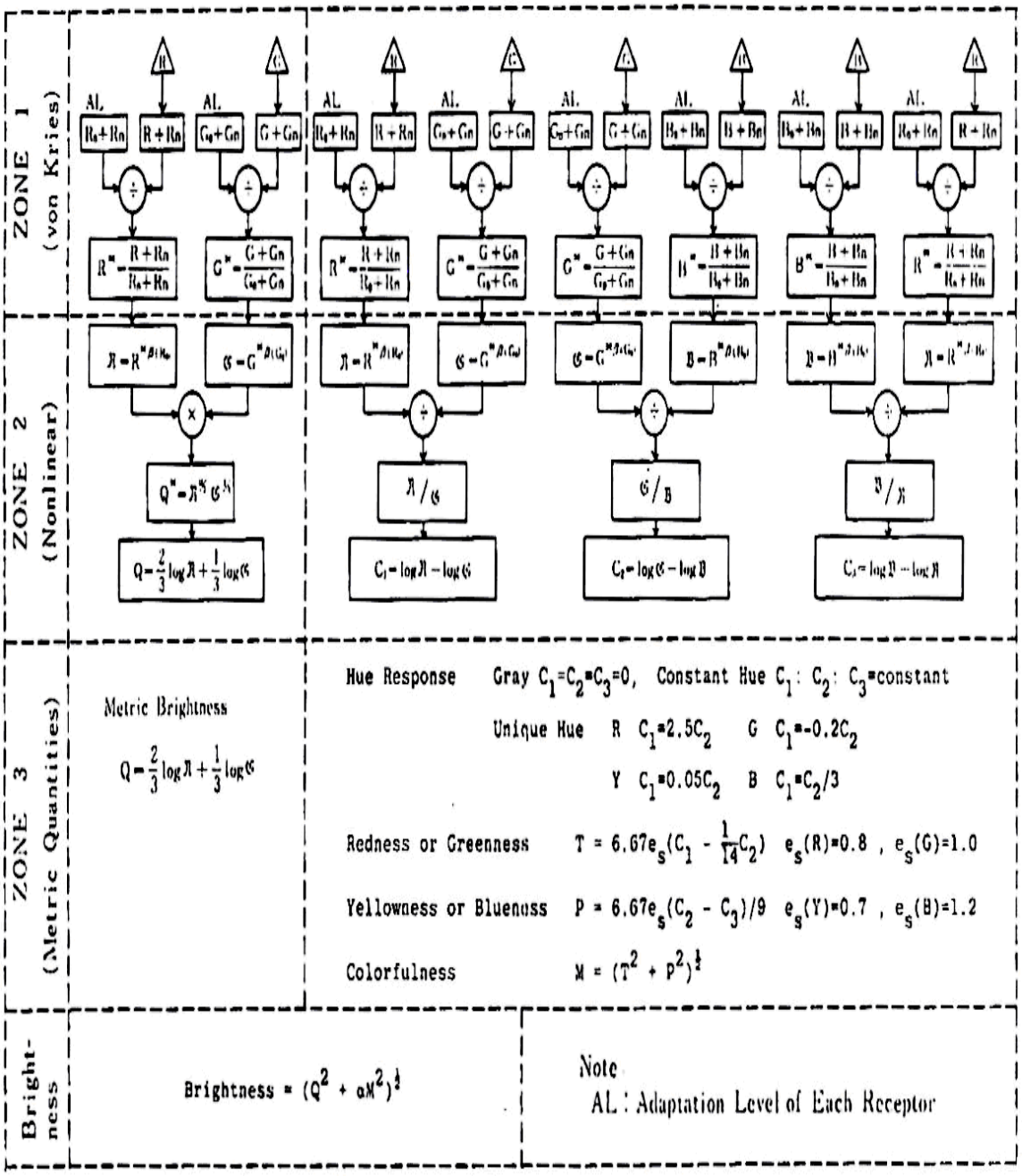

Figure 3.32. Detailed diagram of the Nayatani model. Source: [NAYA_86]

As shown in Figure 3.32, the model has the following steps:

- System inputs: calculation of the fundamental tristimulus values {R,G,B}:

$$\begin{vmatrix} R \\ G \\ B \end{vmatrix} = \frac{E}{100\pi} N \bullet \begin{vmatrix} X \\ Y \\ Z \end{vmatrix} \qquad \text{(eq. 3.32)}$$

$$N = \begin{vmatrix} 0.0711 & 0.9494 & -0.0156 \\ -0.4462 & 1.3173 & 0.0979 \\ 0.0 & 0.0 & 0.9188 \end{vmatrix}$$

$$\begin{vmatrix} R_n \\ G_n \\ B_n \end{vmatrix} = \frac{\rho_n E}{\pi} \begin{vmatrix} 1 \\ 1 \\ 1 \end{vmatrix} \qquad \text{(eq. 3.33)}$$

Where the illumination is characterised by its luminance value E(lx) and ρ_n is an estimation of the noise that is usually of 0.01.

- Zone 1. The Von Kries adaptation transform:

$$I^* = \left(\frac{I + I_n}{I_0 + I_n} \right) \qquad \mathrm{I} \in \{ R, G, B \} \qquad \text{(eq. 3.34)}$$

Where $\{R_o\ G_o\ B_o\}$ model the background values.

- Zone 2. Non-linear characteristics of photoreceptors:

$$I = I^{*\beta(I)} \qquad \text{(eq. 3.35)}$$

$$con \quad \beta(I) = \begin{cases} 16.93 \dfrac{6.469 + 6.362 I_0^{0.4495}}{6.469 + I_0^{0.4495}} & I = \{\mathcal{R}, \mathcal{G}\} \\ 13.28 \dfrac{8.414 + 8.091 I_0^{0.5128}}{8.414 + I_0^{0.5128}} & I = \mathcal{B} \end{cases}$$

- Zone 2B: Chromatic and achromatic pathways: signal combinations of $\{\mathcal{R}, \mathcal{G}, \mathcal{B}\}$ are calculated as seen in the diagram in Figure 3.32, producing $\{Q, C_1, C_2, C_3\}$.

- Zone 3: Uniform colour space model: where brightness and hue (T,P, angle) are defined.[3]

Using the structure of earlier models, the Nayatani et al. model has the following structure:

[3] FAIR_98 provides a more detailed description of these transformations.

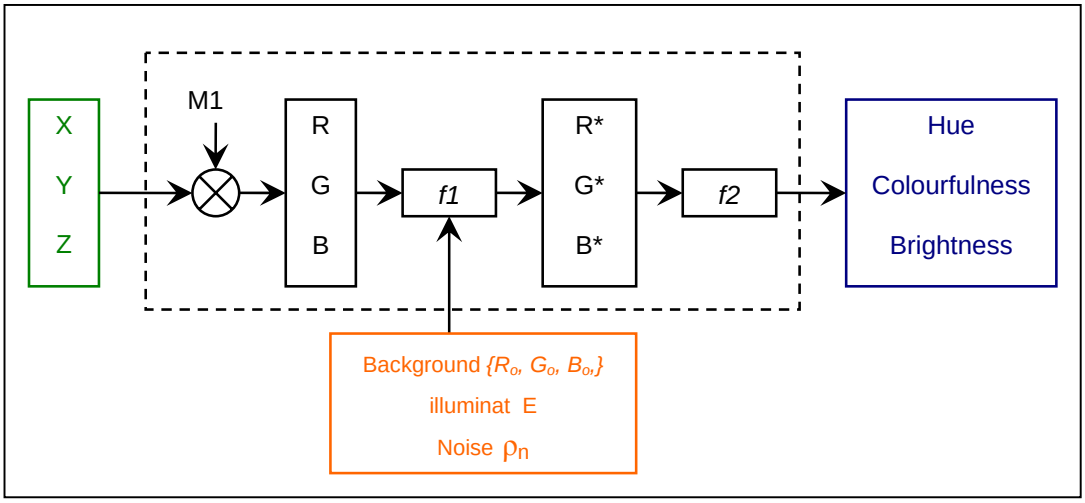

Figure 3.33. NAYATANI model diagram. M1 is the matrix that represents linear transforms while *f1* and *f2* represent non-linear transforms (green inputs, blue outputs, system parameters in orange).

To sum up, the proposed model calculates most relevant colour attributes, predicts the Hunt effect, the Stevens effect and the Helson-Judd effect and can be analytically inverted. On the other hand, it doesn't notify changes in the surrounding areas, is developed for its use in simple patches and doesn't allow to model changes in background colour: simultaneous contrast or surrounding luminance (Bartleson-Breneman equations). Also, it over dimensions the Helson-Judd effect and doesn't include the rod effect [FAIR_98] [NAYA_86].

HUNT

In 1982, R.W.G. Hunt proposed a new colour model that included the effects of the adaptation to the context and the influence of surrounding elements. Subsequently, improvements and different modelled effects have been included [HUNT_82, HUNT_85, HUNT_91, HUNT_94, FAIR_97]. According to [HUNT_91], the model has the following steps:

- Calculation of the basic tristimulus:

$$\begin{vmatrix} R \\ G \\ B \end{vmatrix} = M_H \bullet \begin{vmatrix} X \\ Y \\ Z \end{vmatrix} \qquad \text{(eq. 3.36)}$$

$$M_H = \begin{vmatrix} 0.38971 & 0.68898 & -0.07868 \\ -0.22981 & 1.1834 & 0.04641 \\ 0.0 & 0.0 & 1.0 \end{vmatrix}$$

- Chromatic adaptation:

$$\mathrm{I}_a = B_i\left[f_n(F_L F_i I / I_w) + I_D\right] + 1 \qquad \mathrm{I} \in \{R, G, B\} \qquad \text{(eq. 3.37)}$$

+1 is added to model the noise.

With:

- $$f_n(x) = 40\left[X^{0.73}/(X^{0.73}+2)\right] \qquad \text{(eq. 3.38)}$$

  The function that allows modeling the behaviour for a wide range of luminance as it includes the thresholds for small values and the saturation that is caused in high luminance.

- F_L indicates the adaptation factor to the luminance level. The use of an absolute luminance level allows modeling the Stevens and the Hunt effects.

$$F_L = 0.2k^4 5L_A + 0.1\left(1-k^4\right)^2 \left(5L_A\right)^{1/3}$$
$$k = 1/(5L_A + 1) \qquad \text{(eq. 3.39)}$$

  Where L_A is the luminance of the adapting field (if unknown, use 20% of reference white),

- F_R, F_G, F_B are the chromatic adaptation factors. They represent the fact that chromatic adaptation is often incomplete:

$$F_i = (1 + L_A^{1/3} + h_i)/(1 + L_A^{1/3} + 1/h_i) \quad I \in \{R, G, B\}$$
$$\mathrm{h_i} = \frac{3I_w}{\sum_{i \in \{R,G,B\}} I_w} \qquad \text{(eq. 3.40)}$$

  Where $\{R_W, G_W, B_W\}$; $\{x_W, y_W, Y_W\}$ characterise the reference white (if this value is not available then $\{x_W, y_W\}$ the same as the illumination Y_W =100).

  If the illumination is not taken into account, then the chromatic adaptation is complete and all have a value of 1.

- $\{R_D, G_D, B_D\}$ show the Helson-Judd effect.

$$I_D = f_n(F_L F_G Y_b / Y_w) - f_n(F_L F_i Y_b / Y_w) \quad I \in \{R, G, B\} \qquad \text{(eq. 3.41)}$$

Where Yb corresponds to the background.

In general, this effect doesn't happen, so usually $\{R_D, G_D, B_D\} \equiv \{0, 0, 0\}$

- Cone bleach factor

$$B_i = 10^7 / [10^7 + 5L_A(I_w / 100)] \qquad I \in \{R, G, B\} \qquad \text{(eq. 3.42)}$$

Usually has value 1, if L_A grows considerably, then the B factors decrease until they reach 0 in the limit cases where the cones are fully bleached (retinal burn).

- Calculation of opponent signals: suggests that this stage is done in combination with the signal compression before "leaving" through the optic nerve.

$$\begin{aligned} A_a &= 2R_a + G_a + (1/20)B_a - 3.05 + 1 \\ C_1 &= R_a - G_a \\ C_2 &= G_a - B_a \\ C_3 &= B_a - R_a \end{aligned} \qquad \text{(eq. 3.43)}$$

The amount of -3.05 is included in order to subtract previously introduced noise and +1 is added to include again the presence of noise.

- Colour space:
  - Colour attribute calculation:
    - Hue:

$$\begin{cases} \mathrm{h} = \arctan\left(\dfrac{0.5(C_2 - C_3)/4.5}{C_1 - C_2/11}\right) \\ \mathrm{H} = \mathrm{H}_1 + \dfrac{100 \bullet [(h - h_1)/e_1]}{(h - h_1)/e_1 + (h_2 - h)/e_2} \end{cases} \qquad \text{(eq. 3.44)}$$

    - Lightness:

$$J = 100(\mathrm{Q}/\mathrm{Q}_\mathrm{w})^z \qquad \text{(eq. 3.45)}$$

Where the simultaneous contrast effect is modelled by means of z.

    - Brightness:

$$Q = \{7 \bullet [A + M/100]\}^{0.6} N_1 - N_2 \qquad \text{(eq. 3.46)}$$

uses A and M in order to predict the Helmholtz-Kohlrausch effect and N_1 and N_2 factors for the surround effect in the perceived brightness.

– Saturation:

$$s = 50M /(R_a + G_a + B_a) \quad \text{(eq. 3.47)}$$

– Chroma:

$$C = \ 2.44s^{0.69}\ (Q/Q_w)^n\ (1.64 - 0.29^n) \quad \text{(eq. 3.48)}$$

– Colourfulness:

$$M = CF_L^{0.15} \quad \text{(eq. 3.49)}$$

- Calculation of auxiliary values:

The eccentricity value is defined as:

$$e = e_1 + (e_2 - e_1)\cdot(h - h_1)/(h_2 - h_1) \quad \text{(eq. 3.50)}$$

where subindex 1 indicates the unique colour that has the nearest smallest value and subindex 2 indicates the unique hue that has the nearest greatest value.

	red	yellow	green	blue
h	20.14	90	164.25	237.53
e	0.8	0.7	1.0	1.2
H_1	0	100	200	300

Table 3.1 H and e values for unique hues.

- N_{cb} and N_{bb} represent chromatic induction and luminous background.

$$\begin{aligned} N_{bb} &= N_{cb} = 0.725(1/n)^{0.2} \\ z &= 1 + n^{1/2} \\ n &= Y_b / Y_w \end{aligned} \quad \text{(eq. 3.51)}$$

- Chromatic response:

$$M = \left(M_{YB}^2 + M_{RG}^2\right)^{1/2} \quad \text{(eq. 3.52)}$$

$$\begin{aligned} M_{YB} &= 100 \bullet \left[0.5(C_2 - C_3)/4.5\right]\cdot\left[e_s(10/13)N_c N_{cb} F_t\right] \\ M_{RG} &= 100 \bullet \left[C_1 - (C_2/11)\right]\cdot\left[e_s(10/13)N_c N_{cb}\right] \end{aligned}$$

Where $F_{t=}\frac{L_A}{L_A+0.1}$ models the tritanopia produced with small luminance and N_c is a tabulated value for induction processes.

- Rod adapted response:

$$A_s = 3.05B_s\left[f_n(F_{LS}S/S_W)\right]+0.3 \quad \text{(eq. 3.53)}$$

Where S/ S_W is the scotopic luminance related to the reference white, (if unknown, an approximation can be made with (Y/Y_W)).

- F_{LS} is the adaptation factor to the scotopic luminance level.

$$F_{LS} = 3800j^2(5L_{AS}/2.26)+0.2(1-j^2)^4(5L_{AS}/2.26)^{1/6}$$
$$j = 0.00001/\left[(5L_{AS}/2.26)+0.00001\right] \quad \text{(eq. 3.54)}$$

Where L_{AS} (cd/m^2) is the scotopic luminance of the adaptive field (can be approximated if L_A and the corresponding colour temperature are known).

- Rod bleaching factor:

$$B_S = 0.5/\left\{1+0.3\left[(5L_{AS}/2.26)(S/S_w)\right]^{0.3}+0.5/\left[1+5(5L_{AS}/2.26)\right]\right\} \quad \text{(eq. 3.55)}$$

- Total achromatic signal:

$$A = N_{bb}\left[A_a-1+A_S-0.3+(1+0.3^2)^{1/2}\right] \quad \text{(eq. 3.56)}$$

Where the previously added noise components are subtracted and a new noise component is added.

- Auxiliary brightness values:

$$N_1 = (7A_w)^{1/2}\Big/(5.33N_b^{0.13})$$
$$N_2 = 7A_wN_b^{0.362}/200 \quad \text{(eq. 3.57)}$$

Where N_b corresponds to tabulated values that model induction processes.

The Hunt model has the following structure.

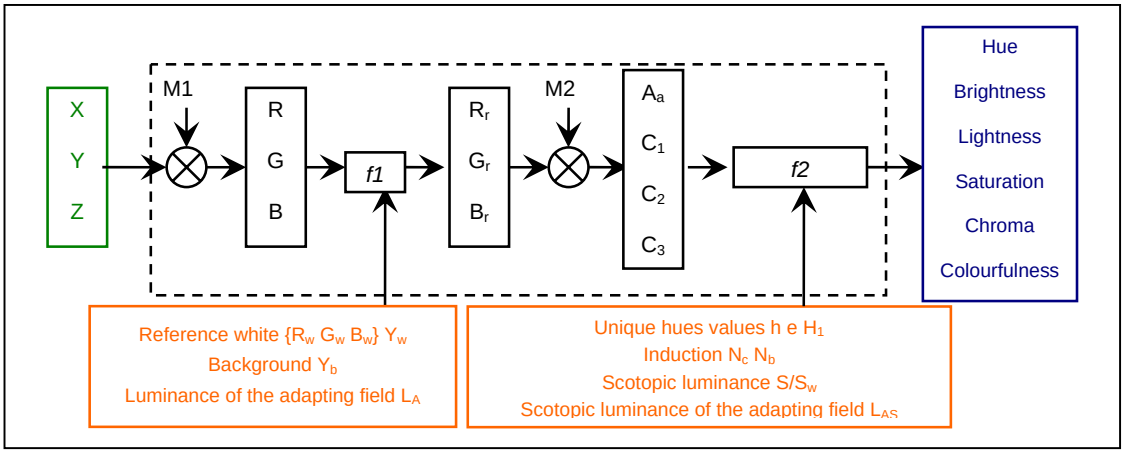

Figure 3.34. Hunt model diagram. Where M1 and M2 are the matrices that represent linear transforms while *f1* and *f2* are the non-linear transforms (green inputs, blue outputs, system parameters in orange).

The definition that establishes the elements to be taken into account when evaluating a colour [HUNT_91] is highly relevant for the model object of this thesis.

1. Stimuli: the element whose colour appearance is going to be evaluated. Experiments normally use a 2º sized stimulus.
2. Proximal field: the adjacent area to the stimulus.
3. Background: the surroundings of the stimulus (immediately adjacent to the stimulus).
4. Surround: the area that is beyond the background and the stimulus.
5. Adapting field: all that surrounds the stimulus.

This is the only model that deals independently with these elements and also the only one that includes the rod effects.

To sum up, the Hunt model predicts multiple effects: Bezold-Brücke, Abney, Helmholtz-Kohlrausch, Hunt, Helson-Judd and Stevens, as well as the simultaneous contrast and the Bartleson-Breneman data. Its complexity allows it to adapt and predict multiple effects, which is at the same time one of its drawbacks due to the inherent difficulty to adjust all of its parameters. Furthermore, it is not an invertible model.

DERRINGTON-KRAUSKOPF-LENNIE

In 1984, Derrington, Krauskopft and Lennie undertook a series of experiments to characterise the neurons in LGN. In order to represent stimuli and later characterise each type of neuron. They defined a space where the chromatic part is based on the chromatic diagram propounded by MacLeod and Boynton, to which they add a third dimension that takes luminance into account.

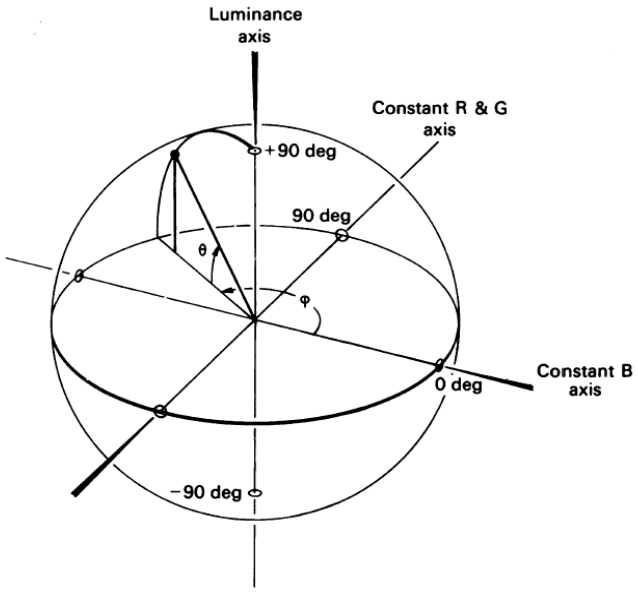

Figure 3.35. Derrington, Krauskopf and Lennie space. Source: [DERR_84]

In order to group the different neuron types in LGN, they take advantage of the fact that two metamere stimuli produce the same neuron activation. The Derrington, Krauskopf and Lennie space, known as DKL, has a plane that goes through the origin and contains all the specific metamers of each neuron. Two types of parvocellular neurons were found in this manner: a large group near an azimuth value of 92.6º with a moderately distributed elevation near an average value of 51.5º and a second group near the azimuth value of 178.4º with an average elevation of 76.7º. Based on these values, they proposed a that the first type corresponds with R-G neurons while the second corresponds with the type B- (R&G).

Later, Lennie and D'Zamura [LENN_88] proposed a signal combination model based on these results. In the first stage there are chromatic opponency cells: centre vs. surround. The second stage combines them in order to create an achromatic and chromatic signal. The following figure shows the model diagram.

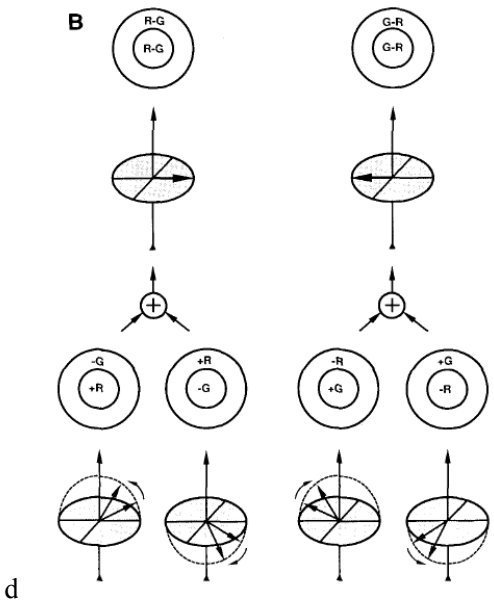

d

Figure 3.36. Lennie and D'Zamura model for the generation of an achromatic signal (A) and a chromatic signal (B) and its representation in the Derrington, Krauskopf and Lennie space. Source: [LENN_88]

DEVALOIS

In 1993, DeValois et al. proposed a four phased model for colour processing based on the primate visual system. The following are the stages of the model [DEVA_93]:

1. Cone signal: the first stage begins in the photoreceptors. The distribution of L:M:S is10:5:1. (At that time, this ratio was not demonstrated but later it has been shown to be very close to reality).

2. Opponency: the second stage assumes the existence of two types of bipolar cells (based on physical data): midget and diffuse. The difference between both lies on the number of photoreceptors that connect with the centre: few or even just one versus multiple.

   Each photoreceptor is connected with four bipolar cells: 2 midget and 2 diffuse, two of them being activation type and two being inhibition type. In this stage, the centre-surround opponency process occurs, which can be generated:

   - In horizontal and/or amacrine cells + ganglion cells.

- In a random or specific manner: made up of signals from different types of photoreceptors or from only one type.

It deems that these 4 types of channels continue to be separate until the cortex (midget or diffuse, activation and inhibition). The signals generated in this phase can be specified in the following manner:

$$L_o = 16L - (10L + 5M + S)$$

$$M_o = 16M - (10L+5M+S) \quad \text{(eq. 3.58)}$$

$$S_o = 16S - (10L+5M+S)$$

3. Perceptual opponency: the third stage combines the centre-surround signals generated in the second phase in order to create colour and luminance signals. The following figure shows how a combination of signals from the earlier stage plus the S component can generate luminance and colour values and a half-wave rectification function (HWR).

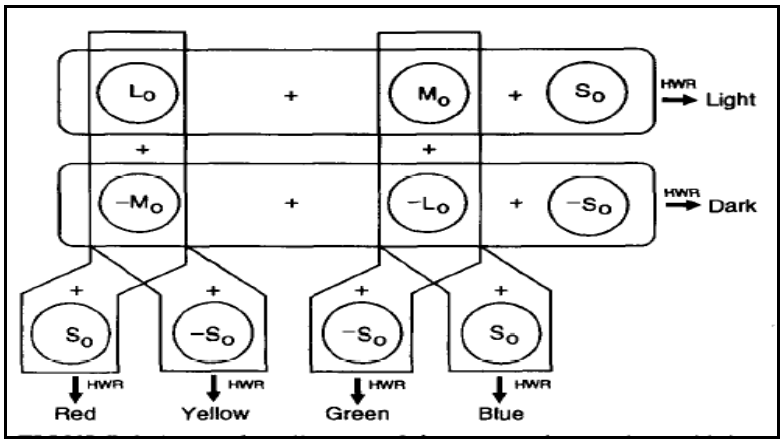

Figure 3.37. Diagram of Stage 3 with HWR. Source: [VALO_93]

Following the diagram in figure 3.37, they obtain:

$$RG = 10L_o - 5M_o + 2S_o = 90L - 1115M + 25S \quad \text{(eq. 3.59)}$$

$$YB = 5M_o - 10L_o + 2S_o = 30L + 95M + 35S$$

4. Colour-selective complex cells: this stage proposes a model of simple and complex V1 cells. The complex cells add the half-wave rectification signal of simple cells (output generated in the previous stage).

The final stages of the model are based on experimental results obtained in LGN and V1 where there is a reduction in the tuning of the red/green and blue/yellow pathways when working with the same stimuli [DEVA_00].

To sum up, it is a model with a biological basis that proposes both a colour information retrieval system as well as one regarding luminance. It states the existence of 2 pathways $+S_o$ and $-S_o$ that generate four colour axis, however the existence of $-S_o$ is not clear and they also don't provide evidence of the existence of these pathways.

RLAB

RLAB was introduced by Fairchild et al. in 1993 with the aim to define a simple colour model that allows the prediction of the colour appearance of a stimulus. It is based on the CIELAB system. It is composed of the following stages:

- Calculation of the basic tristimulus:

$$\begin{vmatrix} L \\ M \\ S \end{vmatrix} = N \bullet \begin{vmatrix} X \\ Y \\ Z \end{vmatrix} \qquad \text{(eq. 3.60)}$$

$$N = \begin{vmatrix} 0.3897 & 0.6890 & -0.0787 \\ -0.2298 & 1.1834 & 0.0464 \\ 0.0 & 0.0 & 1.0 \end{vmatrix}$$

- Calculation of the Von Kries adaptation:

$$A = \begin{vmatrix} a_L & 0 & 0 \\ 0 & a_M & 0 \\ 0 & 0 & a_S \end{vmatrix} \qquad \text{(eq. 3.61)}$$

$$\text{Where} \begin{cases} a_I = \dfrac{p_I + D(1.0 - p_I)}{I_n} \\ p_I = \dfrac{(1.0 + Y_n^{1/3} + i_E)}{(1.0 + Y_n^{1/3} + 1.0/i_E)} \\ i_E = \dfrac{3.0 I_n}{\sum_{I=\{L,M,S\}} I_n} \end{cases} \qquad \forall I \in \{L, M, S\}$$

Y_n being the absolute luminance in cd/m^2, $\{L_n, M_n, S_n\}$ are the white reference values and D is the level of cognitive discount of the illuminant.

- Transform to adapted tristimulus:

$$\begin{vmatrix} X_{ref} \\ Y_{ref} \\ Z_{ref} \end{vmatrix} = R \bullet A \bullet N \bullet \begin{vmatrix} X \\ Y \\ Z \end{vmatrix} \qquad \text{(eq. 3.62)}$$

$$R = \begin{vmatrix} 1.9569 & -1.1882 & 0.2312 \\ 0.3612 & 0.6388 & 0.0 \\ 0.0 & 0.0 & 1.0 \end{vmatrix}$$

- Calculation of values $\{L^R, a^R, b^R\}$:

$$\begin{aligned} L^R &= 100 Y_{ref}{}^{\sigma} \\ a^R &= 430\left(X_{ref}{}^{\sigma} - Y_{ref}{}^{\sigma}\right) \\ b^R &= 430\left(Y_{ref}{}^{\sigma} - Z_{ref}{}^{\sigma}\right) \end{aligned} \qquad \text{(eq. 3.63)}$$

σ being the relative luminance of the surrounding: average value= 1/2.3, dim= 1/2.9 and dark= 1/3.5.

- The remaining colour attributes are calculated as follows:

$$\textit{Hue}\ \text{angle}: h^R = \tan^{-1}(b^R / a^R) \qquad \text{(eq. 3.64)}$$

$$\textit{Chroma}: \quad C^R = \sqrt{\left(a^R\right)^2 + \left(b^R\right)^2} \qquad \text{(eq. 3.65)}$$

$$\textit{Saturation}: \quad S^R = C^R / L^R \qquad \text{(eq. 3.66)}$$

The distance between two points can be measured as in CIELAB.

The model diagram is shown below:

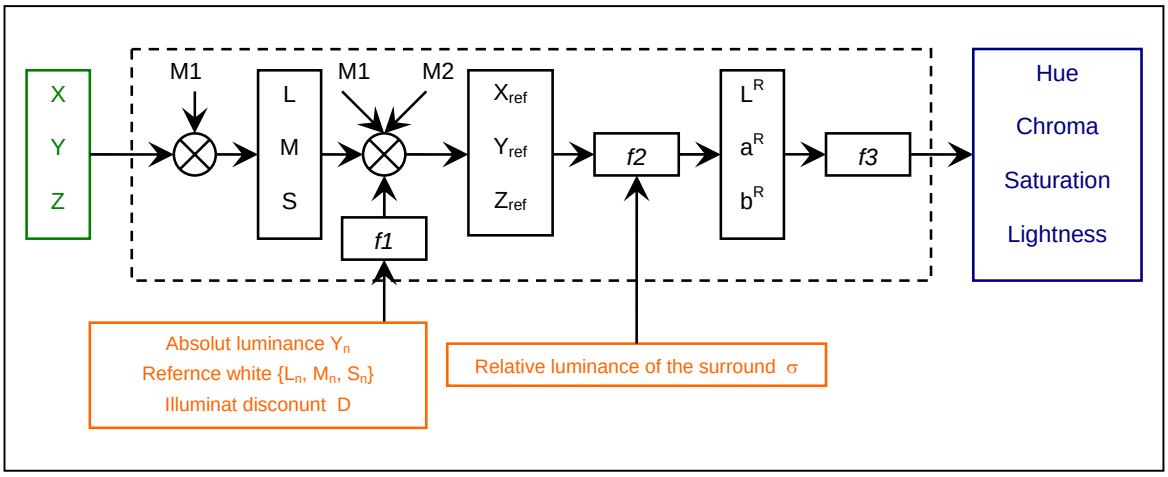

Figure 3.38. RLAB model diagram. Where M1 and M2 are the matrices that represent linear transforms while *f1* and *f2* are the non-linear transforms (green inputs, blue outputs, system parameters in orange).

The advantage of this model lies in its simplicity and the possibility of inversion. At the same time, as it is a simplified model, it doesn't permit to model all the features of colour appearance.

LLAB

LLAB was introduced by Luo et al. in 1996 (1st model). It was built on appearance and colour difference measurements. It has the following stages [LUO_96] [FAIR_97]:

- BFD transform or transformation to the system D65/ 2º observer:

$$\begin{vmatrix} R \\ G \\ B \end{vmatrix} = \begin{vmatrix} 0.8951 & 0.2664 & -0.1614 \\ -0.7502 & 1.7135 & 0.0367 \\ 0.0389 & -0.0685 & 1.0296 \end{vmatrix} \bullet \begin{vmatrix} X/Y \\ Y/Y \\ Z/Y \end{vmatrix} \qquad \text{(eq. 3.67)}$$

$$\begin{aligned} R_r &= \left[D(R_{0r}/R_0)+1-D\right]R \\ G_r &= \left[D(G_{0r}/G_0)+1-D\right]G \\ B_r &= \left[D(B_{0r}/B_0^{\beta})+1-D\right]B^{\beta} \end{aligned} \qquad \text{(eq. 3.68)}$$

Where $\{R_{or}, G_{or}, B_{or}\}$ is the reference white in reference conditions and $\{R_o, G_{or}, B_o\}$ in working conditions and

$$\beta = (B_0 / B_{0r})^{0.0834}$$

$$D = \begin{cases} 0 \text{ non adapted to the illuminant} \\ 1 \text{ adapted to the illuminant} \end{cases}$$

- The inverse transform to that used in equation 3.67 is applied, thus obtaining $\{X_r\ Y_r\ Z_r\}$
- Next, a calculation of L, A and B is made in a similar way to CIELAB:

$$L_L = 116 f\left(\frac{Y_r}{100}\right)^z - 16 \qquad \text{(eq. 3.69)}$$
$$z = 1 + F_L (Y_b / 100)^{1/2}$$

Where z models the effect of lightness contrast, Y_b is the achromatic background value under the illuminant.

$$A = 500\left[f\left(\frac{X_r}{95.05}\right) - f\left(\frac{Y_r}{100}\right)\right] \qquad \text{(eq. 3.70)}$$

$$B = 200\left[f\left(\frac{Y_r}{100}\right) - f\left(\frac{Z_r}{108.88}\right)\right] \qquad \text{(eq. 3.71)}$$

With $\{X_n\ Y_n\ Z_n\}$ as the coordinates of the reference white and

$$f(s) = \begin{cases} \left[\left(0.008856^{1/F_s} - \frac{16}{116}\right) / 0.008856\right] s + \frac{16}{116}, & s \le 0.008856 \\ s^{1/F_s}, & s > 0.008856 \end{cases} \qquad \text{(eq. 3.72)}$$

Where F_S is the induction factor of the surroundings and F_L the lightness induction factor. These are tabulated values.

- The remaining colour attributes are calculated as follows:
  - Hue. $h_L = \tan^{-1}(B / A)$ (eq. 3.73)
  - Chroma: $Ch_L = 25 \ln\left(1 + 0.05(`A^2 + B^2)^{1/2}\right)$ (eq. 3.74)
  - Saturation: $S_L = Ch_L / L_L$ (eq. 3.75)
  - Colourfulness: $C_L = Ch_L S_M S_C F_C$ (eq. 3.76)

With:

$$S_C = 1.0 + 0.47\log(L_L) - 0.057[\log(L_L)]^2$$
$$S_M = 0.7 + 0.02L_L - 0.0002L_L^2 \qquad \text{(eq. 3.77)}$$

F_c is the chromaticness induction factor (tabulated).

With these values, the point coordinates can be calculated:

$$A_L = C_L \cos(h_L) \text{ and } B_L = C_L \sin(h_L) \qquad \text{(eq. 3.78)}$$

The aforementioned has been a description of its main components. This model has been improved over the last years.

The following figure shows the model diagram.

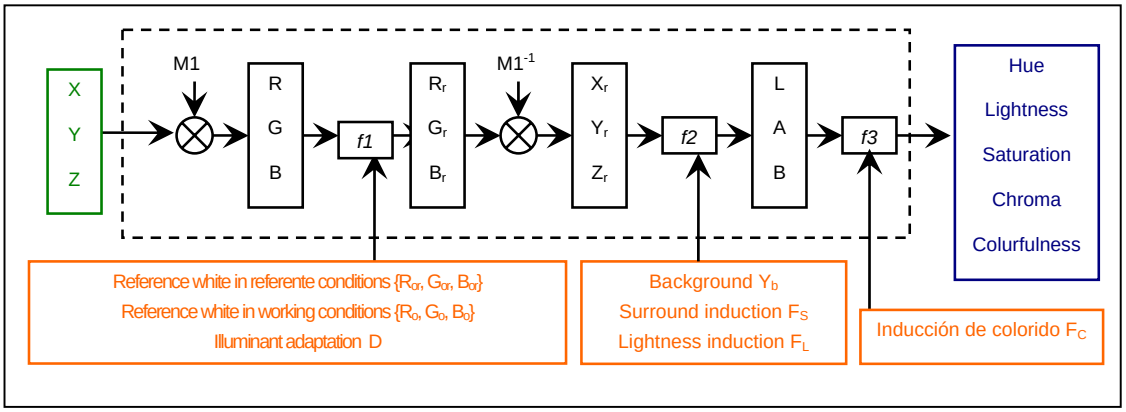

Figure 3.39. LLAB model diagram. Where M1 is the matrix that represents linear transforms while *f1*, *f2* y *f3* represent non-linear transforms (green inputs, blue outputs, system parameters in orange).

This model allows to model the chromatic adaptation, the surround effect as well as the Hunt effect. Its main drawback is that it is not analytically invertible.

CIECAM97

In 1997, CIE approved a proposal for a new model that would encompass the most relevant models to date. The CIECAM97 model includes the Nayatani et al. model, the RLAB model, the LLAB model and the Hunt et al model. The stages of the model are the following [LUO_97]:

- Chromatic adaptation transform:
  - Transformation to the RGB space: applying the Bradford transform. Uses X/Y, Y/Y, Z/Y as inputs.

$$\begin{vmatrix} R \\ G \\ B \end{vmatrix} = M_{BFD} \bullet \begin{vmatrix} X/Y \\ Y/Y \\ Z/Y \end{vmatrix} \qquad \text{(eq. 3.79)}$$

$$M_{BFD} = \begin{vmatrix} 0.8951 & 0.2664 & -0.1614 \\ -0.7502 & 1.7135 & 0.0367 \\ 0.0389 & -0.0685 & 1.0296 \end{vmatrix}$$

  - The degree of chromatic adaptation is calculated as follows:

$$D = \begin{cases} 0 & \text{if chromatic adaptation is complete} \\ 0 & \text{if there is not chromatic adaptation} \\ \frac{1}{2}\left\{1 + F - F/\left[1 + 2\left(L_A^{1/4}\right) + \left(L_A^2/300\right)\right]\right\} & \text{if the adaptation is partial} \\ F - F/\left[1 + 2\left(L_A^{1/4}\right) + \left(L_A^2/300\right)\right] & \text{remaining cases} \end{cases}$$

    Where the luminance of the adapting field is calculated L_A (cd/m) (usually 1/5 of the luminance of a white point) and F is a tabulated parameter (with value 1 in average surroundings that are neither dark nor very dim).

  - The tristimulus values of the working conditions are calculated:

$$I_c = \left[D\left(I_{wr}/I^{p_i}{}_w\right) + 1 - D\right] \mathrm{I}\,|^{p_i} \qquad I \in \{R, G, B\}$$

$$p_i = \begin{cases} \left(\left(I_w/I_{wr}\right)^{0.0834} & \text{si } \mathrm{I} \equiv \mathrm{B} \\ 1 & \text{remaining} \end{cases} \qquad \text{(eq. 3.80)}\ [4]$$

    Where $\{x_w, y_w, Y_w\}$ correspond to the white point in the working conditions $\{x_{wr}, y_{wr}, Y_{wr}\}$ to the white in the reference conditions, which is defined as the equal energy stimulus (1/3, 1/3, 100). These values are included in order to add information about the chromaticity level of the surrounding that is being measured.

[4] When B is negative, B_c must also be negative.

- The cones are transformed to the response space in accordance with Estevez and normalised for the equal energy stimulus:

$$\begin{vmatrix} R' \\ G' \\ B' \end{vmatrix} = M_H M^{-1}{}_{BFD} \bullet \begin{vmatrix} R_c Y \\ G_c Y \\ B_c Y \end{vmatrix} \qquad \text{(eq. 3.81)}$$

$$M_H = \begin{vmatrix} 0.38971 & 0.68898 & -0.07868 \\ -0.22981 & 1.1834 & 0.04641 \\ 0.0 & 0.0 & 1.0 \end{vmatrix}$$

- Dynamic response function: a hyperbolic function is used, as indicated by the measurements of Valeton and Van Norren in the rhesus monkey:

$$I_a' = 40\left(F_L I'/100\right)^{0.73} / \left[\left(F_L I'/100\right)^{0.73} + 2\right] + 1 \qquad \mathrm{I} \in \{\mathrm{R,G,B}\}^{5} \qquad \text{(eq. 3.82)}$$

Where F_L is the luminance level adaptation factor, as defined in the following manner:

$$F_L = 0.2k^4 5L_A + 0.1\left(1-k^4\right)^2 \left(5L_A\right)^{1/3}$$
$$k = 1/(5L_A + 1) \qquad \text{(eq. 3.83)}$$

- Colour space: is similar to that set forth by Hunt with some modifications in order to avoid negative brightness and lightness values.

  - Colour attribute calculation:

    – Hue: $\begin{cases} \mathrm{h} = \arctan(\mathrm{b/a}) \\ \mathrm{H} = \mathrm{H}_1 + \dfrac{100\left[(h-h_1)/e_1\right]}{(h-h_1)/e_1 + (h_2-h)/e_2} \end{cases}$ (eq. 3.84)

    – Lightness: $J = 100(A/A_w)^{c\cdot z}$ (eq. 3.85)

    – Brightness : $Q = (1.24/c)(J/100)^{0.67}(A_w + 3)^{0.9}$ (eq. 3.86)

    – Saturation: $\mathrm{s} = [50(\mathrm{a}^2/\mathrm{b}^2)^{1/2} 100\mathrm{e}(10/13)\mathrm{N_c N_{cb}}]/[\mathrm{R'_a} + \mathrm{G'_a} + (21/20)\mathrm{B'_a}]$

    (eq. 3.87)

[5] If I<0 $I_a' = -40\left(-F_L I'/100\right)^{0.73} / \left[\left(-F_L I'/100\right)^{0.73} + 2\right] + 1 \qquad \mathrm{I} \in \{\mathrm{R,G,B}\}$

– Chroma: $C = 2.44 s^{0.69} (J/100)^{0.67n} (1.64 - 0.29^{n})$ (eq. 3.88)

– Colourfulness $M = C \cdot F_L^{0.15}$ (eq. 3.89)

Where c and N_c are tabulated values that characterise the background and H_i is defined as in Hunt's model (table 3.1).

- Calculation of auxiliary values:

$$Y_{bc} = (0.43231 R_{bc} + 0.51836 G_{bc} + 0.04929 B_{bc}) Y_b \quad \text{(eq. 3.90)}$$

$$Y_{wc} = (0.43231 R_{wc} + 0.51836 G_{wc} + 0.04929 B_{wc}) Y_w \quad \text{(eq. 3.91)}$$

$$N_{bb} = N_{cb} = 0.725 (1/n)^{0.2} \quad \text{(eq. 3.92)}$$

$$z = 1 + F_{LL} n^{1/2} \quad \text{(eq. 3.93)}$$

$$n = Y_{bc} / Y_{wc} \quad \text{(eq. 3.94)}$$

$$a = R_a^{'} - 12 G_a^{'} / 11 + B_a^{'} / 11 \quad \text{(eq. 3.95)}$$

$$b = (1/9)(R_a^{'} + G_a^{'} - 2 B_a^{'}) \quad \text{(eq. 3.96)}$$

The eccentricity value is defined as in Hunt model. See Table 3.1.

$$A = [2R_a^{'} + G_a^{'} + (1/20) B_a^{'} - 2.05] N_{bb} \quad \text{(eq. 3.97)}$$

$$A_w = [2R_{aw}^{'} + G_{aw}^{'} + (1/20) B_{aw}^{'} - 2.05] N_{bb} \quad \text{(eq. 3.98)}$$

Where $\{X_b, Y_b, Z_b\}$ are the background values and F_{LL} is a tabulated value that characterises the background.

The model diagram is shown below:

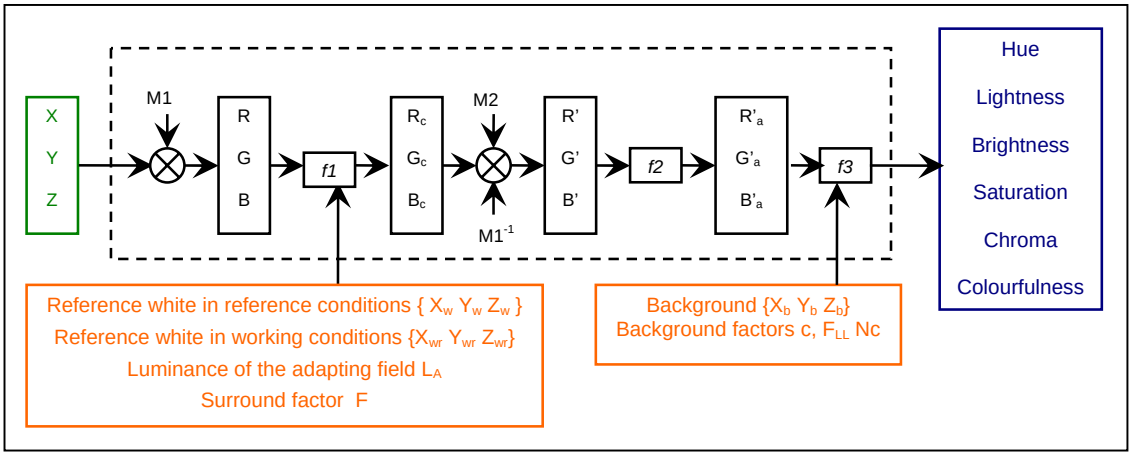

Figure 3.40 CIECAM97 model diagram. Where M1 and M2 are the matrices that represent linear transforms while *f1*, *f2* y *f3* are the non-linear transforms (green inputs, blue outputs, system parameters in orange).

This space combines the most relevant colour appearance models up to their publication date and has allowed the future works to focus in a common model for research in colour appearance models. It is a relatively simple model that allows to predict adaptation effects, the influence of the surround or the effects related to the luminance level.

CHICHILNISKY-WANDELL

In 1999, Chichilnisky and Wandell proposed a hue classification model known as IDO: increment–decrement opponency. The model aims to establish the predominant colour in a series of colour samples visualised in a CRT monitor of 2.5º versus different backgrounds. The classification is based on the results obtained when analysing the samples as red or green and blue or yellow. The model works with differences between the stimulus and background ΔL, ΔM and ΔS (based on the perception curves of cone fundamentals of Stockman, MacLeod & Johnson (1993)). They found asymmetric, non-flat surfaces when representing the boundaries in red vs. green and yellow vs. blue. They proposed a model in which the positive variations regarding the neutral point (e.g. L(+) and negative variations (e.g. L(-)) have different gain factors that depend on the background when modelled. In the case of L it would be as follows:

- The value is established regarding a neutral point:

$$\begin{pmatrix} \dot{L} \\ \dot{M} \\ \dot{S} \end{pmatrix} = \begin{pmatrix} L \\ M \\ S \end{pmatrix} - \begin{pmatrix} \overline{L} \\ \overline{M} \\ \overline{S} \end{pmatrix} \qquad \text{(eq. 3.99)}$$

Where $\{\overline{L}\,\overline{M}\,\overline{S}\}$ characterise the neutral point.

- The signal is split into two components:

$$I^* = \begin{cases} g_I^{(+)}\,\dot{I} & \dot{I} > 0 \\ g_I^{(-)}\,\dot{I} & \dot{I} \le 0 \end{cases} \qquad \forall I \in \{L, M, S\} \qquad \text{(eq. 3.100)}$$

Being $g_I^{(+)}$ and $g_I^{(-)}$ the gain factors that depend on the background.

After this, the values {L*, M*, S*) are combined in order to create the opponency pathways {RG, BY, WB}. This adjustment is based on experimental values. The following figure shows the model diagram.

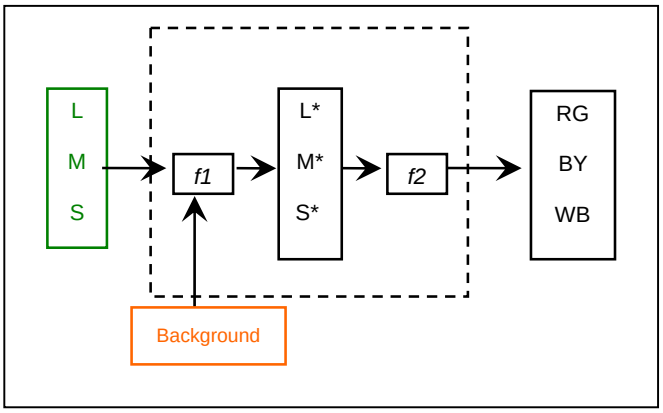

Figure 3.41. Chichilnisky - Wandell model diagram. Where *f1* and *f2* are the non-linear transforms (green inputs, blue outputs and orange system parameters).

One must mention that this model introduces an asymmetric non-linearity in the computation of the {L, M, S} values that is not taken into account by most systems. On the other hand, one must highlight that this is a system for small stimuli and uniform backgrounds.

CIECAM02

The CIECAM02 model was published in 2002 as a revision of the CIECAM97. Multiple colour databases and colour order systems data bases were used in order to select and adjust the functions and parameters. The following are the different stages of the model [MORO_02]:

- Chromatic adaptation transform:
  - Transformation to an intermediate RGB space where the effect of the chromatic adaptation is calculated. This model has selected the CMCCAT2000 transform based on its performance although there was a minimal difference with other options.

$$\begin{vmatrix} R \\ G \\ B \end{vmatrix} = M_{CAT02} \bullet \begin{vmatrix} X \\ Y \\ Z \end{vmatrix} \qquad \text{(eq. 3.101)}$$

$$M_{CAT02} = \begin{vmatrix} 0.7328 & 0.4296 & -0.1624 \\ -0.7036 & 1.6975 & 0.0061 \\ 0.003 & 0.0136 & 0.9834 \end{vmatrix}$$

  - Calculation of the chromatic adaptation effect:

$$D = F\left[1 - \left(\frac{1}{3.6}\right)e^{\left(\frac{-L_A-42}{92}\right)}\right] \qquad \text{(eq. 3.102)}$$

$$I_C = \left[\left(\frac{Y_w D}{I_w}\right) + (1-D)\right] I \qquad I \in \{R, G, B\} \qquad \text{(eq. 3.103)}$$

Where the values $\{R_w\ G_w\ B_w\}$ correspond to the white point and F is a tabulated background value.

  - Transformation to the cone response space using the Hunt-Pointer-Estevez transformation:

$$\begin{vmatrix} R' \\ G' \\ B' \end{vmatrix} = M_H \bullet M_{CAT02}^{-1} \bullet \begin{vmatrix} R_c \\ G_c \\ B_c \end{vmatrix} \qquad \text{(e. 3.104)}$$

$$M_H = \begin{vmatrix} 0.38971 & 0.68898 & -0.07868 \\ -0.22981 & 1.1834 & 0.04641 \\ 0.0 & 0.0 & 1.0 \end{vmatrix}$$

- Dynamic response function: signal compression.

$$I_a^{'} = \frac{400\left(F_L I'/100\right)^{0.42}}{27.13+\left(F_L I'/100\right)^{0.42}} + 0.1 \qquad I \in \{R,G,B\} \qquad \text{(eq. 3.105)}$$

Where F_L is calculated as in CIECAM97.

$$F_L = 0.2k^4 5L_A + 0.1\left(1-k^4\right)^2\left(5L_A\right)^{1/3}$$
$$k = 1/(5L_A+1) \qquad \text{(eq 3.106)}$$

Where L_A (cd/m) is the luminance of the adapting field.

- Colour space:
  - Colour attribute calculation:
    - Hue: $\begin{cases} h = \arctan(b/a) \\ H = H_i + \dfrac{100(h-h_1)/e_1}{(h-h_1)/e_1+(h_2-h)/e_2} \end{cases}$ (eq. 3.107)
    - Lightness: $J = 100(A/A_w)^{c\cdot z}$ (eq. 3.108)
    - Brightness: $Q = (4/c)(J/100)^{1/2}(A_w+4)F_L^{1/4}$ (eq. 3.109)
    - Saturation: $s = 100\sqrt{M/Q}$ (eq. 3.110)
    - Chroma: $C = t^{0.9}\,(J/100)^{1/2}\,(1.64-0.29^n)^{0.73}$ (eq. 3.111)
    - Colourfulness: $M = C \cdot F_L^{1/4}$ (eq. 3.112)

Where c is a tabulated value that depends on the background.

With these values, the point coordinates can be calculated:

$$a_X = X\cos(h)$$
$$b_X = X\sin(h) \qquad X \in \{C,M,S\} \qquad \text{(eq. 3.113)}$$

- Calculation of auxiliary values:

$$a = R_a^{'} - 12G_a^{'}/11 + B_a^{'}/11 \qquad \text{(eq. 3.114)}$$

$$b = (1/9)(R_a^{'} + G_a^{'} - 2B_a^{'}) \qquad \text{(eq. 3.115)}$$

$$e = \left(\frac{12500}{13} N_c N_{cb}\right)\left[\cos\left(h\frac{\pi}{180} + 2\right) + 3.8\right] \qquad \text{(eq. 3.116)}$$

$$t = \frac{e(a^2 + b^2)^{1/2}}{(R_a^{'} + G_a^{'} + (21/20)B_a^{'})} \qquad \text{(eq. 3.117)}$$

$$N_{bb} = N_{cb} = 0.725(1/n)^{0.2} \qquad \text{(eq. 3.118)}$$

$$z = 1.48 + n^{1/2} \qquad \text{(eq. 3.119)}$$

$$n = Y_b / Y_w \qquad \text{(eq. 3.120)}$$

$$A = \left[2R_a^{'} + G_a^{'} + (1/20)B_a^{'} - 0.305\right]N_{bb} \qquad \text{(eq. 3.121)}$$

Where N_c, N_{bb} and N_{cb} are calculated as in the CIECAM 97 model.

The following is a diagram of this model:

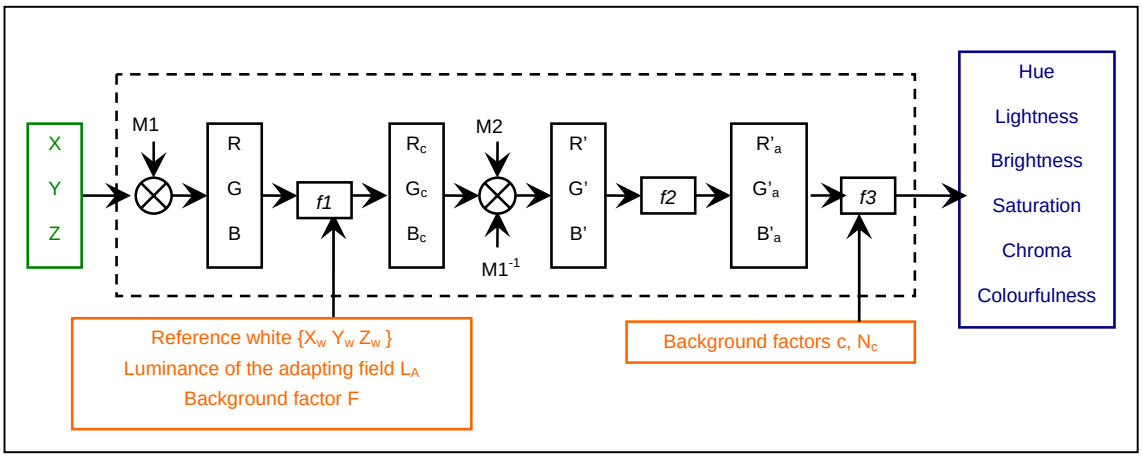

Figure 3.42. Diagram of the CIECAM02 model. Where M1 and M2 are the matrices that represent linear transforms while *f1*, *f2* and *f3* are the non-linear transforms (green inputs, blue outputs, system parameters in orange).

The principal revisions applied to CIECAM02 have been: a new chromatic adaptation, a new compression function and changes in the calculation of colour attributes. The aim of this revision has been to improve the CIECAM97 results, to reduce its complexity, improve its invertibility as well as introduce new elements identified in the human visual system.

5 Colour difference measurements

> *"We must be very careful to transfer, from this point space which we are very much accustomed to regard not only as merely affine, but also as metric, namely Euclidean space, only the affine relations to colour space, not the metric relations, which here are completely unimportant because colour space has its own metric".*
>
> Erwin Schrödinger 1920

The measurement of the difference between two colours has evolved alongside colour models. This section sets forth a summary of the main proposals for the measurement of distances.

If one takes into account a Euclidean three-dimensional space U^3, one can establish a metric that defines the distance between two points as:

$$(\Delta S)^2 = (\Delta U_1)^2 + (\Delta U_2)^2 + (\Delta U_3)^2 \qquad \text{(eq. 3.122)}$$

In a three-dimensional Riemann space, one has:

$$(\Delta S)^2 = k_{11}(\Delta U_1)^2 + k_{22}(\Delta U_2)^2 + k_{33}(\Delta U_3)^2 + k_{12}\Delta U_1 \Delta U_2 + k_{13}\Delta U_1 \Delta U_3 + k_{23}\Delta U_2 \Delta U_3 \qquad \text{(eq. 3.123)}$$

where k_{ij} make that ΔS always positive.

Another different way to define distance, associated to Schrödinger (1920b), consists in defining the distance between two points as the distance which minimises only the number of noticeable steps. This creates a geodesic line between two points. In a Euclidean space, this matches with the straight line but in the Riemann space they are generally curved lines.

Therefore, there are multiple ways of establishing the difference between two colours. When the reference tristimulus were established by the CIE, work began on the transformation of these values in order to measure colour differences and therefore obtain a colour space derived from them.

In 1942, MacAdam presented a set of detectable colour difference measurements, know as the MacAdam ellipses, that reflect the heterogeneity of conventional colour models. In 1946, Stiles propounded the following formula for the measurement of differences based on experiments of the threshold of two colours [STIL_46]:

$$\left(ds^2\right)=\left[\frac{\zeta(R)}{\rho}dR\right]^2+\left[\frac{\zeta(G)}{\gamma}dG\right]^2+\left[\frac{\zeta(B)}{\beta}dB\right]^2 \qquad \text{(eq. 3.124)}$$

With $\zeta(I)=\frac{9}{9+I}\quad I\in\{R,G,B\}$; $\frac{1}{\rho^2}=0.612$; $\frac{1}{\gamma^2}=0.369$; $\frac{1}{\beta^2}=0.0185$

The following figure can be used to compare the results obtained by MacAdam and Stiles:

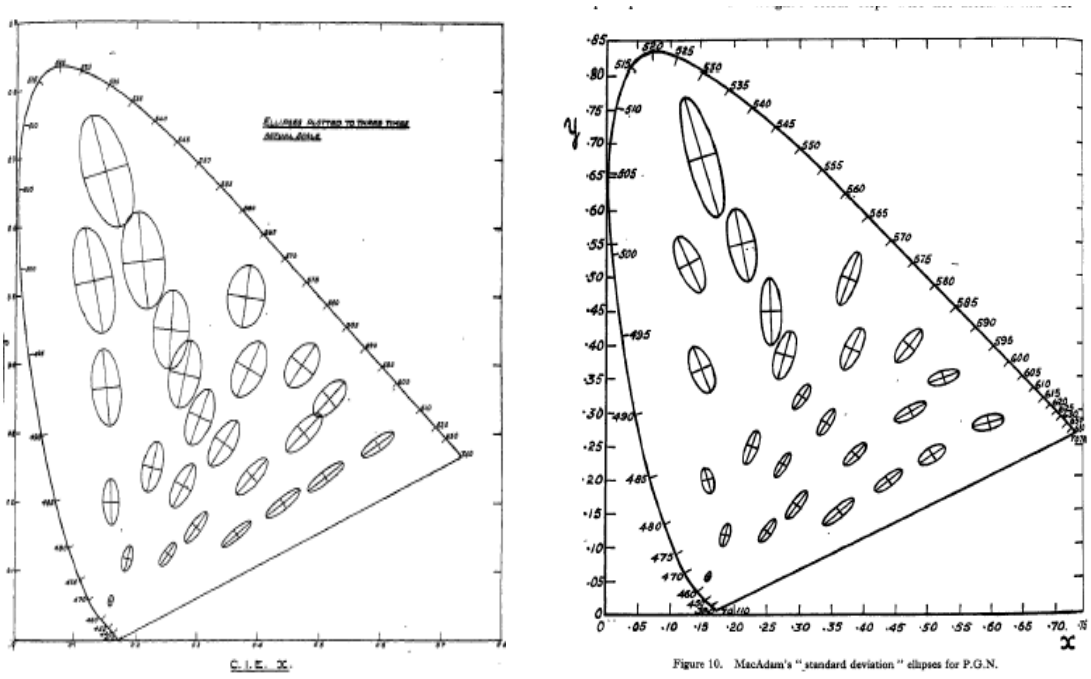

Figure 3.43. Comparison between the values of the MacAdam ellipses and those calculated with equation 3.124. Source: [STIL_46]

After which, MacAdam proposed a non-linear measurement of local differences [MACA_63]:

$$ds=\left[(g_{11}dx)^2+2g_{12}dxdy+(g_{22}dy)^2\right]^{p/2} \qquad \text{(eq. 3.125)}$$

He concluded, based on these results, that a linear transformation of the XYZ space would not give rise to a noticeably uniform space.

The CIE, due to the great variety of difference measurement systems, selected two models as reference: CIELAB and CIELUV (see Section 4.2 of this Chapter).

There has been a continuous flow of new formulas to measure the difference between two colours, however, due to the variety of existing formulas, only the main proposals by CIE will be mentioned:

- CIE94: based on CIELAB values:

$$\Delta E^*_{94} = \left[\left(\frac{\Delta L^*}{k_L S_L} \right)^2 + \left(\frac{\Delta C^*}{k_C S_C} \right)^2 + \left(\frac{\Delta H^*}{k_H S_H} \right)^2 \right]^{1/2} \quad \text{(eq. 3.126)}$$

  Where:

$$C^* = \sqrt{a^{*2} + b^{*2}}$$

$$H^* = \arctan\left(\frac{b^*}{a^*} \right)$$

  $S_L = 1$; $S_C = 1 + 0.045C^*$; $S_H = 1 + 0.015C^*$

  $\{k_L, k_C, k_H\}$ allow to adapt the measurement to the sample size, texture, separation… The following requirements must be met in order to use this measurement: use of a D65 illuminant, 1000lux and an achromatic background with L*=50.

- CIEDE2000: was introduced to measure small or medium differences. It works with CIELAB space values and was adjusted using the BFD-P, Leeds, RIT-DuPont and Witt databases (other databases have also been used for the adjustment of some of the parameters). The following is the formula they obtained [LUO_01]:

$$\Delta E_{00} = \sqrt{\left(\frac{\Delta L'}{k_L S_L} \right)^2 + \left(\frac{\Delta C'}{k_C S_C} \right)^2 + \left(\frac{\Delta H'}{k_H S_H} \right)^2 + R_T \left(\frac{\Delta C'}{k_C S_C} \right) \left(\frac{\Delta H'}{k_H S_H} \right)} \quad \text{(eq. 3.127)}$$

  - Where the CIELAB values are transformed as follows:

$$\begin{aligned} L' &= L^* \\ a' &= (1+G)a^* \\ b' &= b^* \\ C' &= \sqrt{a'^2 + b'^2} \end{aligned} \quad \text{(eq. 3.128)}$$

$$h' = \arctan\left(\frac{b'}{a'}\right)$$

$$\Delta H' = 2\sqrt{C'_a\, C'_b}\,\sin\frac{\Delta h'}{2}$$

Where G is established in order to correct the mistakes in areas near the neutral point.

$$G = 0.5 \bullet \left(1 - \sqrt{\frac{\overline{C}^{*7}_{ab}}{\overline{C}^{*7}_{ab} + 25^7}}\right)$$

Being $\overline{C}^{*}_{ab}$ the arithmetic mean of the samples to compare: a and b.

- The R_T factor is added as it allows to improve the behaviour of the blue area.

$$R_T = -\sin(2\Delta\theta)R_C \qquad \text{(eq. 3.129)}$$

Where

$$\Delta\theta = 30\exp\left\{-\left[\left(\overline{h}_{ab}' - 275^{\circ}\right)/25\right]^2\right\} \qquad \text{(eq. 3.130)}$$

$$R_C = 2\sqrt{\frac{\overline{C}'^{7}_{ab}}{\overline{C}'^{7}_{ab} + 25^7}} \qquad \text{(eq. 3.131)}$$

- The weights of each colour attribute are:

$$S_L = 1 + \frac{0.015(\overline{L}_{ab}' - 50)^2}{\sqrt{20 + (\overline{L}_{ab}' - 50)^2}}$$

$$S_C = 1 + 0.045\overline{C}_{ab}' \qquad \text{(eq. 3.132)}$$

$$S_H = 1 + 0.015\overline{C}_{ab}'\left[\begin{array}{l} 1 - 0.17\cos(\overline{h}_{ab}' - 30^{\circ}) + 0.24\cos(2\overline{h}_{ab}') + \\ 0.32\cos(3\overline{h}_{ab}' + 6^{\circ}) - 0.2\cos(4\overline{h}_{ab}' - 63^{\circ}) \end{array}\right]$$

- The parametric factors are generally deemed k_H=1 y k_C y k_L near to 1 although the performance of the systems can be improved by introducing some adjustments.

CIEDE2000 substantially improves the results obtained by CIE94 and CMC (formula developed by the Society of the Dyers and Colourists (SDC) Colour Measurement

Committee (CMC) based on a broad comparative data base and that is ISO standard on textile applications since 1995).

One must note that the majority of the proposed formulas do not include the effect of the context in colour perception and furthermore, they are designed to measure differences in the perception of large isolated patches of 4º. Although they are usually used to measure differences in colour images [JOHN_03].

Lastly, it is interesting to note that several estimates have been made on the number of colours that we are able to distinguish [KUEH_03]:

- Only taking into account the hue L. A. Jones estimated 128 variations, König-Dieterici 235 and MacAdam 250.
- When including all colour attributes: Titchener estimated that there are 33,000 colours, Indow 7 million and Judd 10 million.

In each case, the differentiation criteria, the degree of certainty... can provide part of the explanation for the disparity.

6 Conclusions

This chapter has set forth the basic concepts of colour theory and some of the colour effects that help explain colour behaviour. The development of a colour model is not as intuitive a process as might seem. The nature of colour and the way to describe it have evolved throughout history. At this time, colour is deemed a perception and not a inherent physical characteristic of objects.

The most relevant colour models have been analysed with special interest placed on colour appearance models. From these, a general working structure has been obtained that shall be used in the development of the colour processing model that is the aim of this thesis:

- Transformation of the chromatic adaptation using XYZ values.
- Dynamic response function.

- Combination of signals in an achromatic and several chromatic pathways.
- Calculation of colour attributes.

This study has also identified the colour attributes that this model must calculate: hue, lightness, brightness, chroma, saturation and colourfulness.

Although at present there is not a universal colour model available, there are approaches and models available for specific problems. The great variety of contexts in which colour perception can be evaluated leads to the fact that there is not a best model for all situations. There are models whose flexibility adapts them to a great number of scenarios while others obtain very good results in specific areas. The following are some of the most relevant issues detected in these varied proposals:

- From a descriptive perspective, Munsell's colour system is especially interesting as it is a system organised according to colour perception. Because of this characteristic, it is one of the most used systems for evaluating new colour model proposals.
- CIELAB and CIELUV systems are widely used in industrial applications due to their simplicity and small number of parameters employed.
- From among colour appearance models, the Hunt model is the most complete.
- CIECAM97 and CIECAM02 are two of the most widely used colour appearance models as they entail a common working proposal for researches in the field.
- Bioinspired models lack systematic generated result evaluations and as a whole remain as theoretical proposals.
- Distance measurements must be configured for each specific application context.

Finally, it is interesting to be able to compare the attributes and effects that are predicted by some of the models.

	CIELAB	LLAB	RLAB	Nayatani	Hunt	CIECAM
Lightness	√	√	√	√	√	√
Brightness				√	√	√
Chroma	√	√	√	√	√	√
Saturation		√	√	√	√	√
Colourfulness		√		√	√	√
Hue angle	√	√	√	√	√	√
Hue		√	√	√	√	√
Helson-Judd effect				√	√	
Stevens effect				√	√	√
Hunt effect		√		√	√	√
Helmholtz-Kohlrausch effect				√	√	
Bartleson-Breneman results		√	√		√	√
Discounting the illuminant		√	√		√	√
Incomplete adaptation			√		√	√
Colour difference	√	√	√			
Others				√	√	

Table 3.2. Model comparison. Source: [FAIR_97]

The development of the model for colour processing shall be looked at in the following chapters, based on the research undertaken in this chapter.

Chapter IV

The retina

"Attempts at devising the "retinal scheme" are as old as modern microscopy. Each such "scheme" reflects the ideas of a particular age. Most retinal schemes have been simply bridges to help us across the chasm of ignorance." S. Polyak 1949

The human visual system begins in the eyes. It is a highly specialised organ that allows us to perceive the reality around us. Each eye has a visual field of approximately 150º with an overlapping area of 120º.

The eye is made up of several different parts. The exterior area of the eye is made up of the cornea (transparent) and the sclera. The iris is behind the cornea and is a set of muscle fibres that is responsible for regulating the size of the pupil that is the opening where light enters the eye.

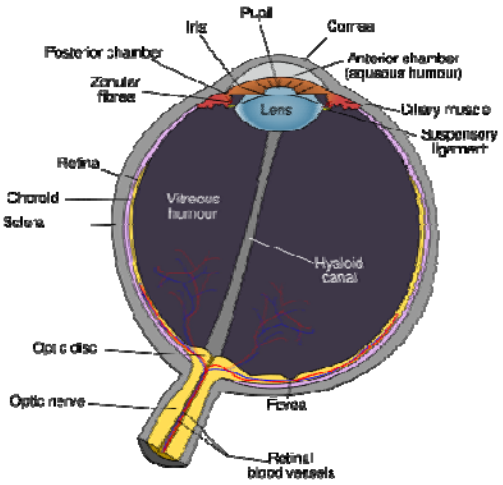

Figure 4.1. Schematic diagram of the human eye. Source: [ERIN]

Behind this is the lens which divides the eye into two chambers, one containing the aqueous humour and the other the vitreous humour that help maintain the spheroid shape of the eye. The cornea has an optical power of 42 dioptres and the crystalline lens of 20 dioptres which can be adjusted by means of the curvature of the lens, a process known as accommodation and which allows focusing nearby objects.

The contact with the sclera occurs in the choroid, a layer of blood vessels and connective tissue. Next is the retina, where one can identify the optic nerve, the macula and the fovea. The retina is composed of layers:

1. Photoreceptor layer: it is light sensitive.
2. Outer nuclear layer: contains the cell nuclei of photoreceptors.
3. Outer plexiform layer: made up of the axons and dendrites of bipolar and horizontal cells as well as the synaptic terminals of photoreceptors.
4. Inner nuclear layer: contains the cell nuclei of amacrine, bipolar and horizontal cells.
5. Inner plexiform layer: is made up of axons and dendrites from amacrine, bipolar and ganglion cells.
6. Ganglion cell layer: contains the cell nuclei of ganglion cells.

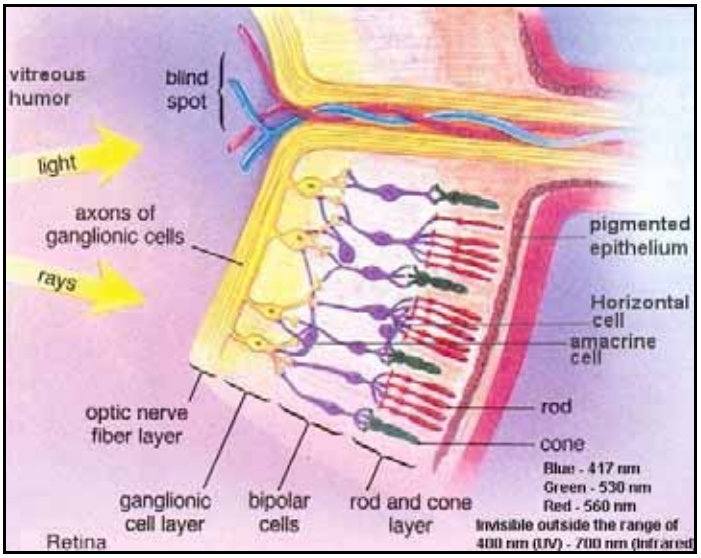

Figure 4.2 Cross-sectional view of the retina that shows the different types of cells. Source: [http://universe-review.ca/R10-16-ANS.htm]

The information provided by 100 million photoreceptors is transmitted by 1 million ganglion cells through the optic nerve. The axons of ganglion cells from the retina join to form the optic nerve.

The range of variation in the light intensity that it is capable of acquiring is of 10^6:1 while the range of the output signal through the optic nerve is 100:1. The retina has specialised in detecting differences to reduce the volume of data to be transmitted through the optic nerve.

This chapter is going to look at the different types of cells that make up the retina, from photoreceptors to ganglion cells finishing in the optic nerve. The objective is to define the input signals of the colour model that is the aim of this thesis and the processing phases of these signals, including:

- The characteristics proper of each cell type and subtype: to define the processes that take place in each of them.
- The cell number and distribution: to scale the model.
- Existing connections: in order to define the connection pathways of the model.

1. Photoreceptors

Photoreceptors are the main light sensitive cells in the retina. The human retina is made up of about 100 million photoreceptors. The following shows the types, sensitivity, distribution and types of connections.

1.1 Types and sensitivity

There are two types of photoreceptors: cones and rods. Rods are saturated with 100 photoisomerizations/s[6] and therefore work in low light intensity while cones need 26,000 photoisomerizations/s and operate in high light intensities.

Human beings have three types of cones and one type of rod. The difference lies in the photopigment that is present in the exterior area of the cones. They are known as L, M and S and are classified according to the absorption wavelength of each: long, medium and short. Although oftentimes they are classified as R, G or B.

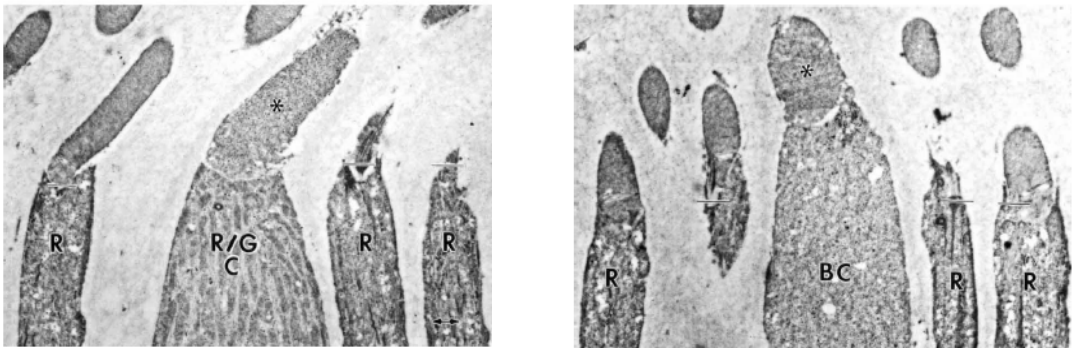

Figure 4.3 Example of cones and rods in the human retina. R/G C is an L or M cones, BC is a S cone and R are rods. Source: [CURC_91]

6 Process initiated by a photon, where the cis-retinal molecule is transformed to the trans- form.

Colour perception is possible because we have more than one type of cone. With only one type it is not possible due to the univariance principle: "*The signals from each cone depend only upon the rate at which it is effectively catching quanta; it does not depend upon the associated wave length.*" [NAKA_66] This entails that the component of light intensity can not be separated from the wavelength component.

However, the wavelength does influence the absorption probability of a photon. The following show the normalised graphs of human photoreceptors along the visible spectrum,

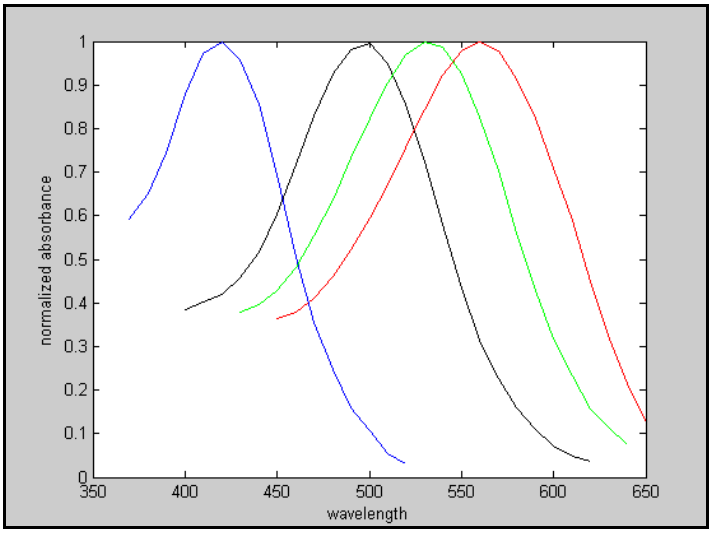

Figure 4.4. Sensitivity of cones and rods of the human being. Blue cones-S, green cones-M, red cones-L, black-rods. Data source: [DART_83].

1.2 Size and distribution

The size and distribution of cones and rods vary according to the retina position. On average, there are 4,6 million cones and 92 million rods [CURC_90a]. The fovea has great cone density and its central area lacks rods. This is the area of greater visual acuity and the area in which we try to focus images with greatest sharpness. The following figure shows the photoreceptor distribution in the fovea and the peripheral area.

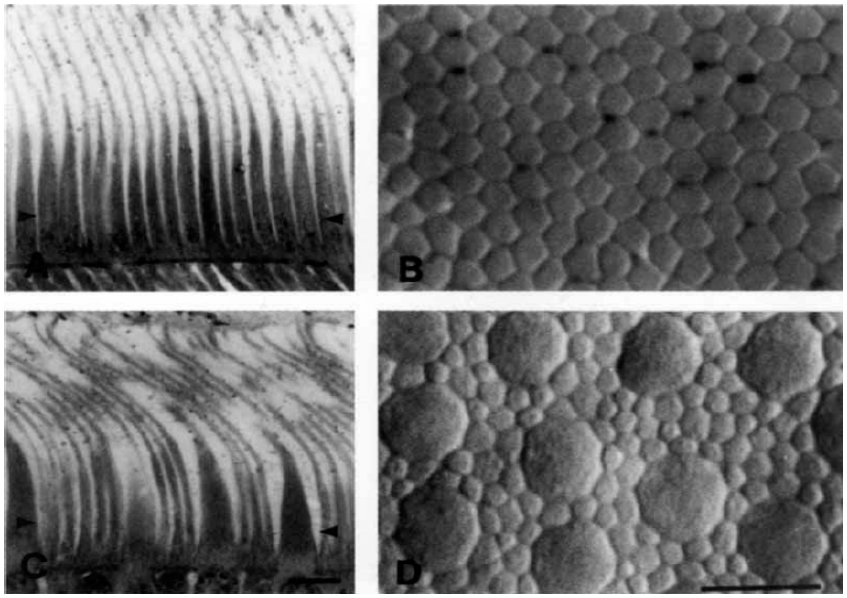

Figure 4.5. Examples of distribution and size of cones and rods. A and B fovea, C and D periphery. Image B only has cones while D has cones and rods (small sized). The arrows in A and C indicate the section where images B and D have been respectively taken. Scale = 10μm.

Source: [CURC_90a]

The distribution is also different in the nasal retina as apposed to the temporal and in the inferior as apposed to the superior. Curcio et al. (1990) have quantified these values in a study on human retinas:

- Maximum cone density: 199,200 cones/mm^2 (though there is great variation between people 100,000-324,000)
- Average cone density: 4,620 cones/mm^2
- Maximum rod density: 176,200 rods/mm^2
- Maximum density eccentricity in rods: 4.1mm
- Average rod density: 94,850 rods/mm^2
- Rod / cone ratio: 20.24.
- Area with no rods: diameter 0.5 mm and known as foveola.

The following images show the great cone concentration in the central zone (white area) which rapidly diminishes when moving away from the centre of the fovea, as well as the foveola that is rod-free (black triangle in image E), the insertion points of the optic nerve (black point in image A), the presence of more cones in the nasal retina (39%) (left side image) than in the temporal (right side image), an approximately equal number between the inferior and superior area, the rod

annulus (orange colour in image C) and the maximum number of rod concentration known as hot spot (red colour in image C).

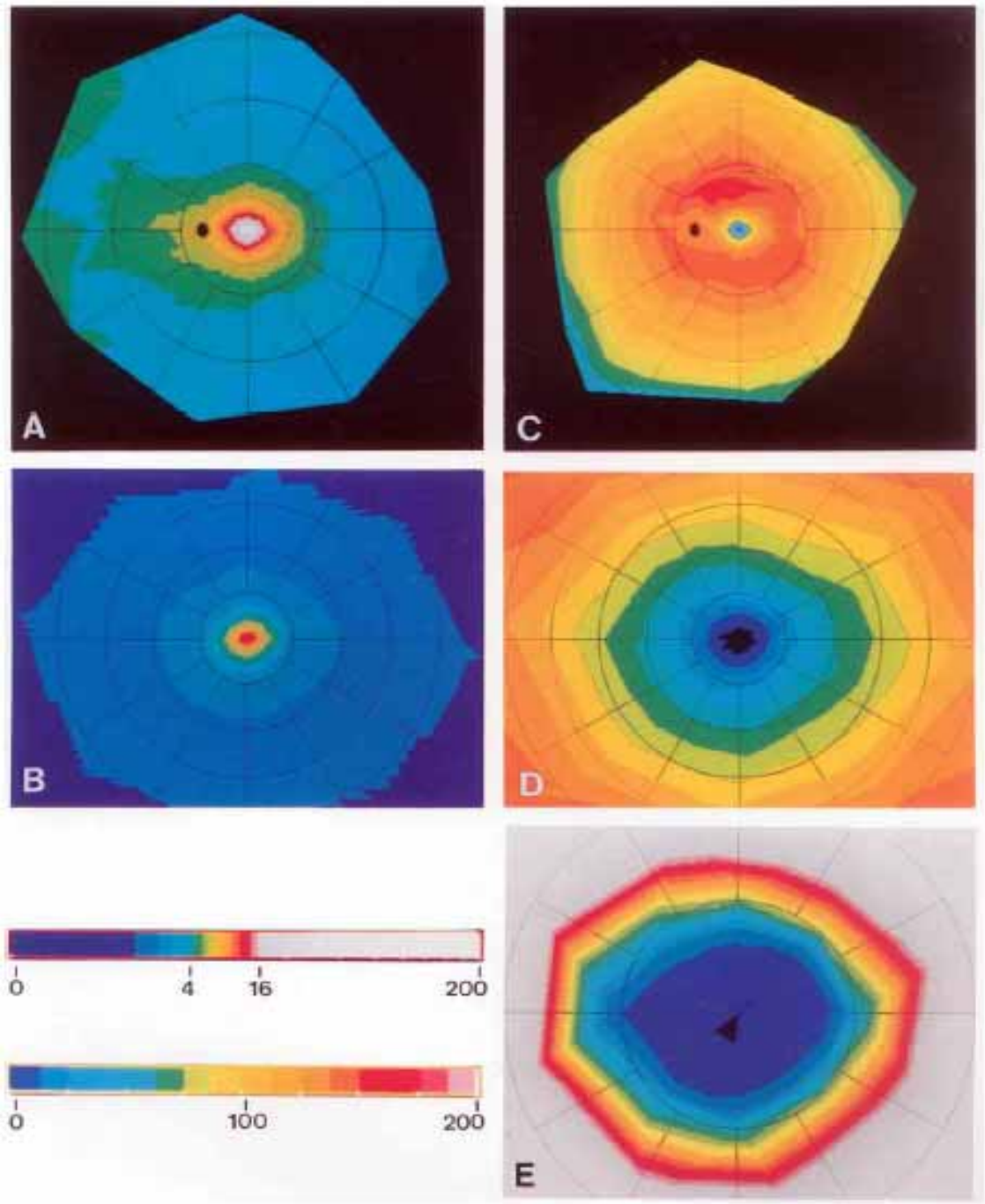

Figure 4.6 Average density values of photoreceptors in the retina A. Cones in the entire retina. B. Cones in the fovea. C. Rods in the entire retina. D. Rods in the central zone. E. Rod-free area (black triangle) 100-200μm from the centre of the fovea. Upper scale applicable to A and E, lower scale applicable to B, C and D. Source: [CURC_90a]

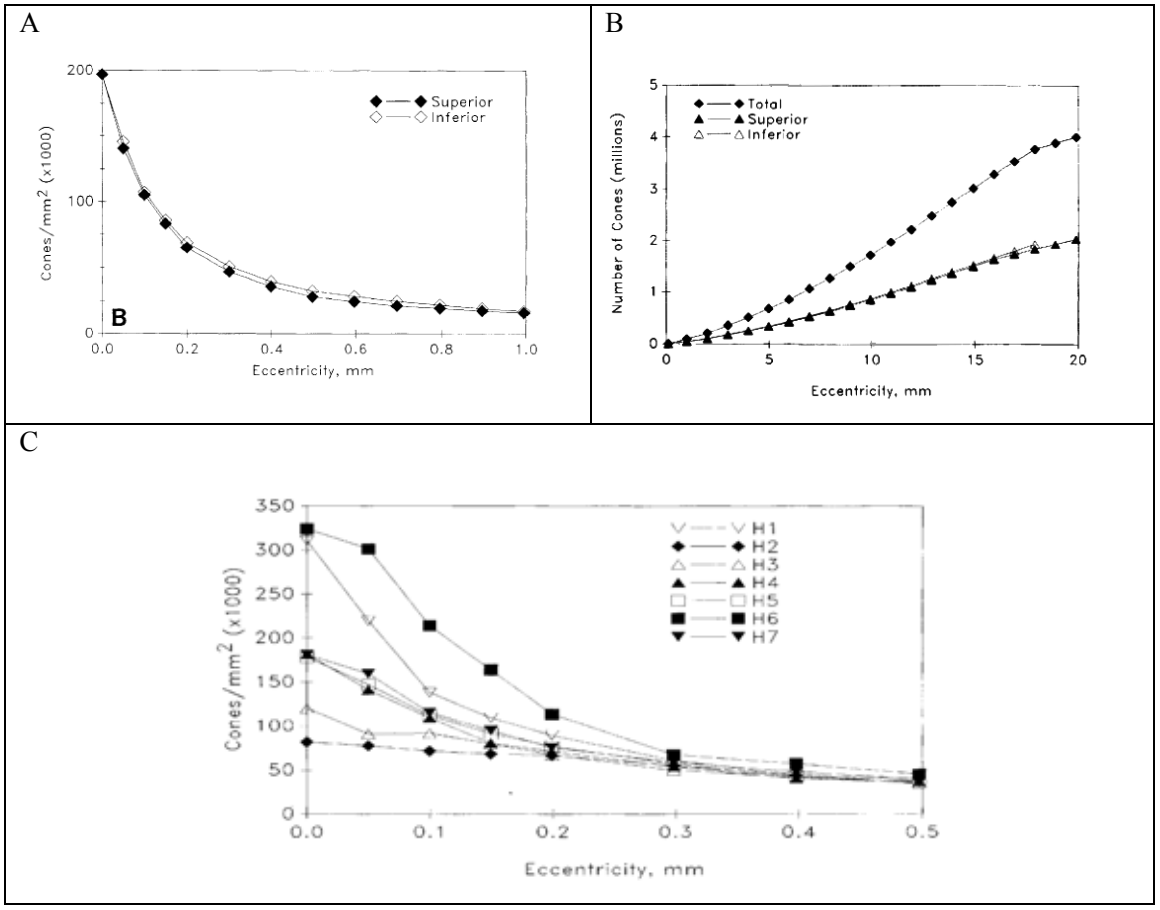

Figure 4.7. A. Cone density in the central zone of the retina: number in the superior and inferior half. B. Number of cones based on the eccentricity: total amount and number in the upper and lower half. C. Cone density per mm^2 based on the eccentricity for several people H1-H7. Source: [CURC_90a]

These measurements have allowed the estimate of the number of cones in the fovea (1.5mm diameter), which is 97,460. This means a circle diameter with 352 cones or a square with 313 cones per side. These measurements can be compared with the measurements of some camera formats: vga with 345,000 pixels or qvga with 76,800 pixels [POLY_41, CURC_90a].

One must bear in mind that this is not a uniform organisation, as the concentration decreases with the eccentricity. .

Once having the average number of cones, an analysis of the distribution must be made in accordance with its type: L, M or S. The following are distribution examples. These do not follow a homogeneous pattern and the L:M:S ratio also widely varies with each person. Furthermore, the

ratio varies with the retina position. The estimated average relation from L to M is 1.6 to 1, while the number of S cones is 7% of the total in the retina [CURC_91a].

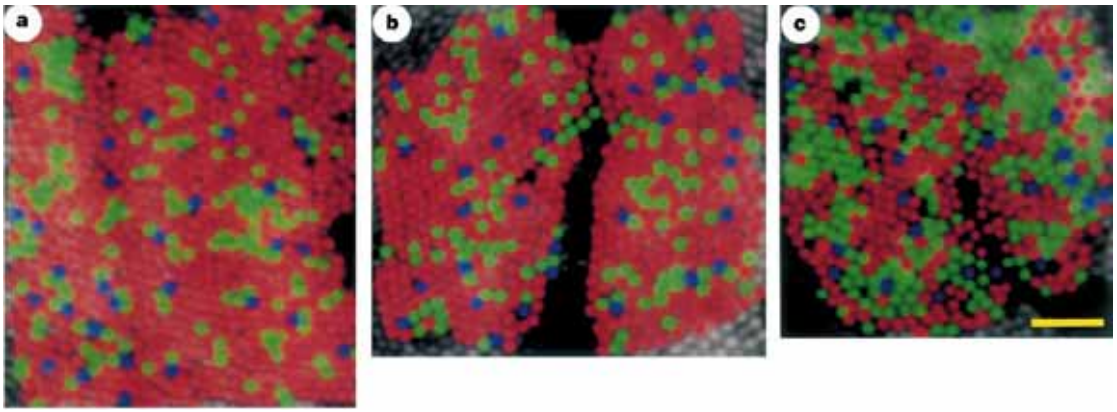

Figure 4.8 Example of cone distribution in the human retina, L (in red), M (in green) and S (in blue). A and B correspond to subject 1(L=75.8%, M=20.0%, S=4.2%) and C to subject 2 (L=50,6%, M= 44,2%, S=5,2%), all with a 1º of eccentricity. Scale = 5 minutes of degree. Source: [ROOR_99]

The following figure of Curcio et al. (1991) shows the S cone distribution. They are scarce in the central area of the fovea and the maximum density is annulus shaped with a density of over 2,000 cones/mm^2.

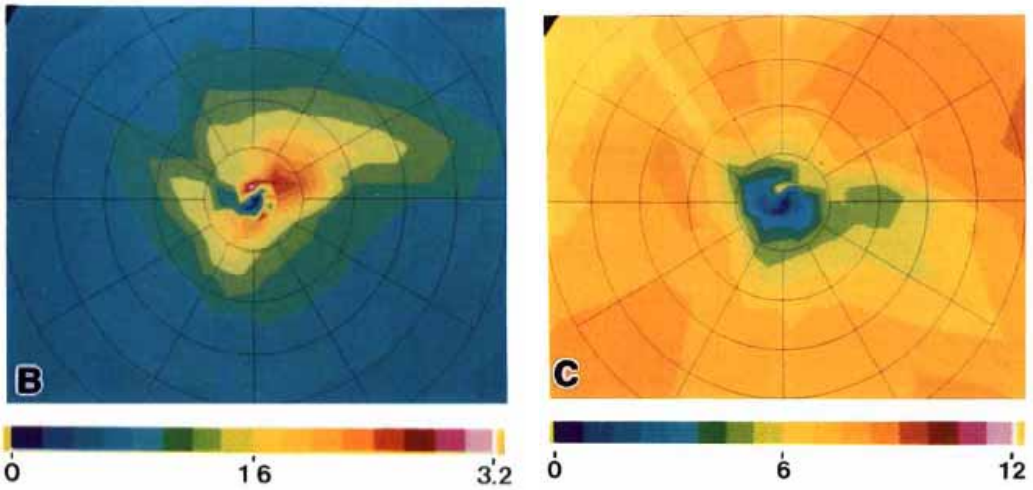

Figure 4.9 Left) S cone distribution, showing an absence in the central area of the fovea. Right) Ratio of S cones to the total number of cones. It increases as the eccentricity increases. Source: [CURC_91]

1.3 Connections

The synaptic ends of cones are known as cone pedicles. These are one of the most complex synapses of the central nervous system WÄSS_04]. Cones also have a pedicle with multiple invaginations with each having an associated synaptic ribbon. Two horizontal cells are connected in this invagination, one at each side, as well as one or more bipolar cells (this connection is known as an invaginating connection). This set is known as triad. Besides this one, there are other types of bipolar cell connections known as: semi-invaginated, basal or plane that is associated to a triad and a basal not associated to a triad. The number of synaptic ribbons per cone in the fovea has been estimated at 21,4±1,6, while in the periphery at 41,8 ± 3 [CHUN_96]. On the other hand, the total number of connections that can be established in a pedicle can reach 500 [WÄSS_04]. The following figure shows the structure of a cone pedicle.

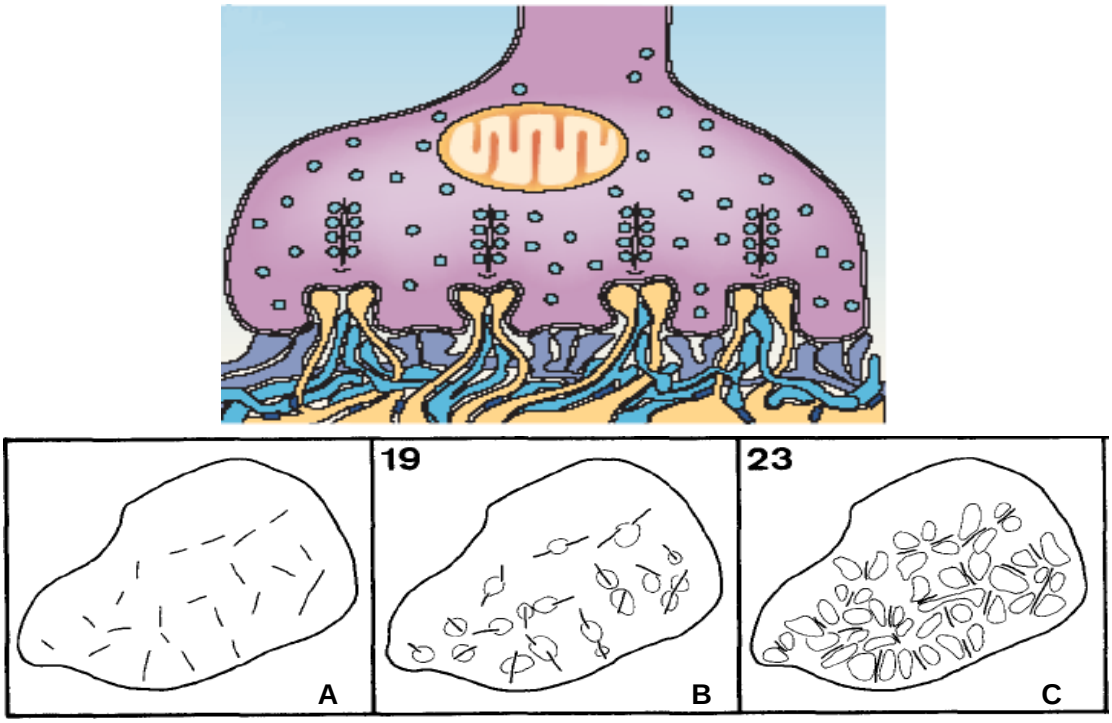

Figure 4.10. Above) Schematic drawing of the connections of a cone pedicle. One can observe the synaptic ribbons, the invaginations with two horizontal cells (beige) and invaginated bipolar types (blue) and bipolar with basal connections (purple). Below) Horizontal side view of the pedicle in the fovea which shows A) synaptic ribbons, B) bipolar cells over synaptic ribbons (total of 19) and C) paired horizontal cells with synaptic ribbons (total of 23 triads). Source: [WÄSS_04, CHUN_96]

Furthermore, L and M cones are connected to other apposed cones and to rods through gap junctions. In turn, S cones are barely connected to other types of photoreceptors by means of this type of synapses [WÄSS_04].

At the same time, rods have a spherule that contains a sole synaptic ribbon that has up to 7 connections to horizontal and bipolar cells [WÄSS_04]. Each rod is connected to between 2 and 5 bipolar cells and each bipolar makes a connection with between 30 and 50 rods [RODI_98]. The following shows the structure of a rod spherule.

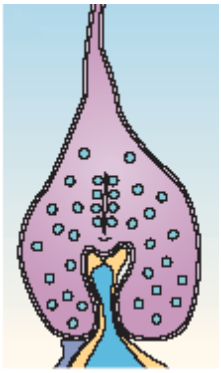

Figure 4.11. A rod spherule representation (colour code as in figure 4.10). Source: [WÄSS_04].

1.4 Conclusions

The human retina has three cone types (L, M and S) and one type of rod. Each of them permits to perceive the surroundings under different light conditions: cones for photopic levels and rods for scotopic levels (more sensitive than cones) [BEAR_06]. Signals from two or more types of cones are necessary in order to perceive colours, although a normal perception is that which uses signals from all 3 types of cones. From a chemical-electrical activation perspective, darkness can be considered as the stimulus that activates the photoreceptors.

There are about 92 million rods and about 5 million cones in a human retina (although this varies from person to person). The distribution of cones and rods throughout the retina is different. The area known as fovea concentrates the greatest cone densities. This is the zone of greatest visual acuity in the retina and is the limit of the resolution in the visual system (estimated between 47,5 and 86,3 cycles/º). The distribution also varies depending on the cone type. The L, M and S spatial pattern is deemed non-homogeneous and the average estimated ratios according to each type in L: M: S; 57.2: 35.8: 7.

The fovea has an average diameter of 1.5mm (5º) and according to measurements on human retinas; the total estimate can be placed at 97,460 cones (not evenly distributed). Based on these values, the average size that each cone has associated can be calculated to be 0,6 arc minutes. Other estimates propose an approximation of a cone through a Gaussian with σ_c=0.8´, value based on the average distance between cones as measured by Campbell & Gubish (1966) [LEBE_07]. Whereas [OYST_99] estimates a field of 0.5 minutes of degree.

2. Horizontal cells

Horizontal cells are the laterally interconnecting neurons in the outer plexiform layer.

2.1 Types

There are two types of horizontal cells: H1 and H2, although some propose a third type [KOLB_94]. Horizontal cells type H1 have large nuclei and thick dendrites that branch forming clusters that are composed of two arbours. A small dendritic arbour near the nucleus of the cell that connects with cones L and M and a second telodendritic arbour which is at a distance of over 1mm away and is connected with rods. Due to the distance between the two types of arbours, these can be deemed to be electrically isolated. Horizontal cells type H2 have a smaller nucleus than that of H1, have thin dendrites and are connected to S cones and some L and M cones. [RODI_98, DACE_96, AHNE_94]

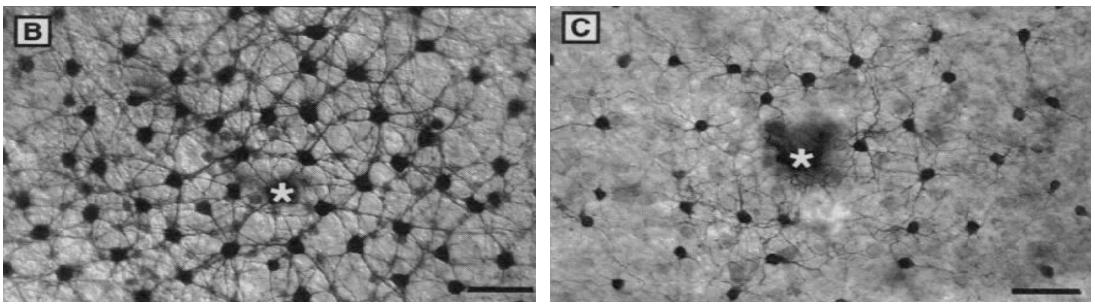

Figure 4.12 Images of H1 (left) and H2 (right) type cells which show how they are interconnected due to the transmission of the marker used. The asterisk shows the points where the electrophysiological measurements were performed. Sample of a macaque retina 11mm from the fovea. Scale: 50μm. Source: [DACE_96]

2.2 Connections and distribution

Horizontal cells are connected to photoreceptors in the invaginations present in the cone pedicles, laterally flanking the synaptic ribbons. The photoreceptor to horizontal cell connection retains its sign while the horizontal- photoreceptor reverses sign.

The human retina has about 500,000 horizontal cells according to some estimates [OYST_99]. The following show the number of horizontal cells based on its eccentricity.

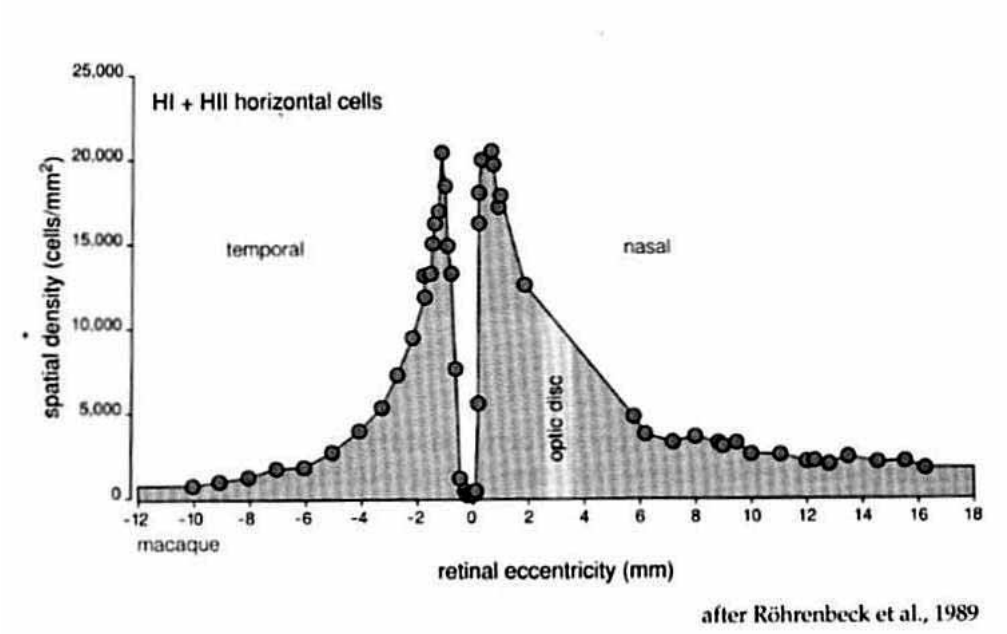

Figure 4.13. Number of macaque horizontal cells based on its eccentricity. Source: [RODI_98]

The H1:H2 distribution varies according to the eccentricity. The ratio near the fovea is 4:1 and 2:1 in the periphery. With these values and with the number of photoreceptors, the following can be estimated [WÄSS_00, AHNE_94b, RODI_98]:

- Each cone is connected with 3,7 H1 in the fovea and 7,5 in the periphery. Each cone establishes on average 6 to 8 connections with each H1 horizontal cell.
- Each cone is connected with about 2,2 H2 in the fovea and between 2,7 and 3,7 H2 in the periphery. Each L and M cone establishes an average of 1 to 5 connections with each H2 cell while the S cones establish between 3 and 9 connections.

The sizes of the dendritic fields vary with the eccentricity and type. The following graph shows the average H1 and H2 sizes.

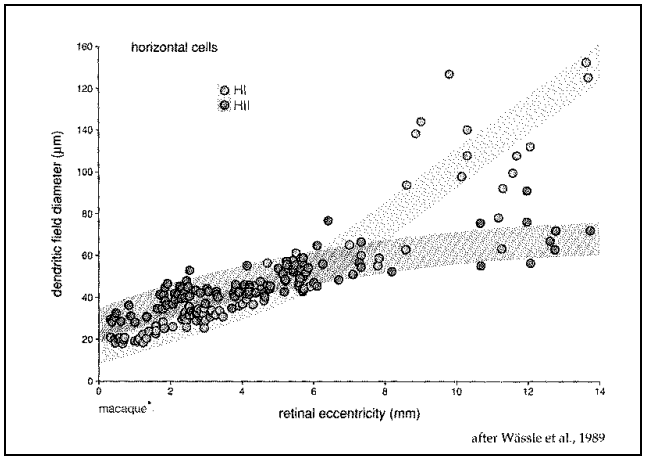

Figure 4.14. Size of the arbours of H1 and H2 cells depending on the eccentricity. Source: [RODI_98]

When studying the human retina, (Ahnelt and Kolb (1994)) measured to 11mm of eccentricity the following dendritic fields: H1 (60µm x40µm /80µm x60µm) and H2 (66µm x 46µm), slightly smaller than those reflected in the previous figure (macaque data).

On the other hand, the second arbour of the H1 cells spans an area of 700 rods, each of which are connected with two different H1[RODI_98].

H1 cells establish multiple connections with L and M cones, while H2 cells have disperse connections with L and M cones and dense with S cones, as can be seen in Figure 4.15. Furthermore, the number of connections decreases with the distance to the nucleus [DACE_96, AHNE_94]. Each type of horizontal cell is also interconnected through gap junctions. Additionally, receptive fields are deemed to vary due to the changes caused in the electrical connections due to chemical variations which could be related with the levels of luminous intensity [WEIL_00].

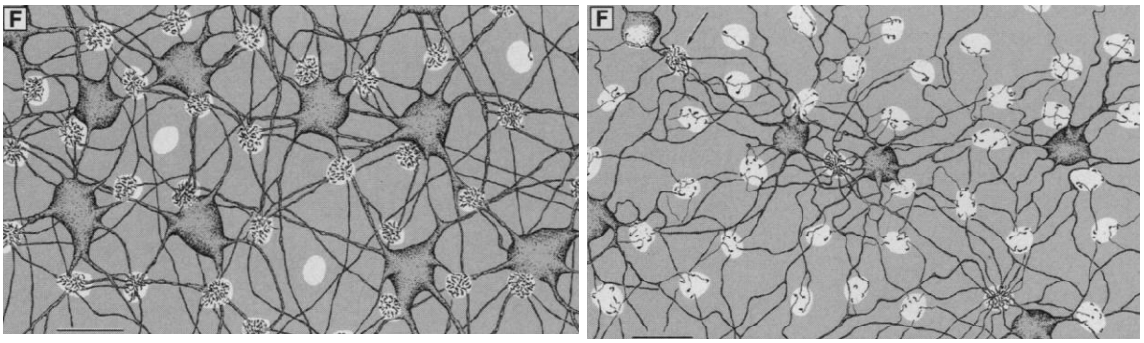

Figure 4.15. Example of H1 (left) and H2 (right) cells. Different connection density can be seen in the cone pedicles (lighter coloured circles). Source: [DACE_96]

2.3 Conclusions

The human retina has at least two types of horizontal cells. The first is known as H1 and has two separate connection zones. On one end, it is connected to L and M cone types, while on the other, it is connected to the rods. The second type, H2, establishes connections solely with cones, especially type S. Estimates account about 500,000 horizontal cells and H1:H2 ratio in the fovea is 4:1. The average size of the H1 in the fovea is of 20 µm, while the average size of the H2 is of 30 µm.

Horizontal cells hyperpolarise with the presence of light. Horizontal cells are considered to exert lateral inhibition on photoreceptors. There are several interpretations to explain these connections, although all have a basis in common: they don't seem to modulate the general level of intensity but rather the presence of borders [RODI_98], they increase the contrast between apposed zones [MASL_01] or adjust the system response to the quantity of light [MASL_01].

Behavioural models of horizontal cells, such as [PACK_02], have been created that employ 2 exponentials. One of the exponentials represents the effect of the direct connections of the horizontal cell with the cones and the second represents the effect of the connections with other horizontal cells.

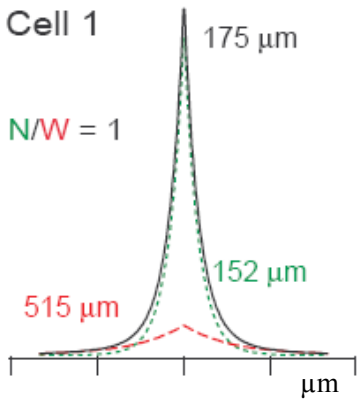

Figure 4.16. Behavioural model of a horizontal cell through the weighted sum that better suits the experimental measurements (black) of two exponential functions (red and green). Source: [PACK_02]

On the other hand, [HATE_07] presents a model of the cone horizontal chain that models spatial and temporal behaviours, through control chains with feedback effects.

3. Bipolar cells

Bipolar cells are retinal neurons that have their nucleus in the inner nuclear layer and establish postsynaptic connections with photoreceptors and presynaptic connections with amacrine and ganglion cells [BOYC_91a].

3.1 Types

Primate retinas have at least 10 types of bipolar cells that are different in both the type and number of photoreceptors with which they connect as well as the shape and level of the axon arbour. The receptive field can be divided into centre and surround, which have opposite effects. The following show the different types of bipolars [DOWL_87, BOYC_91a, WÄSS_04, BACC_07]:

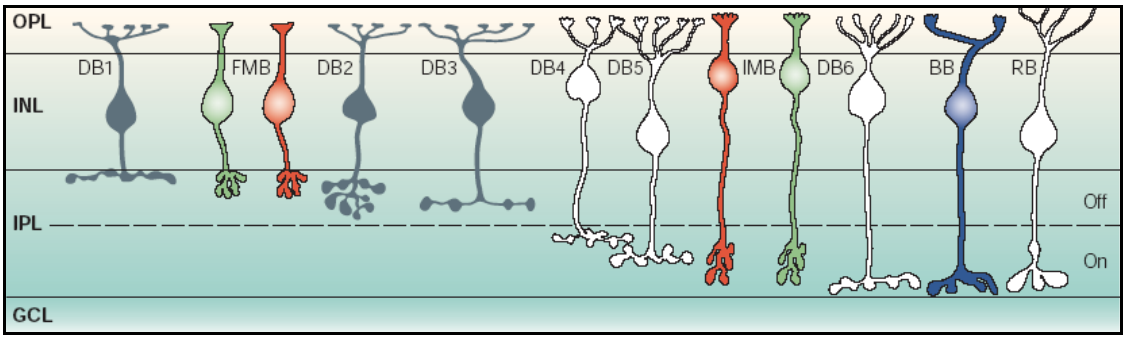

Figure 4.17. Bipolar cell types. Source: [WÄSS_04]

1. Midget bipolar: type of bipolar cell in the fovea that is characterised by its connection to one cone, having the possibility to connect with more than one in the periphery. They can be classified into:
    a. Invaginated or IMB: the axon terminals branch in the inner half of the internal plexiform layer: layer b (sublamina ON), are the central element in the triads.
    b. Flat or FMB: the axon terminals branch in the outer half: layer a (sublamina OFF). They establish basal contacts with cones.
2. S cone bipolars or BB: establish invaginated contacts with S type photoreceptors. The localisation of axon branches in layer b suggests that they are a bipolar cell of type ON.

Additionally, a second type of BB type OFF is considered to exist but still hasn't been verified.

3. Diffuse bipolar: are connected to cone sets. They are classified into 6 types based on the characteristics of the axon arbours.
    a. OFF type (branch in the a layer of the inner plexiform layer) [HOPK_95]:
        - DB1: have an extended axon and a set of fine dendrites.
        - DB2: have a stratified axon and its dendrites establish flat connections in the base of the cone pedicle.
        - DB3: the axon seems to form an irregular shape cord. They establish flat contacts in the pedicle base which are associated and not associated to triads.
    b. ON type (arborise in the b layer of the inner plexiform layer) [HOPK_95]:
        - DB4: the axon is usually star-shaped, the dendrites establish invaginated contacts with the cone pedicles.
        - DB5: establish invaginated contacts and the axons keep a close stratification.
        - DB6: have broad arbours both in the axon as well as in the dendrites.

    Figure 4.17 shows their morphology and stratification areas.
4. Rod bipolars or RB: are bipolar cells that are connected to rods. They are ON type cells.

An additional type has been established. It is known as giant bistratified bipolar cell and it establishes an extended basal union with cones, with an receptive field that is 3 times greater than diffuse bipolar cells [RODI_ 98, OYST_99].

Other sources indicate an additional classification based on whether they generate transient responses (transmit high frequency signals) and others that generate sustained signals (for low frequencies). One of the most common explanations is that its purpose is to optimise the bandwidth of the optic nerve. Masland (2001) suggests that in this manner two pathways that reach ganglion cells are created.

3.2 Connections and distribution

The signal that reaches bipolar cells comes from the photoreceptors and from the actions of horizontal cells. The following shows the connections established by the different types of bipolar cells:

1. Midget bipolar: 1 cone in the fovea, 1 or more in the periphery. Despite making connections with only one cone, they have multiple connections in the cone pedicle.
2. S cone bipolars: 1-3 type S cones [WÄSS_04].
3. Diffuse bipolar: connect in a non-selective manner with L and M cones and at times with S type [WÄSS_04, BOYC_91].
    a. Off type:
        - DB1: between 5 and 8 cones
        - DB2: between 5 and 8 cones
        - DB3: between 8 and 10 cones.
    b. On type:
        - DB4: between 7 and 8 cones.
        - DB5: between 5 and 7 cones.
        - DB6: 10 cones
4. Rod bipolars: connect with 6 rods in the fovea and with about 40 in the periphery [WÄSS_04].

The axon terminals of a bipolar cell establish its connections in the inner interplexiform layer, forming a dyad that has a synaptic ribbon which connects with two ganglion and/or amacrine cells [WÄSS_04]. The synaptic ribbons are smaller than those of photoreceptors and are perpendicularly oriented to the membrane over one of its projections [DOWL_87].

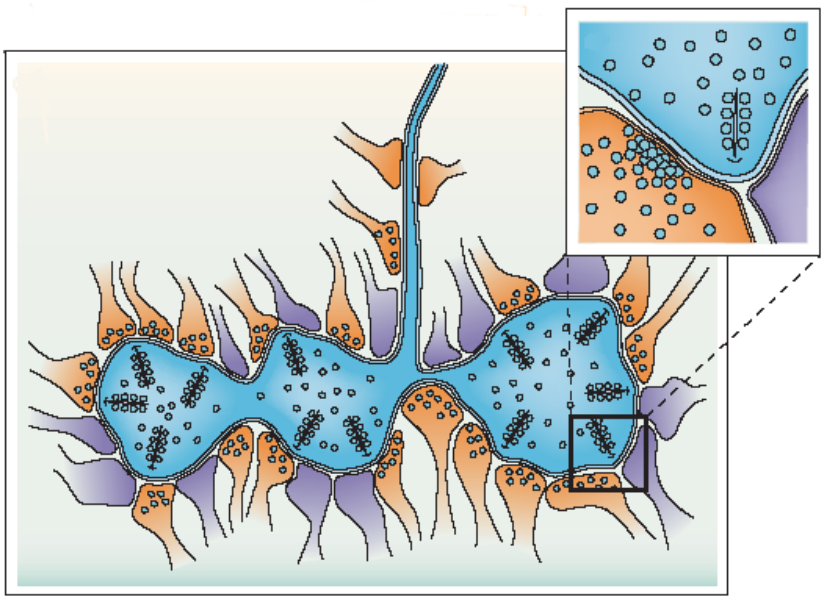

Figure 4.18 Bipolar cell contacts, ganglion cells in purple and amacrine cells in orange. Source: [WÄSS_04]

3.3Conclusions

On average, each photoreceptor is deemed to establish contact with 1 IMB, 1 FMB, 1.6 DBI, 3.6 DB2, 1.6 DB3, 2.8 DB4, 3.8 DB5 and 1.7 DB6, that join with horizontal cells that are connected to that cone [WÄSS_04, BOYC_91B]. Taking into account that a cone has between 20 and 50 synaptic ribbons, it can establish up to 500 connections. The number of cells are much smaller as it establishes multiple contacts with each of them. Taking into account this distribution of connections and cells, the signal captured by photoreceptors is multiplexed towards different information pathways [WÄSS_04, CHUN_96].

Proposals for the modelling of bipolar cells have been made either by means of electric circuits [ATTW_83] or by means of Gaussians [DACE_00]. As this second model (non-electric) is the one which shall be employed in this thesis, a more detailed description is provided. It proposes the use of two Gaussians, one that models the behaviour in the centre and a second which models the surround. The following figure shows both.

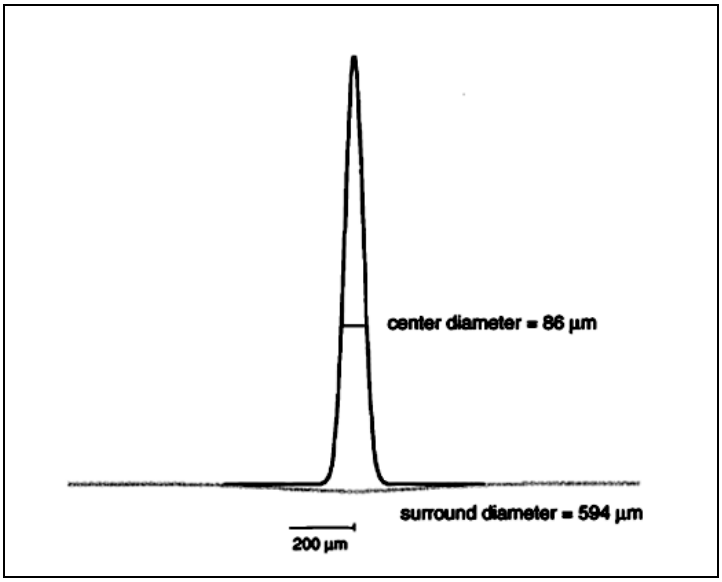

Figure 4.19. Centre/surround structure of a bipolar cell established by two concentric Gaussians. Source: [DACE_00]

Dacey et al. (2000) measured the radii corresponding to the centre (average± SD; 43 ± 8.5µm) and to the surround (average ± SD; 437 ± 61.9µm) (8-14mm eccentricity). As a whole, the surround is 10 times greater than the centre and the weight centre/surround is ~ 1. They propose that the centre/surround opponency that is seen in ganglion cells also happens in bipolar cells. They found that this was 2 to 3 times greater than expected, probably due to electrical connections.

One of the open issues is whether diffuse bipolars establish selective contacts. Along these lines, Boycott and Wässle (1991) propose different possibilities: selective contact by means of different types of receptor in the membrane or non-selective contact transmitting luminosity information.

On the other hand, it is interesting to note, in order to include temporal components of the model in the future, which as all bipolar cell connections in the cone pedicles are not the same. Then one can make a hypothesis by which there are different temporal gaps in each of these connections. In the following figure, Dowling (1987) shows the different types of connections of a ribbon in a cone pedicle. It is noteworthy how he has drawn the FMB on the side of the invaginated process while the FB are farther away and therefore the signal transmission is achieved through different processes.

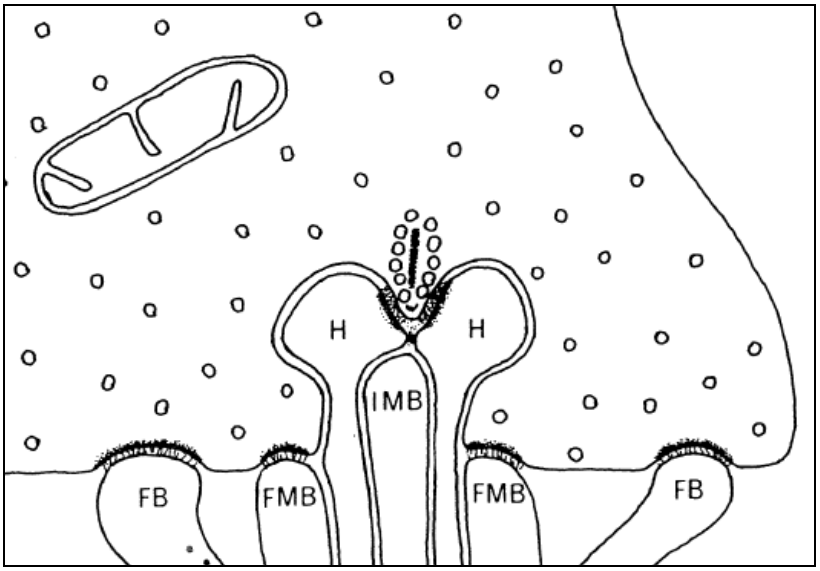

Figure 4.20. Schematic drawing of the connection of bipolar and horizontal cells in a cone pedicle. Source: [DOWL_87]

4. Amacrine cells

Amacrine cells have a cell body situated in the inner nuclear layer and elongations that extend throughout the inner plexiform layer. Their name is due to the fact that it is difficult to find a defined axon in them. [7]

4.1Types

These are one of the lesser known cell types within the retina. The estimates on the number of types range between 30 [MASL_01] and 50 [WÄSS_04]. Different classification criteria have been proposed: based on its morphology (for example, starburst type), according to the type of connections (for example, AII type), based on the type of neurotransmitter (for example, dopaminergic type) or whether they are diffused or stratified [CAJA_ 1893], narrow or wide field diffuse, of transient or sustained response or whether they are mono, bi or multistratified [DOWL_87].

[7] The electron micrographs have shown that these cells proccess have morphological features of axons as weel as dendrites. [DOWL_87]

TABLE 2. Amacrine Cell Types of the Human Retina and Possible Equivalent Cell Types in Other Mammalian Retinas

Type	Sample size	Axon stratification in IPL	Monkey	Cat	Rabbit
A1	Many	S1/2	Knotty 1[1]	A1[2] glycine[4]	
A2	Many	S2	Stratified[6]	A2[2]	
			Knotty bistratified?[1]	GABA[4]	
A3	Many	S2-3	Knotty 2[1]	A3[2] Glycine[5]	
A4	Many	S2,3,4	Knotty 2[1]	A4[2] Glycine[5]	
A5	Few	S4,5	Knotty 3[1]	A5[2]	
			Knotty bistratified?[1]		
			Stratified narrow field[6]		
Small diffuse	Few	S1–5			
AII	Several	a,b	AII[1]	AII[2] Glycine[5]	NFB[3]
			Narrow diffuse[6]		
A8	Few	a,b	Bistratified[6]	A8[2] Glycine[5]	
A12	Several	S5		A12[2] Substance P-IR[11]	Substance P-IR[8]
A14	Few	S2,4/5	Wavy multi-stratified[1]	A14[2]	
Tristratified	Few	S1/2, 2/3,4/5	Wavy multi-stratified[1]		DAPI-3[9]
Wooly	Many	S1–5			
A13	Many	S1–5	A13[1]	A13[2] GABA[4]	
Spiny	Several	S3	Spiny[1]		
			Axon-bearing[15]		
			Unistratified[6]		
Spiny varicose	Several	S3			
ACh	Several	S2, S4	Sa, Sb[1]	Starburst[10]	Starburst[7,14]
Thorny 1	Several	S1	Thorny 1[1]	Indoleamine[19]	
			Dopaminergic[16]		
Thorny 2	Several	S3	Thorny 2[1]	A15[2]	
Wavy	Few	S1	Unistratified[6]		
A18	Many	S1	Type 1 CA[1]	A18[2] TOH-IR[17]	TOH-IR[18]
Semilunar 1	Several	S1	Semilunar 1[1]		
Semilunar 2	Several	S2	Semilunar 2[1]	A19[2]	
			Large uni-stratified[6]	GABA[4]	
Semilunar 3	Several	S4/5	Semilunar 3[1]	A22[2]	
Stellate wavy	Few	S3–4	Stellate wavy[1]		
Stellate varicose	Few	S2–3	Stellate varicose[1]		
			Multistratified[6]		
A17 spidery diffuse	Many	S1–5	Spidery 1[1]	A17[2]	Serotonin[20]
			Wide-field diffuse[6]	GABA[4]	S2[12]
Wiry	Few	S3	Wiry 2[1]	A20[2] Indoleamine[19]	

[1]Mariani ('90).
[2]Kolb et al. ('81).
[3]Dacheux and Raviola ('86).
[4]Pourcho and Goebel ('83).
[5]Pourcho and Goebel ('85).
[6]Boycott and Dowling ('69).
[7]Famiglietti ('83).
[8]Vaney et al. ('89).
[9]Vaney ('90).
[10]Pourcho and Osman ('86).
[11]Pourcho and Goebel ('88).
[12]Vaney ('86).
[13]Mariani and Hokoc ('88).
[14]Tauchi and Masland ('84).
[15]Dacey ('89a).
[16]Dacey ('90).
[17]Kolb et al. ('90).
[18]Brecha et al. ('84).
[19]Wässle et al. ('87).
[20]Sandell and Masland ('86).

Table 4.1. Table showing the different types of amacrine cells in several animals.

Source: [KOLB_92]

Due to the great variety and scarcity of existing data, the followingare the most studied types:

1. AII: small, bistratified, narrow field cells. They establish contacts with bipolar rod cells and connect with ON type bipolar cone cells through electrical connections in the sublamina b and to the OFF type through inhibiting chemical connections in the sublamina a, known as lobular appendages [WASS_95].

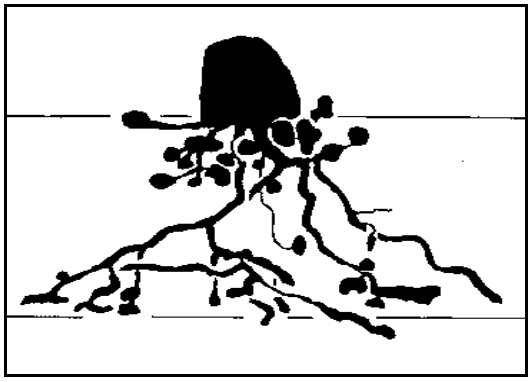

Figure 4.21. Example of an AII cell that shows both types of arbours. Source: [WASS_95]

2. Starburst or cholinergic: are wide-field cells whose name is due to their characteristic shape (see Figure 4.22). They have closely stratified processes within the inner plexiform layer. There are two types, those that are stratified in sublamina a (generate a transient response with the cease of light) and those in sublamina b (generate a transient response with the onset of light). It is believed that they are related to the detection of movement [RODI_89, MASL_05]. Estimates deem that there are about 500,000 in the human retina, with processes of 100μm and an overlapping factor of 10 [OYST_99].

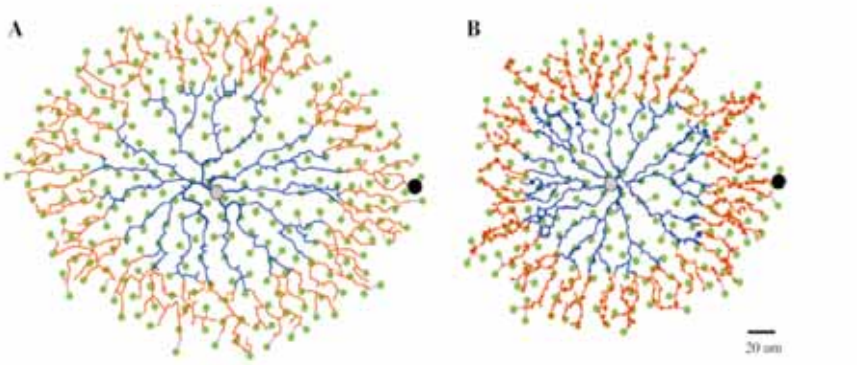

Figure 4. 22. Starburst cell, the cell nucleus in gray and the bipolar cells in green, the arbours in blue and orange. Source: [TUKK_04]

3. Dopaminergic or A18: cells whose neurotransmitter is dopamine. Estimates account for about 10,000. They have few arbour dendrites in fine segments [VICA_97]. They are considered to be related with the response to bright or dim light, thus affecting the electrical connections between horizontal cells [MASL_01].

4. Amacrine A17 or reciprocal amacrine AI: wide-field cells that establish reciprocal connections with rod bipolar cells where they probably modulate the signal transfer [VICA_97, WASS_95].
5. GABAergic amacrine and glycinergic amacrine: are cells that store GABA or glycine and can produce both sustained as well as transient inhibitory responses [VICA_97].

4.2 Connections and distribution

Amacrine cells are connected to bipolar, ganglion, interplexiform and other types of amacrine cells. They establish electrical contacts as well as chemical synapses. They transmit signal both between layers as well as within layers [BACC_07]. Their processes vary in size from 100 μm to over 1,000 μm [OYST_99].

The number of amacrine cells vs. horizontal cells can vary from 4:1 to 10:1 while amacrine: ganglion cells are of 15:1 [MASL_01].

It is noteworthy to mention that there is probably no transmitter in the CNS that can't be found in any of the amacrine cells in the retina [WASS_91].

4.3 Conclusions

When describing amacrine cells, one notices its wide variety and the diversity of functions that they perform (of which we only know a part of). However its importance within the data processing role that takes place in the retina is manifest. The model of this thesis does not include the effects of these cell types, which in the colour chain seem to mainly influence the processes of adaptation. This process is going to be modelled based on colour space models described in Chapter III.

As in earlier cases, models for these cell types have been proposed:

1. Siminoff (1984) presents an amacrine cell action model that divides them into two types: small-field (receive a signal from 1 bipolar) and wide-field (receive a signal from 7 bipolars). He models the feedforward effects to ganglion cells and feedback to bipolar

and horizontal cells. This model obtains that the effect modulates the intensity of the centre and surround signals and in certain configurations incorporates a transient phase.

2. Tukker et al. (2004) propose a starburst model that shows how they can generate the direction selectivity effect.

5. Ganglion cells

Ganglion cells are retina neurons whose cell nuclei are in the innermost layer of the retina. Their dendrites are located in the inner plexiform layer and its axons are grouped together forming the optic nerve.

5.1 Types

There are between 10 and 25 types of ganglion cells, although estimates show that 90% of ganglion cells correspond to three types of cells: midget, parasol and bistratified.

1. Midget ganglion cells: are the most numerous ganglion cells. These cells have a small cell nucleus and a small receptive field. They are capable of working with high frequency spatial signals and/or with low temporal frequencies. They generate a sustained signal when presented stimuli. They are estimated to make up to 95% of ganglion cells in the fovea and 45% of ganglion cells in the periphery [DACE_93].

   These correspond with Dogiel's type 3, Polyak's midget, Leventhal et al. (1981) type B or type P [RODI_85] [NASS_09].

   They are classified as [KOLB_91]:

   a. On center: activated when light reaches its centre.

   b. Off center: activated when there is an absence of light in its centre.

2. Parasol cells: have large receptive fields and axons capable of transmitting at high speeds. They can work with low contrast signals, with low spatial frequencies and/or high temporal frequencies. It is estimated that they make up to 10% of ganglion cells (they are between 8 and 10% of the total, except in the nasal retina where they constitute 10% at

7mm of eccentricity and can reach 20% of the total at greater eccentricities [SILV_91]). Its signal is transient [Croo_08b]).

They correspond with Dogiel's type 2, Polyak's parasol types, type A established by Leventhal et al. (1981) and type M [RODI_85] [NASS_09].

They are divided into two main groups according to whether they branch in the inner or outer layer of the inner plexiform layer:

a. On center: activated when light reaches its centre.

b. Off center: activated when there is an absence of light in its centre.

3. Small bistratified cells: have arbours in two layers: inner and outer layers of the inner plexiform layer. [CHIC_99b]

A series of functional differences have been identified between On and Off types that include [CHIC_02]:

- The number of Off type cells is larger than the On type (periphery zone 5:3 /Off: On [DACE_03]).
- The receptive fields of On type cells are 20% larger in diameter than those of Off type cells (20% according to CHIC_02 and 30% according to DACE_03).
- On type cells have a quicker response than Off type with a peak time that is 10% to 20% faster.
- On type cells have a linear type response while Off type have rectified responses.

Additionally, other types of ganglion cells have been found, reaching a total number of varieties which range from 10 to 20 depending on the author [DACE_03, WÄSS_04, CROO_08a, NASS_09]. The classification criteria is based on different parameters, mainly based on morphology although some are being added based on its chemical components:

a) Size of the dendritic field: small, medium, large or giant.

b) Arbour density: dense, moderate, sparse, very sparse...

c) Stratification levels: monostratified, bistratified, diffuse...

d) Arbour structure: thickness, presence of small branches...

e) Presence of specific chemical components such as melanopsin.

The following figure shows examples of different types of ganglion cells. There exists a great variety of shapes and sizes.

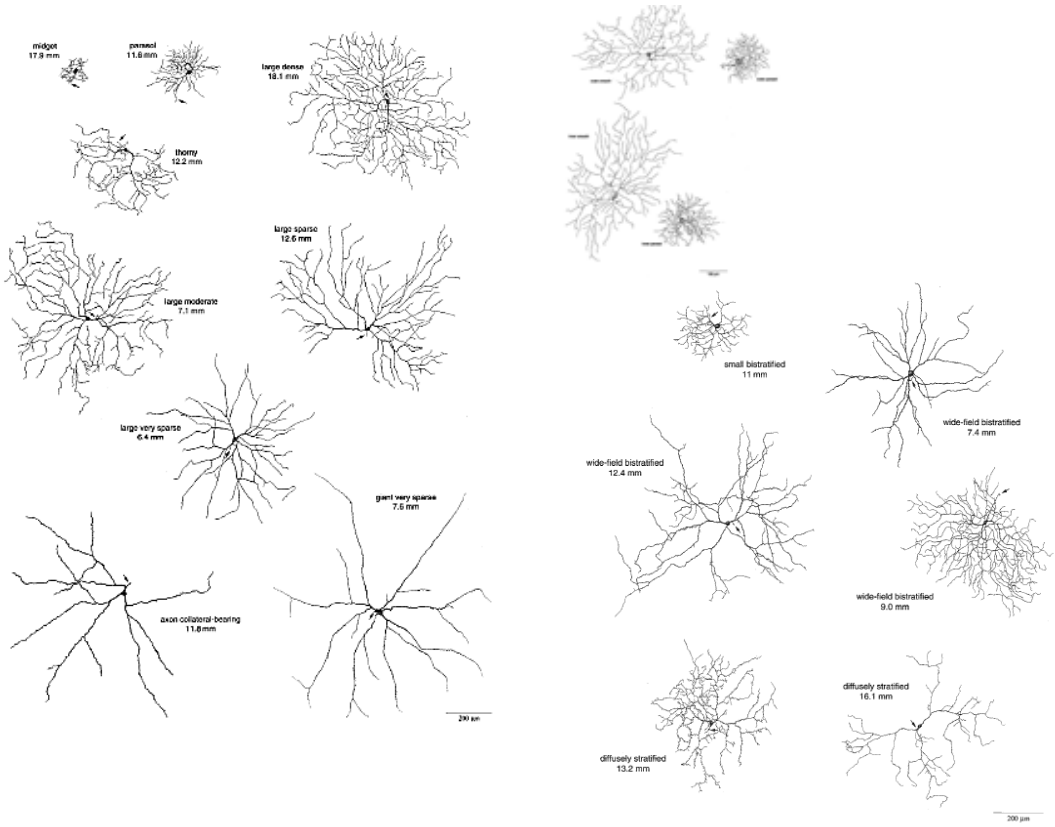

Figure 4.23. Representation of the different types of ganglion cells in the human retina. Sources: [PETE_99] [PETE_00] [CROO_08a].

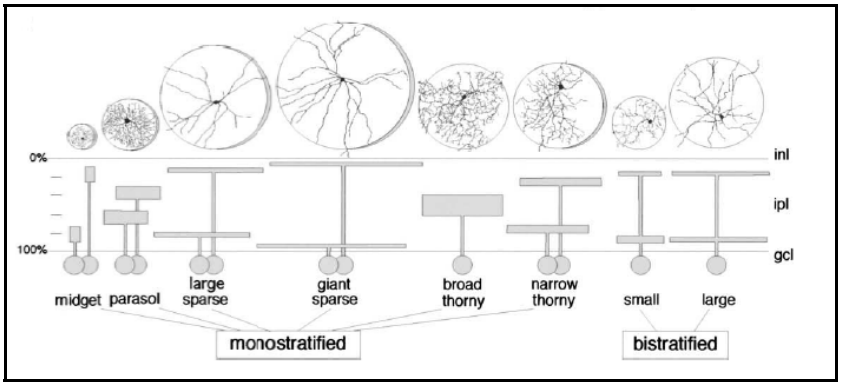

Figure 4.24. Schematic drawing with different types of ganglion cells in primates and their levels of stratification. Source: [DACE_03]

The following are some of the types that have been characterised in primate retinas:

I. Large bistratified cell: the same as the small bistratified cell, it is characterised by being stratified in 2 layers in the inner and outer areas of the inner plexiform layer and is different from the earlier in that it has a large receptive field. Peterson and Dacey (2000) proposed a subclassification in 3 different types based on the arbour shapes and the dendrite structure.

II. Thorny: have a medium-large dendritic field with thick primary dendrites that create secondary dendrites. Their overlapping factor is 1-2. They can be divided into the following types:

    a) Broad: have a transient on-off type response although they don't select the direction.
    b) Narrow: with a dendritic tree that branches very narrowly.

III. Peterson and Dacey (1999) proposed a class whose receptive field is larger than the parasol, which they named wide-field and which in turn are divided into 5 types based on their size and arbour structure:

    a) Large very sparse: stratify in the inner as well as the outer layer. Have a large receptive field (501-1069μm) and very scarcely dense arbours.
    b) Large sparse: have an extremely large receptive field (463-1062μm) and scarcely dense arbours.
    c) Large moderately dense: have a receptive field that is extremely large (523-1034μm) and moderately dense arbours.
    d) Large dense: stratify in the inner as well as the outer layer. They have a large receptive field (501-1069μm) with dense arbours.
    e) Giant very sparse: stratify in the inner as well as the outer layer. They have an extremely large receptive field (1077μm) and very sparse arbours.

IV. Recursives, both monostratified as well as bistratified: are connected with the superior colliculus and possibly to LGN.

V. Biplexiform: cells whose nuclei are in the layer of ganglion cells, whose axon extends throughout the optic nerve and the dendrites, have two processes: one in the inner interplexiform layer that connects with amacrine and bipolar cells and a second in the outer interplexiform layer that connects with rods.

VI. Others:

    a. Diffuse ganglion cells: have dense arbour processes throughout the inner interplexiform layer; mostly have fine dendrites and thorny type components

although part of them have arbours that are less dense and dendrites that are less thorny. [PETE_00]

b. Smooth monostratified ganglion cells: have arbours in the inner and outer layers of the inner plexiform layer, costratified with parasol cells. These are different from the parasol in that they have both a smaller sized cell body and axon and approximately the receptive field diameter is 2 times greater [CROO_08a].

c. Giant sparse monostratified cells: have dendrites well distributed and receive type On signals from L and M cones as well as from rods and S Off type. They have a very regular sustained response that increases with background luminosity. Studies show that they contain melanopsin that allows them to directly react to the luminosity level. They are believed to be related with the control of the circadian rhythms and the diameter of the pupil. [DACE_05]

Therefore, there are multiple types of ganglion cells and different ways to classify them (chromatic vs. achromatic, transient vs. sustained, on vs. off). The following figure is an example of an alternative classification to that earlier shown and presents its possible relations with ganglion cells identified in other animals.

TABLE 3. Ganglion Cell Types of the Human Retina and Possible Equivalent Cell Types in Other Mammalian Retinas

Type	Sample size	Stratification of dendrites	Monkey	Cat	Rabbit
P1a, P1b	Many	S1–2, S5	Midget ganglion long[1]		
			Midget ganglion short[1]		
			Midget ganglion[3]		
P2a, P2b	Many	S2, S3–4	Shrub, small parasol[1]		
			Midget ganglion[3]		
Ma, Mb	Many	S2, S3	Parasol, giant[1]	Beta cells[4]	
			Parasol[3]		
G3a, G3b	Several	S1-2, S3		Gamma cells[2]	
G4	Several	S1–5		G4[2]	OFF—sluggish[8]
G5	Few	S1–5	Small diffuse[1]	G5[2]	
G7	Few	S1, S3		G7[2]	ON-sluggish[8]
G8	Few	S2	Garland[1]	G8[2]	Orientation[7]
G10	Few	S1, S2	Unistratified[5]	G10[2]	
G11	Few	S2, S4	Diffuse[5]	G11[2]	ON-OFF-DS[7,10]
G12	Few	S3		G12[2]	
G16	Few	S5	Garland[1]	G16[2]	
			Unistratified[5]		
G17	Few	S2, S4		G17[2]	Uniformity[7]
G19	Few	S1		G19, delta[2]	
G20	Several	S4–5		G20[2]	
G21	Several	S3		G21[2]	
G22	Few	S1–5		G22[2]	ON-DS[7]
G23	Few	S4–5		G23[2], epsilon[9]	

[1]Polyak ('41).
[2]Kolb et al. ('81).
[3]Rodieck et al. ('85).
[4]Shapley and Perry ('86).
[5]Boycott and Dowling ('69).
[6]Dacey ('89b).
[7]Amthor et al. ('89b).
[8]Amthor et al. ('89a).
[9]Leventhal et al. ('80).
[10]DS, directionally selective.

Table 4.2. Table showing the different types of ganglion cells in several animals. Source: [KOLB_92]

5.2 Connections and distribution

According to the studies of Curcio and Allen (1990), the number of ganglion cells is highly variable among people: 710,000-1,540,000. The maximum density can be found approximately at 1mm from the fovea with average values of 35,100 cells/mm^2. 50% of ganglion cells can be found less than 4.5mm from the fovea, which entails 7.3 % of the total area. The nasal retina has 41% more than the temporal retina. The ratio of cones vs. ganglion cells ranges from 2.9 to 7.5. The following figures show the distribution of ganglion cells in the retina and the eccentricity based density.

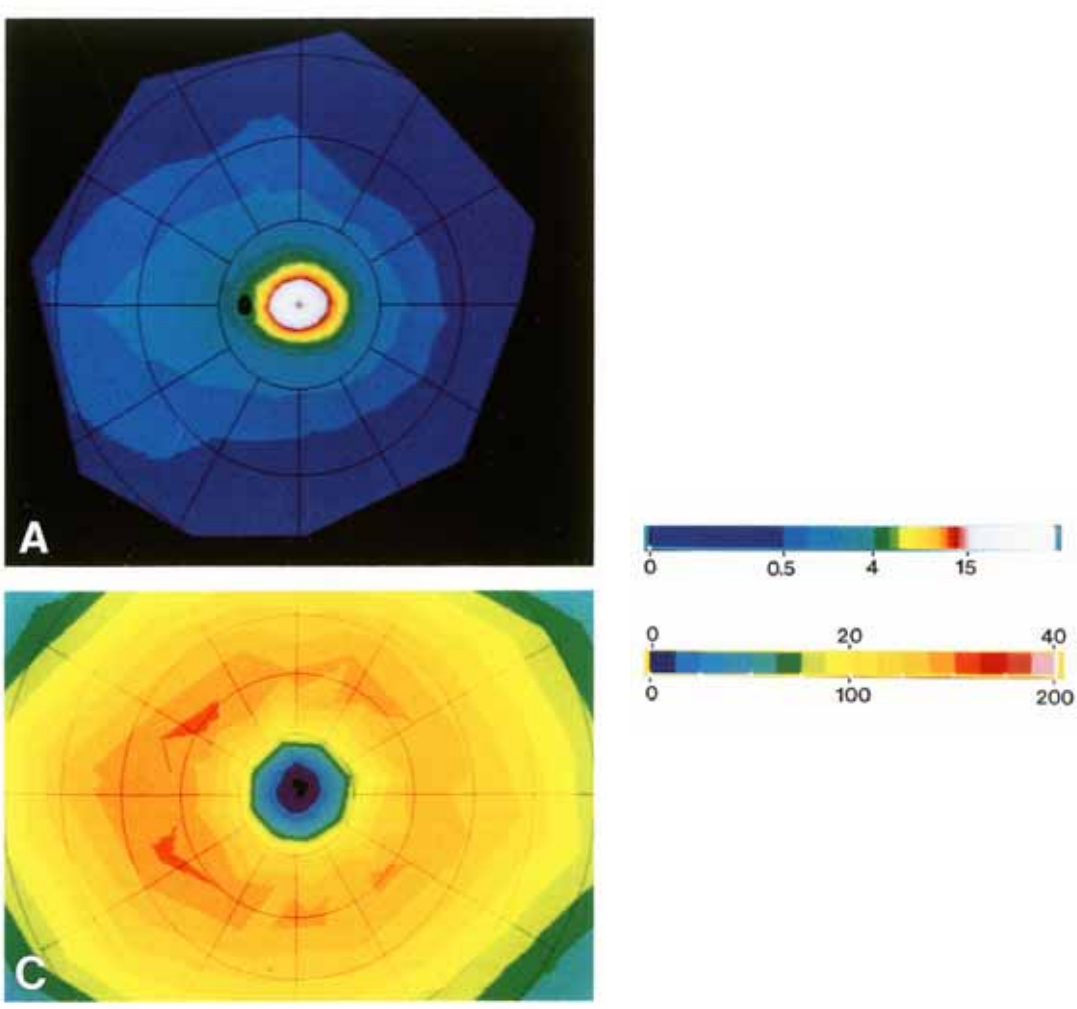

Figure 4.25. Distribution of the ganglion cells in the human retina (above) and area of the fovea (below). Source: [CURC_90b]

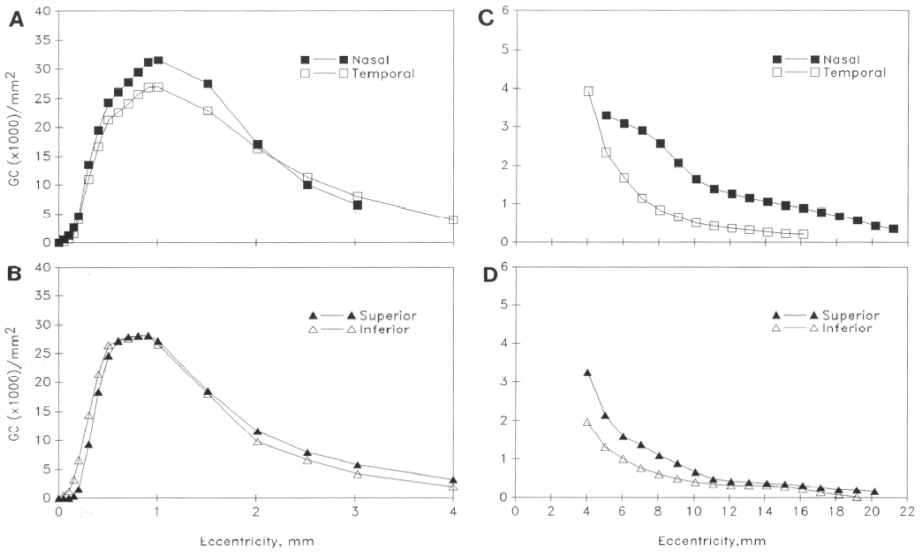

Figure 4.26. Density of ganglion cells in the human retina according to areas. Source: [CURC_90b]

The ganglion cells receive signals from bipolar and amacrine cells, which vary according to the type of ganglion cell. These cells branch in the inner interplexiform layer. As was mentioned earlier, two areas can be distinguished within the inner plexiform layer: the ON and the OFF area (which in turn can be divided into other subsections). On the other hand, the axons of ganglion cells join to form the optic nerve and project towards several areas, including LGN, the superior colliculus, the pretectal area...

The following are the connections established by the different types of ganglion cells:

1. Midget ganglion cells: only have one arbour in the fovea which connects with midget bipolars, the number of arbours increases to 2 or more in the periphery. They are deemed to connect to 1 midget bipolar cell in the fovea and between 1 and 3 in the periphery. The average size of the dendritic field in the human fovea ranges from 5μm to 11μm [DACE_93]. The receptive field is deemed to be between 2 and 3 times bigger than the dendritic tree [KOLB_03]. Likewise, they are connected to amacrine cells (Kolb and Dekorver (1991) estimated that 50% of connections are with these type of cells). The arbour layers locations depend on the type:
    a. On center: arbour in the b layer of the inner plexiform layer and connects with midget invaginated bipolar and amacrine cells. They branch throughout 30% of

the inner plexiform layer between 55% and 85%.[8]. They have an average estimated size in the fovea of 9μm (diameter) [KOLB_03].

b. Off center: arbour in the a layer of the inner interplexiform layer and establish connections with midget bipolar and amacrine cells. They branch throughout 40% of the inner plexiform layer between 10% and 47%. They have an average estimated size in the fovea of 5μm (diameter) [KOLB_03].

2. Parasol cells: have a dendritic field that is greater than that of midget ganglion cells. They make up 10% of ganglion cells in the primate retina. They are considered to be especially important in the perception of movement. They are connected to amacrine cells (both by means of synapse as well as electrical connections) as well as with bipolar cells [JACO_06]. Their average dendritic field size in the fovea ranges from 10 to 80 μm.

   The following figure shows the size variation with the eccentricity of parasol and midget cells.

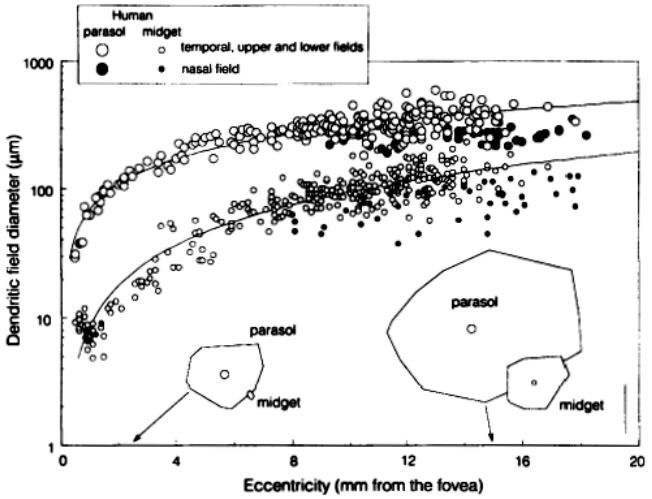

Figure 4.27. Size of midget ganglion and parasol cells depending on their eccentricity. Source: [DACE_92]

Parasol cells are divided into two main groups according to whether they arbour in the inner or outer layer of the inner plexiform layer:

a. On center: arbour in the b layer of the inner interplexiform layer and connect with diffuse bipolar and amacrine cells.

[8] Where 0% is the limit of the inner nuclear layer and 100% the ganglion cell layer. [DACE_03].

b. Off center: arbour in the a layer of the inner interplexiform layer and connect with diffuse bipolar and amacrine cells.

   OFF center parasol cells, like midget ganglion cells, have a greater diameter than ON center cells (30-50%according to [DACE_92]).

3. Small-field bistratified cells: their dendrites arbour into two sets of processes. One in the inner layer and another in the outer layer of the inner plexiform layer, where they receive S type bipolar signals and OFF type diffuse bipolar signals [PETE_00].

   There are different proposals regarding their structure and receptive field:

   a. Crook et. al (2009) propose a coexisting ON OFF field that receives signals from both OFF type diffuse bipolar cell signals as well as S type bipolar cells. The size estimate of the ON/OFF at 3 mm eccentricity in a macaque is: 59.6 ±12.8 μm / 62.5 ± 13.7μm.

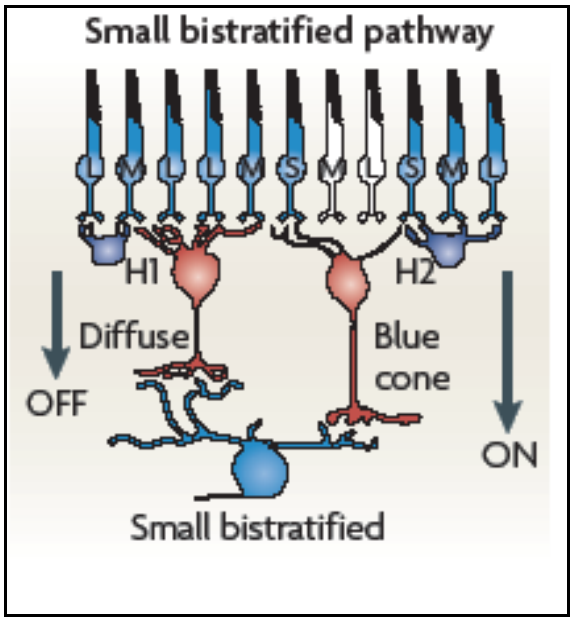

Figure 4.28. Schematic drawing of the connections of small bistratified cells. Source: [NASS_09]

   b. Field et al. (2007) propose a structure of centre/surround in opponency, where the surround is 50% greater than the centre and the effect is generated in horizontal cells.

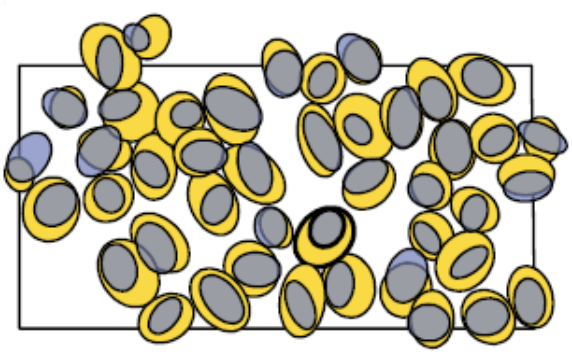

Figure 4.29. Contour boundaries of small bistratified cells: grey S component and yellow L and M component. Gaussian adjustment + 1 SD. Source: [FILE_07]

The following are the average characteristics of the other types of ganglion cells:

I. Large bistratified cell: has a large receptive field: in primates 510μm (modelled with difference of Gaussian)[DACE_03] and in human retinas 682 ± 130 μm [PETE_00]. They constitute 2.7% of ganglion cells that reach LGN [DACE_04], although Peterson and Dacey (2000) suggest that they could also project to the superior colliculus (CS) given the similarities with large bistratified cells of primates.

   The following shows the size variation with the eccentricity of these types of cells both for human as well as primate retinas.

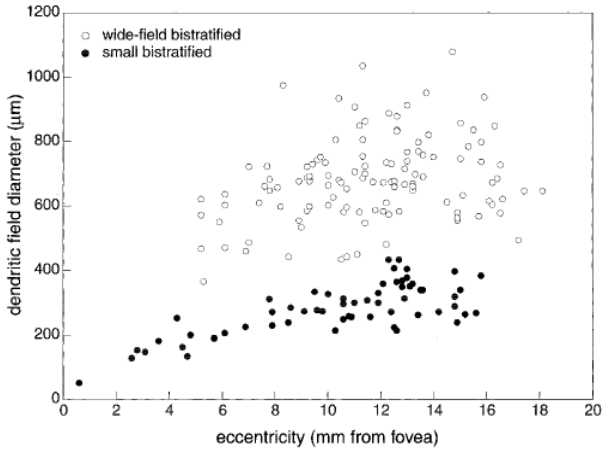

Figure 4.30. Size comparison of small and large bistratified ganglion cells in humans. Source: [PETE_00]

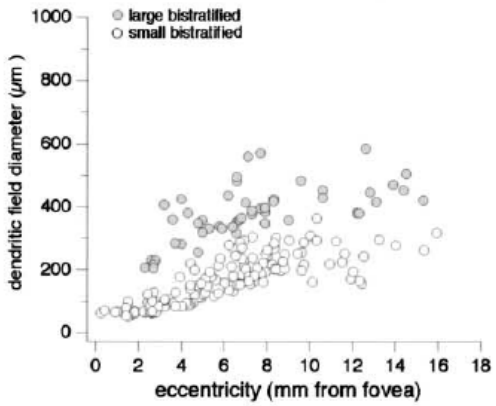

Figure 4.31. Size comparison of small and large bistratified ganglion cells in primates. Source: [DACE_03]

Superimposing both graphs, we can observe that the measurements of the human retina are slightly higher than those of primates.

II. Thorny: are approximately double in diameter than parasol cells with the same eccentricity. They have been identified with retrograde markers from the superior colliculus and LGN. They can be divided into the following types:

   f) Broad: with a thicker dendritic tree that arbours in the centre of the inner interplexiform layer.

   g) Narrow: there are two types according to whether they arbour within the inner or outer limits of the inner interplexiform layer.

   The following figure shows the sizes of both types in accordance with their eccentricity.

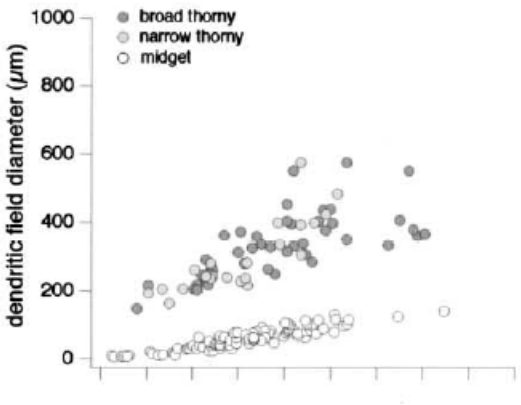

Figure 4.32. Distribution of thorny vs. midget cells. Source: [DACE_03]

III. Wide-field cells: their receptive field is greater than that of parasol, as can be seen in the following figure.

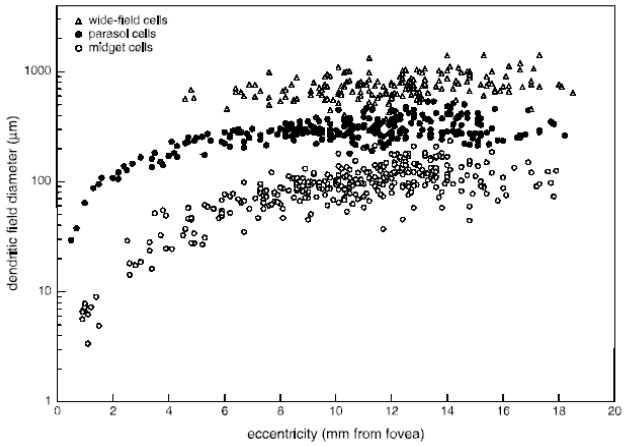

Figure 4.33. Size distribution of wide-field cells vs. parasol and midget cells. Source: [PETE_99]

The following table shows the average characteristics of the 5 types established by Peterson and Dacey.

Table 1. *Wide-field monostratified ganglion cells of the human retina*

Cell group	Sample size	Eccentricity range (mm from fovea)	Mean dendritic field diameter (μm ± S.D.)	Range (μm)	Mean soma diameter (μm ± S.D.)	Range (μm)	Mean number of branch points (±S.D.)	Range
Giant very sparse—inner	5	8.6–15.3	1090 ± 271.1	787–1404	19 ± 2.7	16–22	18 ± 2.9	13–20
Giant very sparse—outer	5	7.6–17.3	1064 ± 227.1	781–1408	23 ± 5.0	16–28	16 ± 2.6	13–19
Total	10	7.6–17.3	1077 ± 236.2	781–1408	21 ± 4.5	16–28	17 ± 2.7	13–20
Large very sparse—inner	44	6.4–18.0	715 ± 141.8	501–1129	20 ± 3.5	13–29	35 ± 4.6	25–43
Large very sparse—outer	14	4.6–14.8	807 ± 160.3	517–1069	19 ± 4.2	15–30	29 ± 4.3	25–42
Total	58	4.6–18.0	737 ± 150.4	501–1129	20 ± 3.7	13–30	33 ± 5.0	25–43
Large sparse[a]	27	4.8–17.1	791 ± 174.0	463–1062	18 ± 3.6	13–28	56 ± 4.9	48–64
Large moderate[a]	48	4.9–15.5	749 ± 126.6	523–1034	18 ± 2.7	13–26	84 ± 6.7	71–97
Large dense—inner	17	7.6–16.6	793 ± 184.3	567–1186	19 ± 3.0	14–26	127 ± 18.5	109–174
Large dense—outer	4	12.9–18.1	712 ± 76.2	643–811	16 ± 1.3	15–18	135 ± 15.6	117–148
Total	21	7.6–18.1	777 ± 170.6	567–1186	18 ± 2.9	14–26	129 ± 17.9	109–174
Thorny[a]	15	8.5–18.5	517 ± 112.7	356–674	17 ± 2.2	15–21	70 ± 12.5	54–88

[a]These are inner stratifying cells only.

Table 4.3. Characteristics of wide-field cells. Source: [PETE_99]

IV. Recursives, both monostratified as well as bistratified: are connected to the superior colliculus and possibly to LGN.

V. Biplexiform: have arbours both in the inner plexiform layer as well as the outer plexiform layer. The following is an example of these.

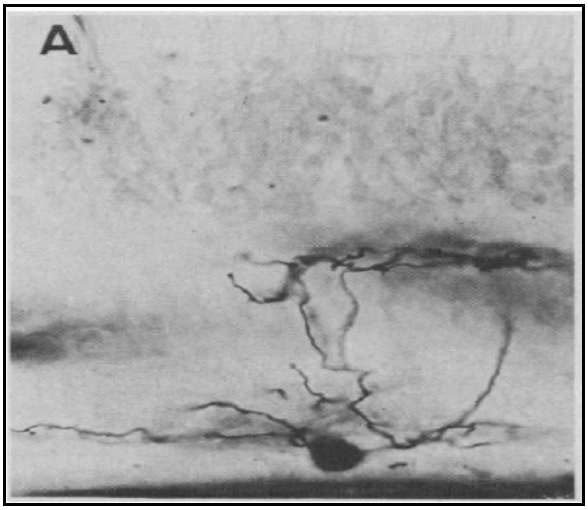

Figure 4.34. Example of Golgi-impregnated biplexiform cell. Source: [MARI_82]

VI. Others:

a. Diffuse ganglion cells: the average size of their dendritic field is 486 ±113 μm [PETE_00].

b. Smooth monostratified ganglion cells: have dendritic fields that are about 1.5 to 3 times greater than parasol cells at the same eccentricity. Figure 4.35 shows the variation in size with the eccentricity. These cells are connected with LGN and the superior colliculus. Crook et al. (2008) propose that these types of cells represent a parallel channel to that generated by parasol cells.

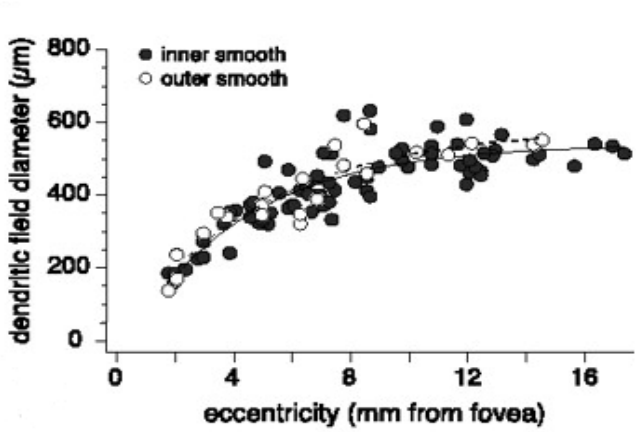

Figure 4.35. Sizes of smooth monostratified cells at different eccentricities. Source: [CROO_08]

c. Giant sparse monostratified cells: have a large receptive field. Figure 4.36 shows the variation with eccentricity. They have been retroactively marked from LGN and the pretectal olivary nucleus (PON) [DACE_05].

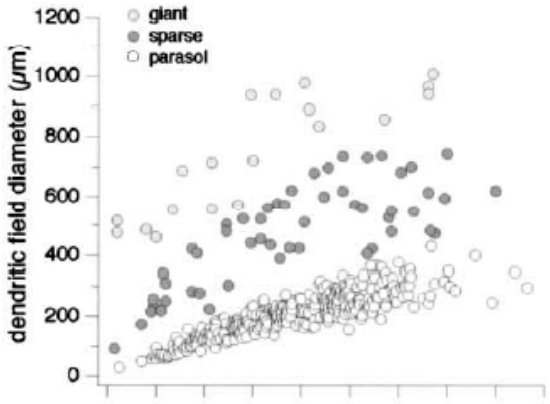

Figure 4.36. Sizes of giant sparse cells versus large sparse and parasol cells. Source: [DACE_03]

Dacey (2004) sets forth an estimate of the connections and percentages of the main types of ganglion cells identified to date in the retina:

TYPE	% at 8 mm eccentricity	CONNECTION
Midget	52	LGN 3, 4, 5 and 6
Parasol	16	LGN1 and 2 SC[9]
Diffuse	3,2	LGN
Giant sparse	2	LGN Pretectal PON Hypothalamus SCN
Recursive	1,9	SC LGN?
Broad thorny	1,2	LGN SC
Thorny	2,4	LGN
Bistratified recursive	4,2	SC
Large bistratified	2,7	LGN
Small bistratified	6,2	LGN KONIO 3 and 4

Table 4.4. Table with the distribution values of the main types of ganglion cells identified to date. Source: [DACE_04]

9 [CROO_08b]

5.3 Conclusions

The retina has a great variety of ganglion cells. The following types should be highlighted: midget, parasol and small- field bistratified. Each point in the field of view of the eye is deemed to be sampled by every type of ganglion cells, that is, each type of ganglion cell has a 100% coverage of the retina [WASS_91].

This section has shown the non-homogeneous distribution of ganglion cells in the retina. Estimates propound that a circle with a radius o f 200 µm (1º) is sampled by about 38,000 ganglion cells and a circle with radius 1mm (5º) by 220,000 ganglion cells (macaque data) [WASS_89].

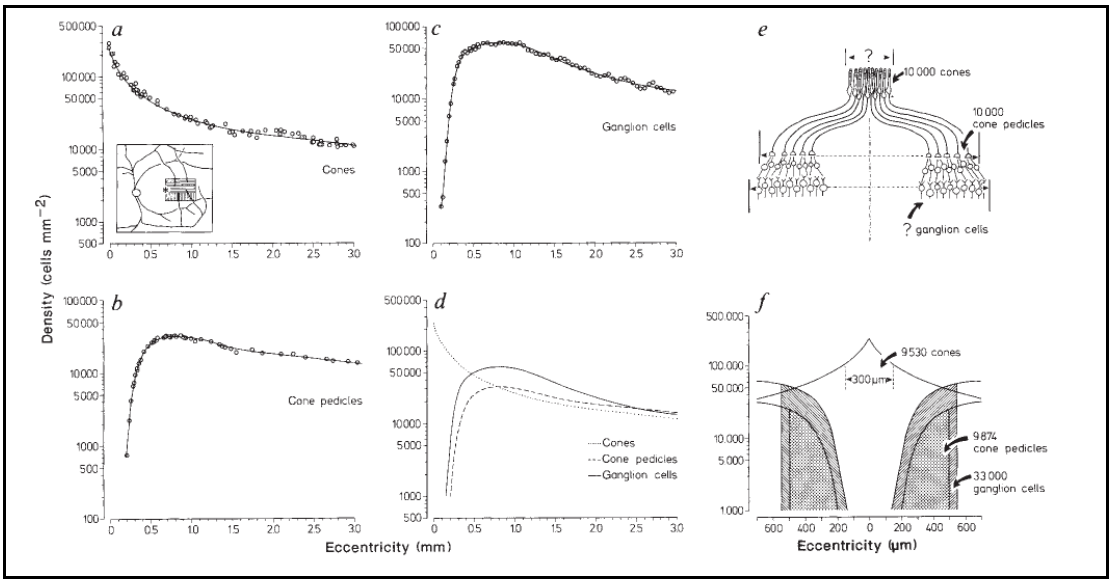

Figure 4.37. Example of distribution of ganglion cells. Source: [WASS_89]

The different types of ganglion cells create a complete "image" of the retina, codifying different types of information, such as movement, brightness contrast, colour information... This way, the different information pathways that are transmitted through the optic nerve are created.

The three pathways deemed as the main ones are: parvocellular, magnocellular and koniocellular. They have their origin in midget cells, parasol cells and small bistratified cells, respectively. In general, ganglion cells are deemed to have a characteristic response with components that have spatial and/or spectral opponency. Figure 4.38 shows the case of spatial opponency. This type of response is known as centre/surround, denoting the opposite effect that is caused by the presence of stimuli in both areas.

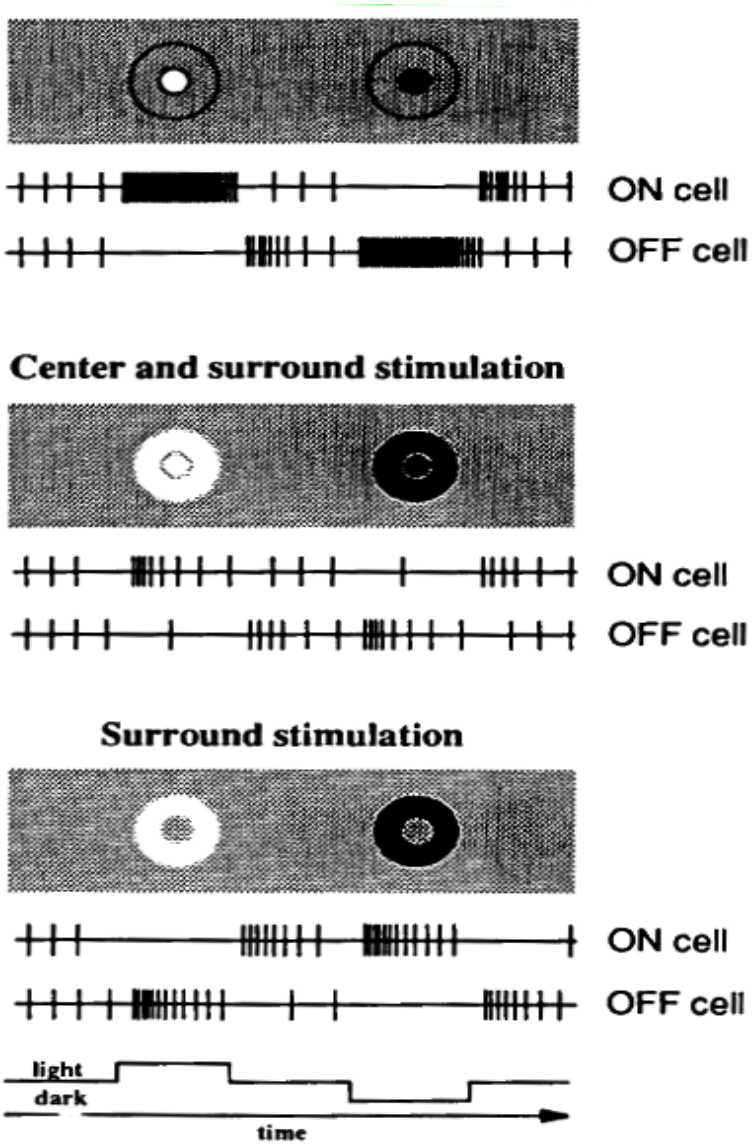

Figure 4.38. Response of ganglion cells. Source: [SCHI_92]

The exact origin of the opponency processes is not clear, although there are theories that include the effect of horizontal cells, of bipolar cells, of amacrine cells and the fact that the connections are selective based on cone type (for example: Ichinose and Lukasiewicz (2005) propose that in the case of the salamander, the effect of the surround in the ganglion cells is influenced by horizontal and amacrine cells. Additionally, they state that each of these elements influences in high levels of lighting: horizontal or in low levels: amacrines.)

In order to be able to identify the components of each pathway and the elements that generate the effects of the centre/surround, Dacey 2000 has proposed connection models for each of them:

- Midget - parvocellular: where the L and M type cones are connected with midget bipolar cells and these in turn with midget ganglion cells.

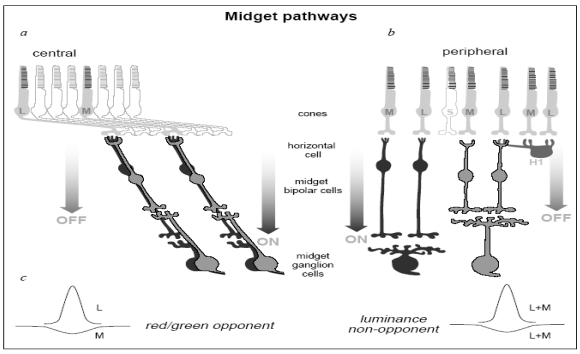

Figure 4.39. Schematic drawing of midget connections. Source: [DACE_00]

- Parasol- magnocellular: where the L and M type cones are connected to diffuse bipolar cells and these to parasol ganglion cells.

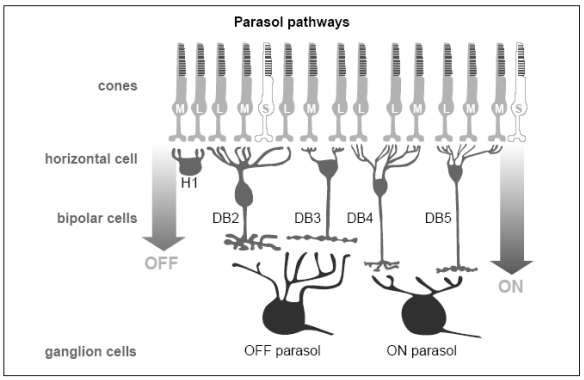

Figure 4.40. Schematic drawing of a parasol connection. Source: [DACE_00]

- Bistratified - koniocellular: where the L and M type cones are connected to diffuse bipolar cells, while the S types are connected to blue bipolar cells. Each of these pathways leads to one of the levels of branches of the bistratified ganglion cells.

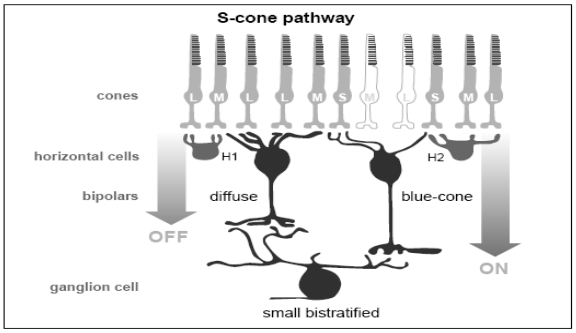

Figure 4.41. Schematic drawing of bistratified cell connection. Source: [DACE_00]

On the other hand, the structure of opponency between centre and surround has been modelled through different mathematical functions. The most common are:

- Difference of Gaussians, proposed by several different authors (Enroth-Cugell and Robson, (1966); Rodieck (1965):

$$f(x,y,\sigma_C,\sigma_P,\kappa_C,\kappa_P)=\frac{\kappa_C}{\sigma_C}\exp\left(-\frac{\left(x^2+y^2\right)}{2\sigma_C^2}\right)-\frac{\kappa_P}{\sigma_P}\exp\left(-\frac{\left(x^2+y^2\right)}{2\sigma_P^2}\right) \qquad \text{(eq. 4.1)}$$

  Where $\sigma_C,\sigma_P,\kappa_C,\kappa_P$ model the sizes and gains of centre and surround.

  Other authors use non-circular symmetries, such as ellipses, that better adjust to the real shape [PASS_02].

- Mexican hat: that can be derived from a Gaussian function (2º derivative normalised)[LOUR_95]:

$$f(x,y,\sigma)=\frac{1}{\sigma^3}\left(1-\frac{\left(x^2+y^2\right)}{\sigma^2}\right)\exp\left(-\frac{\left(x^2+y^2\right)}{2\sigma^2}\right) \qquad \text{(eq. 4.2)}$$

  Where σ models the size.

Besides the models mentioned in this section, there are others that include temporal components and non-linear effects, such as:

- Purpura et al. (1990) model P and M cells with a series of low pass filters. The constants vary for both each cell as well as for the intensity.

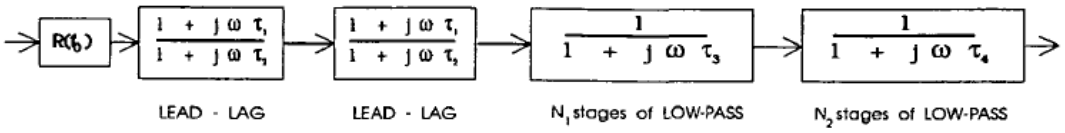

Figure 4.42. Ganglion cell response model. Source: [AWAT_00]

- Lee et al. (1998) propose the existence of a granular structure generated by the non-linear sum of the elements such as midget bipolar cells. This might be the origin of the frequency response effect of the surround.

- Awatramani and Slaughter (2000), propose that in the case of the salamander, the transient and sustained signal components begin in bipolar cells.

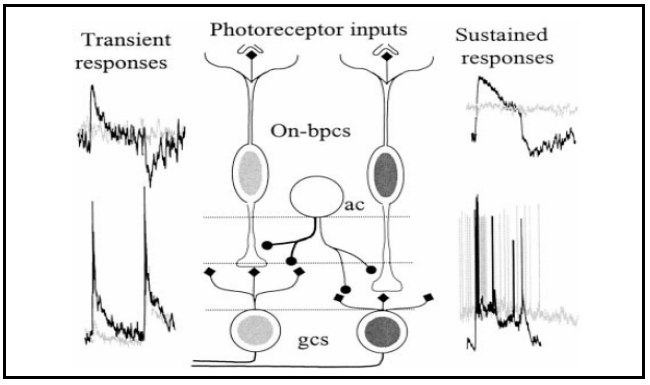

Figure 4.43. Transient and sustained pathways generation model. Source: [AWAT_00]

6. Other cell types

The retina has other types of cells besides those previously mentioned. The following are the most relevant.

6.1 Interplexiform cells

Interplexiform cells are centrifugal type cells that transfer information from the inner interplexiform layer to the outer layer. In most cases, the nucleus is in the inner nuclear layer. Their function is unknown though it is deemed that in the case of the human retina, it is related with the processes of amacrine, bipolar and/or horizontal cells [DOWL_87].

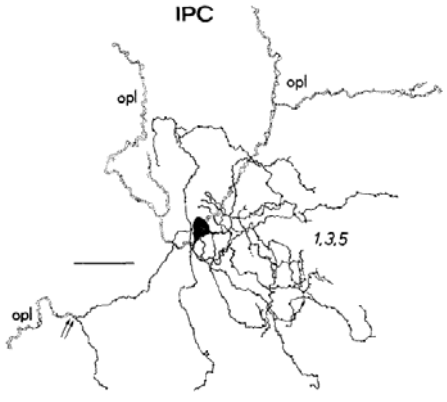

Figure 4.44. Example of an interplexiform cell in the human retina. Source: [KOLB_92]

6.2 Glial cells

There are different types of glial cells in the retina [DOWL_87, KOLB_09]:

1. Müller cells: the most common glial cells in the retina. They span vertically throughout all the layers of the retina, from the outer limiting to the inner limiting membrane. Its nucleus is in the inner nuclear layer. Although their functions are not clear, they seem to include: metabolic support to the retina neurons, guidance through generation and processes modulation of neurotransmitters and ions. [NEWM_96, BARR_03]
2. Retina astrocytes are located almost exclusively in the layer of the fibres of the optic nerve. These cells have an elongated nuclear cell and a set of radial processes.
3. Microglial cells have small nucleus with short and irregular processes. They are distributed throughout the multiple layers of the retina.

7. Output signals from the retina and conclusions

> *"This can be conceived in the sense that the individual components present in the organ of vision are completely independent of one another and each is fatigued or adapted to its own function. But if the real physiological equipment is considered, on which the process are based, it is permissible to doubt whether things are so simple. At any rate, the possibility has to be considered that thought influences the formation of the substances of vision, changes the circulation, and spreads sensitive substances by diffusion; maybe other things modify the states of the exposed areas and their surroundings and there create conditions that do not obey such simple rules".* J. von Kries 1902

The retina has 100 million photoreceptors and 1 million ganglion cell signals. Both due to this and to the wide range of work luminosity, the visual system must compress the original signal before sending it through the optic nerve. In order to do so it processes the information and creates a set of specialised pathways [NASS_09].

Different types of neurons present in the retina have been looked at in this chapter, although it is clear that all of the existing subtypes still have not been identified, many are known:

a) Photoreceptors:
    a. Cones.
    b. Rods
b) Horizontal cells:
    a. HI.
    b. HII.
c) Bipolar cells:
    a. Midget bipolar:
        i. Invaginated, IMB.
        ii. Flat, FMB.
    b. S cone bipolars, BB.
    c. Diffuse bipolar.
        i. Type Off:
            – DB1.
            – DB2.
            – DB3.
        ii. Type On:
            – DB4.
            – DB5.
            – DB6.
    d. Rod bipolars, RB.
d) Amacrine cells:
    a. AII.
    b. Starburst or cholinergic.
    c. Dopaminergic or A18.
    d. Amacrine A17 or reciprocal amacrine AI.
    e. GABAergic amacrine and glycinergic amacrine.

f. …

e) Ganglion cells:

a. Midget ganglion cells:

i. On center.

ii. Off center.

b. Parasol cells:

i. On center.

ii. Off center.

c. Small bistratified cell.

d. Large bistratified cell.

e. Thorny:

i. Broad.

ii. Narrow.

f. Wide-field:

i. Giant very sparse.

ii. Large very sparse.

iii. Large sparse.

iv. Large moderate.

v. Large dense.

g. Recursives: monostratified and bistratified.

h. Biplexiform.

i. Diffuse ganglion cells.

j. Smooth monostratified ganglion cells.

k. Giant sparse ganglion cells.

f) Others: interplexiform cells.

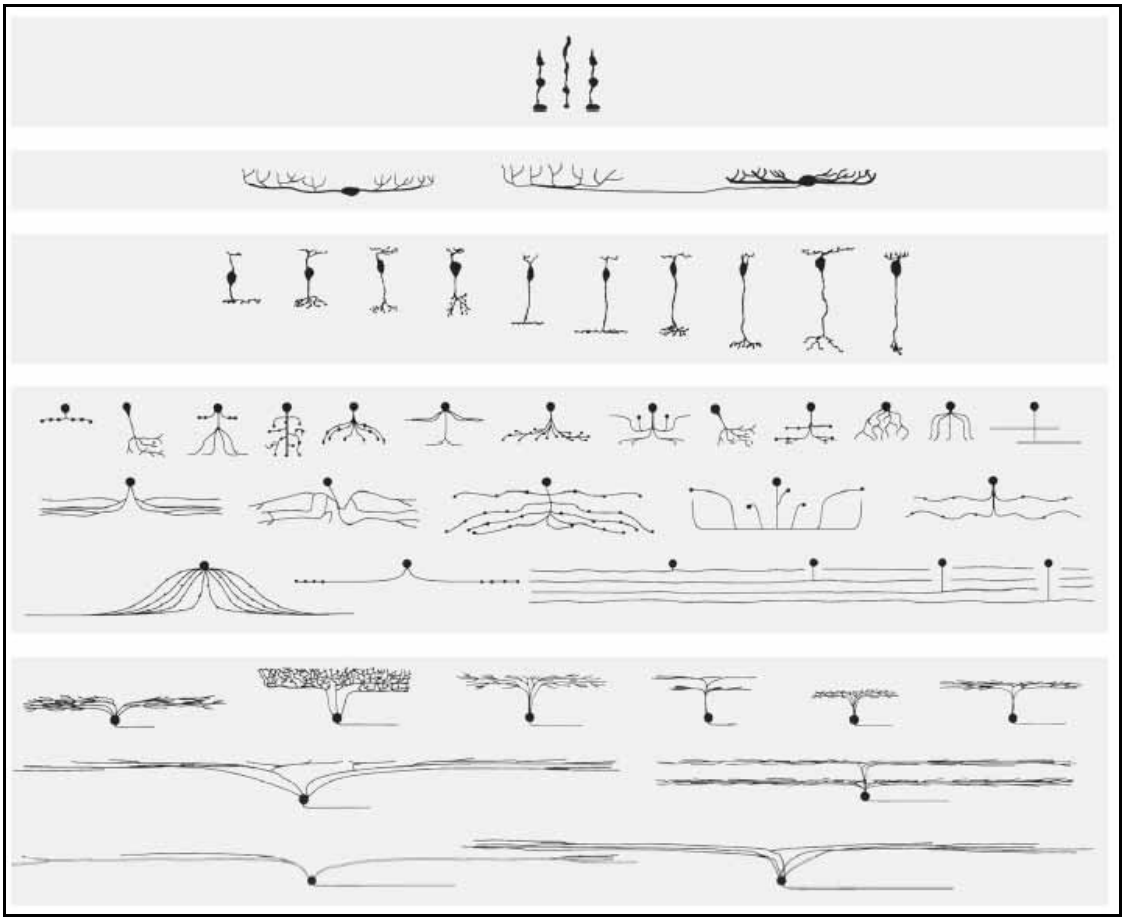

Figure 4.45. Example of sets of cells present in the retina of mammals. From top to bottom: photoreceptors, horizontal cells, bipolar cells, amacrine cells and ganglion cells. Source: [MASL_01]

Only photoreceptors and one type of ganglion cell, of all the types of cells present in the retina, have been identified as light sensitive. On the other hand, only ganglion cells and some amacrine generate action potentials while the rest generate changes of potential in the membrane. Along these lines, it is noteworthy to mention that action potentials are only generated when there is an activation signal at the input of a cell, that is, they only transmit positive signals. From photoreceptors, the visual system generates two signal lines: one whose activation signal is the presence of a luminous stimulus and another whose activation signal is the absence of a luminous stimulus, in reference to an "average" level or background. As a general rule, horizontal and Off type bipolar cells can be said to hyperpolarize when presented light, while On type depolarise. In this way, On type ganglion cells are activated when presented more luminous stimuli than the background, while Off type are activated when presented darker stimuli than the background [WÄSS_04]. As was mentioned in Section 5 of this Chapter, there are certain differences in the

size, transmission speed and delay differences in the signals of On and Off pathways (Balasubramanian and Sterling (2009) propose that this asymmetry is related to the characteristics of natural images).

One must bear in mind that cell density is not homogeneous, thus each type of cell has a specific distribution. The fovea has a high cell concentration which allows it to reach its maximum levels of visual acuity. This high concentration generates that a zone whose area is 2% of the total represents 40% of the total of V1 [OYST_99].

Spikes that originate in the retina are transmitted to LGN in the dorsal thalamus, hypothalamus, pretectum in the mesencephalon and the superior colliculus in the tectum. There are different pathways that are related to the perception of shapes, colours, movements or adjustments of the size of the pupil. Although it seems that each function does not fall upon a sole pathway. The three main pathways that reach LGN are:

- Parvocellular or P pathway: mainly related to signals generated in midget ganglion cells. It is a pathway that is capable of transmitting high frequency spatial signals and signals with colour opponency. It is considered to be related to the detailed perception of shapes and possibly with colour.
- Magnocellular or M pathway: mainly related with signals generated in the parasol ganglion cells. It is a pathway capable of transmitting high frequency temporal signals and low contrast signals. It is considered to be related with the perception of movement.
- Koniocellular or K pathway: mainly related with signals generated in the small-field bistratified ganglion cells. It is considered to be associated with colour perception.

Regarding colour, it is everyday more widely accepted that the information of cones is segregated in two different pathways (one related with S cones and the other with L and M cones) which were generated in different stages of the evolution of primates, the chromatic capacity being a relatively new feature in the evolutionary process. [DACE_00b]

There are many unresolved issues. These are the most relevant regarding the development of the model:

- Can the results of the human visual system be assimilated to that of Old World monkeys?

  Throughout this chapter data relating to humans and other primates has been provided. Although there are differences between species (for example, Dacey and Peterson (1992) stated that in the periphery, human parasol cells are 90% larger than those of macaques,

while midget cells are similar) as far as has been determined by our current state of knowledge of the visual system, both visual systems have similar overall visual capacities. [DACE_00]

- Regarding midget cells, is the centre/surround signal controlled by a sole type of photoreceptor outside the fovea?

  Up to now, there haven't been conclusive results that allow us to state that midget cells outside the fovea receive signals from only one type of cone. However, different authors have tried to resolve this issue by means of experiment evaluations that allow to define whether the results could correspond to specific or mixed connections:

  – Lennie et al. (1991) presented a study that proposed that the connection to the centre is established only with one type of cone.

  – Dacey (1993) analysed the dendritic trees of ganglion cells and superimposed them to the arbours of bipolar cells finding that ganglion cells have selective contacts.

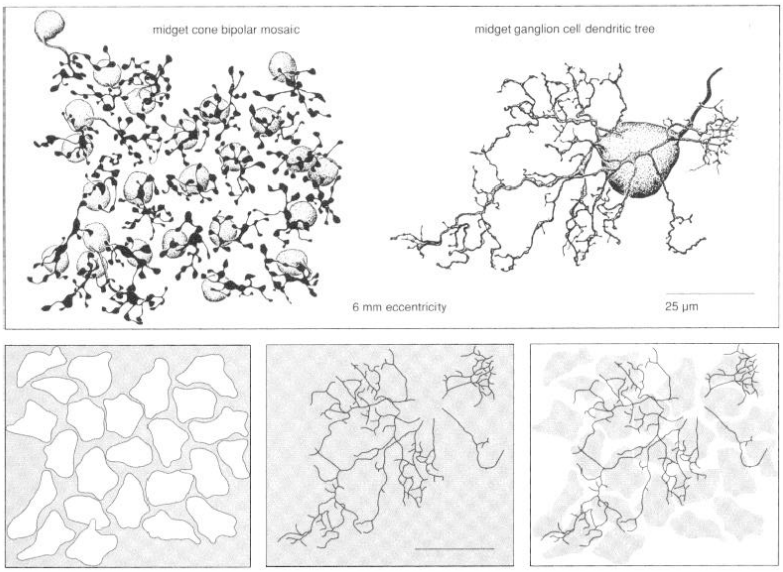

Figure 4.46 Above) Bipolar cells and midget ganglion cell arbours. Below) Representations of the arbours and their superimposing. Source: [DACE_93]

  – Martin et al. (2001) analysed the sensitivity of midget cells in the fovea and the periphery. They obtained similar results for both regions thus infering that the connections are specific. They proposed that the distribution of the dendritic arbours can be the basis of the specific connections of L or M and

that the loss in the capacity for colour discrimination lies in postretinian mechanisms.

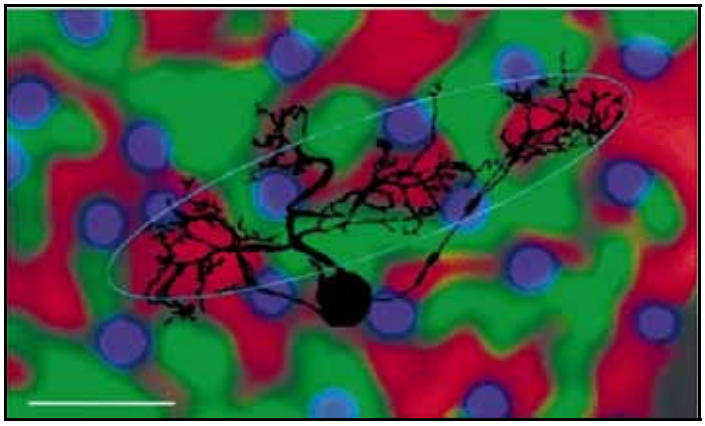

Figure 4.47. Representation of the dendritic tree of a midget ganglion cell of a macaque superimposed on the photoreceptor mosaic. Scale: 50mm. Source: [MART_01]

- Vakrou et al. (2005) measured the variation in chromaticity sensitivity between the centre and the surround and found that there wasn't an important variation in perception, from which they deduced that there must not be specific connections.

- Are signals codified based on the number of nervous spikes or are there other factors involved?

  Although as a general rule work is based on the number of spikes, the fact that other factors represent relevant information is each time becoming more widely accepted:

  - Field and Chichilnisky (2007) introduced a revision of the circuits and codification of the retina and noted how simultaneous or synchronised neuron activation could codify information.
  - Gollisch and Meister (2008) propose codification ways through the temporal relation of signals.

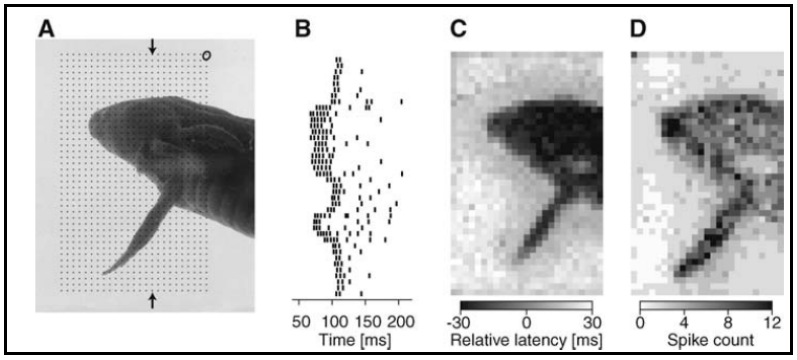

Figure 4.48. Response of OFF type ganglion cells: A) Image shown B) Spikes generated by the cells in the line with the arrows in image A. C) Gray scale representation of the difference in the activation of the stimulus. D) Gray scale representation of the number of nervous impulses.

In conclusion and to summarise, the human visual system can be said to begin in the eyes, specifically with the photoreceptors: cones and rods. The existence of more than one type of cone is what later allows the perception of colour. The cell layers that compose the retina make transformations of the photoreceptor signal in order to finally generate the output signal through ganglion cells. The set of output signals are specialised in the detection of specific features such as the presence of contrast, detection of movement or colour attributes.

Chapter V

From the retina to the cortex

> *"[…] the great enigma in the organisation of the brain was the way in which the nervous ramifications ended and in which the neurons were mutually connected. Repeating a simile already used, it was a case of finding out how the roots and branches of these trees in the gray matter terminate, in that forest so dense that, by a refinement of complexity, there are no spaces in it, so that the trunks, branches, and leaves touch everywhere."*
>
> Santiago Ramón y Cajal (1917)

A brief chapter on the stages that take place after the retina in the visual process has been included in order to place the signals that are generated in the retina and transmitted through the optic nerve.

Signals from each eye are transmitted through the optic nerve and are combined in the optic chiasm where the axons coming from the nasal retina cross towards the corresponding contralateral side and continue through the right optic track (where the information of the left side of the visual field is kept) and left optic track (right side of the visual field).

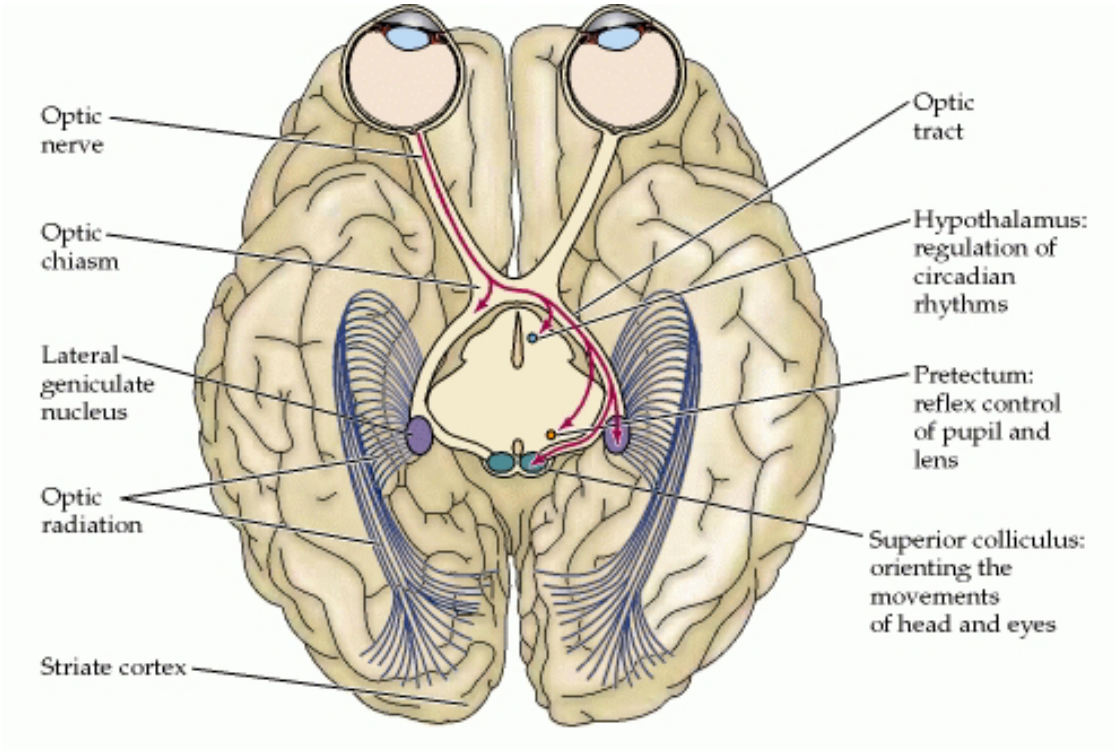

Figure 5.1. Schematic drawing of the visual system. Source: [PURV_01]

The greater part of axons reach the lateral geniculate nucleus (LGN) in the dorsal thalamus. Other destinations are: the hypothalamus that is associated with the control of the circadian rhythms, the pretectum in the midbrain that controls both the size of the pupil as well as some ocular

movements and the superior colliculus in the tectum that controls the eye and head movement in order to direct the glare towards specific positions. [BEAR_06].

LGN projects towards the cortex, specifically towards the primary visual area or V1 and from there to the remaining areas of the cortex, first going through areas V2, V3, V4, V5, IT... At present, the different attributes that we perceive visually are deemed to go across the so-called dorsal and ventral streams. Each is specialised in a task: shape detection (and probably colour) and movement detection. As the following figure shows, these are neither exclusive "pathways" or unidirectional processes.

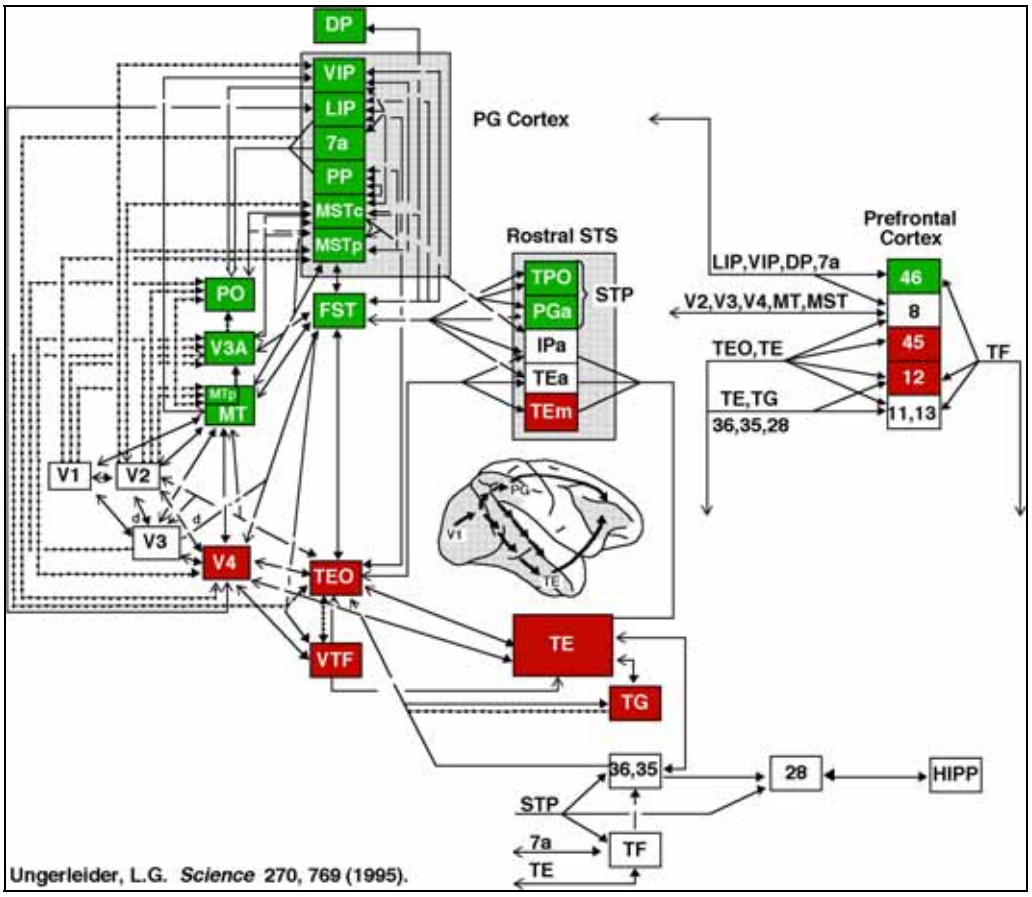

Figure 5.2. Schematic drawing of the different areas of the visual cortex. Source: [UNGE_95b]

The following sections show the main areas of the visual system after going through the retina and the optic nerve.

1. Lateral geniculate nucleus

The lateral geniculate nucleus (LGN) is the main signal receptor from the retina. It has six layers. Half belong to the ipsilateral temporal area and the other half to the contralateral nasal area (this separation can be seen in the following figure)

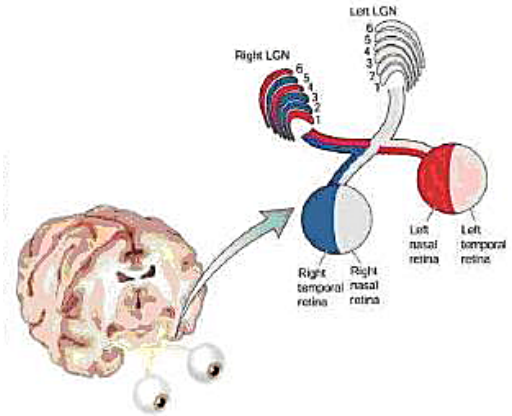

Figure 5.3. Schematic drawing of the connection from the retina to LGN. Source: [BEAR_06]

Layers 1 and 2 are made up of large cells while layers 3, 4, 5 and 6 are made up of smaller cells. The interlaminar cells are also included as part of LGN. In summary, many authors agree on the existence of three parallel channels within LGN that are also physically linked to the different types of layers:

- Parvocellular pathway: made up of small chromatic cells that have low sensitivity and transmission speed. Approximately receive 70% of the signals originated in the retina through the projections of midget ganglion cells. The signals are usually continuous in nature [REID_02]. Although at first two cell types were considered to exist in these layers red vs. green and blue vs. yellow (see [DERRI_85]), later studies have considered that the blue vs. yellow cells correspond to a third independent pathway [LENN_05].
- Magnocellular pathway: made up of large achromatic cells that are highly sensitive and have high transmission speeds. They receive approximately 10% of the signals originated in the retina through the projections of parasol type ganglion cells. The signals are usually transient in nature [REID_02].

- Koniocellular pathway: made up of small cells that approximately receive 8% of the signals originated in the retina through the projection of the small and large bistratified ganglion cells [HEND_00]. Lennie and Movshon (2005) noted that the cells activated by the signal of S photoreceptors are found in these intermediate areas although at times they can be displaced to annex areas. This can explain the reason why at the beginning they were not identified as an independent pathway. This pathway is associated with the stream that brings information from the blue channel [MART_97]. The signals are usually continuous in nature [REID_02].

The following figure shows a diagram with the distribution of these pathways in LGN.

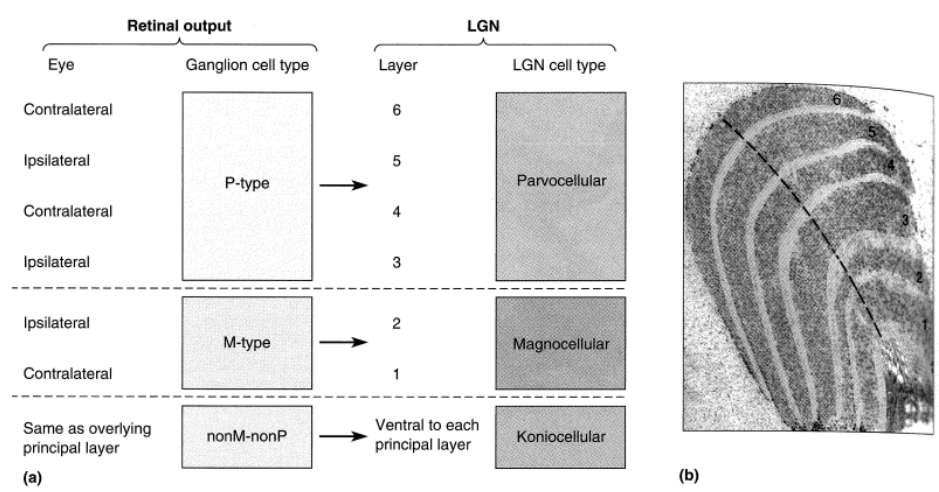

Figure 5.4. A) Organisation of LGN: entries from the retina, its destination in LGN and its possible groupings in the parvocellular, magnocellular and koniocellular pathways. B) Identification of LGN layers. Source: [BEAR_06]

In general, LGN cells are deemed to reproduce signals which come from the retina, which coupled with its better accessibility, has made them the object of multiple research. Regarding the model of this thesis, the proposed classifications of cells that are in this area are of particular interest. The following shows two of these classifications, both from 1966. The first is a reference in many later research and in the study of centre vs. surround opponency and the second classification is related with the processing and models of colour through the analysis of the responses to different wavelengths.

a) In 1966, Wiesel and Hubel identified the following cell types in LGN of the rhesus monkey:
   - Dorsal layers:
     - Type I: colour opponency centre vs. surround.

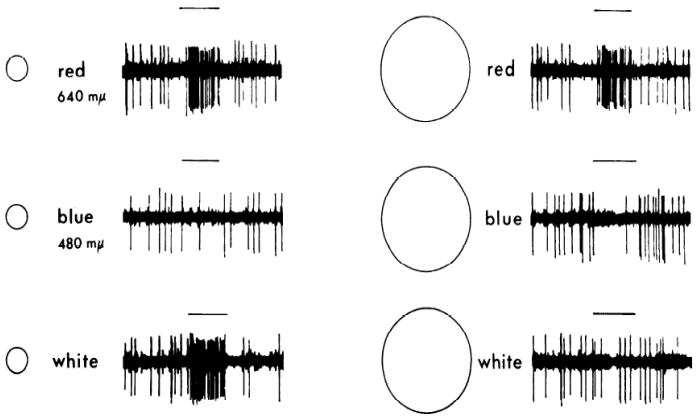

Figure 5.5. Sample of a type I neuron in LGN that shows the sensitivity to red and white stimuli and the dependence with the size of that stimulus. Source: [WIES_66]

     - Type II: colour opponency without spatial opponency, where the receptive fields of each colour component are superimposed.

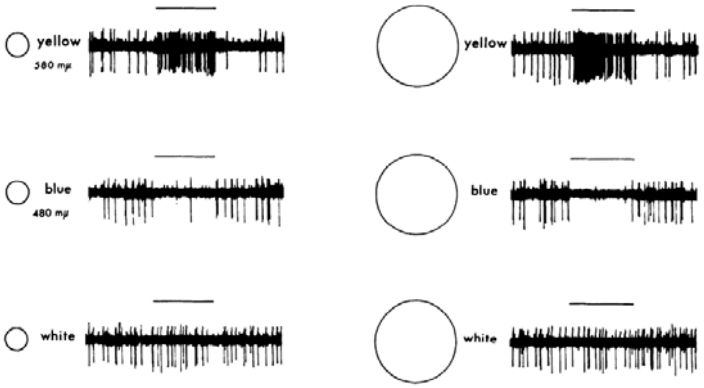

Figure 5.6. Example of type II neuron in LGN that shows the sensitivity to red and white stimuli and the scarce dependence on the size of the stimuli. Source: [WIES_66]

     - Type III: spatial opponency centre/surround with achromatic nature.

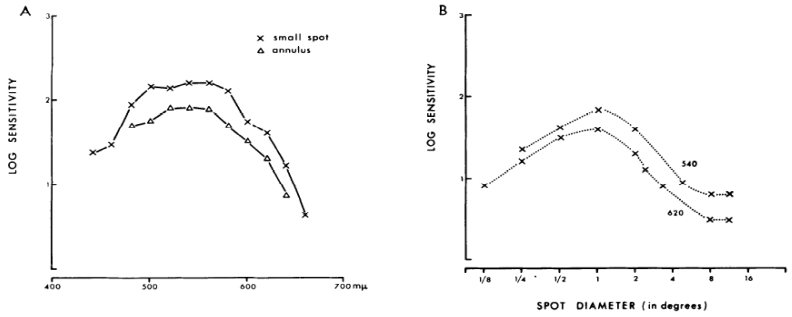

Figure 5.7. Example of a type III neuron in LGN. Left) Response to small stimuli and annulus depending on the wavelength. Right) Response to circle type stimuli depending on the diameter, two wavelengths 540 nm and 630 nm. Source: [WIES_66]

- Ventral layers:
  - Type III: similar to those identified in the dorsal layers.
  - Type IV: centre / surround opponency with brief response signals.

b) On the other hand, De Valois et al. (1966) proposed a cell classification in LGN based on colour opponency:
   - 4 cell types with colour opponency: (+R –G), (+G –R), (+Y –B) y (+B –Y); where + means activation and - means inhibition.
   - Cells without colour opponency that have a similar response in all spectrum wavelengths.

   The following figure shows an example of the measurements obtained when projecting stimuli throughout the visible spectrum.

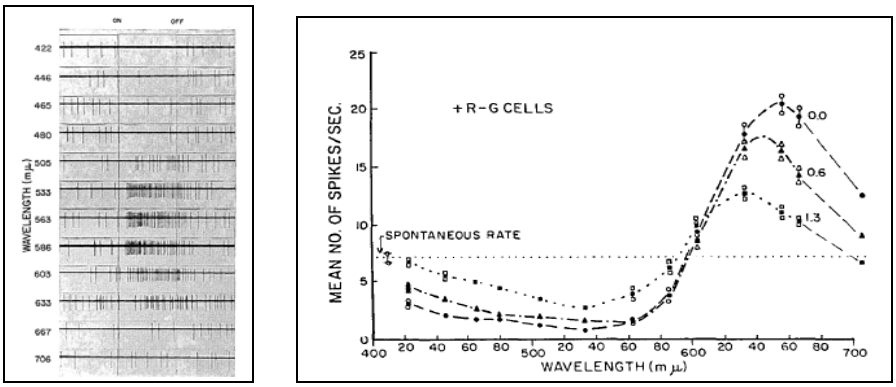

Figure 5.8. Left) Example of cell type (+Y-B): cell measurement obtained with stimuli of different wavelengths. Right) Average cell response (+R-G) for different wavelengths. The dotted horizontal line represents the cell state in the absence of stimuli. Source: [DEVA_66]

From the perspective of the model of this thesis, it should be noted that in LGN the segregation of the visual system in multiple pathways continues and that there are cells with centre vs. surround opponency as well as chromatic opponency. At this point of the visual system there continue to be diverging opinions on whether the surround receives either specific or mixed signals [REID_02].

Lastly, it is important to note that, historically, LGN has been considered a mere transmitter of the signal of the retina to the cortex due to the fact that the measurements of the signals produced in LGN cells are very similar to those generated in retinal ganglion cells. However, they have a characteristic that has not been explained to date: 80% of all signals that reach LGN come from the primary visual cortex (they also receive signals from the brain stem associated with attention and which seem to modulate the response of LGN to visual stimuli).

2. Cortex

The next stage in the visual system is the cortex. It is a layer of about 2mm thickness and has numerous gyri and sulci. Originally it was divided into six layers from I to VI. However, as nine can be easily identified, subregions have been added to the main layers. The following image shows these layers.

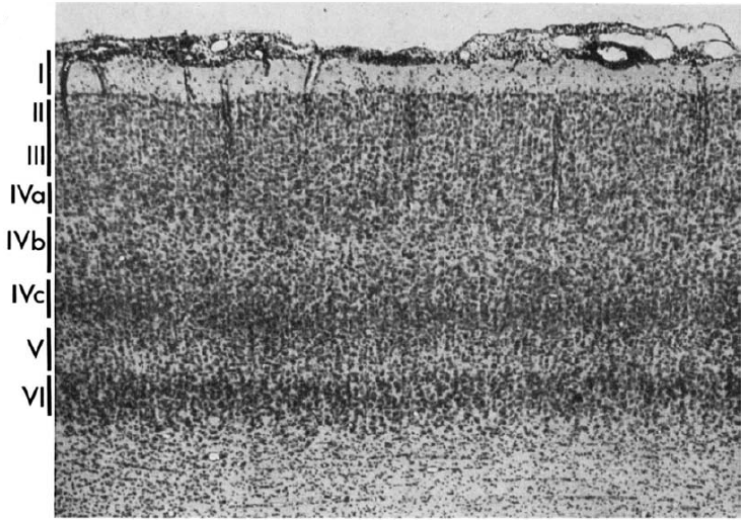

Figure 5.9. Sample of V1 of a rhesus monkey which shows how layer I is mainly composed of axons and dendrites. Source: [HUBE_72]

On the other hand, 32 different areas have been identified that are linked to the processing of visual information and that make up over 50% of the cortex [VANE_94]. The following figure shows the main areas from different perspectives.

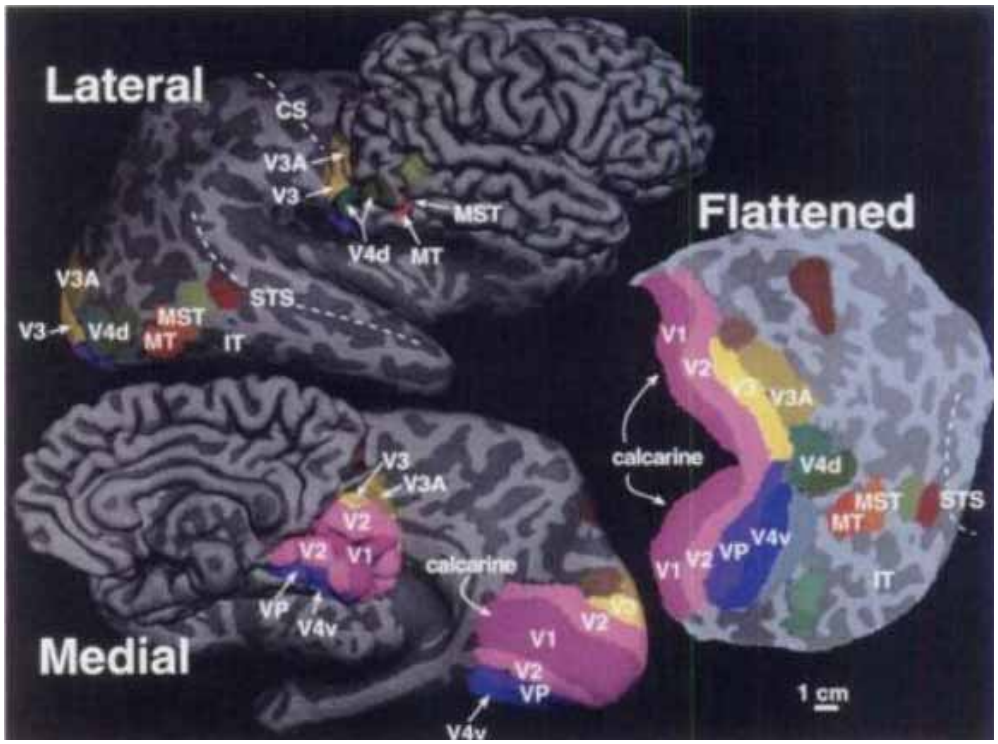

Figure 5.10. Different views of the visual areas of the human brain. The image on the right corresponds to a flattened view of the different areas related with visual perception Source: [BEAR_06]

Their inter-relationships and the processes of each are still to be detailed in-depth. However, there already are organisational proposals, such as that proposed by Felleman and colleagues. Anyhow, one of the most widely accepted issues is the existence of two pathways for the flow of information that are organised in a hierarchical manner [MISH_83, DEYO_88]:

- Dorsal stream: dedicated to the processing of movement and to action recognition, includes areas V1, V2, V3 and MT and higher areas in the visual system. It can be considered as a continuation of the magnocellular pathway from LGN.
- Ventral stream: dedicated to the processing of shapes and object recognition, includes areas V1, V2, V3, V4 and higher areas in the visual system. This pathway is also considered to process colour information. It is identified as the continuation of the parvocellular and koniocellular pathways.

2.1 V1

The first visual area is known as V1, striate cortex o Brodmann area 17. The different pathways from LGN reach different layers within V1 (at these first stages, signals continue to be segregated). This is the visual area of the cortex that has been the object of most research. It has a very characteristic structure [BEAR_06]:

- The signals from LGN reach different sublayers within the layer IV [HUBE_72, HUBE_90, CHAT_03]:
    - The magnocellular pathway is mainly projected to layer 4Cα.
    - The parvocellular pathway is mainly projected to layer 4Cβ (main projection), IVa and a few to layer I.
    - The koniocellular pathway is mainly projected to layer 4A.

    The following figure shows the main and secondary projections. One can see that although there is a main pathway/pathways, the are numerous interlayer connections (there are also horizontal connections inside the layers).

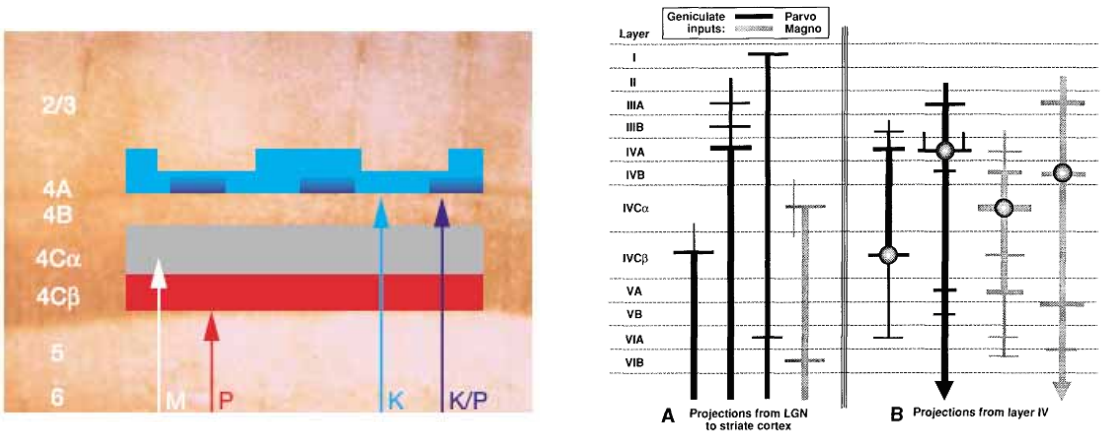

Figure 5.11. Connection structure of LGN to V1. Left) Main connections. Source: [CHAT_03]. Right) General connections that reach layer IV and go out from layer IV. Source: [LENN_88]

- Ipsilateral and contralateral signals continue to be separated in the IVC layer and can be identified as separate stripes, known as ocular dominance columns. The signals from both retinas are combined in other layers of V1 [HUBE_72].

A great number of signal transformations take place in the primary visual cortex from entries projected from LGN. V1 has neurons that are sensitive to lines with specific orientations. In a vertical section of V1, all orientation sensitive cells respond to the same degree of inclination, thus they form column shaped groupings. On the other hand, throughout the cortex plane, the optimal orientation angle varies in a gradual manner. Additionally, neurons can be found within these groups that are selective to these lines but that are also sensitive to direction and to movement (especially if they move perpendicularly to that line) [HUBE_72].

The following figure shows a column scheme, the set of different orientations and the connections from LGN.

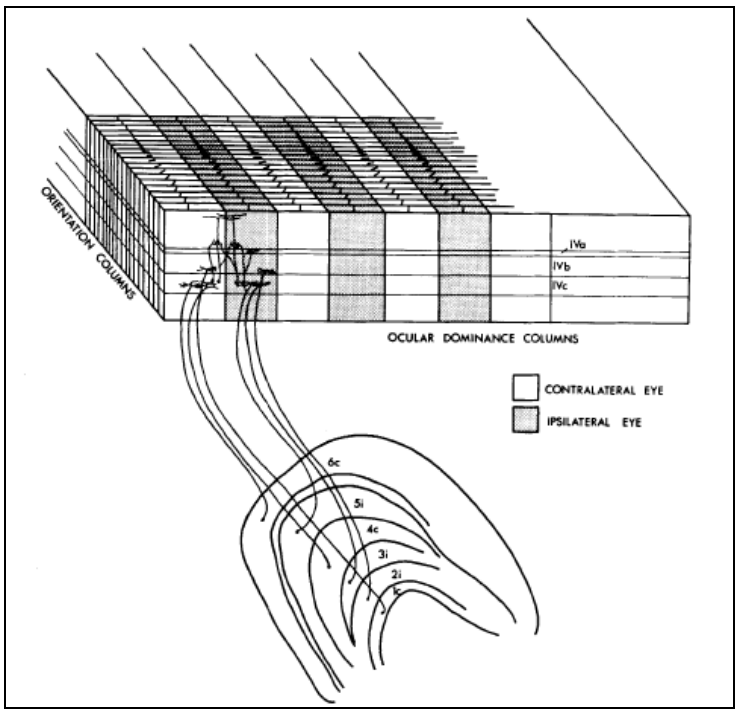

Figure 5.12. Diagram of a possible LGN - cortex connection proposed by Hubel and Wiesel in 1972. Source: [HUBE_72]

- Layers II and III have areas of high concentration of cytochrome oxidase shaped in groupings, known as blobs, that spread as columns in layers IVB, V and VI. Blobs have most of the colour sensitive neurons outside layer IVC. Blobs tend to be monocular and there are no blobs in layers 4A and 4C. [LIVI_84]

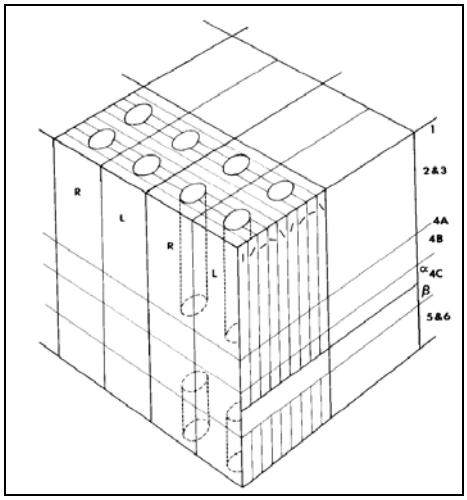

Figure 5.13. Scheme of the modules of V1. Source: [LIVI_84] (modified from Hubel and Wiesel, 1977).

In an area of 2mm x 2mm, 16 blobs can be found, two complete sets with different ocular dominance and a complete sampling of the 180º possible orientations. V1 is considered to be composed of thousands of these types of sets [BEAR_06].

Continuing with the cell-type analysis present in the visual system, the following shows the most relevant classifications proposed for cells in area V1.

From a functional point of view, two types of neurons have been established: simple and complex. Simple cells are mainly specialised in the detection of linear stimuli in specific directions and locations while complex cells detect these stimuli irrespective of their location within the receptive field. Furthermore, simple cells are modelled via a half-wave rectifier while complex use full-wave rectifier.

From a colour processing perspective, some authors have identified other types of cells besides those identified in LGN (Type I, II, ...) although there are diverging opinions on whether there really exist sets of cells with these characteristics [MICH78, LIVI_84, TSO_88, LENN_90, BILL_91 BILL_95, CONW_01, GEGE_03, JOHN_04]:

- Cell with double opponency: have centre vs. surround opponency and also each zone has chromatic opponency. Among the functions of these types of cells are the phenomena of colour constancy and simultaneous colour contrast. (Johnson et al. (2008) also add those of oriented double opponency.) (Conway and Livingstone (2006) noted that on and off photoreceptor signals could be separately wired.)

- ¾ of double opponency: similar to the previous type where colour opponency in the surround is weaker and even achromatic.

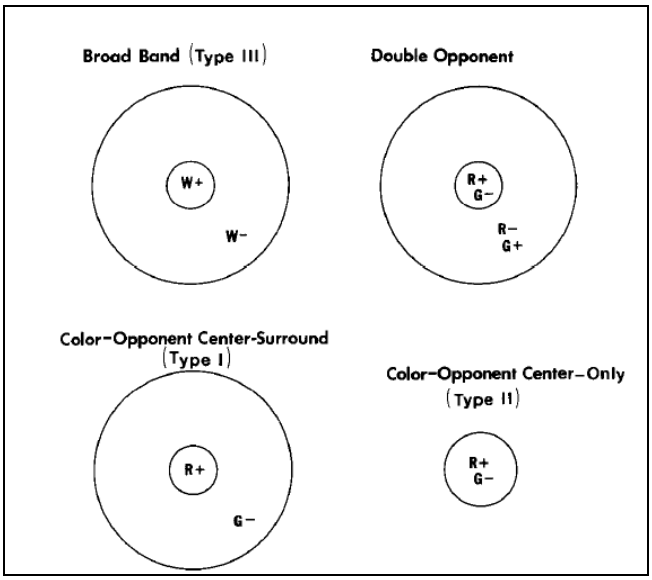

Figure 5.14. Diagram of different cell types in LGN and V1. Source: [HUBE_90]

Proposals have been made for the generation of these type of configurations with retina output signals that are of interest as work models:

a) Billock (1991) proposed a multiplexed signal model. The chromatic information and the signal of the edge presence can be transferred through opponent cells (simple). The following figure shows how this multiplexing is achieved.

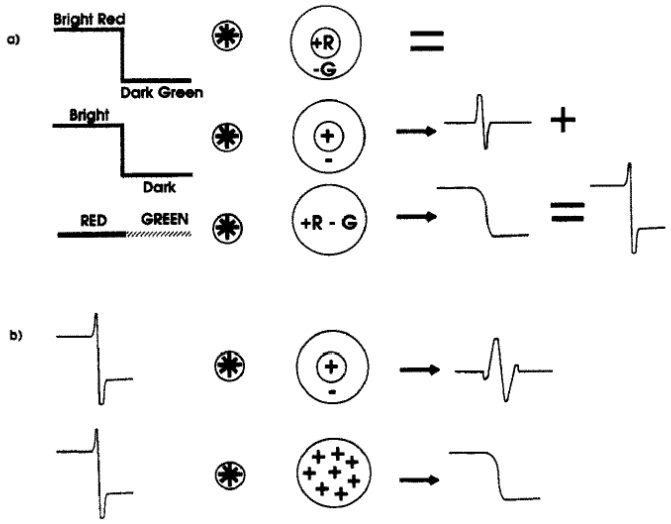

Figure 5.15. Proposal for information multiplexing (chromatic and achromatic) in a sole signal. Source: [BILL_1991]

b) Huble and Livingstone (1987) proposed two models of double opponency generation that arise in a direct manner: one proposal is the combination of two opponent cells (simple) with opposed chromatism and another is the combination of simple opponent cells in an area of circular configuration where there would be opposed chromatisms. Both raise serious issues, the first clearly doesn't show the centre vs. surround opponency while the second case probably also doesn't generate effects in centre vs. surround opponency through an indiscriminate connection of all cells in an area, although there will always be doubts on whether the connection are modulated afterwards.

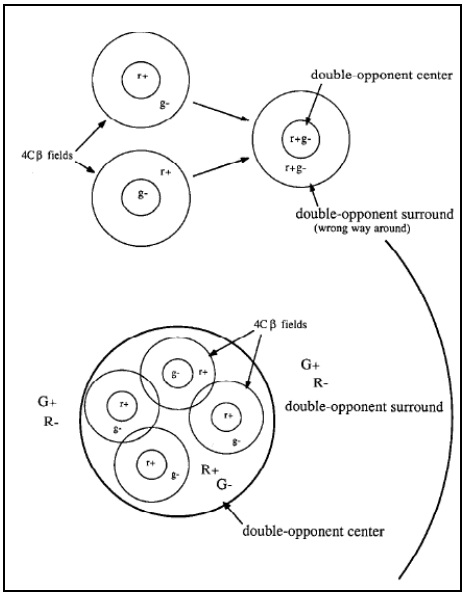

Figure 5.16. Example of two possible circuits to build double opponent cells.
Source: [HUBE_87]

c) Conway and Livingstone (2006) proposed a generation model of cells sensitive to oriented lines and to cells with double opponency through different cell combinations based on linear and circular spatial organisation. In the case of double opponents it is not clear how to make the connections through the centre and through the surround with a annulus structure.

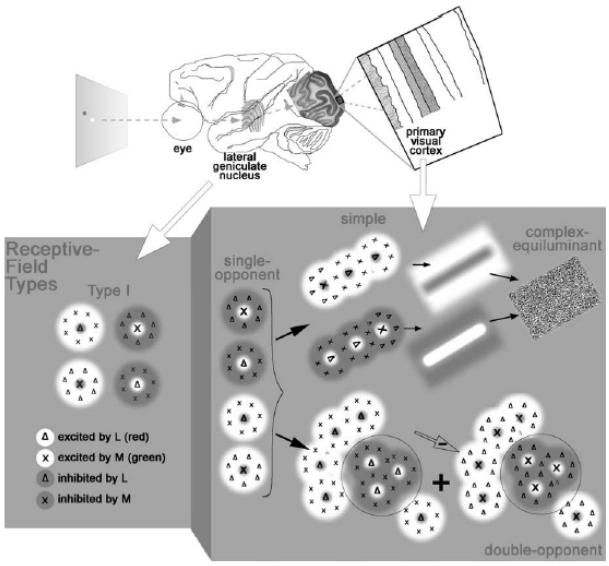

Figure 5.17. Schematic drawing of the connection from LGN to V1. Double opponent cells have 1º centre / 1.7º surround and would be made up of combinations of type I cells of 0.24 – 0.5º. Source: [CONW_06]

V1 is the main entry gate of the visual system to the cortex. It is an area with a column structure that is very typical with sensitive cells to oriented stimuli and to colour elements. Some researchers work with Gabor filters to model oriented lines (see Serre (2006) as an application example) and although proposals have been set forth for chromatic stimuli there still is not one that is widely accepted.

2.2 Beyond the striate cortex

Most visual signals reach the cortex through V1 and are transmitted on to the following areas in the visual system: V2, V3, V4, MT… V1 project mainly to V2 although also directly to V3. The main projection areas of V2 and V3 are V4 and MT (see figure 5.2).

As we continue through the visual areas, each neuron is shown to be influenced by an area of greater size of the visual field and optimal stimuli become more complex. For example, the receptive fields in V4 are greater than in V1 (at 1º of eccentricity they are four times larger (16x in are a) and at 3º they are six times larger) [DESI_85].

A brief look at the visual areas involved in the parvocellular pathway is necessary as the parvocellular pathway and the ventral stream are deemed as the areas that deal with chromatic signals:

- V2 (or area 18) there are greater density bands, known as stripes, which alter between broad, narrow and interstripes. The blobs in V1 are connected to the narrow stripes while the interblobs are connected to the interstripes. Additionally and in any case, stripe-stripe and interstripe- interstripe connection are also known [LIVI_84]. The following shows a schematic drawing of the possible hierarchy of connections.

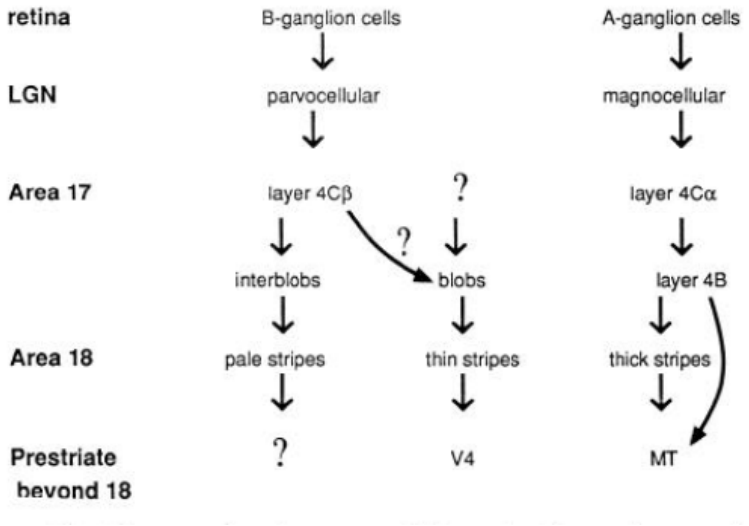

Figure 5.18. Proposed scheme of the connection from the retina to V2 and from there to V4 and MT. Source: [HUBE_87]

As in other cases, there are other possible interpretations (see Sinich and Horton (2005) for a revision).

- Cells sensitive to stimuli with varied shapes have been found in V4. A double effect of convergence (different areas of V2 are projected to the same areas of V4) and divergence (the same area is projected towards several areas of V4) is originated from the narrow stripes and interstripe of V2 [DESI_85]. The following is a proposal by Felleman and colleagues of the processing scheme.

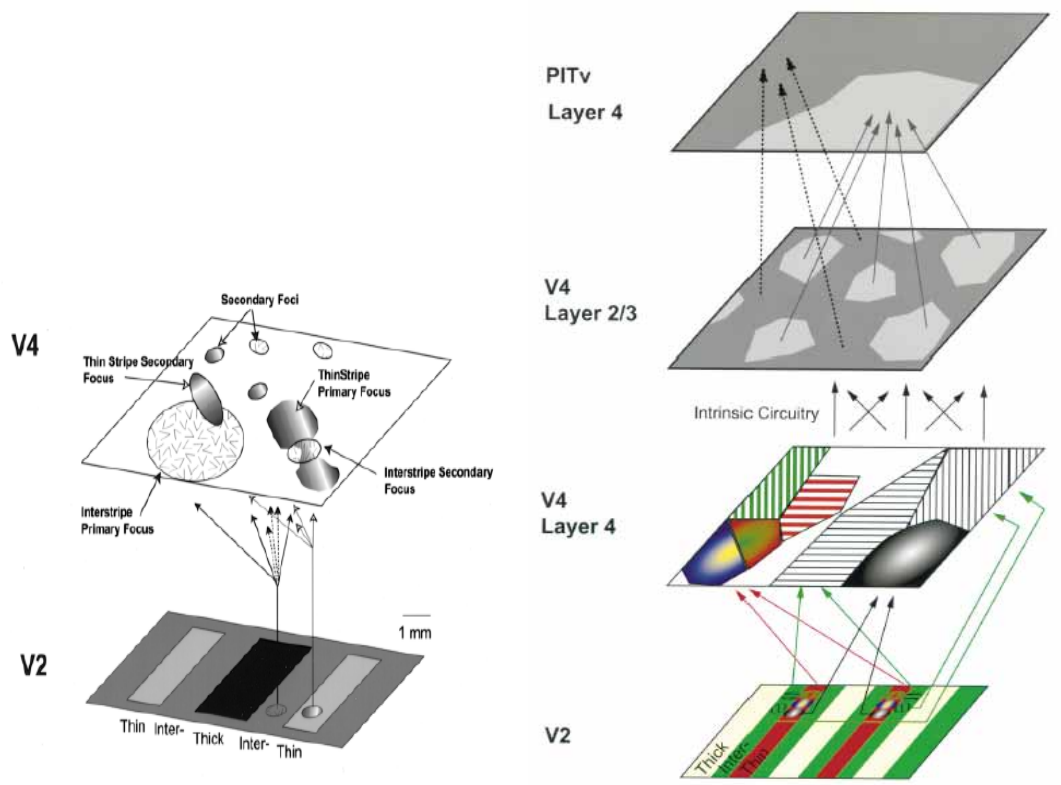

Figure 5.19. Left) Each area of V2 is projected to a main area of V4 and to several secondary that are meshed with the opposite primaries. Source: [XIAO_99]. Right) Schematic diagram of the feedforward conditions from V2 to V4. Source: [FELL_ 97]

Conway et al. (2007) set forth the division of the V4 areas into glogs (highly colour sensitive) and interglogs (shape sensitive) and formulated the hypothesis that glogs receive signals from narrow stripes. They noted that they had found these two types of areas (glogs v. interglogs) in V4 and that this feature could explain the contradictory results that identified V4 both as a specific as well as non-specific area for colour processing.

- V4 projects towards the inferior temporal cortex (IT) which has great receptive fields and from IT towards the frontal and temporal lobes where they probably combine with other types of non-visual information [SERR_06]. IT could be dedicated to gathering information from V4 and generating a representation of shapes and contours.

Regarding colour, several options have been set forth regarding what is the area of the cortex where the processing of chromatic signals are combined in order to generate the hue perception:

Zeki (1980) identified sensitive neurons to specific colour stripes in V4 although later studies have questioned its validity, while Xiao et al. (2003) propose that V2 already has neuron groups that are tuned to hue.

3. Conclusions

Similarly to what was presented in Chapter IV on the retina, precise knowledge is still lacking on the processes that take place in the first areas of the visual cortex. However, some of the basic pieces are being identified.

From the retina, the segregation of information continues in multiple pathways towards the layered structure of LGN and towards V1.

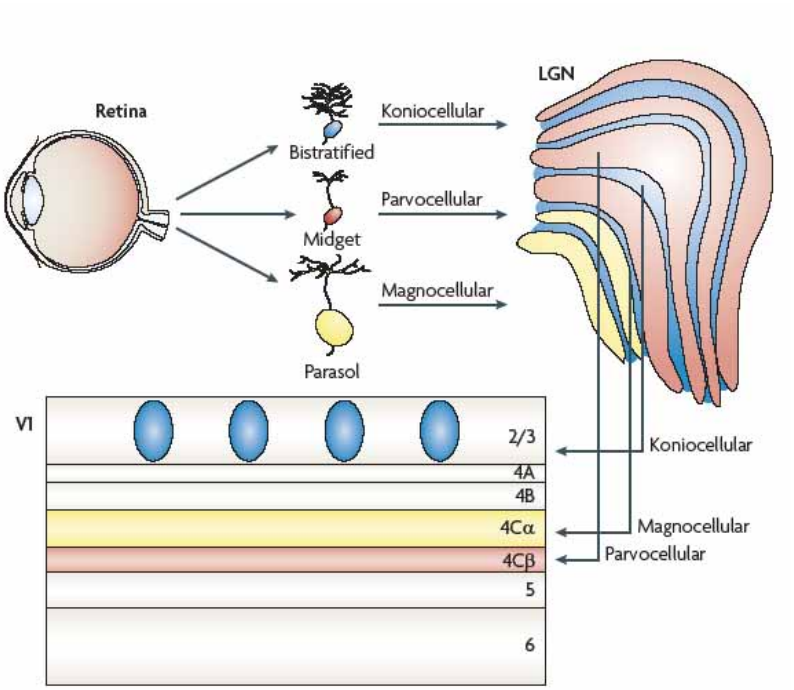

Figure 5.20. Schematic drawing of the pathways from the retina to V1. Source: [NASS_09]

There is once again a layered structure in the primary visual area which also has ipsilateral and contralateral columns as well as oriented columns and blob columns.

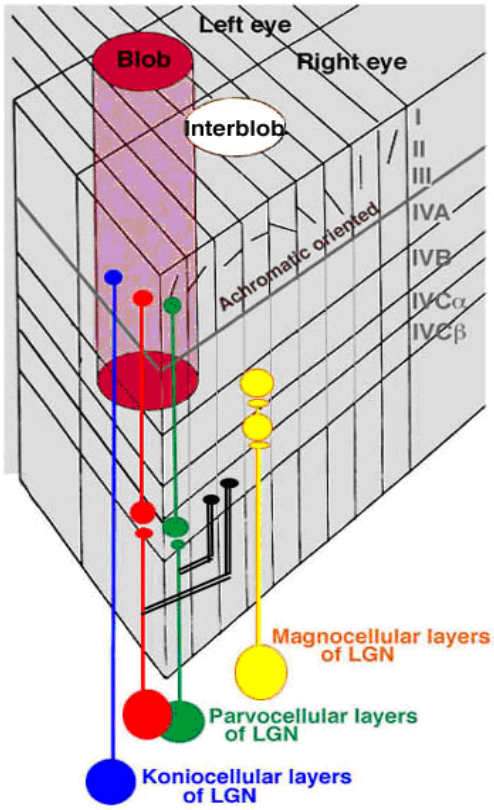

Figure 5.21 V1 structure. Source: [WEBV]

V1 projects to both narrow and wide stripes in V2 as well as to intermediate zones and from there towards V4, MT and higher areas.

The following figure shows an organisational proposal that shows the main areas, the sequence of processes and the selective stimuli in each area. Three pathways reach from LGN: M (high temporary resolution, low spatial resolution), P (high spatial resolution, low temporal resolution) and K (low spatial resolution). These branch into two streams when they reach the cortex: one deals with the location of elements and the other with their identification. The first begins in V1 where it identifies simple shapes (segment orientation) and the difference in signal wavelength. It progressively coordinates more complex shapes and colour components in its following stages. The second processing stream begins by identifying orientation and direction. As it advances through the visual system, it detects each time more complex movement patterns.

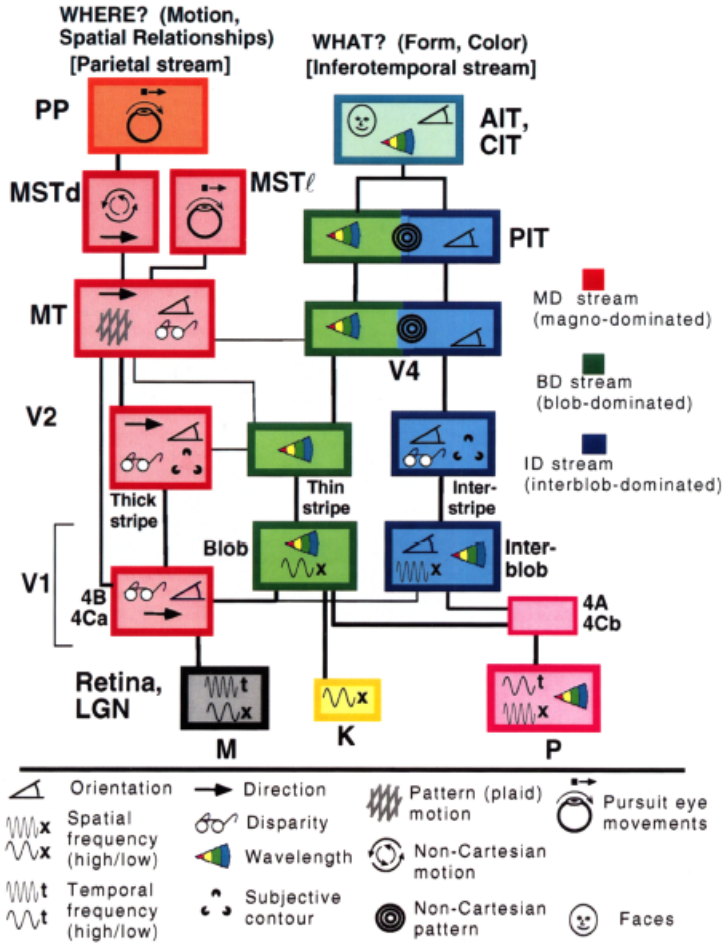

Figure 5.22. Hierarchical sequence of processes in the macaque. The main streams have been named based on their origin in LGN. Dorsal and ventral streams are used in latter areas of the hierarchical vision. Source: [VANE_94]

Before finishing this chapter, three additional issues must be mentioned. Although three main pathways are deemed to exist (parvocellular, magnocellular and koniocellular) other proposals, such as Masland et al. (2007), indicate the existence of up to 12 different pathways. Another way of interpreting the processing as edges and colours is that set forth by DeYoe et al. (1994) where the aim would be to identify an object's boundary and hence its shape and the interior features of the surfaces (where other attributes such as texture would be taken into account besides colour). Last, despite some proposals (Zeki (1980), Xiao et al. (2003), Stoughton and Conway (2008)), at present there is no conclusive evidence on which is the place or the area in the visual system that has the representation of colour hues.

Chapter VI

Functional model of the retina

This chapter presents a functional model of the human retina. The model is based on the analysis of the retina and the latter phases in the visual system that have been undertaken in this study. The main objective is to model the processes that take place in the retina with chromatic component signals. This first version of the model shall not include temporal components that may be part of future works.

Firstly, other retina models are analysed. Then a model scheme with the different stages and structure is presented. Next, its parameters are compiled based on anatomical and physiological data. Those parameters that are not directly available will be estimated. Then, the results obtained in each layer of the model when presented a set of stimuli shall be shown. Finally, the results of the model when presented sample images shall be presented. The chapter concludes with the conclusion section.

1. General models

This section aims to present the most relevant retina models that have been submitted to date. The retina is a highly complex organ. There is no proposal that models it in its entirety. Therefore, each model looks at one or more of the following issues:

- Connection structure.
- Nature of the connections.
- Temporal behaviour.
- Achromatic and chromatic pathways.

Many of the models make proposals on the structure and nature of the retina connections. These models aim to define what could be labelled as the retina architecture.

The structure of the models begins in the photoreceptor layer. Some proposals model it as a square grid (as a conventional image), others as a hexagonal [SIMI_91, HEAR_95], some by means of random models [MOMI_06, DEVA_93] while others are based on real samples of the retina [LEBE_07]. Horizontal and bipolar cells can be found in the second layer of this architecture. Some models place the opponency streams in this layer [SIMI_91], while others attribute it to the amacrine cell effect [LEBE_07]. Some models, after this stage, include it in the amacrine cell layer. Ganglion cells are situated in the final stage.

There are models that specify the number of connections between the different types of cells on this structure, such as DEVA_93, HENN_02, MOMI_06, SAGL_08 and SHAH_96. Additionally, different subtypes can be found within each of these types of cells, such as: on and off type cells [SAGL_08], different types of ganglion, amacrine and bipolar cells [BALY_02], type P and M ganglion cells [DEVA_93], midget bipolar and diffuse as well as P and M type ganglion cells [SHAH_96] or midget, parasol and bistratified ganglion cells [HATE_02].

The cells that make up this architecture have different levels of detail. Each cell is labelled according to its spatial behaviour and at times can also include its temporal behaviour. The most common spatial models are made up of a combination of different size and amplitude Gaussians [RODI_65, LEBE_07, XU_02, WOHR_08, HENN_02]. There are other proposals such as the Mexican hat [SAGL_08] or the use of Gaussian derivatives [GHOS_08]. The following figure shows these functions.

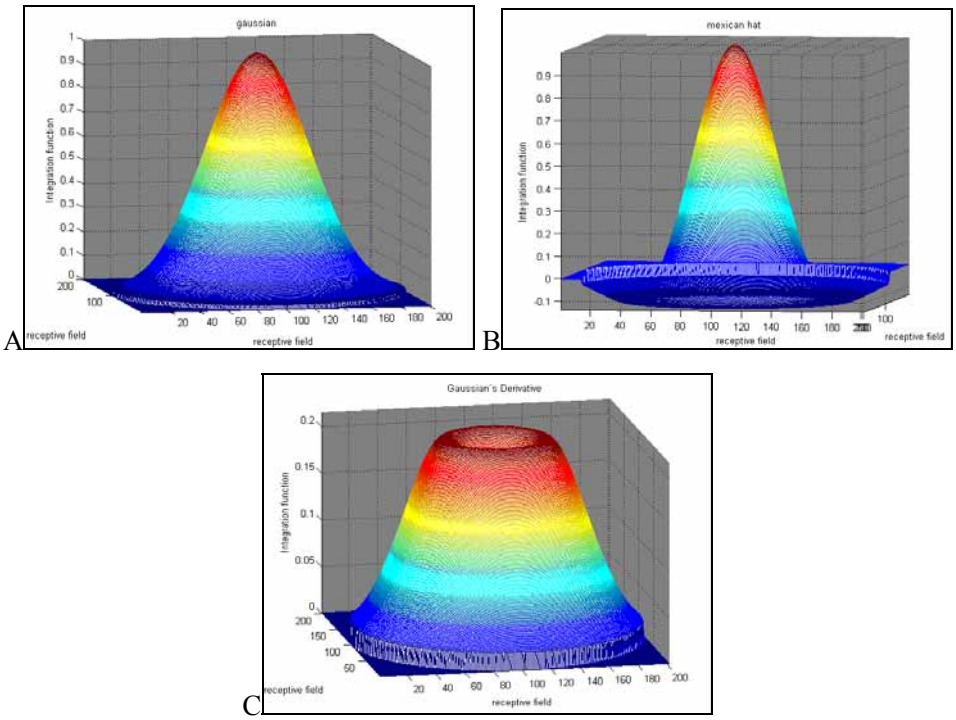

Figure 6.1. Representation of the different spatial modelling functions of a cell's receptive field. A) Gaussian function. B) Mexican hat. C) First order derivative of a Gaussian.

The set of stimuli that reach the cell's receptive field (x and y axis) are integrated in a weighted manner based on their position in the receptive field and according to the function that models its behaviour. This can be expressed in the following manner:

$$Cell\ stimulus = \int_{\text{Cell receptive field}} f_{\text{spatial model}}(x, y) * \text{Stimulus}(x, y) \qquad \text{(eq. 6.1)}$$

The cell's temporal behaviour allows comparing the model results in dynamic processes directly with the neurophysiological measurements, although this entails substantially increasing their complexity (usually the overall complexity is reduced by simplifying other aspects of the model). The models with temporal components are based on equations with partial derivatives that include feedback and feedforward components. The most common strategies in models with temporary components are: integration and fire models (IF) and linear-nonlinear models (LN) (see [KOCH_99] for a summary).

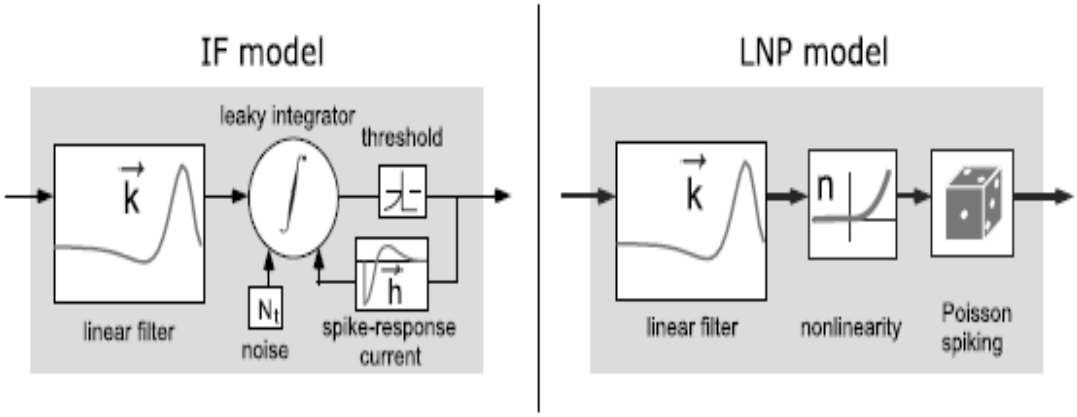

Figure 6.2. Left) Integration and fire model. Right) Linear-nonlinear model. Source: [PILL_05]

Although earlier models are applied to different cell types, in the case of photoreceptors, specific functions are used such as photoreceptor signal compression based on the equations of Naka-Rushton and Valeton and Van Norren, where the exponential factors and the constants are adjusted [SHAH_96, SAGL_08, VALB_08, KUNK_09].

The most common functions for connecting the different cells layers are the weighted sum and subtraction of signals. However, some authors [ZAGH_04, GROS_95, DIAZ_08] use division, such as the shunt inhibition model or the gain inhibition that has been previously described and used in other applications [CARA_94, HEEG_96, TORRE_78].

Spikes are produced as the output of ganglion cells. The most common function of transformation to generate spikes is by using exponential functions [PILL_08], Poisson processes or Gamma distributions [MEIS_99].

Models with colour components

As a whole, retina models that have been developed up to date are focused on achromatic components. In the case of the different colour retina models entail variable abstraction levels on a physiological reality. These models can be classified according to three types:

A. Those models that include chromatic pathways as an extrapolation of the behaviour of achromatic components and that habitually are represented as an opponency channel red vs. green [LEBE_07, BARR_96] and additionally another yellow vs. blue channel [SIMI_91, VALB_08, ANDR_03, DIAZ_08, HATE_02].

B. The theoretical proposals that establish a cell connection scheme in order to reproduce cell features that are observed in physiological experiments. The majority include post-retina stages in LGN and the cortex [DEVA_93, MICH_78, VALB_08].[10]

C. Mixed models, which include a bioinspired part and another of colour attribute calculations without a direct basis on anatomical or physiological measurements [GUTH_91, KUNK_09, RUDE_98].

2. Model introduction

The present model proposes a human retina architecture that establishes cell layers, number of connections and their nature as well as the spatial characterisation of each cell. This retina structure is based on anatomical and physiological data.

The aim of this model is to identify and analyse the different pathways that reach LGN and the cortex from the retina with a special interest in those of chromatic nature. In order to achieve this, the model generates a set of output channels from the retina through different types of ganglion cells. In this way, a set of output signals from the model are obtained that have spatial as well as specific chromatic features, which differentiates it from models that extrapolate achromatic channels results to the chromatic channels or that integrate the centre surround opponency idea in the red vs. green and yellow vs. blue channels (A type models in the previous section).

Regarding theoretical and mixed proposals (type B and C models), this model is not limited to a scheme proposal but rather provides detailed description of the connections, sizes and layers that

[10] It is worth to mention that there are several proposals on how LGN signals are combined in the cortex (see chapter V section)

are present in the retina and generates responses of each cell type to a stimulus. Furthermore, the model is not ascribed to only simple or very controlled stimuli but rather accepts real images as entries.

All this entails that this model reaches a level of detail that present day colour models have not reached to date. It is noteworthy to mention that this model provides a second contribution regarding other proposals, that is, it can be used with complex real stimuli. This feature is of special relevance for machine vision systems as the model will be able to be used in real situations.

3. Model structure

> "*The underlying retinal anatomy is followed, the characteristics of the physiological models, however, are kept simple*" Bálya et. al 2002

The following shows the model structure and its different elements. As with every model, there is a simplification of the true nature of the aim of the research. Part of this simplification is achieved through hypothesis and previous considerations on its reach and context. This model has taken into account the following:

- The model is ascribed to the fovea area. Given the variations that are present in the different areas of the retina, the model will represent the fovea area, as most studies on colour perception are ascribed to the central area of the field of vision (2º or 10º) and as midget ganglion cells are only connected to one photoreceptor in this area.

  Effects related to the central area of the fovea that are free of S type cones are not included.

- The system is structured in layers that are sequentially organised. Similar to what has been studied regarding the retina (see Chapter IV), the model generates pseudo images (images meaning ordered spatial representation of the field of view) for each layer and cell type. The set of output signals of each layer is combined in the next layer according to the connections of each cell type.

- The only layer that has lateral transmission is that of horizontal cells. There has not been a specific modelling of the connections between same type cells, whose reach and modulation are not known at the time of writing of this thesis. However, the Gaussian functions are slightly extended beyond the cell dendrite field, as a first approach to this effect.
- Amacrine cells are not included as they seem, a priori, to be related to temporal processes.

  The following figure shows a schematic drawing of the layers that are included in the model and the information flow.

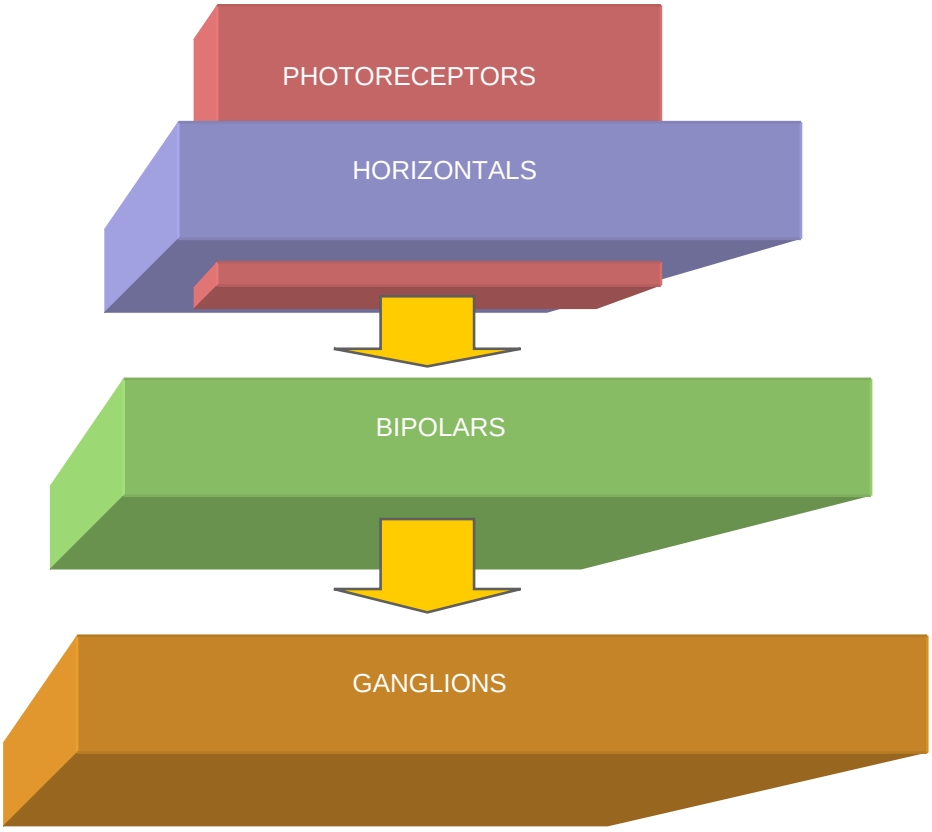

Figure 6.3. Diagram of information flow and connections between model layers.

- Each cell incorporates signals within its receptive field through the use of a Gaussian. Although there are other proposals such as the Mexican hat or the derivates of Gaussian models, most retinaL cell characterisation systems use Gaussian models.

- The output signal of each layer is deemed homogenous in all of its axon arbours. The reason to use this simplification is that some output arbours are very compact, such as photoreceptor pedicles, which decreases the possible variation in the output signal.

  The following figure shows the concept of a Gaussian integration and a homogeneous output.

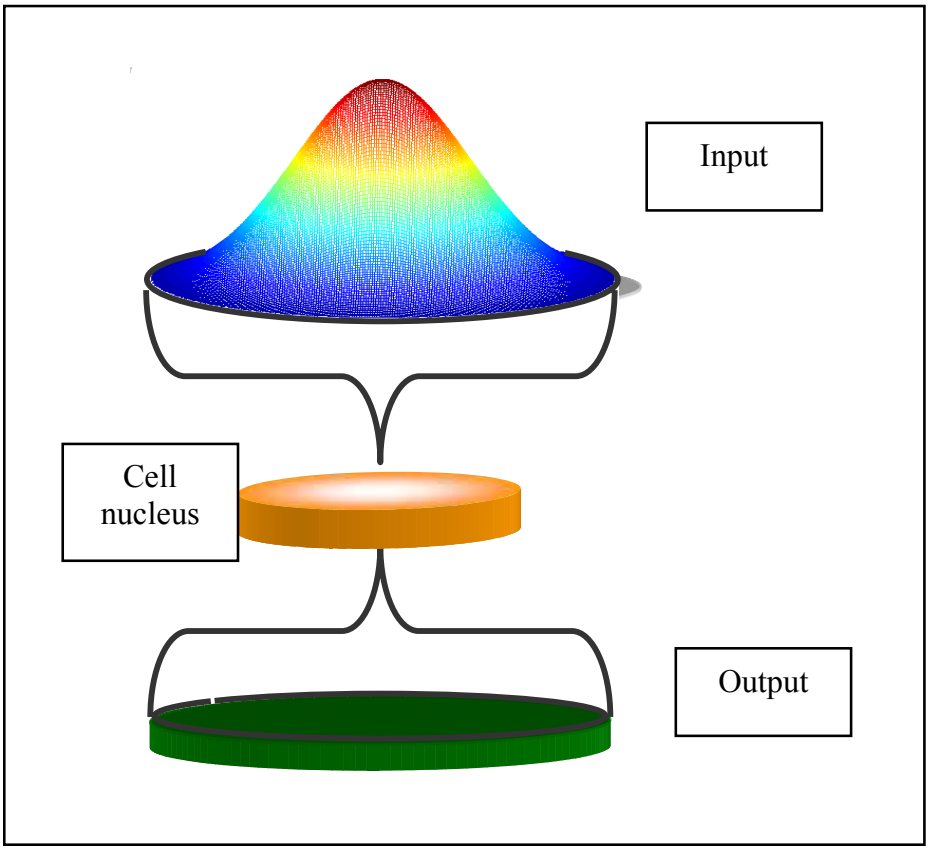

Figure 6.4. Schematic drawing of the weighted entry of a Gaussian and a constant output.

- All cells work with continuous signals except the output of ganglion cells that generate spikes as output. This is one of the specific features of the retina.
- The cell distribution in each layer shall be homogeneous, marked by the cell density and the overlapping factor. This is a simplification taken in order to be able to trace the connections with the upper and lower layers of the model in accordance with the average values available in scientific publications.

- There will be 3 layers of photoreceptors each point is sampled by only one type of cone, either L, M or S, but the model will have three layers. The average percentage of each of the photoreceptors that are present in a retina shall be used in order to adjust the weights of the different photoreceptors.
- The type on and off cells shall be the same size for each cell type. Although there are size differences in their average values, the model will simplify this issue by establishing the same size for both types.

Some of these entail an important reduction in the processes undertaken in the retina but have been included in order to obtain a functional simplified model.

The following shows a general diagram of the model. It represents the input signals of the system, the different cell types, the data flow between different layers and the set of outputs of the system. The input signals are colour images characterised by their XYZ or RGB values (which are transformed into their XYZ values). These values are transformed to the LMS photoreceptor space where each value indicates the input signal that each photoreceptor receives. In turn, these initial values are integrated over the receptive field of each photoreceptor (see equation 6.1). Next are the horizontal cells that receive the signals generated by the photoreceptors.

The signal of photoreceptors and that of horizontal cells are integrated in the stage of bipolar cells. Different types of bipolar cells are generated depending on the sizes of the receptive fields and the signal combinations of the different types of photoreceptors and horizontals.

Finally, the set of output signals of the model set are obtained from the signals generated by ganglion cells. Each type of ganglion cell receives a specific combination of signals from different types of bipolar cells.

The ways to combine signals in the model shall be set out in the following section: *Model parameters.*

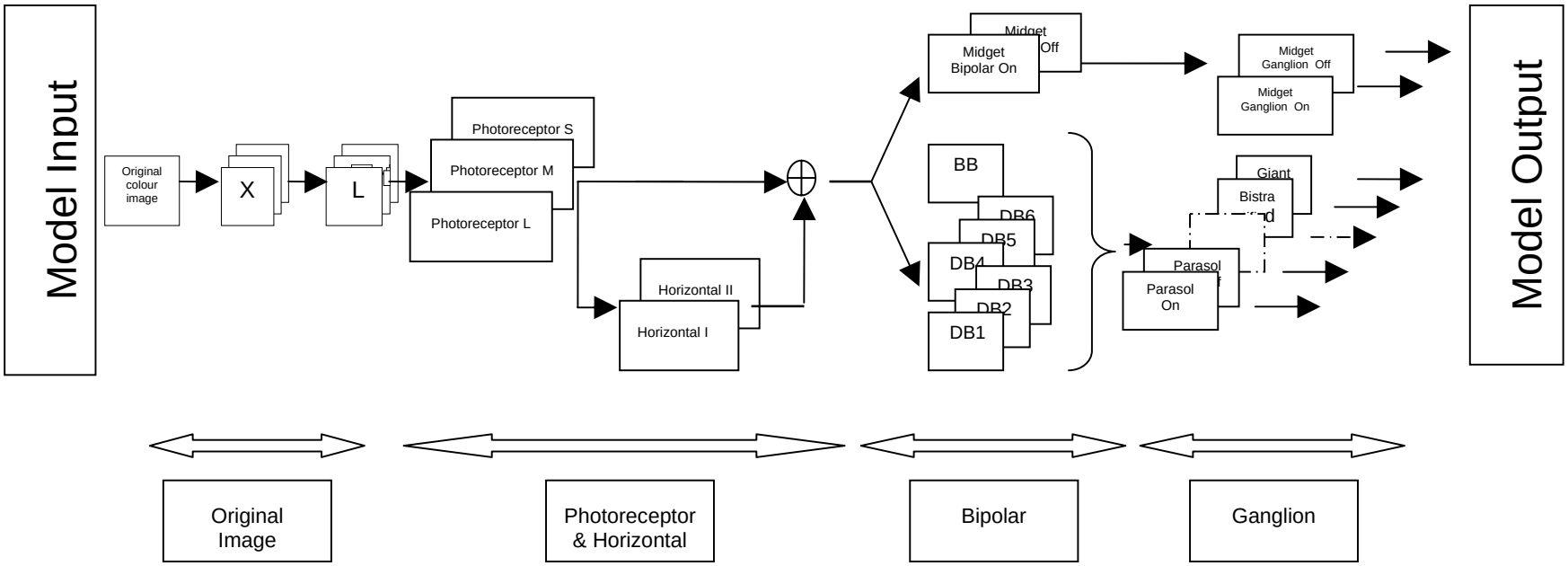

Figure 6.5. Model diagram. The different layers, information flows and their relationships with the different cell types are shown. BB: bipolar blue; DB1-DB6: bipolar diffuse type 1 to 6.

4. Model parameters.

The model proposed in figure 6.5 contains the following parameters:

- **General parameters:**

  - The system's input signals are between 0 and 1. In order to do so, the signals must be normalised regarding their maximum and minimum values. The model will be used with conventional colour images where the maximum and minimum values are 255 and 0 for each colour plane.

  - The relationship between the image pixels and the size of photoreceptors. This parameter can be adjusted according to the selected level of detail. A high value shows the influence of mesh cells while low values speed the processing times. (This value shall be known as RADIUS_PIXEL_SCALE).

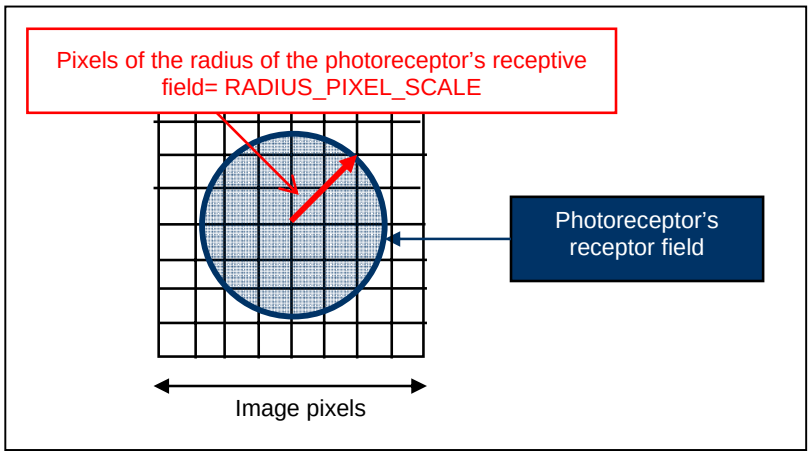

Figure 6.6. Relationship between an image's pixels and the size of photoreceptors.

- **Cell parameters**

  Each type of cell present in each layer is characterised by:

  Parameter type 1. Type of cells to which it is connected and their weights which indicate the contribution of each cell type to the input signal of the cell to which they connect.

  Parameter type 2. Integration radius: indicates the circular area within which the connections with the cells of the earlier layer are established and which constitute

their input. This parameter can be defined by the diameter of the dendritic field or by the number of cells connections established in the immediately preceding layer.

The following image shows a cell connection scheme and the set of cell connections established in the immediately preceding layer. Each cell is represented according to the scheme of figure 6.4, its inputs in blue, the nucleus in orange and the outputs in green.

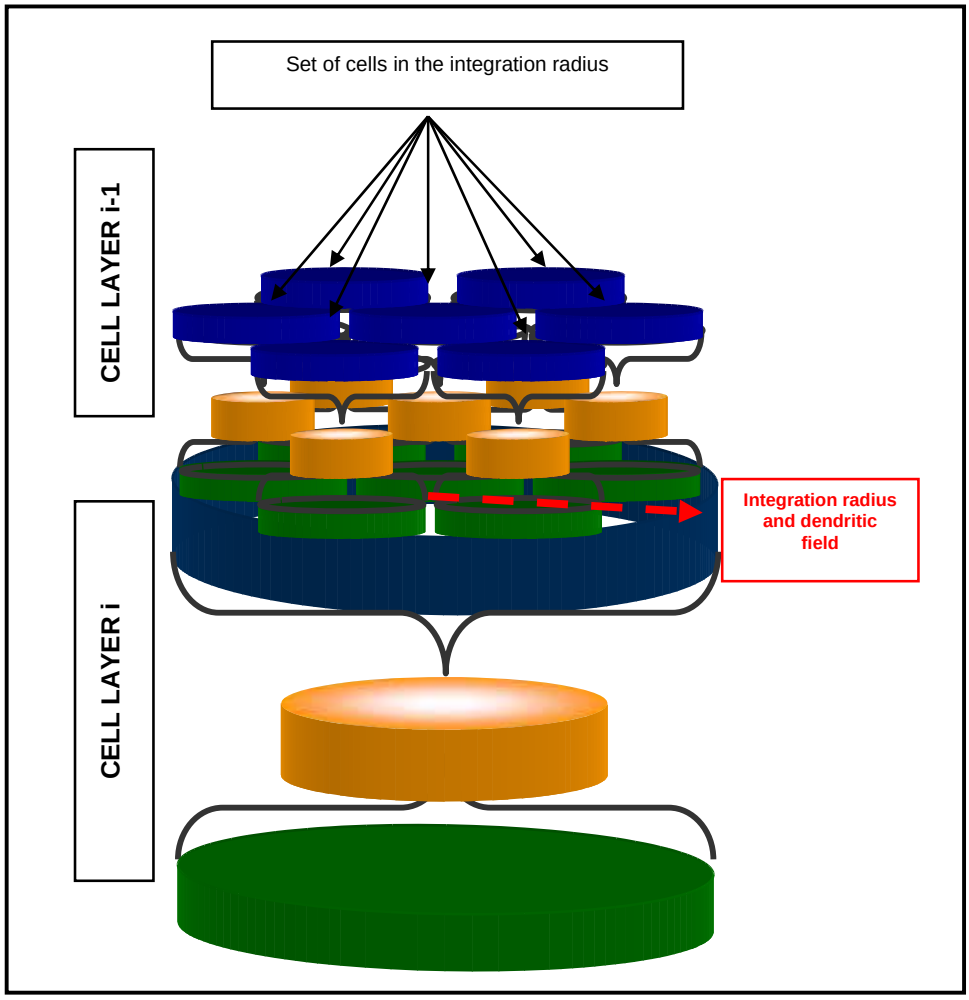

Figure 6.7. Definition of the integration radius through the representation of a cell and the set of connections established in the previous layer. Each cell is represented according to the scheme of figure 6.4, its inputs in blue, the nucleus in orange and the outputs in green.

Parameter type 3. Cell distribution or mesh. Each cell is placed in a specific position within the xy plane of the retina: $\{x_{cell}, y_{cell}\}$. The z coordinate sets the depth within the retina where each cell type can be found. The set of cell positions that belong to a same cell type constitute the distribution or mesh. This parameter is defined by the cell density and/or the overlapping factor, which is the number of cells of a certain type that sample a point in the retina.

The following figure shows an example of the relationship between the overlapping factor and the (mesh) positions of two types of cells in consecutive layers. A set of type i-1 cells (blue coloured circles) and a sample of type i cells (green coloured circles) are represented.

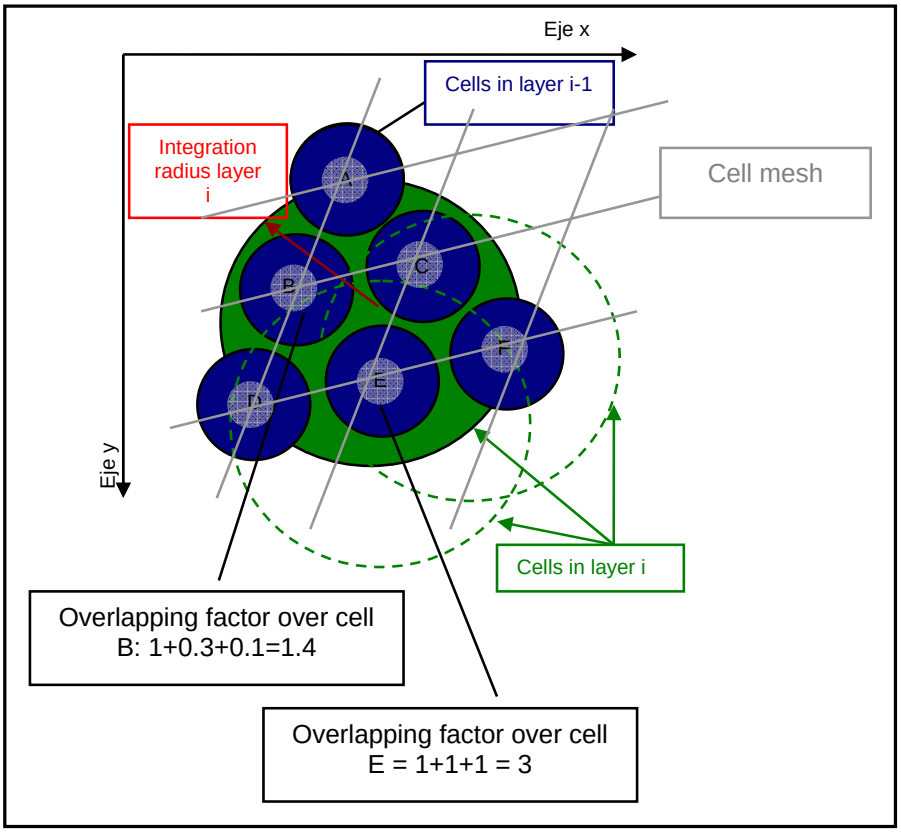

Figure 6.7. Representation of the overlapping factor of cell in layer i. Each cell is placed in a specific position $\{x_{cell}, y_{cell}\}$. This set of positions make up the distribution or mesh of each cell type.

4.1 Cell parameters: biological data

The following will provide information on the parameters needed for the model, specifically the type 1 to 3 parameters of the previous section. Some are directly taken out of chapter IV and others need additional calculations that are shown below.

First, the data obtained in the retina study related with the cell parameters of the model will be compiled (see Chapter IV).

The number of connections with the immediately superior layer is going to be used in order to be able to establish the size of the dendritic fields of the different cells. This way, the fields of the remaining layers can be calculated based on the receptive fields of photoreceptors as a unit of reference. The available information sources for this calculation are:

- Dendritic field or integration field: physical size of the dendritic arbours.
- Receptive field: size of the stimulus with influence in the cell. It is larger than the dendritic field as it includes the effect of interneuron connections both in the same as well as in previous layers.
- Number of connections with cells in the previous layers (its receptive field can be established if one knows this information plus the cell distribution in the previous layer).

The overlapping factor, which is the number of same-type cells that sample a point in the retina, is going to be used in order to calculate the distribution. An additional data is the number of cells of each type which.

Table 6.1 shows these data for the different cell types included in the model. All data for all types is not available. The aim of the model is to define a general processing structure in the retina, although it is highly probable that the parameters will vary not only within the class (within the primate order) but also between different individuals belonging to a same class. The optimisation of the values of the integration radius, the number of connections and the spatial distribution based on the results of colour perception are considered as an additional project.

Cell types		Number of connections with the previous layer	Overlapping factor	Dendritic field diameter	Diameter of the receptive field	Units
Photoreceptors	Cones	1 cone can connect with 15 diffuse bipolars and with 2 midget bipolars	1	1-4 µm (b) Average size in the fovea: 4.8 µm / 0.7'	--	4.6 million (a) (maximum 200,000unid /mm^2)
	Rods	700 HI (m) 2-5 rod bipolars (each bipolar 50-60 rods) (i)	1	1 µm (b) near the fovea	--	92 million (a)
Horizontals	HI	- According to size 17 cones (e) - According to receptive field 162 cones (d) *50-60 rods (i)	3.7 near the fovea (f)	- 20µm (e) - 18-20 µm (p) {40-60µm in the periphery (p)} - 60µm x 40µm (11mm exc.) (c)	122µm at 4mm exc.[11] (x3 DF (e)) 309 µm 11mm exc. (d)	500.000 (g) Ratio fovea 4:1 (HI: HII)(f) (max. 20. 000units /mm^2 (e)) - if used with the overlapping factors and the ration of units cone/ horizontal 46/110
	HII	According to 40 cones (e)	2.2 near the fovea (f)	- 30µm (e) - 66µm x46µm (11mm exc.) (c)	--	

[11] Receptive field measured at 0.1 of the maximum value of the difference of two exponentials as in [d]

Cell types			Number of connections with the previous layer	Overlapping factor	Dendritic field diameter	Diameter of the receptive field	Units
Bipolars	Midget		1 cone	1	--	Centre=42µm (5-10 cones) Periphery= 467µm (8-14mm exc.)(j)	--
	Diffuse	DB1	9 cones (6-7 mm exc.) (i)	1.6 (i)	--	Centre=92µm (20-30 cones) Periphery= 743µm (8-14mm exc.)(j)	Maximum 64,000 units /mm^2 In the fovea about 42,000 units (l)
		DB2	6.4 cones (6-7mm exc.) (i)	3.6 (i)	--		
		DB3	9 cones (6-7mm exc.) (i)	1.63 (i)	--		
		DB4	7.25 cones (6-7mm exc) (i)	2.8 (i)	--		
		DB5	6.6 cones (6-7mm exc) (i)	3.8 (i)	--		
		DB6	10 cones (6-7mm exc) (i)	1.7 (i)	--		
	Blue		1-3 (6-7mm exc) (i)	1.2 (i)	--	--	--
	Rod type		30-50 rods (i) 6 rods in the fovea and with about 40 in the periphery (ee)	2-5 (i)	--	--	--

Cell types		Number of connections with the previous layer	Overlapping factor	Dendritic field diameter	Diameter of the receptive field	Units
Midget		1 (fovea) 1-3 periphery (x)	Overall, there has been a consideration of 1, although there are new proposals; 1.4-2.3 (dd)	- Off 5µm On 9µm (s) - 10 x 17 / 20 x 27 (4mm exc.) - 25 x 18 /54 x 32 (12mm exc.) (s) - 20µm (1.5 mm exc.) (r))	- (2-3 x DF) (s) - 0.03º centre (9µm) 0.18º periphery(v)	80% of a total of 1.07 million (o) Maximum 35,100 /mm^2 (o) There are about 54,000 in the fovea, although they are probably displaced (y)
Parasol		--	3.4 (m) 2-7 (dd)	- 10µm - 80µm (1.5mm exc.) (r) - 30µm (w)	0.1º - 30µm centre / 0.72º - 216µm peri(v)	8-10% of the total (z)
Bistratified	Small			- 50µm in the fovea 200µm in the peri(x)	41µm -80µm component S-On 39µm -79µm component LM- Off (k)	
	Large			- 525µm (6mm exc.) Estimated 275µm in the fovea (aa)		
Large sparse				Off 791± 174 (4.8 - 17.1mm exc.) (cc)		

	Giant sparse			Off 1090±271 (8.6 - 15.3mm exc) On 1064 ±227 µm (7.6 - 17.3mm exc.) (cc)		
	Broad thorny		1-2 (bb)	517 ±113 µm (8.5 - 18.5mm exc.) (cc)		
	Narrow Thorny					

Table 6.1. Data showing cell sizes and overlapping for cells included in the model.

REFERENCES:

a) CURC_90a	i) BOYC_91	q) DACE_92	y) CURC_90b
b) WAND_95	j) DACE_00	r) RODI_85	z) SILV_91
c) ANHE_94b	k) CROO_09	s) KOLB_03	aa) PETE_00
d) PACK_02	l) MART_92	t) KOLB_91	bb) DACE_04
e) RODI_98	m) WASS_91	u) JACO_96	cc) PETE_99
f) WASS_00	n) LEE_98	v) KRON_94	dd) PERR_84
g) OYST_99	o) CURC_90	w) CALK_07	ee) WÄSS_04
h) DACE_96	p) KOLB_92	x) DACE_93	

4.2 Cell parameters: model

A detailed description of each of the cell layers of the model is going to be presented with the data gathered in the previous sections and based on the diagram shown in Figure 6.5.

4.2.1 Connections

The model is organised in cell layers. The input layer is that of photoreceptors and the output is that of ganglion cells. Each layer receives signals that are transformed and transmitted to the next element in the cell chain, except for horizontal cells that establish and receive the signal from and towards photoreceptors. The flow diagram and the connections with the layers formed by different cell types were shown in Figure 6.3.

The following shows the connections established by each cell type:

- Horizontal cells:

Horizontal	HI	HII
Photoreceptor	Type L and M cones Rods	Type L, M and S cones

Table 6.2. Connections between horizontal cells and photoreceptors.

Type I horizontal cells: taking into account the ratio L:M, 1.6:1, the relative weights are: 61.5: 38.5.

Type II horizontal cells: have 50% of the signals from S type cones and the remainder L and M type. The relative weights are L: M: S = 30.7: 19.3: 50.

- Bipolar cells:

Bipolar	Midget	Diffuse						Blue	Rods
		DB1	DB2	DB3	DB4	DB5	DB6		
Photoreceptor	L or M cones	L, M and/or S cones						S cones	Rods

Table 6.3. Connections between bipolar cells and photoreceptors.

Midget bipolar cells only receive signals from one type of photoreceptor (100% of the signal).

Diffuse bipolar cells receive signals from all photoreceptors within their reach. The weights are established according to the relative percentage of each photoreceptor. L: M: S, 57.2: 35.8: 7.

- Ganglion cells:

  Midget ganglion cells are connected to 1 midget bipolar which belongs to either type On or Off.

  In order to provide a definition of the remaining connections between bipolar and ganglion cells, one must analyse the positions in which the axons of bipolar cells branch and the positions in which the dendritic arbours of ganglion cells branch. In order for a bipolar cell to be connected to a ganglion cell both positions must coincide (bipolar axon and ganglion dendrite).

  The heights of both arbours have been represented in the internal plexiform layer (IPL) in order to analyse these connections. The distance that separates the arbour from the inner nuclear layer (INL) have been used to establish a measurement reference, 100% being the distance between the INL layer and the ganglion cell layer (GCL). The heights shown are obtained from the works of [BOYC_91] and [DACE_93 and DACE_03].

  The following figure shows the analysis of the connections. Each type of ganglion cell arbours in a stripe that is represented through a vertical rectangle of a specific colour. Some types of ganglion cells have two subtypes: on and off and therefore have two rectangles associated in different positions. Furthermore, the width of these rectangles is proportional to the size of its dendritic tree. The axon arbours of diffuse bipolar cells are represented as grey coloured horizontal stripes with different textures, while blue bipolar cells are represented by a bluish stripe. Type on and off midget bipolar cells are represented by a green line.

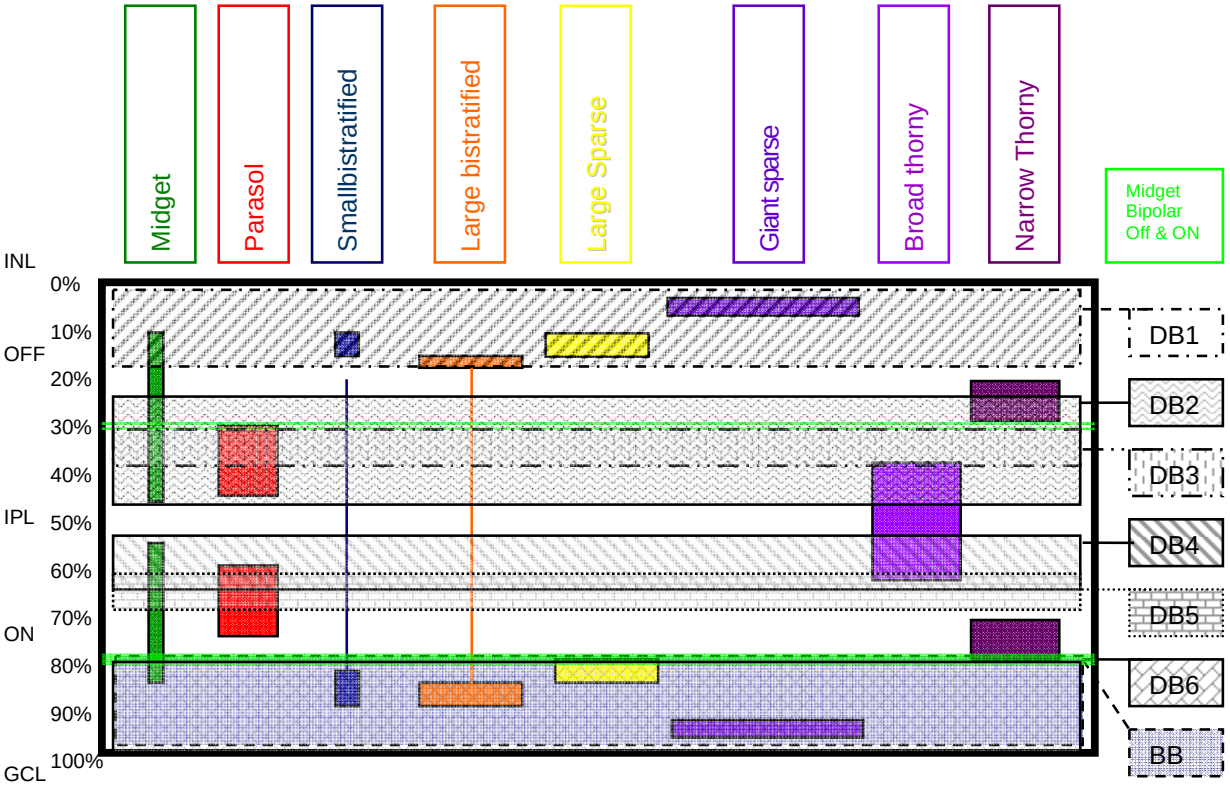

Figure 6.8. Representation of the arbour layers of ganglion cell dendrites and arbours of bipolar cell axons. Sources: Bipolar arbours: [BOYC_91] and ganglion arbours: [DACE_93 and DACE_03].

An estimation of the connections between the different types of ganglion and bipolar cells can be reached based on the areas of intersection.

Ganglion	Midget		Parasol		Bistratified	Large sparse		Giant sparse		Broad thorny	Narrow Thorny	
Bipolar	Off	On	Off	On		Off	On	Off	On		Off	On
	Midget Off type	Midget Off type	DB2 DB3	DB4 DB5	DB1 ⊕ BB DB6	DB1	DB6 BB	DB1	DB6 BB	DB2 DB4 DB5? DB3?	DB2	--

Table 6.4. Connections between ganglion and bipolar cells.

These results match with the results widely accepted for midget cells. The weight is unique, 100% based on red or green type.

The analysis of parasol cells matches with the proposal of DACE_00. Calkins and Sterling (2007), regarding Parasol Off type, identify an area in the fovea with 60% of the connections to DB3 60% and 40% to DB2.

The small-field bistratified cells are going to be built by adding blue bipolars with type DB1 diffuse bipolars, taking into account the combination of the results of table 6.4 and the results of [CROO_09]. It is deemed that blue bipolars connect only with bistratified cells.

In the remaining cases when there is more than one type, the weights shall be homogenously distributed among the different types of cells:

- Parasol type On DB4: DB5, 50: 50.
- Large sparse and giant sparse: On 100% DB6; Off 100% DB1
- Thorny DB2: DB4, 50:50.

4.2.2 Integration radius

In order to calculate the integration radius of each cell type, one can use: either the number of connections with the preceding layer or the dendritic diameter (see data in table 6.1).

- Horizontal cells:
  - Type I horizontal cells are connected to about 17 photoreceptors.
  - Type II horizontal cells are connected in a radius of 39 photoreceptors.

- Bipolar cells:
  - Midget bipolar cells are connected with a sole type L or M photoreceptor in the fovea.
  - Diffuse cells connect with L, M and/or S photoreceptors.
    - DB1: average of 5.9 L, M and/or S photoreceptors
    - DB2: average of 6.4 L, M and/or S photoreceptors
    - DB3: average of 9 L, M and/or S photoreceptors
    - DB4: average of 7.25 L, M and/or S photoreceptors
    - DB5: average of 6.6 L, M and/or S photoreceptors
    - DB6: average of 10 L, M and/or S photoreceptors

- Blue bipolar cells: establish contact with1 to 3 S photoreceptors (in order to establish contact with that number of S photoreceptors one would need an area ranging from 14 to 43 photoreceptors, as S type make up 7% of the total).

- Ganglion cells: the sizes of the dendritic files are available directly.
  - Parasol cells: 10 µm
  - Bistratified ganglion cells:
    - Midget: 50 µm.
    - Large: 275 µm.
  - Large sparse ganglion cells: 791µm (4.8 -17.1mm exc.).
  - Giant sparse ganglion cells: 1,077 µm (7.6 -17.3mm exc.).
  - Thorny ganglion cells 517 ±113 µm (8.5 -18.5mm exc.).

  Midget ganglion cells are connected to 1 midget bipolar which belongs to either type On or Off.

The integration radius establishes the value of the Gaussian radius = 2*σ. However, the model expands the influence area of each cell up to 2*R (4*σ), in order to model small lateral connections between same type cells.

On the other hand, a cell's receptive field is defined as the area of the field of view that when activated generates a change in the output signal of that cell. This area is greater than the integration field as it includes the areas of all cells to which it is connected.

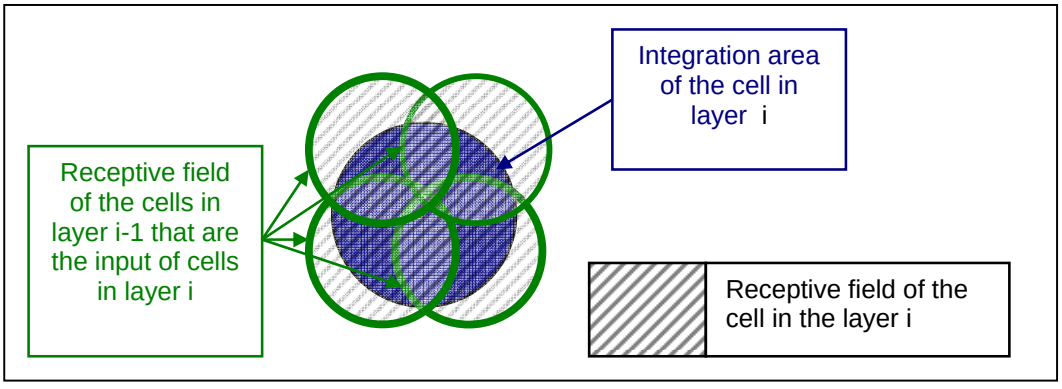

Figure 6.9. Representation of the receptive field of a cell versus the integration field.

4.2.3 Cell distribution

The third parameter to take into account in the model is the distribution of cells of each type within their corresponding layer. A regular mesh is going to be used that establishes the distance between cell centres.

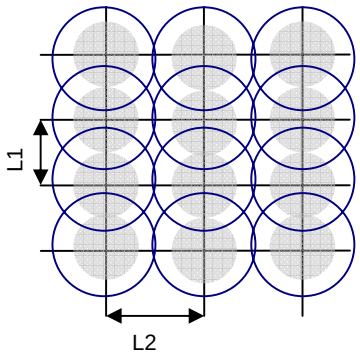

Figure 6.10. Diagram of a rectangular mesh. The cell centres are shown in grey. The integration fields are shown in blue. The parameters that characterise them have been identified.

A second type of hexagonal mesh is going to be used with photoreceptors.

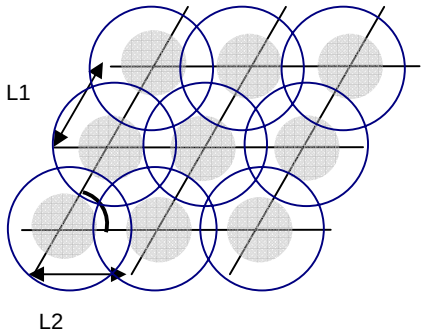

Figure 6.11. Diagram of a hexagonal mesh. The cell centres are shown in grey while the integration fields are shown in blue. The parameters that characterise them have been identified.

These two proposals correspond to the observation of the distribution structure of photoreceptors and the habitual distribution of pixels in digital images.

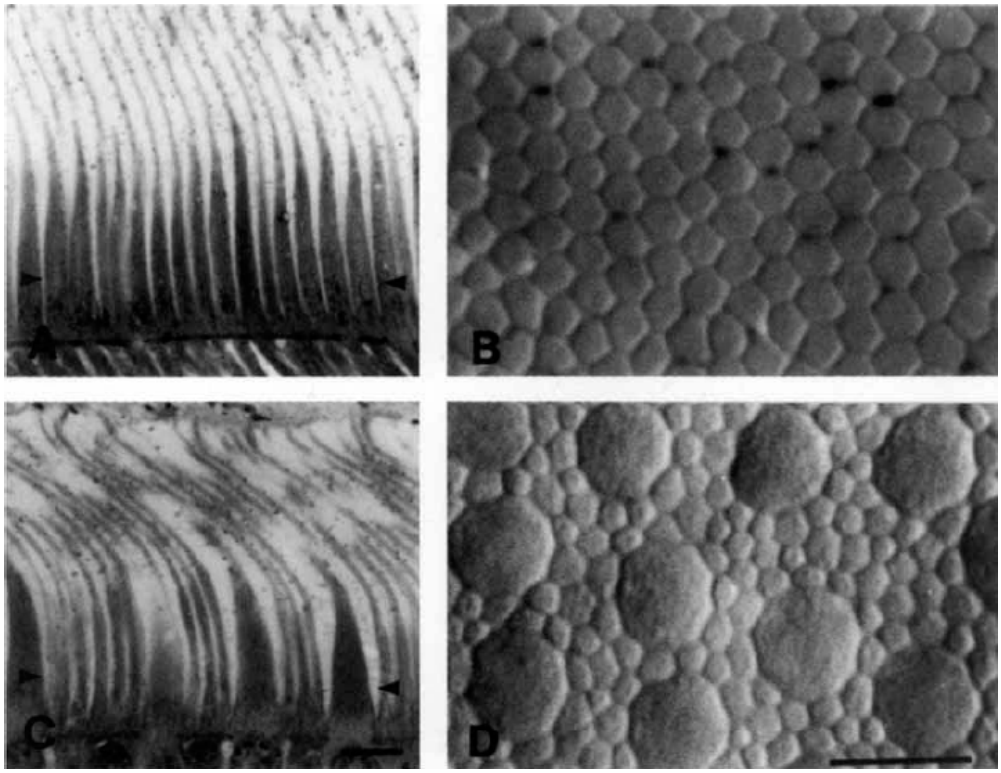

Figure 6.12. Photoreceptors: the photoreceptor images show a hexagonal mesh shaped structure (which can cover the entire surface in an optimal manner). Source: [CURC_90a]

Different cases have been identified in order to establish the sizes of the mesh.

1) Unique mesh model: where each mesh position always has a cell of every type. This mesh is based on the photoreceptor distribution in a rectangular shaped mesh. The overlapping factors do not match with the physiological data but this is a simpler computational model.

2) Model coherent with the factors of anatomical coverage[12]. Although it is highly likely that the cell distribution is irregular, the model works with both types of mesh shown in figures 6.10 and 6.11 (hereinafter, Rectangular and Hexagonal).

   An overlapping factor of 1 (each point is sampled by only one cell of each type) is used with photoreceptors and ganglion cells. The mesh parameters (rectangular and hexagonal) are proportional to the cell radii:

   - Rectangular $L1 = L2 = 2*R$ (eq. 6.2)
   - Hexagonal $L1 = L2 = \sqrt{3}*R$ (eq. 6.3)

[12] See figure 6.7 that describes the coverage factor

In order to calculate the parameters of the cell mesh with an overlapping factor different to 1, an overlapping (or coverage) function is established as the sum of the area that each of the cells to be calculated overlaps the cells in the previous layers, normalised through the division by the area of the cell to be calculated:

$$Overlapping\ \ factor\ _j = \frac{\sum_{\forall Cell \text{ in layer } j-1} Area_{Overlapped}}{Area_{Céll\ j}} \qquad \text{(eq. 6.4)}$$

In order to obtain the values for each mesh and its overlapping factor, a function to be optimised is established. The aim is that the overlapping be optimally uniform near the real anatomical value. For this, the maximum and minimum overlapping values in the set of type j cells are measured and then compared with the real value. In this way, the variation band of the overlapping factor values is limited.

$$f_j^{OPTIMUS} = abs(Overlapping\ \ factor_j^{MAX} - Overlapping\ \ factor_j^{REAL}) + abs(Overlapping\ \ factor_j^{REAL} - Overlapping\ \ factor_j^{MIN}) \qquad \text{(eq. 6.5)}$$

The use of weighted values (λ) of the average value and the standard deviation have also been analysed, but it does not allow limiting the variation in values as it generates solutions with great local differences.

$$f_j^{OPTIMUS} = abs(Overlapping\ \ factor_j^{MEAN} - Overlapping\ \ factor_j^{REAL}) + \lambda \cdot std(Overlapping\ \ factor_j) \qquad \text{(eq. 6.6)}$$

Below is an example of the calculation of the overlapping factor of horizontal cells on photoreceptors. The radii of the dendritic fields, integration area of horizontal cells, are shown in red. The centres of photoreceptors are shown in orange while the blue scales the variation of the overlapping factor in relation to the real value.

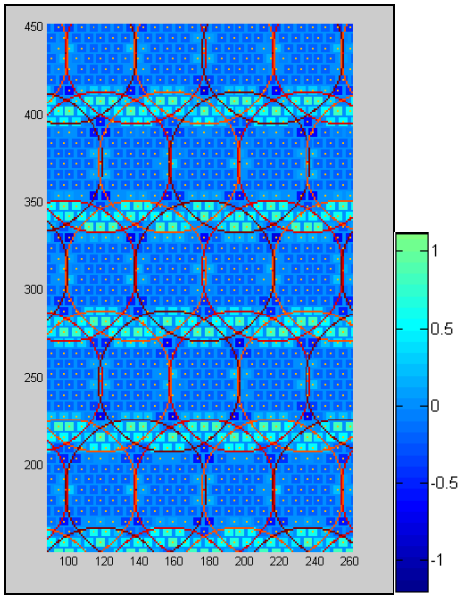

Figure 6.13. Example of coverage of horizontal cells type II vs. photoreceptors. In orange: centre of photoreceptors. In red integration area of a horizontal cell. The blue hues show the difference in the physiologically estimated coverage.

The L1 and L2 values that cause optimal overlapping factors are shown hereunder (in accordance with equations 6.2 and 6.3 or the optimisation function described in equation 6.5, depending on whether the overlapping factor is equal to 1 or not). The (L1, L2) values are scaled with the factor that associates the number of pixels with the radius of a photoreceptor RADIUS_PIXEL_SCALE, for example, parameters (1,1) corresponds to a radius pixel scale of (RADIUS_PIXEL_SCALE, RADIUS_PIXEL_SCALE).

- **Photoreceptors**: The radius of the receptive field has been established as the mesh size.

Cell type	**Parameters** (x RADIUS_PIXEL_SCALE)	
	Rectangular photoreceptors	Hexagonal photoreceptors
Photoreceptors	(2, 2)	(√3, √3)

Table 6.5. Parameters (L1, L2) of the rectangular and hexagonal meshes of photoreceptors.

- **Horizontals**: The overlapping factor over photoreceptors has been calculated.

Cell type		**Parameters** (x RADIUS_PIXEL_SCALE)	
		Rectangular photoreceptors	Hexagonal photoreceptors
Horizontal	HI	(2, 6)	(3, 4)
	HII	(7, 9)	(7.8, 9)

Table 6.6 Parameters (L1, L2) of the horizontal cell meshes over the rectangular or hexagonal photoreceptor mesh.

- **Bipolars**: The overlapping factor over photoreceptors has been calculated.

Cell type			**Parameters** (x RADIUS_PIXEL_SCALE)	
			Rectangular photoreceptors	Hexagonal photoreceptors
Bipolars	Midget		(2, 2)	(√3, √3)
	Diffuse	DB1	(2.8, 3)	(3, 3.2)
		DB2	(1.6, 2)	(2, 2.6)
		DB3	(3, 3.6)	(3, 5.2)
		DB4	(2, 2.6)	(2.4, 2.6)
		DB5	(1.8, 2)	(1.8, 2.6)
		DB6	(3.6, 4.4)	(3, 5.2)
	Blue		(6, 7)	(6, 7.8)

Table 6.7. Parameters (L1, L2) of the bipolar cell meshes over the rectangular or hexagonal photoreceptor mesh.

- **Ganglion**: the overlapping factor is deemed 1, therefore the size of the mesh is equal to the radius of the integration field.

Cell type			Parameters (x RADIUS_PIXEL_SCALE)	
			Rectangular photoreceptors	Hexagonal photoreceptors
Ganglion	Midget		(2, 2)	(√3, √3)
	Parasol		(12.5, 12.5)	(10.83, 10.83)
	Bistratified	P	(20.84, 20.84)	(18.05, 18.05)
		G	(114.58, 114.58)	(99.23, 99.23)
	Large sparse		(158, 158)	(136.83, 136.83)
	Giant sparse		(212, 212)	(183.60, 183.60)
	Thorny		(103.4, 103.4)	(89.55, 89.55)

Table 6.8. Parameters (L1, L2) of the ganglion cell meshes over a rectangular or hexagonal photoreceptor mesh.

Note: the mesh is built from the image's centre point. This way, there will always be a cell of each type in that point regardless of the model parameters.

4.2.4 Connection functions between layers and spikes generation

The output signals of the different layers are calculated through the weighted sum of the input signals to that layer.

If one wants to calculate the signal of a type j cell. First, the total signal generated by the type i cells that connect to the above mentioned type j cell are calculated. Each cell is weighted by a Gaussian factor that represents the distance of that connection to the centre of the type j cell. Second, all types of cells that connect with the type j that is going to be calculated are added, the weight factor is established according to the relative number of connections of each type with the type j cell. The following equation describes this calculation:

$$Signal_{\text{Cell type j}} = \sum_{\substack{\forall \text{ Cell connected} \\ \text{to the cell} \\ \text{type j}}} w_{\text{Cell type i over cell type j}} \sum_{\substack{\forall \text{ cell type i} \\ \text{in the integration field} \\ \text{of the cell type j}}} w(\textit{relative position } i, j)_{\text{Gaussian}} * Signal_{\text{Cell type i}}$$

(eq. 6. 7)

The weights of the sums have been defined in section 4.2.1.

In the case of the connections between the photoreceptors, the horizontals and bipolar cells, two possibilities can be used: weighted sum and shunt type or divisive inhibition. The shunt function is calculated in the following manner. As in the earlier case, when calculating the signal of a type j cell, a calculation is made of the total signal that reaches that cell (exactly as described in the earlier case) from the type i cells (excitatory signal) and type k (inhibitory signal). Both signals are divided and a gain factor is applied. The following equation shows this calculation:

$$Signal_{Cell\ type\ j} = w_{\text{divisive factor for type j}} \frac{\sum_{\substack{\forall \text{ Cell type i in the integration} \\ \text{field of the cell type j}}} w(\text{relative position i, j})_{\text{Gaussiana}} * Signal_{Cell\ type\ j}}{\sum_{\substack{\forall \text{ Cell type i in the integration} \\ \text{field of the cell type k}}} w(\text{relative position k, j})_{\text{Gaussian}} * Output_{Cell\ type\ k}} \quad \text{(eq. 6.8)}$$

Where j are to bipolar cells, i the photoreceptors and k the horizontals.

The on and off pathways of the model are split in the bipolar cell stage. The following function is used for this:

$$Signal_{bipolar\ on} = Signal_{bipolar\ input} - \overline{Signal_{bipolar\ input}} \quad \text{(eq. 6.9)}$$

$$Signal_{bipolar\ off} = \overline{Signal_{bipolar\ input}} - Signal_{bipolar\ input} \quad \text{(eq. 6.10)}$$

where $\bar{x}$ symbol represents the average value of variable x.

On the other hand, the conversion function of continuous signals to spikes that is going to be used is the exponential function.

$$f(x) = A \cdot e^{B \bullet x} \quad \text{(eq. 6.11)}$$

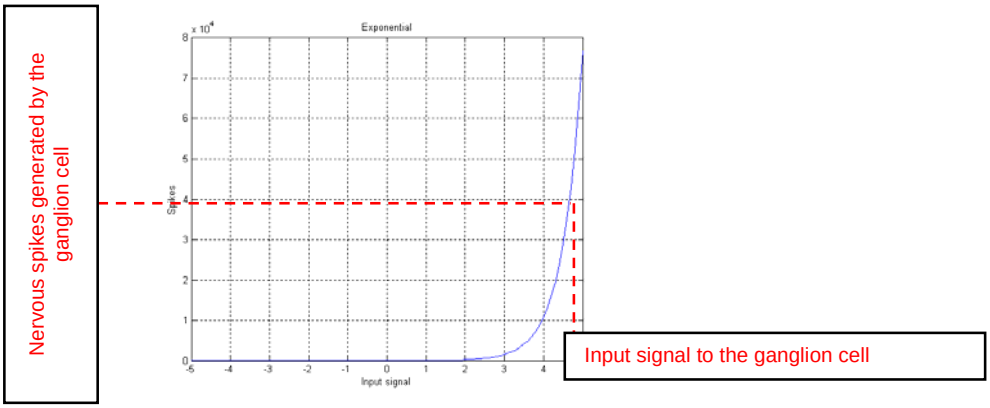

Figure 6.14. Example of the exponential function for the generation of spikes. Abscissas: input signal. Ordinates: number of nervous impulses generated.

4.2.5 Model inputs

The present work is a bioinspired model. The input signals to the retina are the values {L, M, S}. The common values used in colour works are CIE XYZ or the digital values RGB.

The transformation matrix that is going to be used is the Hunt-Pointer-Estevez matrix.

$$\begin{pmatrix} L \\ M \\ S \end{pmatrix} = \begin{bmatrix} 0.38971 & 0.68898 & -0.07868 \\ -0.22981 & 1.1834 & 0.04641 \\ 0.0 & 0.0 & 1.0 \end{bmatrix} \bullet \begin{pmatrix} X \\ Y \\ Z \end{pmatrix} \qquad \text{(eq. 6.12)}$$

This is the most common matrix in colour appearance models (see Chapter III).

5. Evaluation / parameter selection

The previous section has presented the model's parameters. More than one option has been proposed for some of them. At this time, unique values are going to be selected for each parameter in order to evaluate the results of the model regarding physiological data. As previously mentioned, the evaluation of optimal parameters shall be looked at in future works.

a) Mesh parameters: the homogeneity of signals in an image with constant value has been analysed in order to select the mesh for the trial phase.

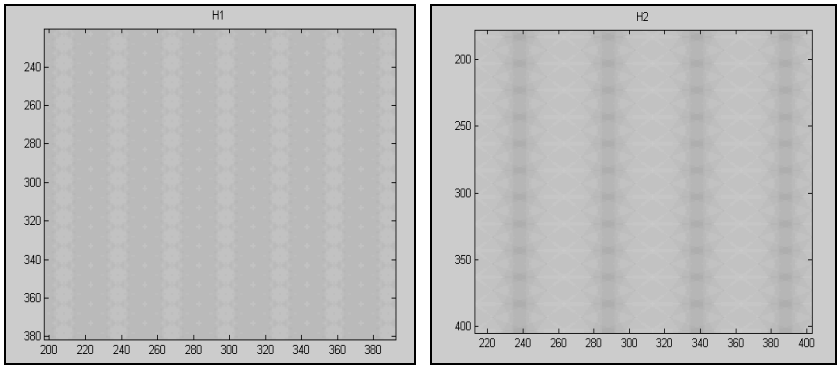

Figure 6.15. Output signal generated by type I and II horizontal cells in response to an average grey image with a mesh adjusted to the anatomical overlapping factor.

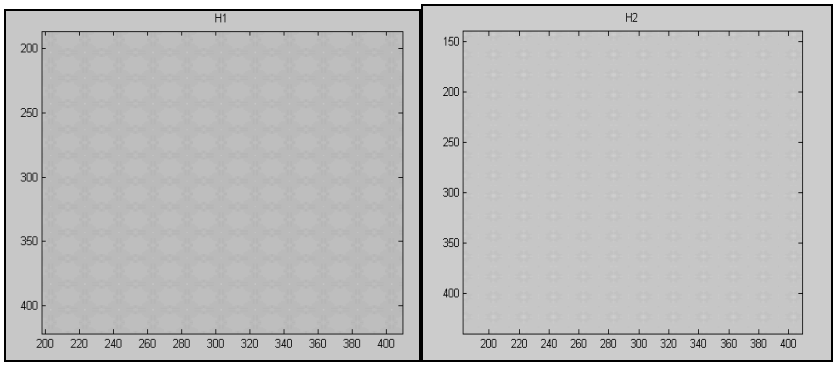

Figure 6.16. Output signal generated by type I and II horizontal cells in response to an average grey image with the unique mesh.

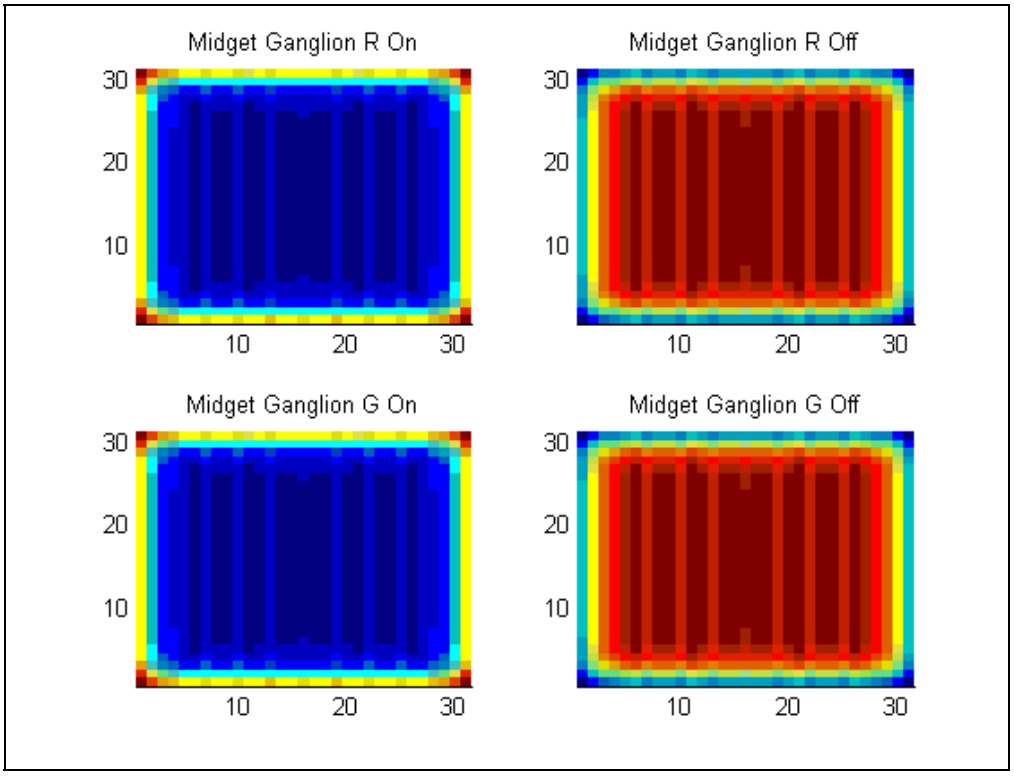

Figure 6.17. Result generated by midget ganglion cells (spikes) in response an average grey image with a mesh adjusted to the anatomical overlapping factor.

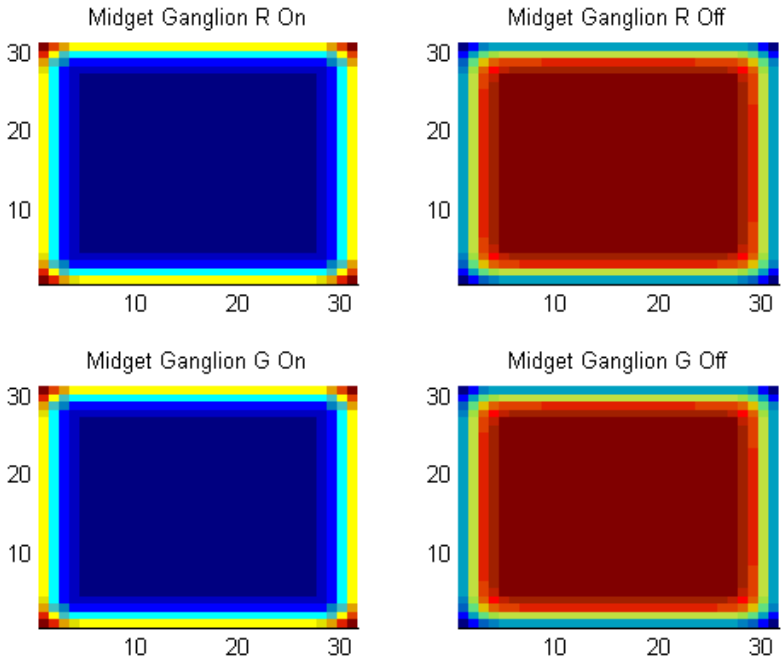

Figure 6.18. Result generated by midget ganglion cells (spikes) in response to an average grey image with the unique mesh.

When using the mesh adjusted to the overlapping factor shows the generation of non-homogeneities as vertical lines that appear in the stage of horizontal cells and continue in the ganglion cell stage. This is caused by the rectangular structure of this mesh. In the case of a unique mesh, these processes are not noticeable (variations appear in the stage of horizontal cells but are almost unnoticeable in the last stage). [13]

Therefore, the unique mesh shall be used.

b) Selection of the extension of lateral connections in photoreceptors.

The aim is to establish a minimum sampling of any given point in the field of view of the model. Therefore, the sampling of each point is calculated based on both the distribution of photoreceptors (photoreceptor mesh) and the size of the Gaussian associated to each photoreceptor. The following are the values for three sizes of Gaussian:

I.) Gaussian Radius = 1* RADIUS_PIXEL_SCALE. Minimum value = 0.07316.

[13] The variations in the borders are due to the fact that the system deems that the original image has a frame of zero value.

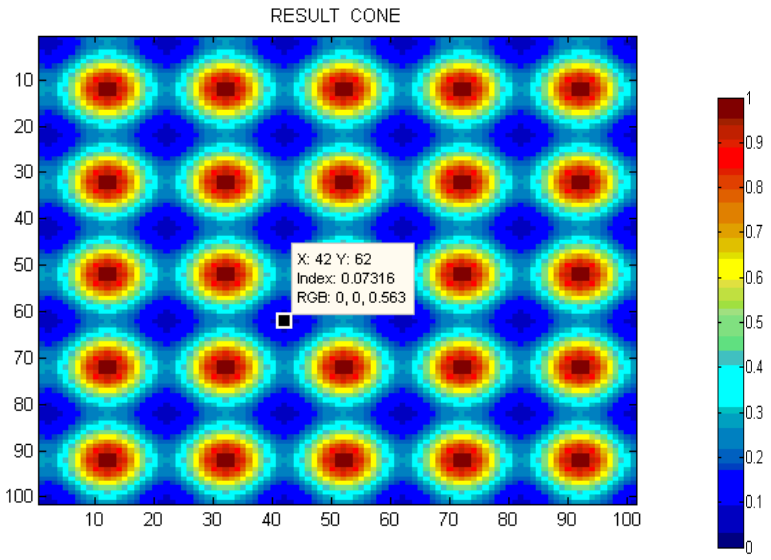

Figure 6.19. Sampling factor of the field of view with a Gaussian radius of 1* RADIUS_PIXEL_SCALE.

II.) Gaussian radius = 1.5* RADIUS_PIXEL_SCALE. Minimum value = 0.605.

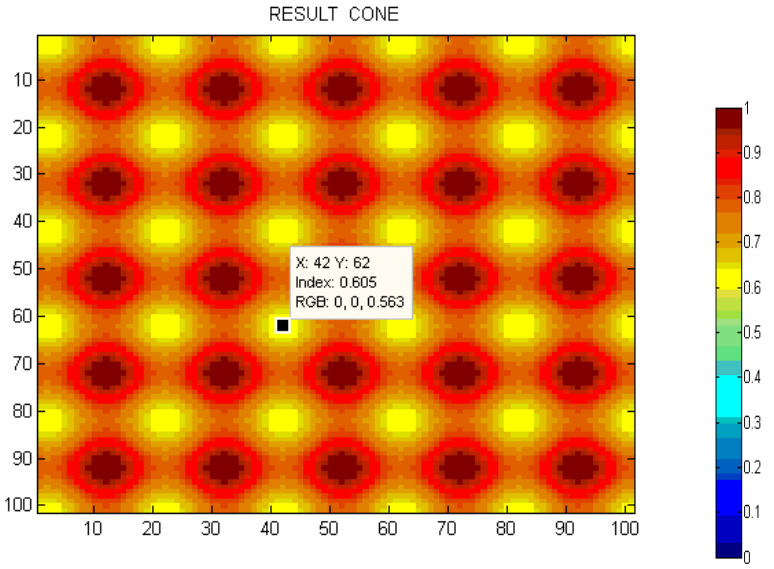

Figure 6.20. Sampling factor of the field of view with a Gaussian radius of 1.5* RADIUS_PIXEL_SCALE.

III.) Gaussian radius = 2* RADIUS_PIXEL_SCALE. Minimum value = 0.944.

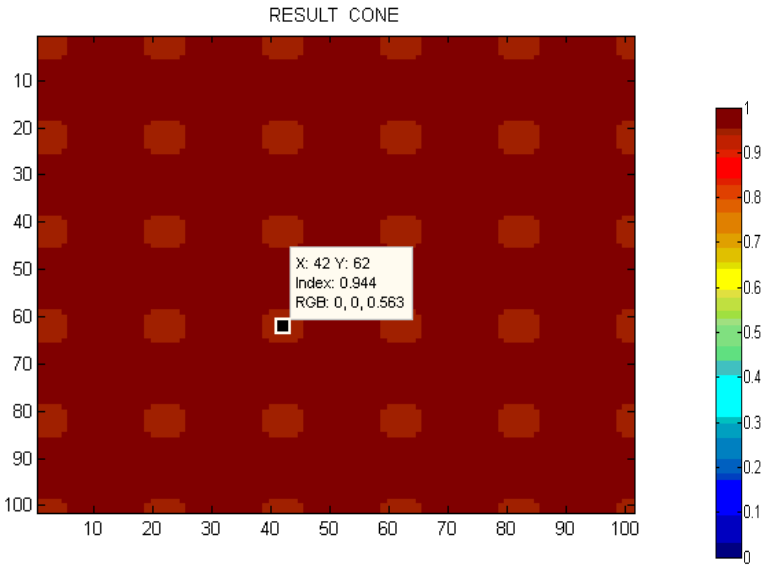

Figure 6.21. Sampling factor of the field of view with a Gaussian radius of 2* RADIUS_PIXEL_SCALE.

Figure 6.15 shows areas with a very low sampling factor while the minimum in the case II is at 60% and in case III is at 94%.

Based on these values, the chosen value of the Gaussian of photoreceptors is 1.5*RADIUS_PIXEL_SCALE as it has an acceptable minimum value. The use of a bigger radius does not seem necessary.

The remaining cell types shall use a Gaussian radius equal to the cell radius because as these stages are posterior to photoreceptors and have overlapping factors that are equal to or greater than 1.

6. Model: output signals generated by each cell type.

The output signals generated by each cell type of the model when presented a set of stimuli is going to be presented and analysed in order to check both the behaviour in the different layers of the model and their relation with physiological measurements.

The purpose of the analysis of the signals generated by the different cell types when presented different stimuli is the following:

- Achromatic stimuli: analyse the structural behaviour of the system. This includes the study of the sizes of the different cell radii and the connections between layers (number and function). This can be used to verify the characteristics of the receptive field: the presence of centre vs. surround process and the total reach of the area of influence of each cell type. It also allows for the comparison of the model results with real physiological measurements.
- Chromatic stimuli: analyse cell types with a selective response to visible spectrum bands as well as processes in chromatic opponency that are described in scientific publications.

The following are the stimuli that are going to be used and are those most commonly used in retina studies[14]:

Achromatic stimuli

1) Spot: set of white circles with a growing radius whose centre coincides with the centre of the cell mesh.

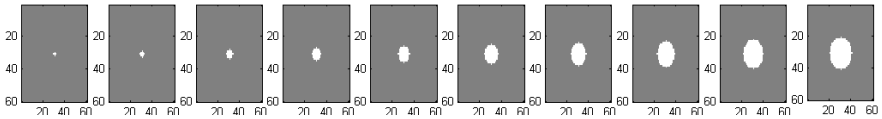

Figure 6.22. Example of different white coloured spots that are presented to the system as stimuli.

2) Annulus: set of white circular annulus with a growing internal radius. The centre coincides with the centre of the cell mesh. The external radius of the annulus is: 310 pixels.[15]

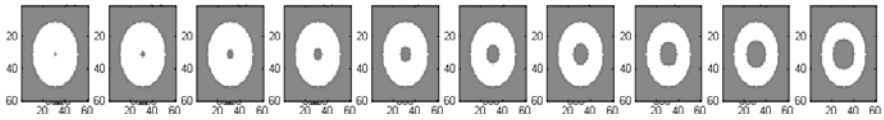

Figure 6.23. Example of different white coloured annulus that are provided into the system as stimuli.

3) Grid: composed of white and black stripes of variable width.

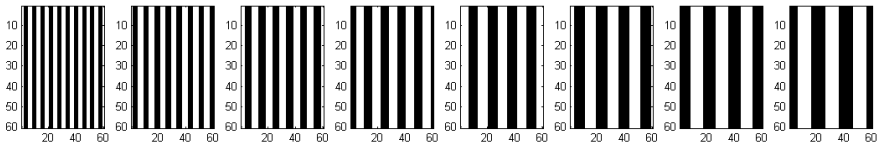

Figure 6.24. Example of different grids that are presented to the system as stimuli.

[14] All cases shall use an average grey background.

[15] In the case of big cells this size will be increased.

Chromatic stimuli:

4) Response in the visible spectrum: analyses the output of each cell when presented stimuli in different wavelengths of the visible spectrum (from 400nm to 850 nm). The values used as a basis are the XYZ Judd values (1951) modified by Vos (1978) as they appear in http://cvrl.ucl.ac.uk/.

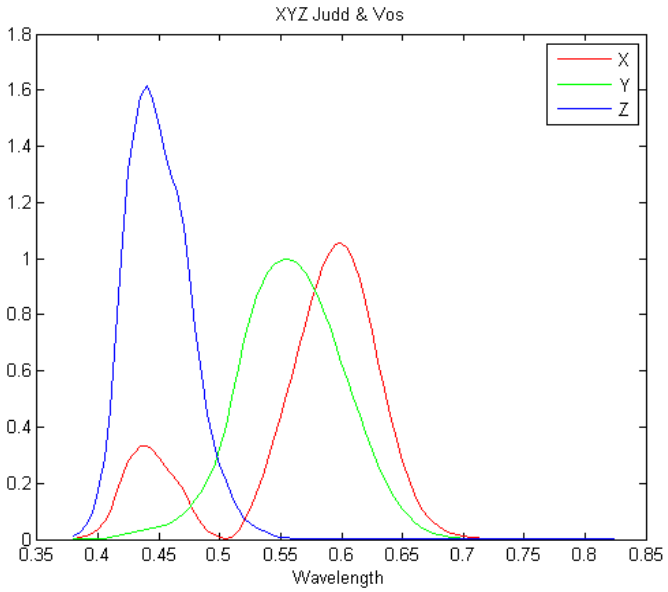

Figure 6.25. XYZ values throughout the visible spectrum. 1931 CIE XYZ values modified by Judd (1951) and Vos (1978).

The Y values throughout the spectrum are compared with the results of each cell type. The output values of each cell type of the model shall be normalised to a maximum value of 1 in order to ease the comparison with Y values.

5) Centre-surround opponency: set of spot + annulus with different colour combinations. The radius of the spot and the interior radius of the annulus are equal to the radius of each cell being studied while the exterior radius of the annulus is twice that radius.

The Y value in the CIE XYZ space must be established in order to work in similar conditions for all colours. The value Y=0.5 has been set and the following chromatic stimuli have been defined.[16]

[16] The value Y=0.5 has not been set in white and black stimuli as this would entail having a continuous grey spot.

{L, M, S}					
Red	{1, 0.20066,0}	Blue	{0.5, 0.5, 1}	"White"	{0.75, 0.75,0.75}
Green	{0, 0.79, 0}	Yellow	{0.5, 0.5, 0}	Black	{0,0,0}

Table 6.9. Base stimuli for chromatic opponency.

The following are the sample of stimuli established with the values in the previous table. The {L, M, S} values are represented directly, not the {R, G, B}. Therefore, the colours that are used in this document are not real representations of colours.

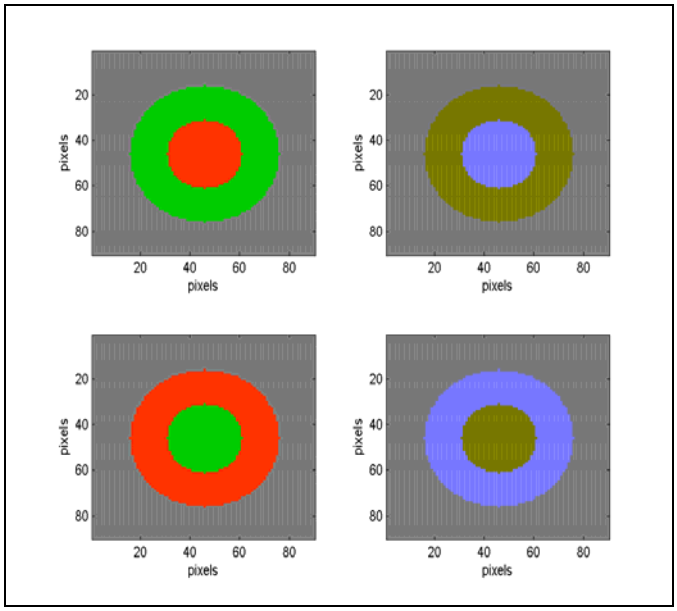

Figure 6.26 Example of stimuli set with chromatic opponency.

The model, in this analysis, uses the parameter RADIUS_PIXEL_SCALE with a value of 10 (10 pixels = photoreceptor radius). A=4.27 and B=1.96 have been used in the exponential function for spike generation (equation 6.11).

Following the model responses for each cell type when presented the proposed stimuli will be presented. First, the structure of each receptive field is shown. Next, the outputs signals obtained for each cell layer will be shown.

6.1 Photoreceptors

The structure of the receptive field of photoreceptors is simple. It is modelled by a Gaussian function. As has been mentioned in the previous section, the Gaussian radius was selected in order to avoid having areas with low sampling. This causes a certain overlapping between the receptive fields of adjacent photoreceptors. In order to see this effect, the result of Gaussian receptive fields of the photoreceptor network is shown.

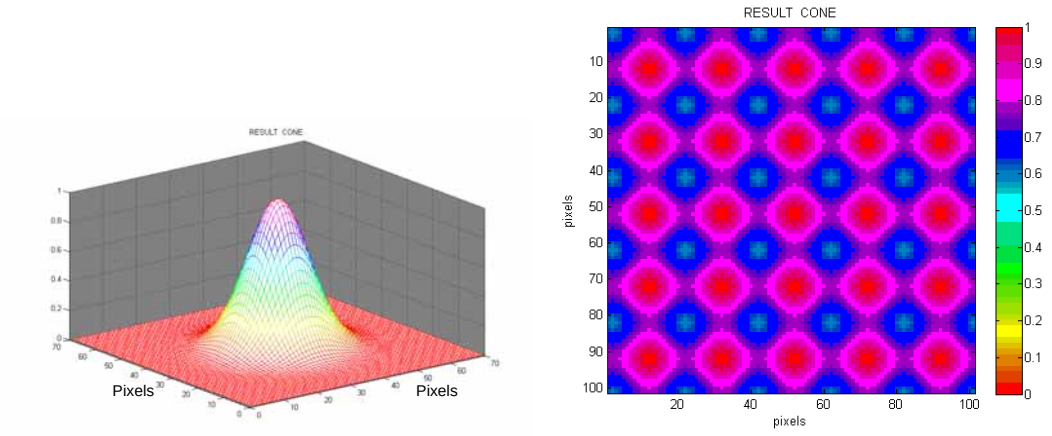

Figure 6.27. Structure of photoreceptor's receptive field. Left) Function of the receptive field. Right) Distribution of the photoreceptor's Gaussian receptive fields on a rectangular mesh.

The photoreceptor signals are calculated according to the following equations, using the parameters described in earlier sections:

$$\text{Photoreceptor type L} = \int_{\substack{\text{Integration field}\\ \text{of the photoreceptor}}} \exp(-2*(x^2+y^2)/15^2)*\text{L plane of the image(x,y)}$$

(eq. 6.13)

$$\text{Photoreceptor type M} = \int_{\substack{\text{Integration field}\\ \text{of the photoreceptor}}} \exp(-2*(x^2+y^2)/15^2)*\text{M plane of the image(x,y)}$$

(eq.6.14)

$$\text{Photoreceptor type S} = \int_{\substack{\text{Integration field}\\ \text{of the photoreceptor}}} \exp(-2*(x^2+y^2)/15^2)*\text{S plane of the image(x,y)}$$

(eq. 6.15)

The following shows the output signals of photoreceptors when presented different stimuli. The graphs show the values generated by a photoreceptor centred in the stimulus. This first stage does

not include the influence of horizontal cells. In order to be activated by the presence of light, the signal that appears in the graphs is the opposite of the biological signal.

1) Spot

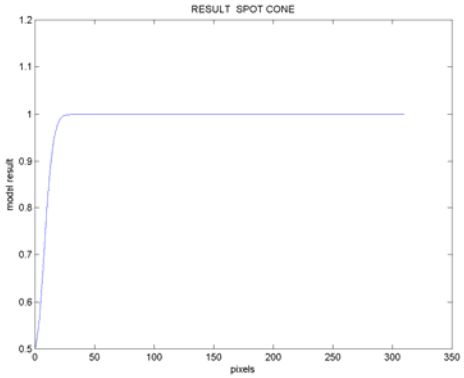

Figure 6.28. Output signal of a photoreceptor when presented a white coloured spot with a variable radius.

When presenting a grey stimulus (Grey: 0.5, 0.5, 0.5) the output value of the system is 0.5. When the spot's radius is increased, a greater area of the photoreceptor's receptive field is covered until it is completely covered, thus generating the maximum response (value 1) when the stimulus is equal to the size of the receptive field. In this first stage, additional cells in the receptive field do not have influence.

2) Annulus

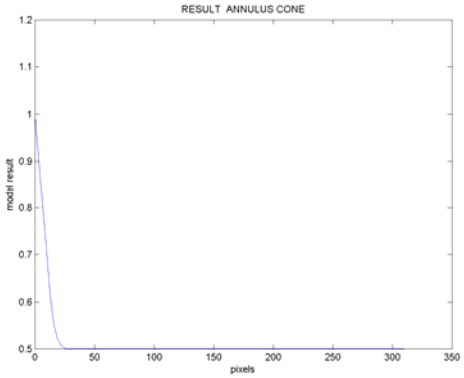

Figure 6.29. Output signal of a photoreceptor when presented a white coloured annulus with a variable inner radius.

This case begins with a annulus with a null interior circle (that is, a completely white circle) that surpasses the limits of the photoreceptor's receptive field. Therefore, a maximum output value (1) is generated. As the radius of the inner circle increases, the area of the white annulus which covers the photoreceptor decreases and thus the response value of this photoreceptor. The limit value of 0.5 is generated when the inner radius reaches the size of the Gaussian associated to the photoreceptor (the inner circle with an average grey level).

This stage does not have processes of centre vs. surround.

3) Grid

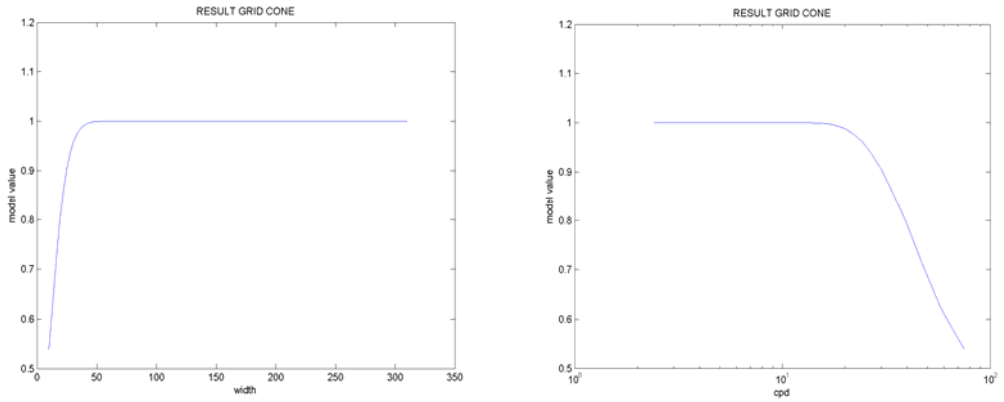

Figure 6.30. Output signal of a photoreceptor when presented a variable size grid. Left) Abscissas: grid width in pixels. Right) Abscissas cycles per degree (5º equal 1.5mm).

The values are near 0.5 (the combination of white and black provides a similar result to that of an average grey) in meshes of small width. As the size of the mesh increases, the band centred in the photoreceptor (white coloured) covers a greater area of the cell receptive field and thus the generated signal increases. When the mesh is greater than the integration radius of the photoreceptor, then the maximum value of 1 is reached (all the photoreceptor's field is covered by a white stimulus).

4) Visible spectrum

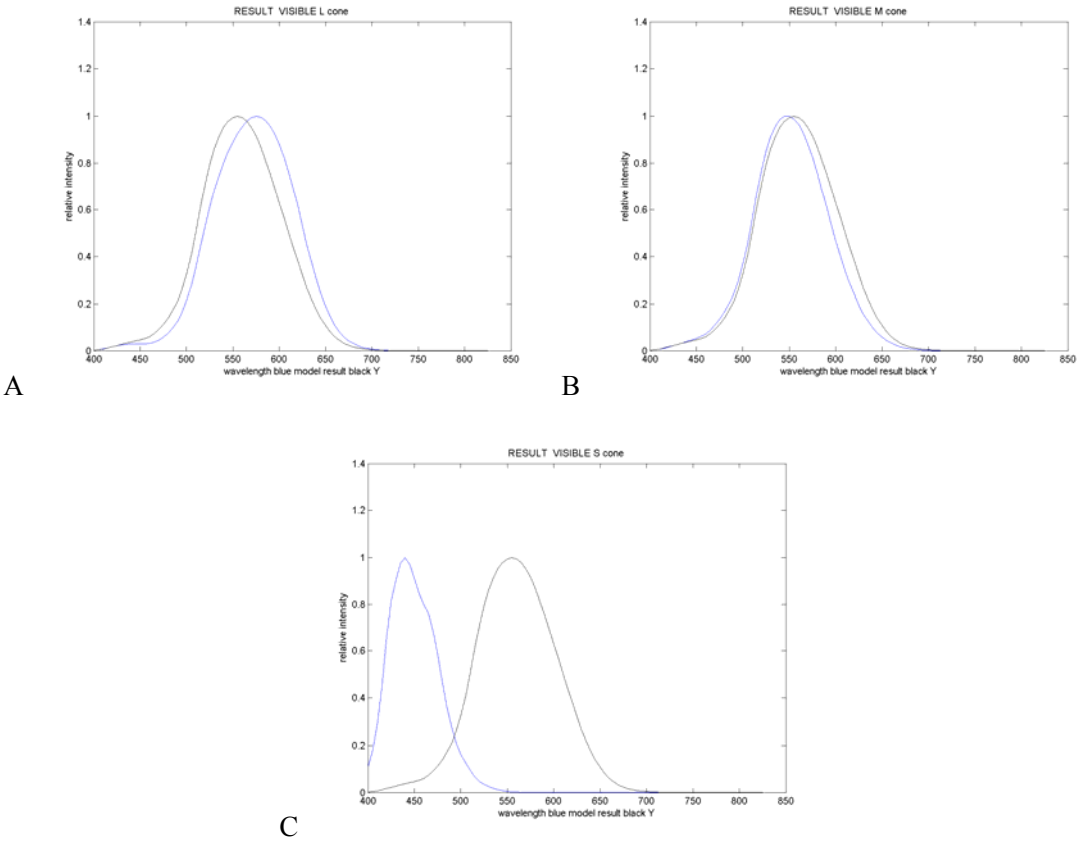

Figure 6.31. Photoreceptor's response throughout the visible spectrum. Blue; model result, black: Y. A) Photoreceptor type L. B) Photoreceptor type M. C) Photoreceptor type S.

Each photoreceptor responds to specific bandwidths along the visible spectrum. As can be seen in the case of type L photoreceptors, the band is displaced towards red wavelengths regarding the Y value, whereas with type M, the variation is in the opposite direction. Type S photoreceptors show a clear response in the blue area, separated from Y. Therefore, type L photoreceptor is especially responsive in the yellow, orange and red areas; while type M is responsive in the green and type S is responsive in the blue area.

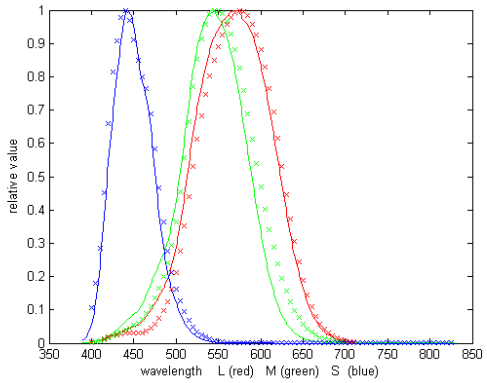

Figure 6.32. Comparison between the model results (straight line) and the Stockman & Sharpe data (2000) for photoreceptors (crosses). Red: L; green: M; blue: S.

The results shown are approximately equal to the proposed values for photoreceptors. The differences are due to the use of a transformation matrix (eq. 6.12) as an approximation to the transformation {XYZ} to {LMS}.

5) Opponency

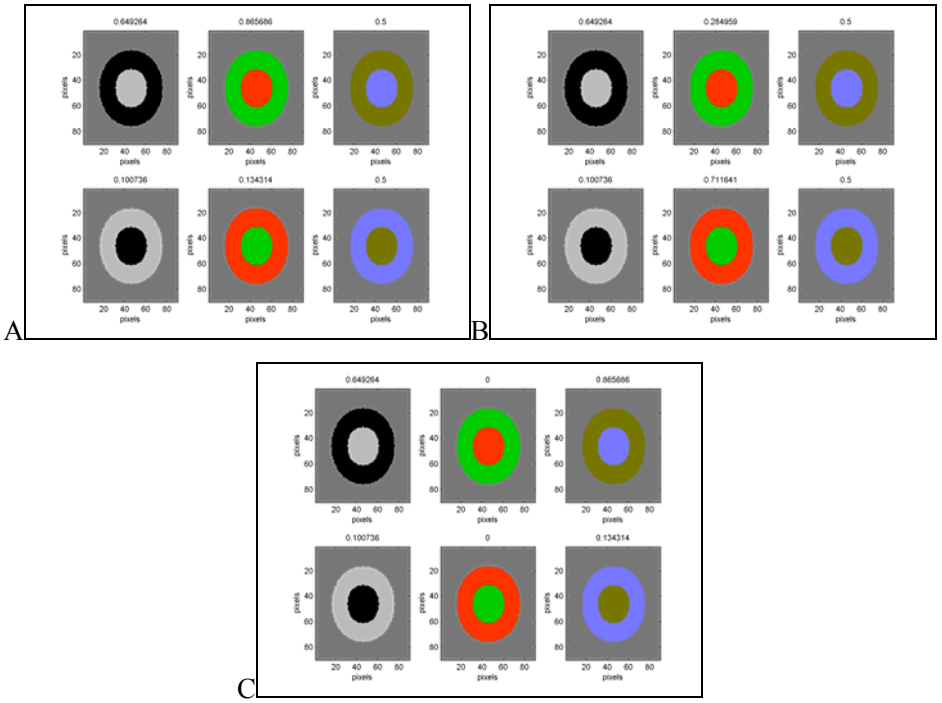

Figure 6.33. Output signal of a photoreceptor when presented different stimuli with chromatic opponency, photoreceptor's output signal represented by the numerical value above each figure. A) Type L. B) Type M. C) Type S.

The results shown are proportional to the stimulus of each channel. Type M has a value that is less than L and S as the green stimulus was set to 0.79 instead of 1 in order to obtain the same Y. It is important to remember that Gaussian receptive fields extend up to $\pm 2*R_{cell}$ and that the stimuli in opponency are circles with R_{cell} radius so the annulus also covers part of the receptive field of the cell to be studied. This explains, for example, the non-null response of type S when presented a blue annulus with a yellow centre.

This stage has no presence of opponency as has been seen with achromatic stimuli.

The coherence of the response of the layer of isolated photoreceptors has been verified through the response to different stimuli. These results are consistent with physiological studies that define receptive fields through Gaussian models and the response of each photoreceptor throughout the visible spectrum.

This can be summed up in that these are cells with a homogeneous receptive field (without opponency) and of a chromatic nature.

6.2 Horizontal cells

The structure of the receptive field of horizontal cells includes the influence proper of its entry function (a Gaussian) plus the fact that it receives the signal from the photoreceptors that contact that horizontal cell. The following figure shows the characteristics of this field, with the general shape of a Gaussian field modulated by the photoreceptor's own fields.

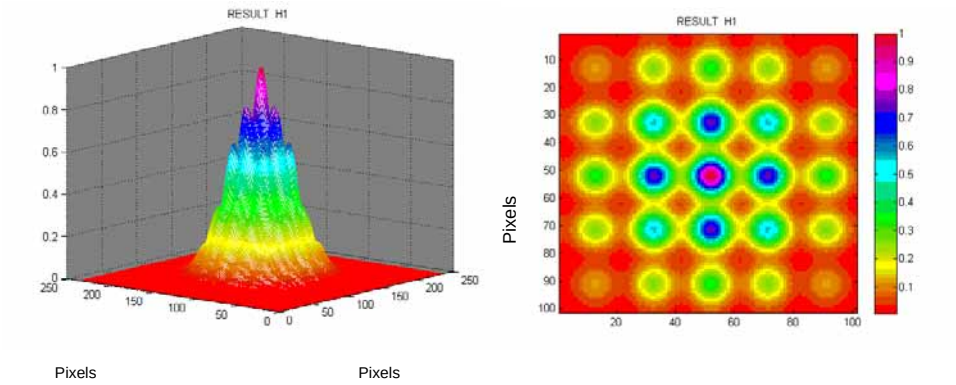

Figure 6.34. Representation of the receptive field of a horizontal cell where the integration of its dendritic field, shaped as a Gaussian, is superimposed on the receptive fields of the cones to which it connects. Left) 3D view. Right) Top View.

Taking the set of parameters described in the previous sections, the signals of horizontal cells are calculated in the following manner:

$$\text{Horizontal type I} = \int_{\substack{\text{Integration field of}\\ \text{horizontal cell type I}}} \exp(-2*(x^2+y^2)/41.23^2)*\begin{Bmatrix} 0.615*\text{L Photoreceptor signal} \\ +0.385*\text{M Photoreceptor signal} \end{Bmatrix}$$

(eq. 6.16)

$$\text{Horizontal tipo II} = \int_{\substack{\text{Integration field of}\\ \text{horizontal cell type II}}} \exp(-2*(x^2+y^2)/62.45^2)*\begin{pmatrix} 0.307*\text{L Photoreceptor signal} \\ +0.193*\text{M Photoreceptor signal} \\ +0.5*\text{S Photoreceptor signal} \end{pmatrix}$$

(eq. 6.17)

The following are the response of horizontal cells to the basic stimuli:

1) Spot

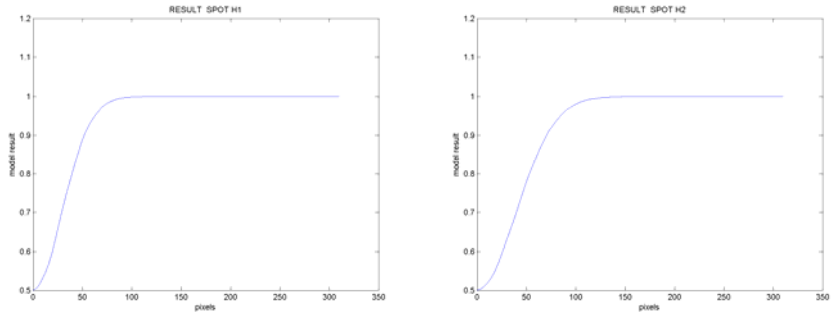

Figure 6.35. Signal generated by the horizontal cells when presented a white spot with a variable radius. Left) HI. Right) HII.

A similar behaviour to that mentioned for photoreceptors is shown, scaled to the size of each horizontal cell and with a slight curve undulation due to subfields introduced by the photoreceptors.

It begins with a value of 0.5 when presented an average grey stimulus. As the size of the white spot increases, the output signal grows, in both cases reaching the maximum value when the size of the stimulus completely covers the area of influence of their receptive fields.

2) Annulus

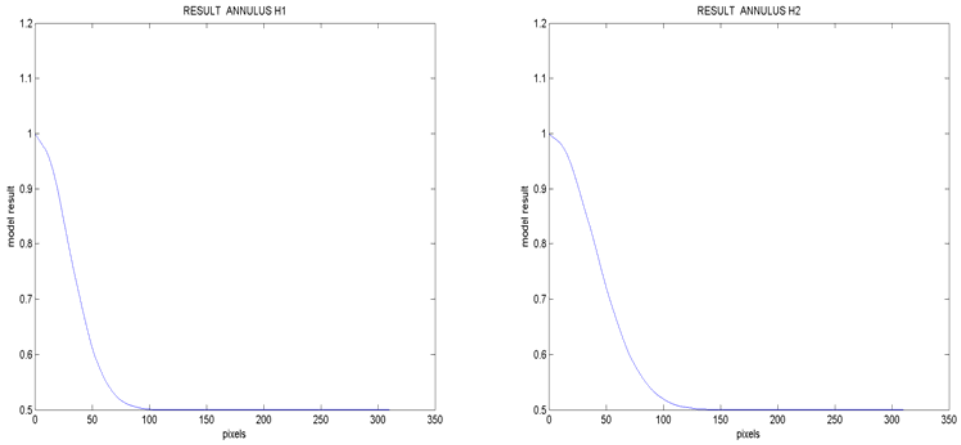

Figure 6.36. Signal produced by horizontal cells when presented a white annulus with a variable inner radius. Left) HI. Right) HII.

The behaviour observed in the case of photoreceptors with the undulation due to the photoreceptor fields is shown again by the horizontal cells when presented a annulus shaped stimulus. The signal begins with a maximum value of 1 when presented a white annulus with a null inner radius in both types of horizontal cells. When the inner radius of the annulus is increased, the signal decreases until it reaches a limit value of 0.5, when it reaches the limits of the receptive fields.

There is no centre vs. surround opponency.

3) Grid

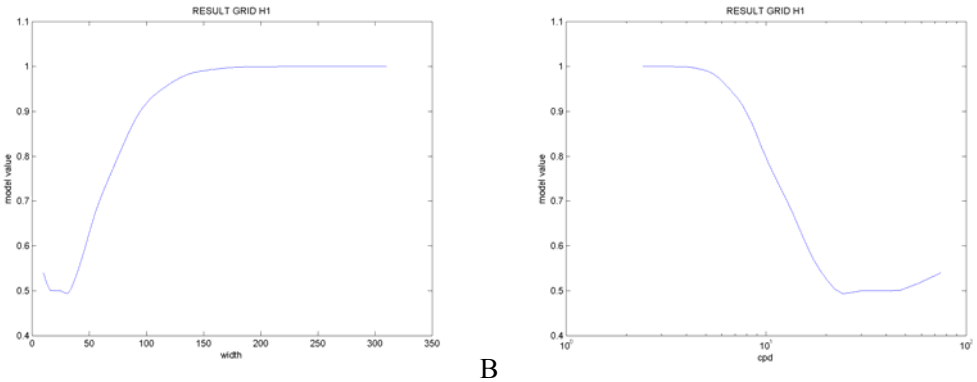

A B

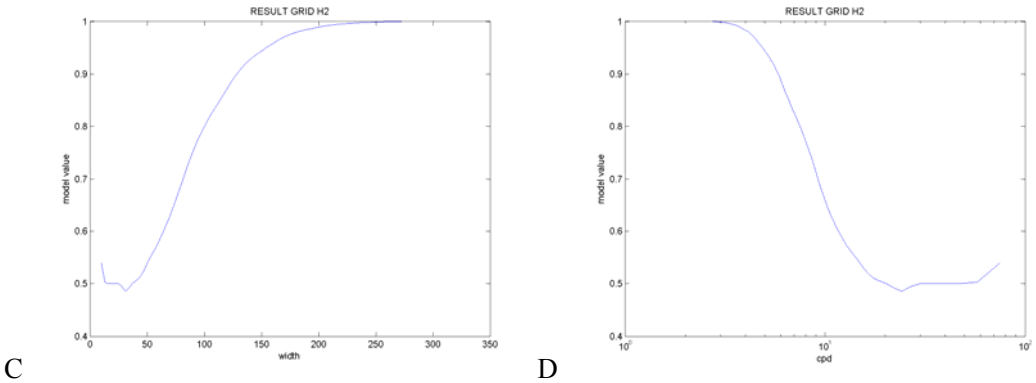

C D

Figure 6.37. Signal generated by horizontal cells when presented a variable size grid. A) HI. Abscissas: grid width in pixels. B) HI Abscissas cycles per degree. C) HII. Abscissas: grid width in pixels. D) HII Abscissas cycles per degree (5º equal 1.5mm).

The behaviour is similar to that of photoreceptors, adapted to its receptive field radius and modulated by the photoreceptor sampling. When the size of the mesh is small, there are small variations due to the subsampling of the photoreceptors present in the field of the horizontal cell. As the size of the grid increases, the signal is stabilised and begins to progressively grow. The maximum value is reached when the white stripe centred on the cell covers the cell's entire receptive field.

4) Visible spectrum

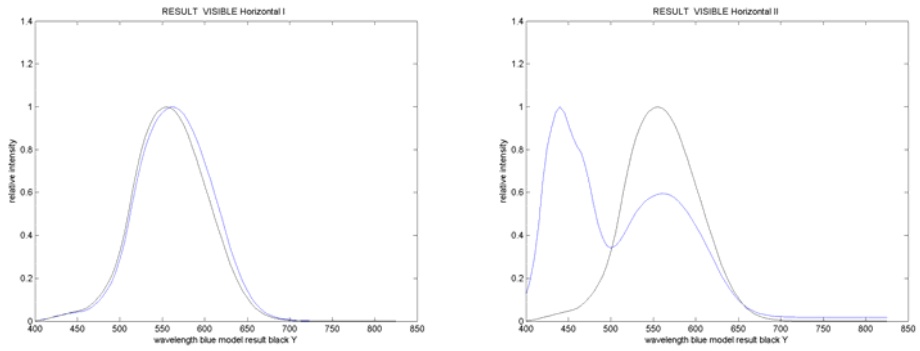

Figure 6.38. Response of the horizontal cells when presented stimuli along the visible spectrum. Blue: model result, black: Y. Left) HI. Right) HII.

In the HI case, the combined effect of photoreceptors type L and M is shown (maximum around 560 nm). One must remember that HI horizontal cells receive 61.5 % of the signal from type L photoreceptors and 38.5 % from type M (see equation 6.16).

Type HII also includes the effect of type S photoreceptor (new maximum in 440 nm). Type II horizontal cells receive 50 % of the signals from type S photoreceptors, 30.7 % from type L and 19.3 % from type M (see equation 6.17).

These results are consistent the measurements taken in horizontal cells when presented chromatic stimuli. As the following figure shows, type HI horizontal cells are activated with red and green stimuli whereas type HII are activated with red, green and especially blue stimuli (greater size of the generated signal). The model, as happens in the case of photoreceptors, works with signals that are activated by the presence of light, unlike physiological signals.

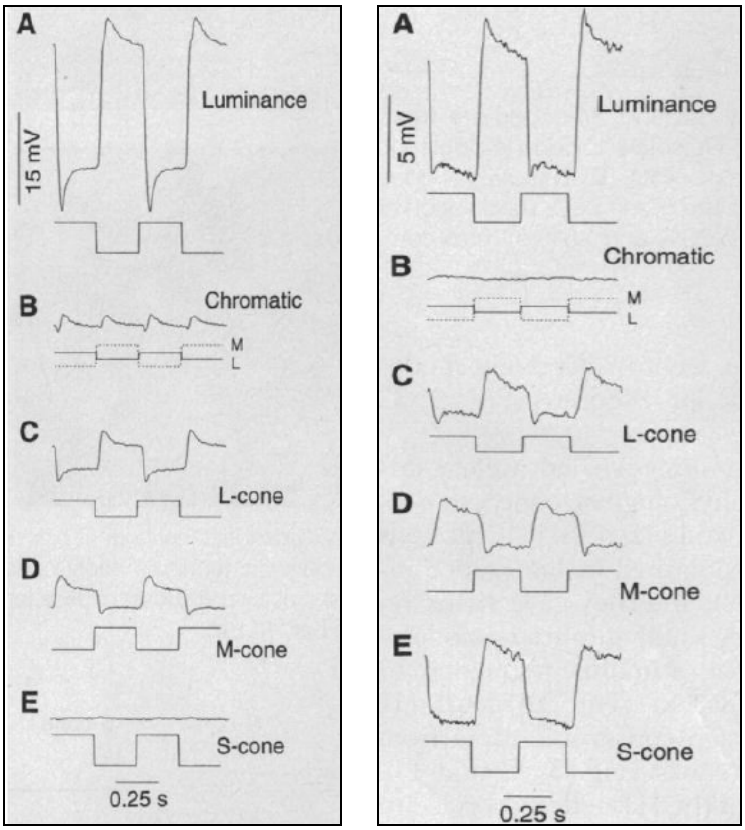

Figure 6.39. Horizontal cell response to chromatic stimuli. Left) HI. Right) HII. Source: [DACE_96]

5) Opponency

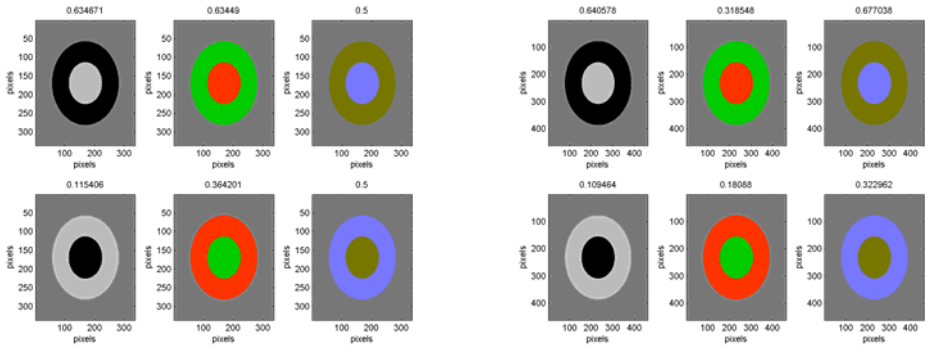

Figure 6.40. Signal produced by horizontal cells when presented stimuli with chromatic opponency. Output signal of each horizontal cell is represented by a numerical value above each figure Left) HI. Right) HII.

The response is different for each colour combination as the horizontal cells of type I and II receive signals from different photoreceptors with different weights. The same as for previous chromatic stimuli, the influence of the L and M values on type HI cells is verified while type II add the S value.

The results of horizontal cells when presented different stimuli have been presented. Their coherence is checked against physiological data. One can notice the influence, although small, of the modulation proper of photoreceptors within the receptive flied of the horizontal cell.

Therefore, they are a set of cells with a homogeneous receptive field (do not have opponency) and with partial chromatic nature.

6.3 Midget bipolar cells

The structure of the receptive field of midget bipolar cells includes an activation effect through a sole photoreceptor and an inhibition effect through the set of horizontal cells to which the photoreceptor is connected to. The structure of this field can be seen below, with a central activation area and the inhibition area of the surrounding horizontal cells.

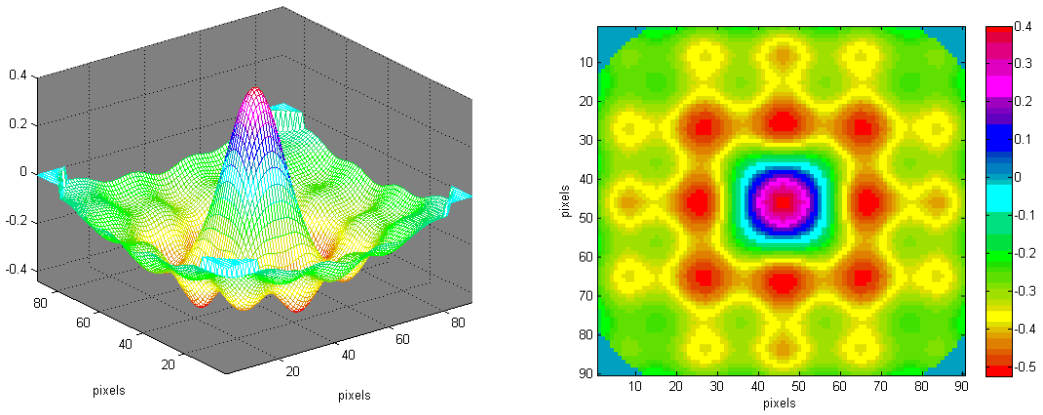

Figure 6.41. Representation of the receptive field of a midget bipolar cell where the integration of its dendritic field, shaped as a Gaussian, is superimposed on the receptive fields of the horizontal cells to which it connects, which in turn are modulated by the photoreceptor fields in its area of influence. Left) 3D view. Right) Top View.

Midget bipolar cells have 4 subtypes: R On, R Off, G On and G Off, depending on the type of photoreceptor they connect to and according to whether they establish invaginated or basal connections with that photoreceptor (see Chapter IV, section 3).

The signals of the different subtypes of midget bipolar cells can be calculated in two different ways based on the set of parameters mentioned in earlier sections: subtraction and division. The following shows the calculations of these signals.

a) Subtraction mode

$$\text{Midget bipolar R} = \int_{\substack{\text{Integration field of}\\ \text{the midget bipolar cell}}} \exp(-2*(x^2+y^2)/10^2)*\left(\begin{array}{l}\text{L Photoreceptor signal}\\ -0.6*(0.8*\text{Horizontal I Signal}+0.2*\text{Horizontal II Signal})\end{array}\right)$$

(eq. 6.18)

$$\text{Midget bipolar G} = \int_{\substack{\text{Integration field of}\\ \text{the midget bipolar cell}}} \exp(-2*(x^2+y^2)/10^2)*\left(\begin{array}{l}\text{M Photoreceptor signal}\\ -0.6*(0.8*\text{Horizontal I Signal}+0.2*\text{Horizontal II Signal})\end{array}\right)$$

(eq. 6.19)

b) Division mode

$$\text{Midget bipolar R} = \int_{\substack{\text{Integration field of}\\ \text{the midget bipolar cell}}} \exp(-2*(x^2+y^2)/10^2)*0.6\left(\frac{\text{L Photoreceptor signal}}{(0.8*\text{Horizontal I Signal}+0.2*\text{Horizontal II Signal})}\right)$$

(eq. 6.20)

$$\text{Midget bipolar G} = \int_{\substack{\text{Integration field of}\\ \text{the midget bipolar cell}}} \exp(-2*(x^2+y^2)/10^2)*0.6\left(\frac{\text{M Photoreceptor signal}}{0.8*\text{Horizontal I Signal}+0.2*\text{Horizontal II Signal}}\right) \quad \text{(eq. 6.21)}$$

In both cases, the type On and Off are calculated as follows:

$$\text{Midget bipolar R On} = \text{Midget bipolar } R - \overline{\text{Midget bipolar } R} \quad \text{(eq. 6.22)}$$

$$\text{Midget bipolar R Off} = \overline{\text{Midget bipolar } R} - \text{Midget bipolar } R \quad \text{(eq. 6.23)}$$

$$\text{Midget bipolar G On} = \text{Midget bipolar } G - \overline{\text{Midget bipolar } G} \quad \text{(eq. 6.24)}$$

$$\text{Midget bipolar G Off} = \overline{\text{Midget bipolar } G} - \text{Midget bipolar } G \quad \text{(eq. 6.25)}$$

Where the $\bar{x}$ symbol represents the average value of variable x. The response, in this case, is the same as that when presented an average grey stimulus (0.5, 0.5, 0.5).

The results of midget bipolar cells type R On are going to be shown for achromatic stimuli as they are structurally similar and therefore a representative sample of the set,. The remainder (type R Off, G On and G Off) shall only be included in chromatic stimuli where there are substantial differences in their responses.

The results with both options of photoreceptor-horizontal-bipolar connection modes are included: subtraction and division (see subsection 4.2.4). These modes have not been included in the two previous cell types as they are not affected by these options.

The following shows the results of the model's bipolar cells when presented the set of test stimuli.

1) Spot

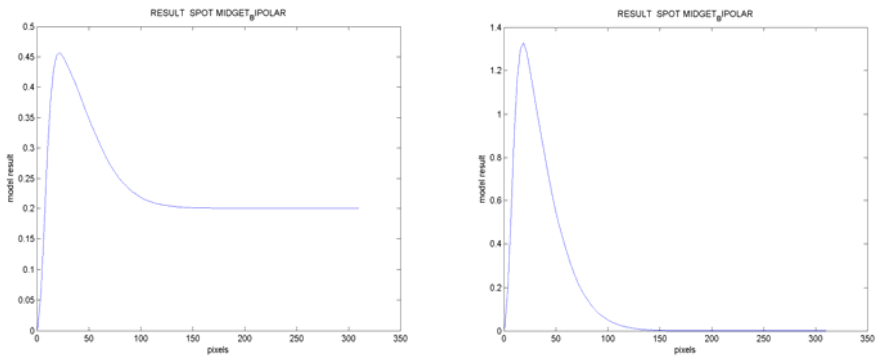

Figure 6.42. Response of a midget bipolar cell type R On when presented a variable radius white spot. Left) Subtraction mode. Right) Division mode.

A change can be seen regarding previous types. In this case, the signal begins with the reference value 0 (one must remember that in this stage the on and off pathways are split, which causes the neutral or average (average grey) stimulus to generate an output 0, see equations 6.9 and 6.10. The signal begins to increase as the spot grows, it covers a greater area of the receptive field of the associated photoreceptor while at the same time of the set of connected horizontal cells. It reaches a maximum value from which the influence of the set of horizontal cells which have a greater field of influence begin to make the signal decrease until it reaches its limit value that is reached when the spot covers the entire receptive field of the midget bipolar cell.

This behaviour is shown in physiological measurements of midget bipolar cells. The following figure shows these measurements.

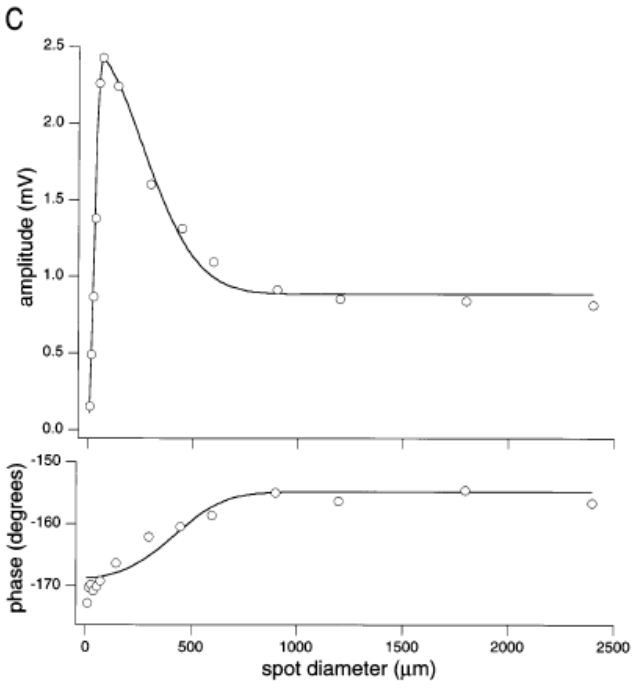

Figure 6.43. Physiological measurement of the response of midget bipolar cells type Off when presented a variable radius spot (the signal is a spot that is activated with a 2.44Hz frequency, the shown signal represents the values of the negative cycles, which accounts for the positive behaviour on the axis). Source: [DACE_00]

The difference between the subtraction and the division modes is that both begin with a null signal but the subtraction mode has a non-null limit value whereas the division is null. In this case, the results of figure 6.43 have greater similarity with the subtraction mode.

2) Annulus

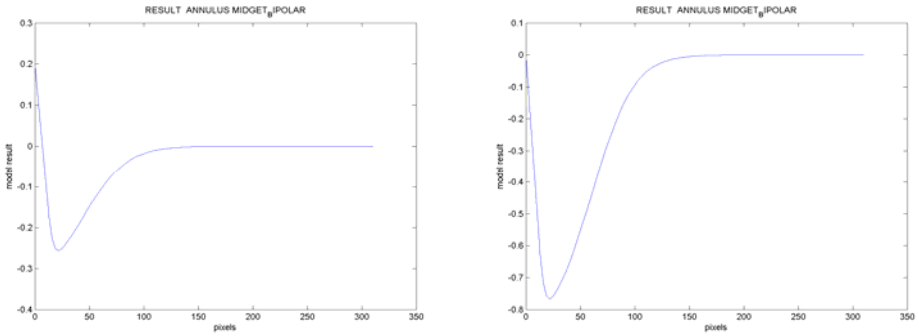

Figure 6.44. Response of a midget bipolar cell type R On when presented a white annulus with a variable inner radius. Left) Subtraction mode. Right) Division mode.

The signal begins with a completely white spot and therefore matches with the limit value of the spot in the earlier case (different for subtraction and division modes). When the interior radius of the annulus is increased, the central area of the photoreceptor and the set of horizontals covered by the white annulus decreases and thus the cell response. The minimum value is reached when the influence of the set of horizontals decreases. The limit value 0 is reached as a response to an average grey stimulus.

The following figure shows the physiological response of a midget bipolar cell type Off when presented a variable radius annulus. The signal generated by the model is consistent these measurements.

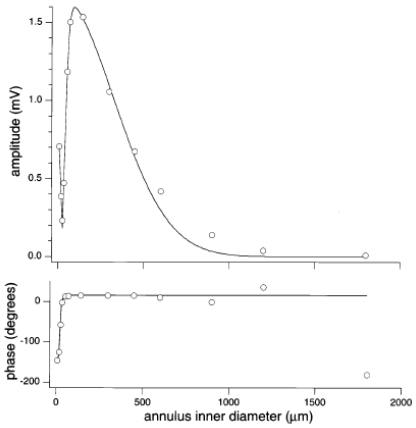

Figure 6.45. Physiological measurement of the response of midget bipolar cells type Off when presented a variable radius annulus (the signal is a spot that is activated with a 2.44Hz frequency, the shown signal represents the values of the negative cycles, which accounts for the positive behaviour on the axis). Source: [DACE_00]

The response has greater similarity with the division mode in this case.

3) Grid

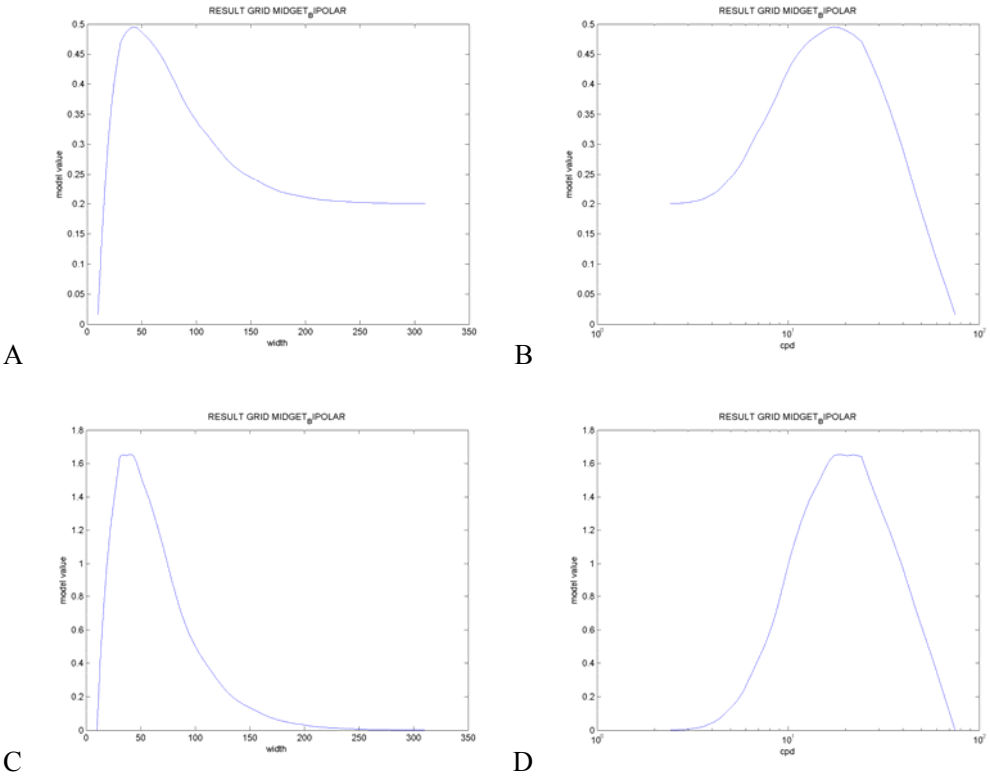

Figure 6.46. Response of a midget bipolar cell type R On when presented a variable size grid. A) Abscissas: grid width in pixels, subtraction mode. B) Abscissas: cycles per degree, subtraction mode. C) Abscissas: grid width in pixels, division mode. D) Abscissas: cycles per degree, division mode.

The response of midget bipolar cells when presented a grid that increases its size begins with a value that is approximately null (0). When the grid size increases, the area of the receptive field covered by the white stripe centred in the cell increases and thus increases the value of the output of the cell until a maximum value, from which the influence of horizontal cells causes the signal to decrease to the limit value of the white stimulus.

The values of physiological measurements are similar to those generated by the model. The following are these measurements.

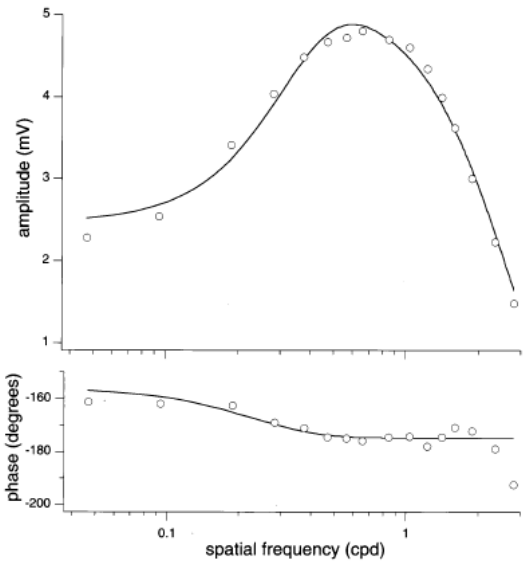

Figure 6.47. Physiological measurement of the response to midget bipolar cells when presented a variable grid. Source: [DACE_00]

The measurements have greater similarity to the subtraction mode in this case.

4) Visible spectrum

a) Subtraction mode

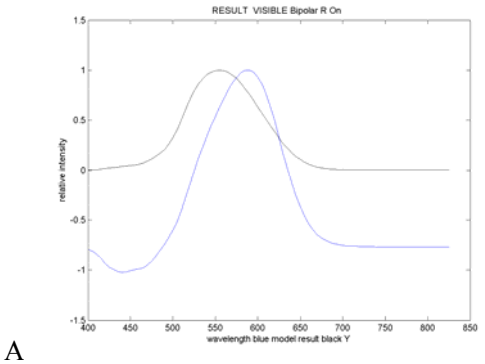

A

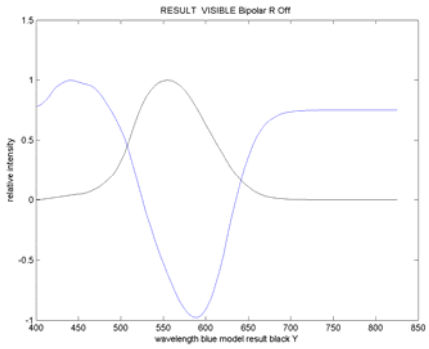

B

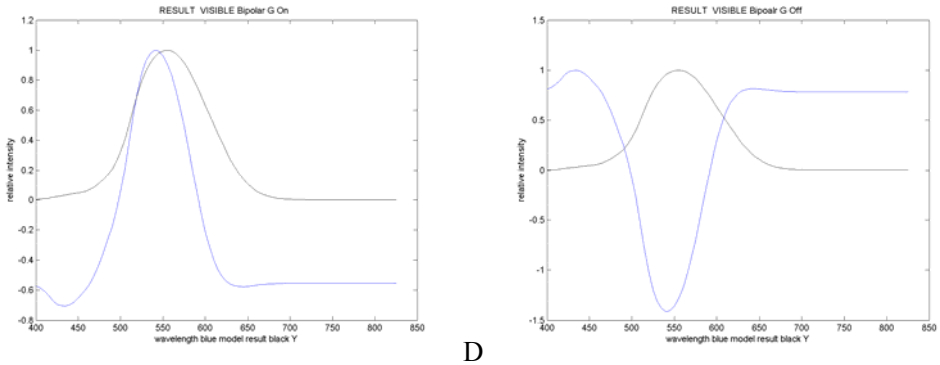

C D

Figure 6.48. Response of midget bipolar cells when presented stimuli throughout the visible spectrum. Blue: model result, black: Y. A) Cell type R On. B) Cell type R Off. C) Cell type G On. D) Cell type G Off. Subtraction mode.

The signals of midget bipolar cells respond to different bandwidths of the visible spectrum:

- R On: active response (positive) from 530 nm to 635 nm.
- G On: active response between 500 nm and 590 nm.
- R Off: complementary active response to R On: 400 nm to 530 nm and from 635nm to 825 nm.
- G Off: complementary active response to G On: 400nm to 500nm and from 590nm to 825nm.

b) Division mode

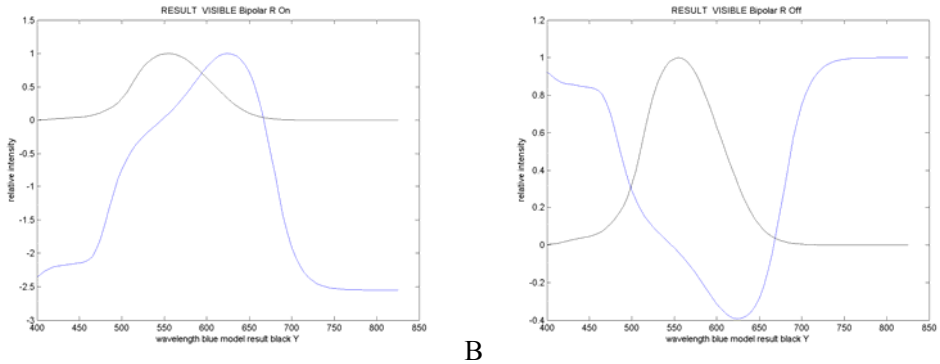

A B

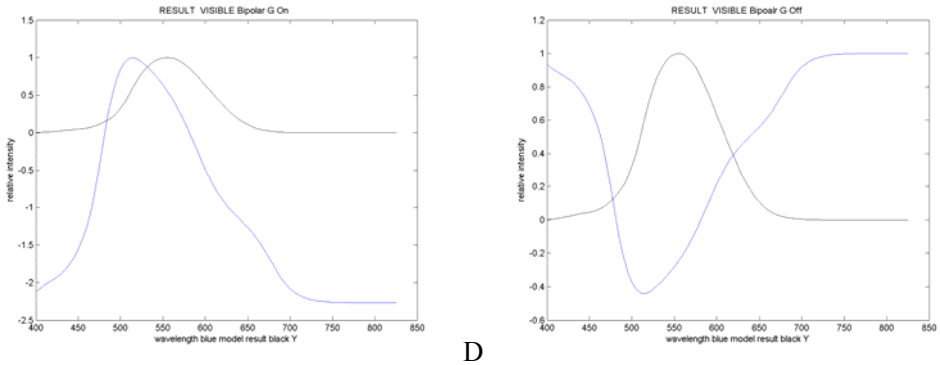

C D

Figure 6.49. Response of midget bipolar cells when presented stimuli throughout the visible spectrum. Blue: model result, black: Y. A) Cell type R On. B) Cell type R Off. C) Cell type G On. D) Cell type G Off. Division mode.

As happened in the earlier mode, the signals of midget bipolar cells respond to different bandwidths of the visible spectrum:

- R On: active response (positive) of 550 a 665nm.
- G On: active response between 485 nm and 580 nm.
- R Off: complementary active response to R On.
- G Off: complementary active response to G On.

When comparing the results with the Y values throughout the spectrum, one notices that, in both modes, type R are displaced towards the red area regarding the Y values (as happens with type L photoreceptors) and type G are displaced towards the opposite direction (as happens with type M photoreceptors). Based on these results, these can be classified as cells with a distinct chromatic nature.

5) Opponency

a) Subtraction mode

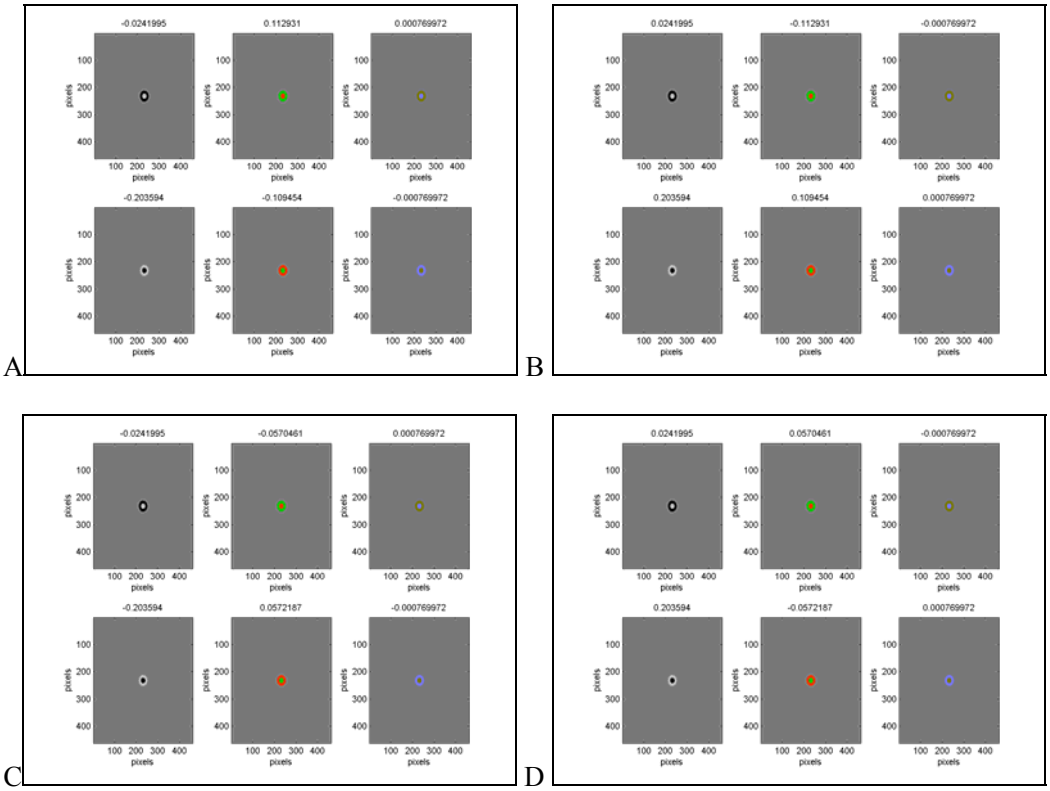

Figure 6.50. Response of midget bipolar cells when presented stimuli in opponency, the numeric values above each figure represent the output signal. Subtraction mode. A) R On. B) R Off. C) G On. D) G Off.

b) Division mode

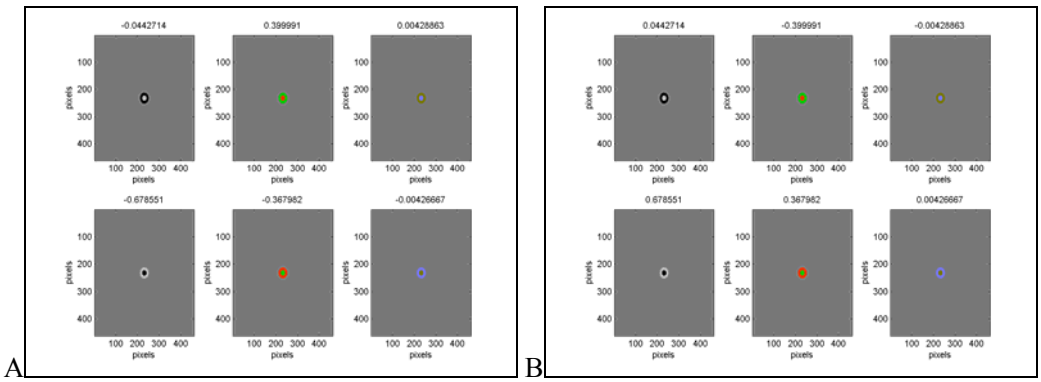

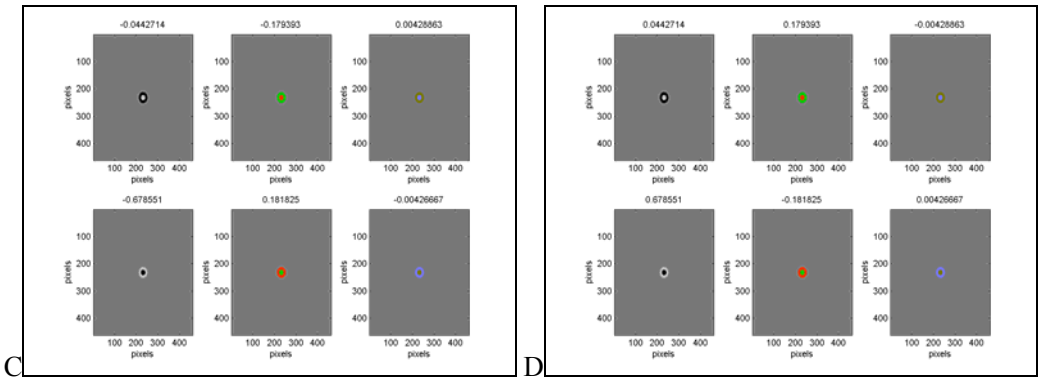

Figure 6.51. Response of midget bipolar cells when presented stimuli in opponency, the numeric values above each figure represent the output signal. Division mode. A) R On. B) R Off. C) G On. D) G Off.

Each subtype of midget bipolar cell type On especially responds to one of the stimulus in chromatic opponency for R On, red in the centre and green in the surround (red vs. green) and for G On, green in the centre and red in the surround. Given that the response is less when presented a white vs. black stimulus, it defines a chromatic opponency process.

Off type have a maximum response to black stimulus in the centre and white in the surround as these are activated by smaller values than average stimuli.

The presence of two areas in opponency within the receptive field has been verified through achromatic stimuli: centre and surround.

The difference between the subtraction and division mode has been shown. In the first case, the cell responds differently to homogeneous stimuli: grey image or white image (≈large sized white spot) while in the second, it responds similarly when presented both stimuli. On the other hand, the division mode highlights more those signals produced in the changes.

The generated results by the model are consistent with the physiological data. The subtraction or division mode can not be selected based on these data.

The case of chromatic stimuli has shown how each midget bipolar cell subtype responds to different bands of the visible spectrum and elements in opponency. Type R On is activated in the orange and red area while type G On is activated in the green area. Type Off responds to the spectrum bands that are complementary to the type On. Each subtype responds to their associated

stimulus in opponency and are consistent with the studies that identify cells with opponency red vs. green.

Therefore, these are cells with opponency centre vs. surround with a distinct chromatic character.

6.4 Diffuse bipolar cells

The structure of the receptive field of diffuse bipolar cells includes the set of photoreceptors from which they receive the signal and the signal in opponency of the set of horizontal cells that are connected to these photoreceptors (the fields of the horizontals are in turn modulated by the photoreceptors from which they receive the signal). All this set is modulated by the Gaussian integration function of the diffuse bipolar cell. The following shows this receptive field. The central area, unlike the previous case, isn't a pure Gaussian but rather shows the modulation of each photoreceptor.

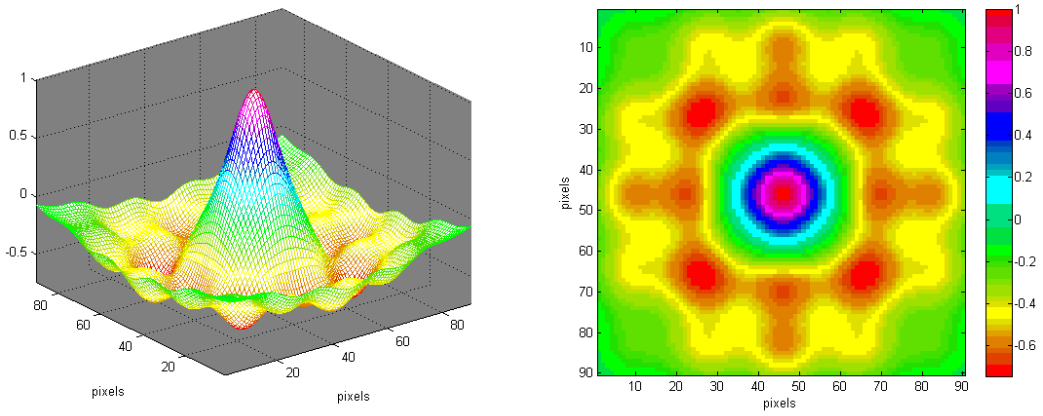

Figure 6.52. Representation of the receptive field of a bipolar diffuse cell where the integration of its dendritic field, shaped as a Gaussian, is superimposed on the receptive fields of the cones and horizontals to which it connects. Left) 3D view. Right) Top View.

Taking into account the previously mentioned parameters, the signals of the different subtypes of diffuse bipolar cells can be calculated in two ways: subtraction and division. The following shows the calculations of these signals.

a) Subtraction mode

$$\text{Bipolar DBX} = \int_{\substack{\text{Integration field}\\ \text{of the difusse}\\ \text{bipolar DBX}}} \exp\left(\frac{-2*(x^2+y^2)}{DifusseRadiusX^2}\right) * \begin{pmatrix} [0.572*\text{L Photoreceptor Signal} - 0.6*(0.8*\text{Horizontal I Signal} + 0.2*\text{Horizontal II Signal})] \\ +[0.358*\text{M Photoreceptor Signal} - 0.6*(0.8*\text{Horizontal I Signal} + 0.2*\text{Horizontal II Signal}) \\ [0.07*\text{S Photoreceptor Signal} - 0.6*(\text{Horizontal II Signal})] \end{pmatrix}$$

(eq. 6.26)

b) Division mode

$$\text{Bipolar DBX} = \int_{\substack{\text{Integration field}\\ \text{of the difusse}\\ \text{bipolar DBX}}} \exp\left(\frac{-2*(x^2+y^2)}{DifusseRadiusX^2}\right) * 0.6 * \begin{pmatrix} [0.572*\text{L Photoreceptor Signal}/(0.8*\text{Horizontal I Signal} + 0.2*\text{Horizontal II Signal})] \\ +[0.358*\text{M Photoreceptor Signal}/(0.8*\text{Horizontal I Signal} + 0.2*\text{Horizontal II Signal}) \\ [0.07*\text{S Photoreceptor Signal}/(\text{Horizontal II Signal})] \end{pmatrix}$$

(eq. 6.27)

Where X= {1..6}. The integration radii are different for each type of diffuse bipolar cell DB1=24.29; DB2=25.29; DB3= 30; DB4=26.92; DB5= 25.69; DB6=31.62.

Finally, the signals of the different subtypes of diffuse bipolar cells are calculated as follows.

$$\text{Difusse Bipolar DB1} = \overline{Bipolar\ DB1} - Bipolar\ DB1 \quad \text{(eq. 6.28)}$$

$$\text{Difusse Bipolar DB2} = \overline{Bipolar\ DB2} - Bipolar\ DB2 \quad \text{(eq. 6.29)}$$

$$\text{Difusse Bipolar DB3} = \overline{Bipolar\ DB3} - Bipolar\ DB3 \quad \text{(eq. 6.30)}$$

$$\text{Difusse Bipolar DB4} = Bipolar\ DB4 - \overline{Bipolar\ DB4} \quad \text{(eq. 6.31)}$$

$$\text{Difusse Bipolar DB5} = Bipolar\ DB5 - \overline{Bipolar\ DB5} \quad \text{(eq. 6.32)}$$

$$\text{Difusse Bipolar DB6} = Bipolar\ DB6 - \overline{Bipolar\ DB6} \quad \text{(eq. 6.33)}$$

The following shows and analyses the responses of the model's diffuse bipolar cells when presented the set of stimuli.

1) Spot

a) Subtraction mode

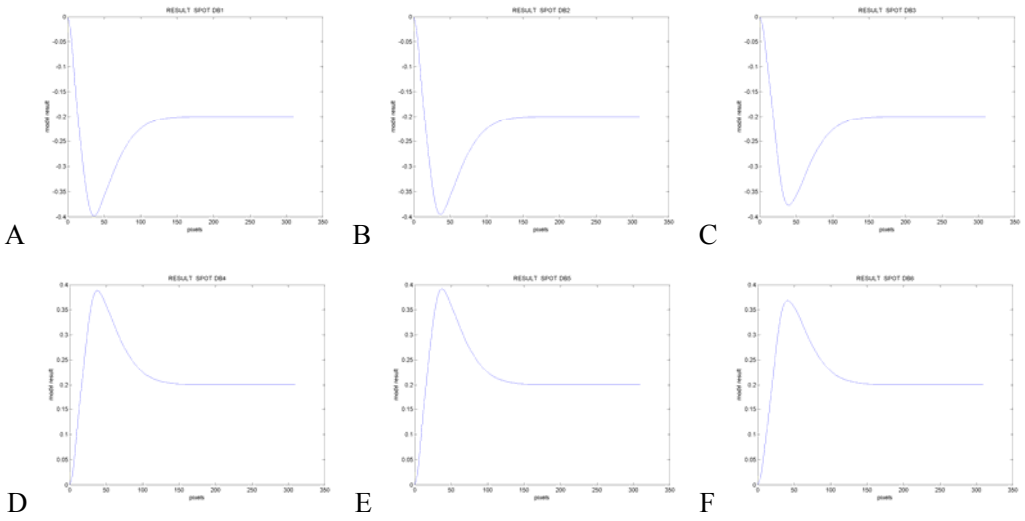

Figure 6.53. Response of diffuse bipolar cells when presented a variable radius white spot. A) Type DB1. B) Type DB2. C) Type DB3. D) Type DB4. E) Type DB5. F) Type DB6. Subtraction mode.

b) Division mode

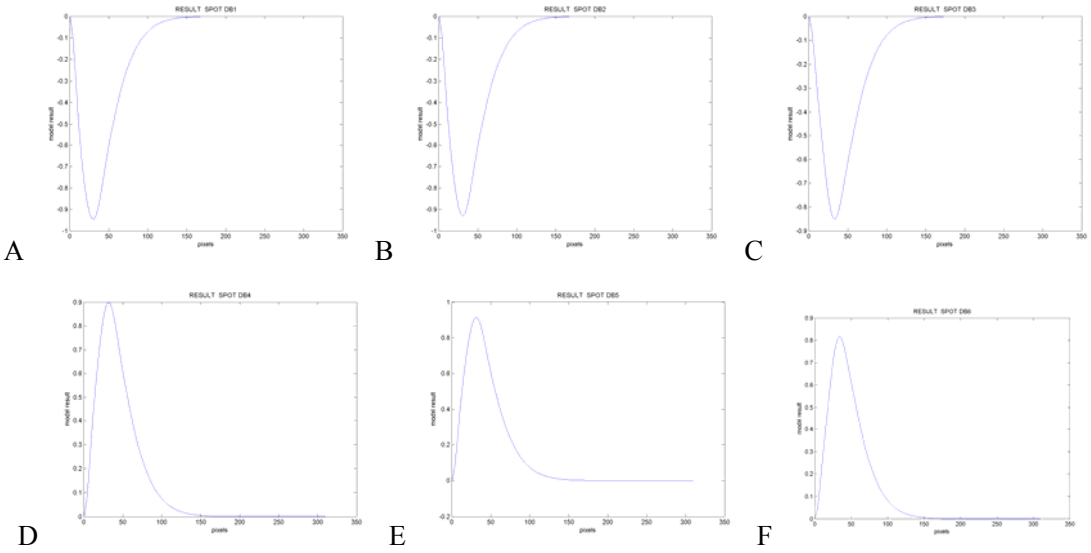

Figure 6.54. Response of diffuse bipolar cells when presented a variable radius white spot. A) Type DB1. B) Type DB2. C) Type DB3. D) Type DB4. E) Type DB5. F) Type DB6. Division mode.

The response of diffuse cells has a similar behaviour to that of midget bipolar cells, scaled in each case to the cell size of each diffuse bipolar cell that is being studied. There are two types of diffuse bipolar cells, those that are activated when presented stimuli with greater intensity than the average (DB4, DB5 and DB6) and those that are activated when presented stimuli of lesser intensity than the average (DB1, DB2 and DB3). All begin with a response 0 when presented an average grey stimulus. DB4, DB5 and DB6, when the spot radius is increased, they begin to increase the generated signal until the influence of the surround reverses the tendency of growth. From this moment, the output signal tends to the limit value generated by a white coloured spot that covers the cell's entire receptive field. As happened in the previous case, the subtraction mode has a limit value that is not zero while the division mode is indeed zero.

The signals of DB1, DB2 and DB3 cells decrease with the increase in the radius of the white spot (when the spot is black, the same behaviour as in the case of DB4-DB6 can be observed). When the radius increases enough, the influence of horizontal cells overcomes the photoreceptors and begins to increase the value of the output signal, showing a tendency towards the limit value of a white spot that covers its entire receptive field. The limit values are opposite to the limit values of DB4 to DB6. In the division case, they match as both are null.

2) Annulus

a) Subtraction mode

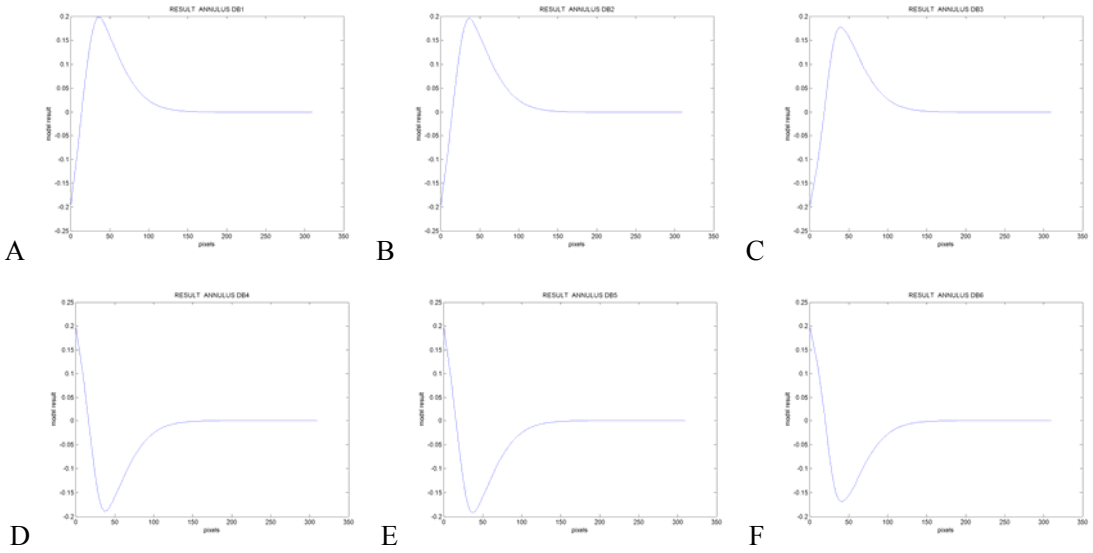

Figure 6.55. Response of diffuse bipolar cells when presented a white annulus with variable inner radius. A) Type DB1. B) Type DB2. C) Type DB3. D) Type DB4. E) Type DB5. F) Type DB6. Subtraction mode.

b) Division mode

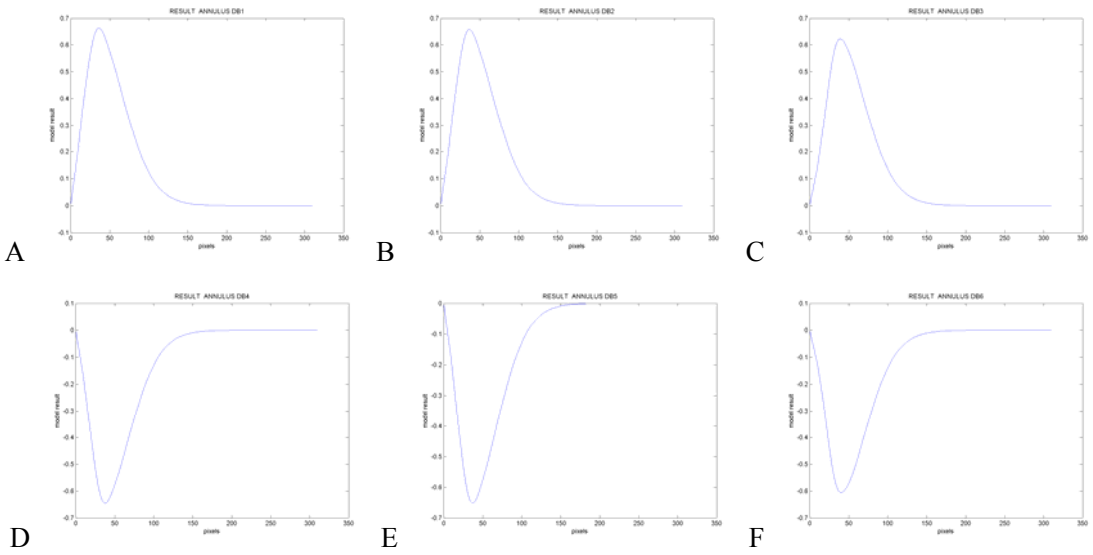

Figure 6.56. Response of diffuse bipolar cells when presented a white annulus with variable inner radius. A) Type DB1. B) Type DB2. C) Type DB3. D) Type DB4. E) Type DB5. F) Type DB6. Division mode.

The results, in the case of a annulus shaped stimulus, have the same characteristics that in the case of midget bipolars, scaled to their cell sizes. All begin in the limit values of the white spot stimulus. The signals, in DB4 to DB6 cases, decrease as it has less coverage of the active field covered by the white stimulus when the size of the inner radius of the annulus increase. It reaches a size where the influence of the surround decreases and the signal begins to grow until it reaches the value for the average grey stimulus. The signal, in DB1 to DB3 cases, grows as the average grey stimulus increases the coverage of the receptive field area, when the inner radius increases. This is due to the fact that these cells detect stimuli that are below average and therefore the average grey stimulus is more active in them than the white stimulus. Finally, it reaches a maximum value and later decrease until it reaches its limit response value for an average grey stimulus.

3) Grid

a) Subtraction mode

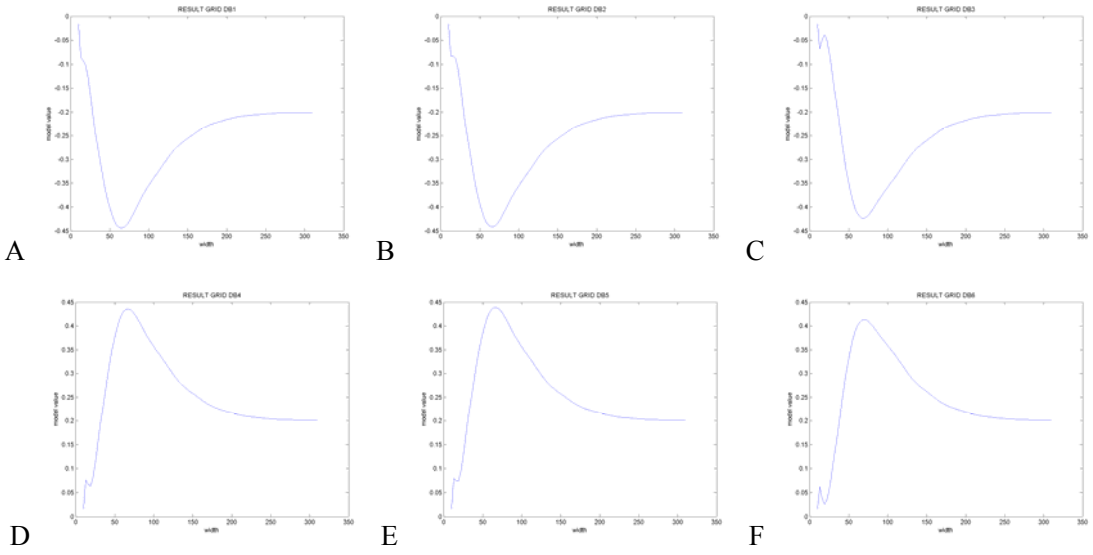

Figure 6.57. Response of diffuse bipolar cells when presented a variable size grid. Abscissas: grid width in pixels. A) Type DB1. B) Type DB2. C) Type DB3. D) Type DB4. E) Type DB5. F) Type DB6. Subtraction mode.

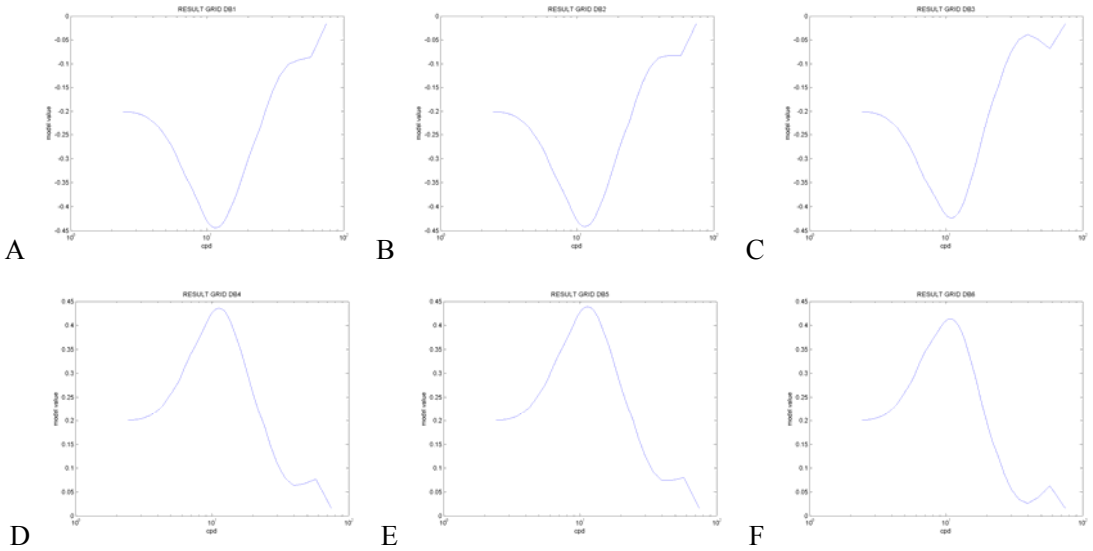

Figure 6.58. Response of diffuse bipolar cells when presented a variable size grid. Abscissas: cycles per degree A) Type DB1. B) Type DB2. C) Type DB3. D) Type DB4. E) Type DB5. F) Type DB6. Subtraction mode.

b) Division mode

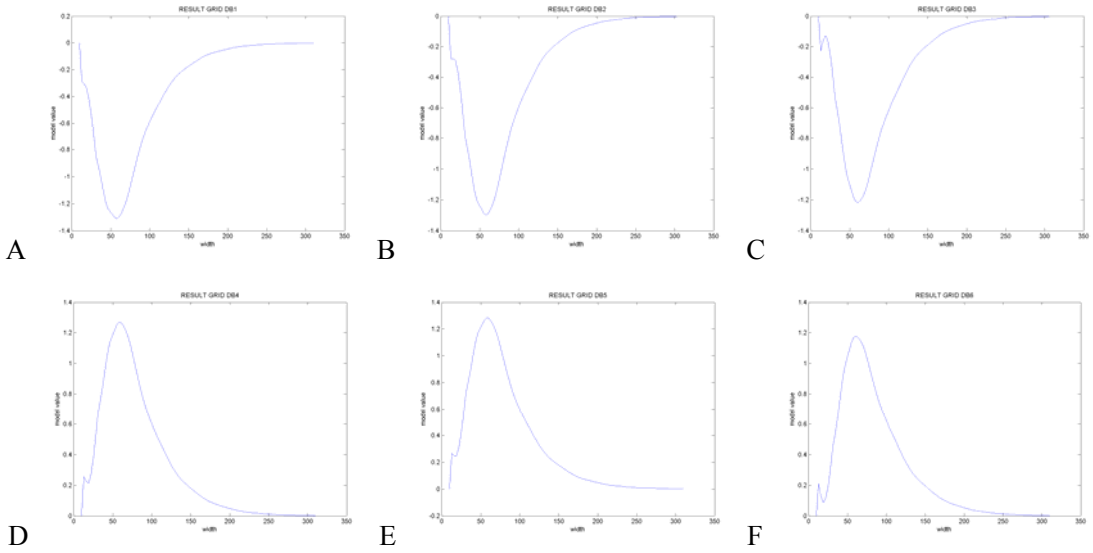

Figure 6.59. Response of diffuse bipolar cells when presented a variable size grid. Abscissas: grid width in pixels. A) Type DB1. B) Type DB2. C) Type DB3. D) Type DB4. E) Type DB5. F) Type DB6. Division mode.

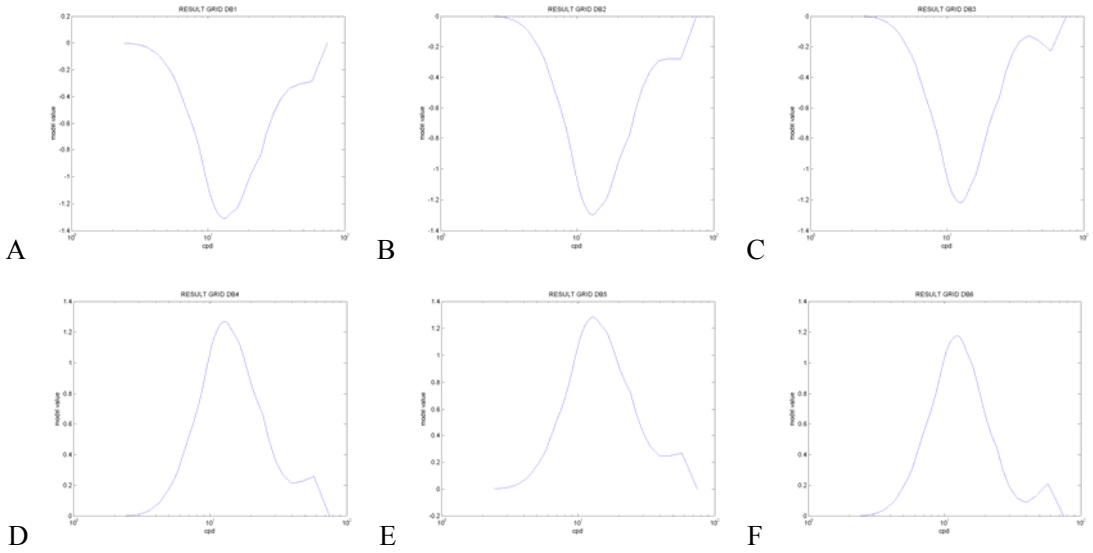

Fig. 6.60. Response of diffuse bipolar cells when presented a variable size grid. Abscissas: cycles per degree A) Type DB1. B) Type DB2. C) Type DB3. D) Type DB4. E) Type DB5. F) Type DB6. Division mode.

All 6 subtypes behave in a similar manner (except for the growth sign) when presented a variable size grid. When the bar width is increased, the area of the receptive field covered by the white bar centred in the cell grows, increasing the output signal (decreasing for DB1 to DB3) until the bar

covers a greater area of the surround. The signal's growth tendency reaches a maximum when the influence of the surround begins to exceed the centre's. Finally it shows a tendency to reach the limit value generated by diffuse bipolar cells when presented a white stimulus over the entire receptive field.

4) Visible spectrum

a) Subtraction mode

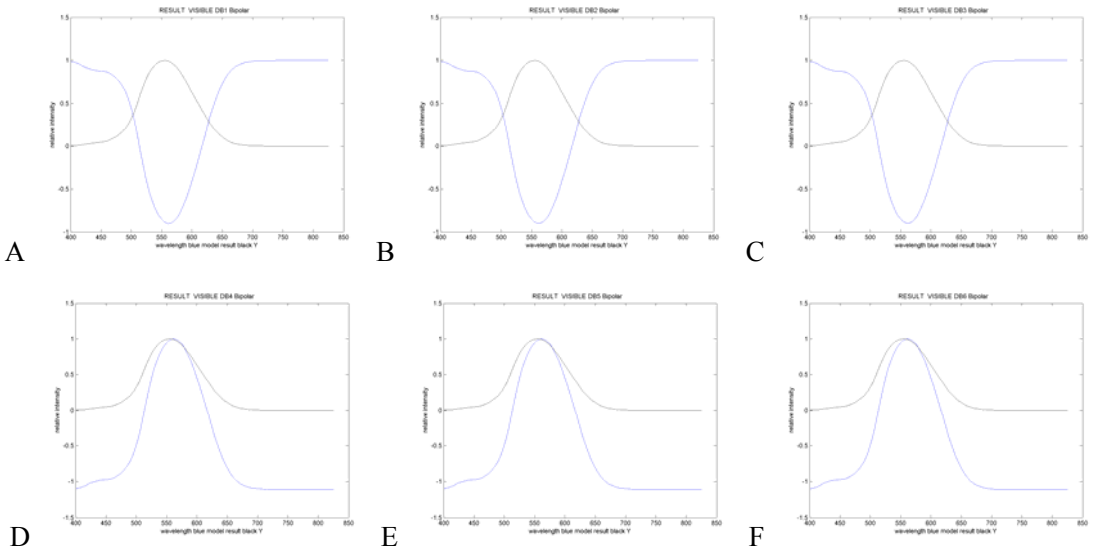

Figure 6.61. Response of diffuse bipolar cells when presented stimuli along the visible spectrum. Blue: model result, black: Y. A) Type DB1. B) Type DB2. C) Type DB3. D) Type DB4. E) Type DB5. F) Type DB6. Subtraction mode.

b) Division mode

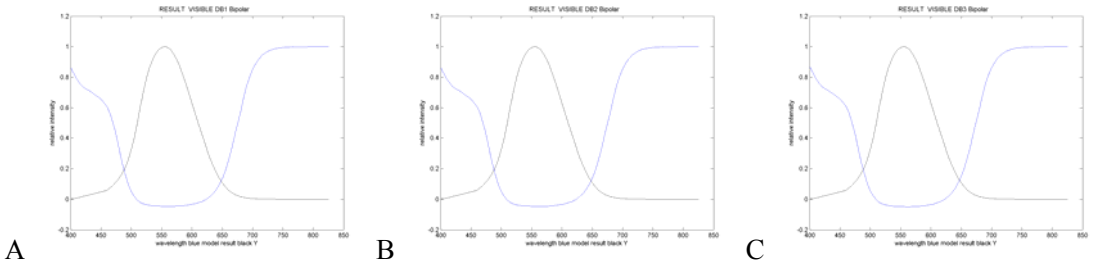

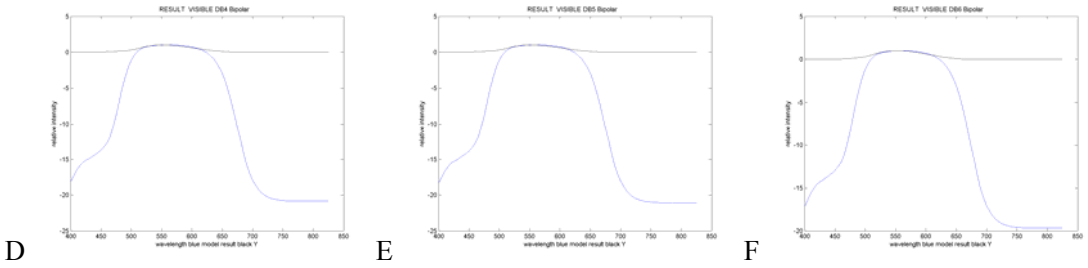

D E F

Figure 6.62. Response of diffuse bipolar cells when presented stimuli along the visible spectrum. Blue: model result, black: Y. A) Type DB1. B) Type DB2. C) Type DB3. D) Type DB4. E) Type DB5. F) Type DB6. Division mode.

The signals generated by diffuse bipolar cells have an activation band (cases of positive activation DB4-DB6) that is very similar to the Y values. Therefore, they can be classified as cells with an achromatic nature.

The activation band in the divisive mode, which matches with that of the subtraction mode, has more homogeneous output values.

5) Opponency

a) Subtraction mode

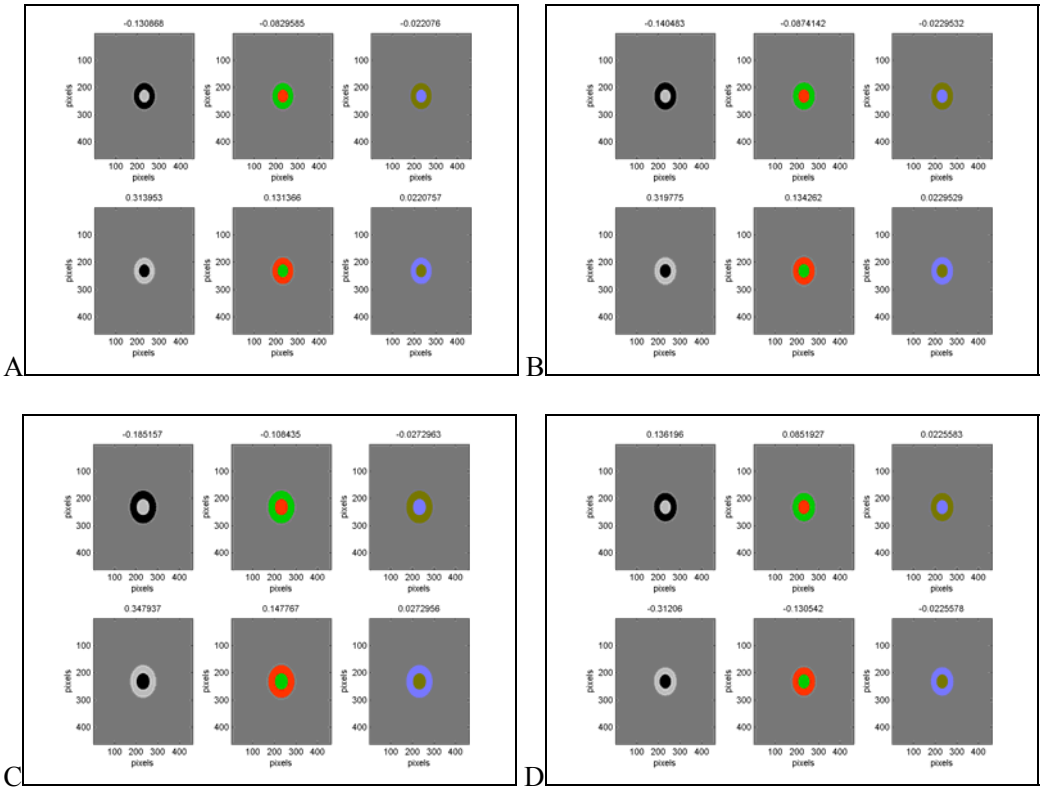

A B

C D

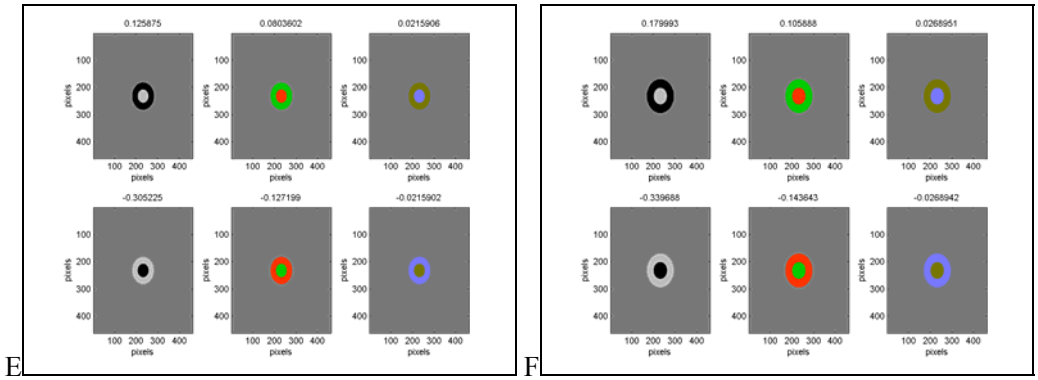

Figure 6.63. Response of diffuse bipolar cells when presented stimuli in opponency. Output signal is represented by the numerical data above each figure. A) Type DB1. B) Type DB2. C) Type DB3. D) Type DB4. E) Type DB5. F) Type DB6. Subtraction mode.

b) Division mode

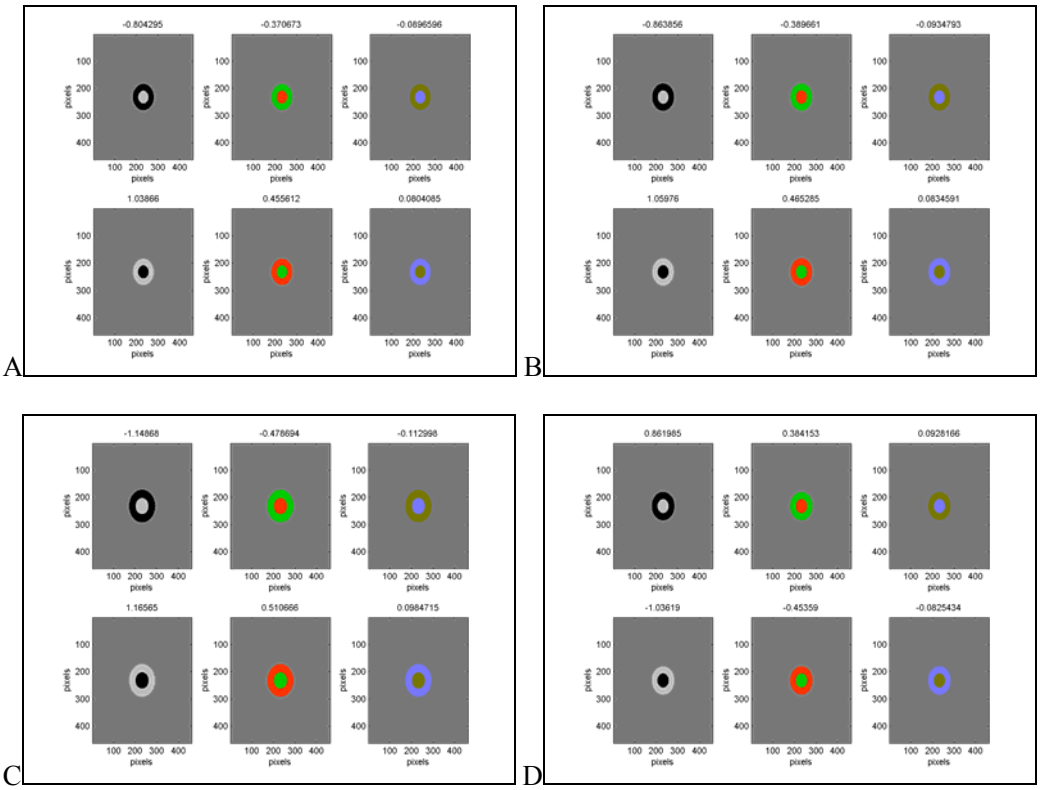

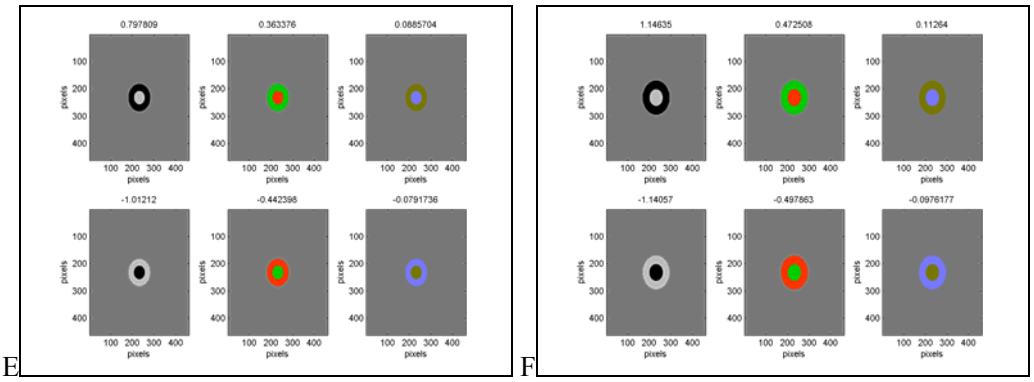

Figure 6.64. Response of diffuse bipolar cells when presented stimuli in opponency. Output signal is represented by the numerical data above each figure. A) Type DB1. B) Type DB2. C) Type DB3. D) Type DB4. E) Type DB5. F) Type DB6. Division mode.

One can observe how diffuse bipolar cells with a negative activation, DB1 to DB3, generate a maximum output when presented a black achromatic stimulus in the centre and white in the surround. On the other hand, DB4 to DB6 cells prefer a white achromatic stimulus in the centre and black in the surround. These results match those obtained throughout the visible spectrum, indicating that these are cells with achromatic nature.

There are two subtypes of diffuse bipolar cells: those that are activated when presented stimuli whose intensity is greater than average and those that are activated when presented lesser than average stimuli.

A behaviour in centre and surround opponency is shown when presented achromatic stimuli. Their response to chromatic stimuli when presented a wide band of the visible spectrum allows classifying them as achromatic.

The difference between the subtraction and division mode is similar to that observed in midget bipolar cells.

6.5 Blue bipolar cells

The structure of the receptive field of blue bipolar cells includes the influence in the central area of the set of photoreceptors to which it connects as well as the set of horizontal cells (in turn modulated by photoreceptors to which it connects) in inhibition mode. This set is modulated by

the Gaussian integration function of the blue bipolar cell. The following figure shows the structure of the receptive field.

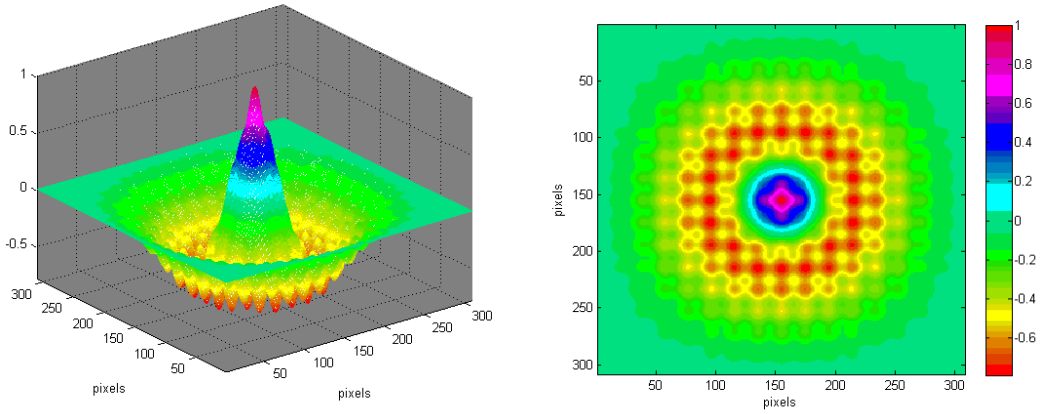

Figure 6.65. Representation of the receptive field of a blue bipolar cell where the integration of its dendritic field, shaped as a Gaussian, is superimposed on the receptive fields of the cones and horizontals in opponency to which it connects. Left) 3D view. Right) Top View.

The signals of the blue bipolar cells, taking into account the parameters mentioned before, can be calculated in two ways: subtraction and division. The following shows the calculations of these signals.

a) Subtraction mode

$$\text{Blue Bipolar} = \int_{\substack{\text{Integration field}\\ \text{of blue bipolar cell}}} \exp\left(\frac{-2*(x^2+y^2)}{28.5^2}\right)*\left(\text{S Photoreceptor Signal} - 0.6*\text{Horizontal II Signal}\right) - \overline{\textit{Blue Bipolar}}$$

(eq. 6.34)

b) Division mode

$$\text{Blue Bipolar} = \int_{\substack{\text{Integration field}\\ \text{of blue bipolar cell}}} \exp\left(\frac{-2*(x^2+y^2)}{28.5^2}\right)*0.6\left(\frac{\text{S Photoreceptor Signal}}{\text{Horizontal II Signal}}\right) - \overline{\textit{Blue Bipolar}}$$

(eq. 6.35)

The signals generated by the model's blue bipolar cells when presented the set of stimuli are presented next.

1) Spot

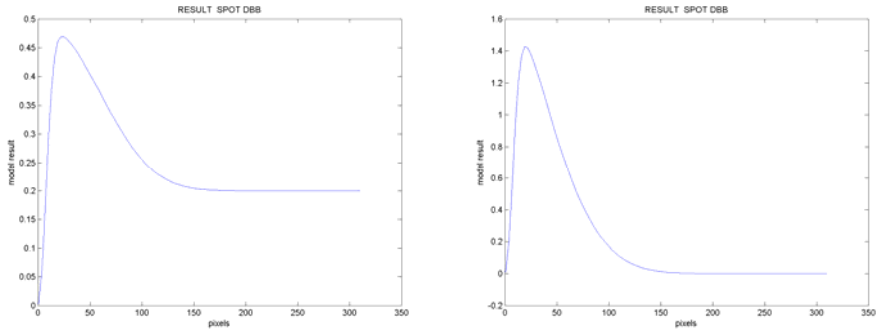

Figure 6.66. Response of a blue bipolar cell when presented a white spot with a variable radius. Left) Subtraction mode. Right) Division mode.

The response of blue bipolar cells when presented a white spot has the same structure as that of midget and diffuse bipolar cells, scaled to their cell size. They begin with a value 0 for an average grey stimulus. The signal increases as the radius increases and the white spot covers a greater area of the receptive field. It reaches a maximum value after which the influence of the surround wins over that of the centre and the signal begins to decrease towards the limit value of a white spot that covers the entire receptive field.

2) Annulus

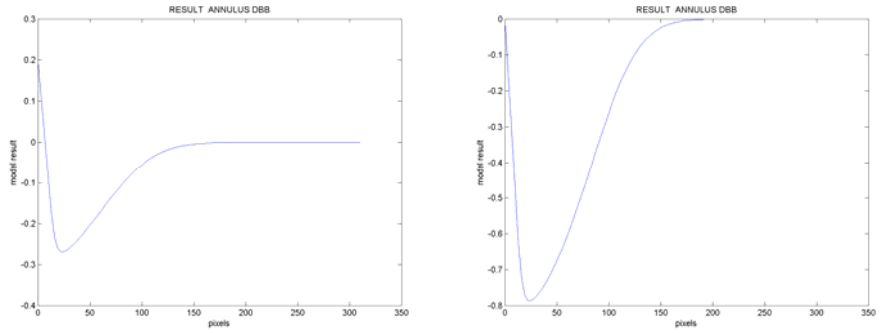

Figure 6.67. Response of a diffuse bipolar cell when presented a white annulus with a variable interior radius. Left) Subtraction mode. Right) Division mode.

The annulus shaped stimuli generate a response that begins with the limit value for a white stimulus that covers the entire receptive field. As the inner radius of the annulus increases, the signal decreases until it reaches a minimum after which the effect of the surround decreases and thus the signal increases, once again having a tendency towards the limit value of an

average grey stimulus. The response of blue bipolar cells when presented this type of stimulus is similar to that generated by other bipolar cells.

3) Grid

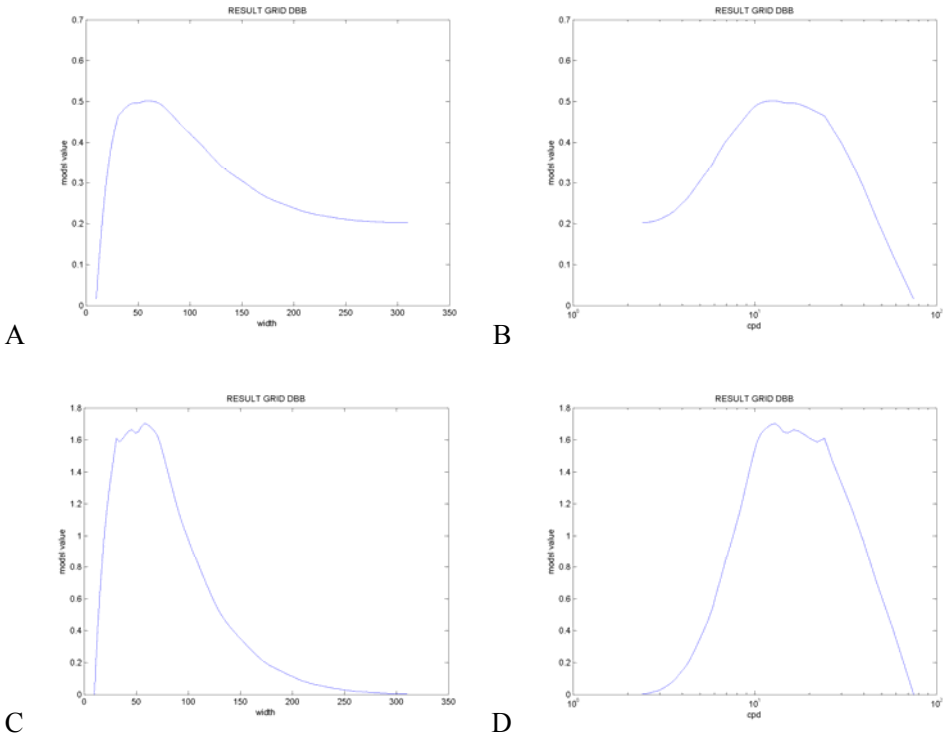

A B C D

Figure 6.68. Response of a blue bipolar cell when presented a variable size grid. A) Subtraction mode. Abscissas: grid width in pixels. B) Subtraction mode. Abscissas: cycles per degree C) Division mode. Abscissas: grid width in pixels. D) Division mode. Abscissas: cycles per degree.

Blue bipolar cells, when presented a variable size grid, respond in a similar manner as midget and diffuse bipolar cells. When the bar width is small, the generated signal tends to have a null value. When the bar width is increased, the signal increases up to its maximum value, as the white bar centred in the cell covers a greater area of the receptive field. When the influence of horizontal cells exceeds that of the centre, the signal decreases having a tendency towards the limit value for the white stimulus.

4) Visible spectrum

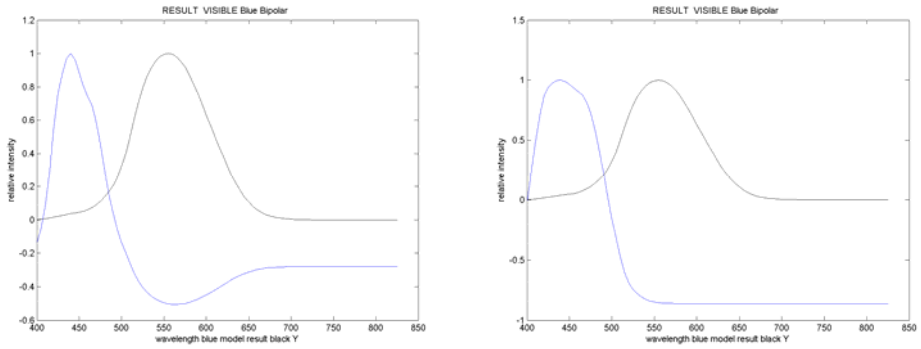

Figure 6.69. Response of a blue bipolar cell when presented stimuli along the visible spectrum. Left) Subtraction mode. Right) Division mode.

The signal of the blue bipolar cells along the visible spectrum responds to a band in the blue area in both modes: between 410 nm and 490 nm in the subtraction mode and between 400 nm and 495 nm in the division mode. This behaviour indicates that this is a cell with a chromatic nature.

5) Opponency

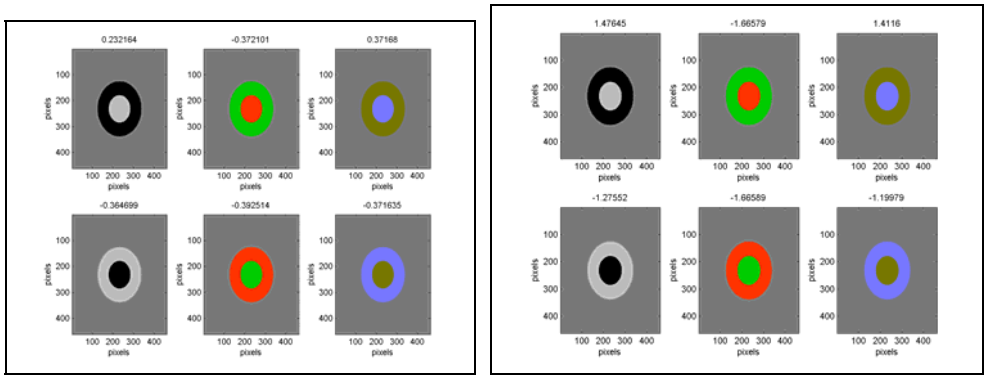

Figure 6.70. Response of a blue bipolar cell when presented stimuli in opponency. Output signal is represented by the numerical data above each figure. Left) Subtraction mode. Right) Division mode.

Blue bipolar cells, in subtraction mode, especially respond to opponency stimuli in blue vs. yellow. On the other hand, in the division mode, blue bipolar cells especially respond to opponency stimuli white vs. black and blue vs. yellow.

Achromatic stimuli, in the case of blue bipolar cells, indicate a process in spatial opponency centre vs. surround. This is a common feature of bipolar cells.

The structural difference between the subtraction and division modes is similar to that observed in midget bipolar cells.

Chromatic stimuli along the visible spectrum indicate that these are cells with chromatic nature.

There exists a slight difference, from the chromatic point of view, between the subtraction and division modes as the cells especially respond to the blue vs. yellow stimulus in the former whereas in the division they also respond to the white vs. black stimulus.

Therefore, these cells have opponency processes in centre-surround of a chromatic nature.

6.6 Midget ganglion cells

The structure of the receptive field of midget ganglion cells is equal to that of midget bipolar cells as they receive the signal directly from a midget bipolar cell. It has the influence of a central photoreceptor and a set of horizontal cells to which it connects. The following figure shows the receptive field.

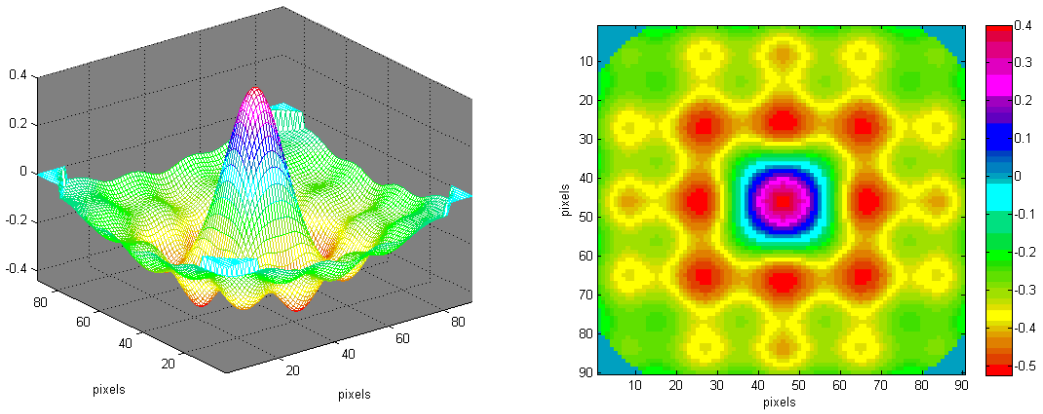

Figure 6.71. Representation of the receptive field of a midget ganglion cell. Left) 3D view. Right) Top View.

The functions for the generation of spikes of the different subtypes of midget ganglion cells, given the parameters presented in earlier sections, are the following:

$$\text{Midget ganglion R On} = 4.27 * \exp\left\{1.96 * \int_{\substack{\text{Integration field of}\\ \text{midget ganglion cell}}} \exp(-2*(x^2+y^2)/10^2) * \text{Midget bipolar R On}\right\} \quad \text{(eq. 6.36)}$$

$$\text{Midget ganglion R Off} = 4.27 * \exp\left\{1.96 * \int_{\substack{\text{Integration field of}\\ \text{midget ganglion cell}}} \exp(-2*(x^2+y^2)/10^2) * \text{Midget bipolar R Off}\right\} \quad \text{(eq. 6.37)}$$

$$\text{Midget ganglion G On} = 4.27 * \exp\left\{1.96 * \int_{\substack{\text{Integration field of}\\ \text{midget ganglion cell}}} \exp(-2*(x^2+y^2)/10^2) * \text{Midget bipolar G On}\right\} \quad \text{(eq. 6.38)}$$

$$\text{Midget ganglion G Off} = 4.27 * \exp\left\{1.96 * \int_{\substack{\text{Integration field of}\\ \text{midget ganglion cell}}} \exp(-2*(x^2+y^2)/10^2) * \text{Midget bipolar G Offf}\right\} \quad \text{(eq. 6.39)}$$

The following shows the responses of midget ganglion cells when presented the set of stimuli. As in the case of midget bipolars, for achromatic stimuli, the results of the type On cells are shown, as all types are structurally the same. In the case of chromatic stimuli, where responses are different, all types are shown.

The response, in the case of achromatic stimuli, is similar to that of midget bipolar cells. The difference lies in the magnitudes as ganglion cells generate spikes while bipolars generate voltage variations. As section 6.3 has a more detailed analysis of these types of responses, this section only shows the signals without including additional comments.

1) Spot

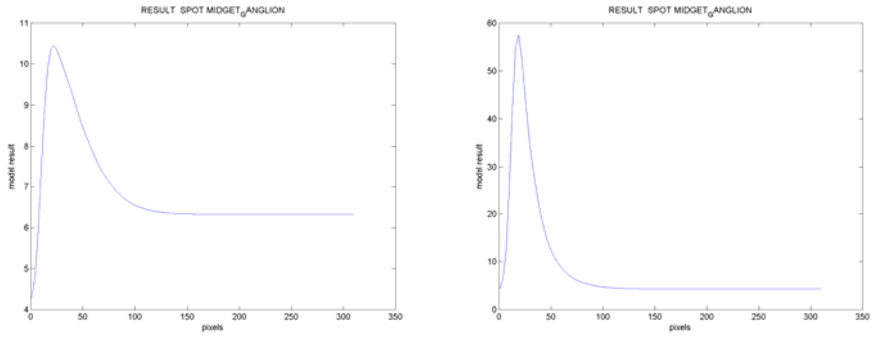

Figure 6.72. Response of a ganglion cell type R On when presented a white spot with a variable radius. Left) Subtraction mode. Right) Division mode.

2) Annulus

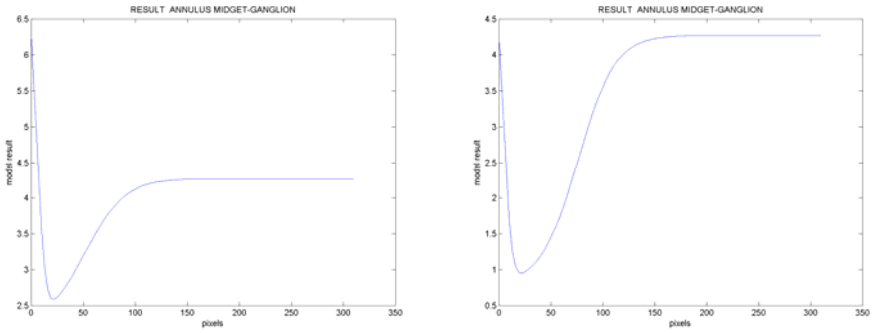

Figure 6.73. Response of a midget ganglion cell type R On when presented a white annulus with a variable radius. Left) Subtraction mode. Right) Division mode.

3) Grid

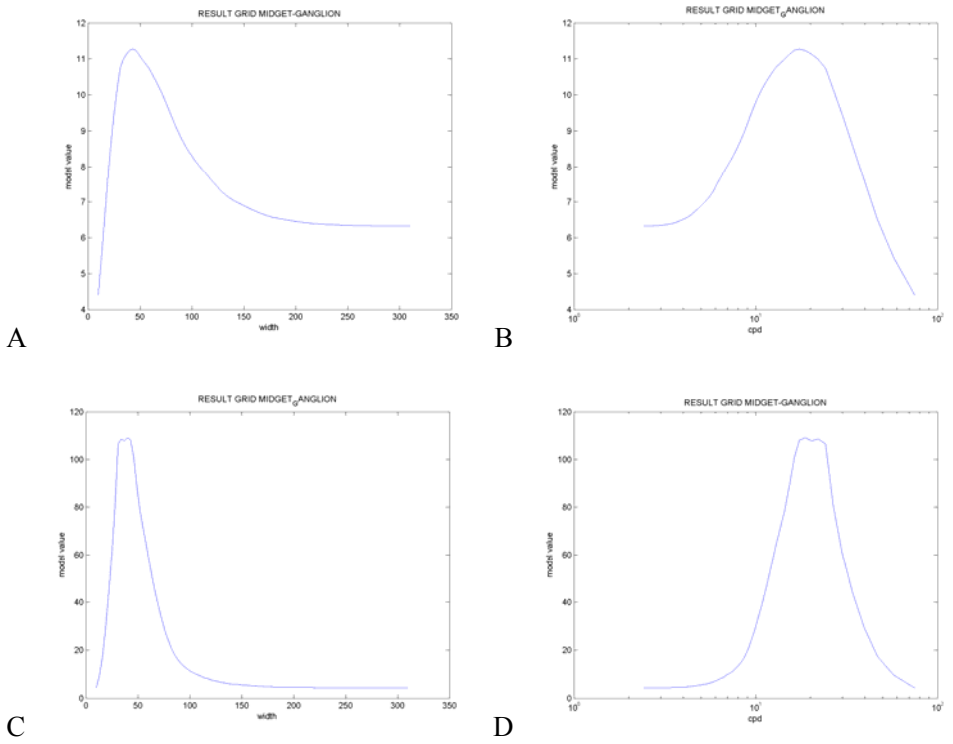

Figure 6.74. Response of a midget ganglion cell type R On when presented a variable size grid. A) Subtraction mode. Abscissas: grid width in pixels. B) Subtraction mode. Abscissas: cycles per degree C) Division mode. Abscissas: grid width in pixels. D) Division mode. Abscissas: cycles per degree.

4) Visible spectrum

a) Subtraction mode

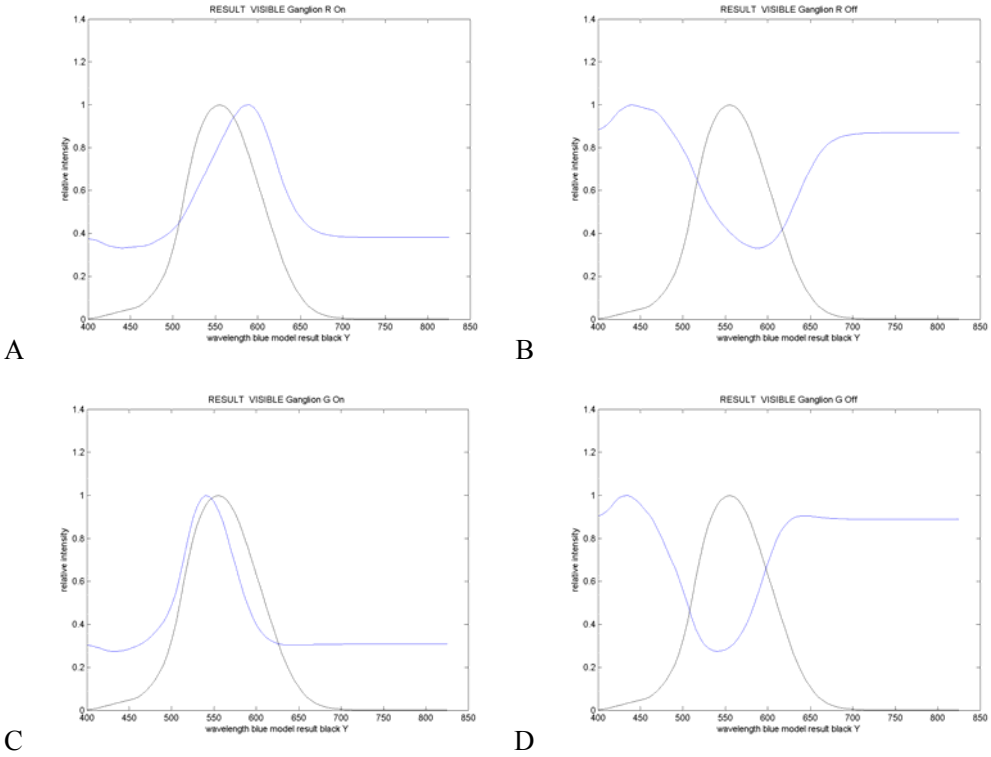

Figure 6.75. Response of midget ganglion cells when presented stimuli along the visible spectrum. Blue: model result, black: Y. A) Type R On. B) Type R On. C) Type G On. D) Type G Off. Subtraction mode.

b) Division mode

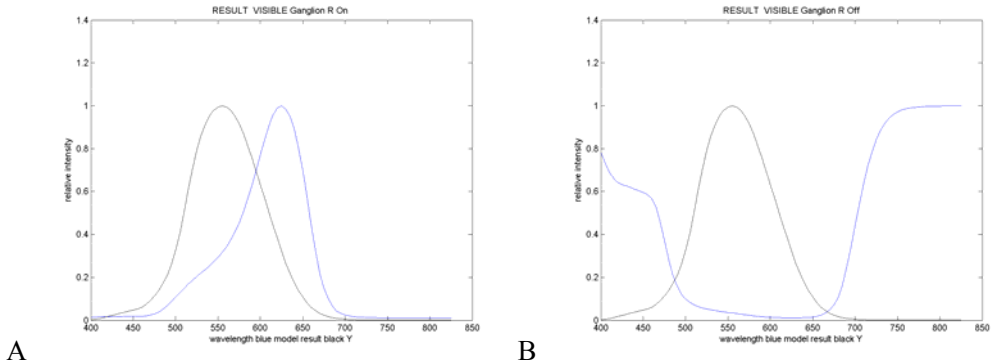

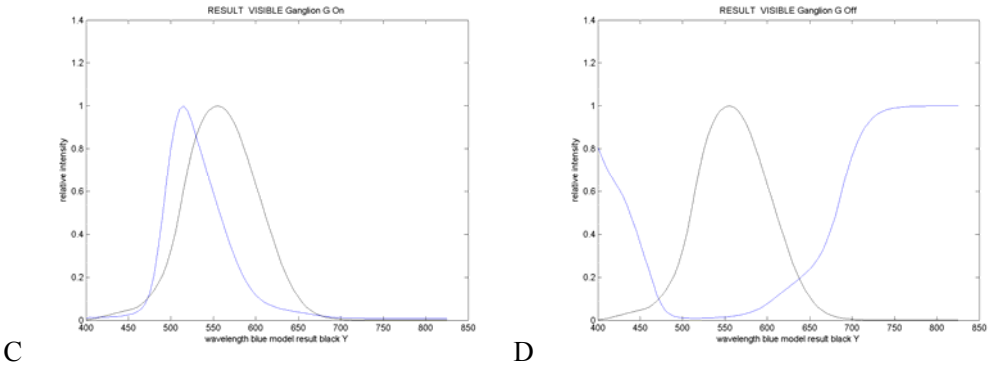

C D

Figure 6.76. Response of midget ganglion cells when presented stimuli along the visible spectrum. Blue: model result, black: Y. A) Type R On. B) Type R On. C) Type G On. D) Type G Off. Division mode.

Each of the midget ganglion cell subtypes responds to a spectrum band. Type R On respond to a band to the right of the peak of the Y values, indicating a preference for orange and red stimuli (530 nm-635 nm in the subtraction mode and between 550 nm and 665 nm in the division mode). On the other hand, type G On respond to a band that is slightly to the left of the maximum Y, in the area of green hues (between 500 nm and 590 nm in the subtraction mode and between 485 nm and 580 nm in the division mode). As in other cases, there is a certain difference between the active bands in the subtraction and division mode.

5) Opponency

a) Subtraction mode

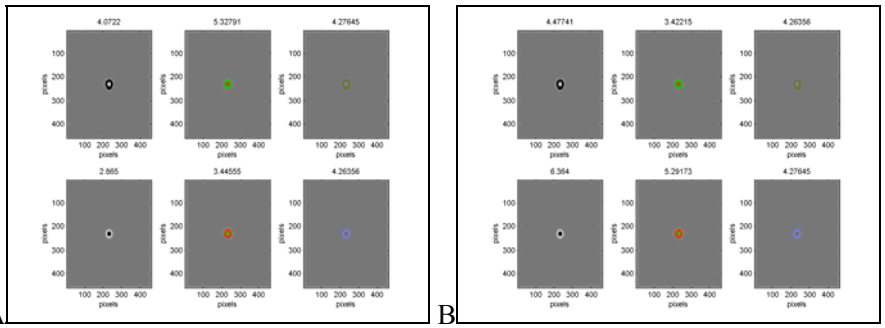

A B

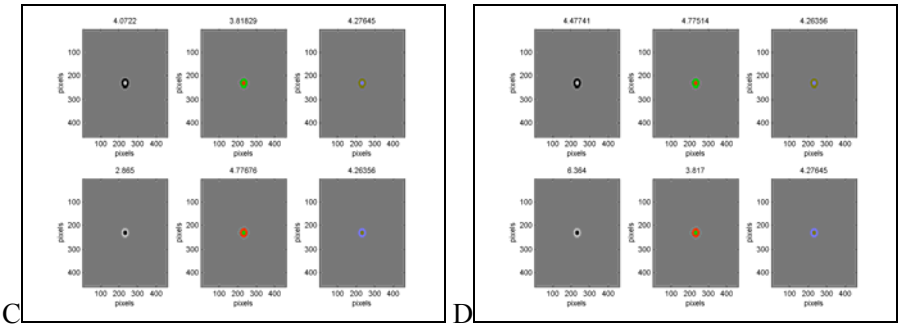

C D

Fig. 6.77. Response of midget ganglion cells when presented stimuli in opponency, output signal represented by the numeric values above each figure. Subtraction mode. A) R On. B) R Off. C) G On. D) G Off.

b) Division mode

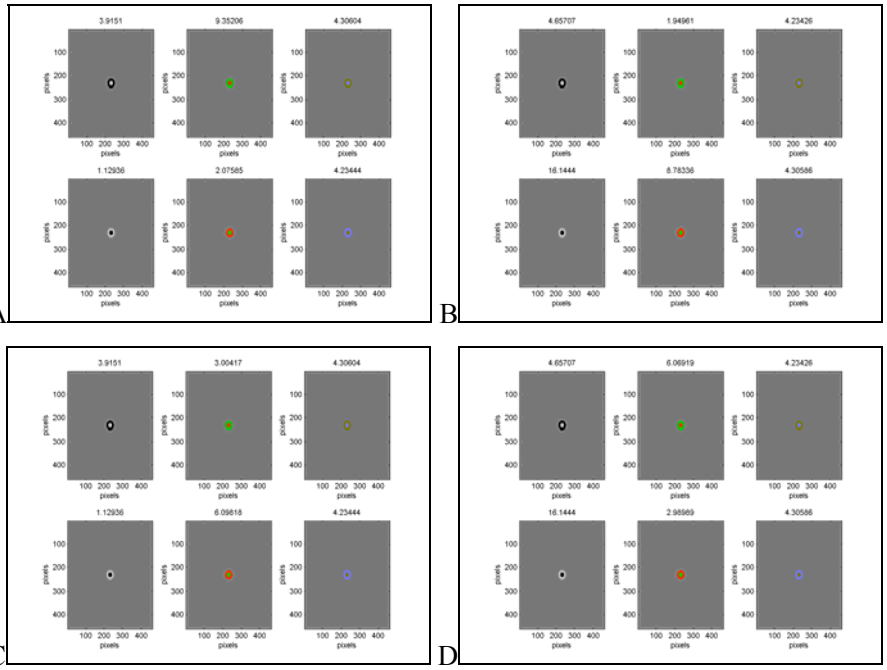

A B

C D

Figure 6.78. Response of midget ganglion cells when presented stimuli in opponency, output signal represented by the numeric values above each figure. Division mode. A) R On. B) R Off. C) G On. D) G Off.

As shown, each cell subtype of positive activation shows a maximum response when presented a chromatic stimulus in opponency: type R to red vs. green and type G to green vs. red. The fact that the response is greater in these cases that in the white vs. black stimulus indicates that these are cells that not only have spatial opponency, centre vs. surround, but also chromatic. The negative activation cells have a maximum response when presented a black vs. white stimulus as this is below the average value.

Midget ganglion cells have a receptive field with spatial opponency: centre vs. surround, as shown by the responses to achromatic stimuli.

Cells type R On respond to a band in the area of the oranges and reds and to the opponent stimuli red in the centre and green in the surround. Type G respond to a band in the green area and to opponent stimuli green in the centre and red in the surround. Therefore, these are cells with a distinct chromatic nature.

To sum up, midget ganglion cells are cells with spatial opponency of chromatic nature: centre vs. surround.

6.7 Parasol ganglion cells

Parasol ganglion cells have a receptive field that receives the signals of the diffuse bipolars in its integration radius. This generates a central area with photoreceptors from which it receives information and a second area with horizontal cells connected to these photoreceptors. All this is modulated by a Gaussian integration function. The following shows the structure of this receptive field.

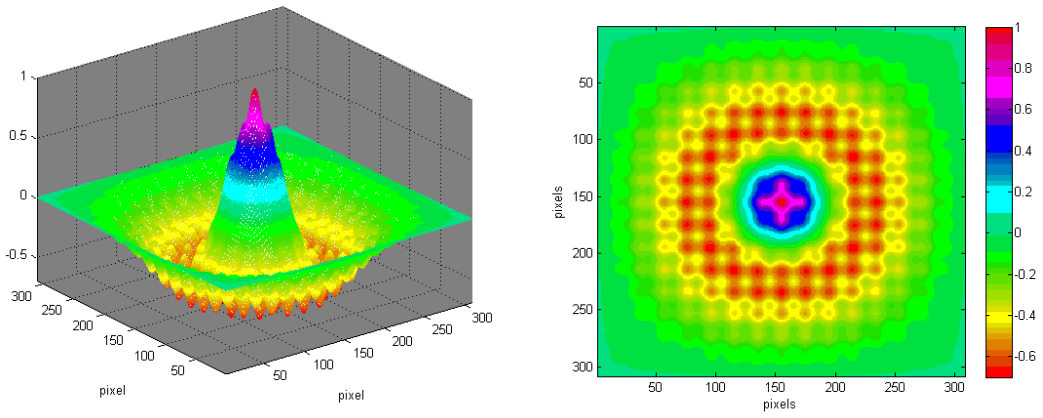

Figure 6.79. Representation of the receptive field of a parasol ganglion cell with a centre that integrates the signal from multiple photoreceptors and a surround generated by the integration of horizontal cells. Left) 3D view. Right) Top View.

The parasol cell signals are calculated as follows. The parameters used are those selected in earlier sections.

$$\text{Parasol ganglion type On} = 4.27 * \exp\left\{1.96 * \int_{\substack{\text{Integration field} \\ \text{of parasol ganglion cells}}} \exp(-2*(x^2+y^2)/62.5^2)*(0.4*\text{Bipolar DB4}+0.6*\text{Bipolar DB5})\right\}$$

(eq. 6.40)

$$\text{Parasol ganglion type Off} = 4.27 * \exp\left\{1.96 * \int_{\substack{\text{Integration field} \\ \text{of parasol ganglion cells}}} \exp(-2*(x^2+y^2)/62.5^2)*(0.4*\text{Bipolar DB2}+0.6*\text{Bipolar DB3})\right\}$$

(eq. 6.41)

The following shows the responses of parasol ganglion cells when presented the set of stimuli. The values of the type On cells are represented in the case of achromatic stimuli, as the type Off are structurally the same.

1) Spot

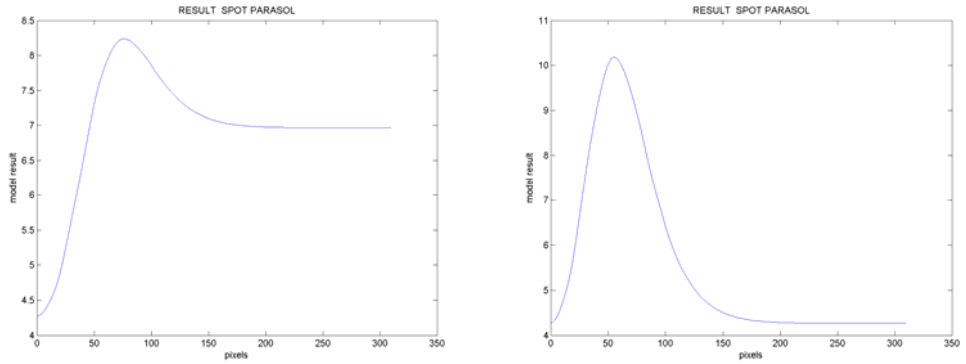

Figure 6.80. Response of a parasol ganglion cell type On when presented a white spot with a variable radius. Left) Subtraction mode. Right) Division mode.

The signal of parasol cells begins in the base value (A value within the exponential function for the generation of nervous spikes, equation 6.11) and continues with an opponency structure, centre vs. surround.

2) Annulus

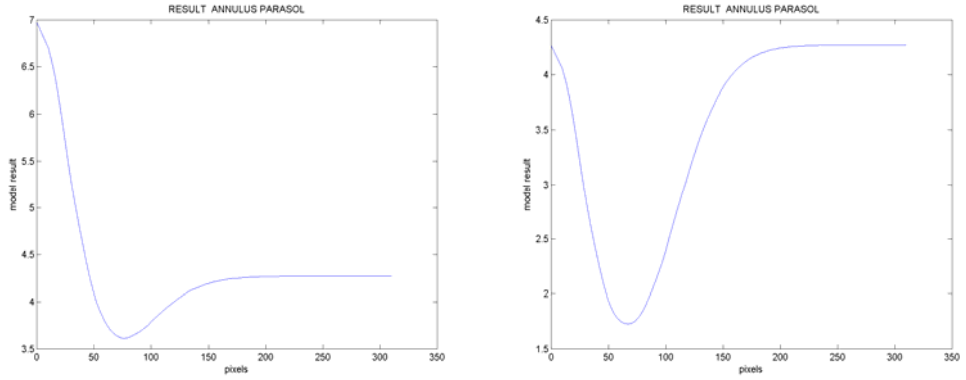

Figure 6.81. Response of a ganglion parasol cell type On when presented a white annulus with a variable radius. Left) Subtraction mode. Right) Division mode.

When presenting a variable inner radius annulus, parasol cells begin with the value of the response to a white stimulus, the signal decreases with the increase of the inner radius of the annulus until the surround influence decreases and the response signal begins to increase towards the limit value generated when presented a grey stimulus. This type of response shows spatial opponency processes, centre vs. surround.

3) Grid

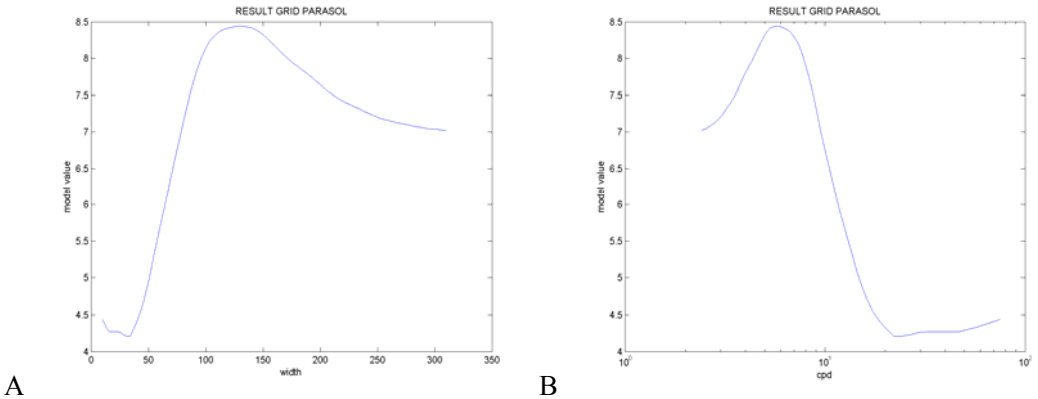

A B

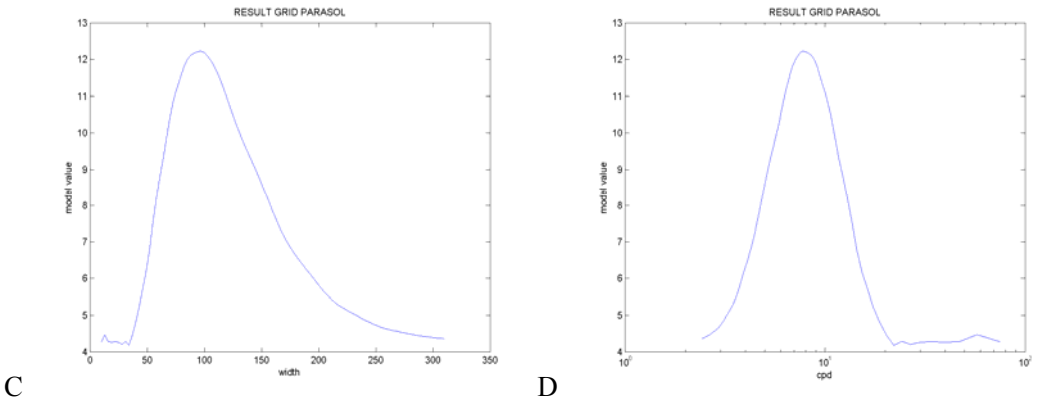

C D

Figure 6.82. Output signals of a parasol ganglion cell type On when presented a variable size grid. A) Subtraction mode. Abscissas: grid width in pixels. B) Subtraction mode. Abscissas: cycles per degree C) Division mode. Abscissas: grid width in pixels. D) Division mode. Abscissas: cycles per degree.

The response of parasol cells, when presented narrow grid, begins oscillating slightly, probably due to the influence of the photoreceptors that modulate the generated signal. After this initial stage, the signal begins to increase in a sustainable manner as the white bar placed in the centre of the cell increases its size, covering a greater area of the receptive field. When this bar reaches a coverage percentage that causes the influence of horizontal cells to exceed those of the centre, the output signal begins to decrease, showing a tendency towards the limit value when presented a white stimulus over the entire receptive field.

The curves provide a larger gradient in the division mode than in the subtraction mode.

4) Visible spectrum

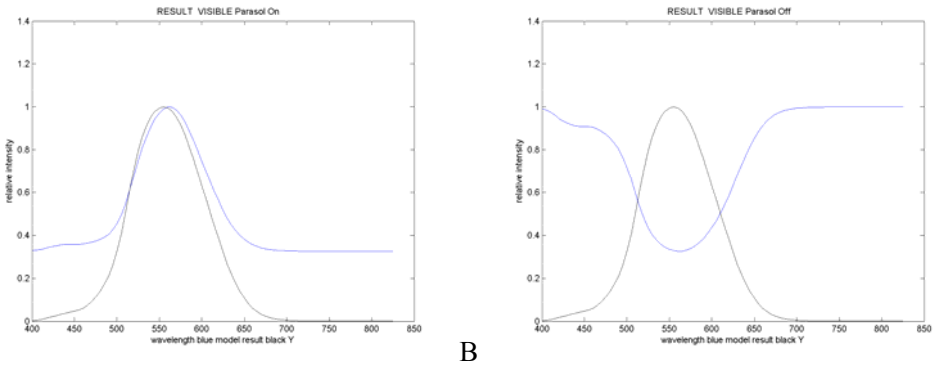

A B

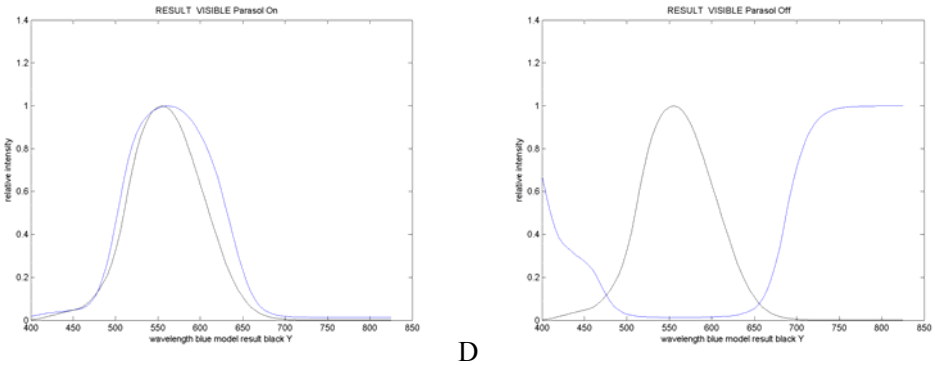

C D

Figure 6.83. Response of parasol ganglion cells when presented stimuli along the visible spectrum. Blue: model result, black: Y. A) Type On, subtraction mode. B) Type Off, subtraction mode. C) Type On, division mode. D) Type Off, division mode.

Type On parasol cells have a similar response to the Y values along the visible spectrum, therefore it can be considered that these are cells of an achromatic nature. Type Off cells respond in a complementary manner to type On.

5) Opponency

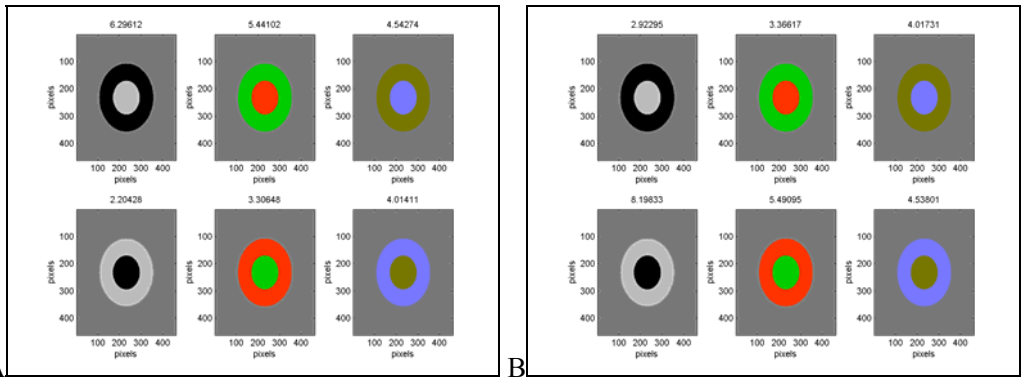

A B

C 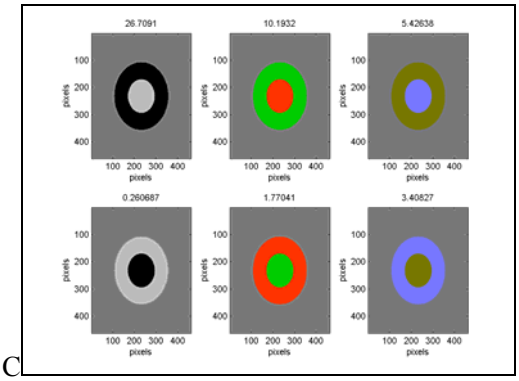 D 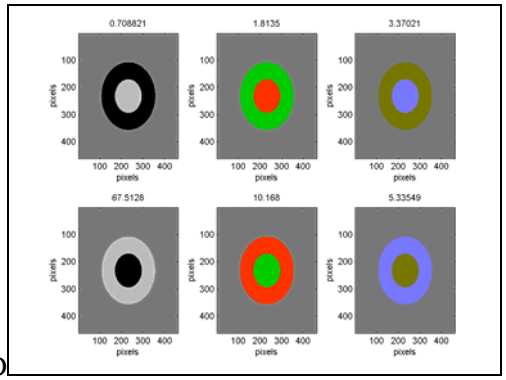

Figure 6.84. Response of parasol ganglion cells when presented stimuli in opponency, output signal represented by the numeric values above each figure. A) Type On, subtraction mode. B) Type Off, subtraction mode. C) Type On, division mode. D) Type Off, division mode.

Based on the responses in opponency, parasol ganglion cells respond with a maximum value when presented stimuli with achromatic opponency: white vs. black for type On and black vs. white for type Off. These results are consistent with those obtained when presented stimuli along the visible spectrum, therefore confirming that these are cells with achromatic nature.

The presence of a process in spatial opponency has been established based on the responses of parasol cells when presented achromatic stimuli: centre vs. surround.

The chromatic stimuli have shown that these are cells with achromatic nature.

The division mode generates a greater gradient between responses, both in stimuli size changes as well as in changes in wavelength.

It is noteworthy to compare the proposal of the receptive field of parasol cells with the analysis undertaken by [CROO_08b] that proposes a structure of "an aggregate of signals" that could explain Fourier's 2º harmonic. The following figure shows the proposal by Crook et al (2008).

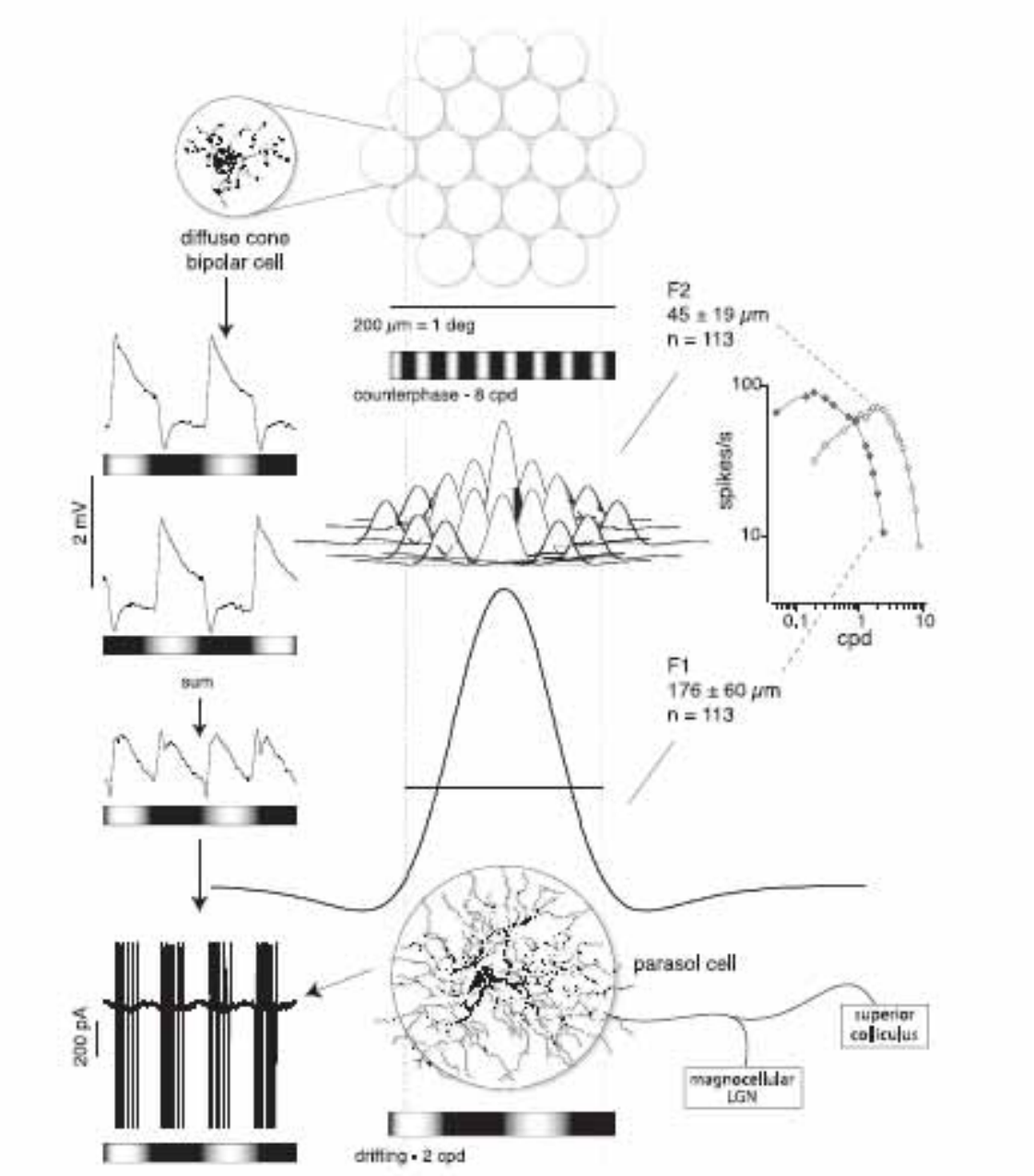

Figure 6.85. Hypothesis of the generation of results by the research of Crook et al (2008). Source: [CROO_08b].

6.8 Small-field bistratified ganglion cells

The structure of the receptive field of small-field bistratified cells includes the influence of two types of bipolar cells. On the one hand, it receives information from blue bipolar cells in its integration radius. On the other, it connects with diffuse bipolar cells type DB1. The following figure shows, first, the part of the receptive field that corresponds to the blue bipolar cells and secondly the one that corresponds to type DB1. Second, it shows the total receptive field of small bistratified cells.

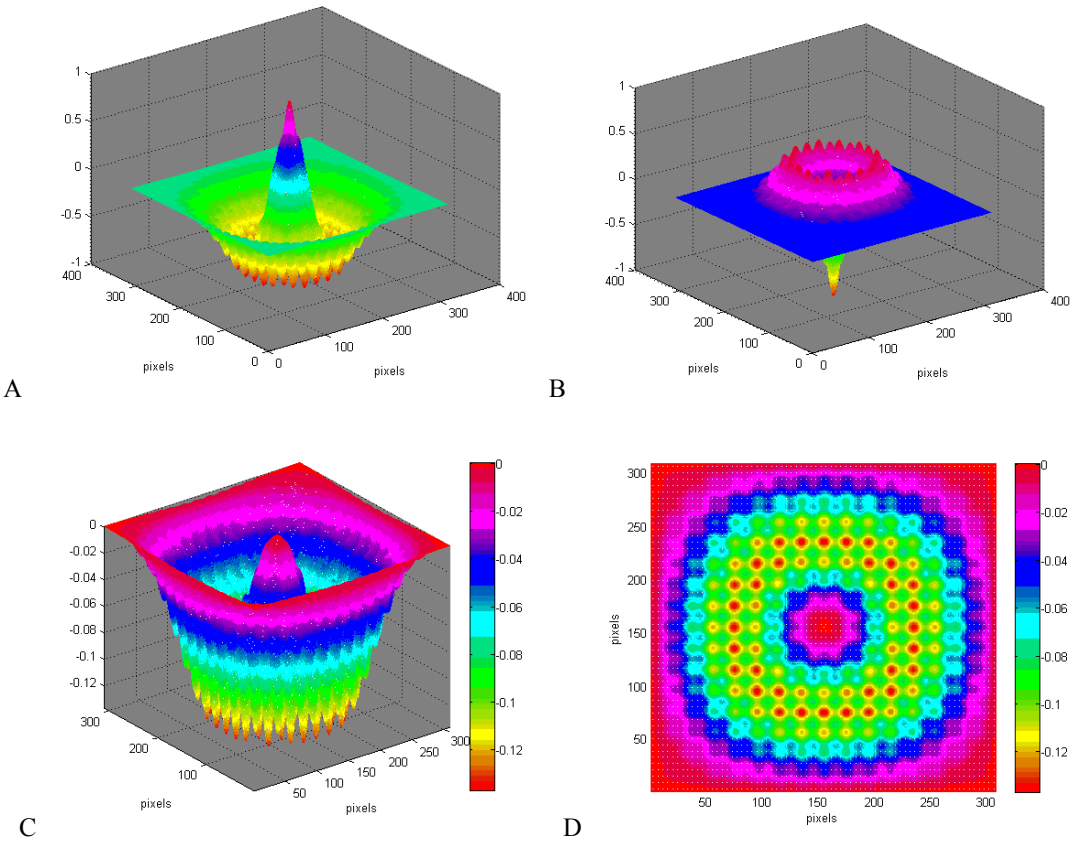

Figure 6.86. A) Area of the receptive field that corresponds to blue bipolar cells. B) Area of the receptive field that corresponds to DB1 bipolar cells. C and D) Receptive field of a small bistratified ganglion cell. C) 3D View D) Top View.

The signals generated by small bistratified cells are calculated in the following manner (the parameters have been described in earlier sections).

$$\text{Small bistratified ganglion} = 4.27 * \exp\left\{1.96 * \int_{\substack{\text{Integration field} \\ \text{of small bistratified} \\ \text{cell}}} \exp(-2*(x^2+y^2)/104.2^2) * (0.5\,\text{Difusse Bipoalr DB1} + 0.5\,\text{Blue Bipolar})\right\}$$

(eq. 6.42)

The following shows the responses of a small bistratified ganglion cell when presented the set of stimuli.

1) Spot

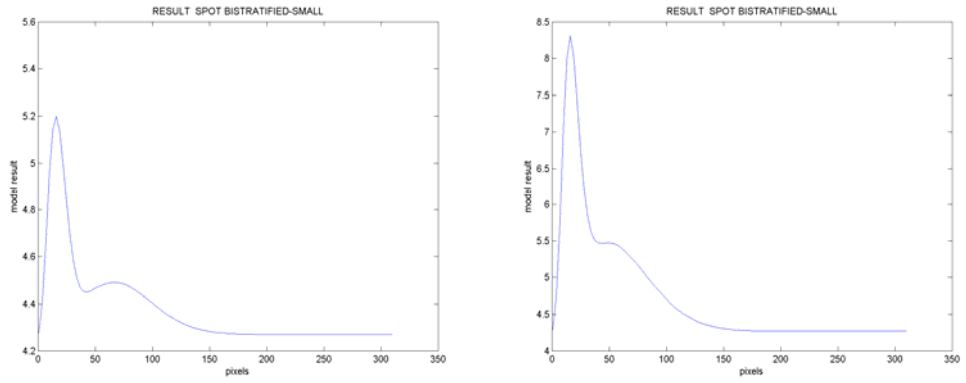

Figure 6.87. Response of a small bistratified ganglion cell when presented a white spot with a variable radius. Left) Subtraction mode. Right) Division mode.

Small bistratified ganglion cells respond to a white spot with a variable radius with a function that has two maximums. When presenting a grey stimulus (spot radius 0) it begins with the base value (value A within the exponential function for spikes generation, equation 6.11). When the spot's radius is increased, a greater area of the receptive fields of blue and DB1 bipolars is covered by this stimulus. In the first phase of the signal of the blue bipolar cells makes the output signal grow until it reaches the first maximum of the graph. After this, the signal decreases to a minimum which coincides with the inflexion point of DB1 bipolar cells (figures 6.53A and 6.54A). When the size of the spot is increased, a new maximum is generated. The signal finishes towards the limit value when presented a white stimulus over the entire receptive field. In this case, the initial and limit values, both in the subtraction as well as the division mode, are equal to the neutral value as there is a double opponency through the integration of two opponency processes centre vs. surround. One comes from blue bipolar cells and the other from DB1 bipolar cells.

2) Annulus

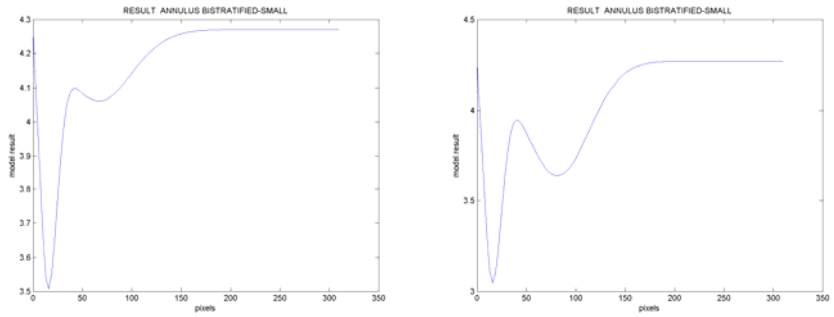

Figure 6.88. Response of a small bistratified ganglion cell when presented a white annulus with a variable radius. Left) Subtraction mode. Right) Division mode.

The response of the small bistratified ganglion cells when presented an annulus has the same morphological characteristics than when presented a spot, with two minimums that show the influence of both types of bipolar cells from which they receive the input signals.

3) Grid

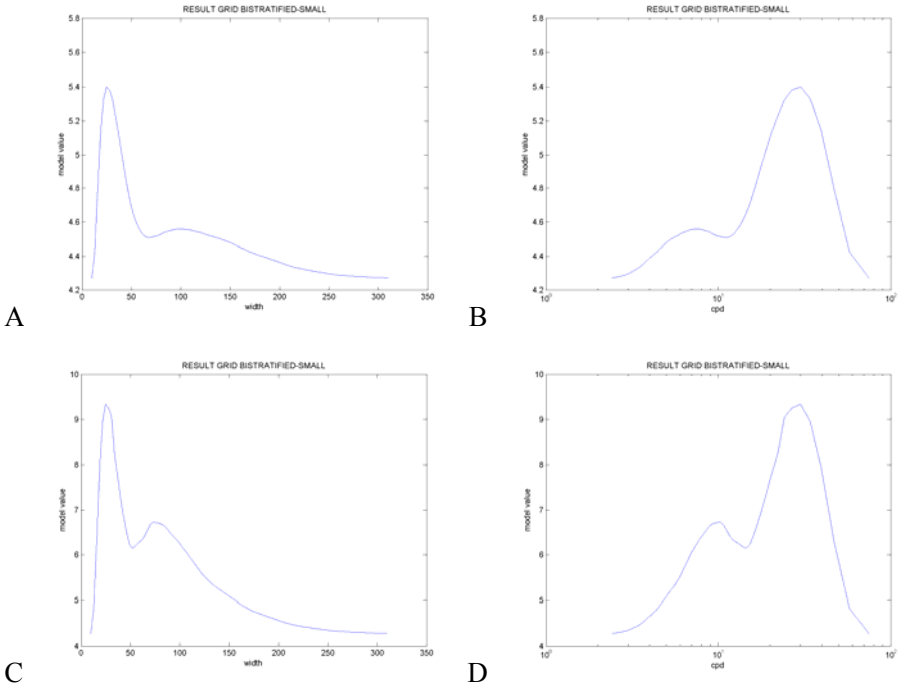

Figure 6.89. Response of a small bistratified ganglion cell when presented a variable size grid. A) Subtraction mode. Abscissas: grid width in pixels. B) Subtraction mode. Abscissas: cycles per degree C) Division mode. Abscissas: grid width in pixels. D) Division mode. Abscissas: cycles per degree.

Bistratified ganglion cells, when presented a variable width grid, show the presence of two processes in opponency centre vs. surround that are superimposed as:

- The initial and limit values are equal both in the subtraction as well as the division mode.
- Two maximums are shown due to the fact that each of the processes in opponency has different integration radii.

4) Visible spectrum

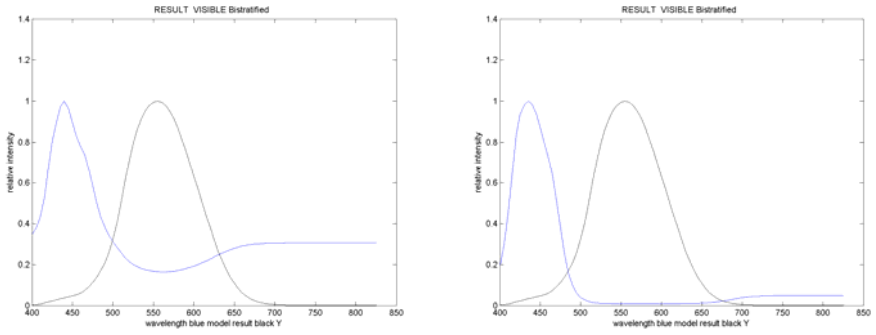

Figure 6.90. Response of small bistratified ganglion cells when presented stimuli along the visible spectrum. Blue: model result, black: Y. Left) Subtraction mode. Right) Division mode

Bistratified ganglion cells have an activation band in the blue area, both in the subtraction as well as in the division mode.

5) Opponency

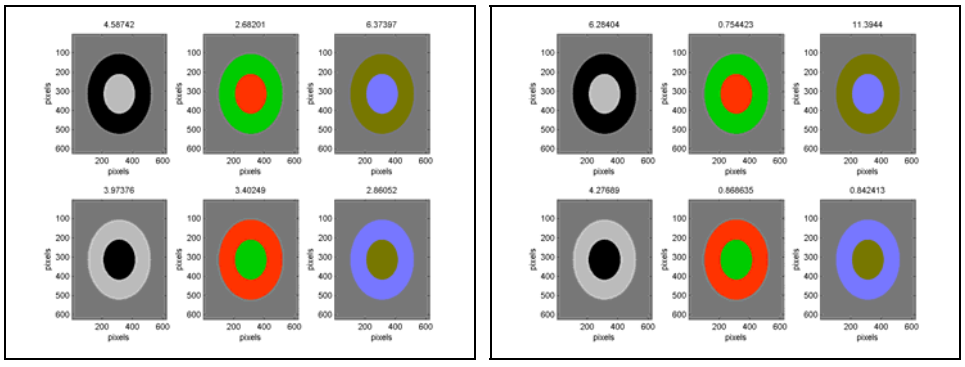

Figure 6.91. Response of a small bistratified ganglion cell when presented stimuli in opponency, output signal represented by the numeric values above each figure. Left) Subtraction mode. Right) Division mode.

Small bistratified ganglion cells, when presented stimuli in opponency, show a maximum response to a blue stimulus in the centre and yellow in the surround. The fact that the yellow surround generates a bigger signal than in the case of white vs. black indicates that these cells respond to stimuli with chromatic opponency of blue vs. yellow type.

A process of double opponency is shown through the results generated by small bistratified cells: spatial opponency centre vs. surround and chromatic opponency that affect the centre and the surround.

Therefore, these cells have opponency processes in centre-surround of a chromatic nature.

6.9 Big ganglion cells

Besides the cells presented until now, other types of ganglion cells have been characterised and identified: large bistratified, large sparse, giant sparse and thorny. These are great size cells and entail a small percentage of the total number of retinal cells. As an example of this set of cells and in order not to greatly extend this section, the results obtained by one of them, thorny type cells (narrow) are going to be presented.

The structure of the receptive field of these type of ganglion cells is similar to that of parasol ganglion cells, as like these, they integrate a set of diffuse bipolar cells. They receive influence from a large number of photoreceptors in the central area and a large set of horizontal cells in the surround. The following figure shows the receptive field.

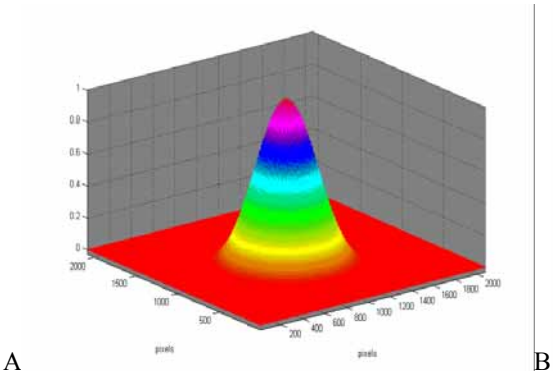

A

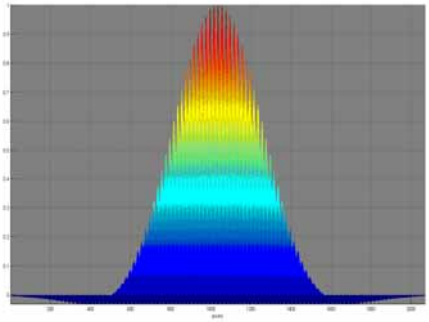

B

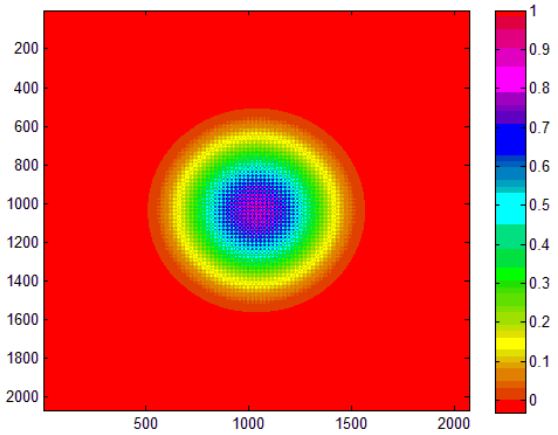

C

Figure 6.92. Representation of the receptive field of a thorny ganglion cell, with a centre that integrates the signal of multiple photoreceptors and a surround generated by the integration of horizontal cells. A) 3D View. B) Side View. C) Top View.

The integration area is great in size, a side view has been added that shows the undulation of photoreceptors in order to appreciate the influence of photoreceptors.

The function for the generation of spikes of the different subtypes of thorny ganglion cells, given the parameters presented in earlier sections, are the following:

$$\text{Thorny ganglion type On} = 4.27 * \exp\left\{1.96 * \int_{\substack{\text{Integration field} \\ \text{of thorny ganglion cell}}} \exp(-2*(x^2+y^2)/517^2) * (\text{Bipolar DB4})\right\} \quad \text{(eq. 6.43)}$$

$$\text{Thorny ganglion type Off} = 4.27 * \exp\left\{1.96 * \int_{\substack{\text{Integration field} \\ \text{of thorny ganglion cell}}} \exp(-2*(x^2+y^2)/517^2) * (\text{Bipolar DB2})\right\} \quad \text{(eq. 6.44)}$$

The following shows the responses of thorny ganglion cells when presented the set of stimuli. As in earlier cases, the results of cells type On are shown for achromatic stimuli: In the case of chromatic stimuli, where responses are different, both types are shown.

In this case, the value used is RADIUS_PIXEL_SCALE=2, due to the computational cost of testing the great size of these cells' receptive field.

1) Spot

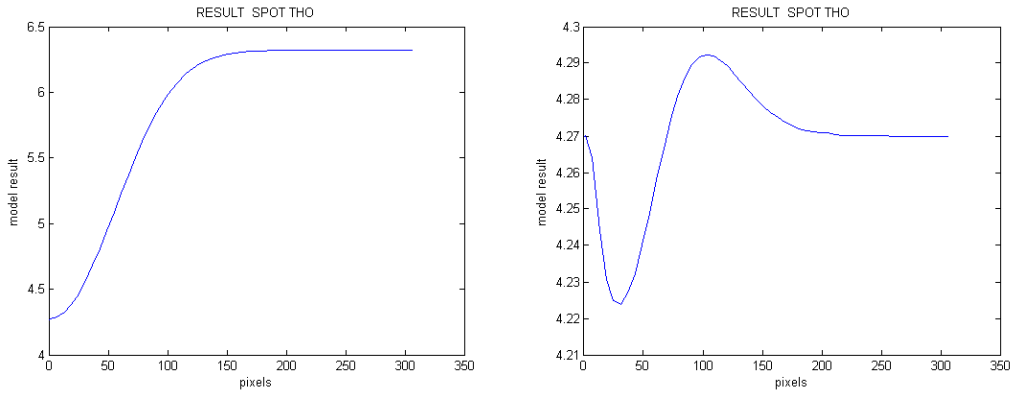

Figure 6.93. Response of a thorny ganglion type On cell when presented a white spot with a variable radius. Left) Subtraction mode. Right) Division mode.

The response of thorny type On cells begins in the base value (parameter A in equation 6.11). It reaches a maximum value when reaching the integration value and tend towards the limit value when increasing the influence of the surround (if one zooms in the maximum area, one can see that this small maximum and later decrease of the generated signal).

The signal, in division mode, has a very small range in variation near the base value (A). It begins in this value and has a small decrease that could be caused by the internal undulation of the receptive field (see figure 6.92B). Subsequently it reaches a maximum level when the white circle reaches the size of the integration radius. From this point, the generated signal decreases showing a tendency towards the limit value as the surround influence increases.

2) Annulus

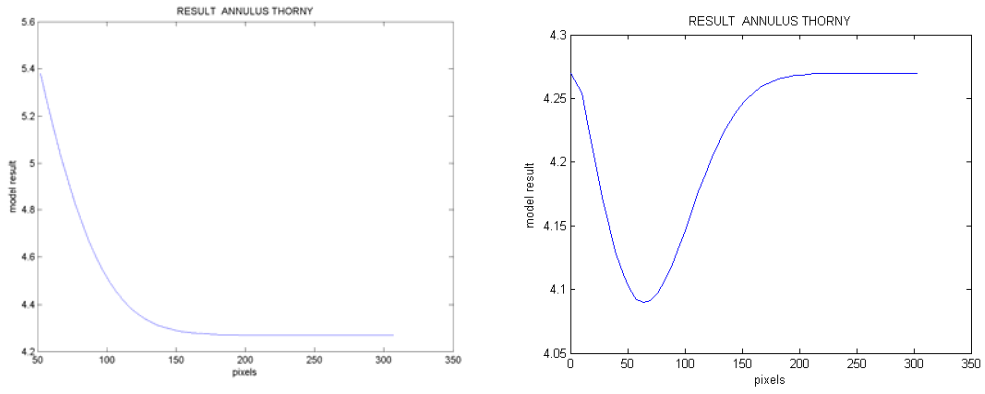

Figure 6.94. Response of a thorny ganglion type On cell when presented a white annulus with a variable radius. Left) Subtraction mode. Right) Division mode.

The signal generated by thorny ganglion cells type On begin in the limit values reached when presented a white stimulus. It decreases as the inner annulus radius increases and the central area changes from white to grey. It reaches a minimum value and then increases again towards the limit value of an average grey stimulus, as the surround influence increases.

In the division mode, the range of variation of the output signal is really small. The signal begins in the limit value for a white image, slightly decreases as the inner circle increase and finishes returning to the A level for a grey image over the complete receptive field.

3) Grid

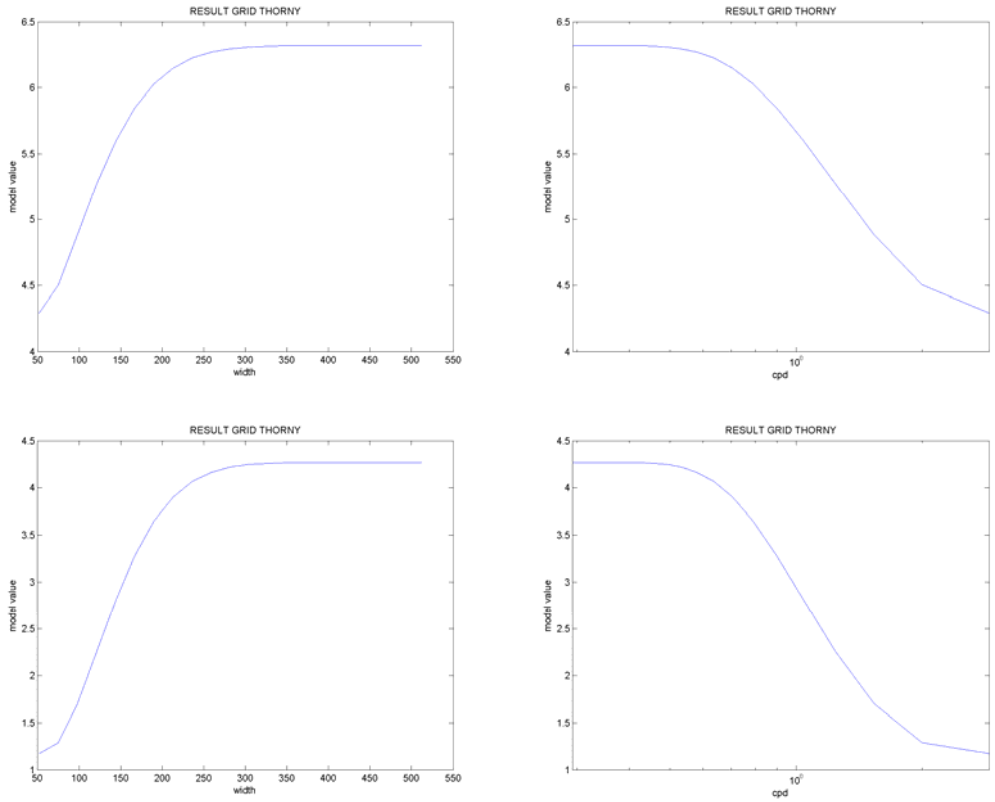

Figure 6.95. Response of a thorny ganglion type On cell when presented a variable size grid. A) Subtraction mode. Abscissas: grid width in pixels. B) Subtraction mode. Abscissas: cycles per degree C) Division mode. Abscissas: grid width in pixels. D) Division mode. Abscissas: cycles per degree.

Thorny type On cells generate a signal that begins near the A limit value and grows as the white stripe covers a greater area of the receptive field, showing a tendency towards the limit

value of a white stimulus covering the entire cell, in a similar manner to that generated when presented a white spot.

4) Visible spectrum

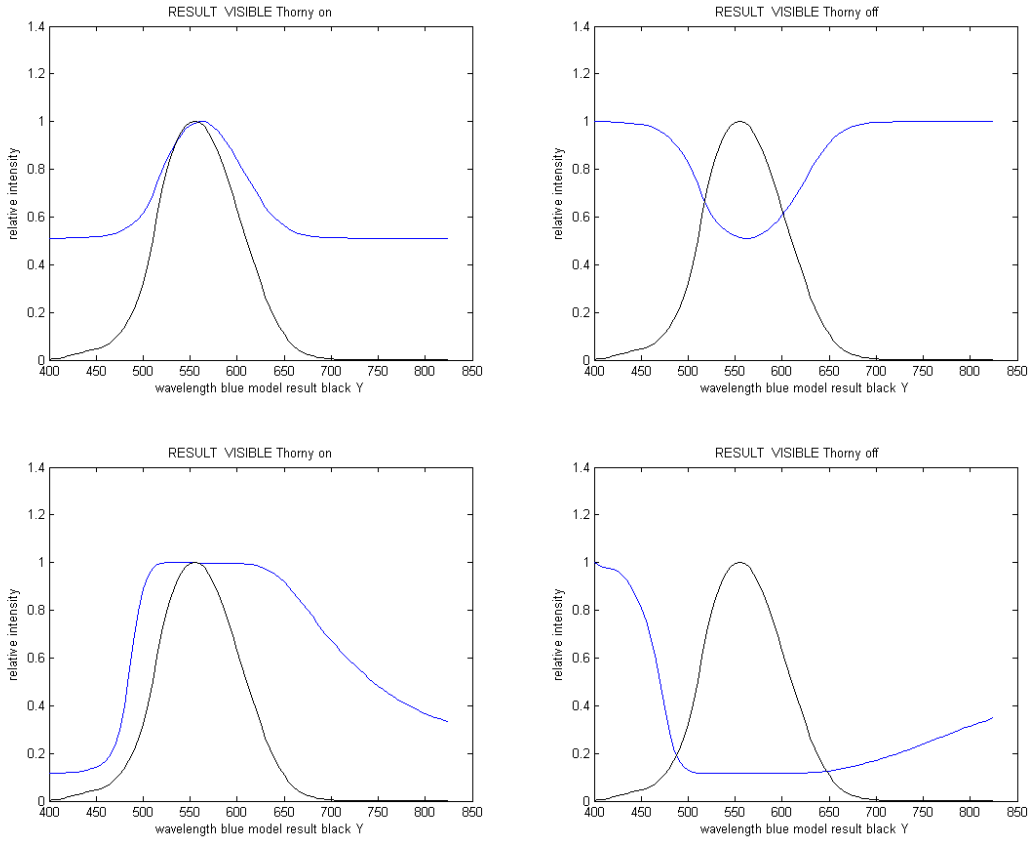

Figure 6.96. Response of thorny ganglion cells when presented stimuli along the visible spectrum. Blue: model result, black: Y. A) Type On, subtraction mode. B) Type Off, subtraction mode. C) Type On, division mode. D) Type Off, division mode.

Thorny type On cells, in subtraction mode, respond in a similar manner to the Y values along the spectrum and type Off have a complementary response to type On. The greater sensitivity wavelength band, in the division mode, is wider. The characteristics of both modes indicate that these are cells with an achromatic character.

5) Opponency

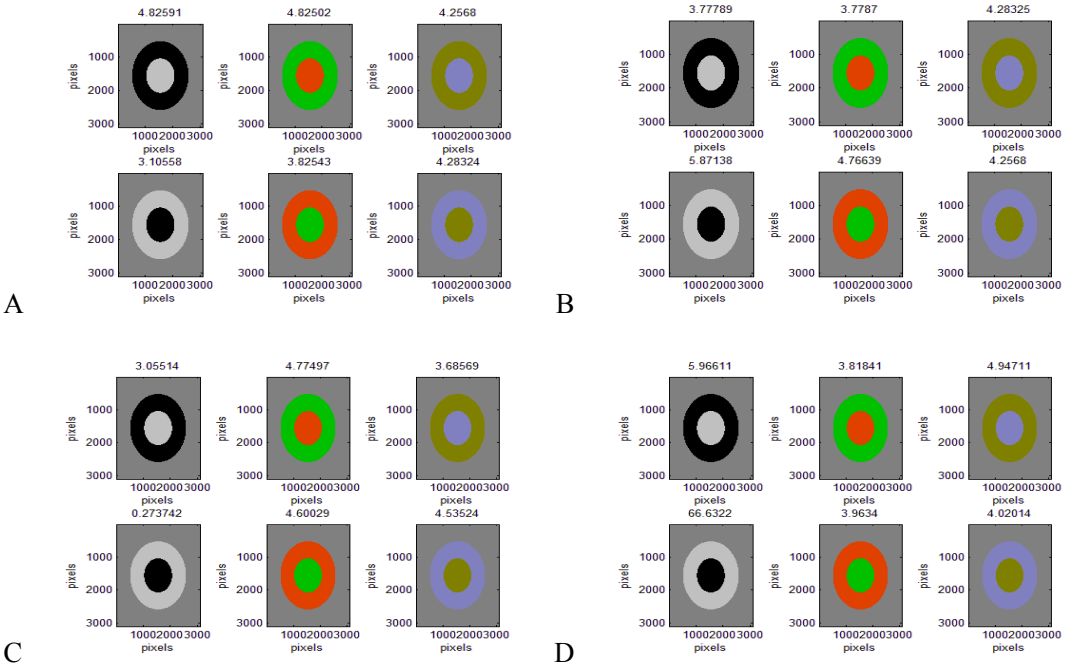

Figure 6.97. Response of thorny ganglion cells when presented stimuli in opponency, output signal represented by the numeric values above each figure. A) Type On, subtraction mode. B) Type Off, subtraction mode. C) Type On, division mode. D) Type Off, division mode.

The analysis of the opponency responses of thorny ganglion cells shows that the subtraction mode generates maximum responses when presented achromatic stimuli in opponency: white vs. black for type On and black vs. white for type Off. This is also applicable for type Off cells in the division mode, however, type On seem to respond better to chromatic stimuli. This is due to the fact that the high sensitivity wavelength band is wider and therefore, in this mode, the signals generated by the chromatic opponency stimuli provide a greater response as these are stimuli with higher overall Y.

Therefore, the results match the values obtained when presented stimuli throughout the visible spectrum. These are achromatic cells.

Taking into account the responses of thorny type cells when presented different stimuli, these can be classified as achromatic cells with a receptive field with two opponency processes: centre and surround.

The response of these type of cells, in the division mode, is affected by their great size, having a band of frequencies in the visible spectrum that is wider than usual, as well as changes in the

response generated with regards to the subtraction mode, possibly generated by the undulation of its receptive field.

7. Application of the model to images

This section shows the results generated by the model when presented image samples. The previous section analysed the responses of different cell types against the set of test stimulus. The results showed a signal generated by only one cell type. The model produces in each cell layer a complete image, that is, each cell from a layer generates a signal, each cell has a place within its layer in such a way that when each generated signal is placed in its position, this in turn produces an image (set of values with spatial relations in a plane).

In order to show the model features, two images have been used as samples. These have been selected to analyse the behaviour when presented an image with different morphologies and colours, particularly the effect in the borders.

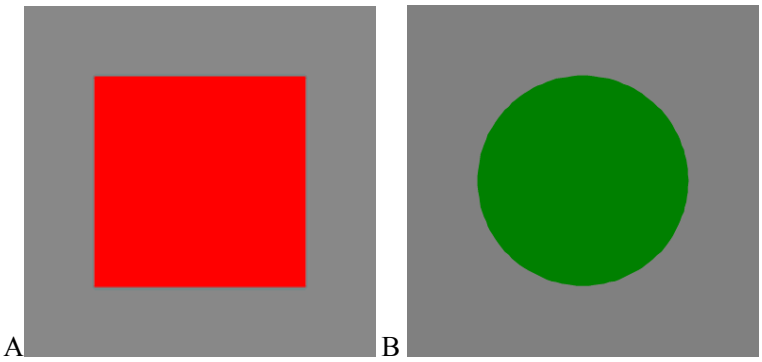

Figure 6.98 Examples of images to be used by the functional retina model.

Below are the results of each cell type when presented image A (red square), as a detailed example.

1. Photoreceptor layer: each photoreceptor receives a signal that is proportional to the original stimulus and generates a homogeneous image as an output. The result is independent of the mode.

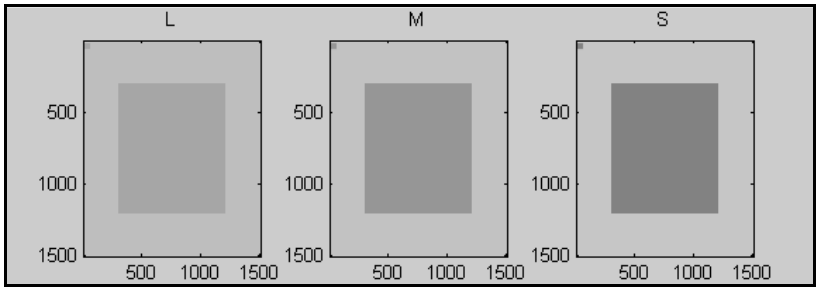

Figure 6.99. Image generated by photoreceptors when presented image A.

2. Horizontal cell layer: HI and HII. The signal is blurry due to the integration process of horizontal cells. The images are homogeneous as was the aim in the selection of the homogeneous mesh (figures 6.15 and 6.16 showed non-homogeneous processes with other meshes). The result is independent of the mode.

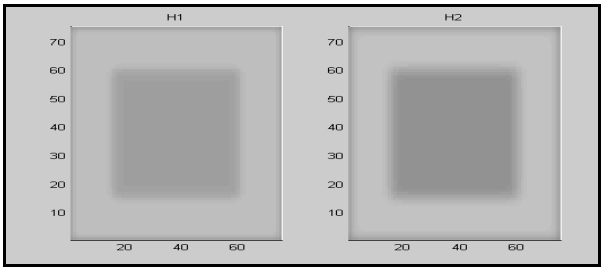

Figure 6.100. Image generated by horizontal cells when presented image A.

3. Bipolar cell layer: midget, diffuse and blue. The generated images are homogeneous in both object and background. The edges zones show processes of edge detection. The division mode highlights more the presence of edges (as was observed in section 6).

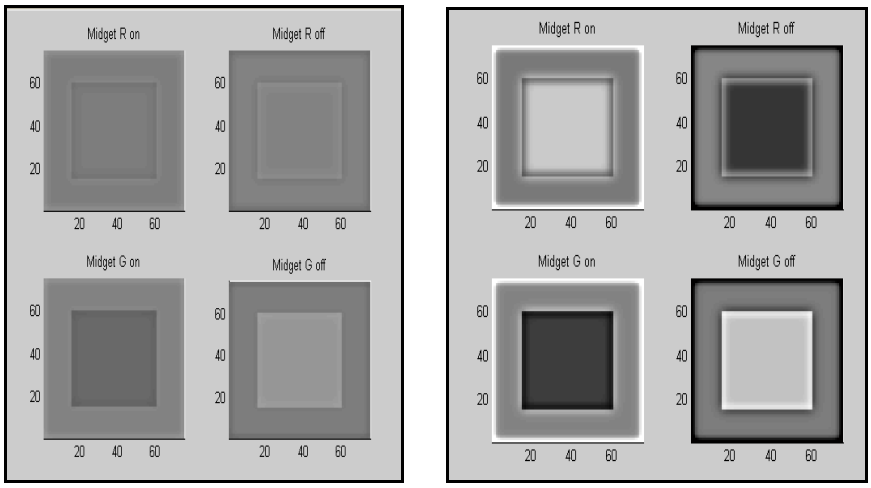

Figure 6.101. Image generated by midget bipolar cells when presented image A. Left) Subtraction mode. Right) Division mode.

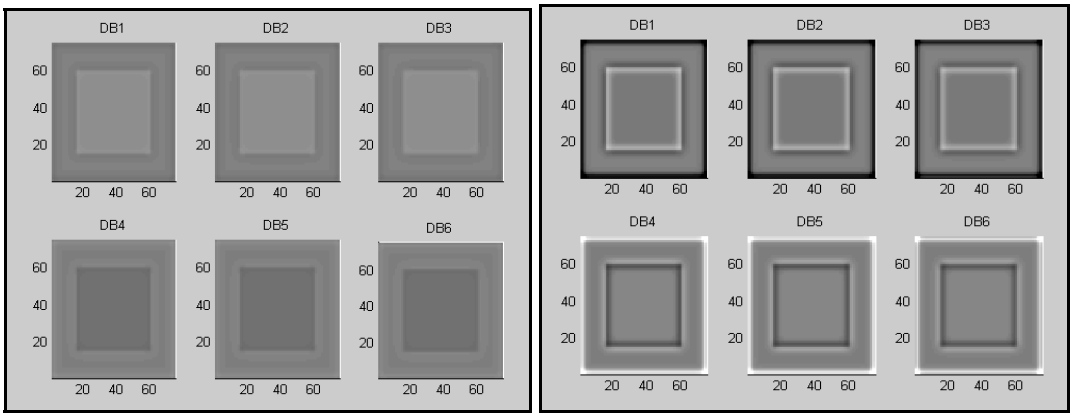

Figure 6.102. Image generated by diffuse bipolar cells when presented image A. Left) Subtraction mode. Right) Division mode.

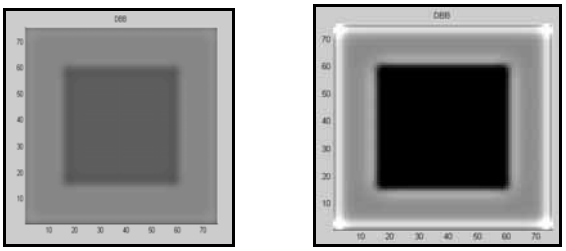

Figure 6.103. Image generated by blue bipolar cells when presented image A. Left) Subtraction mode. Right) Division mode.

4. Ganglion cell layer: midget, parasol, small bistratified and thorny. The generated images represent nervous spikes. The object and background are homogeneous. The object-background transition areas show edge detection. In the image borders, there are effects due to the rounding of the Gaussian functions in these limits (the image is completed with a general frame with level zero). The edges are highlighted more in the division mode, furthermore midget ganglion type R cell show an almost homogeneous image as the object is red (it is not a constant image but the change scale is very small compared to the variations in ganglion type G cells).

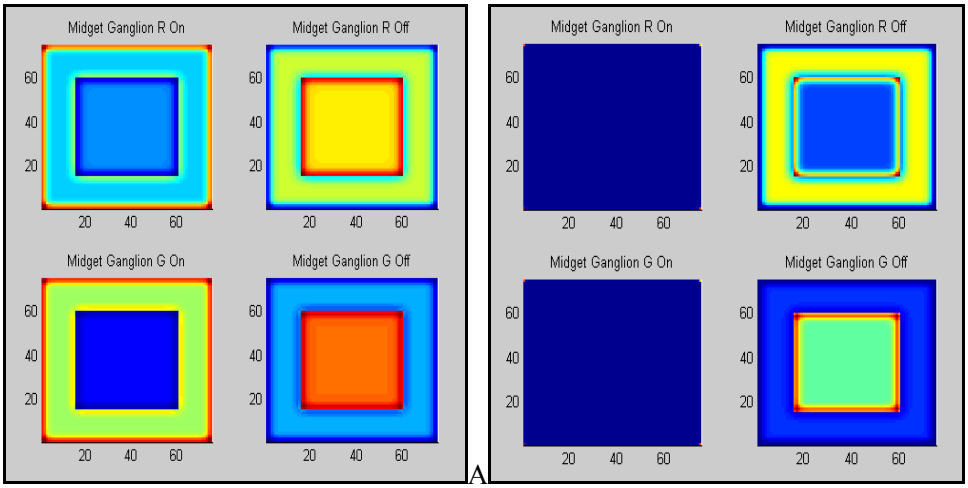

A

Figure 6.104. Image generated by midget ganglion cells when presented image A. Left) Subtraction mode. Right) Division mode.

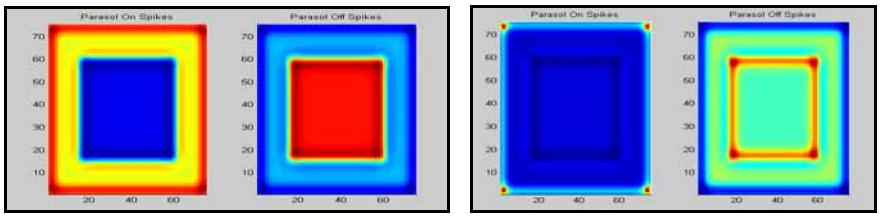

Figure 6.105. Image generated by parasol ganglion cells when presented image A. Left) Subtraction mode. Right) Division mode.

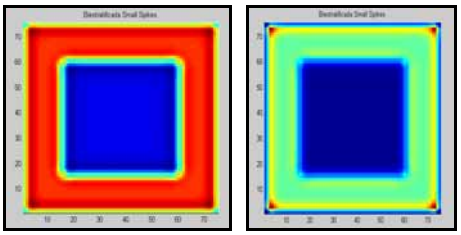

Figure 6.106. Image generated by small bistratified ganglion cells when presented image A. Left) Subtraction mode. Right) Division mode.

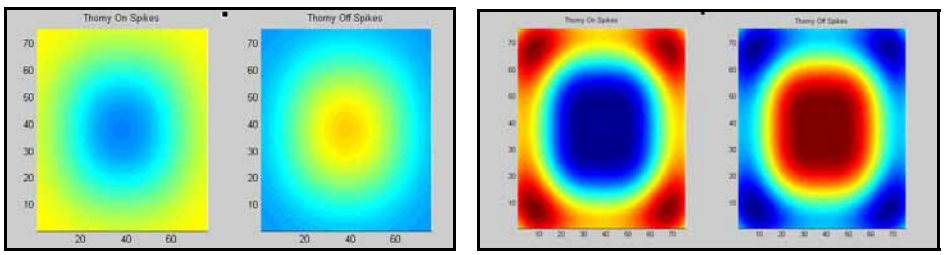

Figure 6.107. Image generated by thorny ganglion cells when presented image A. Left) Subtraction mode. Right) Division mode.

In order to notice the edge detection processes, the image profiles generated by each cell type are shown below (height = size_y/2). In the division mode, the variation scale in the edges is greater than in the subtraction mode.

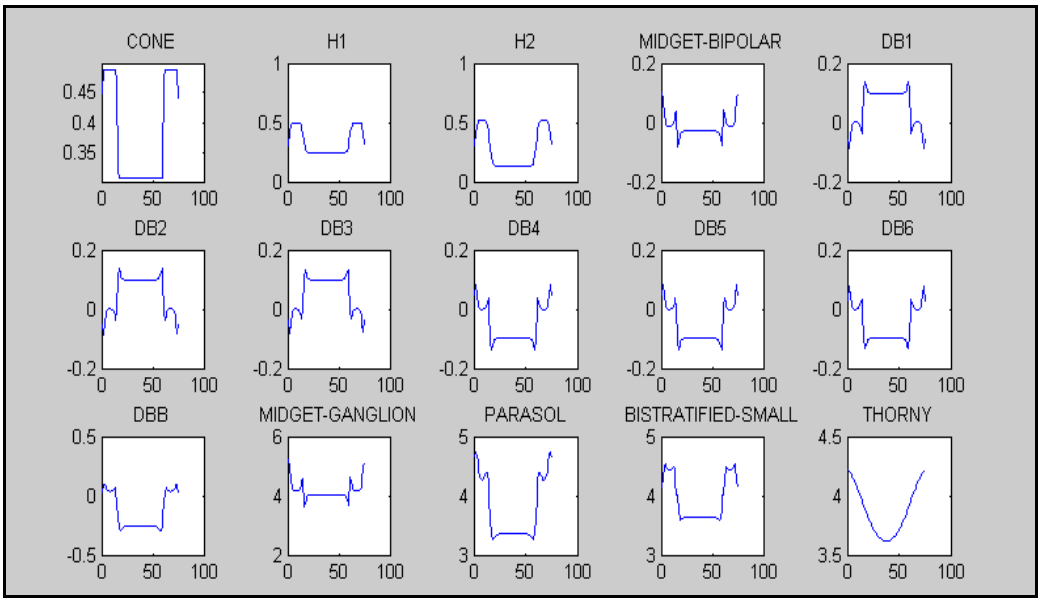

Figure 6.108. Image profiles generated by each cell type when presented image A. (Profile taken in the middle of the image).Subtraction mode.

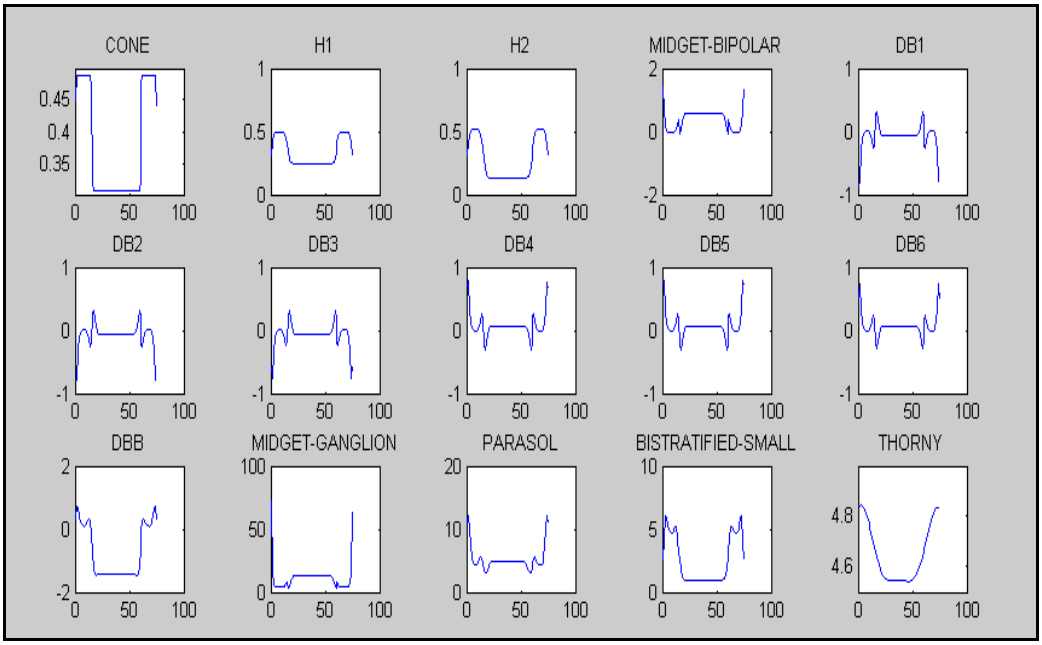

Figure 6.109. Image profiles generated by each cell type when presented image A. (Profile taken in the middle of the image). Division mode.

This figure shows how the edges are detected in the layer of bipolar cells in the layer of ganglion cells. The borders have effects due to the limits proper of the image. The system considers that there is a frame around the image of value 0 necessary for the calculation of the circular integration Gaussian.

The results for image B are represented on the diagram of the model (figure 6.5), subtraction mode. There is a twofold objective when selecting this image. On the one hand, to show the behaviour with other colours and on the other, to show how the system not only detects linear edges but also detects edges in any orientation. This feature is consistent with the fact that it is in the cortex, more specifically in V1, where edge detection in specific orientations occurs. Therefore, it is natural that earlier stages in the visual system detect edges in all directions that later shall be grouped in specific orientations.

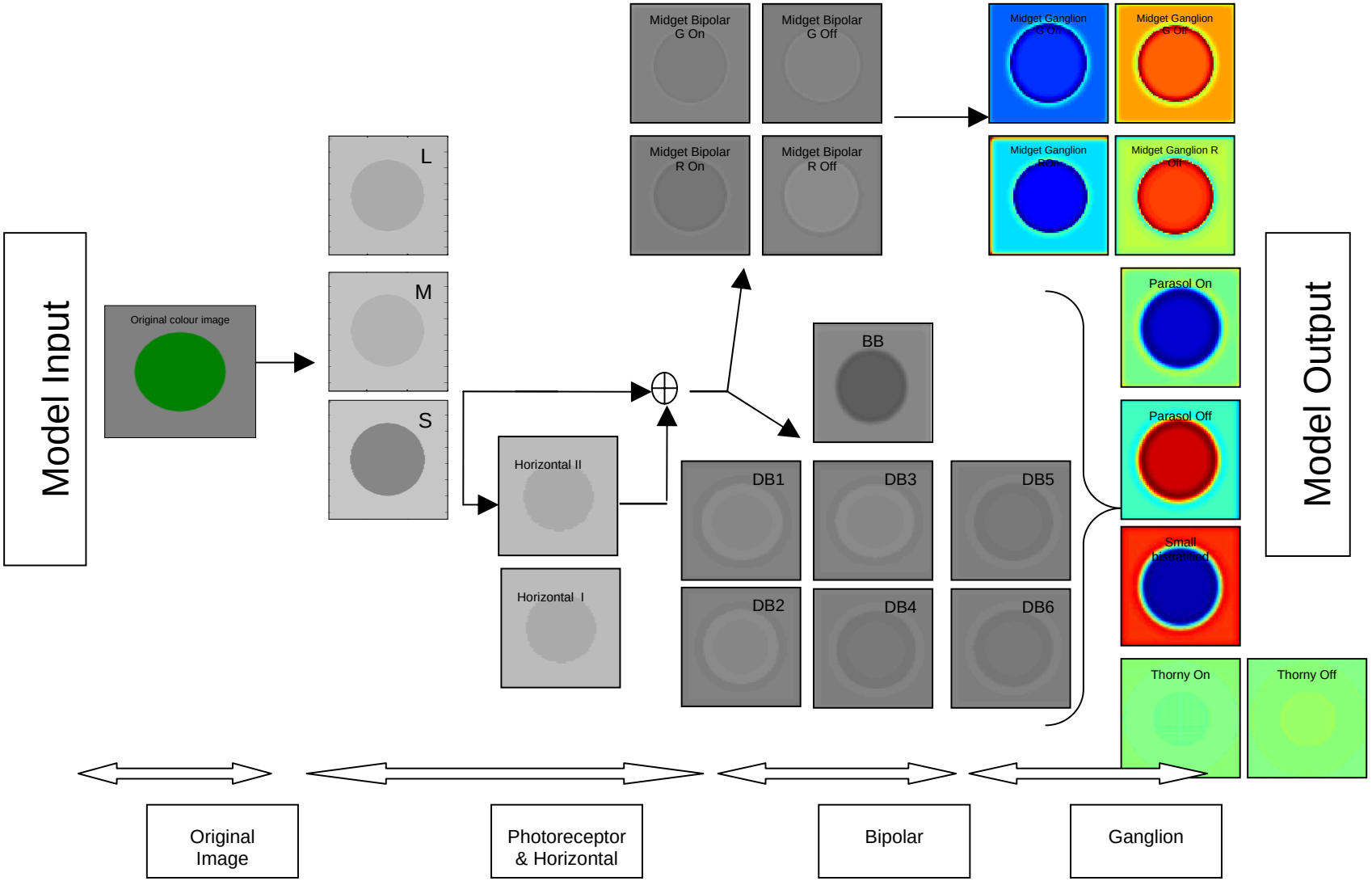

Figure 6.110. Example of images generated by each cell layer on the scheme of the retina model. Subtraction mode.

8. Conclusions

This chapter has presented the retina model. An explanation has been provided on the framework and the simplifications that have been introduced. Within the model, a description has been provided of the set of cells to be modelled, the structure, nature and number of connections that each type of cell establishes as well as the functions of signal generation and the model parameters for the test phase.

A set of test stimuli has been defined in order to analyse the behaviour of each model cell. Achromatic stimuli have been included in order to identify the spatial structure of each cell and a set of chromatic stimuli have been established in order to analyse the character of each cell, that is, to know whether these are highly tuned cells to chromatic or achromatic stimuli.

All this has helped to analyse the functional features of each cell type that has been included in the model:

- Photoreceptors: cells with homogeneous receptive field (without opponency) and with chromatic nature.
- Horizontal cells: cells with homogeneous receptive field (without opponency) and with a partially achromatic nature.
- Midget bipolar cells: cells with opponency centre vs. surround with chromatic nature.
- Diffuse bipolar cells: cells with opponency centre vs. surround with achromatic nature.
- Blue bipolar cells: cells with opponency centre vs. surround with chromatic nature.
- Midget ganglion cells: cells with spatial opponency of a chromatic nature: centre vs. surround.
- Parasol ganglion cells: cells with spatial opponency of chromatic nature: centre vs. surround.
- Small bistratified ganglion cells: cells with spatial opponency of chromatic nature: centre vs. surround.
- Big ganglion cells: cells with opponency centre vs. surround with achromatic nature.

The following these types are shown. The relative sizes of the receptive fields are represented, the presence of opponency processes: centre vs. surround, as well as a cell's most receptive colours.[17]

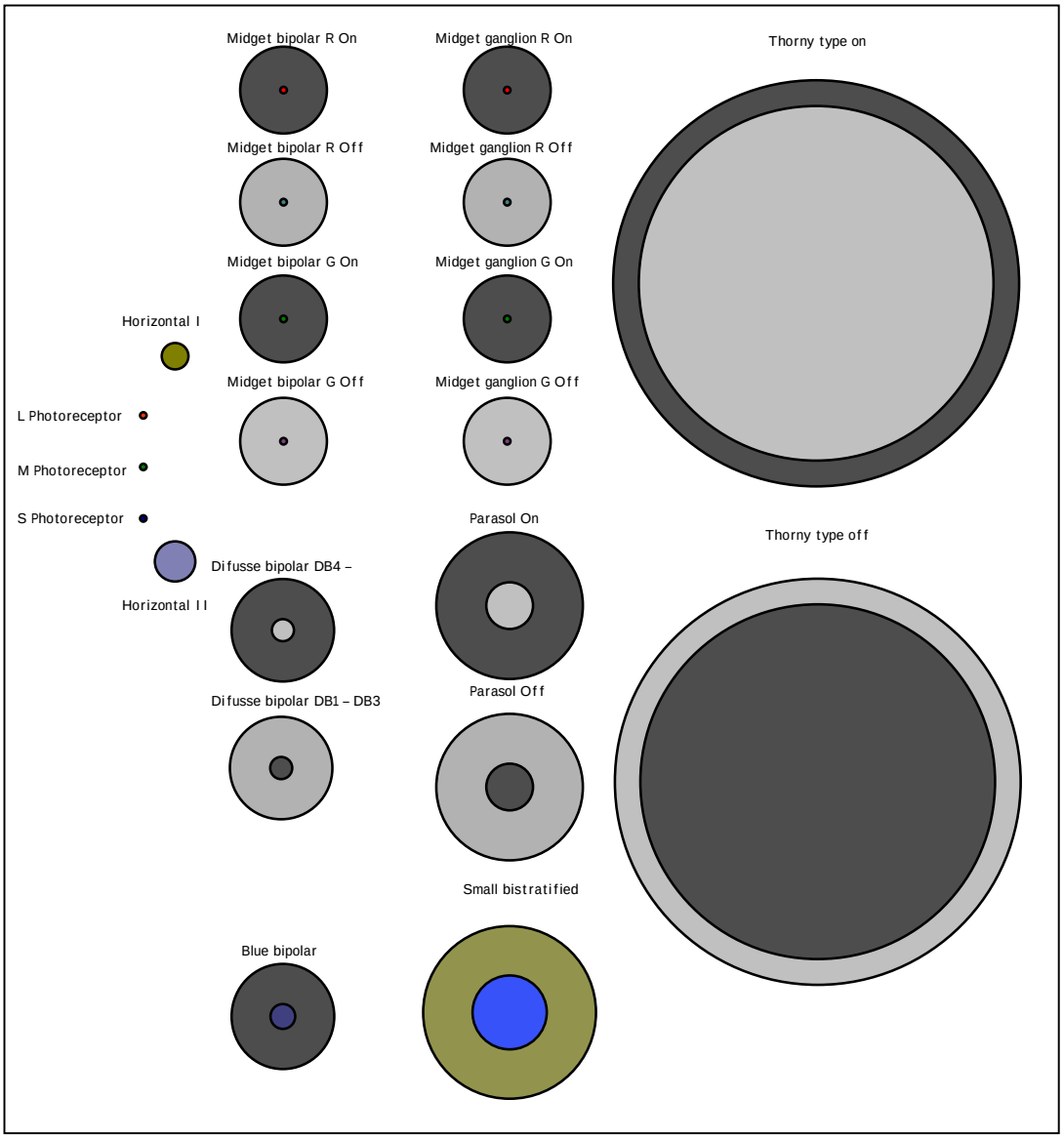

Figure 6.111. Set of cells in the model. Their receptive fields (scaled according to their size), the process type centre vs. surround as well as the set of colours that they are most receptive to are represented.

Based on these features and the model structure, the progression of the different information pathways can be tracked from its origin in photoreceptors to ganglion cells. The following figure

[17] In the case of diffuse bipolar cells an average size has been presented.

shows the flow of information. The pathways that feed the centres have also been identified (arrows that finish in ✦) and the ones for cell peripheries (arrows that finish in ►).

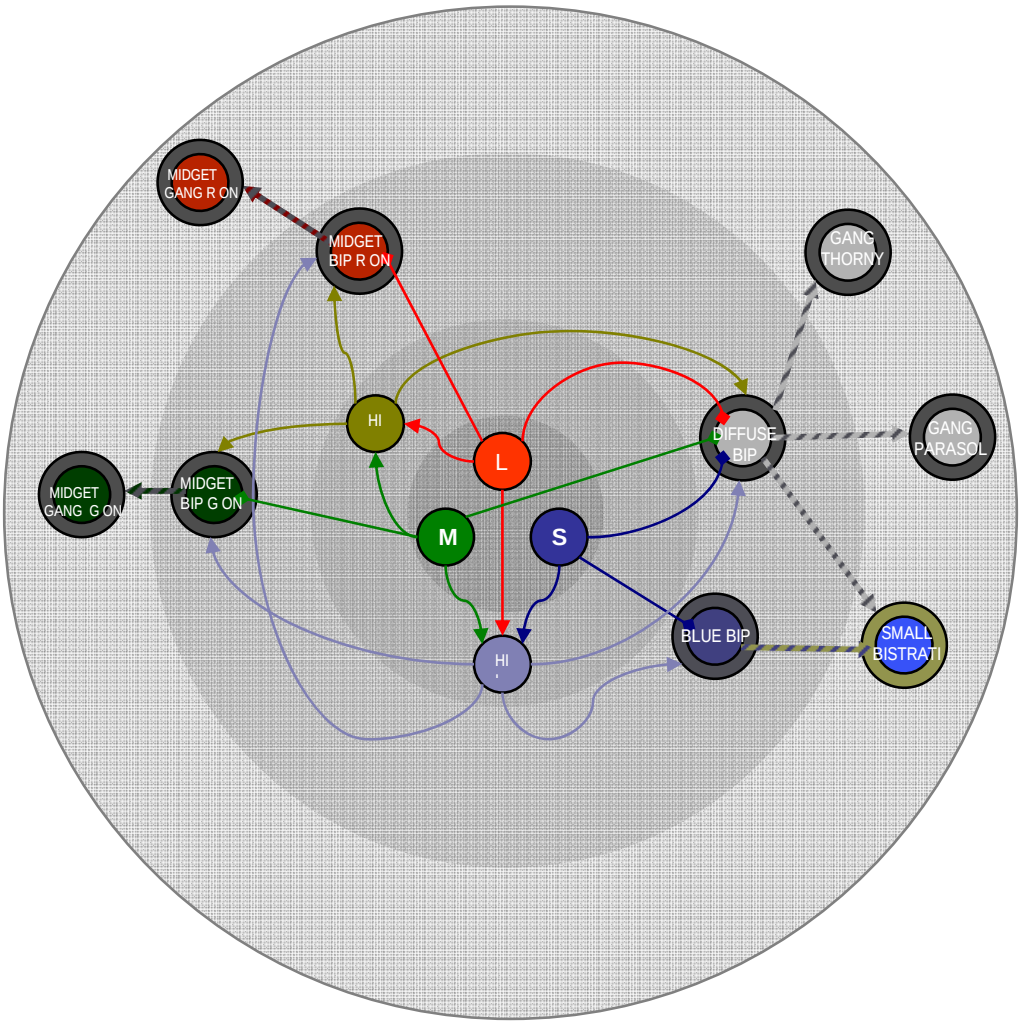

Figure 6.112. Model information flow.

The information flow represented in the previous figure shows the connections between the different cell layers and the influence of each type of photoreceptor in each cell type.

The tests performed have also allowed to compare the model results with real physiological measurements and to attest that the model's results match with these measurements. Besides the comparisons made in section 6 it is interesting to analysis the model regarding other more general features of the retina.

- Generic response of ganglion cells. There are many studies on the response of ganglion cells to circular stimuli. Schiller, in 1992, compiled this behaviour of retina cells. The following figure shows the results observed in this research. It shows how the proposed model is consistent with these representations.

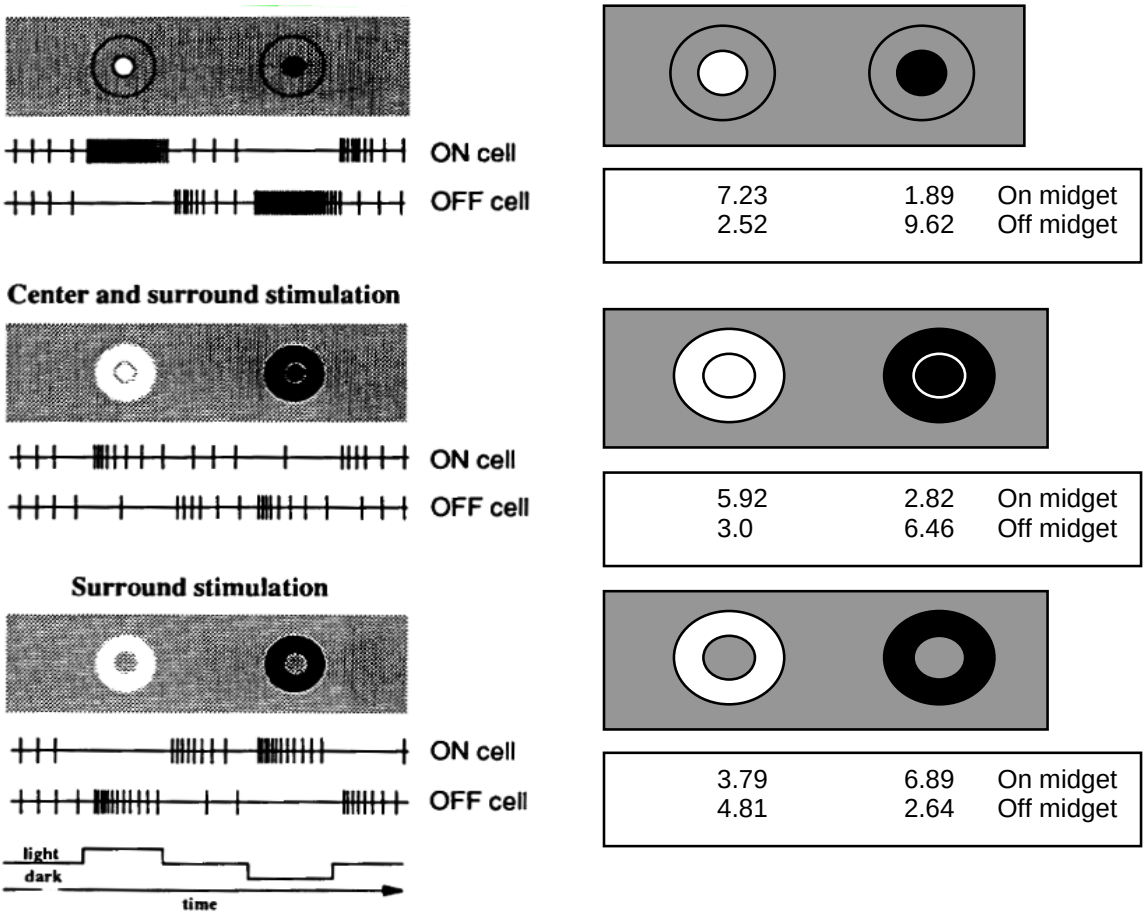

Figure 6.113. Ganglion cell response. Left) Source: [SCHI_92]. Right) Results of midget ganglion cells. The base signal is 4.27 (outputs are considered null below this value).

- Cell types: in chapter V, section 1, some of the cells in LGN were presented. LGN cells have behaviour features that are very similar to ganglion cells.
  - Classification of Wiesel and Hubel (1966).
    - Type I: centre vs. surround colour opponency. The model has identified midget ganglion cells and midget bistratified cells as these types of cells.
    - Type II: colour opponency without spatial opponency, where the receptive fields of each colour component are superimposed. The receptive fields of

small bistratified cells have two areas in opponency but their sizes are very similar, thus depending on the system of experimentation, they could be considered as two superimposed fields.

- Type III: with centre/surround spatial opponency of achromatic nature. Parasol ganglion cells of the model have these features as well as cells with great sizes.
- Type IV: centre/surround opponency with brief response signals. The temporal behaviour has not been included in the model so therefore the presence of this cell type can't be analysed.

- Classification of DeValois et al. 1966:
  - 4 cell types with colour opponency: (+R –G), (+G –R), (+Y –B) y (+B –Y); where + means activation and - means inhibition. These cell types would be the midget ganglion type R and type G cells and the small bistratified ganglion cells of the model. The type (+Y-B) does not have an equivalent in the model as scientific publications have only identified blue bipolar type On cells.
  - Cells without colour opponency that have a similar response in all spectrum wavelengths. This cell type would be the parasol ganglion cells of the model.

- Regarding the achromatic pathway that are parasol cells, it is noteworthy to mention that it has a distribution along the visible spectrum that is very similar to the Y measurements.

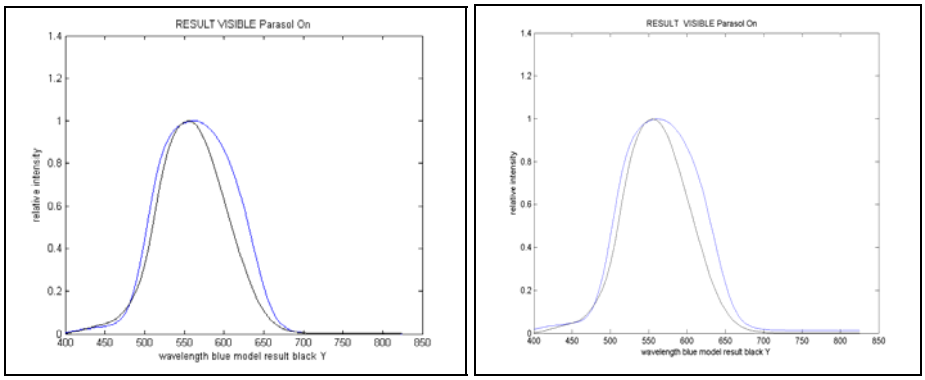

Figure 6.114. Comparison of the output signal of parasol type On cells and signal Y along the visible spectrum. Left) Subtraction mode. Right) Division mode.

- In relation to the processes of edge detection, the fact that the retina detects edges without a specific orientation is consistent with the fact that in V1 there is edge detection in specific orientations. These signals in V1 could be generated through an ordered combination of signals of several cells that detect specific edges coming from the retina.

On the other hand, one must mention that the radii of the receptive fields of real cells are generally greater than those of the model. This is due to two factors. First, the model works on the fovea while many of the available measurements are made at greater eccentricities. Second, it is known that cells establish lateral connections with same type cells. The model has partially included these connections when extending the Gaussian integration functions beyond the integration radius of Gaussians. However, it is possible that these connections may have a greater reach. In any case, the reach of these connections is deemed to be subject to modulations based on the surrounding conditions [WEIL_00].

Regarding the subtraction and division modes, there are no conclusive data on which of the two modes adjusts better to reality. This shall be an issue to study in future works.

Chapter VII

Colour processing model

> *"Color vision has evolved for a number of reasons, including the following: (a) it speeds the process of search and recognition, (b) it allows the identification of important properties of surfaces not otherwise discriminable (e.g. the ripeness of fruit, the pallor of skin), (c) it sometimes permits the perception of contours not otherwise visible, (d) it may also permit the perception of signals near threshold not otherwise visible."*
>
> R. M. Boynton 1977

The aim of this chapter is to define a new model for colour processing that includes the retina model developed in the earlier chapter and to analyse its goodness by comparing it with a reference model such as CIECAM02. In order to do so, the model calculates the colour attributes: hue, lightness, brightness, saturation, chroma and colourfulness of a set of Munsell colour system samples and the results are compared with the values obtained using the reference model.

The aim of this thesis has been to develop new neuroinspired algorithms for colour image processing. Current systems work with RGB values from conventional capture systems and apply either techniques developed for grey level images to each of the pathways (R, G or B) or transform RGB values to other colour spaces where each point is not related to the values that are around it. Although these type of techniques are useful in either very controlled situations (where the illumination is very controlled and the variation gamma of the object to be analysed is small) or simple situations (detect a large sized red circular element), they do not achieve reliable results in more complex situations.

A functional model of the retina has been developed in order to build a system that is capable of analysing colours in a similar manner to that made by human beings (see chapter VI). This model generates, from the image perceived by photoreceptors, a set of output signals or channels.

On the other hand, as shown in chapter III, there are a series of colour attributes that permit the characterisation of colours. This chapter extends the scope of application of the retina model presented in the earlier chapter to the calculation of colour attributes: hue, lightness, brightness, saturation, chroma and colourfulness. This way, taking the functional model of the retina and the architecture of colour appearance models as a basis, a model of colour processing is going to be built that allows to automatically calculate the colour attributes of each point in an image. Furthermore, as shown in the results section on images, this model provides information on the presence of edges in the image as additional information to that provided on colour.

This chapter looks at the following issues. First, an explanation is provided on the need to calculate the colour attributes the colour appearance model that is going to be used as reference and the set of data that are going to be used in order to design the model and to evaluate the results. This phase also presents the work hypotheses for the selection and adjustment of the output channels of the retina model that are necessary in order to calculate the colour attributes.

Second, the results of the combinations of the output channels of the retina model and the final calculation of colour attributes are presented.

Finally, in order to show the information generated by the colour processing model in a real case, the process undertaken by the retina model is shown together with the calculations of the colour attributes, applied to real images.

1. Introduction

Chapter III showed how colour is a perception that bears multiple difficulties in its evaluation. This perception process begins in the photoreceptors in the eye and continues towards the different areas of the cortex. This work has shown a new and innovative retina model that includes different information channels that are transmitted from the retina through the optic nerve. The modelling of the retina cells has specifically defined their connections and structure as well as its integration and signal generation functions. This has allowed the output channels of the model to have very specific spatial and chromatic characteristics. These information channels reach LGN and later the cortex where the final colour perceptions take place.

The obtaining of the output channels of the retina is the first stage in the colour information processing system. A second stage must be added where the calculation of colour attributes from information generated by the retina model.

In order to meet this need, chapter III dealt with the analysis of colour models. More specifically, these colour appearance models presented in chapter III have been the ones which have allowed the identification of the different steps taken for the evaluation of colour attributes:

- Calculation of the chromatic adaptation from the {X, Y, Z} values (where the adaptation to the context is modelled (background, luminance...)).
- Calculation of the non-linear dynamic response.

- Combination of signals in channels.
- Calculation of colour attributes: hue, lightness, brightness, chroma, saturation and colourfulness

Let's look once again to figure 3.24 that specifies these stages:

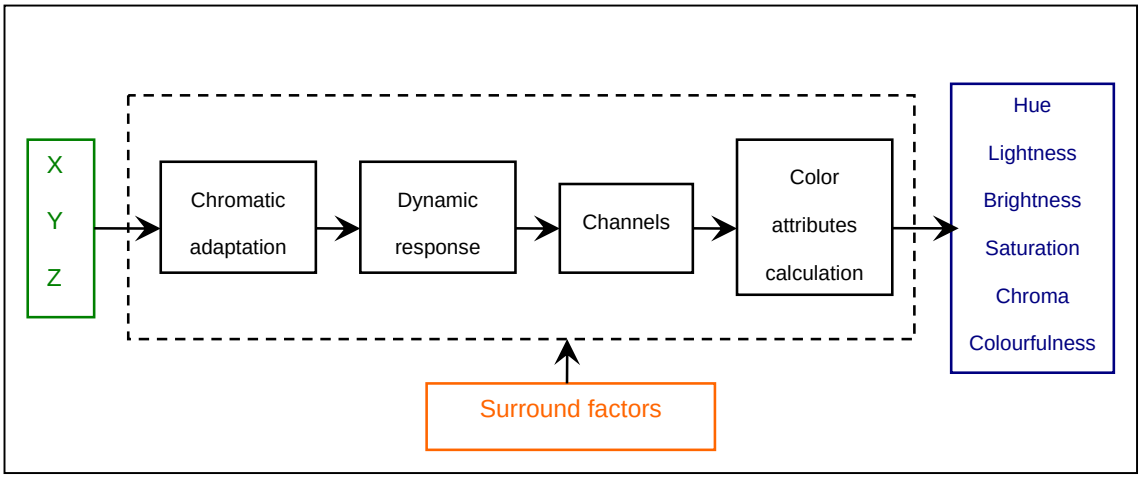

Figure 7.1. Generic structure of colour appearance models.

As mentioned at the beginning of this chapter, the functional model of the retina is going to be integrated with the colour appearance model architecture.

The diagram in figure 7.1 is going to be used in order to generate the colour processing model. The retina model will replace the dynamic response and the channels stages. The following figure shows the diagram of the colour processing model proposed in this work.

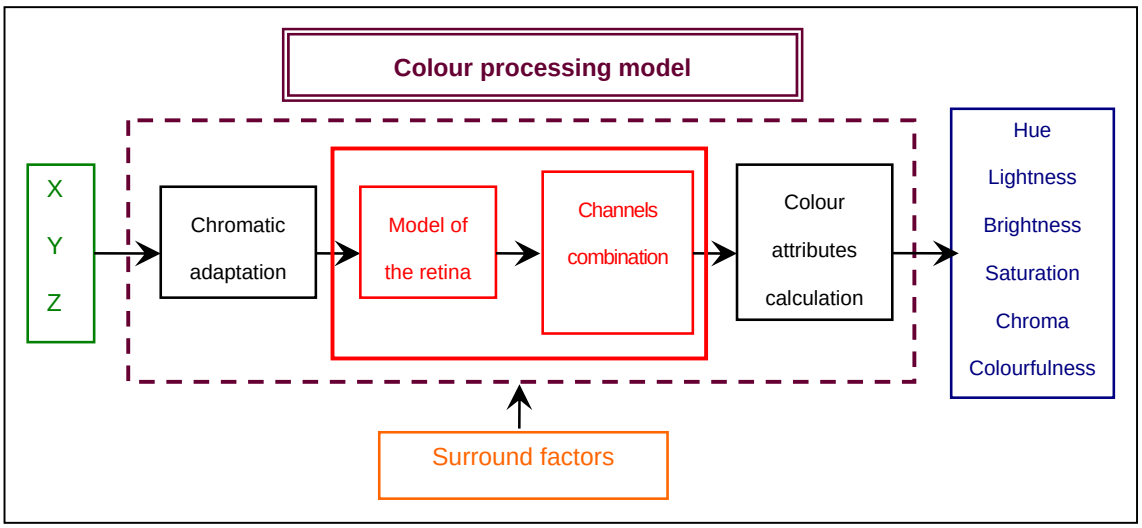

Figure 7.2. Diagram of the colour processing model.

This diagram includes a stage that combines the output channels of the retina model in order to generate chromatic and achromatic channels which are inputs for the calculation of colour attributes.

A reference colour appearance model (CIELAB, Hunt, CIECAM02….) capable of predicting the greatest number of colour and colour effect attributes is selected in order to adjust these combinations.

The set of data employed is a set of samples from Munsell's colour system (shown in chapter III). This colour system was chosen among a multitude of existing models as it generates a homogeneous distribution of samples based on multiple observers' perception evaluations. Precisely because of this, it is one of the most widely used data sets in colour models adjustment and evaluation.

The ideal colour model, when applied to Munsell samples, will generate concentric rings for constant chroma values and straight lines for samples of constant hue. Chapter III presented the CIELAB and CIELUV results using a set of Munsell samples. The CIELAB case was shown in figure 3.28.

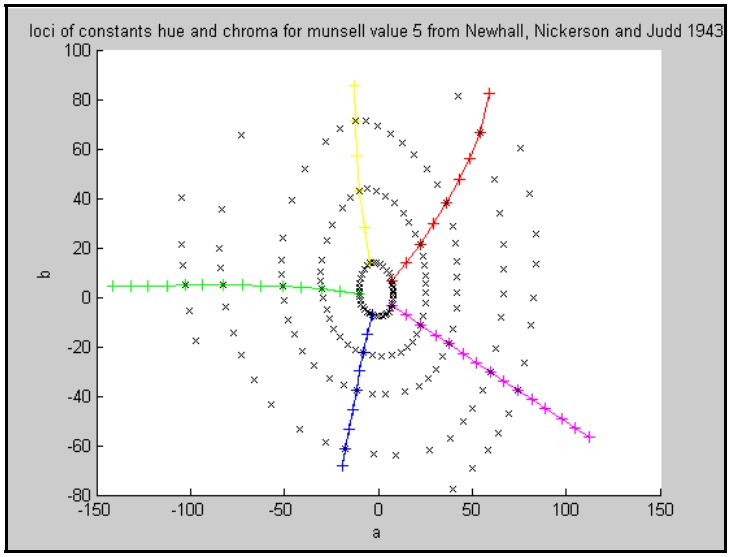

Figure 7.3. Munsell samples with constant chroma (each point of the ovals in black) and constant hue (each point set of the same colour), for a value=5 in CIELAB space.

The image shows that instead of circles there are pseudo-ovals and that the hue lines are curved.

The colour processing model results, given the nature of the Munsell colour system, can be evaluated in two ways:

- Measurement of the circularity level of rings with constant chroma and linearity of the constant hue sets.
- Calculation of the colour attributes of the Munsell samples.

Both cases shall compare the model results with those of the reference colour appearance model and thus shall measure the goodness of fit of the proposed colour processing model.

The data base to be used has been obtained from the Munsell Color Science Laboratory: http://www.cis.rit.edu/research/mcsl2/online/munsell.php, where the values X, Y and Z are provided for the different Munsell samples.

2. Colour appearance model selection

Chapter III, section 4.2 presented the main colour appearance models. Table 3.2 showed an evaluation of the attributes calculated for each model and the effects they are capable of modelling. The most complete was the Hunt model, followed by the CIECAM97 and CIECAM02 models.

In order to select the reference model, it is necessary to define its scope of application. The aim of the colour model that is presented in this work is for its use in the automated processing of images. Usually, these images are codified in three colour channels of 8 bits, that is, the signal varies from 0 to 225. On the other hand, the luminance of the adapting field is considered to be in an intermediate range (if an evaluator has to analyse one of those images, then he would not do it in either low or high brightness conditions). This means that the system's dynamic range of work will be much smaller than the range of work of the human eye 10^6:1. The working hypothesis that is going to be considered is that under these conditions, the effects of rods and the bleaching of cones are very small.

The Hunt model will not be used as a reference model due to the its complexity, its non-invertibility and because some of the advantages of this model over CIECAM97 and CIECAM02 are not applicable in this context.

The following are the differences, in each of their phases, between the CIECAM97 and CIECAM02 models:

- Calculation of the chromatic adaptation:
  - CIECAM97: Bradford transform.
  - CIECAM02: CMCCAT2000 selected versus the Bradford transform based on the results.
- Calculation of the non-linear dynamic response: different exponential factor and constant factors.
  - CIECAM97:

$$I_a^{'} = 40\left(F_L I'/100\right)^{0.73} / \left[\left(F_L I'/100\right)^{0.73} + 2\right] + 1 \qquad \mathrm{I} \in \{\mathrm{R},\mathrm{G},\mathrm{B}\} \qquad \text{(eq. 3.81)}$$

  - CIECAM02:

$$I_a^{'} = \frac{400\left(F_L I'/100\right)^{0.42}}{27.13 + \left(F_L I'/100\right)^{0.42}} + 0.1 \qquad I \in \{R,G,B\} \qquad \text{(eq. 3.104)}$$

- Combination of signals in channels: equal except the constants of A values, which compensate the noise components introduced in functions 3.81 and 3.104 respectively.
  - CIECAM97 and CIECAM02:

$$a = R_a^{'} - 12G_a^{'}/11 + B_a^{'}/11 \qquad \text{(eq. 3.94 and 3.113)}$$

$$b = (1/9)(R_a^{'} + G_a^{'} - 2B_a^{'}) \quad \text{(eq. 3.95 and 3.114)}$$

  - CIECAM97:

$$\mathrm{A} = \ [2\mathrm{R}_a^{'} + \mathrm{G}_a^{'} + (1/20)\mathrm{B}_a^{'} - 2.05]\mathrm{N}_{bb} \qquad \text{(eq. 3.96)}$$

  - CIECAM02:

$$A = \left[2R_a^{'} + G_a^{'} + (1/20)B_a^{'} - 0.305)\right]N_{bb} \qquad \text{(eq. 3.120)}$$

- Colour attribute calculation: differences in the calculation of brightness, saturation, chroma, colourfulness and some auxiliary values.

As can be seen, both models have multiple common elements. Apart from the he phases that the retina model replaces, the chromatic adaptation in CIECAM02 is better than that of CIECAM97, while the calculation of chromatic and achromatic channels are the same in both models. This, coupled with the fact that the CIECAM02 model was proposed as an improvement over CIECAM97 leads one to select the former as the reference model.

The working conditions that are going to be considered are: iluminant C, L_A=100, Y_b=20 and average working conditions.

3. Selection of *a* and *b* channels

The diagram in figure 7.2 has added a stage where the output signals of the retina model are combined in order to create chromatic and achromatic channels. Three work channels *a*, *b* and *A* are going to be established in accordance with normal nomenclature. This section presents the work hypothesis for the generation of *a* and *b* channels, as these are the channels that influence the circularity level of constant chroma rings and the linearity of constant hue points of the Munsell samples.

Before establishing the channels, it is necessary to group the type On and Off signals of each type generated by the functional retina model. Ganglion cells, as previously shown, generate spikes that are proportional to the electric signal they receive. Only positive signals can be codified as these are spikes. In order to solve this limitation, above and below average signals are codified in two different channels: channel On and pathway Off. From a computational perspective, both signals must be joined in a sole information channel. The following criterion is used in order to do so.

$$Given\ \ x\begin{cases} x \geq threshold \rightarrow f(x) = On\ \ Signal \\ x < threshold \rightarrow f(x) = Off\ \ \ Signal \end{cases} \qquad \text{(eq. 7.1)}$$

The original exponential signal from equation 6.11 is transformed in:

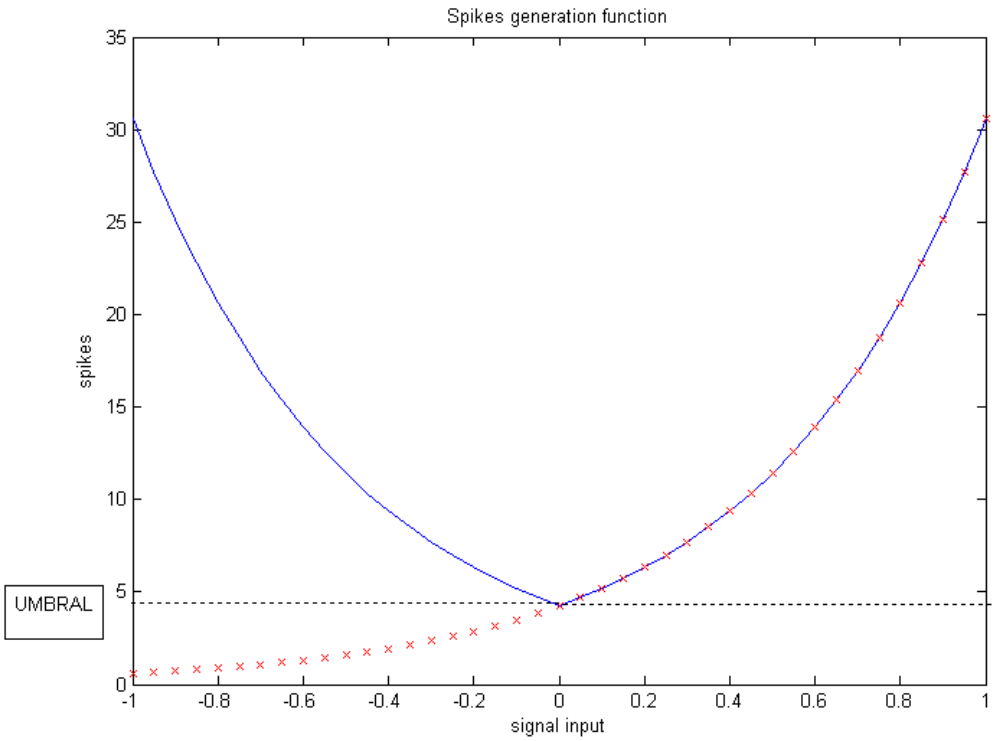

Figure 7.4. Representation of the result from the On and Off channels combination. Blue: Combined output signal. Red: exponential signal type On.

When applying this criterion to the set of output signals of the retina model, the following channels are obtained:

- Midget ganglion type R channel.
- Midget ganglion type G channel.
- Small bistratified ganglion channel.
- Parasol ganglion channel.

We propose two possibilities in order to define the a and b chromatic channels:

a) Hypothesis A: *a* and *b* values are the combination of three chromatic channels of the retina model.

$$a = C_1 \bullet Midget\ ganglion\ R + C_2 \bullet Midget\ ganglion\ G + C_3 \bullet Small\ bistratified \qquad \text{(eq. 7.2)}$$

$$b = C_4 \bullet Midget\ ganglion\ R + C_5 \bullet Midget\ ganglion\ G + C_6 \bullet Small\ bistratified \qquad \text{(eq. 7.3)}$$

This hypothesis follows the calculation criterion used by colour appearance models (see equations 3.113 and 3.114), where a and b are linear combinations of R, G and B.

b) Hypothesis B: channel a is proportional to the midget ganglion type G channel and channel b is proportional to the bistratified ganglion channel. Subchannels type On and Off of each type have an specific exponential function for the generation of spikes.

The type On and Off subchannels are transformed in the following manner:

$$Ganglion\,G\,on = A_1 \exp(B_1 \bullet ganglion\,G\,on\,input) \quad \text{(eq. 7.4)}$$

$$Ganglion\,G\,off = A_2 \exp(B_2 \bullet ganglion\,G\,off\ input) \quad \text{(eq. 7.5)}$$

$$Bistratified\ off = A_3 \exp(B_3 \bullet Bistratified\ off\ input) \quad \text{(eq. 7.6)}$$

$$Bistratified\ off = A_4 \exp(B_4 \bullet Bistratified\ off\ input) \quad \text{(eq. 7.7)}$$

Using equation 7.1 again, these four signals are regrouped in the modified midget ganglion type G and modified bistratified ganglion channels.

A channel that is not present in the retina model has been included: bistratified ganglion type Off. The calculation of this channel is done according to the data of type On channel for values below threshold. The input value of the ganglion cell is recovered from the exponential function (equation 6.11). If the receptive fields in both types are considered equal, then the input values of type On and type Off (before the exponential function) have the following relationship:

$$On\ Type = -Off\ Type \quad \text{(eq. 7.8)}$$

The bistratified ganglion type Off can be calculated, in accordance with this relationship, with their specific function for the generation of nervous spikes: A_4 and B_4 (equation 7.7).

This work hypothesis arises from the analysis of the original influence of each type of photoreceptor on each of the channels. In order to do so, the relative weights of photoreceptor signals that receive each channel have been evaluated using a combination of photoreceptors that feed the centre of each cell and the set of horizontals that feed the surround. This helps to obtain an approximation of the combination of signals {L, M, S} that each ganglion cell receives.

$$Ron \approx K_1 * (3.21*L-M-0.28*S) \quad \text{(eq. 7.9)}$$

$$Gon \approx K_2 * (-0.42*L+M-0.076*S) \quad \text{(eq. 7.10)}$$

$$Bistratified \approx K_3 * (-1.59*L - M + 6.05*S) \quad \text{(eq. 7.11)}$$

$$Parasol \approx K_4 * (1.6*L + M - 60.043*S) \quad \text{(eq.7.12)}$$

Channel G on has a combination similar to channel *a* when comparing the combinations of each channel, while the bistratified channel has a combination similar to channel *b*. This way, when representing the G ganglion value and the bistratified ganglion value of the constant value Munsell samples, the following figure is obtained.

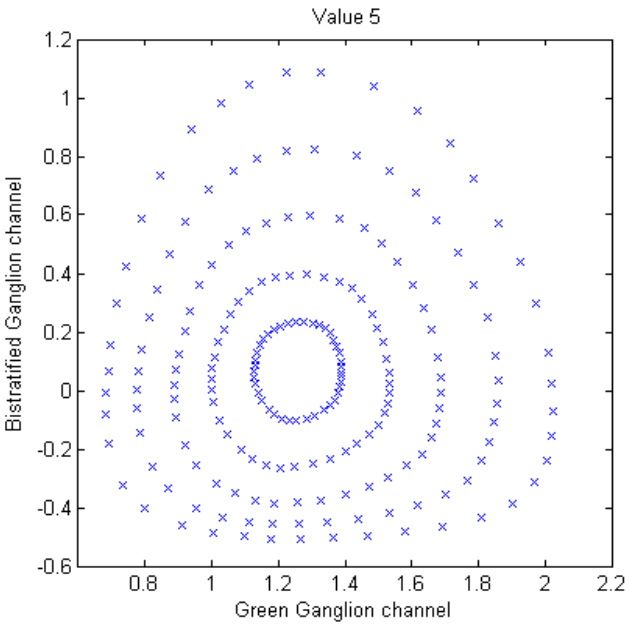

Figure 7.5. Munsell system samples with constant chroma (each oval of points in black), for value=5 where the midget ganglion type G channels is represented in the abscissas axis while the ordinates represents the bistratified ganglion channel.

This direct representation of the results of two of the retina's channels bears a very considerable level of circularity, also taking into account, that it has not been developed for this end. This indicates that the channels identified as sources for *a* and *b* already have ideal characteristics, in the output stage of the retina, for their transformation into channels *a* and *b* of the colour processing model.

In order to improve the circularity level of constant chroma rings, we propose to adjust the exponential function for the generation of spikes for each of the 4 types of ganglion cells in this work (equations 7.4 to 7.7). This adjustment is biologically justified as not all types of cells must have the same parameters in the function for the generation of spikes.

3.1 Target functions to optimise

Both work hypothesis proposed in the earlier section have defined a series of parameters. In order to adjust these. The optimisation of the circularity level of constant chroma ringside going to be used to configure the parameters.

The measurement of the circularity level has been defined as the normalised sum for each constant chroma ring of the squared differences between the average radius of the ring and the radius of each sample. The centre of the rings has been established as the average value of all points of a given Value. The radii are defined as the distance of each point to the average point. The normalisation is achieved by dividing that sum by the average radius of the ring squared, in order to avoid that outer rings have more weight than inner rings. This is shown in the following equations. Number of points

$$a_{centre} = \frac{\sum_{\forall chroma\ j} \sum_{\forall point\ i} a_{point\ i}^{chroma\ j}}{\text{Number of points}} \qquad \text{(eq. 7.13)}$$

$$b_{centr} = \frac{\sum_{\forall chroma\ j} \sum_{\forall point\ i} b_{point\ i}^{chroma\ j}}{\text{Number of points}} \qquad \text{(eq. 7.14)}$$

$$Radius_{point\ i}^{chroma\ j} = \left(\left(a_{centre} - a_{point\ i}^{chroma\ j}\right)^2 + \left(b_{centre} - b_{point\ i}^{chroma\ j}\right)^2\right)^{1/2} \qquad \text{(eq. 7.15)}$$

$$Radius_{mean}^{chroma\ j} = \frac{\sum_{point\ i} Radius_{point\ i}^{chroma\ j}}{\text{Number of points ring j}} \qquad \text{(eq. 7.16)}$$

$$f_{optimise} = \frac{\sum_{\forall chroma\ j} \sum_{\forall point\ i} \left(Radius_{mean}^{chroma\ j} - Radius_{point\ i}^{chroma\ j}\right)^2 / (Radiua_{mean}^{chroma\ j})^2}{\text{Number of points}} \qquad \text{(eq. 7.17)}$$

As the linearity of the constant hue points is also one of the desired characteristics, the use of such measurement as an optimisation function has been pondered. However, the results have not been positive as the optimisation process tends to align both axis either by making {C1, C2, C3} equal to {C4, C5, C6} in hypothesis A or by minimising one of the axis, either making C1 and C2

or C3 and C4 tend towards zero, in hypothesis B. Therefore, its use to establish the configuration parameters of the different channels has been discarded.

4. Results

This section presents the results of the optimisation processes for both work hypotheses. The optimisation processes are going to be performed with data with constant Munsell Value. As a representative sample, the following Values have been chosen: 3, 5 and 7.

The evaluation of the results is going to be made based on the optimisation function and the appearance in the *ab* plane of the set of chroma rings for each Value. The results are going to be analysed by quadrants in order to ease the evaluation of the results in the *ab* plane.

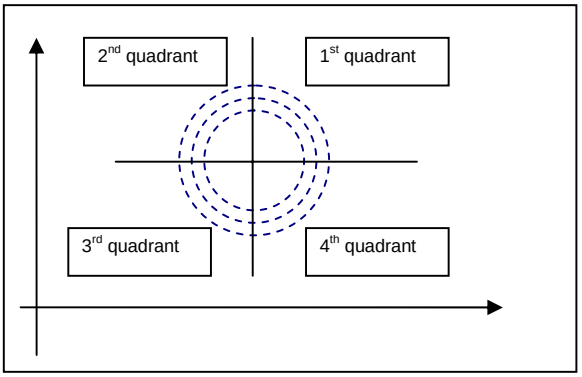

Figure 7.6. Analysis of results by quadrants.

The following shows the optimisation results of these three Values, for each work hypothesis, as well as for the subtraction and division modes. Beginning with Value 5, as it is the middle value.

a) Hypothesis A:

1. Subtraction mode:

   The optimisation is evaluated with Ci in the interval ±1 with $i \in \{1..6\}$, in order to avoid non-desired effects in the optimisation as happened in the case of hue linearity, the interval is limited to values equal or smaller than 1. The evaluation step has been 0.2, due to the equilibrium obtained between results and computational time.

   a. Optimisation results for the set of points with Value 5: the following are the optimal parameters that were obtained.

C1	C2	C3	C4	C5	C6	$F_{optimise}$
-1	-0.2	0.4	-0.8	-0.8	0	0.2037

Table 7.1. Result of the optimisation for Value=5, hypothesis A, subtraction mode.

The representation of this optimisation in the *ab* plane is:

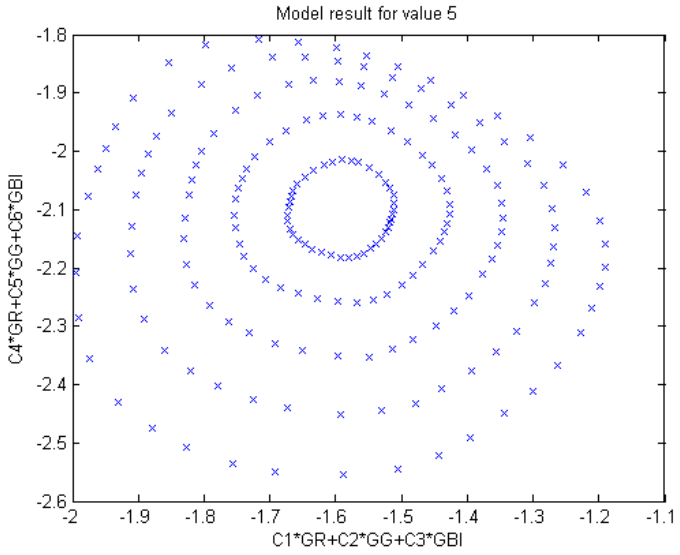

Figure 7.7. Results of the set of points with Value 5 after optimisation, hypothesis A, subtraction mode in the *ab* plane.

The figure shows how the elements in quadrants 2, 3 and 4 are approximately circular whereas quadrant 1 does not have this feature for rings with greater chroma.

b. Optimisation results for a set of points with Value 3: the following are the optimal parameters that were obtained.

C1	C2	C3	C4	C5	C6	$F_{optimise}$
1	0.4	-0.4	-0.2	-0.4	-0.2	0.1425

Table 7.2 Result of the optimisation for Value=3, hypothesis A, subtraction mode.

The representation of this optimisation in the *ab* plane is:

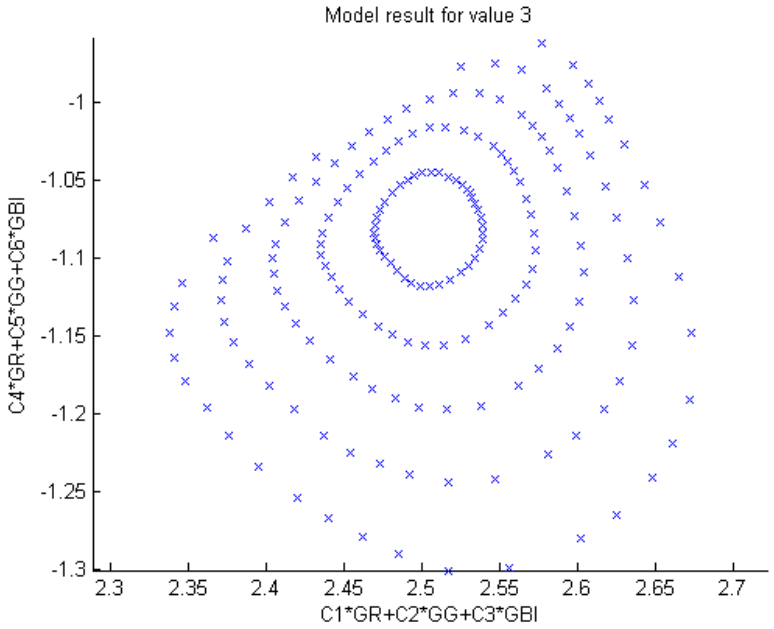

Figure 7.8 Results of the set of points with Value 3 after optimisation, hypothesis A, subtraction mode, in the *ab* plane.

The results show a smaller circularity level than in the earlier case, showing an area with very little circularity in quadrant 2. The level of circularity decreases in rings with greater chroma.

c. Optimisation results for a set of points with Value 7: the following are the optimal parameters that were obtained.

C1	C2	C3	C4	C5	C6	$F_{optimise}$
0.2	-1	0.6	-0.4	-0.8	-0.4	0.0135

Table 7.3 Result for the optimisation for Value=7, hypothesis A, subtraction mode.

The representation of this optimisation in the *ab* plane is:

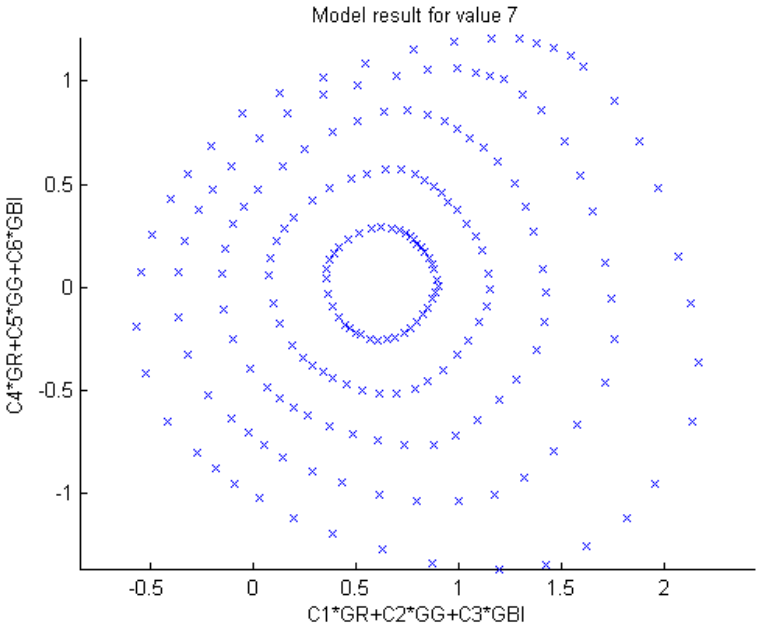

Figure 7.9. Optimisation results of the set of points with Value 7, hypothesis A, subtraction mode, in the *ab* plane.

The results are better than in earlier cases although there continues to be a quadrant that unbalances the final circularity of the rings.

2. Division mode:

   a. Optimisation results for a set of point with Value 5: the following are the optimal parameters that were obtained

C1	C2	C3	C4	C5	C6	$F_{optimise}$
0	-0.6	-0.8	-0.2	-0.8	0.6	0.0072

Table 7.4 Optimisation result for Value=5, hypothesis A, division mode.

The representation of the optimisation in the *ab* plane is:

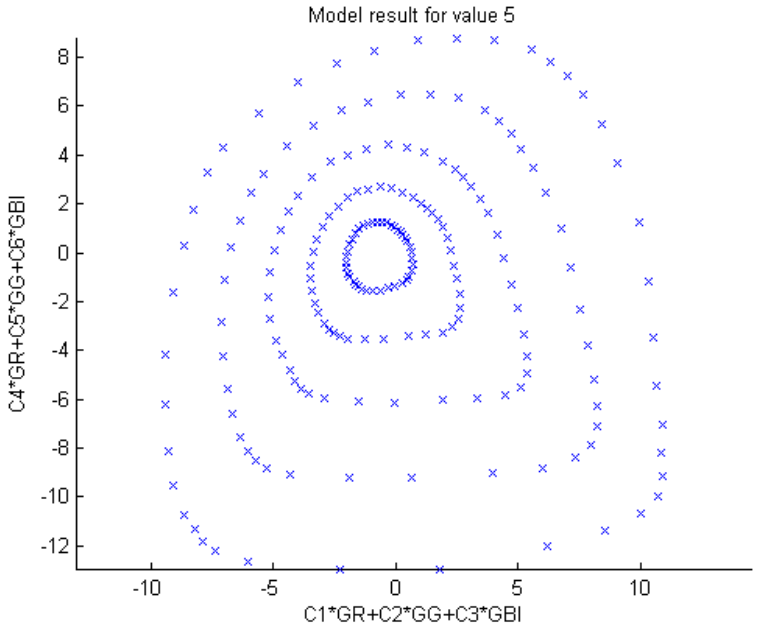

Figure 7.10. Optimisation results of the set of points with Value 5, hypothesis A, division mode in the *ab* plane.

Quadrant 2 shows a high level of circularity while the remaining quadrants generate curves that could be described as a shape between a circle and a rectangle.

b. Optimisation results for a set of points with Value 3: the following are the optimal parameters that were obtained.

C1	C2	C3	C4	C5	C6	$F_{optimise}$
-0.4	-0.8	1	-0.2	-1	-1	0.0097

Table 7.5. Optimisation result for Value=3, hypothesis A, division mode.

The representation of the optimisation in the *ab* plane is:

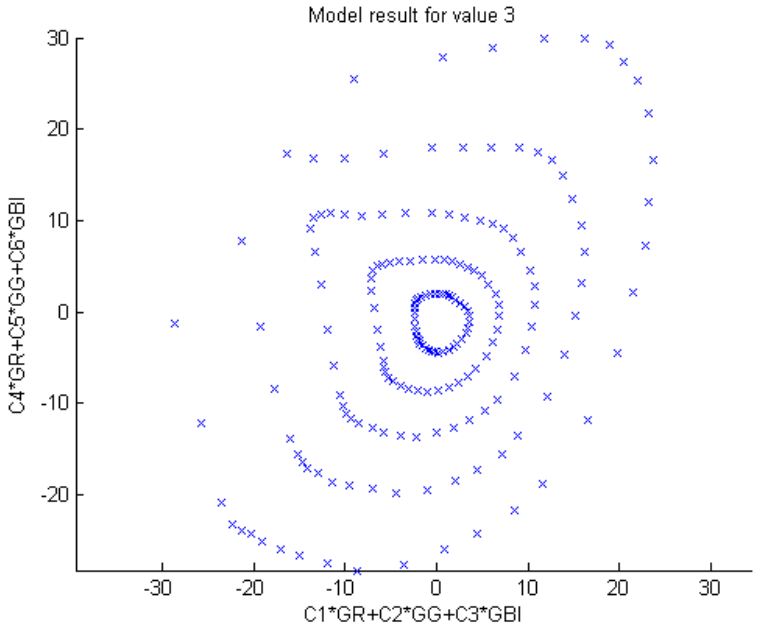

Figure 7.11. Optimisation results of the set of points with Valor 3, hypothesis A, division mode in the *ab* plane.

The results in this case have are not positive as they have shapes that are very far from optimal circles.

c. Optimisation results for a set of points with Value 7: the following are the optimal parameters that were obtained.

C1	C2	C3	C4	C5	C6	$F_{optimise}$
0.2	1	-0.8	-0.2	1	1	0.0084

Table 7.6. Optimisation results for Value=7, hypothesis A, division mode.

The optimisation representation in the *ab* plane is:

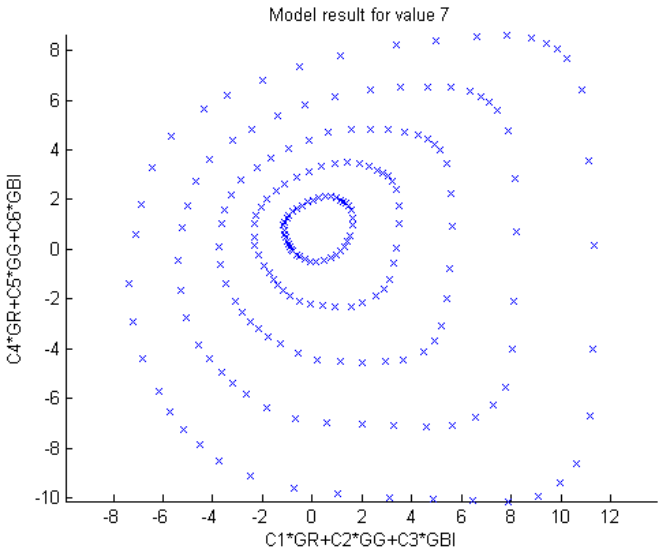

Figure 7.12. Optimisation results of the set of points with Value 7, hypothesis A, division mode in the *ab* plane.

Similar to the results obtained for Value 5, the result is closer to a circular shape but continues to be between the shapes of a rectangle and a true circle.

After analysing the optimisation process results for work hypothesis A, the different quadrants are not compensated and usually there is one that is far away from circular behaviour. On the other hand, vectors {C1, C2, C3} and {C4, C5, C6} have large variations between the different constant Value planes. The best result among the different cases looked at is that of Value 7 and subtraction mode.

b) Hypothesis B:

The optimisation has been carried out with values Ai and Bi in the range 0..2 with $i \in \{1..4\}$. The step selected is 0.4 in order to allow a difference between channels of 1 to 5 and due to the relationship between results and the computational time of the optimisation.

1. Subtraction mode:

    a. Optimisation results for a set of points with Value 5: the following are the optimal parameters that were obtained.

A1	A2	A3	A4	B1	B2	B3	B4	$F_{optimise}$
1.2	1.6	0.8	2	0.8	1.2	0.8	1.6	0.0043

Table 7.7. Optimisation result for Value=5, hypothesis B, subtraction mode.

The optimisation representation in the *ab* plane is:

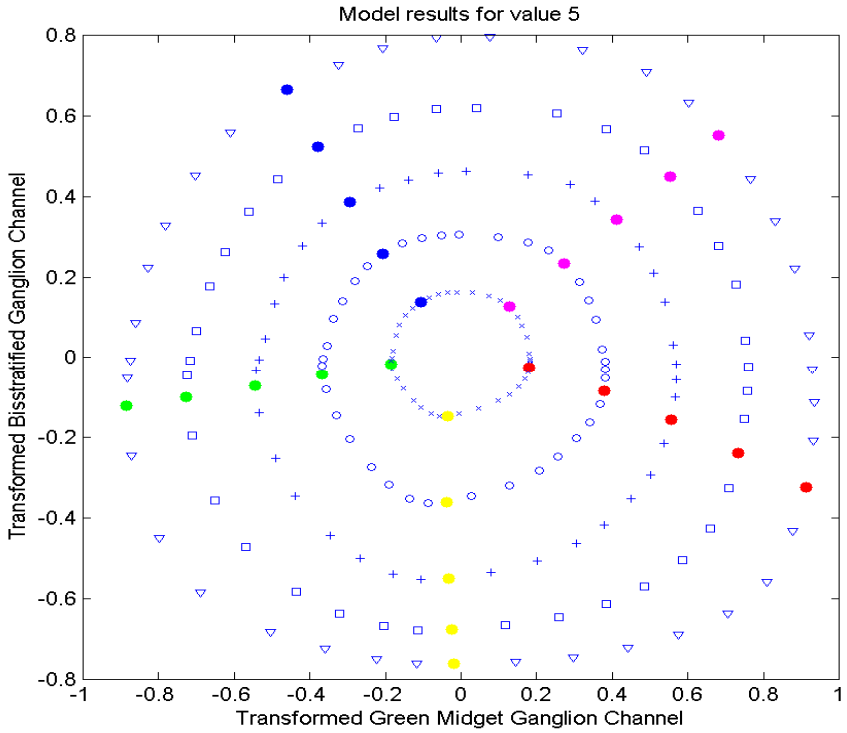

Figure 7.13 Optimisation results of the set of points with Value 5, hypothesis B, subtraction mode in the *ab* plane. Blue constant chroma rings, in different colours, lines with constant hue.

The optimisation results have been extremely good. It has generated a very homogeneous circular structure; furthermore the constant hue points are aligned almost making straight lines.

b. Optimisation for a set of points with Value 3: the following are the optimal parameters that were obtained.

A1	A2	A3	A4	B1	B2	B3	B4	$F_{optimise}$
0.4	0.8	0.4	1.2	0.4	0.8	0.4	1.2	0.0043

Table 7.8. Optimisation result for Value=3, hypothesis B, subtraction mode.

The optimisation representation in the *ab* plane is:

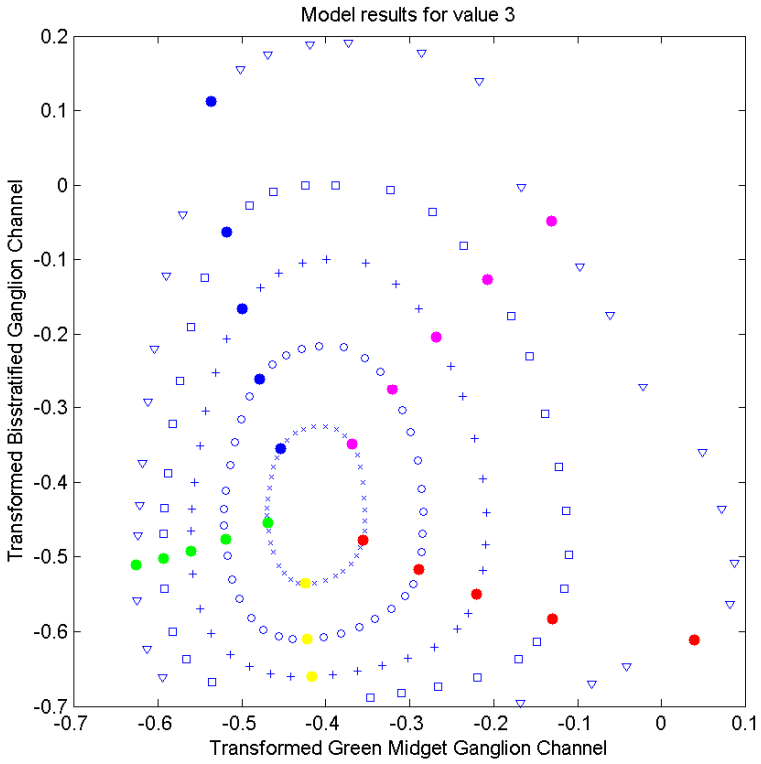

Figure 7.14. Results of a set of points with Value 3 after optimisation, hypothesis A, subtraction mode in the *ab* plane. Blue constant chroma rings, in different colours, constant hue lines.

The result has not been as positive as in the earlier case, as the shapes formed have been ovals instead of circumferences. In quadrant 4, the high chroma rings are far from the desired structure. The constant chroma points make lines which are similar to straight lines except for the points with highest chroma in quadrant 4.

c. Optimisation results for a set of points with Value 7: the following are the optimal parameters that were obtained.

A1	A2	A3	A4	B1	B2	B3	B4	$F_{optimise}$
1.2	1.6	0.8	1.2	0.8	1.2	0.8	1.6	0.0034

Table 7.9. Optimisation result for Value=7, hypothesis B, subtraction mode.

The representation of the optimisation in the *ab* plane is:

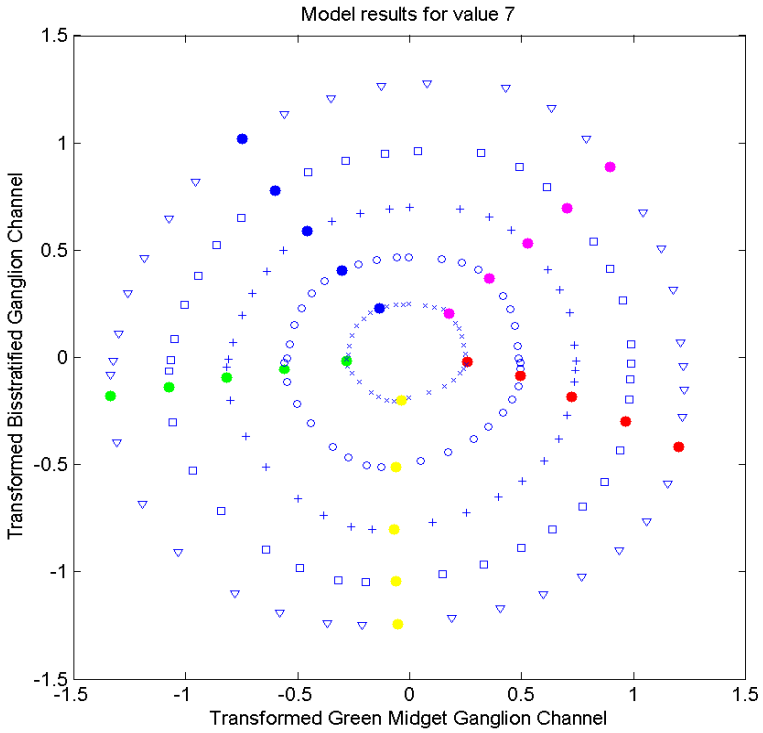

Figure 7.15 Optimisation results of the set of points with Value 7, hypothesis B, subtraction mode in the *ab* plane. Blue constant chroma rings, in different colours, constant hue lines.

The optimisation result has been very positive and is near to the desired circular structure and straight lines in the case of constant hue points. The optimisation parameters are very similar to those obtained in the case of Value=5 (only differs in value A4).

2. Division mode:

   a. Optimisation for a set of points with Value 5: the following are the optimal parameters that were obtained.

A1	A2	A3	A4	B1	B2	B3	B4	$F_{optimise}$
2	2	2	1.2	0.8	1.6	0.8	1.6	0.0060

Table 7.10 Optimisation result for Value=5, hypothesis B, division mode.

The representation of the optimisation in the *ab* plane is:

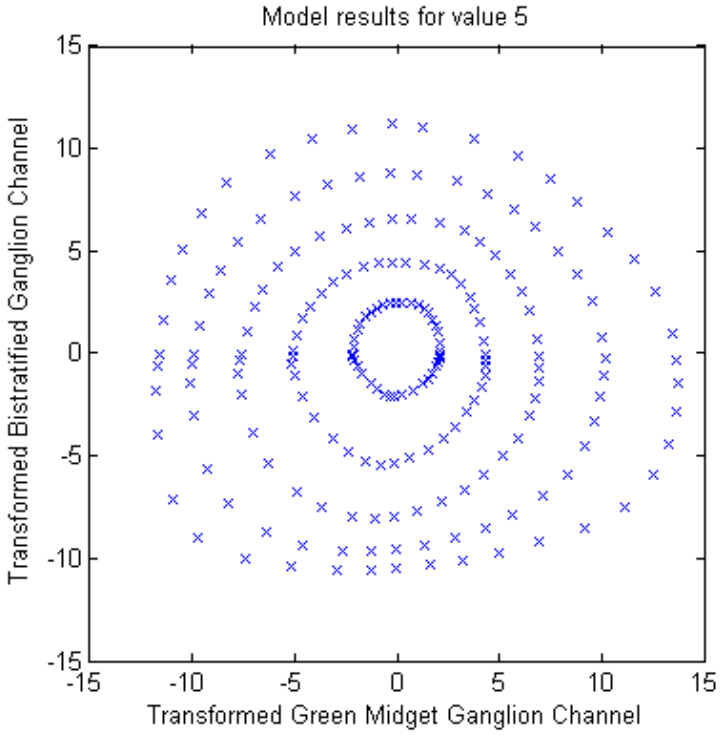

Figure 7.16 Optimisation results of the set of points with Value 5, hypothesis B, division mode in the *ab* plane.

The general shape comes close to that of a circular shape. A certain crowding can be noticed in the quadrant intersections. The lower and left lateral areas are slightly unbalanced. Despite this, the result obtained in this case is also highly satisfactory.

   b. Optimisation results for a set of points with Value 3: the following are the optimal parameters that were obtained.

A1	A2	A3	A4	B1	B2	B3	B4	$F_{optimise}$
1.6	1.2	0.8	0.8	0.4	1.2	0.8	1.2	0.0056

Table 7.11. Optimisation result for Value=3, hypothesis B, division mode.

The representation of the optimisation in the *ab* plane is:

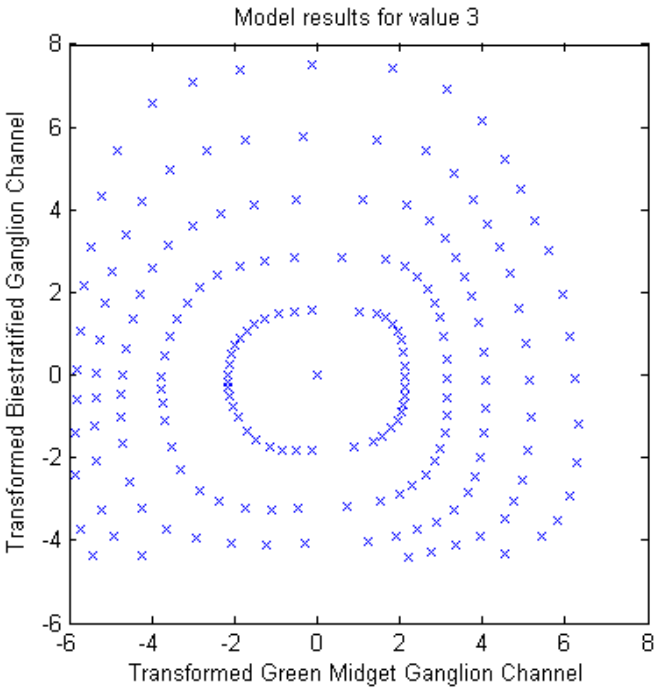

Figure 7.17. Optimisation results for a set of points with Value 3, hypothesis B, division mode in the *ab* plane.

There is a certain gap in the intermediate area. Quadrants 2 and 3 have a shape that comes close to an oval while quadrants 1 and 4 are farther from these types of shapes.

c. Optimisation results for a set of points with Value 7: the following are the optimal parameters that were obtained.

A1	A2	A3	A4	B1	B2	B3	B4	$F_{optimise}$

2	0.8	1.2	0.8	0.4	1.6	0.8	1.2	0.0055

Table 7.12. Optimisation result for Value=7, hypothesis B, division mode.

The representation of the optimisation in the *ab* plane is:

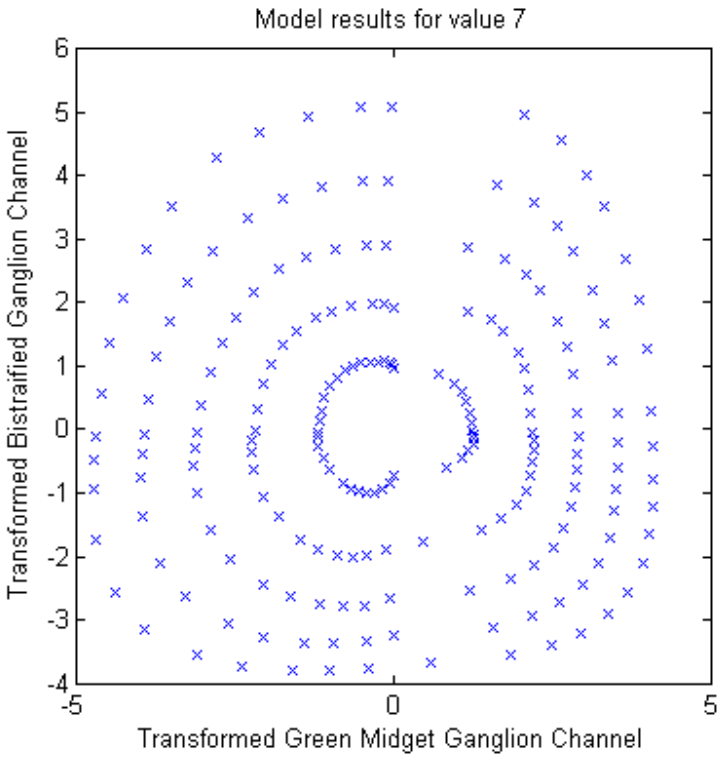

Figure 7.18. Optimisation results for a set of points with Value 7, hypothesis B, division mode in the *ab* plane.

As in the earlier cases, a union gap between quadrants 1 and 4 and quadrants 2 and 3 is found. The general shape is approximately circular.

The results obtained in the optimisations with work hypothesis B have been very positive. Especially in the subtraction mode. The chroma rings have are nearly circles and constant hue lines near straight lines. Furthermore, the configuration parameters have not shown changes based on the Value planes that were obtained in work hypothesis A.

4.1 Result analysis and comparison with CIECAM02

First, it is necessary to present the results obtained by CIECAM02 for the three Value levels used.

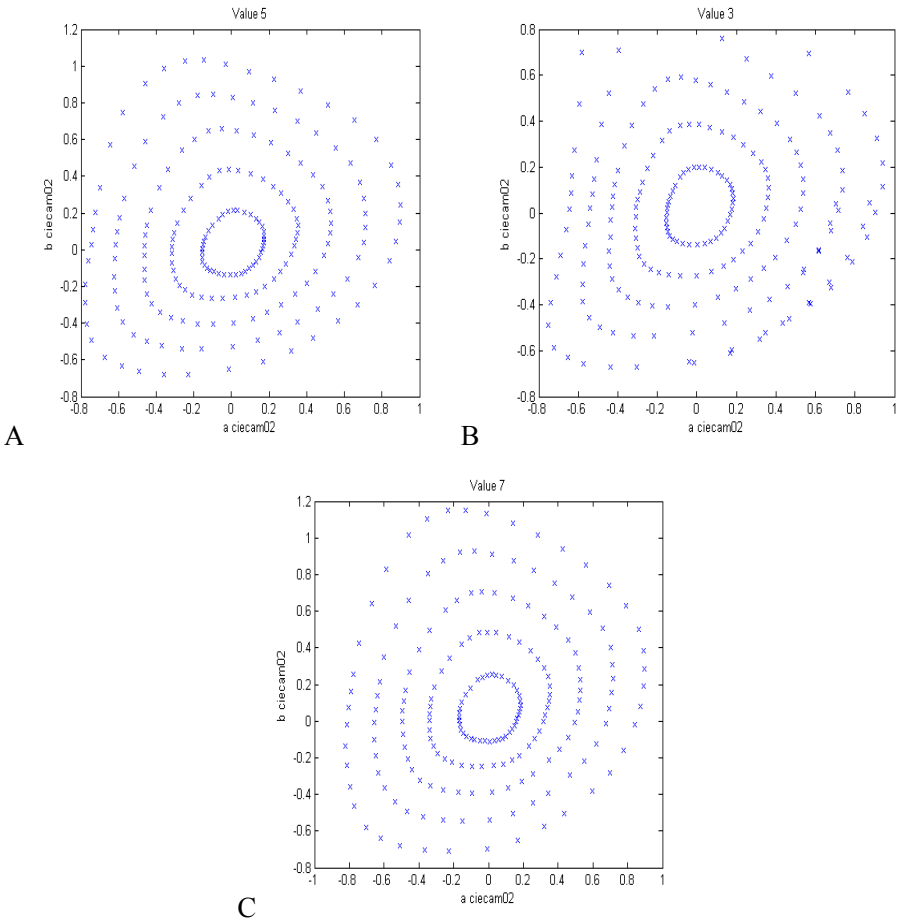

Figure 7.19 Results of the *ab* plane generated by CIECAM02 for points with constant Value. A) Value 5. B) Value 3. C) Value 7.

From the graphs, one can observe how hypothesis B, subtraction mode, has generated rings with shapes closest to circles. In order to make a comparison based on numerical parameters, the following table shows the circularity level results (equation 7.17) obtained in each case.

		Subtraction mode			Division mode		
Value		3	5	7	3	5	7
Circularity levels	Hypothesis A	0.1425	0.2037	0.0135	0.0097	0.0072	0.0084
	Hypothesis B	**0.0043**	**0.0043**	**0.0034**	**0.0056**	**0.0060**	**0.0055**
	Ciecam02	Independent of the mode					
		0.0471	0.0221	0.0392	0.0471	0.0221	0.0392

Table 7.13. Comparison of circularity levels.

The circularity levels obtained through hypothesis B, as demonstrated, are better, particularly in the subtraction mode, when compared with the circularity levels obtained by CIECAM02.

The following shows the sets of points for each Value plane, using the optimisation parameters for Value 5 hypothesis B subtraction mode, in order to analyse the behaviour of the Value=5 optimisation on other value planes.

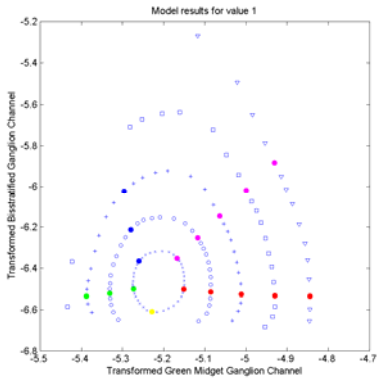

1

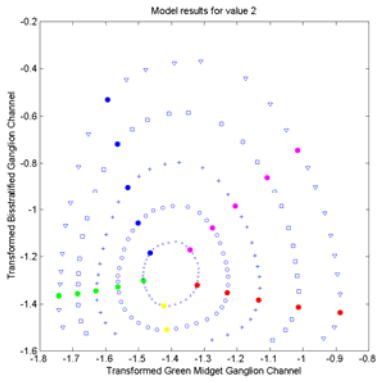

2

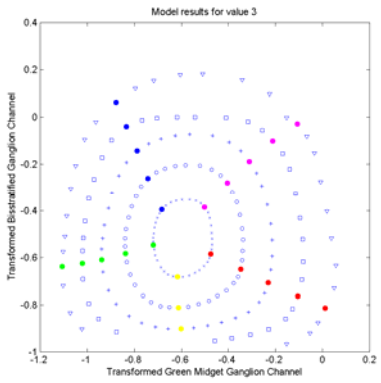

3

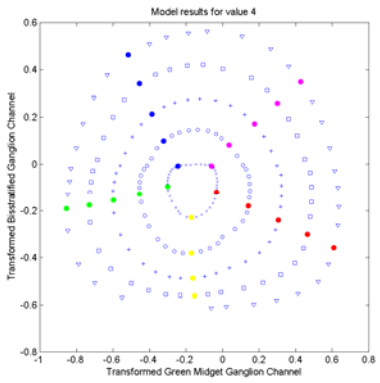

4

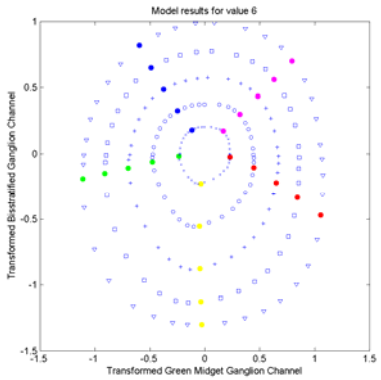

6

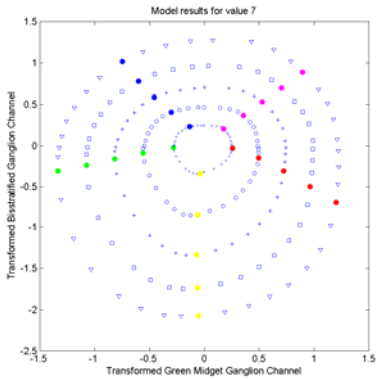

7

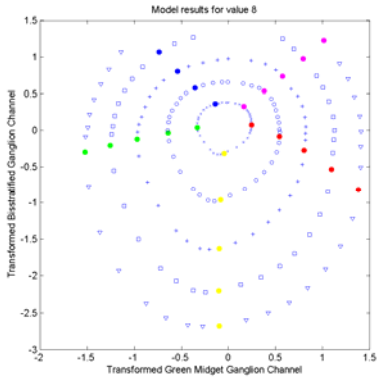

8

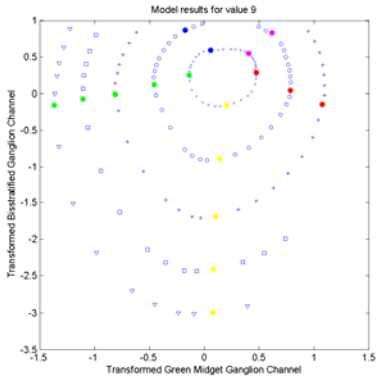

9

Figure 7.20. Results for the set of Munsell samples of constant value in the *ab* plane with the optimisation parameters of hypothesis B for Value 5, subtraction mode. Blue constant chroma rings, in different colours, constant hue lines. 1) Value=1. 2) Value=2. 3) Value=3. 4) Value=4. 6) Value=6. 7) Value=7. 8) Value=8. 9) Value=9.

Values near 5 keep a high circularity level in chroma rings and linearity in constant hue points. Probably the configuration parameters of the exponential function for the generation of spikes

vary according to the intensity level of the point to be evaluated. The evaluation of this issue is not within the objectives set out in this work and therefore shall be dealt with in future works.

The following section completes the model development for colour processing for one work hypothesis and one mode. Hypothesis B and the subtraction mode are chosen based on the results obtained in the *ab* plane.

To sum up, based on the retina model, an *ab* colour space has been generated where the constant chroma rings have shapes that closely resemble circles and constant hue lines that closely resemble straight lines.

The fact that the *a* and *b* channels can be associated with midget type G and bistratified ganglion channels and that the type R channel does not appear to be necessary for the calculation of these channels is at least surprising.

5. Calculation of colour attributes

Channels *a* and *b* have been selected and configured in previous sections. This section defines channel *A* and the model auxiliary parameters.

First, in order to apply the calculation of CIECAM02 colour attributes, it is necessary to scale the a_{model} values, b_{model} values and A_{model} values based on the a_{CIECAM02}, b_{CIECAM02} and A_{CIECAM02}values. The scale factor is established in the following manner:

$$a'_{modelo} = k_1 \bullet a_{modelo} \qquad \text{(eq. 7.18)}$$

$$b'_{modelo} = k_2 \bullet b_{modelo} \qquad \text{(eq. 7.19)}$$

$$A'_{modelo} = k_3 \bullet A_{modelo} \qquad \text{(eq. 7.20)}$$

Such that k_i $i \in \{1..3\}$, minimises the difference between values *a*, *b* and *A* CIECAM02 and the values *a'*, *b'* and *A'* of the model.

The optimization of the points with Value 5 obtains k_1= 0.95. The following figure show the values $a_{CIECAM02}$ and (0.95 *a_{model}).

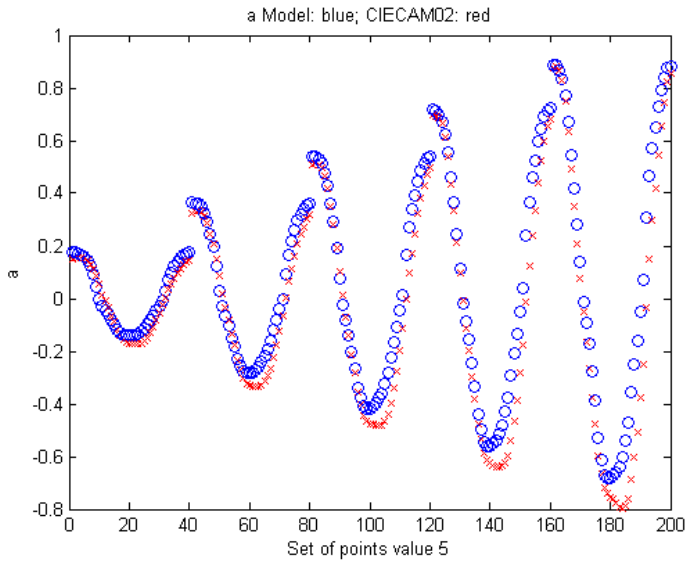

Figure 7.21. Representation of the values $a_{CIECAM02}$ (blue) and (0.95*a_{model}) (red) for all Munsell samples with Value 5.

In a similar manner, for channel *b*: k2= -1.07. Next, the values are represented for $b_{CIECAM02}$ and (-1.07*b_{model}).

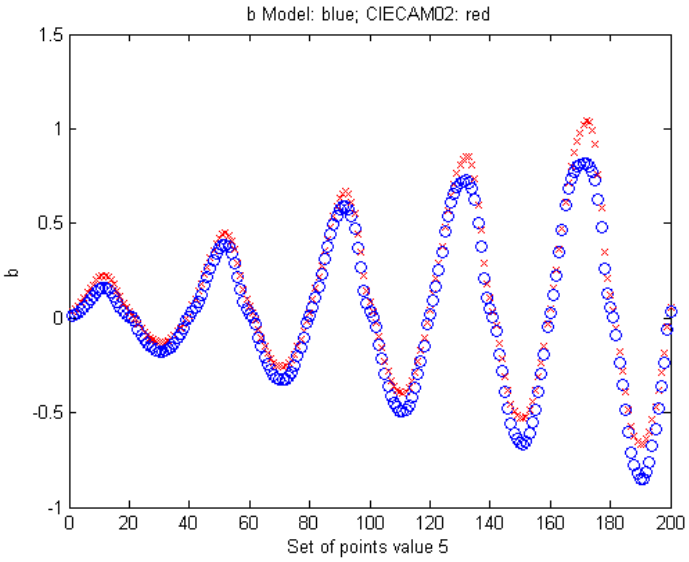

Figure 7.22. Representation of the values $b_{CIECAM02}$ (blue) and (-1.07 *b_{model}) (red) for all Munsell samples with Value 5.

The differences with CIECAM02, in this case, are slightly bigger than in the case of channel *a*.

For the calculation of channel *A*, first, the use of the parasol ganglion channel was considered. However, when trying to adjust the factor of proportionality k_3 (equation 7.20) the results obtained were very distant from $A_{CIECAM02}$. Therefore, the remaining output channels of the retina model were analysed as possible origins of channel *A*. The following figure shows these channels normalised to a maximum value of 1, the aim is to identify that or those channels whose minimums match with those of $A_{CIECAM02}$.

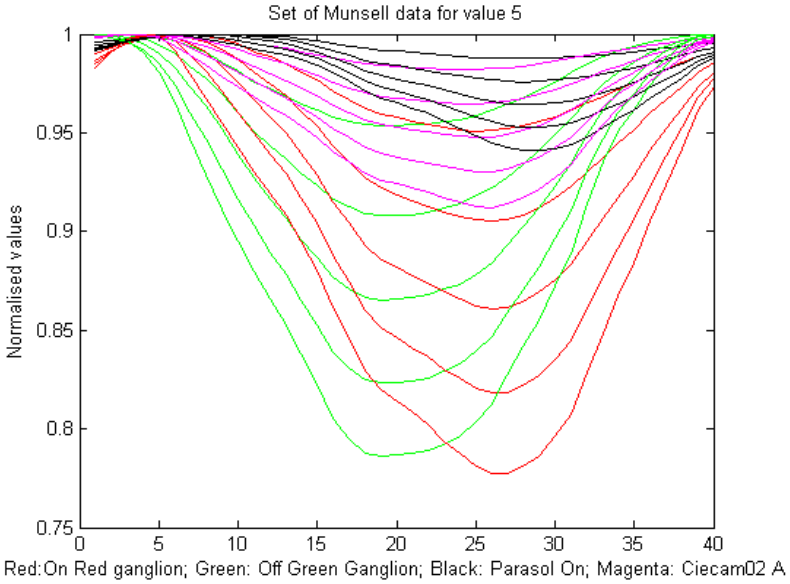

Figure 7.23 Representation of the values of the different channels of the retina model and of $A_{CIECAM02}$ where each curve represents the constant chroma rings with Value=5. Red) Ganglion R On channel. Green) Ganglion G Off channel. Black) Parasol On channel. Magenta) $A_{CIECAM02}$.

This analysis shows that ganglion R On channel is that which has the minimum values in the same points as $A_{CIECAM02}$. In order to adjust the A_{model}, work hypothesis B is applied.

$$A_{model} = A_5 \exp(B_5 \bullet Ganglion\ R\ on\ input) \qquad \text{(eq. 7.21)}$$

The values that minimise the difference with $A_{CIECAM02}$ are A_5=13.05 and B_5=0.35. The following figure shows the representation of the values $A_{CIECAM02}$ and A_{model}.

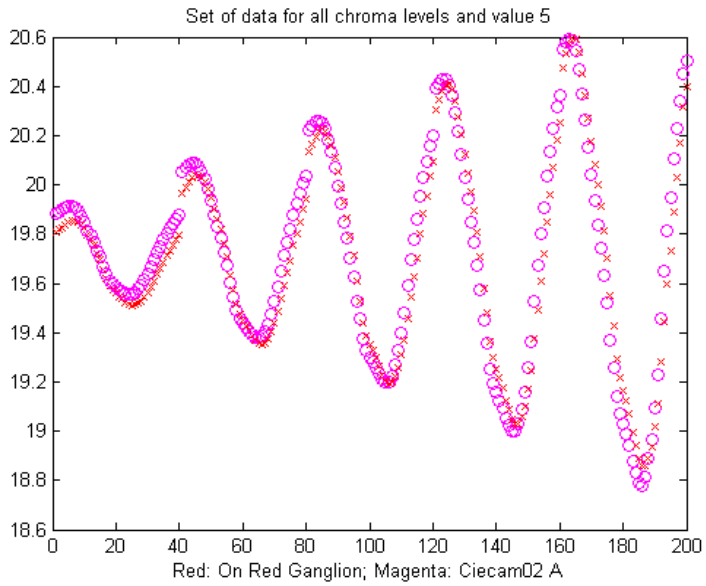

Figure 7.24 Representation of the values $A_{CIECAM02}$ (magenta) and A_{model} (red) for Munsell samples with Value 5.

In order to calculate the colour attributes using CIECAM02, the model needs, besides channels *a*, *b* and *A*, a series of external parameters such as L_A, Y_b, Illuminant and the surround paramenters: F, c and Nc.

CIECAM02 uses in its calculations the parameter t (equation 3.117) that is expressed by means of the internal values {Ra, Ga, Ba} of CIECAM02. A combination of *a*, *b* and *A* is calculated to generate the same sum of {Ra, Ga, Ba}. The combination obtained is:

$$R'a + G'a + (\frac{21}{20})B'a = A - 0.4783a - 4.6957b \qquad \text{(eq. 7.22)}$$

Once the channels, parameters and functional relationships are established, the colour attributes can be calculated according to the calculations of CIECAM02 (see equations 3.106 a 3.121) from chapter III).

The adjustments have been calculated for Value =5. Given the work illuminant, the reference white would be in Value levels higher than the work Value 5. Therefore, the optimisation parameters for Value 5 do not adjust to the value Aw (relative to the reference white) calculated by CIECAM02. This is a constant value for all Munsell samples, thus the Aw value that is going to be used in the following phases is that generated by CIECAM02. The development of a model that works with multiple Value levels is not the object of this thesis, which researches the

structure and viability of a neuroinspired colour processing model. This shall be looked at in future works.

The following shows the results obtained for Munsell samples with Value 5 and for each colour attribute, both those generated by the colour processing model as well as by CIECAM02:

a) Hue: $$\begin{cases} h = \arctan(b/a) \\ H = H_i + \dfrac{100(h-h_1)/e_1}{(h-h_1)/e_1 + (h_2-h)/e_2} \end{cases} \quad \text{(eq. 3.107)}$$

The following figure shows the results obtained for hue, by the model (in blue) and by CIECAM02 (in red) for samples with Value=5 and Chroma= 2, 4, 6, 8 and 10.

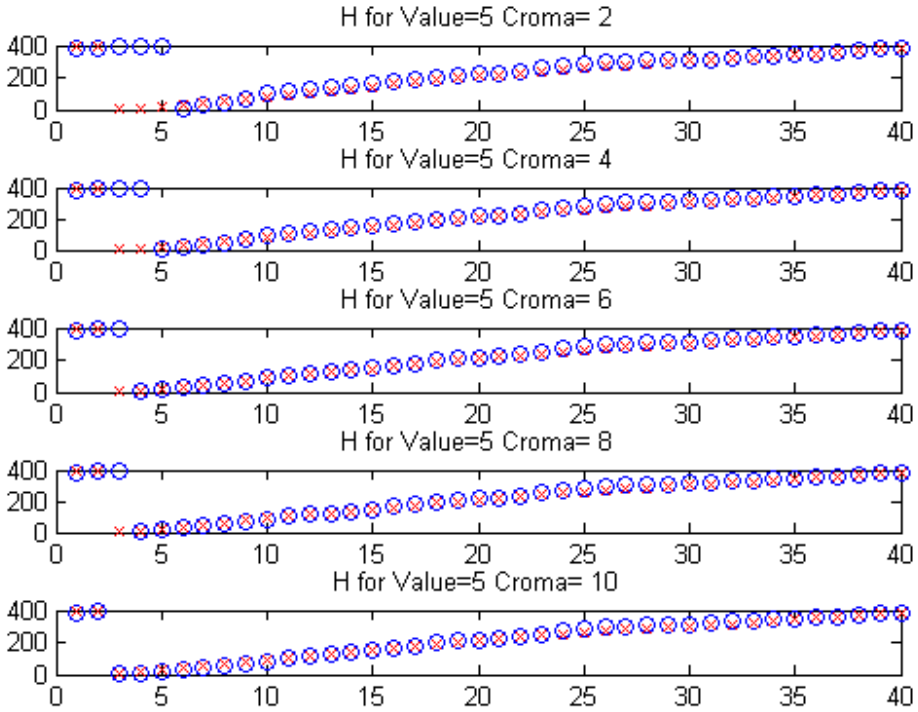

Figure 7.25. Representation of the hue values for Munsell samples with Value 5 and different chroma. Blue) Model. Red) CIECAM02.

The hue values calculated by the model are very near to those generated by CIECAM02. The hue values generated for each set of Munsell data with Value 5 and the same hue (for example the set of values with hue Munsell 5R) have been measured in order to evaluate the results. Munsell's plane of Value 5 has 40 different hues. The following graph shows the average value and

standard deviation obtained by the model and by CIECAM02 for each of the 40 sets of constant hue.

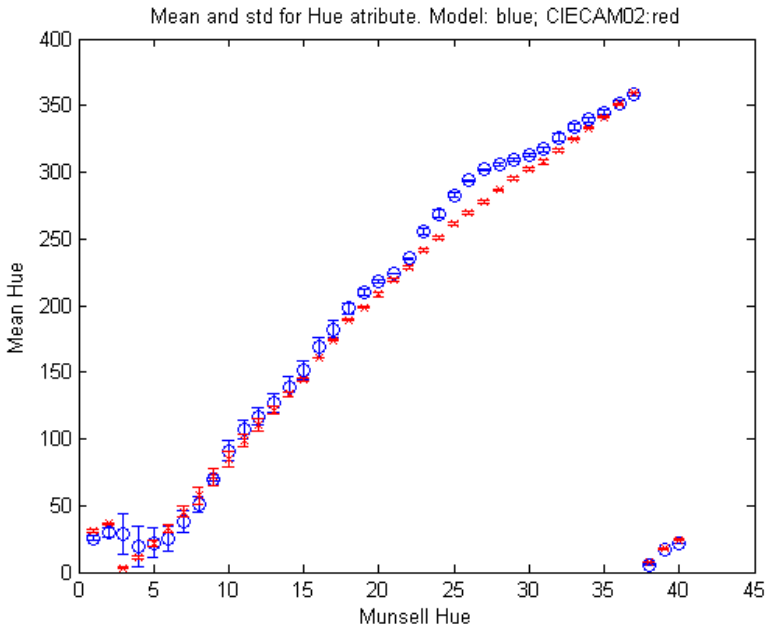

Figure 7.26. Representation of the average hue values and standard deviation of Munsell's constant hue sets with Value 5. Blue) Model. Red) CIECAM02.

The dispersion obtained by CIECAM02 is less than that of the model. However, the constant hue lines appear more proximate to straight lines in the model than in the case of CIECAM02. The following figure shows these lines.

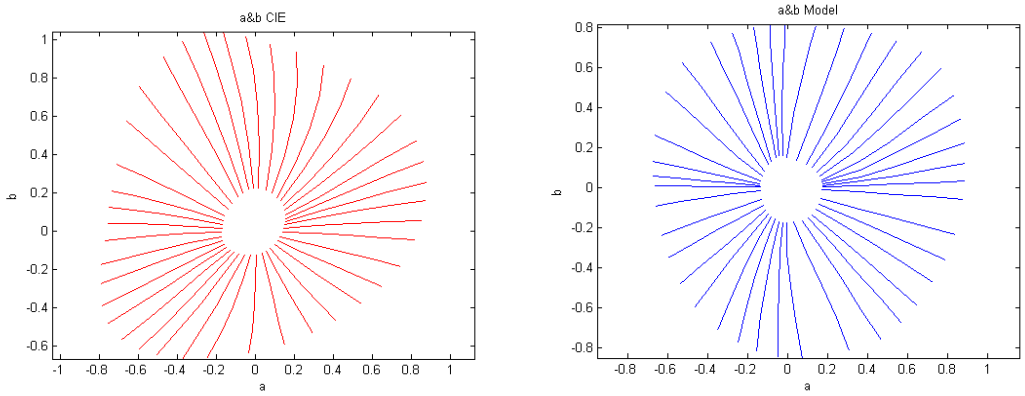

Figure 7.27. Representation of the constant hue lines for Munsell samples with Value 5 in the *ab* plane. Red: CIECAM02. Blue: Model.

Based on these results, the straight line that is closest to each of the constant hue lines has been calculated and the distance of each point in the line to the straight line has been measured. The following graph shows the average distances and the standard deviation obtained for each of the 40 sets of constant hue.

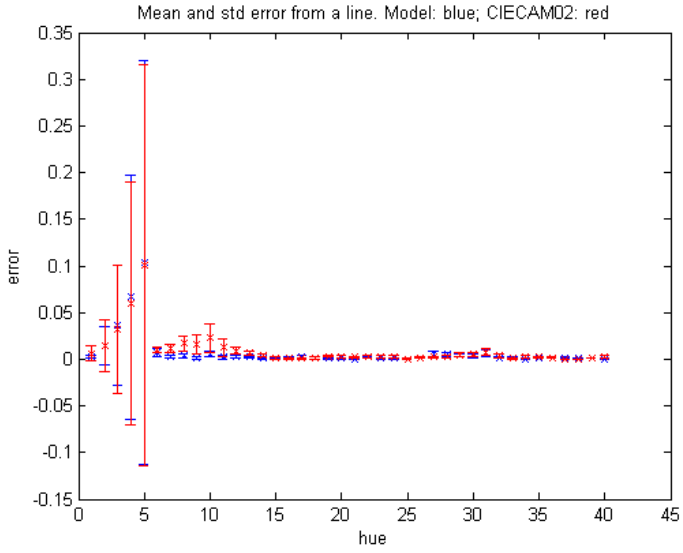

Figure 7.28. Representation of the average distance and standard deviation to the straight lines for constant hue sets of Munsell samples with Value 5 in the *ab* plane. Red: CIECAM02. Blue: Model.

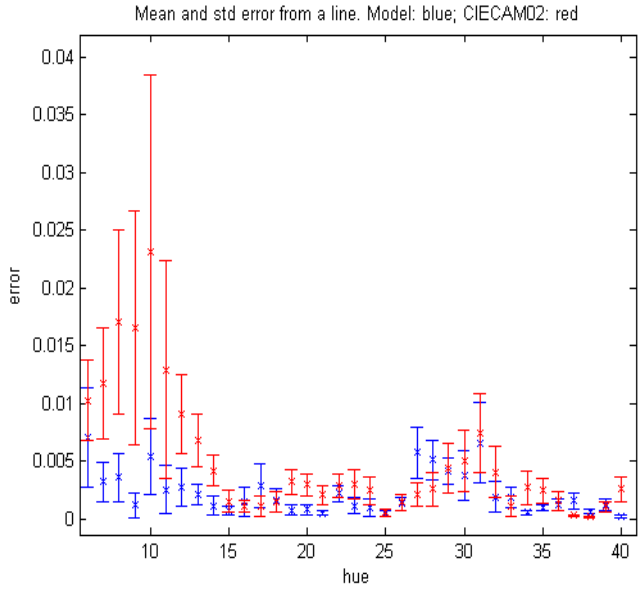

Figure 7.29. Enlargement of figure 7.27 for sets from 5 to 40. Red: CIECAM02. Blue: Model.

This shows how the lines generated by the model are closer to straight lines than those of CIECAM02. The average distance per point is:

- Model= 0.0029;
- CIECAM02= 0.0047;

When evaluating the linearity in this case, the model results are better than those of CIECAM02.

b) Lightness: $J = 100(A/A_w)^{c \cdot z}$ (eq. 3.108)

The following figure shows the results obtained for lightness, by the model (in blue) and by CIECAM02 (in red), for points with Value=5 and Chroma= 2, 4, 6, 8 and 10.

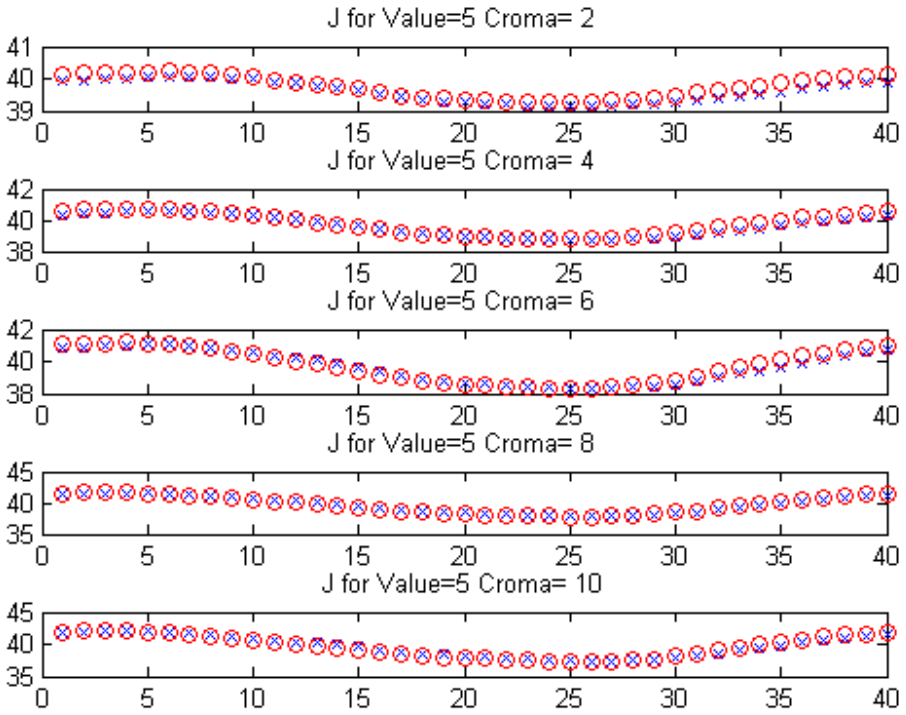

Figure 7.30. Representation of the lightness values for Munsell samples with Value 5 and different chroma. Blue) Model. Red) CIECAM02.

The average values and standard deviation of J generated by the model and by CIECAM02 have been evaluated:

- Model: average J= 39.6498; std=1.0757;
- CIECAM02: average J= 39.7040; std=1.1305;

The values obtained are very similar, being the model's values slightly better.

c) Brightness: $Q = (4/c)(J/100)^{1/2}(A_w + 4)F_L^{1/4}$ (eq. 3.109)

The following figure shows the brightness results obtained by the model (in blue) and by CIECAM02 (in red), for points with Value=5 and Chroma= 2, 4, 6, 8 and 10.

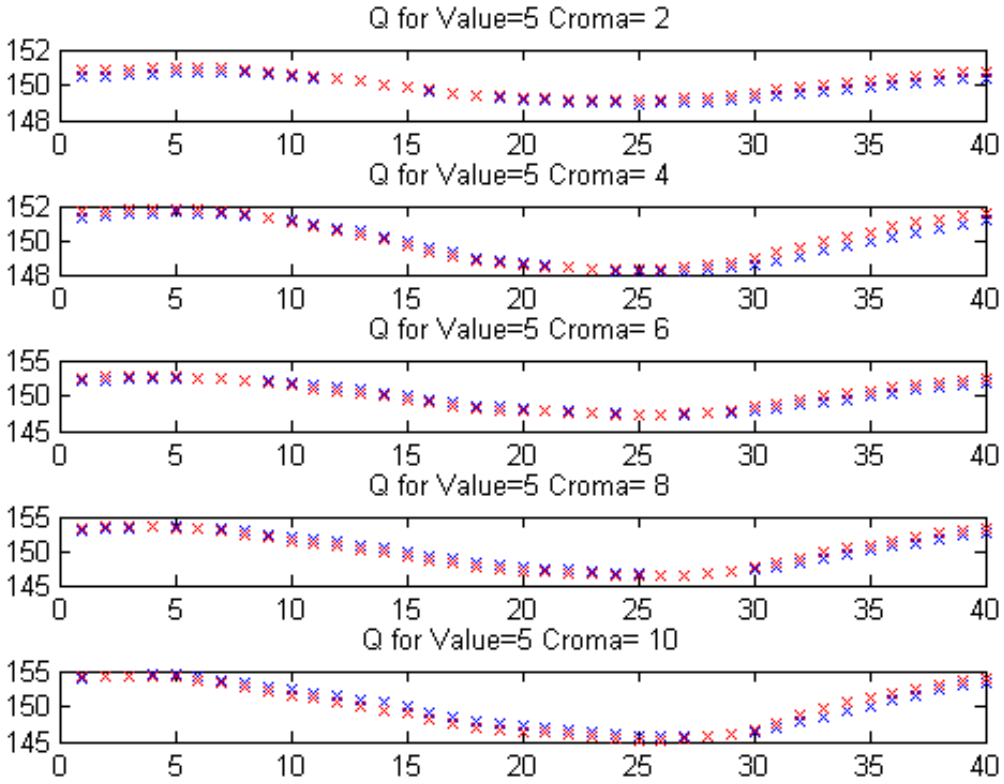

Figure 7.31 Representation of the brightness values for Munsell sample with Value 5 and different chroma. Blue) Model. Red) CIECAM02.

The model's and CIECAM02's average values and the standard deviation of Q have been evaluated:

- Model: average Q= 149.9150; std=2.0330;

- CIECAM02: average Q= 149.9679; std=2.1370;

The values obtained are very similar, being the model's values slightly better.

d) Saturation: $s = 100\sqrt{M/Q}$ (eq. 3.110)

The following figure shows the saturation results obtained by the model (in blue) and by CIECAM02 (in red), for points with Value=5 and Chroma= 2, 4, 6, 8 and 10.

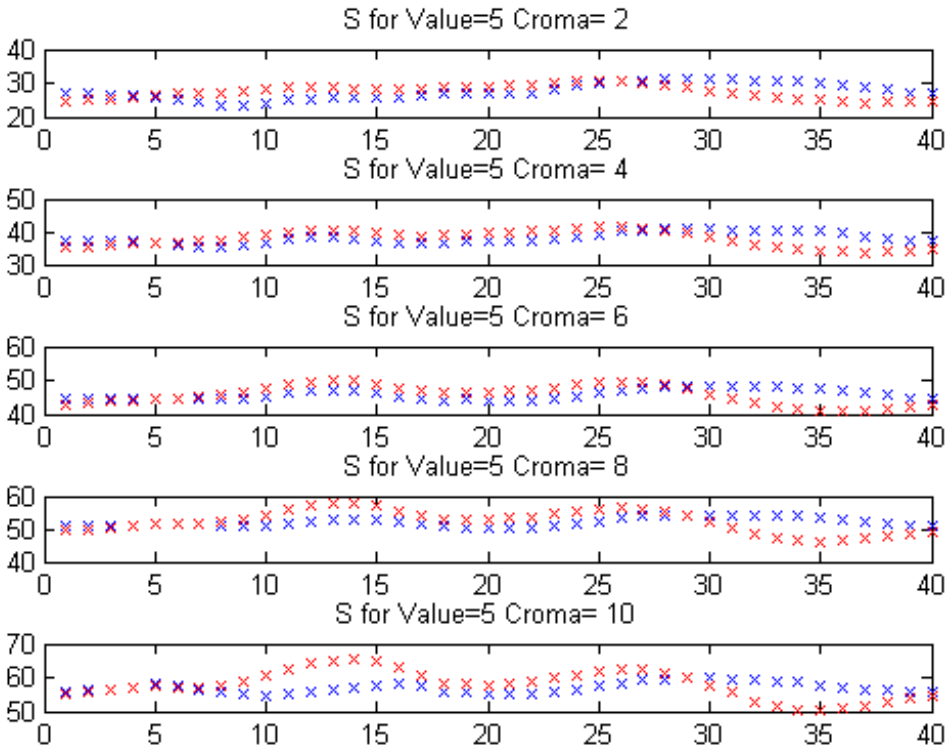

Figure 7.32 Representation of the saturation values for Munsell samples with Value 5 and different chroma. Blue) Model. Red) CIECAM02.

The following figure shows the same data together, where each group of points corresponds to a different level of chroma.

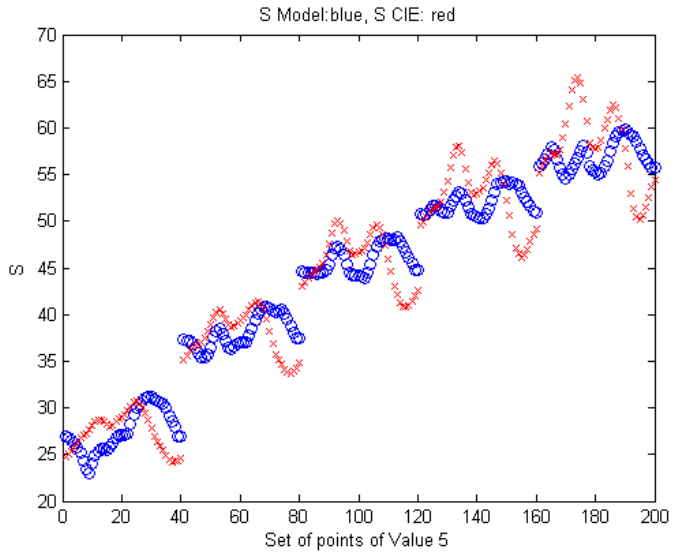

Figure 7.33 Representation of the saturation values for Munsell samples with Value 5. Each cloud of points is associated with a level of Munsell chroma. Blue) Model. Red) CIECAM02.

The values obtained have a certain degree of similarity, although they show differences in some of the points. The aS and bS values have been calculated in order to evaluate this attribute (equation 3.113). The following figure represents the generated values.

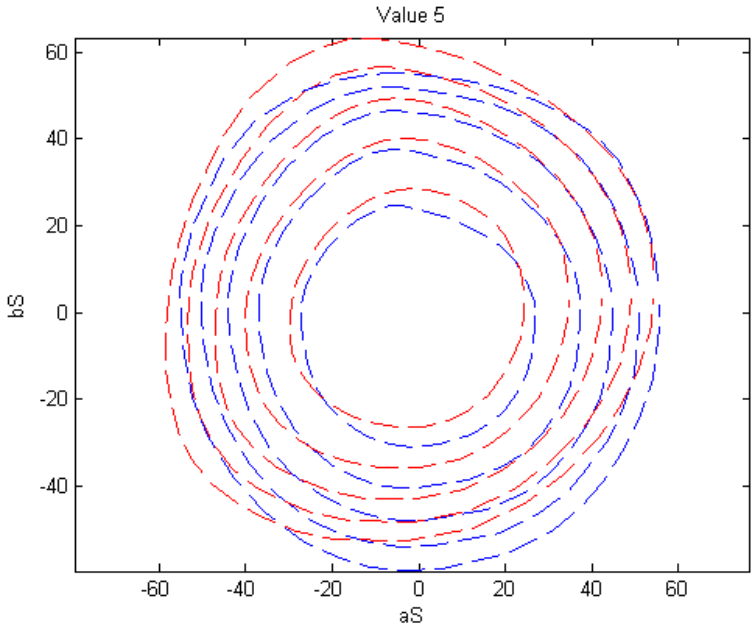

Figure 7.34. Representation of the aS and bS values for the Munsell samples with Value 5, where each ring corresponds to a Munsell chroma level. Blue) Model Red) CIECAM02.

The level of circularity of the results has been evaluated using these data:

- Model=0.023;
- CIECAM02=0.045;

The model results have a circularity level that is greater than those of CIECAM02.

e) Chroma: $C = t^{0.9} (J/100)^{1/2} (1.64 - 0.29^{n})^{0.73}$ (eq. 3.111)

The following figure shows the chroma results obtained by the model (in blue) and by CIECAM02 (in red), for points with Value=5 and Chroma= 2, 4, 6, 8 and 10.

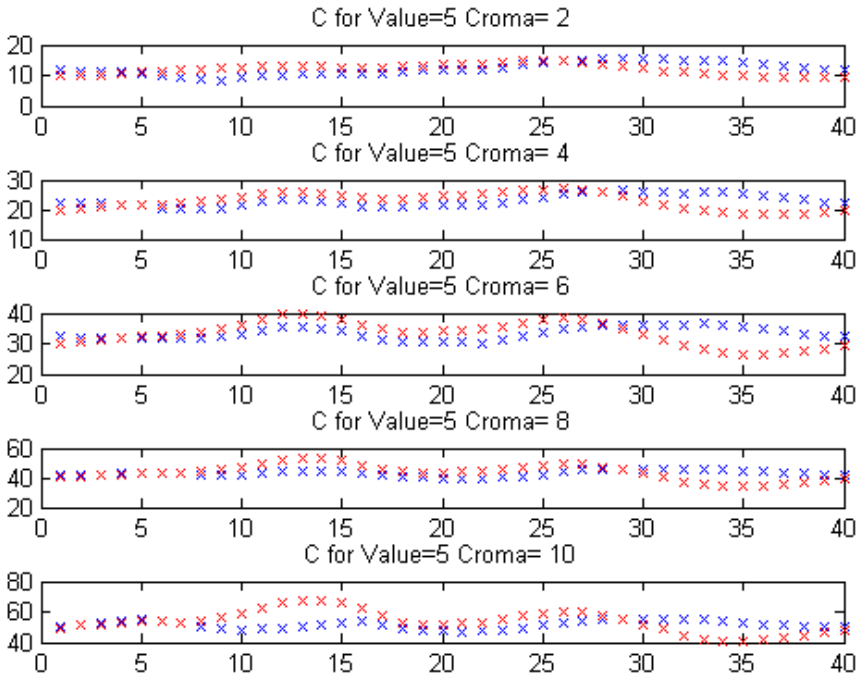

Figure 7.35. Representation of the chroma values for Munsell samples with Value 5 and different chroma. Blue) Model. Red) CIECAM02.

The dispersion of the results with respect to the Munsell chroma values is going to be evaluated. The following figure is obtained by representing the values for each level of Munsell chroma.

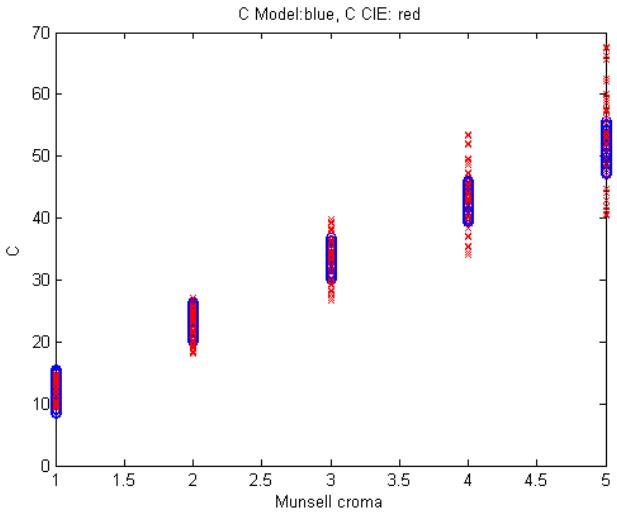

Figure 7.36. Representation of the chroma values for Munsell samples with Value 5 with respect to the associated Munsell chroma values. Blue) Model. Red) CIECAM02.

The values generated by the model, as shown, for most of the levels of Munsell chroma are more grouped in the model than in the case of CIECAM02. A calculation of the average value and standard deviation has been made in order to evaluate the grouping level. The following figure shows these results.

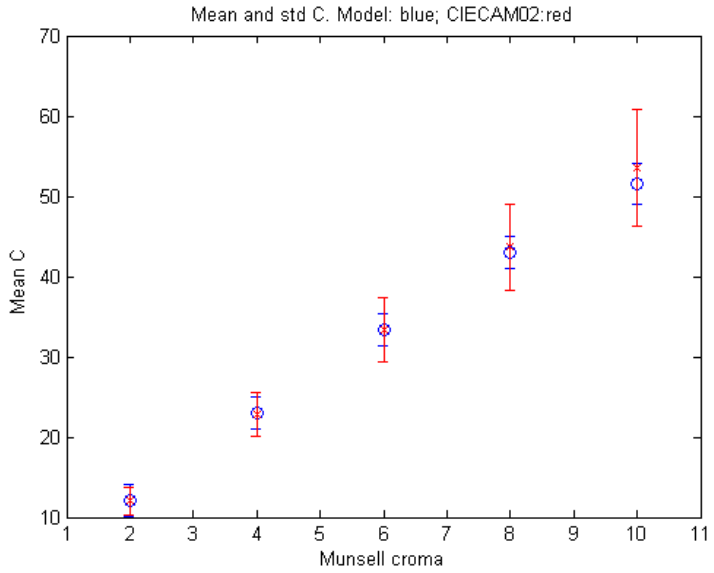

Figure 7.37 Representation of the average value and standard deviation of C for the set of points associated with the different levels of Munsell chroma and Value=5. Blue) Model. Red) CIECAM02.

The results obtained by the model, as shown, are better than those generated by CIECAM02.

f) Colourfulness: $M = C \cdot F_L^{1/4}$ (eq. 3.112)

The following figure shows the colourfulness results obtained by the model (in blue) and by CIECAM02 (in red) for points with Value=5 and Chroma= 2, 4, 6, 8 and 10.

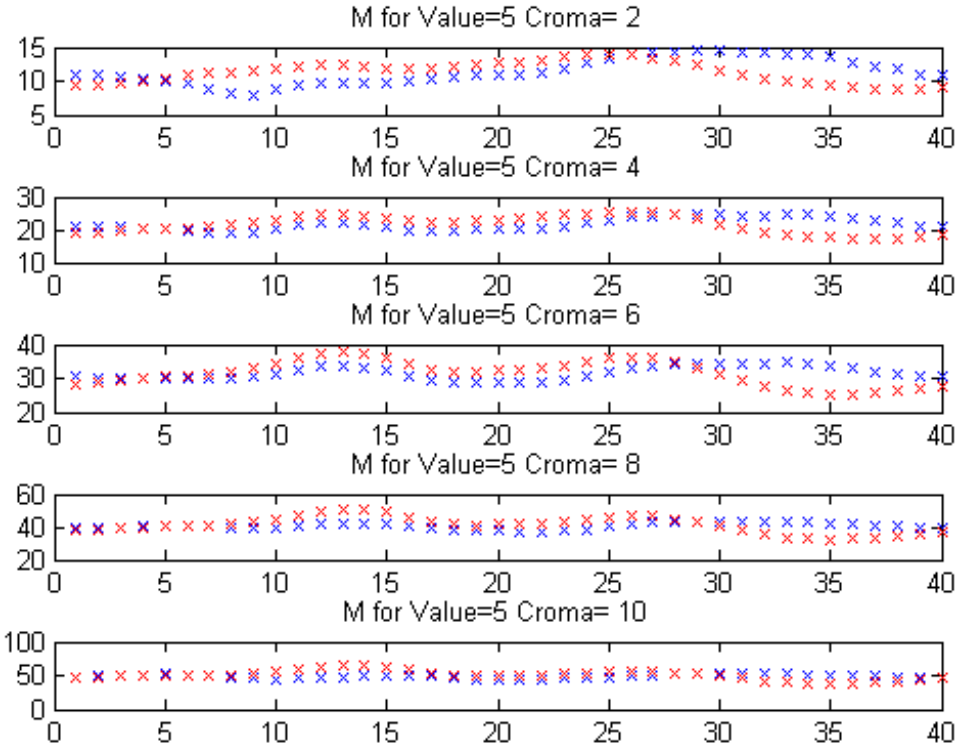

Figure 7.38 Representation of the colourfulness values for the Munsell samples with Value 5 and different chroma. Blue) Model. Red) CIECAM02.

The following figure shows these data together, where each group of points corresponds to a different chroma level.

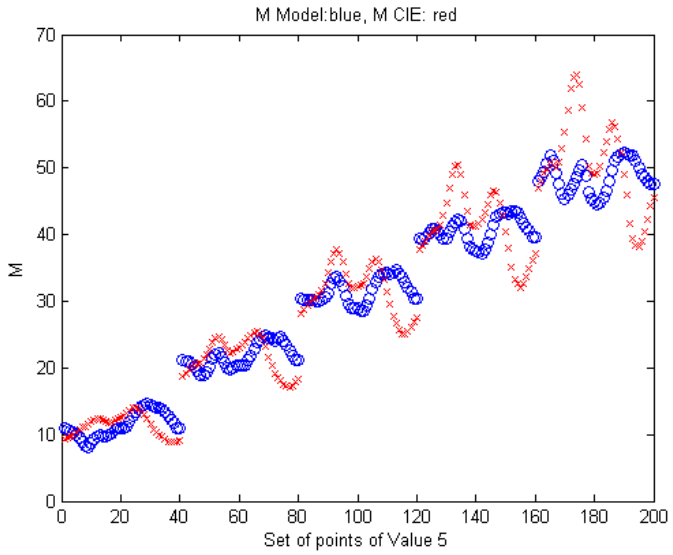

Figure 7.39 Representation of the colourfulness values for all Munsell samples with Value 5. Each cloud of points is associated to a Munsell chroma level. Blue) Model. Rojo) CIECAM02

As has happened with saturation levels, the values that have been obtained for colourfulness have a certain degree of similarity. Values aM and bM are going to be evaluated (equation 3.113). The following figure shows the generated values.

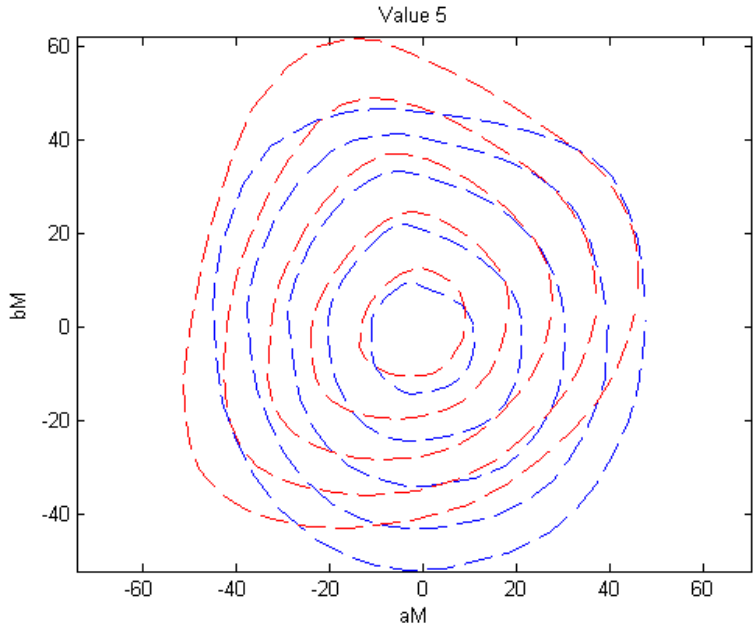

Figure 7.40. Representation of the aM and bM values for Munsell samplea with Value 5 where each ring corresponds to a Munsell chroma level. Blue) Model. Red) CIECAM02.

The level of circularity of the results has been evaluated using this data:

- Model=0.0086;
- CIECAM02=0.016;

The model results have a circularity level that is greater than those of CIECAM02.

5.1 Conclusions

This section has presented the calculations of colour attributes and the results obtained by the colour processing model. Below is a summary of the model results when compared with those generated by CIECAM02 (🡅 better results than CIECAM02, 🡇 worse results than CIECAM02):

- Hue: values are very close to those generated by CIECAM02.
  - 🡇 Greater dispersion in hue for samples with constant Munsell hue.
  - 🡅 Constant hue lines closer to straight lines.
- Lightness practically equal values to those generated by CIECAM02.
  - 🡅 Less dispersion in generated values.
- Brightness: practically equal values to those generated by CIECAM02.
  - 🡅 Less dispersion in generated values.
- Saturation: values in the same levels as those generated by CIECAM02.
  - 🡅 Greater circularity in generated values.
- Chroma: similar values to those generated by CIECAM02.
  - 🡅Less dispersion in chroma levels for constant chroma Munsell samples.
- Colourfulness: values in the same levels as those generated by CIECAM02.
  - 🡅 Greater circularity of generated values.

The obtained results have been very satisfactory, as they are not only equiparable to those obtained by the CIECAM02 model, but in many occasions they are better.

6. Real images

Two images have been selected as examples in order to show the image processing capacity of the colour processing model. The first is composed of a set of colour stripes. This is a simple manner to link each colour with the generated attributes.

Figure 7.41. Image C, example of the application of the colour processing model.

The following figure shows the colour attributes generated by the colour processing model for each point in example image C.

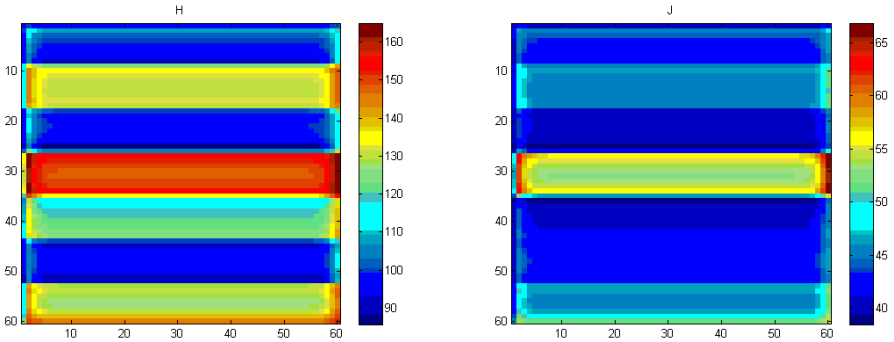

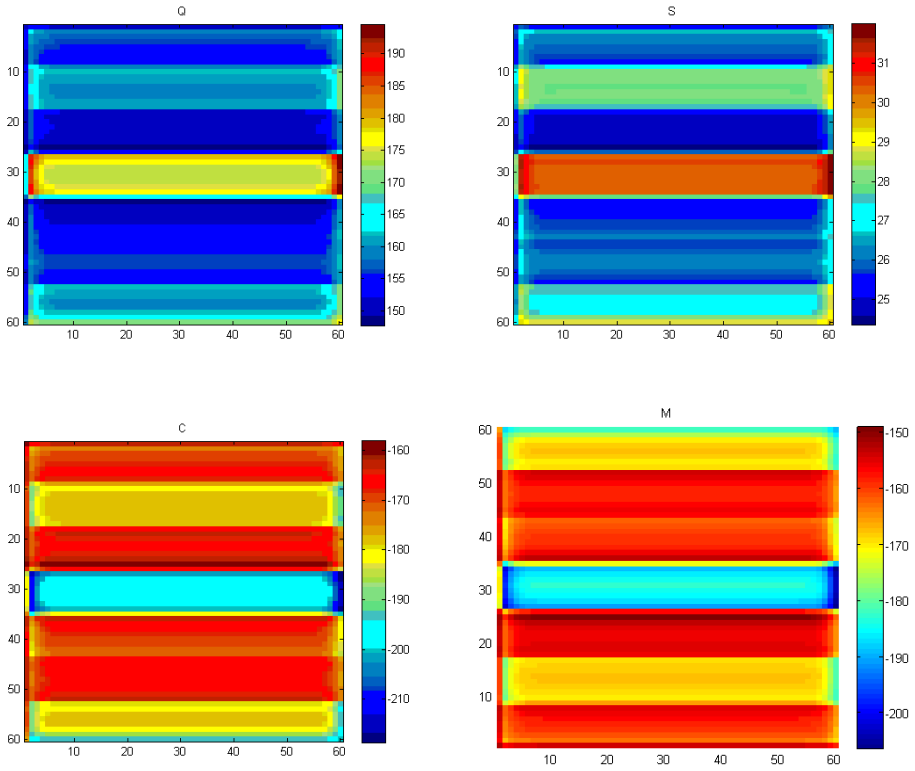

Figure 7.42. Images of the colour attribute values for each point in image C. Each image has its value scale on its right. H: hue. J: lightness. Q: brightness. S: saturation. C: chroma. M: colourfulness.

As can be observed, each colour is classified in a different manner by the system, through a combination of its colour attributes. The central areas of the bands are homogeneous for each colour attribute, showing border detection processes in the transition borders between bands. These homogeneity and border detection characteristics that are part of the model shall be particularly useful when applied to image segmentation and to the detection and classification of objects.

A comment must be made on how the colour processing model has defined a background level. It is supposed to be a constant grey level but the colours in this image does not comply with it as the colours are surrounded by other different colours. The background value is foreseen to be integrated to the calculation in a dynamic manner in future model versions.

The second example image has been selected to show the complete processing chain that is done by the system also including the results of colour attributes and the images generated by each type

of cell of the functional retina model. This image has been selected as it combines colour presence with varied shapes.

Figure 7.43. Image D, example of the application of the colour processing model.

The following shows the images generated in each cell layer of the retina model:

1. Photoreceptor layer: the generated image is proportional to the LMS planes of the original image, slightly modulated by the process of the integration of the receptive field of each photoreceptor.

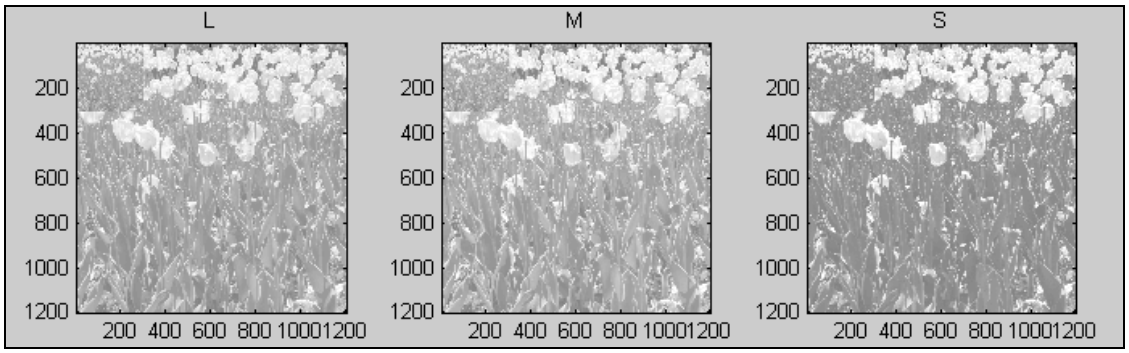

Figure 7.44 Image generated by photoreceptors when presented image D.

2. Horizontal cell layer: the image is slightly blurry as the integration fields of horizontal cells are bigger than those of photoreceptors.

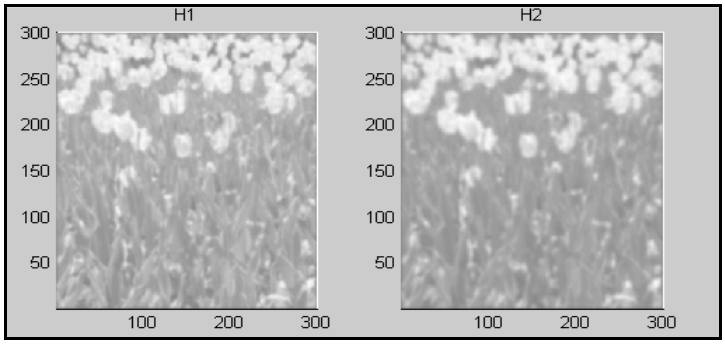

Figure 7.45. Image generated by horizontal cells when presented image D.

3. Bipolar cell layer: one notices how the flowers are above the threshold value and therefore appear highlighted in the type On cells while the stems and leaves are below the threshold and therefore are highlighted by the type Off cells. The objects in the edges show edge detection processes.

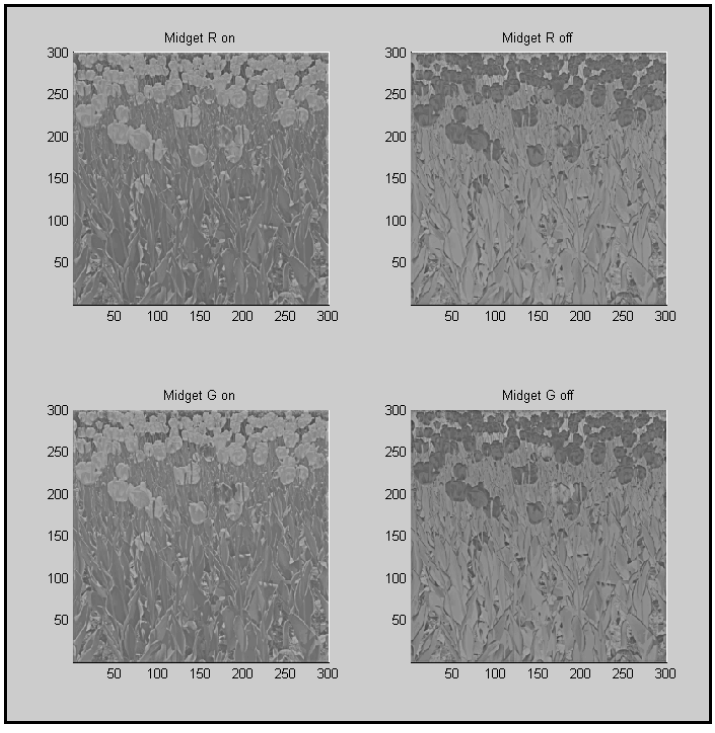

Figure 7.46. Image generated by midget bipolar cells when presented image D.

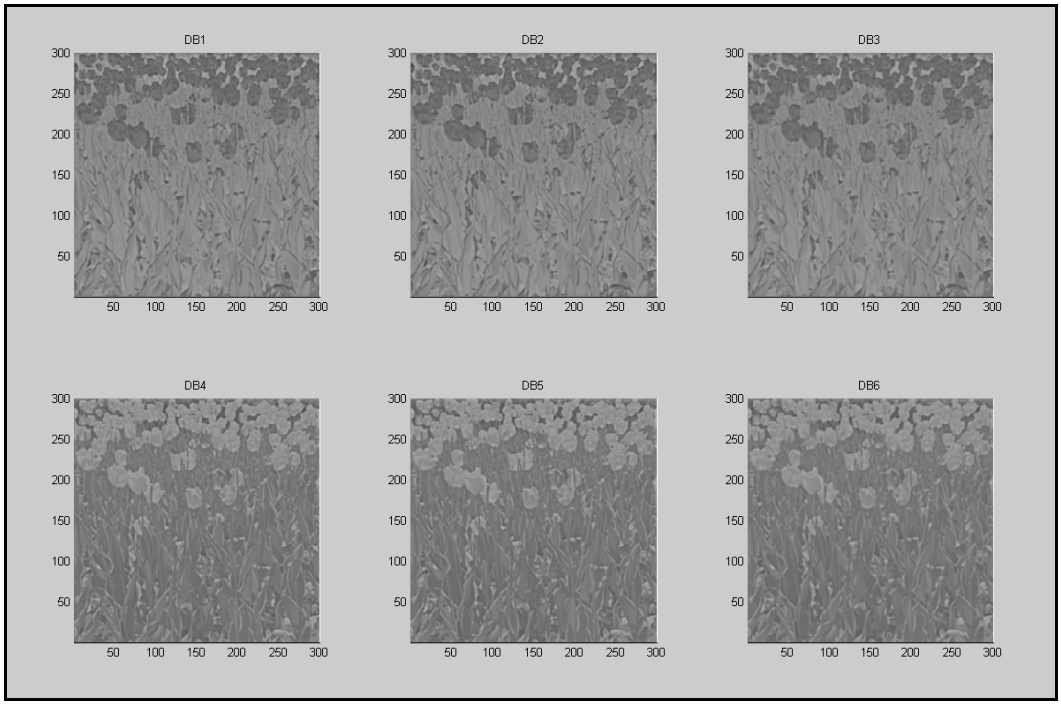

Figure 7.47. Image generated by diffuse bipolar cells when presented image D.

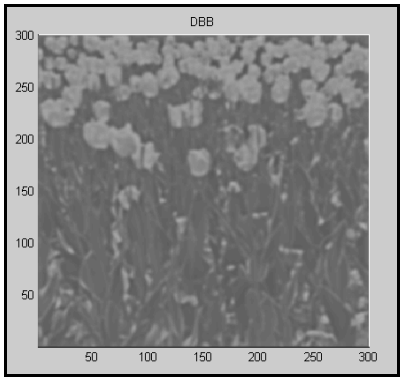

Figure 7.48. Image generated by blue bipolar cells when presented image D.

4. Ganglion cell layer: as happens with bipolars, flowers are highlighted by type On cells while the stems and leaves are highlighted by type Off. The edge detection processes appear more clearly in these types of images of spikes. The differences between chromatic type R and G cells and bistratified cells are confirmed, due to the differences in the original colours of the image. Thorny type cells are of great size and perform integration processes on wide areas of the image.

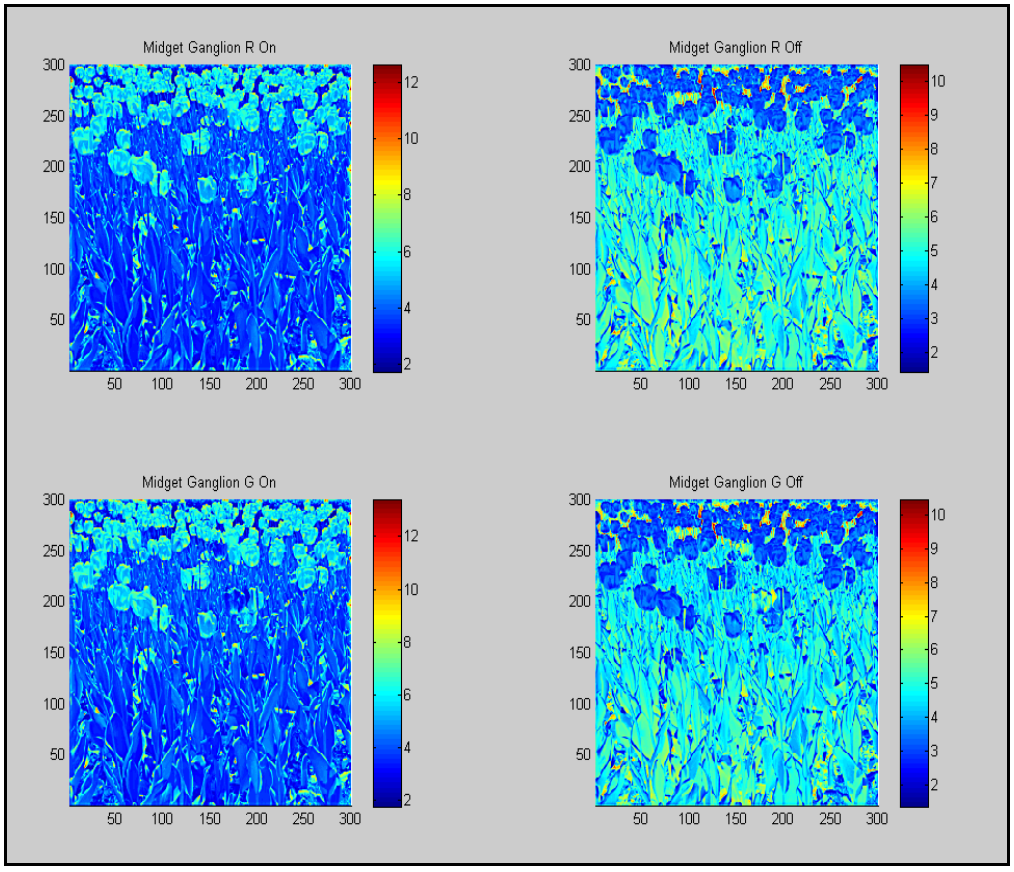

Figure 7.49. Image generated by midget ganglion cells when presented image D.

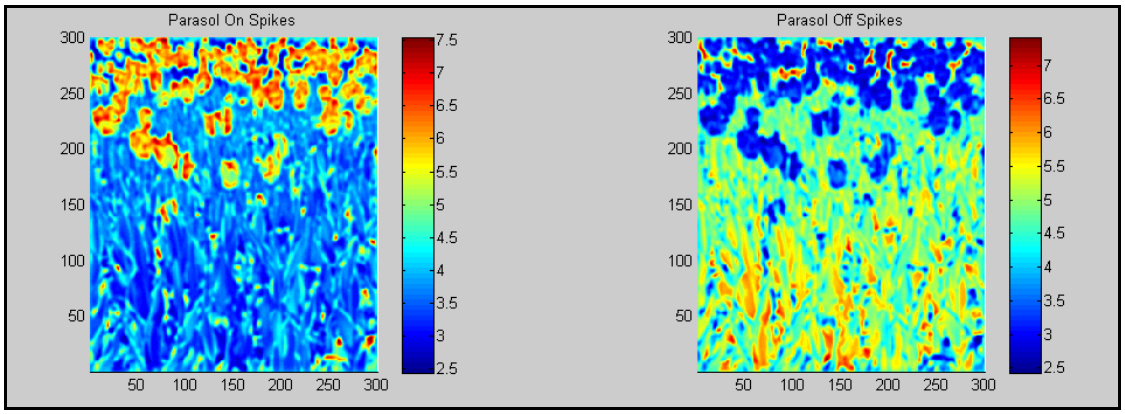

Figure 7.50. Image generated by parasol ganglion cells when presented image D.

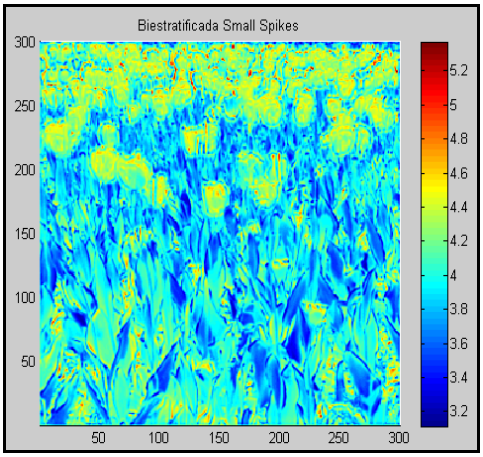

Figure 7.51. Image generated by the small bistratified ganglion cells when presented image D.

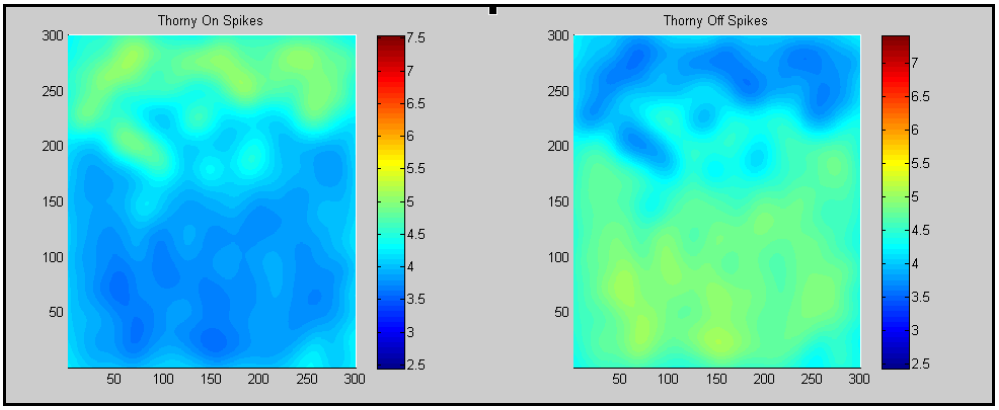

Fig. 7.52. Image generated by thorny ganglion cells when presented image D.

Colour attributes

The colour attributes of the image points have been calculated using the output channels generated by the retina model.

1. Hue: the image shows how white flowers are classified in similar hue levels, red flowers in another hue level and lastly, stems and the dark background areas in another two different levels. The edge areas have different hues than the objects that they belong to.

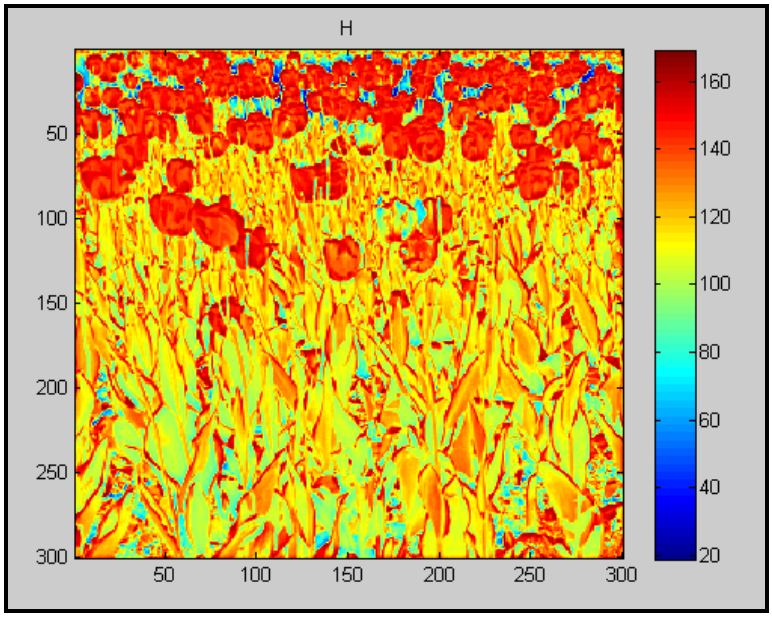

Figure 7.53. Image of hue levels produced by the colour processing model when presented image D.

2. Lightness: as happened in the previous case, the 4 types of objects present in the image (white and red flowers, stems and background) are identified. This image especially highlights the flower edges.

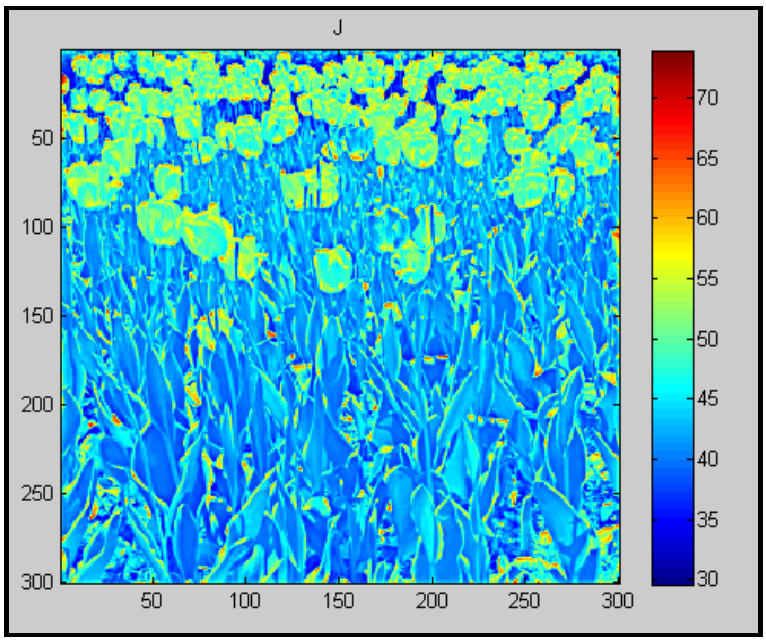

Figure 7.54. Image of lightness levels produced by the colour processing model when presented image D.

3. Brightness: the brightness of the scene is quite homogeneous and the edges of the flowers and the background are highlighted.

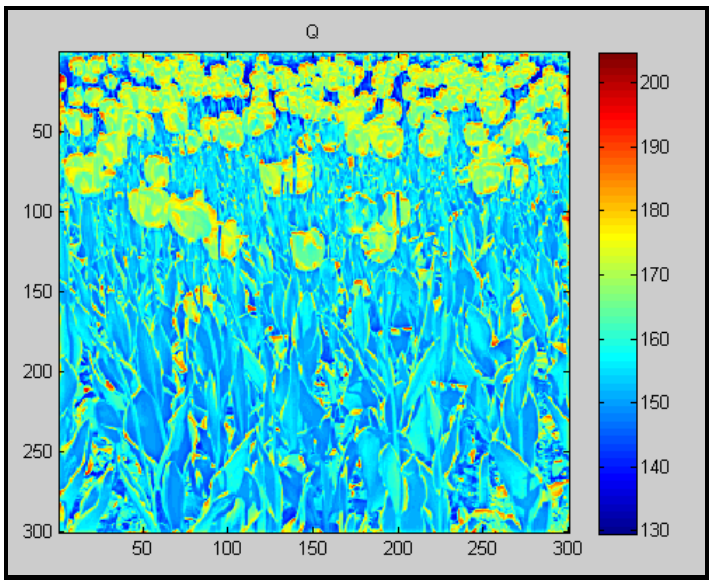

Figure 7.55. Image of brightness levels produced by the colour processing model when presented image D.

4. Saturation: the saturation plane differentiates 3 main categories, compared with the 4 originals. In this case, red flowers and stems have similar saturation levels as their original colours are two categories of solid colours.

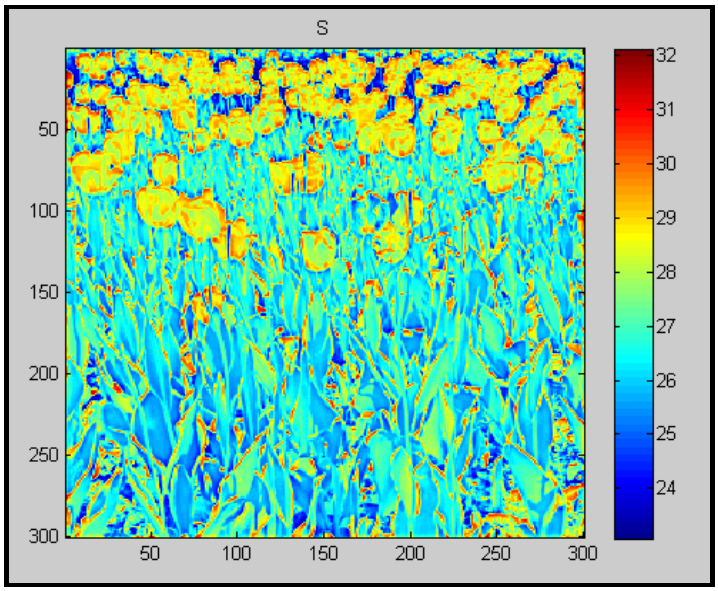

Figure 7.56. Image of saturation levels produced by the colour processing model when presented image D.

5. Chroma: in the chroma plane, all the 4 original objects are distinguishable and can be even identified two subptypes within the stems, those of a darker green and those of a lighter green.

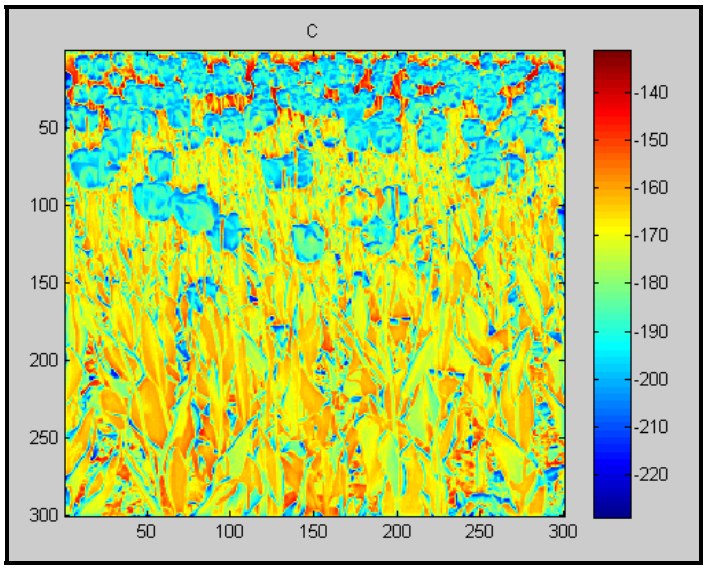

Figure 7.57. Image of chroma levels produced by the colour processing model when presented image D.

6. Colourfulness: the comments on the chroma plane are applicable to the colourfulness plane.

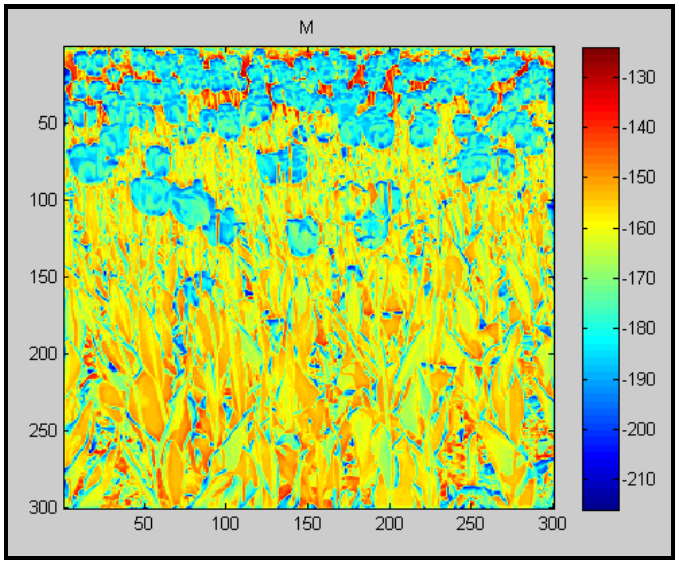

Figure 7.58. Image of colourfulness levels produced by the colour processing model when presented image D.

In order to show the complete model, the following figure shows a third example of the processing chain performed by the model where the images generated in each stage are shown.

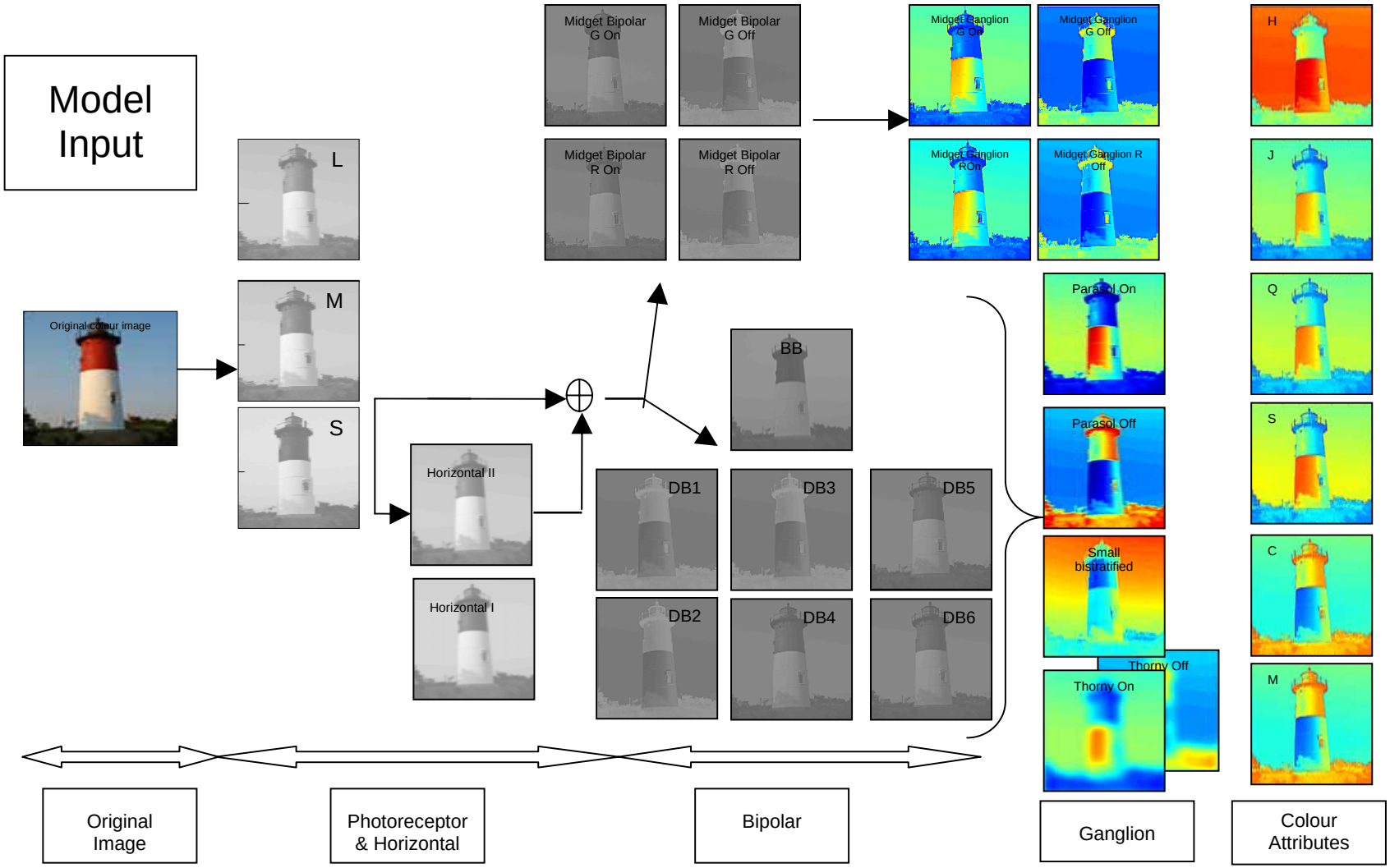

Figure 7.59. Examples of images generated by each cell layer and colour attributes on the expanded diagram of the retina model.

The selected examples show:

- The applicability of the model to real images.
- The stability in hue characterisation.
- The capacity of the system to calculate all 6 colour attributes (hue, lightness, brightness, saturation, chroma and colourfulness).
- The border detection processes.

This set of characteristics positions the system as a tool for great use in processes of:

- Image segmentation, as it provides information on the edges that are present in an image. It obtains the edges that are present not only in achromatic channels (as those that are habitually applied) but also in chromatic channels. On the other hand, as it can characterise each colour area with 6 attributes, it provides greater reliability than RGB, HSI...
- Object detection, as it can group pixel that potentially belong to the same object, using the information of the edges and colour characteristics.
- Characterisation of the elements present in an image, through its surface colours and morphological characteristics. The latter can be calculated based on the detected edges and similar colour areas.
- Object identification: as it has some colour attributes that are more stable than habitual ones and therefore can be used in identification process in images in different contexts.

The use of the model in these applications shall be looked at in future research works.

7. Conclusions

A new model for colour processing with a bioinspired nucleus based on the functional retina model has been presented throughout this chapter. This model permits the calculation of colour attributes.

The architecture structure of colour appearance models has been used and has been coordinated with the functional model of the retina (figure 7.2).

Work hypotheses have been set for the transformation of the output channels of the retina model in channels *a*, *b* and *A* of colour appearance models. These hypotheses have been configured and tested with Munsell colour sample data. The aim has been to optimise the circularity level of constant chroma rings of Munsell samples. The obtained results indicate:

- **Channel *a*** corresponds with the **midget ganglion type G channel.**
- **Channel *b*** corresponds with the **small bistratified ganglion channel.**
- **Channel *A*** corresponds with the **midget ganglion type R channel**.
- Type On and Off channels have different spike generation functions (equation 6.11).
- Two subchannels need to be defined from the bistratified ganglion channel. The existence of a type Off subchannel is not biologically proven, although it could also be a sole cell type with different behaviours above and below the average threshold.
- The spike generation functions in *a* and *b* cases vary slightly depending on the level of the Munsell Value.
- The spike generation function in channel *A* widely varies based on the level of the Munsell Value.

Under these circumstances, channels *a* and *b* show a very high circularity level and constant hue lines that are nearly straight lines for the Munsell colour samples.

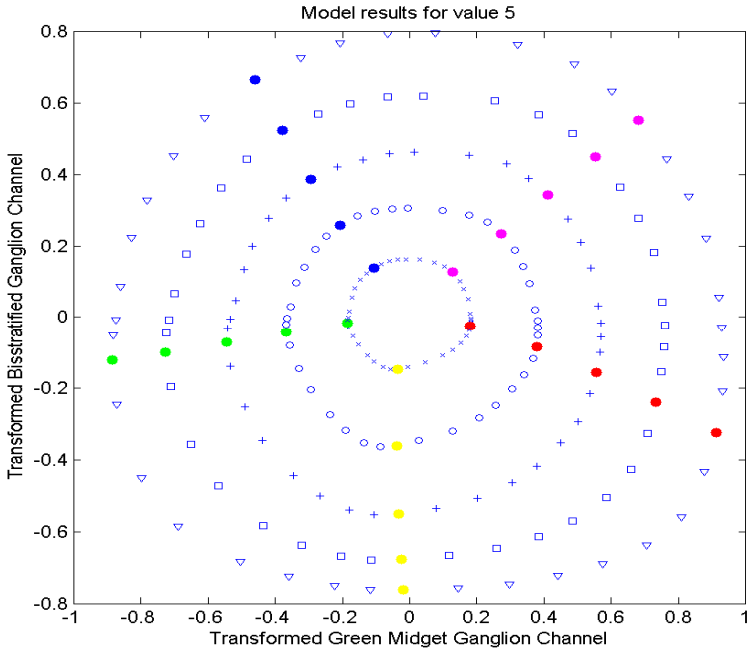

Figure 7.60 Example of Munsell data with Value 5 in the *ab* plane of the colour processing model.

The calculations performed by CIECAM02 to generate colour attribute values have been applied to the *a*, *b* and *A* channels defined for the colour processing model. The results have been evaluated with Munsell samples. The response of the colour processing model has been very positive, generating, **not only results close to those produced by CIECAM02 but in several cases, producing better results.:**[18]

≈ Hue: values very similar to those generated by CIECAM02, greater dispersion in the hue with regard to Munsell hues, but greater linearity in the constant hue lines.

≈ Lightness: practically equal values to those generated by CIECAM02.

≈ Brightness: practically equal values to those generated by CIECAM02.

↑ Saturation: greater level of circularity of the generated values.

↑ Chroma: less dispersion in chroma levels for constant chroma Munsell samples.

[18] ≈ resultados similares a los de CIECAM02, ↑ resultados superiores a los producidos por CIECAM02, ↓ resultados inferiores a los producidos por CIECAM02.

↑Colourfulness: greater level of circularity of the generated values.

Furthermore, it is important to bear in mind that the equations for the calculation of colour attributes are the optimised functions for the CIECAM02 structure (see MORO_02 for databases used). Future works shall look at the adjustment of the calculation functions for colour attributes based on the *a*, *b* and *A* results generated by the model (in a and b cases, the obtained level of circularity is better than that of CIECAM02). This additional development has not been the aim of this work as the main objective has been to define a general model that can encompass the entire chain of colour calculation.

Finally, it is necessary to mention that the channel that was deemed a priori as the source for the *A* channel was the achromatic parasol type ganglion cell channel. However, the midget ganglion type R channel has been that which better adjusts to the $A_{CIECAM02}$ values. On the other hand, another fact that a priori would not have been contemplated is that *a* and *b* channels only need the midget ganglion type G and bistratified ganglion channels, respectively, as sources. It is important to remember that these channels have all three type of photoreceptor components (equations 7.9 to 7.12). Future works shall analyse this characteristic jointly with the direct optimisation of the calculations functions of colour attributes as well as the possible implications regarding colour perception theory.

At the conclusion of this chapter, it is important to emphasize **the capacity of the model developed in this thesis to work with real images**. This opens up a great applicability potential to the model as for example for image segmentation, characterisation or object identification.

Chapter VIII

Conclusions, contributions and future works

The structure and components of a novel colour processing model have been introduced throughout the different chapters of this work. The core of this model is a new functional model of the retina.

Each component has been individually studied, analysed and tested in each of the sections of the thesis. This has provided the final work with the necessary consistency to compare the results of the developed model against consolidated results provided in scientific publications.

This last chapter is going to provide a global vision by stating the conclusions that have been reached throughout this work.

The contributions provided by this research have been set out throughout the work, from the research methodology to the studies and developments reached in each of its stages. This chapter is going to compile the most relevant as a summary.

Finally, the work undertaken in this thesis entails the beginning of new research ways in colour image processing. Some of these have been identified in the development of the work as complementary elements to the research done in this thesis. They will be included in the section of future works.

1. Conclusions

This work has two main conclusions. **The first conclusion is that a retina model can be designed and built with an architecture and set of cell types** with great depth. This permits to characterise the output pathways of the retina, both its spatial as well as its chromatic behaviour. The model has been validated both through an in-depth study as well as through an evaluation of the behaviour of its cell types. The results obtained by the model agree with real neuron measurements and, additionally, the model is consistent with the general characteristics that are currently accepted for the retina: type cells and features, properties of the multiple pathways of information, V(λ)…

The second conclusion has been **that the definition and development of a colour processing model with a bioinspired nucleus (functional model of the retina) results in a colour appearance model with very satisfactory results**: the constant chroma rings of the Munsell samples bear a high circularity level (higher than that obtained by CIECAM02) and the

calculation of colour attributes on Munsell samples provides similar results to those obtained by CIECAM02 and even better.

These two conclusions open the possibilities to new ways to analyse the visual system: on the one hand by placing the attention on the importance of the retina and the processing that takes place inside it, and on the other hand, by providing new ways for colour processing and the channels related with it (versus evaluation techniques of the individual colour point or simplified techniques of centre/surround opponency: red vs. green or blue vs. yellow.)

Besides these two general conclusions, other conclusions have been reached throughout this work that are presented in the following.

A retina model based on biological data can **be established and developed, as shown in Chapter VI.** This conclusion is completed by the following:

- It has been confirmed that an **organised structure of the retina** allows building a model **which permits including different types of cells** with their specific characteristics. The working context has been defined. The hypothesis and assumed simplifications have been listed as in any model.
- The detailed design has allowed the **characterisation of the spatial and chromatic properties of the model's different cell types. The features of the cells have been detailed by the analysis of the responses to a set of stimuli (achromatic: spot, ring and grid; and chromatic: visible spectrum and opponency)**:
  - Photoreceptors: cells with a homogeneous receptive field (without opponency) and chromatic nature.
  - Horizontal cells: cells with a homogeneous receptive field (without opponency) and partial achromatic nature.
  - Midget bipolar cells: cells with opponency centre vs. periphery of chromatic nature.
  - Diffuse bipolar cells: cells with opponency centre vs. periphery of achromatic nature.
  - Blue bipolar cells: cells with opponency centre vs. periphery of chromatic nature.
  - Midget ganglion cells: cells with spatial opponency of chromatic nature: centre vs. periphery.
  - Parasol ganglion cells: cells with spatial opponency of achromatic nature: centre vs. periphery.

  - Small bistratified ganglion cells: cells with spatial opponency of a chromatic nature: centre vs. periphery.
  - Big ganglion cells: cells with opponency centre vs. periphery of achromatic nature.

- **Multiple output pathways** belonging to different subtypes of ganglion cells have been established:
  - Midget ganglions cells.
  - Parasol ganglion cells.
  - Small bistratified ganglion cells.
  - Large bistratified ganglion cells.
  - Big ganglion cells.
- The need for a phase of ganglion cells as a conversion stage of analogic signals (potential variations) to digital signals (nervous spikes), in order to transmit through the optic nerve has been established.
- The presence of output pathways of chromatic and achromatic nature as well as spatial opponency processes centre/surround have been established.
- Additionally, the existence of two pathways, an On and an Off type, has been established. These dual channels are necessary to codify information through nervous spikes that only allow positive data codification.
- It has been shown how information generated by type L and M photoreceptors is processed in different ways to that of type S photoreceptors.
- There has been a verification of how the retina develops a processing that is essential in the visual system. As sample images have shown, **the information transmitted by the ganglion pathways includes information of the edges of the images**.

Finally, it should be noted that the strategy employed in the development and definition of the model **has allowed to better characterise the output channels of the retina** when compared with previous existing models, more specifically in the case of chromatic pathways that are usually defined through simple colour opponency.

As has been shown in Chapter VII, it is **possible to design and implement a colour processing model based on a neuroinspired model of the retina and on the structure of colour appearance models**. Additionally:

- Pathways **a, b and A of the** colour appearance models **can be assigned to three of the channels generated by the retina model**. These channels are:
  - Midget ganglion type G.
  - Small bistratified ganglion.
  - Midget ganglion type R.
- This work has also shown how **the use of an exponential function** (as a generator of spikes) that can adapt its parameters, **allows to obtain a high circularity level** of the chroma rings of the Munsell samples.
- It has been documented how the **use of these adapted ganglion channels permits the calculation of all attributes** that are necessary for the characterisation of a colour: hue, lightness, saturation, chroma and colourfulness. The obtained results on Munsell samples are comparable or even better than those obtained by the colour appearance model CIECAM02.
- The colour processing model has been shown to keep the property of the retina model for **edge detection**.

2. Contributions

This work has generated two main contributions. On the one hand, the **development of a functional model of the retina** that has a detailed architecture as well as a set of assigned cells. The different cell types have been specified both according to their size as well as their distribution, to their established connections and their functionalities. The second main contribution of this thesis is **the design and development of a colour processing model with a bioinspired nucleus**. This model analyses each point in an image and calculates its colour attributes: hue, lightness, brightness, saturation, chroma and colourfulness. Both models have

been validated through systematic testing and have been compared against biological data as well as with other colour appearance models.

The following shows the contributions provided in this work, according to the chapter order, starting with Chapter III, as Chapter II was a basic introduction of the issues that have been dealt with in this thesis.

Chapter III has provided a study on colour theory and colour models. This chapter showed how colour characterisation is not a simple matter. Colour effects presented some of the additional elements that influence the final colour perception: background, surrounding, illumination, luminance…. On the other hand, the analysis made has helped to **identify the stages of colour appearance models** and **the necessary attributes for colour description.** All these elements have set the groundwork for the development of the colour processing model that is the objective of this thesis. These contributions can be summed up as follows:

i. Identification of the structure of colour appearance models.

ii. Identification of the colour attributes that a colour appearance model must calculate.

iii. Analysis of the most relevant colour models that are the reference of this system.

iv. Selection of the set of data for the evaluation of the colour processing model: Munsell colour system.

A thorough study of the retina and its different types of cells was shown in Chapter IV. The following has been analysed: each cell type, subtypes, the connections they establish, their nature, distribution and sizes in the receptive fields. This has allowed the identification and characterisation of the elements that compose the functional model of the retina. Different model proposals for each cell type have also been identified as well as some unresolved issues for which the retina model has had to establish working hypotheses. These contributions can be summed up as:

v. **Identification of the different cell types** of the retina.

vi. **Characterisation of the cell types** through the definition of:

   a. Number of cells in the retina and/or fovea.

   b. Receptive field size.

   c. Number and type of established connections.

   d. Functions of each cell type.

vii. Ganglion cells have been identified as the cells that generate nervous spikes that constitute the signals that are transmitted through the optic nerve.

viii. **Multiple output channels** of the retina have been identified.

ix. Different areas within the retina have been shown: fovea, intermediate area and periphery.

x. Cell modelling techniques have been identified as well as some open issues regarding the retina and its components.

Chapter V has introduced a brief study on the stages of the visual system after the retina. This has placed the retina models and colour processing in a broader context. This has been done in order to both know the characteristics of the neurons in these stages and therefore verify the outputs of the retina model as well as to identify the stages of colour processing in the human visual system. A brief summary of the contributions presented in this chapter are:

xi. The segregation of the information pathways transmitted in the visual system is confirmed.

xii. The neurons in LGN have similar responses to retinal ganglion cells.

xiii. The **main types of cells in LGN have been identified**.

xiv. In V1 there are neurons tuned to oriented lines.

xv. Specific areas for the detection of chromatic stimuli (blobs) can be found in V1.

Chapter VI has shown the design and implementation of the functional model of the retina. Its structure has been described and the connections of each cell type have been provided, along with its distribution and size. This has permitted to obtain a set of retina output channels through the signals generated by the ganglion cells that are transmitted through the optic nerve. A method has been established to allow the calculation of the cell distribution in each layer taking into account the biological overlapping factors. A set of stimuli has been defined in order to analyse the spatial and chromatic features of each cell type and a study has been made of the signal response of each cell type. The level of details of each cell type layer has surpassed those of existing models, particularly those that deal with chromatic channels that usually employ simple concepts of colour opponency. The presence of multiple parallel information pathways completely matches with what is known on the retina to this day. The retina, an organ that is often obviated in the visual processing system, has been shown to have an essential task in perception. The channels generated by the ganglion cells have characteristics that determine all the later processing of

visual data and the excellent results provided by the colour processing model uphold this fact. The set of contributions provided in this chapter can be summarised in the following list:

xvi. Design and development of a functional model of the retina.

xvii. Design of a detailed architecture of the model.

xviii. Definition of a method for the configuration of the cell distribution by means of a mesh that optimally adapts to the biological cell coverage factors.

xix. **Detailed description of all cell types in the model**: sizes, distribution, established connections, receptive fields, connection functions and nervous spike generation function.

xx. Definition of a set of test stimuli for the spatial and chromatic characterisation of each cell type.

xxi. Study of the results provided by the model by means of the signal analysis generated by each cell type when presented the set of previously established test stimuli.

xxii. Characterization of the receptive field of each cell type.

xxiii. Identification of the cells as chromatic or acromatic.

xxiv. Identification and characterization of the main output channels of the retina.

xxv. Use of the model for real images processing.

Chapter VII has introduced a colour processing model based on the functional model of the retina and on the structure of colour appearance models. The channels *a*, *b* and *A*, necessary to generate colour attributes, have been established and configured using the circularity level of constant chroma rings of the Munsell samples as a criterion. These channels correspond to the output channels of the retina model: midget ganglion type G, bistratified ganglion and midget ganglion type R respectively. An *ab* space with a high circularity level has been achieved by modifying the nervous spike generation functions, coming close to the ideal space of the Munsell samples. Finally, colour attributes have been calculated: hue, lightness, brightness, saturation, chroma and colourfulness. The results achieved have been better than those obtained by CIECAM02 (colour appearance model used as reference). Finally, the model has been applied to the calculation of the colour attributes of all the pixels in real colour images. The summary of the contributions of this chapter are:

xxvi. Definition and development of a new colour processing model.

xxvii. Combination of a functional retina model with the structure of colour processing models identified in chapter III.

xxviii. Definition of a work hypothesis for the selection of *a*, *b* and *A* channels of colour appearance models.

xxix. Definition of the adjustment possibilities of the colour model's channels, based on the combination of the output channels of the retina model.

xxx. Definition of the optimisation criteria for the combination of the retina channels.

xxxi. Selection of the channels that make up *a*, *b* and *A* channels of the colour processing models.

xxxii. **Identification of the midget ganglion type G, small bistratified ganglion and the midget ganglion type R** channels as the main channels of the colour processing model.

xxxiii. Improvement in the circularity level of constant chroma rings of the Munsell samples by means of a **modification of the spike generation function**.

xxxiv. Calculation of colour attributes: hue, lightness, brightness, saturation, chroma and colourfulness.

xxxv. Goodness of fit of the colour processing model evaluation through the comparison of the results obtained on Munsell colour samples with the CIECAM02 model's results.

xxxvi. Application of the **colour processing model to real image processing**.

Finally, it is noteworthy to mention that a European patent application has been filed for both the functional retina model as well as for the colour processing model.

3. Future works

The work carried out in this thesis is the beginning of a research line. Throughout these chapters, several research issues have been mentioned that have been set aside for future works in order to

obtain a complete and operational version of the model. The following are these future works with some additional comments.

The first works that will be mentioned are those works that have been identified as extensions and improvements of the functional retina model:

- This first version of the functional model of the retina has not included **temporal components** as the processes related with colour are not influenced by these temporal components at the first stage. However, given the usefulness obtained by the colour processing model when analysing the visual system from its origin in the retina, temporal components will be added to the model in order to analyse the pathways that highly depend on temporal components (such as movement detection). This will also allow comparing the results with live measurements.
- It has been verified how there is not a sole set of parameters for the retina model. A selection of a set of parameters to carry out the study of the signals generated by each cell type was made in Chapter VI, section 5. Other models [SERRE_06] have applied routines for a **systematic optimisation of the parameters** that have obtained improvements in the results of the final model. This systematic study shall be object of future research. The model shall be codified into GPUs in order to perform optimisation routines within reasonable times.
- Each type of neuron establishes **dynamic lateral connections**. The study and inclusion of lateral connection processes between neurons and their dynamic adaptation when facing changes in the context conditions shall also be studied. These types of functionalities will provide greater versatility and range of work to the system.
- Two modes of work have been included in the model: **subtraction mode and division mode**. The tests carried out do not provide conclusive evidence that establish the use of one over the other. The subtraction mode is the most common in scientific publications, however the division mode (or shunt inhibition) has been proposed for use in other areas of the cortex with very satisfactory results. On the other hand, the colour appearance models model the dynamic response through functions in division mode that include a numerator with the direct photoreceptor information and a denominator that depends on surrounding levels. This denominator could correspond with the signals that come from horizontal cells, as happens in the model proposed in the division mode. The analysis of these issues shall be undertaken in future research.

Several areas have been identified in reference to the colour processing model that will be part of future works:

- The model has been adjusted to be compared with the model CIECAM02 for Munsell samples with Value 5. The study of the adjustment parameters of the channels **in different intensity levels** is going to be carried out in order to broaden the range of application of the colour processing model.
- A series of configuration parameters have been established in the model. One of them is the background level value (colour appearance models have been developed in order to evaluate individual colour samples where all surrounding parameters are defined and/or established in a manual manner). Future versions of the model shall include the **automatic calculation of the background values**.
- The functions developed for colour attributes calculation in CIECAM02 model have been used. The input channels have also been configured in reference to CIECAM02 model. As the circularity level obtained for the chroma rings of Munsell samples by the proposed model has been better than those of the CIECAM02 model, it is reasonable to look at **the optimisation of the calculations of colour attributes**. There are multiple databases that could be used for the development and optimisation of these calculations.

Special attention must be placed on the study of the channels that are formed by signals *a*, *b* and *A* of the colour processing model. The three retina channels that correspond with these channels have been identified:

- Channel *a* corresponds with the midget ganglion type G channel.
- Channel *b* corresponds with the small bistratified ganglion channel.
- Channel *A* corresponds with the midget ganglion type R channel.

This fact entails a new approach to colour perception processes and shall be studied in depth. It shall be compared against the optimisation processes both of the parameters of the retina model as well as the calculation functions of colour attributes. The implications and relations in the different areas of the cortex shall also be analysed.

Finally, and as it is one of the great contributions of this work, both the functional model of the retina as well as the colour processing models shall be studied in applications for image segmentation, characterisation and object identification.

References

[AHNE_94] P Ahnelt, H. Kolb. ”Horizontal Cells and Cone Photoreceptors in Primate Retina: A Golgi-Light Microscopic Study of Spectral Connectivity” The Journal of Comparative Neurology. No 343. pp. 387-405. 1994

[AHNE_94b]P. Ahnelt, H. Kolb. “Horizontal Cells and Cone Photoreceptors in Human Retina: A Golgi-Electron Microscopic Study of Spectral Connectivity” The Journal of Comparative Neurology 343 pp. 406-427. 1994

[ALBR_84] T. D. Albright. “Direction and orientation selectivity of neurons in visual area MT of the macaque”. Journal of Neurophysiology, 52(6):1106–1130, Dec. 1984.

[ANDR_03] R. G. D’Andrade, A. K. Romney. “A quantitative model for transforming reflectance spectra into the Munsell color space using cone sensitivity functions and opponent process weights” PNAS, V 100, No. 10, pp. 6281–6286. 2003

[ARAG_02] M. Aragort. “El sistema nervioso central” 2002 www.monografias.com/trabajos11/sisne/sisne.shtml#ne

[ATTW_83] D. Attwell, M. Wilson. “The spatial frequency sensitivity of bipolar cells”. Biol. Cybern. 47, pp. 131-140. 1983

[AWAT_00] G. B. Awatramani, M. M. Slaughter.“Origin of Transient and Sustained Responses in Ganglion Cells of the Retina” The Journal of Neuroscience, , 20(18):7087–7095 2000

[BACC_07] S.A. Baccus. “Timing and computation in inner retinal circuitry”. Ann. Rev. Physiol. Vol 69 pp271-90. 2007

[BALA_09] V. Balasubramanian, P. Sterling. “Receptive fields and functional architecture in the retina”. The Journal of Physiology, Vol. 587, No 12, pp. 2753-2767. 2009

[BALY_02] D. Balya, B. Roska, T. Roska, F.S. Werblin. “A CNN framework ofr modeling parallel processing in a mammalian retina” International journal of circuit theory and applications Nº30 pp. 363- 393. 2002

[BARR_96] Barrow H. G., Bray A. J., Budd J. M. L. “A self organizing model of color blob formation” Neural computation 8, pp. 1427-1448. 1996.

[BARR_03] B. A. Barres. “What is a Glial cell?” GLIA No. 43 pp. 4-5. 2003

[BEAR_06] M. F. Bear, B.W. Connors, M.A. Paradiso. “Neuroscience: Exploring the Brain 3rd edition” Lippincott Willians & Wilkins. 2007

[BI_98] G.Q. Bi and M.M. Poo. “Synaptic modifications in cultured hippocampal neurons: dependence on spike timing, synaptic strength, and postsynaptic cell type”. J. Neurosci., 18. 1998.

[BILL_91] V. A. Billock. “The relationship between simple and double opponent cells” Vision Res. Vol 31 N1 pp 33-42 1991

[BILL_95] V. A. Billock. “Cortical simple cells can extract achromatic information from multiplexed chromatic and achromatic signals in the parvocellular pathway”. Vision Res. Vol 35, N16, pp. 2359-2369. 1995.

[BELM] J. Belmar “Neurociencias” Facultad de Ciencias Biológicas http://www.puc.cl/sw_educ/neurociencias/html/

[BOOT_98] M. C. Booth and E. T. Rolls. “View-invariant representations of familiar objects by neurons in the inferior temporal visual cortex”. Cereb. Cortex, 8, 1998.

[BOYC_91a] B.B. Boycott, H. Wässle. “Morphological classification of bipolar cells of the primate retina”. European Journal of Neuroscience, vol 3, pp. 1069-1088. 1991

[BOYC_91b] B. B. Boycott, J.M. Hopkins. “Cone bipolar cells and cone synapses in the primate retina”. Visual neuroscience,7, pp. 49-60. 1991.

[BOYN_77] R. M. Boynton "Color vision". International encyclopedia of psychiatry, psychology, psychoanalysis and neurology (B. B. Wolman ed.) Vol III pp. 226-230. 1977

[BOYN_96]. R. M. Boynton, "History and current status of a physiologically based system of photometry and colorimetry," J. Opt. Soc. Am. A 13, pp. 1609-1621.1996

[BRAI_08] D. H. Brainard, D. R. Williams, H. Hofer. "Trichromatic reconstruction from the interleaved cone mosaic: Bayesian model and the color appearance of small spots" J Vis. ; V. 8 No. 5 pp. 1–23. 2008

[BUDZ_02] T. Budzichowski http://userpages.umbc.edu/~budzicho/spectrum.gif 2002

[BURK_86] Burkhalter, D. C. Van Essen. "Processing of color, form and disparity information in visual areas VP and V2 of ventral extrastriate cortex in the macaque monkey". J. Neurosci., 6(8), pp. 2327–51. 1986.

[CAJA_ 1893] S. R. Cajal S. R. "La rétine des vertébrés" Cellule 9 pp.119-255. 1893

[CALK_07] D. J. Calkins, P. Sterling. "Microcircuitry for Two Types of Achromatic Ganglion Cell in Primate Fóvea" The Journal of Neuroscience, 27(10):2646-2653. 2007

[CAMP_66] F. W. Campbell, R. W. Gubish. "Optical quality of the human eye". Journal of Physiology 186, pp. 558–578. 1966

[CARA_94] Carandini , D.J. Heeger. "Summation and division by neurons in primate visual cortex" Science 264. pp 1333- 1336. 1994

[CHIC_99] E.J. Chichilnisky, B. A. Wandell "Trichromatic opponent color classification" Vision Research 39, pp. 3444–3458 1999

[CHIC_99b]E. J. Chichilnisky, D. A. Baylor. "Receptive-field microstructure of blue-yellow ganglion cells in primate retina". Nature neuroscience volume 2, no 10, pp.889-893. 1999

[CHIC_02] E. J. Chichilnisky, R. S. Kalmar. "Functional Asymmetries in ON and OFF Ganglion Cells of Primate Retina" The Journal of Neuroscience, April 1, 22(7), pp. 2737–2747. 2002

[CHUN_96] M. Chun, U. Grunert, P. R. Martin, H. Wassle. "The Synaptic Complex of Cones in the Fóvea and in the Periphery of the Macaque Monkey Retina". Vision Res., Vol.36, No.21, pp.3383–3395. 1996

[CONW_01] B. R. Conway. "Spatial structure of cone inputs to color cells in alert macaque primary visual cortex (V-1]" The journal of neuroscience 21(8) pp. 2768-2783. 2001

[CONW_05] B. R. Conway, D. Y. Tsao. "Color Architecture in Alert Macaque Cortex Revealed by Fmri" Cerebral Cortex Advance Access published December 28. 2005

[CONW_06] B. R. Conway, M. S. Livingstone. "Spatial and temporal properties of cone signals in alert macaque primary visual cortex" The journal of neuroscience 26 (42) pp. 10826- 10846. 2006

[CONW_07] Conway B. R., Moeller S., Tsao D. Y. "Specilalized color modules in macaque extrastriate cortex" Neuron 56 pp 560-573 2007.

[CROO_08a] J. D. Crook, B. B. Peterson, O. S. Packer, F.R. Robinson, P.D. Gamlin, J. B. Troy, D.M. Dacey. "The smooth monostratified ganglion cell: evidence for spatial diversity in the Y-cell pathway to the lateral geniculate nucleus and superior colliculus in the macaque monkey." J Neurosci. 26;28 (48), pp. 12654-71. 2008

[CROO_08b] J. D. Crook, B. B. Peterson, O. S. Packer, F. R. Robinson, J. B. Troy, D. M. Dacey. "Y-cell receptive field and collicular projection of parasol ganglion cells in macaque monkey retina." J Neurosci. 29;28(44), pp. 11277-91. 2008

[CROO_09] J.D. Crook, C. M. Davenport, B. B. Peterson, O. S. Packer,. P.B. Detwiler, D. M. Dacey. "Parallel on and off cone bipolar inputs establish spatially coextensive receptive field structure of blue-yellow ganglion cells in primate retina" The Journal of Neuroscience, 29(26):8372– 8387 July 1, 2009

[CURC_90a] C A. Curcio, K. R. Sloan, R. E. Kalina, A. E. Hendrickson "Human photoreceptor topography" The Journal of Comparative Neurology 292, pp. 497-523.1990.

[CURC_90b] C. A. Curcio, K. A. Allen. "Topography of ganglion cells in human retina". The journal of comparative neurology, 300, pp. 5-25. 1990.

[CURC_91] C. A. Curcio, K. A. Allen, K. R. Sloan, C. L. Lerea, J. B. Hurley, I. B. Klock, A. H. Milam. "Distribution and Morphology of Human Cone Photoreceptors Stained With Anti-Blue Opsin" The Journal of Comparative Neurology 312, pp. 610-624. 1991.

[DACE_92] D. M. Dacey, M. R. Petersen. "Dendritic field size and morphology of midget and parasol ganglion cells of the human retina" Proc. Natl. Acad. Sci. USA Vol. 89, pp. 9666-9670. 1992

[DACE_93] D. M. Dacey. "The Mosaic of Midget Ganglion Cells in the Human Retina" The Journal of Neuroscience, December, 13(12), pp. 5334-5355. 1993

[DACE_94] D. M. Dacey, B. B. Lee "The 'blue-on' opponent pathway in primate retina originates from a distinct bistratified ganglion cell type". Nature Vol. 367. pp. 731-735. 1994.

[DACE_96] D. M. Dacey. "Circuitry for color coding in the primate retina" Proc. Natl. Acad. Sci Vol 93, pp. 582-588. 1996

[DACE_00] D. Dacey, O. S. Packer, L. Diller, D. Brainard, B. Peterson, B. Lee. "Center surround receptive field structure of cone bipolar cells in primate retina" Vision Research 40 pp. 1801–1811. 2000

[DACE_00b] D. M. Dacey. "Parallel pathways for spectral coding in primate retina". Annu. Rev. Neurosci.pp.743-775. 2000

[DACE_03] D. M. Dacey, B. B. Peterson, F. R. Robinson, P. D. Gamlin. "Fireworks in the Primate Retina: neurotechnique In Vitro Photodynamics Reveals Diverse LGN-Projecting Ganglion Cell Types". Neuron Vol 37 pp 15-27 2003

[DACE_04] D.M. Dacey. "Origins of perception: retinal ganglion cell diversity and the creation of parallel visual pathways" . In The Cognitive Neurosciences, ed. MS Gazzaniga, Cambridge, MA: MIT Press pp. 281–301. 2004

[DACE_05] D. M. Dacey, H. Liao, B. B. Peterson, F. R. Robinson, V. C. Smith, J. Pokorny3, K. Yau, P. D. Gamlin. "Melanopsin-expressing ganglion cells in primate retina signal colour and irradiance and project to LGN." Nature Vol. 433, pp. 749-754. 2005

[DART_83] J. A. Dartnall, J. K. Bowmaker, J. D. Mollon "Human visual pigments: microspectrophotometric results from the eyes of seven persons" Proc. R. Soc. Lond.. B 220, pp. 115-130. 1983

[DEMA_92] P. DeMarco, J. Pokorny, V. C. Smith. "Full-spectrum cone sensitivity functions for X-chromosome-linked anomalous trichromats" J. Opt. Soc. Am. A Vol. 9, No. 9/September 1992

[DERR_84] A. M. Derrington, J. Krauskopft, P. Lennie "Chromatic mechanisms in lateral geniculate nucleus of macaque" J. Physiol. 357; pp. 241-265. 1984

[DESI_85] R. Desimone, S. J. Schein, J. Moran, L. G. Ungerleider. "Contour, color and shape analysis beyond the striate cortex" Vision Res. Vol 25, Nº 3, pp. 441-452. 1985

[DEVA_93] R. L. De Valois, K. K. De Valois. "A Multi-Stage Color Model". Vision Res. Vol. 33, No. 8, pp. 1053-1065. 1993.

[DEVA_00] R. L. De Valois, N. P. Cottaris, S. D. Elfar, L.E. Mahon, J. A. Wilson. "Some transformation of color information from lateral geniculate nucleus to striate cortex" PNAS Vol 97 Nº 9 pp. 4997-5002. 2000

[DEYO_88] E. A. DeYoe, D. C. Van Essen. "Concurrent processing streams in monkey visual cortex." Trends. Neurosci., 11(5) pp. 219–26, 1988.

[DEYO_94] E. A. DeYoe, D. J. Felleman, D. C. Van Essen, E. McClendon. "Multiple processing streams in occipitotemporal visual cortex" Nature, Vol 371, Nº 8, pp. 151-154. 1994

[DIAZ_08] F. J. Díaz-Pernas, Antón-Rodriguez, J. F. Díez-Higuera, M. Martínez-Zarzuela. "A bio-inspired neural model for colour image segmentation" ANNPR 2008, LNAI 5064, pp. 240-251. 2008.

[DOWN_01] P. E. Downing, Y. Jiang, M. Shuman, N. Kanwisher. "A cortical area selective for visual processing of the human body". Science, 293. 2001.

[DOWS_07] S. Dowshen "Your brain and nervous system" http://www.kidshealth.org/kid/en_espanol/cuerpo/brain_esp.html 2007

[DUBI] M. Dubin. http://spot.colorado.edu/~dubin/index.html "Brodmann Areas in the Human Brain with an Emphasis on Vision and Language"

[EC_07] European Commission "ICT - INFORMATION AND COMMUNICATION TECHNOLOGIES Work Programme 2007-08" 11 June 2007

[ENC_08] Enciclopedia Encarta Copyright 2008

[ENRO_66] C. Enroth-Cugell, J. G. Robson. "The contrast sensitivity of retinal ganglion cells in the cat". Journal of hysiology, 187, pp. 517–522. 1966

[ERIN] Erin_Silversmith. http://wikipedia.com

[FAIR_97] M. D. Fairchild. "Color appearance models." Ed. Addison Wesley Longman 1997

[FAIR_04] M. D. Fairchild. "Color appearance models. 2nd ed." Ed. Wiley 2004

[FAIR_04a] M.D. Fairchild. "Color appearance models CIECAM02 and Beyond" IS&T/SID 12th Color Imaging Conference. 2004

[FELL_91] D. J. Felleman, D. C. van Essen. "Distributed hierarchical processing in the primate cerebral cortex." Cereb. Cortex, 1, pp. 1–47. 1991.

[FELL_ 97] D. J. Felleman, Y. Xiao, E. McClendon. "Modular Organization of Occipito-Temporal Pathways: Cortical Connections between Visual Area 4 and Visual Area 2 and Posterior Inferotemporal Ventral Area in macaque Monkeys" The journal of neuroscience, 17 (9), pp. 3185-3200. 1997

[FIEL_07] G. D. Field, A. Sher, J. L. Gauthier, M. Greschner, J. Shlens, A. M. Litke, E. J. Chichilnisky."Spatial Properties and Functional Organization of Small Bistratified Ganglion Cells in Primate Retina". The Journal of Neuroscience, • 27(48) pp. 13261–13272. 2007.

[FIEL_07b] G.D. Field and E.J. Chichilnisky "Information Processing in the Primate Retina: Circuitry and Coding"Annu. Rev. Neurosci. 30, pp.1–30. 2007

[GEGE_03] K. R Gegenfurtner. "Cortical mechanisms of colour vision" Nature Reviews, Neuroscience, Vol 4. pp. 563- 572. 2003

[GHOS_08] K. Ghosh, K. Bhaumik, S. Sarkar S. "Retinomorphic image processing" Progress in brain research Vol 168. 2008

[GIES_03] M. Giese, T. Poggio. "Neural mechanisms for the recognition of biological movements and action." Nat. Rev. Neurosci., 4, pp.179–192, 2003.

[GOWI_00] B. A. Gowitzke, M. Milner "El cuerpo y sus movimientos: Bases científicas" Ed. Paidotribo, 2000

[GOLL_08] T. Gollisch, M. Meister "Rapid Neural Coding in the Retina with Relative Spike Latencies" Science 319 pp. 1108-1111. 2008

[GROS_95] S. Grossberg S, E. Mingolla, J. Williamson. "Synthetic aperture radar processing by a multiple scale neural system for boundary and surface representation" Neural Networks. Vol 8, Is. 7-8, pp. 1005 – 1028. 1995

[GUTH_91]S. L. Guth "Model for color vision and light adaptation" J. Opt. Soc. Am. A, Vol. 8, No. 6/June 1991

[GUYT_06] A. C. Guyton, J. E. Hall Tratado de fisiologia médica 11 edición Ed. MCGRAW HILL. 2006

[HATE_02] J. H. van Hateren, L. Ruttiger, H. Sun, B. B. Lee. “Processing of Natural Temporal Stimuli by Macaque Retinal Ganglion Cells” The Journal of Neuroscience, Vol 22 (22) 5, pp. 9945–9960. 2002

[HATE_07] J. H. van Hateren ”A model of spatiotemporal signal processing by primate cones and horizontal cells” Journal of Vision 7(3):3, pp:1–19. 2007

[HEEG_96] D. J. Heeger D. J., Simoncelli E. P., Movshon J. A. “ Computational models of cortical visual processing”. Proceedings of the National Academy of Sciences, pp 93, 623-627 1996

[HEND_00] S. H. C. Hendry, R. C. Reid. “THE KONIOCELLULAR PATHWAY IN PRIMATE VISION” Annu. Rev. Neurosci. 23 pp. 127–153. 2000

[HENN_02] M. H. Hennig, K. Funke, F. Wörgötter. “The influence of different retinal subcircuits on the nonlinearity of ganglion cell behaviour” The journal of Neuroscience 22 (19), pp. 8726- 8738. 2002

[HERA_95] J. Herault. “A model of colour processing in the retina of vertebrates: from photoreceptors to colour opposition and colour constancy phenomena”. Neurocomputing 12, pp. 113-129. 1996

[HERR] http://www.herrera.unt.edu.ar/bioingenieria/Temas_inves/sist_nervioso/pagina2.htm

[HIRS_06] J. A. Hirsch, L. M. Martinez. "Circuits that build visual cortical receptive fields." Trends in Neurosciences. 29. 2006

[HOGE_01] R. Hoge. “Primary human visual pathways” adapted from Hubel. Data Acquisition Lab 2001 www.nmr.mgh.harvard.edu Hoge. 2001

[HOPK_95] J. M. Hopkins, B. B. Boycott. “Synapses between primate retina cones and diffuse bipolar cells of a primate retina” Journal of Neurocytology 24, pp. 680-694. 1995

[HUBE_72] D. H. Hubel, T. N. Wiesel. “Laminar and columnar distribution of geniculo-cortical fibers in the macaque monkey” J. Comp. Neur. 146, pp. 421-450. 1972

[HUBE_87] D. H. Hubel, M. S. Livingstone. “Segregation of Form, Color, and Stereopsis in Primate Area 18” The journal of neuroscience 7 (11) pp. 3378 -3415. 1987

[HUBE_90] D. H. Hubel, M. S. Livingstone. “Color and Contrast Sensitivity in the Lateral Geniculate Body and Primary Visual Cortex of the Macaque Monkey” The journal of neuroscience 10(7), pp. 2223-2237. 1990.

[HUNG_05] C. P. Hung , G. K. Kreiman , T. Poggio , J. J. DiCarlo. “Fast Readout of object identity from macaque inferior temporal cortex.” Science 310, 2005.

[HUNT_58] R. S. Hunter “Photoelectric color difference meter” Journal of the optical society of America, Vol 48, N 12, pp.985-995. 1958.

[HUNT_82] R. W. G. Hunt. “A model of colour vision for predicting colour appearance” .Color Research and application Vol 7 pp. 95-112. 1982.

[HUNT_85] R.W.G. Hunt, M.R. Pointer. “A colour appearance transform for the CIE 1931 standard colorimetric observer” Color Research and application Vol 10 p 165-179 1985

[HUNT_91] R. W. G. Hunt “Revised colour-appearance model for related and unrelated colours”. Color Research and application. Vol 16, pp. 146-165. 1991

[HUNT_94] R. W. G. Hunt. “An improved predictor of colourfulness in a model of colour vision”.Color Research and application Vol 19, pp. 23-26. 1994.

[HURV_55] L. M. Hurvich, D. Jameson. “Some Quantitative Aspects of an Opponent-Colors Theory. II. Brightness, Saturation, and Hue in Normal and Dichromatic Vision”, J. Opt. Soc. Am. 45, 602. 1955

[HURV_56] L. M. Hurvich, D. Jameson. “Some Quantitative Aspects of an Opponent-Colors Theory. IV. A Psychological Color Specification System”. Journal of the Optical Society of America. Volume 46, number 6 June, 1956

[ICHI_05] T.Ichinose, P. D. Lukasiewicz. "Inner and outer retinal pathways both contribute to surround inhibition of salamander ganglion cells" J Physiol (Lond) 565: pp..517–535. 2005

[IIBC_99] L. Barbeito, M. Lalinde, D.Jenci, G. Bernasconi, M. Cabezas, C.Nossar, R. Pacheco, D. Waszuk http://iibce.edu.uy/uas/neuronas/abc.htm#Forma. 1999

[IQB_02] Instituto de investigación y Desarrollo Químico-Biológico "Medciclopedia" http://www.iqb.es/neurologia/visitador/v004.htm 2002

[JACO_06] R. Jacoby, D. Stafford, N. Kouyama, D. Marshak. "Synaptic Inputs to ON Parasol Ganglion Cells in the Primate Retina" The Journal of Neuroscience, 16(24) pp. 8041–8056. 1996

[JAME_55] D. Jameson, L. M. Hurvich. "Some Quantitative Aspects of an Opponent-Colors Theory. I. Chromatic Responses and Spectral Saturation", J. Opt. Soc. Am. 45, 546. 1955

[JAME_56] D. Jameson, L. M. Hurvich, "Some Quantitative Aspects of an Opponent-Colors Theory. III. Changes in Brightness, Saturation, and Hue with Chromatic Adaptation" J. Opt. Soc. Am. 46, 405 1956.

[JOHN_03] G. M. Johnson, M.D. Fairchild " A top down description of S-CIELAB and CIEDE2000" Color research and application, Vol 28, I 6, pp 425-435. 2003.

[JOHN_04] E. N. Johnson, M. J. Hawken, R. Shapley. "Cone inputs in macaque primary visual cortex" J. Neurophysiol. 91 pp. 2501- 2514. 2004.

[JONH_08] E. N. Johnson, M. J. Hawken, R. Shapley. "The orientation selectivity of color-responsive neurons in macaque V1" The journal of neuroscience 28(32), pp. 8096-8106. 2008

[KAME_98] M. Kamermans, D. A. Kraaij, H. Spekreijse. "The cone//horizontal cell network: A possible site for color constancy". Visual Neuroscience , 15, pp,787–797. 1998

[KAND_95] E. R Kanddel, J.H. Schwartz, T. M. Jessell. "Essentials of neural science and behaviour". Appleton & Lange. 1995

[KOCH_99] C. Koch. "Biophysics of computation" Oxford university press. 1999

[KOCH_06] K. Koch, J. McLean, R. Segev, M. A. Freed, M. J. Berry II, V. Balasubramanian, P. Sterling. "How much the eye tells the brain" Current Biology 16, pp. 1428-1434. 2006.

[KOLB_91] H. Kolb, L. Dekorver. "Midget Ganglion Cells of the Parafóvea of the Human-Retina: A Study by Electron Microscopy and Serial Section Reconstructions." The journal of comparative neurology. No 303. pp. 617-636. 1991

[KOLB_92] H. Kolb H, K. A. Linberg, S. K. Fisher. "Neurons of the human retina: a Golgi study." J Comp Neurol. 318, pp. 147-87. 1992

[KOLB_94] H. Kolb, E. Fernandez., J. Schouten, A. Ahnelt, K. A. Linberg, S. K Fisher. "Are there three types of horizontal cell in the human retina?" Journal of Comparative Neurology 343, pp. 370–386. 1994.

[KOLB_03] H. Kolb, D. Marshak. "The midget pathways of the primate retina" Documenta Ophthalmologica 106, pp. 67–81. 2003.

[KOLB_09] H. Kolb, E. Fernández, R. Nelson. "Webvision: the organization of the retina and the visual system" http://webvision.med.utah.edu/ última actualización Julio 2009

[KREI_06] G. Kreiman, C.P. Hung, A. Kraskov, R.Q. Quiroga, T. Poggio and J.J. DiCarlo. "Object Selectivity of Local Field Potentials and Spikes in the Macaque Inferior Temporal Cortex". Neuron, Vol. 49, 2006.

[KRIE_02] J. von Kries, "Chromatic Adaptation," Festschrift der Albrecht-Ludwigs-Universität, 1902 [Translation: D.L. MacAdam, The MIT Press (1970), pp. 109-119

[KUEH_03] R. G. Kuehni. "Color space and its divisions: color order from antiquity to the present" John Wiley & Sons Publications. 2003

[KUNK_09] T. Kunkel T, E. Reinhard. "A neurophysiology-inspired steady-state color appearance model" JOSA A, Vol. 26, Issue 4, pp. 776-782. 2009

[LEBE_07] D.S. Lebedev, D.W. Marshack. "Amacrine cell contributions to red-green color opponency in central primate retina: A model study." Visual Neuroscience 24, pp. 535–547. 2007

[LEE_98] B. B. Lee, J. Kremers, T. Yeh. "Receptive fields of primate retinal ganglion cells studied with a novel technique" Visual neuroscience 15, pp. 161-175. 1998.

[LEE_99] B. B. Lee, D. M. Dacey, V. C. Smith, J. Pokorny. "Horizontal cells reveal cone type-specific adaptation in primate retina" PNAS, Vol. 96, Nº 25, pp. 14611–14616. 1999

[LEE_04] B. B. Lee. "Paths to colour in the retina" Clinical and experimental optometry 87. pp. 239-247. 2004

[LENN_88] P. Lennie M. D'Zmura. "Mechanism of color vision"CRC Critical Reviews in Neurobiology Volume 3 Issue 4. 1988.

[LENN_90] P. Lennie, J. Krauskopf, G. Sclar. "Chromatic mechanisms in striate cortex of macaque" The journal of neuroscience, 10(2), pp. 549 -669. 1990

[LENN_91] P. Lennie, P. Willian Haake, D.R. Williams. "The design of chormatically opponent receptive fields". Computational model of visual processing. MIT 1994

[LENN_05] P. Lennie, J. A. Movshon "Coding of color and form in the geniculostriate visual pathway". Optical Society of America A, Vol 22 N10, pp. 2013-2033. 2005

[LEVE_81] A. G. Leventhal, R.W. Rodieck, B. Dreher. "Retinal ganglion cell classes in the Old World monkey: Morphology and central projections." Science, 213 pp.1139-1142. 1981

[LIVI_84] M. S. Livingstone, D. H. Hubel. "Anatomy and physiology of a color system in the primate visual crotex" Journal of neuroscience, 4, pp. 309-356. 1984

[LOGO_96] Logothetis, D.L. Sheinberg. "Visual object recognition." Ann. Rev. Neurosci., 19, pp. 577–621. 1996.

[LOUR_95] T, Lourens "Modeling retinal high and low contrast sensitivity filters" From Natural to Artificial Neural Computation Editor Spannuluser Berlin / Heidelberg, Volume 930.1995

[LUO_96] M. R. Luo, M. Luo, W. Kuo. "The LLAB(l:c) colour model" Color research and application, Vol 21, pp. 412-429. 1996

[LUO_97] M.R.Luo, R.W.G. Hunt. "The estructure of the CIE 1997 colour appearance model (CIECAM97s)" Color research and application. Vol 23, 1998.

[LUO_01] M. R. Luo, G. Cui, B. Rigg "The Development of the CIE 2000 Colour-Difference Formula: CIEDE2000" Color research and application. Vol. 26. 2001

[MACA_42] D. L. MacAdam "Visual Sensitivities to Color Differences in Daylight" Journal of the optic society of America May Volume 32 Number 5. 1942

[MACA_63] D. L. MacAdam. "Nonlinear relations of psychometric scale values to chromaticity differences" Journal of the optical society of America, Vol 53, N 6, pp. 754-757. 1963.

[MACA_74] D. L. MacAdam. "Uniform color spaces" Journal of the optical society of America, Vol 64, N 12, pp. 1691-1702. 1974.

[MACL_79] D. I. A. MacLeod, R. M. Boynton, "Chromaticity diagram showing cone excitation by stimuli of equal luminance", J. Opt. Soc. Am. 69, pp. 1183-1186. 1979

[MARI_82] A. P. Mariani. "Biplexiform Cells: Ganglion Cells of the Primate Retina that Contact Photoreceptors" Science, Vol. 216, No. 4550, pp. 1134-1136. 1982.

[MART_92] P. R. Martin, U. Grünert. "Spatial density and immunoreactivity of bipolar cells in the macaque monkey retina" The journal of comparative neurology 323 pp. 269-287. 1992

[MART_01] P. R. Martin, B. B. Lee, A. J. R. White, S. G. Solomon, Lukas Rüttiger. "Chromatic sensitivity of ganglion cells in the peripheral primate retina" Nature, Vol 410, pp. 933-935. 2001

[MART_95] J. F. Martí Massó. "Neurología. Información para pacientes y familiares." 1995

[MART_97] P. R. Martin, A. J. R. White, A. K. Goodchild, H. D. Wildert, A. E. Sefton. "Evidence that blue on cells are part of the third geniculocortical pathway in primates". European Journal of Neuroscience, vol. 9 pp. 1536-1541 1997.

[MART_06] L. M. Martinez. "The generation of visual cortical receptive fields." Progress in Brain Res. 154, 2006.

[MASL_01] R. H. Masland. "The fundamental plan of the retina" Nature Neuroscience, Vol. 4, No. 9, pp. 877- 886. 2001

[MASL_05] R. H. Masland "The many roles of starburst amacrine cells" TRENDS in Neurosciences, Vol.28, No.8, August 2005

[MASL_07] R. H. Masland, P. R. Martin "The unsolved mystery of vision" Current biology, vol. 17, N. 15, pp. 577-582. 2007

[MAUN_83] J. H. Maunsell , D. C. Van Essen. "Functional properties of neurons in middle temporal visual area of the macaque monkey. I. selectivity for stimulus direction, speed, and orientation". Journal of Neurophysiology, 49(5) pp. 1127–1147. 1983.

[MAXW_856] J. C. Maxwell (1856/1970). "Theory of the perception of colors". Transactions of the Royal Scottish Society of Arts, 4, pp 394-400. Nachdruck aus D. L. MacAdam (Ed.), Sources of color science (pp. 62-66). Cambridge, MA: MIT Press.

[MEIS_99] Meister M, Berry MJ 2nd. "The neural code of the retina". Neuron,.22(3) pp. 435-50.1999

[MICH_78] C. R. Michael. "Color vision mechanisms in monkey striate cortex: dual-opponent cells with concentric receptive fields" Journal of neurophysiology, Vol 41, Nº 3 pp. 572- 588. 1978

[MISH_83] M. Mishkin, L. G. Ungerleider, K. A. Macko. "Object vision and spatial vision: Two cortical pathways". Trends Neurosci. Vol 6, pp. 414- 417. 1983.

[MIT_02] Enciclopedia MIT de ciencias cognitivas. Editorial Síntesis 2002.

[MOMI_06] H. Momiji H., A. A. Bharath, M. W. Hankins, C. Kennard. "Numerical study of short-term afterimages and associate properties in fóveal vision" Vision research, 46, pp. 365-381. 2006

[MORO_02] N. Moroney, M. D. Fairchild, R. W.G. Hunt, C. Li, M. R. Luo, T. Newman "The CIECAM02 Color Appearance Model" IS&T/SID Tenth Color Imaging Conference. Scottsdale, Arizona 2002

[NAKA_66] K. I. Naka, W. A. H. Rushton. "S-potentials from colour units in the retina of fish (cyprinidae)" J. Physiol 185, pp. 536-555. 1966

[NASS_09] J. J. Nassi, E. M. Callaway "Parallel processing strategies of the primate visual system" Nature Reviews Neuroscience Vol. 10. 2009

[NATI_08] National institute of aging "Glosario" http://www.nia.nih.gov/Alzheimers/Publications/LaEnfermedaddeAlzheimer/Glossario/ 2008

[NAYA_86] Y. Nayatani, K. Takaham, H. Sobagaki. "Prediction of color appearance under various adapting conditions". Color research and application, Vol. 11, pp. 62- 71. 1986

[NEWM_96] E. Newman, A. Reichenbach. "The Müller cell: a fucntional element of the retina" TINS Vol. 19, No. 8 pp. 307-312. 1996

[NSF_02] NSF, Converging Technologies for Improving Human Performance NANOTECHNOLOGY, BIOTECHNOLOGY, INFORMATION TECHNOLOGY AND COGNITIVE SCIENCE". Edited by Mihail C. Roco and William Sims Bainbridge, National Science Foundation. June 2002

[ORAM_94] M. W. Oram, D. I. Perrett. ” Modeling visual recognition fromneurobiological constraints”. Neural Netw., 7(6-7) pp. 945–972. 1994.

[PACK_02] O. S. Packer, D. M. Dacey. “Receptive field structure of H1 horizontal cells in macaque monkey retina” Journal of Vision No 2, pp.272-292. 2002

[PASS_02] C. L. Passaglia, J. B. Troy, L. Rüttiger, B. B. Lee. “Orientation sensitivity of ganglion cells in primate retina” Vision Research 42 pp. 683–694. 2002

[PATR_ 02] D. A. Patrone. “Neurología” 2002

[PERR_84] V. H. Perry, R. Oehler, A. Cowey. “Retinal ganglion cells that protect to the dorsal lateral geniculate nucleus in the macaque monkey” Neurosciencde Vol. 12, No. 4, pp. 1101-I 123. 1984

[PETE_99] B. B. Peterson, D. M. Dacey. “Morphology of wide-field, monostratified ganglion cells of the human retina” Visual Neuroscience , 16, pp. 107–120. 1999

[PETE_00] B. B. Peterson, D. M. Dacey. “Morphology of wide-field bistratified and diffuse human retinal ganglion cells” Visual Neuroscience, 17, pp. 567–578. 2000

[PILL_05] J. W. Pillow, L. Paninski, V. J. Uzzell, E. P. Simoncelli, E. J. Chichilnisky. “Prediction and decoding of retinal ganglion cell responses with probabilistic spiking model” The journal of neuroscience, 25(47), pp. 11003-11013. 2005

[PILL_08] J. W Pillow, J. Shlens, L. Paninski, A. Sher, A. M. Litke, E. J. Chichilnisky, E. P. Simoncelli. “Spatio-temporal correlations and visual signalling in a complete neuronal population” Nature, Vol 454, pp. 995-999. 2008

[POLY_49] S. Polyak. (1949). “Retinal structure and color vision”. In F. P. Fischer, A. J. Schaeffer & A. Sorsby (Eds.), Documenta ophthalmologica (Outline of a theory of color measurement for daylight vision) David L. MacAdam, The MIT Press (1970), 246-268.

[PUC] [http://www.puc.cl/sw_educ/neurociencias/html/frame02.html]

[PURD_31] D. McL. Purdy “Spectral Hue as a Function of Intensity” The American Journal of Psychology, Vol. 43, No. 4, pp. 541-559 1931

[PURP_90] K. Purpura, D. Tranchina, E. Kaplan, R. M. Shapley. “Light adaptation in the primate retina: Analysis of changes in gain and dynamics of monkey retinal ganglion cells” Visual Neuroscience , 4, pp. 75-93. 1990

[PURV_01] Edited by Purves D, Augustine G. J., Fitzpatrick D., Katz L. C., LaMantia A, McNamara J. O. y Williams S. M. “Neuroscience” 2nd edition Ed. Sinauer 2001

[RAMO_08] G. Ramón “Sistema nervioso periférico” http://viref.udea.edu.co/contenido/apuntes/gusramon/con_corporal_II/06-periferico.pdf 2008

[REID_02] R. C. Reid, R. M. Shapley. ”Space and time maps of cono photoreceptor signals in macaque lateral geniculate nucleus” The journal of neuroscience, 22 (14) pp. 6158-6175. 2002

[RICH_94] E. Rich, K. Knight. “Inteligencia artificial”. Segunda edición McGraw-Hill 1994.

[RODI_65] R. W. Rodieck. “Quantitative analysis of cat retinal ganglion cell response to visual stimuli”. Vision Research, 5, pp. 583–601. 1965

[RODI_85] R. W. Rodieck, K. F. Binmoeller, J. Dineen “Parasol and Midget Ganglion Cells of the Human Retina” The journal, of comparative neurology, N. 233 pp. 115-132. 1985.

[RODI_89] R. W. Rodieck “Starburst Amacrine Cells of the Primate Retina” the journal of comparative neurology, 285, pp. 18-37. 1989

[RODI_98] R. W. Rodieck. “The first steps in seeing” Ed. Sinauer Associates. 1998.

[RONN_05] A. K. Romney, R. G. D'Andrade. "Modeling lateral geniculate nucleus cell response spectra and Munsell reflectance spectra with cone sensitivity curves" PNAS Vol. 102. No. 45, pp. 16512–16517. 2005

[ROOR_99] A. Roorda, D. R. Williams "The arrangement of the three cone classes in the living human eye" Nature vol 397, 1999

[RUDE_98] D. L. Ruderman, T. W. Cronin, C. Chiao. "Statistics of cone responses to natural images: implications for visual coding" JOSA A, Vol. 15, I 8, pp. 2036-2045. 1998

[SAGL_08] M. Sağlam, Y. Hayashida, N. Murayama. "A retinal circuit model accounting for wide-field amacrine cells" Cognitive Neurodynamics Vol 3 N1 pp. 25-32. 2008

[SCHI_92] P. H. Schiller. "The ON and OFF channels of the visual system" TINS, Vol. 15, No. 3, 1992

[SCHO_20] E. Schrödinger Sc"Grundlinien einer Theorie der Farbenmetrik im Tagessehen," Annalen der Physik, (4), 63, (1920), 397-426; 427-456; 481-520 (Outline of a theory of color measurement for daylight vision) David L. MacAdam, The MIT Press (1970), 134-182.

[SCHÜ_07] Schünke, Schulte, Schumacher, Voll y Wesker. "PROMETHEUS, Texto y Atlas de Anatomía" De. Médica Panamericana, 2007

[SERR_06] T. Serre "Learning a Dictionary of Shape-Components in Visual Cortex: Comparison with neurons, Humans and Machines" 2006

[SERR_07a] T. Serre, A. Oliva, T. Poggio. "A Feedforward Architecture Accounts for Rapid Categorization". Proceedings of the National Academy of Sciences, Vol. 104, No. 15, 2007.

[SERR_07b] T. Serre, L. Wolf, S. Bileschi, M. Riesenhuber and T. Poggio. "Object Recognition with Cortex-like Mechanisms," IEEE Transactions on Pattern Analysis and Machine Intelligence, 29, 3, 2007.

[SERR_06] T. Serre. "Learning a Dictionary of Shape-Components in Visual Cortex: Comparison with Neurons, Humans and Machines." Ph.D. Thesis, MIT, 2006.

[SHAH_96a] S. Shah, M. D. Levine. "Visual information process in the primate cone pathways Part I Model" IEEE transactions on systems, man and cybernetics – Part B Cybernetics, Vol 26, Nº2, pp. 259- 274. 1996

[SHAH_96b] S. Shah, M. D. Levine. "Visual information processin in the primate cone pathways Part II Experiments" IEEE transactions on systems, man and cybernetics – Part B Cybernetics, Vol 26, Nº2, pp. 274- 289. 1996

[SHEV_03] S. K. Shevell Ed. "The science of color" Elsevier, 2003

[SILV_91] L. C. L. Silveira, V. H. Perry. "The topography of magnocellular projecting ganglion cells (m ganglion cells) in the primate retina" Neuroscience Vol. 40, No. 1, pp. 217-237, 1991

[SIMI_84] R. Siminoff. "Influence of amacrine cells on receptive field organization of ganglion cells of the generalizad vertebrate cone retina: electronic simulartion". Biol. Cybern. 50, pp. 213-234. 1984.

[SIMI_91] R. Siminoff. "Simulated bipolar cells in fóvea of human retina" Biological Cybernetics, 64, pp. 497- 504 1991

[SINI_05] L. C. Sincich, J. C. Horton. "The Circuitry of V1 and V2:Integration of Color, Form, and Motion" Annu. Rev. Neurosci.. 28, pp. 303–26. 2005

[SFN] Society For Neuroscience http://web.sfn.org/index.cfm?pagename=brainBackgrounders_main#

[SMIT_75] V. C. Smith, J. Pokorny "Spetral sensitivity of the foveal cone photopigments between 400 and 500 nm" Vis. Res. Vol 13, pp. 161-171. 1975

[STEP_00] Stephen "Frequently asked questions about Colour Physics" www.colourware.co.uk 2000

[STIL_46] W. S. Stiles "A modified Helmholtz line--element in brightness--colour space\ Proceedings of the Physica"l Society of London, 58, pp. 41-65. 1946

[STOC_93] A. Stockman, D. I. A. MacLeod, N. E. Johnson "Spectral sensitivities of the human cones" J. Opt. Soc. Am. A Vol. 10, No. 12. 1993

[STOC_00] A. Stockman, L. T. Sharpe "The spectral sensitivities of the middle- and long-wavelength-sensitive cones derived from measurements in observers of known genotype" Vision Research 40, pp 1711–1737. 2000

[STOU_08] C. M. Stoughtoon, B. R. Conway. "Neural basis for unique hues" Current Biology, Vol. 5, pp. 698-699. 2008.

[SUN_06] H. Sun, H. E. Smithson, Q. Zaidi, B. B. Lee. "Specificity of Cone Inputs to Macaque Retinal Ganglion Cells" J Neurophysiol.; 95(2), pp. 587–588. 2006

[TANA_96] K. Tanaka. "Inferotemporal cortex and object vision." Ann. Rev. Neurosci., 19, pp.109–139. 1996.

[TORR_78]V. Torre, T. Poggio. "A synaptic mechanism possibly underlying direccional selectivity to motion" Proc. Roy. Soc Lond. B 202, pp. 409-416. 1978.

[TSO_88] D. Y. Tsó, D. Gilbert. "The organization of chromatic and spatial interactions in the primate striate cortex" The journal of neuroscience, 8(5), pp. 1712- 1727. 1988.

[TUKK_04] J.J. Tukker, W. Rowland Taylor, R. G. Smith. "Direction selectivity in a model of the startburst amacrina cell" Visual neuroscience 21, pp. 611-625. 2004

[UNGE_94] L.G. Ungerleider, J.V. Haxby. "'What' and 'where' in the human brain." Curr. Op. Neurobiol., 4, pp. 157–165. 1994.

[UNGE_95] A. Martin, J.V. Haxby, F. M. Lalonde, C. L. Wiggs, L. G. and Ungerleider. "Discrete cortical regions mediate knowledge of colors and knowledge of actions". Science, 270, pp. 102-105. 1995

[UNGE_95b] L. G. Ungerleider. "Functional Brain Imaging Studies of Cortical Mechanisms for Memory" Science 270 pp. 769-775. 1995.

[UÑA_04] O. Uña, A. Hernández "Diccionario de Sociología" Ed. ESIC 2004

[URTU_06] C. Urtubia Vicario. "El efecto expansión con una red cuadrada acromática en función de la luminancia y del tamaño". Universitat de Valencia. Servei de Publicacions. 2006

[VAKR_05] C. Vakrou, D. Whitaker, P. V. McGraw, D. McKeefry. "Functional evidence for cone-specific connectivity in the human retina" J Physiol 566, 1, pp. 93–102. 2005

[VALB_08] A. Valberg, T. Seim. "Neural mechanisms of chromatic and achromatic vision" Color Research & Application, Vol 33, I 6, pp. 433- 443. 2008

[VALE_83] J. M. Valeton, D. Van Norren. "Light adaptation of primate cones an análisis base don extracellular data" Vision Res. Vol 23, Nº12, pp. 1539- 1547. 1983

[VANE_94] D. C. Van Essen, J. L. Gallant. "Neural Mechanisms of Form and Motion Processing in the Primate Visual System" Neuron, Vol 13, pp. 1-10. 1994

[VICA_97] C. U. Vicario "Neurobiología de la visión" Ed. UPC 1997

[VOS_71] J. J. Vos, P.L. Walraven "On the derivation of the fóveal receptor primaries" Vision Research 11, pp. 799-818. 1971

[VOS_90] J.J. Vos, O. Estevez and P. L. Walraven. " Improved color fundamentals offer a new view on photometric additivity" Vision Rr. Vol. 30, No. 6, pp. 937-943. 1990

[WAND_95] B. A. Wandell. "Foundations of Vision" Ed. Sinauer Associates, Incorporated 1995

[WASS_89] H. Wässle, U. Grünert, J. Röhrenbeck, B.B. Boycott. "Cortical magnification factor and the ganglion cell density of the primate retina" Nature, Vol 341, pp. 643-646. 1989

[WASS_91] H, Wässle, B. B. Boycott. "Functional architecture of the mammalian retina" Physiological reviews, Vol 71, Nº2, pp. 447-480. 1991

[WASS_95] H. Wässle, U. Grünert, M. Chun, B.B. Boycott. "The rod pathway of the macaque monkey retina: identification of AII-amacrine cells with antibodies against calretinin". The journal of comparative neurology, 361, pp. 537-551. 1995.

[WÄSS_00] H. Wässle, D. M. Dacey, T Haun, S. Haverkamp, U. Grünert, B. B. Boycott."The mosaic of horizontal cells in the macaque monkey retina: with a comment on biplexiform ganglion cells" Visual Neuroscience, 17, pp.591–608. 2000

[WÄSS_04] H. Wässle. "Parallel processing in the mammalian retina" Nature reviews neuroscience Vol. 5 2004.

[WEIL_00] R. Weiler, M. Pottek, S. He, D. I. Vaney. "Modulation of coupling between retinal horizontal cells by retinoic acid and endogenous dopamine" Brain Research Reviews, 32, pp.121–129. 2000.

[WIES_66] T. N. Wiesel, D. H. Hubel "Spatial and chromatic interactions in the latereal geniculate body of the rehsus monkey" J Neurophysiol. 29(6),Ç pp 1115- 1156. 1966

[WIKI_10] www.wikipedia.org 2010

[WOHR_08] A. Wohrer. "Model and large-scale simulator of a biological retina, with contrast gain control". PhD Thesis 2008

[WYSZ_00] G. Wyszecki, W.S. Stiles "Color science: concepts and methods, quantitative data and formulae"2nd edition Ed. JOHN WILEY & SONS, LTD 2000

[XIAO_99] Y. Xiao, A, Zych, D. J. Felleman. "Segregation and convergence of functionally defined V2 thin stripe and interstripe compartment projections to area V4 of macaques". Cerebral cortex, Vol 9, Nº8, pp. 792-804. 1999.

[XU_02] X. Xu, A.B. Bonds, V. A. Casagrande. "Modeling receptive-field structure of koniocellular, magnocellular, and parvocellular LGN cells in the owl monkey (Aotus trivigatus)" Visual Neuroscience, 19, pp. 703-711. 2002.

[YOUN_97] P. A. Young, P.H. Young "Neuroanatomía clínica funcional" Masson 1997

[ZAGH_04] K. A. Zaghloul. "optic nerve signals in a neuromorphic chip I: outer and inner retina model" IEE transactions on biomedical engineering, V 51, N 4, 2004

[ZEKI_80] S. Zeki. "The representation of colours in the cerebral cortex" Nature, Vol 284, pp. 412-418. 1980

[ZREN_81] E. Zrenner, P. Gouras. "Characteristics of the Blue Sensitive Cone mechanism in Primate Ganglion cells". Vision Res., 21, pp. 1605-1609. 1981

http://in.umh.es/

http://www.puc.cl/sw_educ/neurociencias/html/frame02.html ;

http://www.puc.cl/sw_educ/neurociencias/html/frame01.html

http://iibce.edu.uy/uas/neuronas/abc.htm#Forma

http://www.uprm.edu/biology/profs/velez/neurotrans.htm

http://www.herrera.unt.edu.ar/bioingenieria/Temas_inves/sist_nervioso/pagina2.htm

http://www.nia.nih.gov/Alzheimers/Publications/LaEnfermedaddeAlzheimer/Glossario/

http://web.sfn.org/index.cfm?pagename=brainBackgrounders_main#

http://www.iqb.es/neurologia/visitador/v004.htm

http://www.kidshealth.org/kid/en_espanol/cuerpo/brain_esp.html

http://www.elergonomista.com/biologia/snervioso.htm

http://viref.udea.edu.co/contenido/apuntes/gusramon/con_corporal_II/06-periferico.pdf

http://webvision.med.utah.edu/Color.html

f